frontiers | Research Topics

Advances in radiotherapy for head and neck cancer

Edited by
Giuseppe Carlo Iorio, Nerina Denaro, Isacco Desideri, Umberto Ricardi, Valerio Nardone and Lorenzo Livi

Published in
Frontiers in Oncology

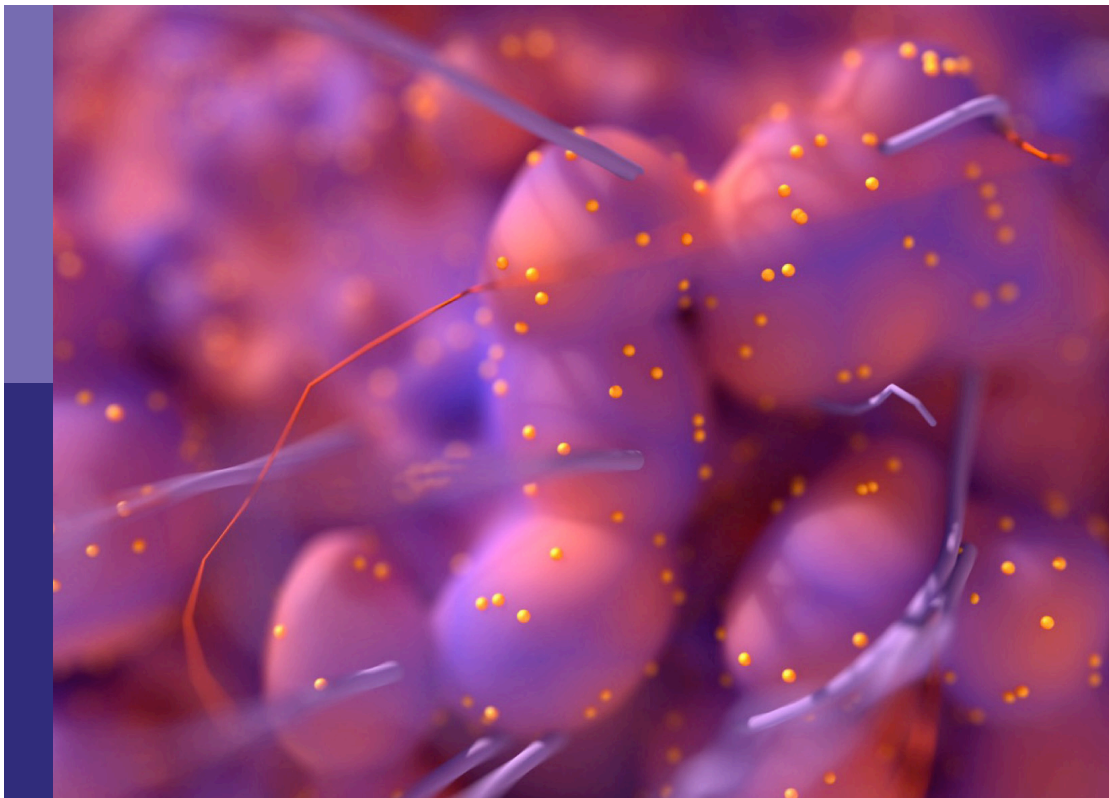

ISSN 1664-8714
ISBN 978-2-8325-5044-1
DOI 10.3389/978-2-8325-5044-1

About Frontiers

Frontiers is more than just an open access publisher of scholarly articles: it is a pioneering approach to the world of academia, radically improving the way scholarly research is managed. The grand vision of Frontiers is a world where all people have an equal opportunity to seek, share and generate knowledge. Frontiers provides immediate and permanent online open access to all its publications, but this alone is not enough to realize our grand goals.

Frontiers journal series

The Frontiers journal series is a multi-tier and interdisciplinary set of open-access, online journals, promising a paradigm shift from the current review, selection and dissemination processes in academic publishing. All Frontiers journals are driven by researchers for researchers; therefore, they constitute a service to the scholarly community. At the same time, the *Frontiers journal series* operates on a revolutionary invention, the tiered publishing system, initially addressing specific communities of scholars, and gradually climbing up to broader public understanding, thus serving the interests of the lay society, too.

Dedication to quality

Each Frontiers article is a landmark of the highest quality, thanks to genuinely collaborative interactions between authors and review editors, who include some of the world's best academicians. Research must be certified by peers before entering a stream of knowledge that may eventually reach the public - and shape society; therefore, Frontiers only applies the most rigorous and unbiased reviews. Frontiers revolutionizes research publishing by freely delivering the most outstanding research, evaluated with no bias from both the academic and social point of view. By applying the most advanced information technologies, Frontiers is catapulting scholarly publishing into a new generation.

What are Frontiers Research Topics?

Frontiers Research Topics are very popular trademarks of the *Frontiers journals series*: they are collections of at least ten articles, all centered on a particular subject. With their unique mix of varied contributions from Original Research to Review Articles, Frontiers Research Topics unify the most influential researchers, the latest key findings and historical advances in a hot research area.

Find out more on how to host your own Frontiers Research Topic or contribute to one as an author by contacting the Frontiers editorial office: frontiersin.org/about/contact

Advances in radiotherapy for head and neck cancer

Topic editors

Giuseppe Carlo Iorio — University of Turin, Italy
Nerina Denaro — IRCCS Ca 'Granda Foundation Maggiore Policlinico Hospital, Italy
Isacco Desideri — University of Florence, Italy
Umberto Ricardi — University of Torino, Italy
Valerio Nardone — University of Campania Luigi Vanvitelli, Italy
Lorenzo Livi — Department of Radiotherapy, Careggi Hospital, Italy

Citation

Iorio, G. C., Denaro, N., Desideri, I., Ricardi, U., Nardone, V., Livi, L., eds. (2024). *Advances in radiotherapy for head and neck cancer*. Lausanne: Frontiers Media SA. doi: 10.3389/978-2-8325-5044-1

Table of contents

frontiers | Frontiers in Oncology

TYPE Editorial
PUBLISHED 07 June 2024
DOI 10.3389/fonc.2024.1437237

OPEN ACCESS

EDITED AND REVIEWED BY
Timothy James Kinsella,
Brown University, United States

*CORRESPONDENCE
Giuseppe Carlo Iorio
beppecarlo.iorio@gmail.com

RECEIVED 23 May 2024
ACCEPTED 31 May 2024
PUBLISHED 07 June 2024

CITATION
Iorio GC, Denaro N, Livi L, Desideri I, Nardone V and Ricardi U (2024) Editorial: Advances in radiotherapy for head and neck cancer.
Front. Oncol. 14:1437237.
doi: 10.3389/fonc.2024.1437237

Editorial: Advances in radiotherapy for head and neck cancer

Giuseppe Carlo Iorio[1]*, Nerina Denaro[2], Lorenzo Livi[3], Isacco Desideri[3], Valerio Nardone[4] and Umberto Ricardi[1]

[1]Department of Oncology, Radiation Oncology, University of Turin, Turin, Italy, [2]Medical Oncology Unit, Fondazione IRCCS Ca' Granda Ospedale Maggiore Policlinico, Milan, Italy, [3]Department of Experimental and Clinical Biomedical Sciences "Mario Serio", University of Florence, Florence, Italy, [4]Department of Precision Medicine, University of Campania "L. Vanvitelli", Naples, Italy

KEYWORDS

HNC (head and neck cancer), radiotherapy, radiation oncology, cancer care, personalized oncology

Editorial on the Research Topic
Advances in radiotherapy for head and neck cancer

Modern Radiotherapy (RT) plays a key role in Head and Neck Cancer (HNC). More precise delivery techniques, increasing employment of hadrontherapy, and artificial intelligence (AI) support characterize modern RT, enabling safer treatments with enhanced therapeutic window. Nonetheless, multidisciplinary care paths are necessary to manage HNC patients undergoing RT. This Research Topic features 14 articles exploring the advances in RT for HNC, covering both clinical and technological aspects in this complex oncologic scenario.

The first manuscript by Chen is a remarkable review of one of the topics at the forefront of HNC research: the human papillomavirus (HPV-)related oropharyngeal squamous cell carcinoma RT de-escalation (1). Chen appropriately highlighted how, while enthusiasts argue that the data robustly supports the integration of de-escalation into contemporary practice, skeptics point out that the published data is still relatively preliminary and makes it difficult to make definitive recommendations.

Two manuscripts reported the role of hadrontherapy in HNC (Adeberg et al. and Rampinelli et al.). Hadrontherapy offers advantages in dose distribution and improved radiobiology that may significantly improve the treatment safety and outcomes of certain HNCs (2–4). The retrospective analysis by Adeberg et al. assessed the outcomes and treatment-related toxicity following intensity-modulated RT (IMRT) and a Carbon Ion RT (CIRT) boost for salivary duct carcinoma (SDC). The study showed that multimodal therapy approaches with surgery followed by IMRT and CIRT boost for SDC leads to good local and locoregional disease control. The use of proton therapy reirradiation for HNC is increasing (5). However, reports are heterogeneous, and outcomes can be difficult to interpret (5). Rampinelli et al. assessed outcomes and toxicities of different treatment modalities (including proton therapy) for recurrent nasopharyngeal carcinoma (NPC) in a non-endemic area. A total of 140 patients treated in Italy from 1998 to 2020 were retrospectively assessed. In this series, favorable cases with lower age, comorbidity rate, and stage underwent preferentially endoscopic surgery, as well as patients with shorter

disease-free interval from primary treatment. More complex cases underwent re-RT, distributed between photon-based RT and proton therapy. Noteworthy, regarding the intricate context of recurrent NPC, a Chinese multicentre randomized phase 3 trial (published in 2021) demonstrated that endoscopic surgery significantly improved overall survival compared with re-IMRT in patients with resectable local recurrence (6).

Three manuscripts focused on how radiation oncologists should set up multidisciplinary care paths to limit the severity of side effects and encourage tailored monitoring strategies for HNC patients (Santo et al.; He et al.; Patel et al.).

Patients with HNC are at a high risk of malnutrition at the time of diagnosis, and nutritional support or intervention is often needed during and after RT to avoid jeopardizing treatment outcomes (7). Therefore, the role of a multidisciplinary team is to share the outcomes to assess the proper supportive path. The literature overview by Santo et al. highlighted that adequate nutritional screening, assessment, and interventions might increase treatment adherence. Cognitive behavioral therapy (CBT) has already been confirmed to be an effective psychological treatment to avoid or decrease the occurrence of adverse effects in patients with proven malignancies (8). In this regard, the prospective study by He et al. showed that CBT reduced the occurrence, latency, and severity of oral mucositis during chemoradiation therapy for locoregional advanced NPC. A too-often neglected HNC treatment-related toxicity is financial toxicity. Unplanned hospitalizations and emergency department (ED) visits during RT can lead to treatment breaks, leading to a financial burden on patients and the healthcare system (9). Patel et al. retrospectively analyzed the occurrence of ED visits, unplanned hospitalizations, and treatment breaks in HNC patients (n=376) undergoing RT in relation to pain and opioid use as well as other clinical, treatment, and socioeconomic characteristics. The authors found that patients with factors such as heavy opioid use, black race, receipt of concomitant chemotherapy, and lower socioeconomic class may require closer monitoring during RT.

Moving into the "technical" section, this Research Topic is rounded out by two articles (Zong et al.; Cai et al.) focusing on NPC clinical target volume (CTV) optimization and organs-at-risk (OARs) refinement, and a final set of six articles (Luan et al.; Lucido et al.; Gu et al.; Li et al.; Liu et al.; Huang et al.) highlighting advances in machine learning(ML)/deep learning(DL), radiomics and dosiomics.

In terms of modern RT target volumes refinement and optimization for NPC patients, a phase III trial published in 2022 demonstrated that the elective ipsilateral upper-neck irradiation (UNI), sparing the uninvolved lower neck, provided similar regional control and resulted in less toxicity compared with standard whole-neck irradiation (WNI) in patients with N0-N1 disease (10). The retrospective study by Zong et al. aimed to determine the diagnostic value of diffusion-weighted imaging (DWI) and to elucidate the clinical characteristics of medial group retropharyngeal lymph nodes (RLNs) based on multimodal imaging. Additionally, the authors intended to explore the feasibility of optimizing the CTV60 boundary based on the characteristics of medial group RLNs. Among the findings, DWI demonstrated superiority in displaying lymph nodes. Moreover, based on the low incidence of the medial RLNs, CTV60 of medial group RLNs from the skull base to the upper edge of C2 emerged as feasible, leading to dosimetric advantages for protecting swallowing structures. Cai et al. aimed to assess the effects of accessory parotid gland (APG) on the dosimetry of the parotid glands (PGs) during NPC RT and evaluate its predictive value for late xerostomia. Noteworthy, the APG is rarely mentioned in the literature (11). Cai et al. suggested the potential benefits of considering the APG and PGs as a single OAR during RT for NPC. With APG included, the predictive power of the dosimetric parameters for xerostomia tended to improve, although no significant differences were observed. Manual labeling of HN OARs is time-consuming and subjective (12). Therefore, DL segmentation methods have been widely used. However, the accuracy of commercial autosegmentation systems still needs to be evaluated and improved (13).

Luan et al. proposed a parallel network architecture called PCG-Net, which incorporates both convolutional neural networks and a Gate-Axial-Transformer to capture local information and global context effectively. The PCG-Net outperformed other methods, improving the accuracy of HN OARs segmentation and potentially treatment planning for HNC patients. In the setting of using a DL-based autosegmentation model to reduce contouring time without compromising contour accuracy, Lucido et al. conducted a blinded randomized trial employing two HNC expert radiation oncologists and using retrospective de-identified patient data. DL autosegmentation demonstrated significant time-savings for OARs contouring while improving agreement with the institutional gold standard. On the other hand, DL for RT dose prediction has been reported for different tumor sites, but the influence of multiple different levels of input information on the ability to predict dose has not been adequately investigated. A generative adversarial network (GAN) is a class of ML frameworks and a prominent framework for approaching generative AI.

A GAN generates realistic predictions using two concurrent generative and discriminative neural networks (14, 15). Gu et al. used a three-dimensional deep GAN to predict dose distributions for locally advanced HNC RT and achieved results that were highly similar to the clinical plans.

Radiomics is a new research field that decodes tumor phenotypes by quantitatively analyzing image features extracted from medical images, seeking personalized clinical decision-making and better patient stratification (16–20).

Li et al. analyzed the recurrence patterns and reasons in patients with NPC treated with IMRT and investigated the feasibility of radiomics for the analysis of radioresistance. The authors found that radiomic analysis can serve as an imaging biomarker to facilitate early salvage for NPC patients at risk of in-field recurrence. Using methods similar to radiomics, dosiomics analyzes the spatial features of the 3-dimensional patient-specific dose distribution, providing better predictions of radiation-induced results (21, 22). Liu et al. demonstrated that a comprehensive modeling approach combining radiomics, dosiomics and clinical components displayed better predictive values for locoregional recurrence risk following

RT than any single factor for locoregionally advanced hypopharyngeal squamous cell carcinoma.

Finally, radiomics and dosiomics can predict treatment-related toxicity for HNC patients. Huang et al. showed that radiomics and dosiomics features (from the planning computed tomography) are correlated with the incidence of grade 4 radiation-induced lymphopenia (G4-RIL) in NPC patients. Noteworthy, RIL has been proven to be a prognostically significant toxicity, affecting survival outcomes in several solid tumors (23, 24). To conclude, this Research Topic presents evidence of the clinical and technological advances in RT for HNC. This broad collection of articles summarizes these exciting active research areas while underscoring the current advances.

Author contributions

GI: Conceptualization, Investigation, Writing – original draft, Writing – review & editing, Data curation, Methodology, Project administration, Supervision, Validation, Visualization. ND: Conceptualization, Writing – review & editing. LL: Conceptualization, Writing – review & editing. ID: Conceptualization, Writing – review & editing. VN: Conceptualization, Writing – review & editing. UR: Conceptualization, Writing – review & editing.

Conflict of interest

The authors declare that the research was conducted in the absence of any commercial or financial relationships that could be construed as a potential conflict of interest.

The author(s) declared that they were an editorial board member of Frontiers, at the time of submission. This had no impact on the peer review process and the final decision.

Publisher's note

References

1. Iorio GC, Arcadipane F, Martini S, Ricardi U, Franco P. Decreasing treatment burden in HPV-related OPSCC: A systematic review of clinical trials. *Crit Rev Oncol Hematol.* (2021) 160:103243. doi: 10.1016/j.critrevonc.2021.103243

2. Laramore GE. Role of particle radiotherapy in the management of head and neck cancer. *Curr Opin Oncol.* (2009) 21:224–31. doi: 10.1097/cco.0b013e328329b716

3. Garden AS, Weber RS, Morrison WH, Ang KK, Peters LJ. The influence of positive margins and nerve invasion in adenoid cystic carcinoma of the head and neck treated with surgery and radiation. *Int J Radiat Oncol Biol Phys.* (1995) 32:619–26. doi: 10.1016/0360–3016(95)00122-F

4. Jensen AD, Nikoghosyan AV, Poulakis M, Höss A, Haberer T, Jäkel O, et al. Combined intensity-modulated radiotherapy plus raster-scanned carbon ion boost for advanced adenoid cystic carcinoma of the head and neck results in superior locoregional control and overall survival. *Cancer.* (2015) 121:3001–9. doi: 10.1002/cncr.29443

5. Lee A, Woods R, Mahfouz A, Kitpanit S, Cartano O, Mohamed N, et al. Evaluation of proton therapy reirradiation for patients with recurrent head and neck squamous cell carcinoma. *JAMA Netw Open.* (2023) 6:e2250607. doi: 10.1001/jamanetworkopen.2022.50607

6. Liu YP, Wen YH, Tang J, Wei Y, You R, Zhu XL, et al. Endoscopic surgery compared with intensity-modulated radiotherapy in resectable locally recurrent nasopharyngeal carcinoma: a multicentre, open-label, randomised, controlled, phase 3 trial. *Lancet Oncol.* (2021) 22:381–90. doi: 10.1016/S1470–2045(20)30673–2

7. Isenring EA, Capra S, Bauer JD. Nutrition intervention is beneficial in oncology outpatients receiving radiotherapy to the gastrointestinal or head and neck area. *Br J Cancer.* (2004) 91:447–52. doi: 10.1038/sj.bjc.6601962

8. Brothers BM, Yang HC, Strunk DR, Andersen BL. Cancer patients with major depressive disorder: testing a biobehav Ioral/Cognitive behavior intervention. *J Consult Clin Psychol.* (2011) 79:253–60. doi: 10.1037/a0022566

9. Noel CW, Forner D, Wu V, Enepekides D, Irish JC, Husain Z, et al. Predictors of surgical readmission, unplanned hospitalization and emergency department use in head and neck oncology: A systematic review. *Oral Oncol.* (2020) 111:105039. doi: 10.1016/J.ORALONCOLOGY.2020.105039

10. Tang LL, Huang CL, Zhang N, Jiang W, Wu YS, Huang SH, et al. Elective upper-neck versus whole-neck irradiation of the uninvolved neck in patients with nasopharyngeal carcinoma: an open-label, non-inferiority, multicentre, randomised phase 3 trial. *Lancet Oncol.* (2022) 23:479–90. doi: 10.1016/S1470–2045(22)00058–4

11. Frommer J. The human accessory parotid gland: its incidence, nature, and significance. *Oral Surg Oral Med Oral Pathol.* (1977) 43:671–6. doi: 10.1016/0030–4220(77)90049–4

12. Kosmin M, Ledsam J, Romera-Paredes B, Mendes R, Moinuddin S, de Souza D, et al. Rapid advances in auto-segmentation of organs at risk and target volumes in head and neck cancer. *Radiother Oncol.* (2019) 135:130–40. doi: 10.1016/j.radonc.2019.03.004

13. Chen X, Sun S, Bai N, Han K, Liu Q, Yao S, et al. A deep learning-based autosegmentation system for organs-at-risk on whole-body computed tomography images for radiation therapy. *Radiother Oncol.* (2021) 160:175–84. doi: 10.1016/j.radonc.2021.04.019

14. Goodfellow IJ, Pouget-Abadie J, Mirza M, Xu B, Warde-Farley D, Ozair S, et al. Generative adversarial networks. *Adv Neural Inf Process Syst.* (2014) 2672–80. doi: 10.48550/arXiv.1406.2661

15. Isola P, Zhu J-Y, Zhou T, Efros AA. Image-to-image translation with conditional adversarial networks. IEEE-Proceedings of the IEEE Conference on Computer Vision and Pattern Recognition (CVPR). (2017) 5967–76. doi: 10.1109/CVPR.2017.632

16. Fave X, Mackin D, Lee J, Yang J, Zhang L. Computational resources for radiomics. *Transl Cancer Res.* (2016) 5:340–8. doi: 10.21037/tcr.2016.06.17

17. Aerts HJ, Velazquez ER, Leijenaar RT, Parmar C, Grossmann P, Carvalho S, et al. Decoding tumour phenotype by noninvasive imaging using a quantitative radiomics approach. *Nat Commun.* (2014) 5:4006. doi: 10.1038/ncomms5006

18. Lambin P, Rios-Velazquez E, Leijenaar R, Carvalho S, van Stiphout RG, Granton P, et al. Radiomics: extracting more information from medical images using advanced feature analysis. *Eur J Cancer.* (2012) 48:441. doi: 10.1016/j.ejca.2011.11.036

19. Gillies RJ, Kinahan PE, Hricak H. Radiomics: images are more than pictures, they are data. *Radiology.* (2016) 278:563. doi: 10.1148/radiol.2015151169

20. Kumar V, Gu Y, Basu S, Berglund A, Eschrich SA, Schabath MB, et al. Radiomics: the process and the challenges. *Magn Reson Imaging.* (2012) 30:1234–48. doi: 10.1016/j.mri.2012.06.010

21. Liang B, Yan H, Tian Y, Chen X, Yan L, Zhang T, et al. Dosiomics: Extracting 3D spatial features from dose distribution to predict incidence of radiation pneumonitis. *Front Oncol.* (2019) 9:269. doi: 10.3389/fonc.2019.00269

22. Wu A, Li Y, Qi M, Lu X, Jia Q, Guo F, et al. Dosiomics improves prediction of locoregional recurrence for intensity modulated radiotherapy treated head and neck cancer cases. *Oral Oncol.* (2020) 104:104625. doi: 10.1016/j.oraloncology.2020.104625

23. Iorio GC, Ricardi U, Dal Pra A. Radiation-induced lymphopenia beyond the COVID-19 pandemic. *Front Oncol.* (2020) 10:617302. doi: 10.3389/fonc.2020.617302

24. Iorio GC, Spieler BO, Ricardi U, Dal Pra A. The impact of pelvic nodal radiotherapy on hematologic toxicity: A systematic review with focus on leukopenia, lymphopenia and future perspectives in prostate cancer treatment. *Crit Rev Oncol Hematol.* (2021) 168:103497. doi: 10.1016/j.critrevonc.2021.103497

frontiers in Oncology

ORIGINAL RESEARCH
published: 21 December 2018
doi: 10.3389/fonc.2018.00648

Use of Radiomics Combined With Machine Learning Method in the Recurrence Patterns After Intensity-Modulated Radiotherapy for Nasopharyngeal Carcinoma: A Preliminary Study

Shuangshuang Li†, Kongcheng Wang†, Zhen Hou, Ju Yang, Wei Ren, Shanbao Gao, Fanyan Meng, Puyuan Wu, Baorui Liu, Juan Liu and Jing Yan**

The Comprehensive Cancer Centre of Drum Tower Hospital, Medical School of Nanjing University and Clinical Cancer Institute of Nanjing University, Nanjing, China

OPEN ACCESS

Edited by:
Radka Stoyanova, University of Miami, United States

Reviewed by:
Bilgin Kadri Aribas, Bülent Ecevit University, Turkey
Andrew Wenhua Ju, The Brody School of Medicine at East Carolina University, United States

***Correspondence:**
Jing Yan
yj20030610@126.com
Juan Liu
liuuar0813@163.com

†These authors have contributed equally to this work

Specialty section:
This article was submitted to Radiation Oncology, a section of the journal Frontiers in Oncology

Received: *18 September 2018*
Accepted: *10 December 2018*
Published: *21 December 2018*

Citation:
Li S, Wang K, Hou Z, Yang J, Ren W, Gao S, Meng F, Wu P, Liu B, Liu J and Yan J (2018) Use of Radiomics Combined With Machine Learning Method in the Recurrence Patterns After Intensity-Modulated Radiotherapy for Nasopharyngeal Carcinoma: A Preliminary Study. Front. Oncol. 8:648. doi: 10.3389/fonc.2018.00648

Objective: To analyze the recurrence patterns and reasons in patients with nasopharyngeal carcinoma (NPC) treated with intensity-modulated radiotherapy (IMRT) and to investigate the feasibility of radiomics for analysis of radioresistance.

Methods: We analyzed 306 NPC patients treated with IMRT from Jul-2009 to Aug-2016, 20 of whom developed with recurrence. For the NPCs with recurrence, CT, MR, or PET/CT images of recurrent disease were registered with the primary planning CT for dosimetry analysis. The recurrences were defined as in-field, marginal or out-of-field, according to dose-volume histogram (DVH) of the recurrence volume. To explore the predictive power of radiomics for NPCs with in-field recurrences (NPC-IFR), 16 NPCs with non-progression disease (NPC-NPD) were used for comparison. For these NPC-IFRs and NPC-NPDs, 1117 radiomic features were quantified from the tumor region using pre-treatment spectral attenuated inversion-recovery T2-weighted (SPAIR T2W) magnetic resonance imaging (MRI). Intraclass correlation coefficients (ICC) and Pearson correlation coefficient (PCC) was calculated to identify influential feature subset. Kruskal-Wallis test and receiver operating characteristic (ROC) analysis were employed to assess the capability of each feature on NPC-IFR prediction. Principal component analysis (PCA) was performed for feature reduction. Artificial neural network (ANN), k-nearest neighbor (KNN), and support vector machine (SVM) models were trained and validated by using stratified 10-fold cross validation.

Results: The median follow up was 26.5 (range 8–65) months. 9/20 (45%) occurred in the primary tumor, 8/20 (40%) occurred in regional lymph nodes, and 3/20 (15%) patients developed a primary and regional failure. Dosimetric and target volume analysis of the recurrence indicated that there were 18 in-field, and 1 marginal as well as 1 out-of-field recurrence. With pre-therapeutic SPAIR T2W MRI images available, 11 NPC-IFRs (11 of 18 NPC-IFRs who had available pre-therapeutic MRI) and 16 NPC-NPDs were subsequently employed for radiomic analysis. Results showed that NPC-IFRs vs.

NPC-NPDs could be differentiated by 8 features (AUCs: 0.727–0.835). The classification models showed potential in prediction of NPC-IFR with higher accuracies (ANN: 0.812, KNN: 0.775, SVM: 0.732).

Conclusion: In-field and high-dose region relapse were the main recurrence patterns which may be due to the radioresistance. After integration in the clinical workflow, radiomic analysis can be served as imaging biomarkers to facilitate early salvage for NPC patients who are at risk of in-field recurrence.

Keywords: intensity-modulated radiotherapy, nasopharyngeal carcinoma, recurrence pattern, radiomic analysis, prediction

INTRODUCTION

The incidence and mortality of nasopharynx cancer (NPC) were estimated to 130,000 and 73,000 worldwide, respectively, in 2018 (1). In China, 60.600 cases were diagnosed with NPC in 2015, responsible for approximately 1.41% of the total incidence of malignancy (2).

Intensity-modulated radiotherapy (IMRT) has served as a major breakthrough in the treatment of head and neck cancer carcinoma (HNC) as it is capable of providing a highly conformal dose distribution with sharp dose gradients. By conforming the doses to the irregular tumor, dose escalation is possible with IMRT, which has greatly improved the therapeutic ratio and local control after radiotherapy (3). However, local-regional recurrence remains the major cause of treatment failure in patients with NPC (4). Although some research has been carried out on the patterns of local-regional recurrence (e.g., out of field, in field, marginal miss) (4–8), few studies have focused on early identification of patients who are at higher risk of in-field recurrence before radiotherapy. Therefore, new tools are needed for further investigation of radiation resistant of NPCs with in-field recurrence.

Radiomics is a new research field to decode tumor phenotype by quantitative analysis of image features extracted from medical images, with the goal of personalized clinical decision making and improving patient stratification. This advanced technology has shown the significant predictive power for gene expression, pathological classification, response to treatment, and prognosis (9–13). By extracting a high-dimensional mineable feature set from MRI images, recent studies on NPC have found that the features are associated with pathological types, progression free survival (PFS), local or distant treatment failure, and treatment response (14). Thus far, to our knowledge, although prior studies (4–8) have been able to explore the recurrence patterns of failure, further radiomic analysis for in-field recurrence has not been performed at present.

In this study, we investigated the potential of MRI-based radiomics in characterizing radioresistance of nasopharyngeal carcinoma (NPC) with in-field recurrence. Specifically, we examined whether radiomic features could distinguish NPC-IFR (NPC with in-field recurrence) from NPC-NPD (NPC with non-progression disease).

MATERIALS AND METHODS

Patients and Tumor Characteristics

This retrospective study was approved by the Nanjing Drum Tower Hospital's ethics committee, and informed consent was waived. Three hundred and six patients administered radiation with IMRT for NPC from July 2009 to August 2016 were reviewed. Inclusion criteria were: (a) biopsy-proven nasopharyngeal carcinoma; (b) absence of metastases; (c) developed with recurrence after IMRT; (d) radiotherapy (RT) for primary disease were administered at Nanjing Drum Tower Hospital; (e) CT, and/or MRI/PET examination were performed before and after RT; (f) completion of planned radiation treatment; (g) follow-up of more than 3 months.

A total of 20 recurrent NPCs who met the criteria were identified. **Table 1** shows the general characteristics of the patients.

Imaging Method

Pretreatment and recurrent MR images were obtained with a 3.0 T MRI unit (Achieva 3.0T X-series, Philips Healthcare, Best, Netherlands) according to a standard clinical acquisition protocol: SPAIR T2W MRI (repetition time [TR], 3,000 ms; echo time [TE], 100 ms; flip angel, 90 degrees; matrix size, 212 × 141; slice thickness 4 mm, in-plane resolution 0.65 mm × 0.65 mm).

TABLE 1 | Baseline characteristics of 20 NPCs with recurrence.

Characteristic	Number of patients (%)
Total	20
Gender	
Male	16/20 (80%)
Female	4/20 (20%)
Age (years)	
Median (range)	51 (41–66 years)
AJCC staging	
III	17/20 (85%)
IVa	3/20 (23%)
Concurrent Chemotherapy	
Yes	20/20 (100%)
No	0/20 (0%)
Radiotherapy technique	IMRT

SPAIR is a kind of fat-suppression techniques which is desirable to remove the fat contribution from MR imaging signal to better visualize pathology or contrast enhanced (15). Tie et al. (16) reported that the addition of fat suppression techniques to T2W MR sequences improves the detection and delineation of head and neck lesions.

Target Delineation and IMRT Treatment Planning

Patients were treated with supine position and immobilized by a thermoplastic head and shoulder mask. CT images with slice thickness of 3 mm were obtained and transferred to Pinnacle software (Philips Medical Systems, Andover, MA, United States) for treatment planning design.

Tumor volumes were defined by both experienced radiologists and radiation oncologists on simulation CT images registered with MRI images. The gross tumor volume (GTV) including primary gross tumor volume (GTVp) and involved lymph nodes (GTVnd), was defined as the visible tumor based on imaging, clinical examination, as well as endoscopic findings. The elective clinical target volume (CTV) was defined to include regions and lymph nodes that have a high risk of tumor involvement. The planning target volume (PTV) was constructed automatically by expanding the corresponding CTV by 3–5 mm according to the immobilization and localization uncertainties.

The range of the total prescribed RT dose was 70–74 Gy. All patients were treated at 2–2.2 Gy daily fractions, one fraction per day, 5 days per week, as shown in **Table 2**. The radiation dose was prescribed to cover at least 96% of PTV. All plans were assessed and confirmed by both senior physicians and oncologists. All patients were treated with external-beam radiation therapy using 6-MV photons, 7–9 radiation fields.

Chemotherapy

The chemotherapy program was performed according to clinicians' assessment of multi-factors, including age, comorbidity, contraindication, tumor extent and social support. One patient (No.10 in **Table 2**) in stage IVa received neoadjuvant chemotherapy with nedaplatin + 5-fluorouracil. All patients received nedaplatin/docetaxel/paclitaxel liposome based concurrent chemotherapy. Adjuvant chemotherapy was delivered to all patients following concurrent chemoradiation. The most common regimen of adjuvant chemotherapy included nedaplatin + 5-fluorouracil or docetaxel + 5-fluorouracil or nedaplatin + 5-fluorouracil+docetaxel or paclitaxel + gemcitabine (17–20).

Image Registration and Recurrence Definition

Local recurrence referred to the disappearance of the primary tumor treated with radical radiation but the presence of new lesions later, while regional recurrence referred to the reappearance of metastatic lymph nodes in the lymphatic drainage area. The local regional recurrences were confirmed by MRI and/or PET scan, or pathological biopsy examination if applicable.

For patients with local regional failure, MRI and/or PET scans obtained at the time of recurrence were registered with pretreatment planning CT, by rigid registration first and then deformable registration and visual assessment, using MIM (MIM Software, Inc., Cleveland, OH, United States). The recurrent tumor volume (V_{recur}) was subsequently identified and delineated by the user blinded to the original tumor volume and isodose distribution.

After V_{recur} was delineated on the pretreatment planning CT, the radiation dosed received by V_{recur} was then obtained by analyzing the dose-volume histogram (DVH). Depending on the position of V_{recur}, the recurrences were classified into occurring inside or outside the high-dose target volume: "in field," in which 95% or more of V_{recur} was within the 95% prescription isodose; "marginal miss," if 20 to 95% of the V_{recur} was inside the 95% prescription isodose; "out of field," if <20% of the V_{recur} was within the 95% prescription isodose (8).

Recurrences were defined as local if the failures occurred inside the primary tumor, and as regional if the failures occurred elsewhere including neck lymph nodes. **Figure 1** shows the type of failures for patients with recurrences.

Image Preprocessing and Radiomic Feature Extraction for NPC

To investigate the feasibility of radiomics for analysis of NPC radioresistance, NPCs with in-field recurrences (NPC-IFR) and with non-progression disease (NPC-NPD) after treatment were enrolled for radiomic analysis. NPC-NPD were met the following inclusion criteria: (a) biopsy-proven nasopharyngeal carcinoma; (b) absence of metastases; (c) RT for primary disease were administered at our institution; (d) completion of planned radiation treatment; (e) followed-up for more than 36 month and has not been lost to date; (f) available of pretreatment SPAIR T2W MR images. A total of 16 recurrent NPC-IFR who met the criteria were identified. **Figure 2** shows the flowchart of using radiomic analysis in NPC-IFR vs. NPC-NPD.

The radiomic features were extracted from pretreatment gross tumor volume. Before using these treatment-planning contours for radiomic research, each contour was manually modified to avoid adjacent air, fat and surrounding organs by two senior board-certified radiation oncologists. In addition, for each contour, gray-level normalization was performed, using a method that normalize the image intensities in a range of $[m - 3s, m + 3s]$ (m, mean value of gray-level in the contours; s, standard deviation of gray-level), to minimize the influence of contrast and brightness variation (21). The gray levels that were located outside the range $[m \pm 3s]$ were excluded for further analysis and the range obtained was subsequently quantized to 6 bits (between 1 and 64) (21). Moreover, the contoured volume with voxel size of $0.65 \times 0.65 \times 4$ mm^3 were resampled to a voxel size of $1 \times 1 \times 1$ mm^3 using cubic interpolation algorithm before feature extraction to unify the voxel size across the cohort.

Radiomic feature computation was performed using pyradiomics V1.3.0 (22). Pyradiomics is an open-source python package for the extraction of radiomic features from two-dimensional (2D) or three-dimensional (3D) medical imaging

TABLE 2 | Details of recurrent patients and their failure patterns.

No.	Primary tumor site	Stage	RT dose (Gy/fr)	Concurrent chemotherapy	Time to failure (Months)	Site of recurrence	Patterns of failure
1	Nasopharynx	III	50 Gy/25 + 20 Gy/10	Nedaplatin	19	Local	In field
2	Nasopharynx	III	50 Gy/25 + 20 Gy/10	Paclitaxel liposome	65	Regional	In field
3	Nasopharynx*	III	44 Gy/20 + 22 Gy/10 + 4 Gy/2	Nedaplatin	14	Local	In field
4	Nasopharynx	III	44 Gy/20 + 22 Gy/10 + 4 Gy/2	Paclitaxel liposome	49	Regional	Marginal
5	Nasopharynx*	III	50 Gy/25 + 20 Gy/10	Nedaplatin	30	Local-regional	In field
6	Nasopharynx*	III	50 Gy/25 + 20 Gy/10	Nedaplatin	17	Local-regional	In field
7	Nasopharynx	III	44 Gy/20 + 22 Gy/10 + 4.4 Gy/2	Nedaplatin	54	Regional	Out of field
8	Nasopharynx*	III	50 Gy/25 + 20 Gy/10	Nedaplatin	8	Local	In field
9	Nasopharynx*	III	44Gy/20 + 22 Gy/10 + 4.4 Gy/2	Docetaxel	34	Local-regional	In field
10	Nasopharynx*	IVa	44 Gy/20 + 22 Gy/10 + 6.6 Gy/3	Nedaplatin	26	Local	In field
11	Nasopharynx	III	66 Gy/30 + 4 Gy/2	Docetaxel+ oxaliplatin	27	Local	In field
12	Nasopharynx*	III	50 Gy/25 + 20 Gy/10	Nedaplatin	11	Regional	In field
13	Nasopharynx*	III	50 Gy/25 + 20 Gy/10	Docetaxel	41	Regional	In field
14	Nasopharynx	IVa	50 Gy/25 + 20 Gy/10 + 4 Gy/2	Cetuximab+ Nedaplatin	26	Local	In field
15	Nasopharynx*	III	50 Gy/25 + 20 Gy/10	Nedaplatin	26	Regional	In field
16	Nasopharynx	IVa	44 Gy/20 + 22 Gy/10 + 4.4 Gy/2	Docetaxel	51	Regional	In field
17	Nasopharynx	III	50 Gy/25 + 20 Gy/10	Oxaliplatin	41	Regional	In field
18	Nasopharynx*	III	44 Gy/20 + 22 Gy/10 + 4.4 Gy/2	Nedaplatin	33	Local	In field
19	Nasopharynx*	III	50 Gy/25 + 20 Gy/10	Paclitaxel liposome	14	Local	In field
20	Nasopharynx	III	50 Gy/25 + 20 Gy/10 + 4 Gy/2	Nedaplatin	23	Local	In field

**11 NPC-IFRs (in field recurrence) with pre-treatment MRI images available are subsequently used for radiomic analysis*

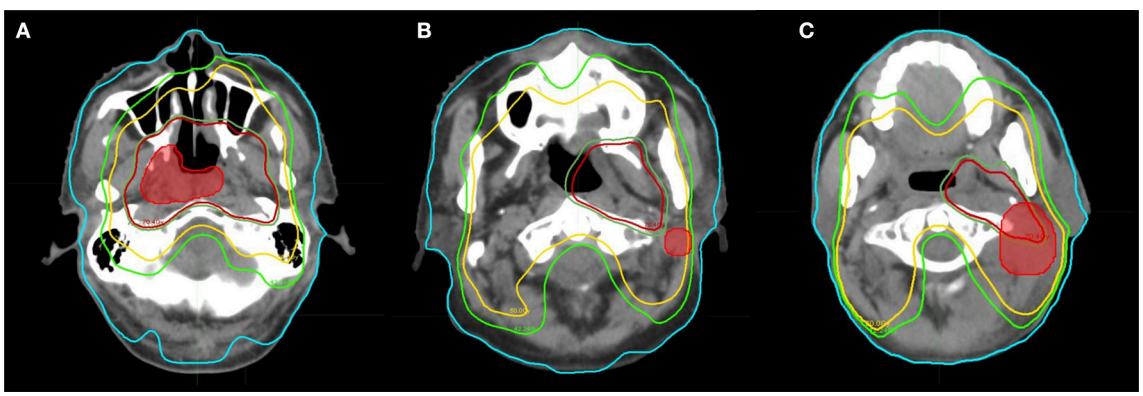

FIGURE 1 | Patterns of failure for patients with recurrence, with the accumulated dose and site of recurrence. **(A)** In field. **(B)** Out of field. **(C)** Marginal.

data. With this package, the following methods were used for feature computation: (1) morphological features: descriptors of shape and size; (2) intensity histogram (IH): describe the distribution of voxel intensities within the contoured volume; (3) five texture matrices: *a*. gray-level co-occurrence matrix (GLCM, 13 angles in 3D [26-connectivity], distance = 1 voxel); *b*. gray level size zone matrix (GLSZM, 13 angles in 3D, distance = 1 voxel); *c*. gray level run length matrix (GLRLM, 13 angles in 3D); *d*. neighboring gray tone difference matrix (NGTDM, neighborhood size: 3 × 3 × 3 voxels); *e*. gray level dependence matrix (GLDM, distance = 1 voxel). As for GLCM, GLSZM, and GLRLM, each feature was calculated on each angle separately, after which the mean value of the feature was obtained. (4) Laplacian of Gaussian (LoG)-filtration and Wavelet-transform features: all the aforementioned texture matrices can also be calculated on a derived image, obtained by applying LoG band

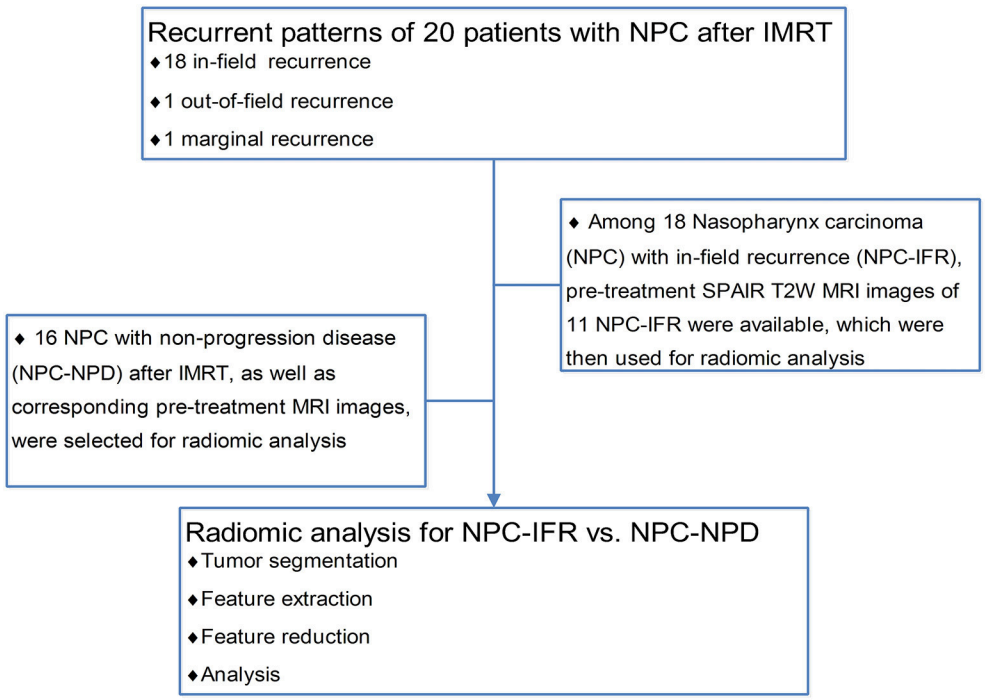

FIGURE 2 | Flowchart of using radiomic analysis in recurrent pattern.

pass filter and wavelet filter on the original image. In particular, LoG filter was applied on the contoured volumes for enhancing fine to coarse texture (filter width: fine, $\sigma = 0.5$; medium, $\sigma = 1.5$; coarse, $\sigma = 2.5$) and wavelet filter was applied to focus features on the different decomposition and approximation level of the original contoured volumes.

Overall, as for each contoured volume, quantitative radiomic features were calculated from original image and derived image, using five principal algorithms: morphological-based (shape and size), IH-based (intensity histogram), texture-based (GLCM, GLSZM, GLRLM, GLDM), LoG filter-based ($LoG_{\sigma=0.5/1.5/2.5}$_GLCM, $LoG_{\sigma=0.5/1.5/2.5}$_GLSZM, $LoG_{\sigma=0.5/1.5/2.5}$_GLRLM, $LoG_{\sigma=0.5/1.5/2.5}$_GLDM), and Wavelet transform—based ($Wavelet_{level}$_GLCM, $Wavelet_{level}$_GLSZM, $Wavelet_{level}$_GLRLM, $Wavelet_{level}$_GLDM). A complete list of the features was shown in **Supplementary Table S1**. **Figure 3A** shows the workflow of radiomic analysis for NPC-IFR. **Figure 3B** shows the example of GLCM textural feature maps calculated from 2D slices.

Statistical Analysis

Statistical analysis was performed using R statistical and computing software version 3.3.2 (http://www.rproject.org, R Foundation for Statistical Computing, Vienna, Austria).

Inter-observer variability in measurement of MRI radiomic features was evaluated by calculating intraclass correlation coefficients (ICC) (ICC $<$ 0.40, poor; 0.40 $\leq$ ICC $<$ 0.60, moderate; 0.60 $\leq$ ICC $<$ 0.80, good; ICC $\geq$ 0.80, excellent), using "irr" package (ver. 0.84 in R software). It was calculated for assessment of feature reproducibility in repeated delineation and then features with ICC $<$ 0.8 were removed. Additionally, for the aforementioned selected features (ICC $\geq$ 0.80), we also compute Pearson correlation coefficient (PCC) by conducting a correlation matrix, to quantify the pair-wise correlations. In this work, for example, if two features appeared a strong correlation ($|PCC| \geq 0.80$), we look at the mean absolute correlation coefficient of each feature (with the remaining features) and remove the feature with the largest mean absolute correlation. Using the above methods, influential feature sets were generated with high reproducibility and low redundancy.

Statistical significance of each influential feature for discrimination between NPC-IFR and NPC-NPD was analyzed using Kruskal-Wallis test. The Benjamini-Hochberg method was performed to correct *P*-values for multiple testing. $P < 0.05$ were considered significant. Diagnostic performance of the significant features was assessed by using receiver operating characteristic (ROC) curve and the area under the curve (AUC) analysis. All the significant features were selected for further analysis.

Feature Reduction and Radiomic Machine-Learning Classifiers

Prior to classification, principal component analysis (PCA) was used to further reduce the feature vector dimensions and to increase the discriminative capability. Those principal components that sufficiently accounted for 85% of the significant feature subset variability were selected for further modeling. Next, supervised machine-learning classifiers (ANN, KNN, and

SVM) were then established and validated with the stratified 10-fold cross-validation in Weka (University of Waikato, Hamilton, New Zealand) to evaluate how well these predictive models would perform with the subset of the components derived from PCA method. The associated metrics including false positives (FP), true positives (TP), accuracy, and matthews correlation coefficient (MCC) were calculated for model evaluation.

RESULTS

Patterns of Recurrence

A total of 20 NPC patients with recurrence were met the inclusion criteria. During a median follow up period of 26.5 months, 9 patients had local recurrences, 8 patients had regional recurrences, and 3 patients had local-regional recurrences. As for the patterns of recurrence, 18 (90%), 1 (5%), and 1 (5%)

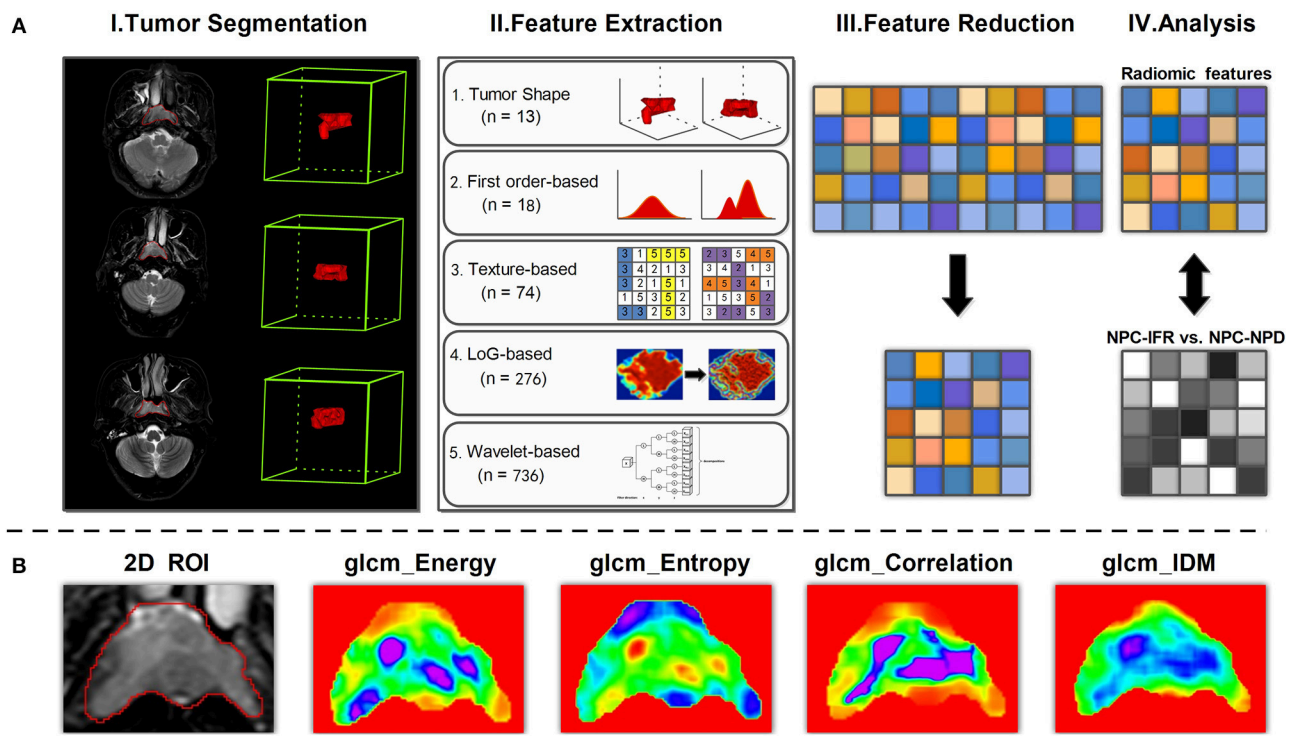

FIGURE 3 | (A) Workflow of radiomic analysis for discrimination between NPC-IFR (NPC with in-field recurrence) and NPC-NPD (NPC with non-progression disease). I, Image segmentation was performed on SPAIR T2W MR images. II, Features were extracted from the tumor contours on the MR images using shape, first order, texture, LoG and wavelet-based method. III, Principal component analysis (PCA) was performed on significant features for dimension reduction. IV, For the analysis, principal components derived from significant features were combined with supervised machine learning method for prediction of NPC-IFR vs. NPC-NPD. **(B)** Examples of feature maps computed from two-dimensional tumor region by using GLCM method (e.g., Energy, Entropy, Correlation, InverseDifferenceMoment [IDM]).

TABLE 3 | Features show statistical difference between NPC-IFR and NPC-NPD.

Feature	*P* value	Standard error	95% CI	AUC	Sens	Spec
glcm_CT	0.046	0.099	0.541–0.891	0.744	0.818	0.687
W_{HLL}_gldm_DE	0.023	0.084	0.643–0.949	0.835	0.909	0.750
W_{HLH}_F_RMS	0.023	0.079	0.636–0.946	0.830	0.909	0.687
W_{HLL}_glcm_CP	0.032	0.093	0.591–0.922	0.790	0.909	0.625
W_{HLL}_ngtdm_Complexity	0.041	0.094	0.559–0.903	0.761	0.909	0.625
W_{HLH}_glcm_IMC	0.041	0.096	0.553–0.899	0.756	0.727	0.750
W_{HLL}_gldm_SDLGLE	0.048	0.104	0.523–0.879	0.727	0.636	0.875
W_{LLH}_ngtdm_Strength	0.048	0.126	0.523–0.879	0.727	0.727	0.875

glcm, gray-level co-occurrence matrix; CT, cluster tendency; W_{HLL}, volume with a wavelet high-pass filter along x-direction, a low-pass filter along y-direction and a low-pass filter along z-direction; gldm, gray-level dependence matrix; DE, dependence entropy; RMS, root mean squared; CP, cluster prominence; ngtdm, neighboring gray-tone difference matrix; IMC, informational measure of correlation; SDLGLE, small dependence low gray Level emphasis; CI, confidence interval; AUC, area under the curve; Sens, Sensitivity; Spec, Specificity; NPC-IFR, NPC with in-field recurrences; NPC-NPD, NPC with non-progression disease.

patients were identified as in-field failures, marginal, and out-of-field failures, respectively. Details of recurrent patients and their local or/and regional failure are summarized in **Table 2**. As shown in **Table 2**, 18 NPCs developed in-field recurrences (NPC-IFR). Among these 18 NPC-IFRs, 11 cases with pre-treatment MRI images available were then used for radioresistance analysis by radiomics method.

Predictive Capabilities of Radiomic Features for NPC-IFR

In addition to these 11 patients with NPC-IFR, 16 NPC patients with non-progression disease (NPC-NPD), as well as the corresponding MR images were also enrolled in this study for exploring the predictive power of the imaging features. **Supplementary Table S2** showed the general characteristics of

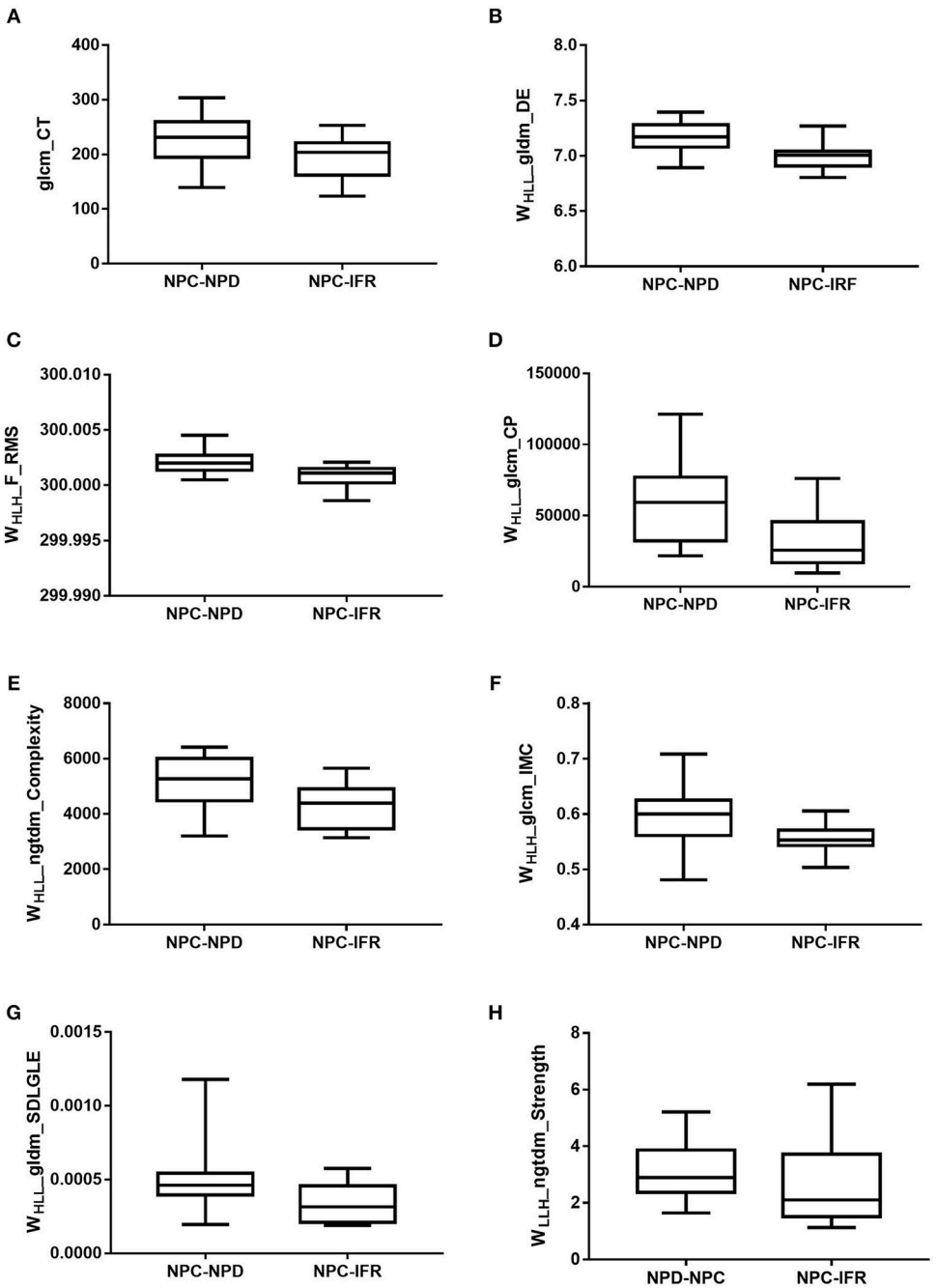

FIGURE 4 | Box plots of amplitude features, successfully differentiating NPC-IFR from NPC-NPD. **(A)** glcm_CT ($P = 0.046$); **(B)** WHLL_gldm_DE ($P = 0.023$); **(C)** WHLH_F_RMS ($P = 0.023$); **(D)** WHLL_glcm_CP ($P = 0.032$); **(E)** WHLL_ngtdm_Complexity ($P = 0.041$); **(F)** WHLH_glcm_IMC ($P = 0.041$); **(G)** WHLL_gldm_SDLGLE ($P = 0.048$); **(H)** WLLH_ngtdm_Strength ($P = 0.048$).

NPC-NPDs. A total of 1117 imaging features, preprocessed with or without $LoG_{\sigma=0.5/1.5/2.5}$ and wavelet filter, were computed from each of the 27 cases (11 NPC-IFR, 16 NPC-NPD). Of the complete radiomic feature set, influential features were yielded by calculating ICC and PCC values. Results of the Kruskal-Wallis test revealed that 8 features (1 texture feature, 7 wavelet feature; *P*-value: 0.023–0.048) were capable of differentiating between NPC-IFR and NPC-NPD. **Table 3** summarizes the details of the corresponding significant features and **Figure 4** presents their distribution, as well as **Figure 5** shows the PCC values among them. In order to assess the diagnostic performance of the significant features, ROC analysis was used and the associated AUC values were obtained (range from 0.727 to 0.835). **Figure 6A** displays the ROC curves of all significant features.

Supervised Classification

After radiomic quantification and feature reduction process, we found that the first three principal components were most significant on the basis of PCA method (with the accumulated variance of the components was 85.43%). **Figure 6B** shows the distribution of the patients using the three components. Supervised machine-learning algorithms (ANN, KNN, and SVM) were performed on these three components and the efficiency of classification was validated by stratified 10–fold CV, with the results showed that ANN, KNN and SVM obtained the accuracies of 0.812, 0.775, and 0.732, respectively. The predictive results of the models are presented in **Table 4**.

DISCUSSION

Understanding the failure patterns for NPC patients treated with IMRT plays a central role in radiotherapy planning optimization and patient clinical management. Prior works have documented the different failure patterns for HNC patients. Oksuz et al. (8) and Johansen et al. (7), for example, analyzed the recurrence patterns among HNC patients treated with radical (chemo-)

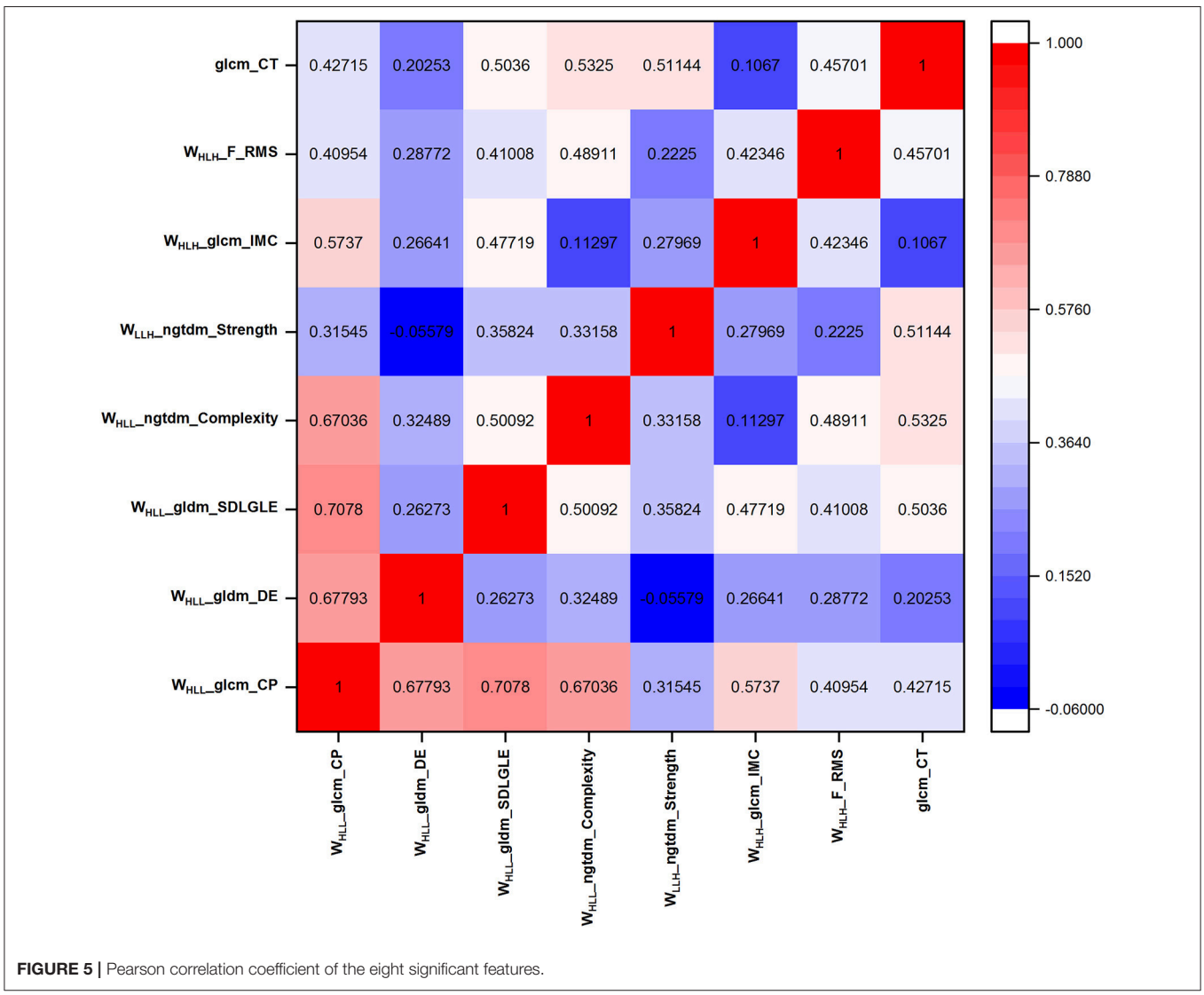

FIGURE 5 | Pearson correlation coefficient of the eight significant features.

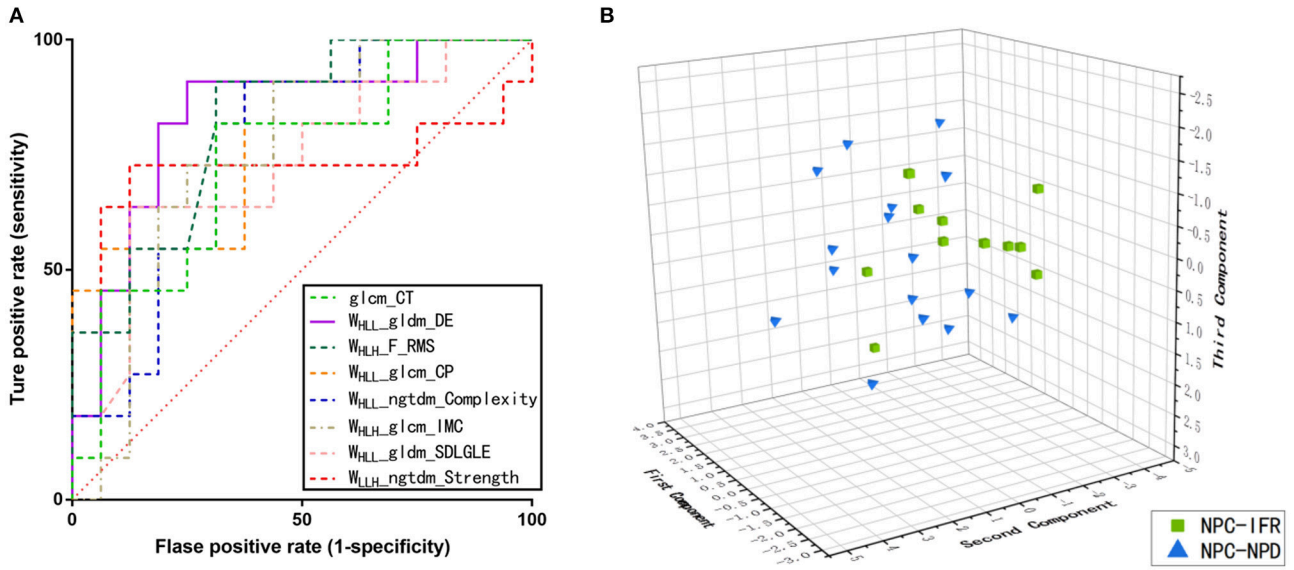

FIGURE 6 | (A) Receiver operating characteristics (ROC) curves on the basis of the significant features. **(B)** Three-dimensional scatter plot of the NPC-IFR and NPC-NPD by using three principal components derived from the above eight significant features.

TABLE 4 | Summary of Classification Results Obtained from stratified 10-Fold cross-validation on two classification groups by ANN, KNN, and SVM model.

Algorithm	TP rate	FP rate	Precision	*F*-measure	MCC	Accuracy
ANN	0.815	0.231	0.814	0.813	0.613	0.812
KNN	0.778	0.210	0.790	0.780	0.559	0.775
SVM	0.741	0.292	0.738	0.738	0.457	0.732

ANN, artificial neural network; KNN, k-nearest neighbor; SVM, support vector machine; FP, false-positive; TP, true-positive; MCC, matthews correlation coefficient

radiotherapy. They reported that "in field" failures were the majority of recurrence. Similarly, "in field" failures are the main patterns of local-regional recurrence for NPC (4–6), suggesting that it may be related to the radioresistance of tumor cells. A review such as that conducted by Hong et al. has shown that radioresistance may be responsible for NPC local-regional recurrence (23). Therefore, new tools should be developed to quantify heterogeneity within tumors for further analysis of radioresistance. Radiomic analysis is emerging as a new method to quantify the tumor heterogeneity, Ganeshan et al. has found that texture features are associated with tumor hypoxia and angiogenesis (24). To data, there have been few studies to explore the power of radiomics for predicting "in field" failures of NPC. Promising results have been presented for predicting local failure of NPC patients using radiomic-based method (25). However, a major problem with the above research was that the therapeutic regimen and local failure pattern of NPC patients were not specified in detail. It has yet to investigate whether causes of in-field recurrence was due to insufficient tumor volume delineation or tumor heterogeneity.

This study set out with the aim of analyzing the recurrence patterns and reasons in patients with NPC treated with IMRT and investigating the predictive power of MRI-based radiomic features for radioresistance. In present study, 1 patient developed with "marginal" recurrence and 1 patient occurred with "out of field" recurrence, which may due to the risk of marginal miss for IMRT and/or inadequate target volume delineation. Moreover, "in field" failure was the major recurrence pattern (90%, 18/20) and similar to the reports from other centers (4–8). It may be questioned whether heterogeneity within tumors may cause of "in field" recurrence. Therefore, in current work, we further analyzed 1117 radiomic features extracted from tumor volumes for 27 NPC patients (11 NPC-IFRs, 16 NPC-NPDs) and found that 8 parameters were able to discriminate between NPC-IFR and NPC-NPD, with AUC values range from 0.727 to 0.835. These findings suggested that there is a significant difference within the tumor tissue between NPC patients who resisted to radiation vs. those who do not, and these potential differences can be detected and quantified by using the radiomic parameters extracted from pretreatment MRI images. The radiomic features were mathematical measurement concerned with the distribution of gray levels within the tumor region that reflects underlying pathophysiologic and phenotypic characteristics (26). In other words, the studied radiomic features in this work captured tumor heterogeneity at local macro- and micro-scale, using the data-characterization algorithms, indirectly characterizing areas of hemorrhage, necrosis, high cell density, myxoid change, and hypoxia. Thus, with this context,

tumor heterogeneity induced radioresistance could be predicted by radiomic analysis. Our work presents one of the first attempts to employ the pretreatment imaging biomarkers for prediction of "in field" failures for NPC patient (NPC-IFR).

In addition, we showed as well that the radiomic features combined with machine learning algorithms was strongly predictive and validated among NPC patients (NPC-IFD vs. NPC-NPD), and was associated with radioresistance. To minimize the over-fitting or bias, we performed a series of pre-processing: feature reproducibility and correlation evaluation, as well as principal component analysis. After the pre-processing procedures and machine-learning process, the three models achieved high accuracies (ANN: 0.812; KNN: 0.775; SVM: 0.732) on the basis of the selected attributes. A possible physiologic explanation for these observations is the difference in intratumoral heterogeneity between NPC-IFD and NPC-NPD, which can be captured by radiomic features. These findings extend those of Zhang et al. (25), we not only analyzed the recurrence patterns for NPC patients but also demonstrated that machine-learning models trained with the radiomic features described have the potential to predict the risk of NPC patients developing "in field" recurrence. This work thus indicates the benefit gained form radiomic analysis could potentially speed up the development of personalized medicine.

Several limitations are worth noting in this work, namely the small patient cohort in a single center and the retrospective nature of the analysis. Due to the relative small simple size, an independent external validation of the radiomic models was not performed. Future prospective study is needed to verify the work with a much larger prospective cohort of patients. In addition, although recent radiomic works have shown the promising results in different cancers, the radiomic-biology correlations have not yet to be determined. Therefore, other extensions of this work would be to incorporate the biological data of tumor, to explore the potential mechanism further.

In conclusion, MR imaging-based radiomic features combined with supervised machine-learning algorithms were found to early discriminate NPC patients with or without "in field" recurrence before IMRT. These findings suggest the potential value for radiomics to provide a quantitative, objective measurement of NPC patients who had a higher risk to develop "in field" recurrence, with advantage of low cost, using existing MR imaging data, without subjecting patients to extra radiation exposure or imaging.

ETHICS STATEMENT

Ethical approval was given by the medical ethics committee of Nanjing Drum Tower Hospital with the following reference number No. 2018-016-09.

AUTHOR CONTRIBUTIONS

SL, KW, and ZH: Conception and design. JuY and JL: Administrative support. JiY, BL, WR, SG, JL, and FM: Provision of study materials or patients. SL, KW, ZH, and WR: Collection and assembly of data. SL and ZH: Data analysis and interpretation. All authors manuscript writing and final approval of manuscript.

SUPPLEMENTARY MATERIAL

The Supplementary Material for this article can be found online at: https://www.frontiersin.org/articles/10.3389/fonc.2018.00648/full#supplementary-material

REFERENCES

1. Bray F, Ferlay J, Soerjomataram I, Siegel RL, Torre LA, Jemal A. Global cancer statistics 2018: GLOBOCAN estimates of incidence and mortality worldwide for 36 cancers in 185 countries. *CA Cancer J Clin*. (2018) 68:394–424. doi: 10.3322/caac.21492
2. Chen W, Zheng R, Baade PD, Zhang S, Zeng H, Bray F, et al. Cancer statistics in China, 2015. *CA Cancer J Clin*. (2016) 66:115–32. doi: 10.3322/caac.21338
3. Lee N, Puri DR, Blanco AI, Chao K. Intensity-modulated radiation therapy in head and neck cancers: an update. *Head Neck*. (2007) 29:387–400. doi: 10.1002/hed.20332
4. Wang L, Guo Y, Xu J, Chen Z, Jiang X, Zhang L, et al. Clinical analysis of recurrence patterns in patients with nasopharyngeal carcinoma treated with intensity-modulated radiotherapy. *Ann Otol Rhinol Laryngol*. (2017) 126:789–97. doi: 10.1177/0003489417734229
5. Li J-X, Huang S-M, Jiang X-H, Ouyang B, Han F, Liu S, et al. Local failure patterns for patients with nasopharyngeal carcinoma after intensity-modulated radiotherapy. *Radiat Oncol*. (2014) 9:87. doi: 10.1186/1748-717X-9-87
6. Kong F, Ying H, Du C, Huang S, Zhou J, Chen J, et al. Patterns of local-regional failure after primary intensity modulated radiotherapy for nasopharyngeal carcinoma. *Radiat Oncol*. (2014) 9:60. doi: 10.1186/1748-717X-9-60
7. Johansen S, Norman MH, Dale E, Amdal CD, Furre T, Malinen E, et al. Patterns of local-regional recurrence after conformal and intensity-modulated radiotherapy for head and neck cancer. *Radiat Oncol*. (2017) 12:87. doi: 10.1186/s13014-017-0829-5
8. Oksuz DC, Prestwich RJ, Carey B, Wilson S, Senocak MS, Choudhury A, et al. Recurrence patterns of locally advanced head and neck squamous cell carcinoma after 3D conformal (chemo)-radiotherapy. *Radiat Oncol*. (2011) 6:54. doi: 10.1186/1748-717X-6-54
9. Fave X, Mackin D, Lee J, Yang J, Zhang L. Computational resources for radiomics. *Transl Cancer Res*. (2016) 5:340–8. doi: 10.21037/tcr.2016.06.17
10. Aerts HJ, Velazquez ER, Leijenaar RT, Parmar C, Grossmann P, Carvalho S, et al. Decoding tumour phenotype by noninvasive imaging using a quantitative radiomics approach. *Nat Commun*. (2014) 5:4006. doi: 10.1038/ncomms5006
11. Lambin P, Rios-Velazquez E, Leijenaar R, Carvalho S, van Stiphout RG, Granton P, et al. Radiomics: extracting more information from medical images using advanced feature analysis. *Eur J Cancer* (2012) 48:441. doi: 10.1016/j.ejca.2011.11.036
12. Gillies RJ, Kinahan PE, Hricak H. Radiomics: images are more than pictures, they are data. *Radiology* (2016) 278:563. doi: 10.1148/radiol.2015151169
13. Kumar V, Gu Y, Basu S, Berglund A, Eschrich SA, Schabath MB, et al. Radiomics: the process and the challenges. *Magn Reson Imaging* (2012) 30:1234–48. doi: 10.1016/j.mri.2012.06.010
14. Jethanandani A, Lin TA, Volpe S, Elhalawani H, Mohamed AS, Yang P, et al. Exploring applications of radiomics in magnetic resonance imaging of head and neck cancer: a systematic review. *Front Oncol*. (2018) 8:131. doi: 10.3389/fonc.2018.00131

15. Del Grande F, Santini F, Herzka DA, Aro MR, Dean CW, Gold GE, et al. Fat-suppression techniques for 3-T MR imaging of the musculoskeletal system. *Radiographics* (2014) 34:217–33. doi: 10.1148/rg.341135130
16. Tien RD, Hesselink J, Chu P, Szumowski J. Improved detection and delineation of head and neck lesions with fat suppression spin-echo MR imaging. *Am J Neuroradiol*. (1991) 12:19–24.
17. Tang C, Wu F, Wang R, Lu H, Li G, Liu M, et al. Comparison between nedaplatin and cisplatin plus docetaxel combined with intensity-modulated radiotherapy for locoregionally advanced nasopharyngeal carcinoma: a multicenter randomized phase II clinical trial. *Am J Cancer Res*. (2016) 6:2064.
18. Tang L-Q, Chen D-P, Guo L, Mo H-Y, Huang Y, Guo S-S, et al. Concurrent chemoradiotherapy with nedaplatin versus cisplatin in stage II–IVB nasopharyngeal carcinoma: an open-label, non-inferiority, randomised phase 3 trial. *Lancet Oncol*. (2018) 19:461–73. doi: 10.1016/S1470-2045(18)30104-9
19. Zheng J, Wang G, Yang GY, Wang D, Luo X, Chen C, et al. Induction chemotherapy with nedaplatin with 5-FU followed by intensity-modulated radiotherapy concurrent with chemotherapy for locoregionally advanced nasopharyngeal carcinoma. *Jpn J Clin Oncol*. (2010) 40:425–31. doi: 10.1093/jjco/hyp183
20. Cao K-J, Zhang A-L, Ma W-J, Huang P-Y, Luo D-H, Xia W-X. Nedaplatin or cisplatin combined with 5-fluorouracil for treatment of stage III-IVa nasopharyngeal carcinoma: a randomized controlled study. *Chinese J Oncol*. (2011) 33:50–2. doi: 10.3760/cma.j.issn.0253-3766.2011.01.011
21. Collewet G, Strzelecki M, Mariette F. Influence of MRI acquisition protocols and image intensity normalization methods on texture classification. *Magn Reson Imaging* (2004) 22:81–91. doi: 10.1016/j.mri.2003.09.001
22. van Griethuysen JJ, Fedorov A, Parmar C, Hosny A, Aucoin N, Narayan V, et al. Computational radiomics system to decode the radiographic phenotype. *Cancer Res*. (2017) 77:e104–7. doi: 10.1158/0008-5472.CAN-17-0339
23. Hong B, Lui VWY, Hashiguchi M, Hui EP, Chan ATC. Targeting tumor hypoxia in nasopharyngeal carcinoma. *Head Neck* (2013) 35:133–45. doi: 10.1002/hed.21877
24. Ganeshan B, Goh V, Mandeville HC, Ng QS, Hoskin PJ, Miles KA. Non-small cell lung cancer: histopathologic correlates for texture parameters at CT. *Radiology* (2013) 266:326–36. doi: 10.1148/radiol.12112428
25. Zhang B, He X, Ouyang F, Gu D, Dong Y, Zhang L, et al. Radiomic machine-learning classifiers for prognostic biomarkers of advanced nasopharyngeal carcinoma. *Cancer Lett*. (2017) 403:21. doi: 10.1016/j.canlet.2017.06.004
26. Cook GJR, Siddique M, Taylor BP, Yip C, Chicklore S, Goh V. Radiomics in PET: principles and applications. *Clin Transt Imaging* (2014) 2:269–76. doi: 10.1007/s40336-014-0064-0

Conflict of Interest Statement: The authors declare that the research was conducted in the absence of any commercial or financial relationships that could be construed as a potential conflict of interest.

frontiers in Oncology

ORIGINAL RESEARCH
published: 20 December 2019
doi: 10.3389/fonc.2019.01420

Intensity Modulated Radiotherapy (IMRT) With Carbon Ion Boost in the Multimodal Treatment of Salivary Duct Carcinoma

Sebastian Adeberg[1,2,3,4], Paul Windisch[1], Felix Ehret[1], Melissa Baur[1], Sati Akbaba[1,2], Thomas Held[1,2], Denise Bernhardt[1,2], Matthias F. Haefner[1,2], Juergen Krauss[5], Steffen Kargus[6], Christian Freudlsperger[6], Peter Plinkert[7], Christa Flechtenmacher[8], Klaus Herfarth[1,2,4], Juergen Debus[1,2,3,4,5] and Stefan Rieken[1,2,4]*

[1] Department of Radiation Oncology, Heidelberg University Hospital, Heidelberg, Germany, [2] Heidelberg Institute for Radiation Oncology, Heidelberg, Germany, [3] Clinical Cooperation Unit Radiation Oncology, German Cancer Research Center (DKFZ), Heidelberg, Germany, [4] Heidelberg Ion-Beam Therapy Center, Heidelberg, Germany, [5] National Center for Tumor Diseases, Heidelberg, Germany, [6] Department of Oral and Maxillofacial Surgery, Heidelberg University Hospital, Heidelberg, Germany, [7] Department of Otorhinolaryngology, Heidelberg University Hospital, Heidelberg, Germany, [8] Department of Pathology, Heidelberg University Hospital, Heidelberg, Germany

OPEN ACCESS

Edited by:
Brian Timothy Collins, School of Medicine, Georgetown University, United States

Reviewed by:
Michael Andrew Samuels, University of Miami, United States
Heng-Hong Li, Georgetown University, United States

****Correspondence:***
Sebastian Adeberg
sebastian.adeberg@med.uni-heidelberg.de

Specialty section:
This article was submitted to Radiation Oncology, a section of the journal Frontiers in Oncology

Received: *09 August 2019*
Accepted: *29 November 2019*
Published: *20 December 2019*

Citation:
Adeberg S, Windisch P, Ehret F, Baur M, Akbaba S, Held T, Bernhardt D, Haefner MF, Krauss J, Kargus S, Freudlsperger C, Plinkert P, Flechtenmacher C, Herfarth K, Debus J and Rieken S (2019) Intensity Modulated Radiotherapy (IMRT) With Carbon Ion Boost in the Multimodal Treatment of Salivary Duct Carcinoma. Front. Oncol. 9:1420. doi: 10.3389/fonc.2019.01420

Background: To assess outcomes and treatment related toxicity following intensity-modulated radiotherapy (IMRT) and a Carbon Ion Radiotherapy (CIRT) boost for salivary duct carcinoma (SDC).

Methods: Twenty-eight consecutive patients with SDC who underwent a postoperative (82%) or definitive (18%) radiation therapy between 2010 and 2017 were assessed in this retrospective single-center analysis. CIRT boost was delivered with median 18 Gy(RBE) in 6 daily fractions, followed by an TomoTherapy®-based IMRT (median 54 Gy in 27 daily fractions). Treatment-related acute toxicity was assessed according to CTCAE Version 4.

Results: Tumors were most commonly located in the major salivary glands ($n = 25$; 89%); 23 patients (82%) received previous surgery (R0: 30%; R1: 57%; R2: 4%; RX: 19%). Median follow-up was 30 months. Four patients (14%) experienced a local relapse and 3 (11%) developed locoregional recurrence. The two-year local control (LC) and locoregional control (LRC) was 96 and 93%, respectively. Median disease-free survival (DFS) was 27 months, metastasis-free survival (MFS) was 69 months, and overall survival (OS) was 93 months. Acute grade 3 toxicity occurred in 11 patients (mucositis, dermatitis, xerostomia; $n = 2$ each (7%) were the most common) and 2 osteonecroses of the mandibular (grade 3) occurred. No patients experienced grade $\geq$4 toxicities.

Conclusions: Multimodal therapy approaches with surgery followed by IMRT and CIRT boost for SDC leads to good local and locoregional disease control. However, the frequent occurrence of distant metastases limits the prognosis and requires optimization of adjuvant systemic therapies.

Keywords: radiation therapy, bimodal radiotherapy, carbon ion radiotherapy, toxicity, salivary gland, intensity-modulated radiotherapy

INTRODUCTION

SDC were first described by Kleinsasser and colleagues in 1968 as a separate group of "adenocarcinomas" of the salivary gland displaying a histopathological resemblance to ductal carcinoma of the breast; the World Health Organization recognized these tumors as a distinct tumor entity in 1991 (1, 2). Since then, SDC refer to rare but highly aggressive tumors originating from the ductal epithelium of major salivary glands (3). Malignant salivary gland tumors (MSGT) have an estimated annual incidence rate of 1 to 1.2 per 100,000 (4). SDC account for approximately 1% to 3% of all malignant salivary gland tumors and mostly occur during the fifth to seventh decade of life; men are predominantly affected (4–14). Current treatment options include surgery, systemic therapy, radiation and targeted therapy. Surgical management typically involves complete surgical resection and lymphadenectomy; depending on the tumor localization and stage, this can include parotidectomy, submandibular excision, ipsilateral, and contralateral neck dissection. Owing to its rarity and often poor response, the role of systemic therapies has only been investigated in case series and small clinical trials (15, 16).

Despite the advancements in surgery, systemic therapy and radiotherapy, the prognosis of SDC remains meager (6). Despite showing trends toward improved local control, especially the role of adjuvant radiotherapy remains unclear (6, 17–20). These tumors are currently treated in analogy to other MSGT. In the adjuvant setting, radiotherapy plays a role in patients with higher risk disease, e.g., perineural invasion (PNI), R+, T3/4 tumors. Additionally, definitive radiotherapy is a valuable alternative for unresectable cases. In the adjuvant setting, dose response relationships were described for both LRC (21) and LC (22) in MSGTs. Here, high-linear energy transfer (LET) radiation therapy (e.g., with charged particles such as carbon ions) can lead to improved tumor control rates in other head/neck malignancies as compared to standard photon therapy (22, 23). The objective of this retrospective, single-institutional study is to provide further clinical data and prognostic factors regarding intensity modulated radiotherapy (IMRT) with carbon ion radiotherapy (CIRT) in patients with SDC.

MATERIALS AND METHODS

Patient Population

Patient records, surgical reports, histological work-up, and radiotherapy treatment plans of patients with SDC who underwent IMRT-CIRT between August 2010 and November 2017 in the Department of Radiation Oncology, University Hospital and at the Heidelberg Ion-Beam Therapy Center (HIT) were evaluated retrospectively. A subset of patients (18%) with locoregional advanced disease or unresectable received a primary radiotherapy.

Radiation Therapy

Treatment planning was performed using native and contrast enhanced CT/MRI. Patients were immobilized with individualized thermoplastic head masks. Technical details of CIRT are described elsewhere (24, 25). Treatment planning for CIRT was performed using Syngo PT Planning, Version 13 (Siemens, Erlangen, Germany) and TomoTherapy®-Planning Station (Accuray, Sunnyvale, CA, USA) for photon radiotherapy planning. Patients were treated with a fixed horizontal beam/gantry for CIRT utilizing 1-2 coplanar/non-coplanar beams.

All patients received combined IMRT and CIRT. The base plan was performed using a helical intensity-modulated radiotherapy (IMRT) with daily image guidance (TomoTherapy®, Accuray, Sunnyvale, CA, USA), with 5 daily fractions per week (**Figure 1**).

Target Volume Delineation and Dose Prescription

Target delineation was based on native/contrast enhanced CT scans fused with contrast-enhanced MRI. Two clinical target volumes (CTV1/CTV2) were outlined. CTV2 comprised the macroscopic tumor and/or tumor bed. CTV1 included CTV2 as well as local growth patterns; ipsilateral nodal levels II-III were included into the CTV1 as well. A 3 mm margin was added to the CTVs to generate the planning target volumes (PTVs).

Organs at risk such as the spinal cord, contralateral parotid gland, temporomandibular joints, and the optic system were constrained per QUANTEC data (26). CTV1 received a median dose of 54 Gy (range: 50–56 Gy) in 2 Gy daily doses (1.8 Gy to 2.0 Gy) (median equivalent dose in 2 Gy fractions (EQD2) of 50 Gy). CTV1 was to be covered by the 90% isodose line. A sequential CIRT boost was applied to the CTV2 utilizing an intensity-controlled active raster-scanning technique, in 3 Gy [relative biological effectiveness (RBE)] fractional doses up to a median combined EQD2 (Equivalent dose in 2Gy fractions) $= D\frac{[d+(\alpha/\beta)]}{[2+(\alpha/\beta)]}$ (where, D = total dose given in Gy, d = dose per fraction in Gy, and α/β = is assumed to be 2) of 78.5 Gy (range 78.5–80 Gy). We aimed for the CTV2 to be covered by the 95% isodose line. The following equation was used to calculate biologically effective dose (BED) $= nd(1 + \frac{d}{\alpha/\beta})$ (where n is the number of fractions, d is fractional dose (in Gy), and α/β is assumed to be 2). The total CIRT dose of 18–24 Gy (RBE) corresponds to a BED of 45–60 Gy.

Follow Up

Patients were monitored on treatment weekly with toxicity assessments (CTCAE classification v.4). Follow-up included a clinical examination by an otorhinolaryngologist and contrast enhanced MR-imaging of the head and neck every 3 months for the first 2 years after radiotherapy, every 6 months until the fifth year after treatment, and annually thereafter. Staging CTs were performed yearly to exclude distant metastases.

Survival, Local, and Locoregional Control

Local control (LC) and locoregional control (LRC) rates were calculated by Kaplan-Meier estimates, from the start of therapy until local tumor progression/death and/or nodal failure. Patients without tumor progression and patients lost to follow-up were censored.

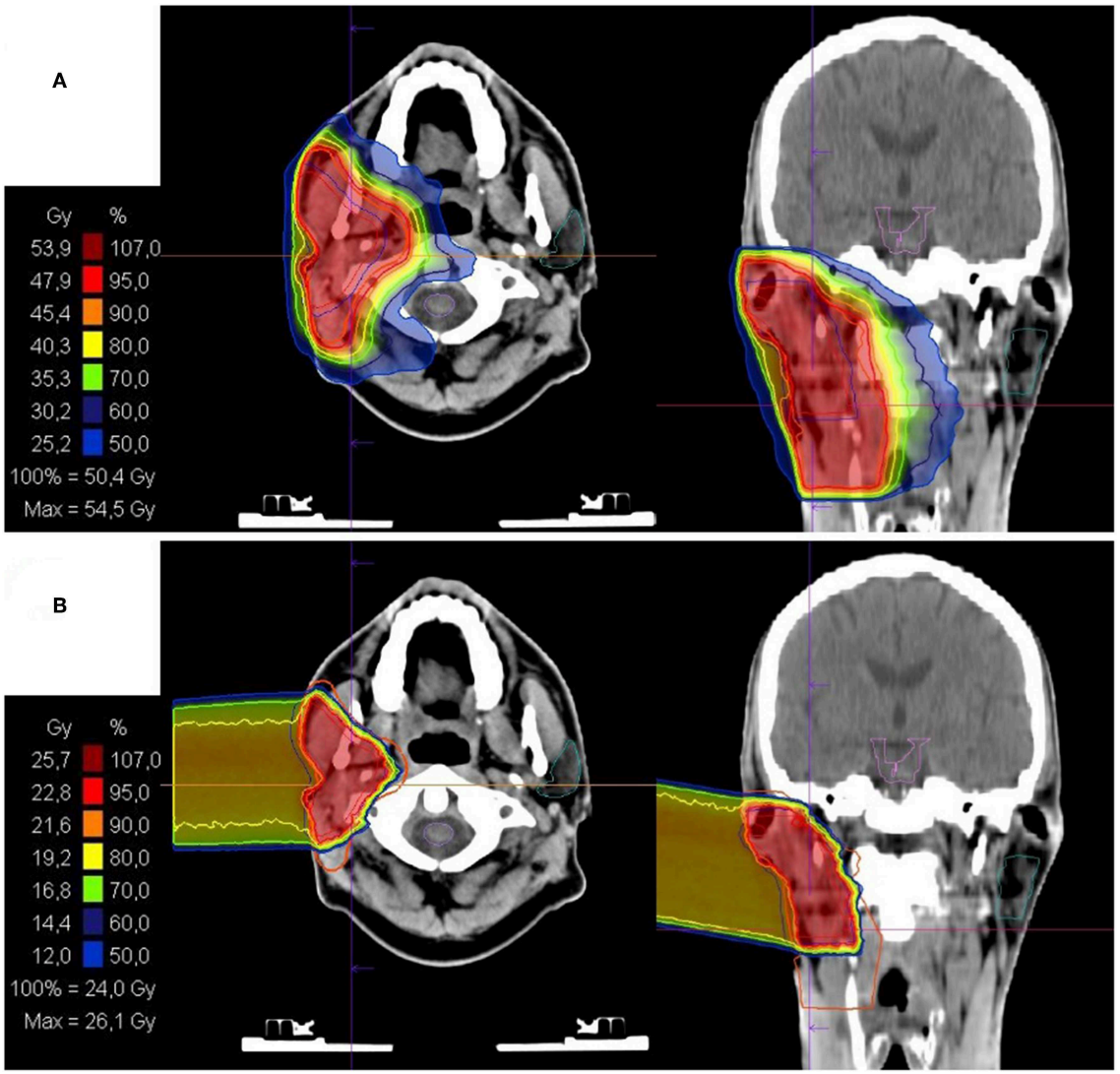

FIGURE 1 | Bimodal radiotherapy treatment plan: **(A)** intensity modulated radiotherapy (IMRT) base plan with 50Gy in 2Gy/fraction and **(B)** active raster-scanning carbon ion radiotherapy (CIRT) boost plan with 28Gy (RBE) in 3Gy (RBE)/fraction. Treatment was delivered as a definite radiotherapy in a patient with a recurrent rcT2 rcN2b cM0 salivary duct carcinoma (SDC) of the right parotid gland. CIRT was applied with one lateral beam. Histopathological work up revealed Her2neu and androgen receptor (AR) positivity. Therefore, the patient received an adjuvant therapy with trastuzumab and bicalutamide.

Metastasis-free survival (MFS) and disease-free survival (DFS) were calculated by Kaplan-Meier estimates, defined from the start of therapy until distant metastases occurred or progression/relapse at any location, respectively. Patients without events and those lost to follow-up were censored.

Overall Survival (OS) was calculated by Kaplan-Meier estimates, from the start of therapy until death or last contact (alive subjects were censored).

Data Analysis

The log-rank test for univariate analysis was performed to assess prognostic factors for survival. Statistical analyses were performed using SigmaPlot™ (Systat Software GmbH, Germany) software, and a p-value of <0.05 was considered statistically significant.

RESULTS

Treatment Setup and Tumor Characteristics

Detailed patient characteristics are depicted in **Table 1**. Overall 28 consecutive patients were included with a median age of 69 years (range 41–83 years). 79% ($n = 22$) of tumors were localized in the parotid gland.

Twenty-three patients (82%) underwent surgical resection (parotidectomy, $n = 17$; mastoidectomy, $n = 4$; modified neck dissection, $n = 20$) followed by postoperative radiotherapy. Five patients (18%) received a definitive radiotherapy. Median clinical target volume (CTV) and planning target volume (PTV) dimension of the CIRT boost was 120cc (range 36–639cc) and 187cc (range 63–817cc). Median time interval between surgery

TABLE 1 | Clinical characteristics of the study cohort ($n = 28$).

Parameter	Median (range or %)
Age (years)	69 (41–83)
KPS	90 (60–100)
Gender	
Male	25 (89%)
Female	3 (11%)
Primary location	
Parotid gland	22 (79%)
Submandibular gland	2 (7%)
Minor salivary glands	2 (7%)
Sublingual gland	1 (4%)
Lacrimal gland	1 (4%)
T classification	
T1	2 (7%)
T2	3 (11%)
T3	10 (36%)
T4	13 (46%)
N classification	
N0	9 (32%)
N1	2 (7%)
N2	14 (50%)
N3	2 (7%)
NX	1 (4%)
M classification	
M1	1 (4%)
PNI	
Yes	14 (50%)
No	6 (21%)
n.e.	8 (29%)
LV	
Yes	11 (39%)
No	10 (36%)
n.e.	7 (37%)
Resection status	
R0	7 (30%)
R1	13 (57%)
R2	1 (4%)
Rx	2 (9%)
Her2neu	
Positive	14 (50%)
Negative	10 (36%)
n.e.	4 (14%)

PNI, perineural invasion; LV, lymphovascular invasion; n.e., not examined; KPS, Karnofsky performance status.
Numbers may not add to 100% owing to rounding and multiple categorizations for single specimens.

and commencement of radiotherapy was 57 days (range: 30–135 days). Complete surgical resection (R0) was achieved in 7 patients (30%). The majority of tumors initially presented at advanced stages (T3, $n = 10$, 36% and T4, $n = 13$, 46%) and with lymph node involvement (N1, $n = 2$, 7%; N2, $n = 14$, 50%; N3, $n = 2$, 7%). PNI (50%) and lymphovascular invasion (LVI) (39%) was common. Her2neu was positive in 14/24 tested patients (58%). tumor tissues were positive for androgen receptors Most (19/23, 83%). Adjuvant systemic therapy with the antiandrogen agent bicalutamide was delivered to 7 patients and bicalutamide with trastuzumab in 5 patients.

Survival and Local Control

After a median follow-up of 30 months (range: 8–109 months), 17 patients (61%) were still alive. Local tumor progression was observed in 3 patients (11%) and nodal failure was observed in 4 patients (14%). Median LC and LRC were not reached (**Figure 2**). The actuarial 2-year LC and LRC was 96 and 93%, respectively. Distant metastases occurred in 9 patients (32%) over the course of disease. Median metastasis-free survival (MFS) was 69 months (range: 4–102).

The most frequent location of distant metastases was pulmonary (21%) and osseous (14%) areas. Metachronous distant metastases occurred in 4 patients (21%). In one patient, preexisting bipulmonary metastases were progressive. Overall, the median disease-free survival (DFS) was 27 months (range: 4–107 months). Median overall survival (OS) was 93 months (range: 9–109 months) (**Figure 3**). Five cases who underwent definitive radiotherapy did not experience a local relapse during follow-up, but 3 of 5 experienced distant metastases after 6, 7, and 15 months. Patient and tumor characteristics between definitive and postoperative treated patients did not differ significantly. Here median DFS ($p = 0.23$) and OS ($p = 0.58$) did not show statistical differences, even though patient cohorts were rather small for comparison.

Prognostic Factors

On univariate analysis larger CTV and PTV dimension of the CIRT boost (both continuous variates) were prognostic for impaired DFS ($p = 0.026$ and $p = 0.003$), MFS ($p = 0.006$ and $p = 0.007$) and OS ($p = 0.005$ and $p = 0.005$). Nodal involvement was prognostic for poor DFS ($p = 0.022$), MFS ($p = 0.044$) (**Figure 4**) and showed a trend toward impaired OS ($p = 0.059$). LVI was associated with impaired DFS ($p = 0.045$) and OS ($p = 0.041$) (**Figure 4**). Other known prognostic factors like T-stage, Her2neu, PNI, age, adjuvant systemic therapies and resection status did not show a correlation with any endpoint.

Treatment Related Toxicities

Acute grade 1 and 2 fatigue, mucositis, xerostomia, and dermatitis were commonly observed in the study cohort. Ten acute grade 3 toxicities [two each (7%) of mucositis, dermatitis, xerostomia; and one each (3%) of dysphagia, odynophagia, dysgeusia, nausea/emesis] occurred in 7 patients (25%). In 11 patients (58%) a preexisting facial palsy remained stable during/after radiotherapy. Regarding late adverse event, two osteonecroses of the mandibular jaw occurred 24 and 32 months after radiotherapy. In one patient a surgical intervention was necessary (grade 3) and led to satisfactory long-term results. Overall, no acute or late grade $\geq$4 toxicities were reported.

TABLE 2 | Overview of the literature regarding management of salivary duct carcinoma.

Authors/Study	Year	Sample size (number of patients)	Median time of follow-up (months)	Local control (%)	Received surgery (number of patients)	Received radiotherapy (number of patients)	Node positive tumors (number of tumors)	Results
Afzelius et al. (27)	1987	12	NR	NR	12	12	5	Average survival: 21.7 months DOD: 7/12 (58%)
Brandwein et al. (28)	1990	12	NR	NR	12	6	8	DOD: 45% (5/11) within 10 years
Delgado et al. (29)	1993	15	NR	NR	15	9	10	DOD: 53% (8/15)
Kumar et al. (30)	1993	11	NR	NR	11	10	3	NR
Barnes et al. (31)	1994	13	24 (for 12/13)	92	13	5	7	DOD: 23% (3/13)
Grenko et al. (32)	1995	12	NR	NR	12	8	8	DOD: 33% (4/12) Median 12.5 months
Lewis et al. (9)	1996	26	NR	65	25	15	17	DOD within 3 years: 77% (20/26) Mean survival: 36 months 2-year survival: 58% 5-year survival: 30%
Guzzo et al. (15)	1997	26	36	64	25	18	15	2-year survival: 43% 5-year survival: 11.5%
Hosal et al. (33)	2003	15	34	79	15	14	11	DOD: 57% (8/14) Mean time to recurrence: 17 months
Jaehne et al. (7)	2005	50	NR	52	49	36	28	Average OS: 56.2 months Average time from first treatment to local recurrence: 17.4 months DOD: 56% (28/50) 5-year survival rate stage I: 42% 5-year survival rate stage II: 40% 5-year survival rate stage III: 30.8% 5-year survival rate stage IV: 23.2%
Kim et al. (20)	2012	35	48	63 (5-year)	35	35	26	Cause-specific death rate: 31.4% 5-year survival: 55.1% 5-year DFS: 47.4%
Shinoto et al. (19)	2013	25	44 (for 14/25)	67 (5-year)	25	25	15	5-year DFS: 45% 5-year survival: 47%
Jayaprakash et al. (6)	2014	228	53 (for survivors)	NR	223	166	111	DOD: 30% (70/228) after 10 years Median OS: 79 months 5-year DSS: 64% 10-year DSS: 56%
Shi et al. (34)	2014	38	39	NR	30	14	14	5-year DSS: 45% 5-year RFS: 30%
Roh et al. (35)	2014	56	71	87	44	47	40	Median DMFS: 36 months Median DSS: 48 months Median OS: 48 months

(Continued)

TABLE 2 | Continued

Authors/Study	Year	Sample size (number of patients)	Median time of follow-up (months)	Local control (%)	Received surgery (number of patients)	Received radiotherapy (number of patients)	Node positive tumors (number of tumors)	Results
								Median OS: 48 months Median PFS: 16 months 5-year DMFS rate: 36% 5-year DSS rate: 44% 5-year OS rate: 42% 5-year PFS rate: 29%
Nakashima et al. (36)	2015	26	31	NR	26	19	20	3-year OS rate: 54% 5-year OS rate: 48.1%
Huang et al. (10)	2015	11	NR	NR	11	8	6	Mean OS time: 72.8 months 2-year OS rate: 75%
Schmitt et al. (37)	2015	28	NR	NR	28	11	20	Median DFS: 3.24 years Median OS: 4.65 years 5-year DFS: 49.2% 5-year OS: 49.3%
Luk et al. (8)	2016	23	26	NR	23	22	14	DOD: 43% (10/23) 5-year DFS: 36% 5-year DSS: 43%
Johnston et al. (38)	2016	54	68	83 (5-year)	53	49	44	5-year distant control: 48% 5-year OS: 43%
Otsuka et al. (39)	2016	141	36	90	134	83	71	3-year DFS: 38.2 % 3-year OS: 70.5%
Gilbert et al. (40)	2016	75	55	NR	71	61	54	Median DFS: 2.7 years Median OS: 3.1 years
Mifsud et al. (41)	2016	17	37	NR	17	17	13	Median OS: 49 months 3-year OS: 35.5% 3-year RFS: 34.4%
Breinholt et al. (11)	2016	34	28	NR	31	26	20	5-year DSS: 42% 5-year OS: 32% 5-year RFS: 35%
Haderlein et al. (18)	2017	67	26	NR	45	38	33	5-year DFS: 58.1% 5-year DMFS: 65.2% 5-year OS: 56.9%
Beck et al. (42)	2018	15	NR	100	15	14	9	2-year OS: 93%
Boon et al. (14)	2018	177	26	NR	162	149	120	Median DFS: 23 months Median DMFS: 26 months Median OS: 51 months
Anwer et al. (43)	2018	12	12	NR	11	10	3	10-month DFS: 75% 20-month DFS: 25%
Current study Adeberg et al.	2019	28	30	96	23	28	18	Median DFS: 27 months Median DMFS: 69 months Median OS: 93 months Grad 3 toxicity: 21%

DOD, dead of disease; NR, not reported; OS, overall survival; DFS, disease-free survival; DSS, disease-specific survival; RFS, recurrence-free survival; DMFS, distant metastasis-free survival.

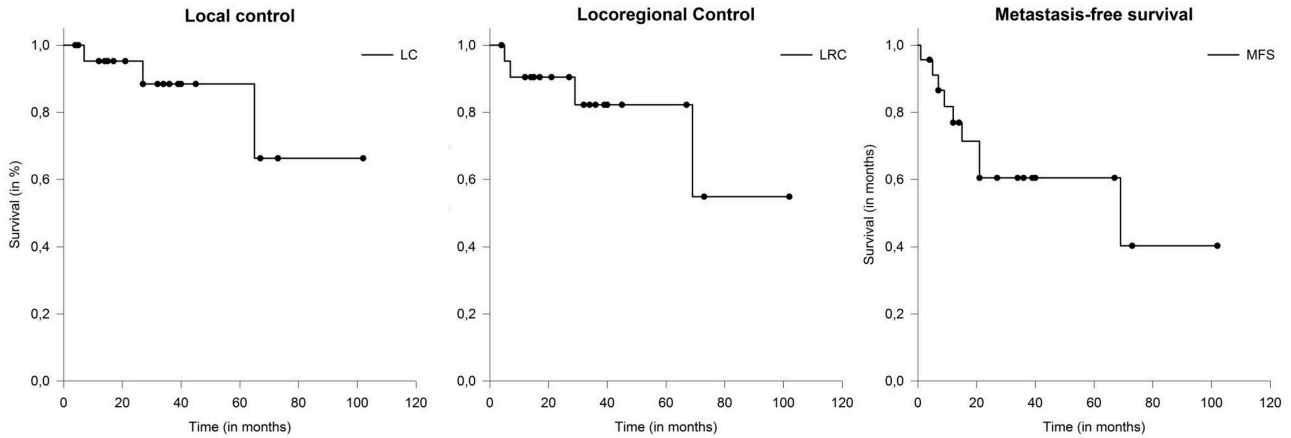

FIGURE 2 | The actuarial 2-year LC and LRC was 96 and 93%, respectively. Metastasis-free survival (MFS) in patients with salivary duct carcinoma (SDC) 69 months.

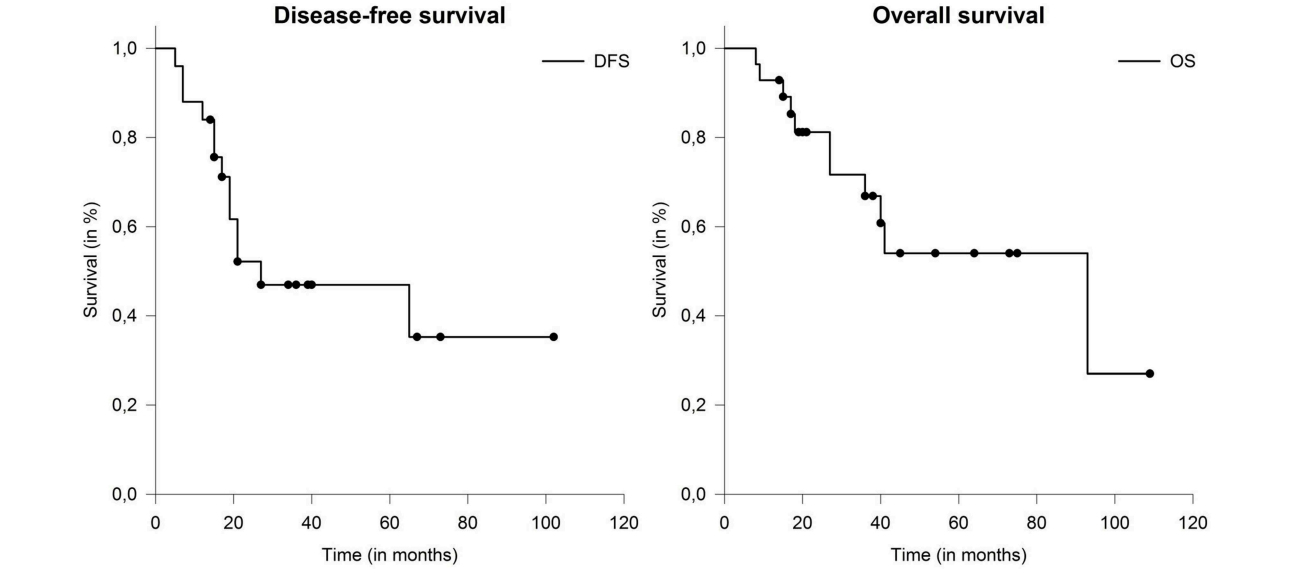

FIGURE 3 | Median disease-free survival (DFS) and overall survival (OS) in patients with salivary duct carcinoma (SDC) were 27 and 93 months.

DISCUSSION

Although surgery combined with IMRT and CIRT resulted in appropriate LC and LRC, prognosis of patients with SDC is limited by the high rate of distant metastases underlined by a poor MFS in our cohort.

However, even when definitively treated, SDCs are linked to a meager prognosis with most of the patients dying within 5 years of diagnosis (7, 9, 14, 39, 40, 44). High rates of local recurrence (15–55%) and distant metastases (33–62%) account for the worse outcome (33). Local approaches should thus include radical surgical resection e.g., with parotidectomy and neck dissection whenever possible.

Postoperative radiotherapy in SDC is mainly performed as extrapolations from head and neck tumors including MSGT. However, larger series that focus on the predictors and outcome after radiotherapy are lacking. Smaller series report of 5-year LC, DFS, and OS rates of 67, 45, and 47% after adjuvant radiotherapy with a median photon dose of 60Gy. The authors advise including nerves tracked to the skull base if PNI is presented (19). The addition of radiotherapy can reduce local recurrence rates from approximately 30 to 10% without impacting OS (21). Summarizing various single institution experiences, LC rates were encouraging after surgery and postoperative radiotherapy (17, 20).

Overall a benefit for radiotherapy dose escalation for MSGTs has been shown, for instance in adenoid cystic carcinoma (ACC) (45, 46). The data for the subgroup of SDC, however, is unclear. The current study presents the first data of advanced radiation techniques with IMRT and high-LET CIRT.

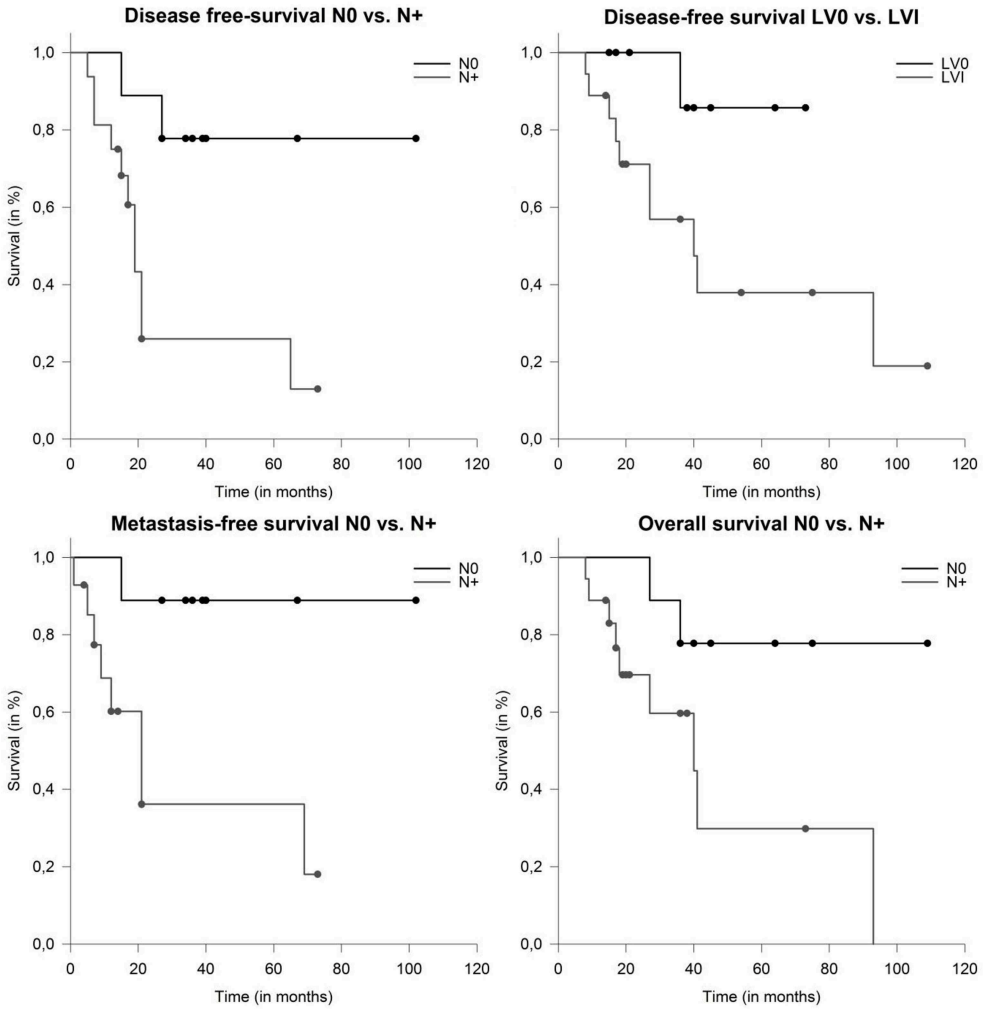

FIGURE 4 | Median disease-free survival (DFS) depending on nodal involvement ($p = 0.009$) and lymphovascular involvement ($p = 0.045$). Metastasis-free survival and overall survival (OS) in patients with salivary duct carcinoma (SDC) depending on nodal involvement ($p = 0.02$ and $p = 0.039$).

With regard to local control in these relatively radioresistant tumors, high-LET radiotherapy seems to be beneficial. In this context, the biophysical advantages with its steep dose-gradient and superior relative biological effectiveness (RBE) allow for safer dose-escalation, like previously described in other tumor entities of the head and neck (47–52) Furthermore the high physical conformity, compared to photons and decreased lateral scattering as with other particles lead to decreased dose to normal tissue (53). This potentially translates into improved local control by means of safer dose escalation combined with improved sparing of organs at risk. Despite negative prognostic factors in the majority of patients in our cohort, LC and LRC rates of 96 and 93% after 2 years were favorable compared to other reports in the literature (7, 9, 15, 36, 43). Our experiences of relatively low DFS and MFS are supported by previous series (6, 7, 14, 39, 40).

In the largest database analysis of 228 patients with SDC treated between 1973 and 2008, lymph node involvement, age, large tumor size, and tumor grade were associated with worse disease-specific survival (median OS was 79 months) (6). In another large national registry study in the Netherlands, OS, DFS, and MFS were 51, 23, and 26 months. Herein, the majority of patients (68%) initially presented with lymph node involvement, which is in line with our findings that greater boost volumes and nodal involvement were associated with inferior DFS and OS (14).

Clinical outcomes of 141 patients of a multi-institutional study cohort in Japan, where 59% of patients underwent postoperative radiotherapy, revealed that N+ was associated with lower OS and that the most common treatment failure was distant metastases in 39% (39). These results are consistent with the current study and underline the urgent need for improved systemic therapy.

A histopathological review of 75 cases, with the majority (81.3%) of patients receiving (chemo)radiotherapy, showed that PNI, LVI, and/or extracapsular spread were negative prognostic factors. The addition of chemotherapy to radiotherapy did not improve outcomes (40).

Additionally, there is no consensus on the role of systemic therapy in SDC in general (54–56). However, androgen receptors are found in 80 to 90% of SDC, as well as 30 to 70% expressing the human epidermal growth factor receptor (EGFR) and Her2neu, making the tumor a target for androgen deprivation therapy and monoclonal antibodies like cetuximab or trastuzumab, respectively (14, 40, 57–61). Recently, adjuvant androgen deprivation in patients with androgen receptor positive SDC has been shown do have a positive impact on DFS and seems to influence OS (62). In a histopathologic study of 50 SDC cases, expression of Her2neu was associated with a more aggressive course of disease (7). In this study, a significant proportion of the assessed tumors were positive for Her2neu and a subset received non-standardized trastuzumab as adjuvant treatment. Furthermore, the majority of tumors assessed were positive for androgen receptors, and received bicalutamide. However, the treatment period, intervals, and combinations thereof were extremely heterogenous, likely why no effect of any systemic therapy in the current analysis could be shown. Moreover, 50 to 70% of tumors expressing the EGFR-receptor may show benefit to EGFR-targeted therapy (56, 61, 63, 64). The high tendency for aggressive growth and patterns of failure demand the optimization of adjuvant treatment regimens. However, prospective trials remain elusive due to the rarity of the disease, even in a multicenter setting. A detailed list of series on surgical treatment and radiotherapy for SDC is provided in **Table 2**.

Toxicities herein were acceptable. In a retrospective analysis of patients with minor MSGT, several higher-grade toxicities were described, including dysphagia, xerostomia and also hearing loss, which were influenced by the target volume (65). Schulz-Ertner et al. described severe toxicity rates under 5% if radiotherapy is performed with modern techniques like IMRT combined with CIRT (66). Data of high-LET radiotherapy with neutrons produce late toxicities in approximately 10% (67), which is higher compared to these data, although follow up was relatively short herein. Furthermore, the retrospective design and the small patient sizes may add additional biases. In addition, adjuvant therapies were non-standardized and unmonitored herein. Despite these limitations, this is the first study to evaluate advanced radiation techniques using high-LET radiotherapy in SDC. Overall, the combination of surgical resection with neck dissection followed by dose-escalated radiotherapy with IMRT and CIRT leads to good LC. However, the high rate of distant metastases requires optimization of systemic therapies.

CONCLUSIONS

Overall, the combination of surgical resection with neck dissection followed by dose-escalated radiotherapy with IMRT and CIRT leads to good local control rates. Larger tumor size and nodal involvement were associated with inferior disease control and survival. However, the limiting factor in patients with SDC is the high rate of distant mestastases, which is why adjuvant therapy need to optimized.

DATA AVAILABILITY STATEMENT

All datasets generated for this study are included in the article.

ETHICS STATEMENT

The study was conducted in accordance with the Declaration of Helsinki. The study was approved by the ethics committee University Heidelberg (S-421/2015). Due to the retrospective nature of the evaluation of the performed standard therapy and the sole use of anonymized data, no study specific informed consent was necessary according to the local ethical guidelines.

AUTHOR CONTRIBUTIONS

SAd and PW: conceptualization. SAd, PW, and FE: methodology. SAd: formal analysis. SAd, PW, SAk, MB, TH, and DB: investigation. SAd and FE: writing—original draft preparation. SAd, JD, and SR: supervision. All authors: writing—review and editing.

FUNDING

This work was supported by Heidelberg University young investigator grants to DB. We thank Thomas Mielke for excellent technical assistance.

REFERENCES

1. Kleinsasser O, Klein HJ, Hubner G. [Salivary duct carcinoma. A group of salivary gland tumors analogous to mammary duct carcinoma]. *Archiv fur klinische und experimentelle Ohren- Nasen- und Kehlkopfheilkunde.* (1968) 192:100–5.
2. Udager AM, Chiosea SI. Salivary duct carcinoma: an update on morphologic mimics and diagnostic use of androgen receptor immunohistochemistry. *Head Neck Pathol.* (2017) 11:288–94. doi: 10.1007/s12105-017-0798-x
3. Barnes L, Eveson JW, Reichart, P, Sidaransky, D. *Pathology and Genetics of Head and Neck Tumours. WHO Classification of Tumours, 3rd Edition.* Lyon: IARC Press (2005).
4. Boukheris H, Curtis RE, Land CE, Dores GM. Incidence of carcinoma of the major salivary glands according to the WHO classification, 1992 to 2006: a population-based study in the United States. *Cancer Epidemiol Biomarkers Prev.* (2009) 18:2899–906. doi: 10.1158/1055-9965
5. Tamaki T, Dong Y, Ohno Y, Sobue T, Nishimoto H, Shibata A. The burden of rare cancer in Japan: application of the RARECARE definition. *Cancer Epidemiol.* (2014) 38:490–5. doi: 10.1016/j.canep.2014.07.014
6. Jayaprakash V, Merzianu M, Warren GW, Arshad H, Hicks WL, Rigual NR, et al. Survival rates and prognostic factors for infiltrating salivary duct carcinoma: analysis of 228 cases from the surveillance, epidemiology, and end results database. *Head Neck.* (2014) 36:694–701. doi: 10.1002/hed.23350
7. Jaehne M, Roeser K, Jaekel T, Schepers JD, Albert N, Loning T. Clinical and immunohistologic typing of salivary duct carcinoma: a report of 50 cases. *Cancer.* (2005) 103:2526–33. doi: 10.1002/cncr.21116
8. Luk PP, Weston JD, Yu B, Selinger CI, Ekmejian R, Eviston TJ, et al. Salivary duct carcinoma: clinicopathologic features, morphologic spectrum, and somatic mutations. *Head Neck.* (2016) 38(Suppl. 1):E1838–47. doi: 10.1002/hed.24332
9. Lewis JE, McKinney BC, Weiland LH, Ferreiro JA, Olsen KD. Salivary duct carcinoma. Clinicopathologic and immunohistochemical review

of 26 cases. *Cancer.* (1996) 77:223–30. doi: 10.1002/(SICI)1097-0142(19960115)77:2<223::AID-CNCR1>3.0.CO;2-N
10. Huang X, Hao J, Chen S, Deng R. Salivary duct carcinoma: a clinopathological report of 11 cases. *Oncol Lett.* (2015) 10:337–41. doi: 10.3892/ol.2015.3176
11. Breinholt H, Elhakim MT, Godballe C, Andersen LJ, Primdahl H, Kristensen CA, et al. Salivary duct carcinoma: a Danish national study. *J Oral Pathol Med.* (2016) 45:664–71. doi: 10.1111/jop.12426
12. Simpson RH. Salivary duct carcinoma: new developments–morphological variants including pure in situ high grade lesions; proposed molecular classification. *Head Neck Pathol.* (2013) 7(Suppl. 1):S48–58. doi: 10.1007/s12105-013-0456-x
13. Wee DT, Thomas AA, Bradley PJ. Salivary duct carcinoma: what is already known, and can we improve survival? *J Laryngol Otol.* (2012) 126(Suppl. 2):S2–7. doi: 10.1017/S0022215112000412
14. Boon E, Bel M, van Boxtel W, van der Graaf WTA, van Es RJJ, Eerenstein SEJ, et al. A clinicopathological study and prognostic factor analysis of 177 salivary duct carcinoma patients from The Netherlands. *Int J Cancer.* (2018) 143:758–66. doi: 10.1002/ijc.31353
15. Guzzo M, Di Palma S, Grandi C, Molinari R. Salivary duct carcinoma: clinical characteristics and treatment strategies. *Head Neck.* (1997) 19:126–33. doi: 10.1002/(SICI)1097-0347(199703)19:2<126::AID-HED7>3.0.CO;2-6
16. Takahashi H, Tada Y, Saotome T, Akazawa K, Ojiri H, Fushimi C, et al. Phase II trial of trastuzumab and docetaxel in patients with human epidermal growth factor receptor 2-positive salivary duct carcinoma. *J Clin Oncol.* (2019) 37:125–34. doi: 10.1200/JCO.18.00545
17. Kim TH, Kim MS, Choi SH, Suh YG, Koh YW, Kim SH, et al. Postoperative radiotherapy in salivary ductal carcinoma: a single institution experience. *Radiat Oncol J.* (2014) 32:125–31. doi: 10.3857/roj.2014.32.3.125
18. Haderlein M, Scherl C, Semrau S, Lettmaier S, Hecht M, Erber R, et al. Impact of postoperative radiotherapy and HER2/new overexpression in salivary duct carcinoma: a monocentric clinicopathologic analysis. *Strahlentherapie und Onkologie.* (2017) 193:961–70. doi: 10.1007/s00066-017-1196-8
19. Shinoto M, Shioyama Y, Nakamura K, Nakashima T, Kunitake N, Higaki Y, et al. Postoperative radiotherapy in patients with salivary duct carcinoma: clinical outcomes and prognostic factors. *J Radiat Res.* (2013) 54:925–30. doi: 10.1093/jrr/rrt026
20. Kim JY, Lee S, Cho KJ, Kim SY, Nam SY, Choi SH, et al. Treatment results of post-operative radiotherapy in patients with salivary duct carcinoma of the major salivary glands. *Br J Radiol.* (2012) 85:e947–52. doi: 10.1259/bjr/21574486
21. Terhaard CH. Postoperative and primary radiotherapy for salivary gland carcinomas: indications, techniques, and results. *Int J Radiat Oncol Biol Phys.* (2007) 69(Suppl. 2):S52–55. doi: 10.1016/j.ijrobp.2007.04.079
22. Garden AS, Weber RS, Morrison WH, Ang KK, Peters LJ. The influence of positive margins and nerve invasion in adenoid cystic carcinoma of the head and neck treated with surgery and radiation. *Int J Radiat Oncol Biol Phys.* (1995) 32:619–26. doi: 10.1016/0360-3016(95)00122-F
23. Jensen AD, Nikoghosyan AV, Poulakis M, Höss A, Haberer T, Jäkel O, et al. Combined intensity-modulated radiotherapy plus raster-scanned carbon ion boost for advanced adenoid cystic carcinoma of the head and neck results in superior locoregional control and overall survival. *Cancer.* (2015) 121:3001–9. doi: 10.1002/cncr.29443
24. Combs SE, Burkholder I, Edler L, Rieken S, Habermehl D, Jäkel O, et al. Randomised phase I/II study to evaluate carbon ion radiotherapy versus fractionated stereotactic radiotherapy in patients with recurrent or progressive gliomas: the CINDERELLA trial. *BMC Cancer.* (2010) 10:533. doi: 10.1186/1471-2407-10-533
25. Rieken S, Habermehl D, Haberer T, Jaekel O, Debus J, Combs SE. Proton and carbon ion radiotherapy for primary brain tumors delivered with active raster scanning at the Heidelberg Ion Therapy Center (HIT): early treatment results and study concepts. *Radiat Oncol.* (2012) 7:41. doi: 10.1186/1748-717X-7-41
26. Bentzen SM, Constine LS, Deasy JO, Eisbruch A, Jackson A, Marks LB, et al. Quantitative Analyses of Normal Tissue Effects in the Clinic (QUANTEC): an introduction to the scientific issues. *Int J Radiat Oncol Biol Phys.* (2010) 76(Suppl. 3):S3–9. doi: 10.1016/j.ijrobp.2009.09.040
27. Afzelius LE, Cameron WR, Svensson C. Salivary duct carcinoma–a clinicopathologic study of 12 cases. *Head Neck Surgery.* (1987) 9:151–6. doi: 10.1002/hed.2890090304
28. Brandwein MS, Jagirdar J, Patil J, Biller H, Kaneko M. Salivary duct carcinoma (cribriform salivary carcinoma of excretory ducts). A clinicopathologic and immunohistochemical study of 12 cases. *Cancer.* (1990) 65:2307–14. doi: 10.1002/1097-0142(19900515)65:10<2307::AID-CNCR2820651024>3.0.CO;2-1
29. Delgado R, Vuitch F, Albores-Saavedra J. Salivary duct carcinoma. *Cancer.* (1993) 72:1503–12. doi: 10.1002/1097-0142(19930901)72:5<1503::AID-CNCR2820720503>3.0.CO;2-K
30. Kumar RV, Kini L, Bhargava AK, Mukherjee G, Hazarika D, Shenoy AM, et al. Salivary duct carcinoma. *J Surg Oncol.* (1993) 54:193–8. doi: 10.1002/jso.2930540315
31. Barnes L, Rao U, Krause J, Contis L, Schwartz A, Scalamogna P. Salivary duct carcinoma. Part I. A clinicopathologic evaluation and DNA image analysis of 13 cases with review of the literature. *Oral Surg Oral Med Oral Pathol.* (1994) 78:64–73. doi: 10.1016/0030-4220(94)90119-8
32. Grenko RT, Gemryd P, Tytor M, Lundqvist PG, Boeryd B. Salivary duct carcinoma. *Histopathology.* (1995) 26:261–6. doi: 10.1111/j.1365-2559.1995.tb01440.x
33. Hosal AS, Fan C, Barnes L, Myers EN. Salivary duct carcinoma. *Otolaryngol Head Neck Surg.* (2003) 129:720–5. doi: 10.1016/S0194-5998(03)01386-X
34. Shi S, Fang Q, Liu F, Zhong M, Sun C. Prognostic factors and survival rates for parotid duct carcinoma patients. *J Cranio Maxillo Fac Surg.* (2014) 42:1929–31. doi: 10.1016/j.jcms.2014.08.001
35. Roh JL, Lee JI, Choi SH, Nam SY, Kim SO, Cho KJ, et al. Prognostic factors and oncologic outcomes of 56 salivary duct carcinoma patients in a single institution: high rate of systemic failure warrants targeted therapy. *Oral Oncol.* (2014) 50:e64–6. doi: 10.1016/j.oraloncology.2014.08.010
36. Nakashima T, Yasumatsu R, Toh S, Hashimoto K, Shinoto M, Nakamura K, et al. Is there a role of adjuvant treatment for salivary duct carcinoma? *J Laryngol Otol.* (2015) 129 (Suppl. 2):S98–101. doi: 10.1017/S0022215114002965
37. Schmitt NC, Sharma A, Gilbert MR, Kim S. Early T stage salivary duct carcinoma: outcomes and implications for patient counseling. *Otolaryngol Head Neck Surg.* (2015) 153:795–8. doi: 10.1177/0194599815601659
38. Johnston ML, Huang SH, Waldron JN, Atenafu EG, Chan K, Cummings BJ, et al. Salivary duct carcinoma: treatment, outcomes, and patterns of failure. *Head Neck.* (2016) 38 (Suppl. 1):E820–6. doi: 10.1002/hed.24107
39. Otsuka K, Imanishi Y, Tada Y, Kawakita D, Kano S, Tsukahara K, et al. Clinical outcomes and prognostic factors for salivary duct carcinoma: a multi-institutional analysis of 141 patients. *Ann Surg Oncol.* (2016) 23:2038–45. doi: 10.1245/s10434-015-5082-2
40. Gilbert MR, Sharma A, Schmitt NC, Johnson JT, Ferris RL, Duvvuri U, et al. A 20-year review of 75 cases of salivary duct carcinoma. *JAMA Otolaryngol Head Neck Surg.* (2016) 142:489–95. doi: 10.1001/jamaoto.2015.3930
41. Mifsud M, Sharma S, Leon M, Padhya T, Otto K, Caudell J. Salivary duct carcinoma of the parotid: outcomes with a contemporary multidisciplinary treatment approach. *Otolaryngol Head Neck Surg.* (2016) 154:1041–46. doi: 10.1177/0194599816636812
42. Beck ACC, Lohuis P, Al-Mamgani A, Smit LA, Klop WMC. Salivary duct carcinoma: evaluation of treatment and outcome in a tertiary referral institute. *Eur Arch Oto-Rhino-laryngol.* (2018) 275:1885–92. doi: 10.1007/s00405-018-5000-x
43. Anwer AW, Faisal M, Adeel M, Waqas O, Abu Bakar M, Qadeer S, et al. Clinicopathological behavior and treatment-related outcome of rare salivary duct carcinoma: the shaukat khanum memorial cancer hospital experience. *Cureus.* (2018) 10:e3139. doi: 10.7759/cureus.3139
44. Gnepp DR HJ, Simpson RHW, Eveson J. Salivary and lacrimal glands. In: Gnepp DR, editor. *Diagnostic Surgical Pathology of the Head and Neck. 2 ed.* Philadelphia: Saunders Elsevier (2009). doi: 10.1016/B978-1-4160-2589-4.00006-1
45. Laramore GE, Krall JM, Griffin TW, Duncan W, Richter MP, Saroja KR, et al. Neutron versus photon irradiation for unresectable salivary gland tumors: final report of an RTOG-MRC randomized clinical trial. Radiation Therapy Oncology Group. Medical Research Council. *Int J Radiat Oncol Biol Phys.* (1993) 27:235–40. doi: 10.1016/0360-3016(93)90233-L

46. Douglas JG, Koh WJ, Austin-Seymour M, Laramore GE. Treatment of salivary gland neoplasms with fast neutron radiotherapy. *Arch Otolaryngol Head Neck Surg.* (2003) 129:944–8. doi: 10.1001/archotol.129.9.944
47. Akbaba S, Mock A, Hoerner-Rieber J, Held T, Katayama S, Forster T, et al. Treatment outcome of a combined dose-escalated treatment regime with helical tomoTherapy(R) and active raster-scanning carbon ion boost for adenocarcinomas of the head and neck. *Front Oncol.* (2019) 9:755. doi: 10.3389/fonc.2019.00755
48. Akbaba S, Lang K, Held T, Herfarth K, Rieber J, Plinkert P, et al. Carbon-ion radiotherapy in accelerated hypofractionated active raster-scanning technique for malignant lacrimal gland tumors: feasibility and safety. *Cancer Manag Res.* (2019) 11:1155–66. doi: 10.2147/CMAR.S190051
49. Akbaba S, Lang K, Bulut OC, Held T, Rieken S, Plinkert P, et al. The role of organ- and function-preserving radiotherapy in the treatment of adenoid cystic carcinoma of the larynx. *Head Neck.* (2019) 41:2208–14. doi: 10.1002/hed.25678
50. Akbaba S, Heusel A, Mock A, Held T, Lang K, Hoerner-Rieber J, et al. The impact of age on the outcome of patients treated with radiotherapy for mucoepidermoid carcinoma (MEC) of the salivary glands in the head and neck: a 15-year single-center experience. *Oral Oncol.* (2019) 97:115–23. doi: 10.1016/j.oraloncology.2019.08.018
51. Akbaba S, Ahmed D, Lang K, Held T, Mattke M, Hoerner-Rieber J, et al. Results of a combination treatment with intensity modulated radiotherapy and active raster-scanning carbon ion boost for adenoid cystic carcinoma of the minor salivary glands of the nasopharynx. *Oral Oncol.* (2019) 91:39–46. doi: 10.1016/j.oraloncology.2019.02.019
52. Adeberg S, Akbaba S, Lang K, Held T, Verma V, Nikoghosyan A, et al. The Phase 1/2 ACCEPT trial: concurrent cetuximab and intensity modulated radiation therapy with carbon ion boost for adenoid cystic carcinoma of the head and neck. *Int J Radiat Oncol Biol Phys.* (2019). doi: 10.1016/j.ijrobp.2019.09.036
53. Weber U, Kraft G. Comparison of carbon ions versus protons. *Cancer J.* (2009) 15:325–32. doi: 10.1097/PPO.0b013e3181b01935
54. Dimery IW, Legha SS, Shirinian M, Hong WK. Fluorouracil, doxorubicin, cyclophosphamide, and cisplatin combination chemotherapy in advanced or recurrent salivary gland carcinoma. *J Clin Oncol.* (1990) 8:1056–62. doi: 10.1200/JCO.1990.8.6.1056
55. Lewis AG, Tong T, Maghami E. Diagnosis and management of malignant salivary gland tumors of the parotid gland. *Otolaryngol Clin North Am.* (2016) 49:343–80. doi: 10.1016/j.otc.2015.11.001
56. Williams MD, Roberts DB, Kies MS, Mao L, Weber RS, El-Naggar AK. Genetic and expression analysis of HER-2 and EGFR genes in salivary duct carcinoma: empirical and therapeutic significance. *Clin Cancer Res.* (2010) 16:2266–74. doi: 10.1158/1078-0432.CCR-09-0238
57. D'Heygere E, Meulemans J, Vander Poorten V. Salivary duct carcinoma. *Curr Opin Otolaryngol Head Neck Surgery.* (2018) 26:142–51. doi: 10.1097/MOO.0000000000000436
58. Masubuchi T, Tada Y, Maruya S, Osamura Y, Kamata SE, Miura K, et al. Clinicopathological significance of androgen receptor, HER2, Ki-67 and EGFR expressions in salivary duct carcinoma. *Int J Clin Oncol.* (2015) 20:35–44. doi: 10.1007/s10147-014-0674-6
59. Takase S, Kano S, Tada Y, Kawakita D, Shimura T, Hirai H, et al. Biomarker immunoprofile in salivary duct carcinomas: clinicopathological and prognostic implications with evaluation of the revised classification. *Oncotarget.* (2017) 8:59023–35. doi: 10.18632/oncotarget.19812
60. Shimura T, Tada Y, Hirai H, Kawakita D, Kano S, Tsukahara K, et al. Prognostic and histogenetic roles of gene alteration and the expression of key potentially actionable targets in salivary duct carcinomas. *Oncotarget.* (2018) 9:1852–67. doi: 10.18632/oncotarget.22927
61. Keller G, Steinmann D, Quaas A, Grunwald V, Janssen S, Hussein K. New concepts of personalized therapy in salivary gland carcinomas. *Oral Oncol.* (2017) 68:103–13. doi: 10.1016/j.oraloncology.2017.02.018
62. van Boxtel W, Locati LD, van Engen-van Grunsven ACH, Bergamini C, Jonker MA, Fiets E, et al. Adjuvant androgen deprivation therapy for poor-risk, androgen receptor-positive salivary duct carcinoma. *Eur J Cancer.* (2019) 110:62–70. doi: 10.1016/j.ejca.2018.12.035
63. Fan CY, Melhem MF, Hosal AS, Grandis JR, Barnes EL. Expression of androgen receptor, epidermal growth factor receptor, and transforming growth factor alpha in salivary duct carcinoma. *Arch Otolaryngol Head Neck Surg.* (2001) 127:1075–9. doi: 10.1001/archotol.127.9.1075
64. Williams MD, Roberts D, Blumenschein GR Jr, Temam S, Kies MS, Rosenthal DI, et al. Differential expression of hormonal and growth factor receptors in salivary duct carcinomas: biologic significance and potential role in therapeutic stratification of patients. *Am J Surg Pathol.* (2007) 31:1645–52. doi: 10.1097/PAS.0b013e3180caa099
65. Salgado LR, Spratt DE, Riaz N, Romesser PB, Wolden S, Rao S, et al. Radiation therapy in the treatment of minor salivary gland tumors. *Am J Clin Oncol.* (2014) 37:492–7. doi: 10.1097/COC.0b013e31827e54e5
66. Schulz-Ertner D, Nikoghosyan A, Didinger B, Münter M, Jäkel O, Karger CP, et al. Therapy strategies for locally advanced adenoid cystic carcinomas using modern radiation therapy techniques. *Cancer.* (2005) 104:338–44. doi: 10.1002/cncr.21158
67. Stannard C, Vernimmen F, Carrara H, Jones D, Fredericks S, Hille J, et al. Malignant salivary gland tumours: can fast neutron therapy results point the way to carbon ion therapy? *Radiother Oncol.* (2013) 109:262–8. doi: 10.1016/j.radonc.2013.08.013

Conflict of Interest: SAd and DB received grants from Accuray International Sàrl outside the submitted work. DB received grants from Novocure outside the submitted work. JD received grants from CRI–The Clinical Research Institue GmbH, View Ray Inc., Accuray International Sàrl, Accuray Incorporated, RaySearch Laboratories AB, Vision RT limited, Merck Serono GmbH, Astellas Pharma GmbH, Astra Zeneca GmbH, Solution Akademie GmbH, Ergomed PLC Surrey Research Park, Siemens Healthcare GmbH, Quintiles GmbH, Pharmaceutecal Research Associates GmbH, Boehringer Ingelheim Pharma GmbH Co, PTW-Freiburg Dr. Pychlau GmbH, Nanobiotix AA outside the submitted work.

The remaining authors declare that the research was conducted in the absence of any commercial or financial relationships that could be construed as a potential conflict of interest.

frontiers | Frontiers in Oncology

TYPE Original Research
PUBLISHED 11 November 2022
DOI 10.3389/fonc.2022.958961

OPEN ACCESS

EDITED BY
Rakesh Kapoor,
Post Graduate Institute of Medical Education and Research (PGIMER), India

REVIEWED BY
Silviu Albu,
Iuliu Haţieganu University of Medicine and Pharmacy, Romania
Michael Andrew Samuels,
Banner Health, United States

*CORRESPONDENCE
Xiao-Li Yu
yuxiaoli3@mail.sysu.edu.cn

†These authors have contributed equally to this work and share first authorship

SPECIALTY SECTION
This article was submitted to Radiation Oncology, a section of the journal Frontiers in Oncology

RECEIVED 01 June 2022
ACCEPTED 24 October 2022
PUBLISHED 11 November 2022

CITATION
Cai X-L, Hu J, Shi J-T, Chen J-S, Bai S-M, Liu Y-M and Yu X-L (2022) Contouring the accessory parotid gland and major parotid glands as a single organ at risk during nasopharyngeal carcinoma radiotherapy. *Front. Oncol.* 12:958961. doi: 10.3389/fonc.2022.958961

Contouring the accessory parotid gland and major parotid glands as a single organ at risk during nasopharyngeal carcinoma radiotherapy

Xin-Ling Cai[1†], Jiang Hu[2†], Jun-Tian Shi[3,4], Jin-Shu Chen[3,4], Shou-Min Bai[3,4], Yi-Min Liu[3,4] and Xiao-Li Yu[3,4*]

[1]Department of Radiation Oncology, Shenshan Medical Center, Sun Yat-Sen Memorial Hospital, Sun Yat-Sen University, Shanwei, China, [2]Department of Radiation Oncology, Sun Yat-Sen University Cancer Center and State Key Laboratory of Oncology in Southern China, Collaborative Innovation Center of Cancer Medicine, Guangzhou, China, [3]Guangdong Provincial Key Laboratory of Malignant Tumor Epigenetics and Gene Regulation, Sun Yat-sen Memorial Hospital, Sun Yat-sen University, Guangzhou, China, [4]Department of Radiation Oncology, Sun Yat-sen Memorial Hospital, Sun Yat-sen University, Guangzhou, China

Background and purpose: No research currently exists on the role of the accessory parotid gland (APG) in nasopharyngeal carcinoma (NPC). We thereby aimed to assess the effects of APG on the dosimetry of the parotid glands (PGs) during NPC radiotherapy and evaluate its predictive value for late xerostomia.

Material and methods: The clinical data of 32 NPC patients with radiological evidence of the APG treated at Sun Yat-sen Memorial Hospital between November 2020 and February 2021 were retrospectively reviewed. Clinically approved treatment plans consisted of only the PGs as an organ at risk (OAR) (Plan1), while Plan2 was designed by considering the APG as a single organ at risk (OAR). The APG on Plan1 was delineated, and dose–volume parameters of the PGs alone (PG-only) and of the combined structure (PG+APG) were analyzed in both plans. The association of such dosimetric parameters in Plan1 with xerostomia at 6–9 months post-radiotherapy was further explored.

Results: Fifty APGs were found, with a mean volume of 3.3 ± 0.2 ml. Significant differences were found in all dosimetric parameters between Plan1 and Plan2. The mean dose and percentage of OAR volumes receiving more than 30 Gy significantly reduced in Plan1 itself (PG-only vs. PG+APG, 39.55 ± 0.83 Gy vs. 37.71 ± 0.75 Gy, and 62.00 ± 2.00% vs. 57.41 ± 1.56%, respectively; $p < 001$) and reduced further in Plan2 (PG+APG, 36.40 ± 0.74 Gy, and 55.54 ± 1.61%, respectively; $p < 0.001$). Three additional patients met the dose constraint in Plan1, which increased to seven in Plan2. With APG included, the predictive

power of the dosimetric parameters for xerostomia tended to improve, although no significant differences were observed.

Conclusion: APG is anatomically similar to the PGs. Our findings suggest the potential benefits of treating the APG and PGs as a single OAR during radiotherapy (RT) of NPC by improving PG sparing.

KEYWORDS

nasopharyngeal carcinoma, accessory parotid gland, dosimetry analysis, contouring, xerostomia

Introduction

Nasopharyngeal carcinoma (NPC) is a radiosensitive cancer characterized by its unique geographic distribution, with particularly high incidences in Southern China (1, 2). While radiotherapy (RT) represents the mainstay treatment for non-metastatic NPCs, radiation-induced xerostomia is a common long-term complication that can greatly affect the quality of life of patients (3). Despite the advent of more advanced RT techniques such as intensity-modulated RT (IMRT), the incidence of grade III–IV xerostomia remained between 13.9% and 27.5% among patients with mild-to-severe skull-base invasion (4). This is mainly attributed to radiation damage of the salivary glands, particularly the parotid glands (PGs). Accurate delineation of the PGs is thus the cornerstone for their protection during RT.

Increasing attention has been paid to the protection of the PGs during RT. Several studies have developed the split-parotid delineation approach to spare specific regions of the organ, including the stem and progenitor cells and the superficial lobe (5–7). However, the accessory parotid gland (APG), which has been found as a fairly common anatomical variant with a prevalence of 21%–56% (8, 9), is rarely mentioned in the literature. Based on cadaveric studies, no appreciable histopathological differences from the PGs have been reported (8), and both serous and mucous acini have been identified, suggesting that APG may have similar functions as PGs (9). In most cases, the APG drains into Stensen's duct (parotid duct) through an accessory duct (10). Nonetheless, current guidelines for the delineation of organs at risk (OAR) (11, 12) do not account for the APGs, and whether they should be included in the target volume of PGs remains unknown.

A strict dose constraint is essential to minimize the radiation exposure of the PGs. Recent guidelines have recommended a mean dose (Dmean) of ≤26 Gy, with maximum acceptance criteria of <30 Gy for ≥50% (D50≤30Gy) of at least one gland (12). However, with large tumors and gross nodal involvement, compromise of the PGs is often required to ensure adequate dose delivery to the target area. In addition, we observed clinical inconsistencies between xerostomia and dosimetric parameters of the PGs in patients with APGs. As such, the effects of considering APG as a homologous organ of the PGs on the dosimetry of the PGs, and subsequently the development of xerostomia, represent a question that needs to be addressed.

Our study thereby aimed to compare the dosimetric parameters of the PGs based on the inclusion of the APG during RT planning and evaluate its influence on late xerostomia development among NPC patients.

Materials and methods

Patients

The clinical and radiological data of biopsy-proven NPC patients treated at Sun Yat-sen Memorial Hospital between November 2020 and February 2021 were retrospectively collected. The inclusion criteria were as follows: 1) NPC stage I–IVa according to the 8th edition of the American Joint Committee on Cancer (AJCC8), 2) radiological evidence of the APG, 3) definitive treatment with IMRT, and 4) completion of treatment. Exclusion criteria were as follows: 1) lost to medical records and 2) incompletion of treatment. This study was approved by the local ethics committee of the institute.

Target delineation and dose prescription

Contrast-enhanced CT imaging (SOMATOM Definition, Siemens Healthcare, Forchheim, Germany) was performed for IMRT planning. All patients were immobilized in the supine position with a head–neck–shoulder thermoplastic mask and a vacuum bag. The scans ranged from the superior margin of the

frontal sinus to 2 cm below the clavicle with a slice thickness of 3 mm. Delineation of target volumes and OARs was performed based on recent international guidelines (11–13). The gross tumor volume included the primary tumor volume and any enlarged regional lymph nodes confirmed on CT and magnetic resonance imaging. The high-risk clinical target volume was defined as the gross tumor volume plus a 5–10-mm margin and the entire nasopharyngeal mucosa. The low-risk clinical target volume was defined as the high-risk clinical target volume plus a 5–10-mm margin and encompassed low-risk sites of microscopic extension such as the skull base, clivus, sphenoid sinus, parapharyngeal space, pterygoid fossae, posterior nasal cavity, pterygopalatine fossae, retropharyngeal nodal regions, and the elective neck area from level IB to V. A 3-mm margin was used to generate the corresponding planning target volume (PTV) and planning OAR volume (PRV).

IMRT was administered in 33 fractions, five fractions per week. The radiation doses to the gross tumor volume and the high- and low-risk clinical target volumes were 70, 60, and 54 Gy, respectively (PTV70Gy, PTV60Gy, and PTV54Gy, respectively). The dosimetric objectives of the PGs were set as either V30 ≤ 50% for at least one PG, or Dmean ≤ 26 Gy. The dosimetric parameters of other OARs were determined according to Radiation Therapy Oncology Group (RTOG) protocols 0225 and 0615 (14, 15).

APG delineation and dosimetric data collection

At this stage of analysis, two treatment plans were involved—Plan1 and Plan2. Plan1 represented the clinically approved treatment plans obtained from the Varian Trilogy system (Eclipse, version 13.5; Varian Medical Systems, Palo Alto, CA), whereby only the PGs were contoured (and protected) as an OAR. The APG was then outlined (without any attempts made to protect the gland) (Figure 1) to allow for dosimetric evaluation of the APG and the PGs and APG combined (PG+APG). Delineation of the APG was performed by two clinicians with >10 years of RT experience in NPC, and any disagreements were discussed and resolved by consensus. Plan2 was subsequently designed by intentionally treating the APG as an OAR. The target and OAR dose criteria from Plan1 were retained. All patients were treated using Plan1, while Plan2 was created for comparative purposes.

The dosimetric data of PG-only and PG+APG of both plans were subsequently compared. Dosimetric parameters were retrieved

FIGURE 1
Delineation of the parotid glands (purple) and accessory parotid gland (cyan).

from dose–volume histograms and included the following: Dmean; the dose to 50% of the OAR volume (D50); percentage of the OAR volume receiving more than 26, 30, 33, and 45 Gy (V26, V30, V33, and V45, respectively); and the absolute OAR volume receiving lower than 20 Gy (V20cc).

Xerostomia evaluation

Xerostomia was graded according to the RTOG late toxicity scale (16). The presence of xerostomia was evaluated at 6–12 months post-RT, and its association with all relevant dosimetric parameters in each of the two delineation approaches was compared. Clinically significant xerostomia was defined as those grades ≥2.

Statistical analysis

All dosimetric parameters were compared using either the paired-samples T-test, Wilcoxon rank-sum test, or McNemar's test, while clinical characteristics and xerostomia rate were compared using Fisher's exact test. The predictive value of dosimetric parameters for xerostomia was assessed using the receiver operating characteristic (ROC) analysis, and areas under the ROC curve (AUCs) were compared using Delong's test.

All statistical analyses were performed using SPSS Statistics version 23.0 and MedCalc version 12.0. Two-tailed p-values < 0.05 were considered statistically significant.

Results

Patient characteristics

Among a total of 136 NPC patients treated with IMRT at our hospital, 32 were identified to have the APG (23.53%) and were included in our study. A total of 50 APGs were found and were unilateral and bilateral in 14 and 18 patients, respectively. The mean age was 51 years (range, 29–71 years). The mean maximum diameter of LNs ipsilateral to the APG was 2.52 ± 0.25 cm. Locally advanced NPCs (stage III–IVa) were demonstrated in approximately 85% of the patients.

All baseline and clinical characteristics of the included patients are summarized in Table 1.

PG, APG, and target-overlapping volumes

The mean volumes were as follows: APG, 3.3 ± 0.2 ml (range, 1.3–8.6 ml); PG, 29.4 ± 1.3 ml (range, 15.8–47.7 ml); and PG+APG, 32.9 ± 1.4 ml (range, 19.0–56.0 ml). No overlaps between the APG and the target volumes were observed. In contrast, target-overlapping PG volumes were 0.60(0.20–1.00) ml, 0.55(0.20–1.00) ml, and 7.1 (6.0–9.1) ml for PTV70Gy, PTV60Gy, and PTV54Gy, respectively.

Comparison of dosimetric parameters based on APG involvement

All dosimetric parameters between Plan1 and Plan2 are summarized in Table 2. A significantly higher Dmean of APG was observed in Plan1 compared to Plan2 (24.79 ± 0.85 Gy vs. 14.22 ± 0.41 Gy; $p < 0.001$). Both the Dmean and D50 of PG-only were significantly higher than that of PG+APG in Plan1 (39.55 ± 0.83 Gy vs. 37.71 ± 0.75 Gy; 39.31 ± 1.21 Gy vs. 35.37 ±

TABLE 1 Clinicopathological characteristics.

Variable	N = 32	
Sex	n	(%)
Male	23	71.88%
Female	9	28.13%
Age		
≥56	13	40.63%
<56	19	59.38%
Maximum diameter of unilateral LN*		
>2.5 cm	22	44.00%
≤2.5 cm	28	56.00%
T stage,		
T1	4	12.50%
T2	8	25.00%
T3	13	40.63%
T4	7	21.88%
N stage		
N0	3	9.38%
N1	8	25.00%
N2	18	56.25%
N3	3	9.38%
Clinical stage		
I	2	6.25%
II	3	9.38%
III	19	59.38%
IVa–b	8	25.00%
Clinical levels of LN*		
No	1	2.00%
II	11	22.00%
II–III	31	62.00%
II, IV	1	2.00%
II –IV	6	12.00%
Treatment, n (%)		
InC+CCRT	30	93.75%
CCRT	2	6.25%

LN, lymph node; CCRT, concurrent chemoradiotherapy; InC+CCRT, induction chemotherapy followed by concurrent chemoradiotherapy.
*Lymph nodes ipsilateral to the accessory parotid gland, N = 50.

1.15 Gy, respectively; $p < 0.001$). Significant improvement was observed in all dosimetric parameters between PG-only in Plan1 and PG+APG in both Plan1 and Plan2 (Table 2 and Figure 2). Significant improvement was also observed in the corresponding dosimetric parameters of PG+APG in Plan2 compared to Plan1 ($p < 0.001$). In Plan2, all the dosimetric parameters of PG-only, except for V26, were lower than those in Plan1 (Figure 2).

Overall, more favorable mean dosimetry was observed for the combined structures in Plan1. In Plan1, the PG+APG delineation approach associated with three additional patients who met the dose constraint for V30, resulting in a slight improvement in the rate that met the dose restriction of the PGs (37.5%, 12/32 vs. 46.9%, 15/32; $p > 0.05$). All three patients had stage III–IVa NPC and grade 0–1 xerostomia, two of whom exhibited bilateral APGs. The maximum diameter of LNs ipsilateral to the APG ranged between 1.2 and 6.9 cm among these patients. In Plan2, the V30 of four additional patients improved to meet the dose criteria, resulting in significant improvement in dose constraint fulfillment rate (37.5%, 12/32 vs. 59.4%, 19/32; $p < 0.05$). Of these seven patients, V30 of PG-only in Plan1 and that of PG+APG in Plan2 ranged between 51.2% and 61.7% and 41.4% and 49.6%, respectively (Figure 3). At 6 months follow-up, five of them exhibited grades 0–1 xerostomia, while two reported grade 2 xerostomia.

Xerostomia and the predictive value of dosimetric parameters

Grades 0–1 xerostomia was reported in 25 patients (grade 0, n = 9; and grade 1, n = 16), grade 2 xerostomia was reported in 5, while grade 3–4 xerostomia was not observed. Two patients were lost to follow-up. The clinical characteristics of patients based on

TABLE 2 Comparison of dosimetric parameters of PG-only and PG+APG in Plan1 and Plan2.

Variable	Plan 1			Plan2	
	PG-only	PG+APG	p-value	PG+APG	p'-value
Dmean (Gy)					
Mean	39.55 ± 0.83	37.71 ± 0.75	<0.001	36.40 ± 0.74	<0.001
Range	29.49–65.61	27.66–60.52		26.77–57.52	
D50 (Gy)					
Mean	39.31 ± 1.21	35.37 ± 1.15	<0.001*	34.31 ± 1.14	<0.001
Range	23.89–68.71	20.44–67.50		20.07–64.94	
V26 (%)					
Mean	68.07 ± 1.64	64.39 ± 1.62	<0.001	61.78 ± 1.55	<0.001
Range	47.00–99.84	41.74–94.57		41.40–94.20	
V30 (%)					
Mean	62.00 ± 2.00	57.41 ± 1.56	<0.001*	55.54 ± 1.61	<0.001
Range	42–99	36.99–89.76		36.80–88.30	
V33 (%)					
Mean	57.91 ± 1.68	52.80 ± 1.52	<0.001*	51.29 ± 1.62	<0.001
Range	38.89–98.81	34.22–87.63		33.50–85.00	
V45 (%)					
Mean	44.16 ± 1.77	39.18 ± 1.54	<0.001	37.25 ± 1.53	<0.001
Range	25.92–95.80	23.31–82.85		22.20–82.10	
V<20 (cc)					
Mean	6.65 ± 0.61	7.99 ± 0.73	<0.001	9.16 ± 0.76	<0.001
Range	0–19.99	0.05–25.27		1.20–25.10	
Organ Volume (cc)					
Mean	29.36 ± 1.28	32.85 ± 1.37	<0.001*	–	
Range	15.80–47.70	19.00–56.00		–	

PG-only, the parotid glands as an organ at risk; PG+APG, the parotid glands and accessory parotid gland as a single organ at risk; Dmean, mean dose; D50, dose of 50% OAR volume; V26, percentage of the OAR volume that received ≥ 26 Gy; V30, percentage of the OAR volume that received ≥ 30 Gy; V33, percentage of the OAR volume that received ≥ 33 Gy; V45, percentage of the OAR volume that received ≥ 45 Gy; V20cc, the OAR volume receiving < 20 Gy.

* Paired-sample T-test.

p = p-value of dosimetric parameters of PG-only and PG+APG in Plan1.

p' = p-value of dosimetric parameters of PG+APG in Plan1 and PG+APG in Plan2.

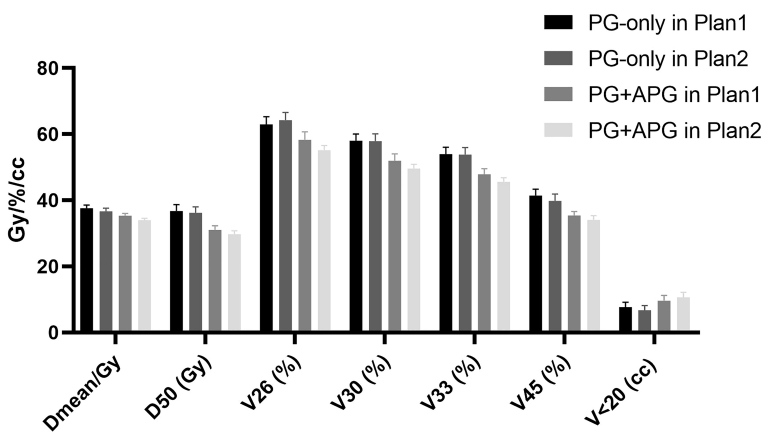

FIGURE 2
Dosimetric parameters in Plan1 and Plan2.

the development of clinically significant xerostomia are shown in Table 3. Patients who underwent induction chemotherapy and concurrent chemoradiotherapy (InC+CRRT) were associated with significantly higher rates of grade 2–3 xerostomia compared to those who underwent CCRT alone ($p < 0.05$).

In Plan1, the AUCs of Dmean, D50, V30, V33, and V20cc of PG+APG tended to increase compared to those of PG-only, although no significant differences were shown. The AUCs of V26 and V45 for PG-only and PG+APG remained similar (Table 4).

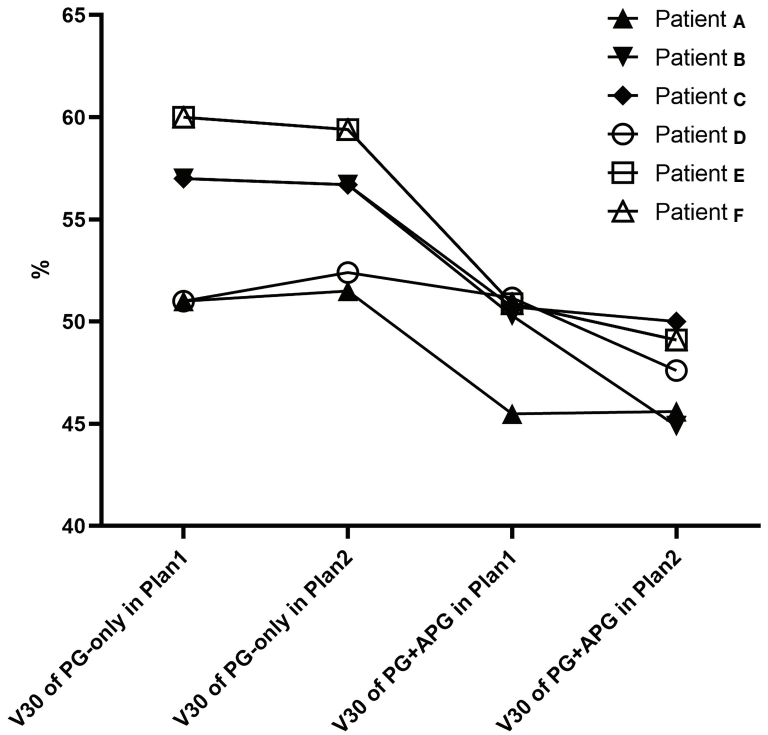

FIGURE 3
V30 of seven patients that improved and met the PG dose restriction standard in Plan1 (patients E–G) and Plan2.

TABLE 3 Association between xerostomia and clinical characteristics.

Variable	≥ Grade 2		Grade 0–1		p-value
Sex	n	(%)	n	(%)	0.859
Male	3	60.0%	19	76.0%	
Female	2	40.0%	6	24.0%	
Age					>0.999
≥56	3	60.0%	16	64.0%	
<56	2	40.0%	9	36.0%	
Maximum diameter of unilateral LNs					0.138
>2.5 cm	4	80.0%	9	36.0%	
≤2.5 cm	1	20.0%	16	64.0%	
T-stage					0.364
T1–2	2	40.0%	9	36.0%	
T3–4	3	60.0%	16	64.0%	
N-stage					0.300
N0–1	2	40.0%	7	28.0%	
N2–3	3	60.0%	18	72.0%	
Clinical stage					0.183
I–II	2	40.0%	3	12.0%	
III–IVa	3	60.0%	22	88.0%	
Clinical levels of LN					>0.999
No	0	0.0%	1	4.0%	
II	1	20.0%	7	28.0%	
II–III	4	80.0%	14	56.0%	
II, IV	0	0.0%	2	8.0%	
II–IV	0	0.0%	1	4.0%	
Treatment					0.023
InC+CCRT	3	60.0%	25	100.0%	
CCRT	2	40.0%	0	0.0%	

AUC, area under the curve; 95% CI, 95% confidence interval; PG-only, parotid glands as an organ at risk; PG+APG, the parotid glands and accessory parotid gland as a single organ at risk; Dmean, mean dose; D50, dose of 50% OAR volume; V26, percentage of the OAR volume receiving ≥ 26 Gy; V30, percentage of the OAR volume that received ≥ 30 Gy; V33, percentage of the OAR volume that received ≥ 33 Gy; V45, percentage of the OAR volume that received ≥ 45 Gy.

Discussion

The salivary glands consist of three major pairs of glands, namely, the PGs, submandibular glands, and sublingual glands, with 65% of saliva produced by the PGs (17). Given that the submandibular glands are often located within the target volume during RT and that the sublingual glands are usually difficult to recognize, preservation of the PGs is of great importance. The APG functions similarly to the PGs and demonstrates no appreciable histopathological differences (8). To our knowledge, the role of APG preservation during RT for NPC has not been explored. As such, our study represents the first in assessing the effects of treating the APG and PGs as a single OAR in NPC radiotherapy.

Heterogeneity exists in the prevalence and location of the APG in the population, as more than one APG may be found unilaterally, adjacent to a single PG, or deviate from its expected location (18). The prevalence of the APG in our study was 23.53%, which was lower than the 33.8% prevalence found in a recent meta-analysis in Asia (18). In addition, a higher prevalence was observed in male compared to female patients. Unlike the findings of Toh et al. (9), bilateral APGs were observed in the majority of our patients (56.3%). This may be due to the smaller sample size of our study and the higher proportion of male patients.

The mean size of the APG has been reported to be 15.8 × 5.0 mm on CT (19) and can range from the size of a pea to that of a kidney bean, as described in the cadaveric study by Frommer (8). Our results were in accordance with such findings. In the study by Pujol-Olmo et al., the PGs demonstrated a mean height and width of 66.37 and 46.84 mm, respectively (20). A longitudinal volumetric study found that the mean volume of PGs ranged between 28.7 and 32.2 ml (21), which was consistent with our data (mean, 29.4 ± 1.3 ml; range, 15.8–47.7 ml). While the PGs were found to be larger compared to the APG, there was a great extent of overlap with PTV54Gy (mean, 28.36%), rendering most of the organ exposed to a radiation dose ≥54 Gy. In contrast, no overlap between the APG and the target volume

TABLE 4 Receiver operating characteristic (ROC) analysis of dosimetric parameters in Plan1 for xerostomia.

Variable	AUC/95% CI	p-value
Dmean		0.264
PG-only	0.552 (0.210–0.894)	
PG+APG	0.608 (0.270–0.946)	
D50		0.050
PG-only	0.512 (0.198–0.826)	
PG+APG	0.624 (0.294–0.954)	
V26		>0.999
PG-only	0.616 (0.273–0.959)	
PG+APG	0.616 (0.282–0.950)	
V30		0.596
PG-only	0.600 (0.267–0.933)	
PG+APG	0.640 (0.309 –0.971)	
V33		0.512
PG-only	0.592 (0.265–0.919)	
PG+APG	0.640 (0.306–0.974)	
V45		>0.999
PG-only	0.584(0.263–0.905)	
PG+APG	0.584 (0.252–0.916)	
V20cc		0.952
PG-only	0.472(0.100–0.844)	
PG+APG	0.504(0.161–0.874)	

AUC, Area under the curve; 95% CI, 95% confidence interval; PG-only, parotid glands as an organ at risk; PG+APG, the parotid glands and accessory parotid gland as a single organ at risk; Dmean, mean dose; D50, dose of 50% OAR volume; V26, percentage of the OAR volume receiving ≥ 26 Gy; V30, percentage of the OAR volume that received ≥ 30 Gy; V33, percentage of the OAR volume that received ≥ 33 Gy; V45, percentage of the OAR volume that received ≥ 45 Gy.

was observed, indicating that protection of the APG may be easily achieved. A study revealed that partial volume thresholds for the prediction of reduced salivary flow were V45 < 24% and V30 < 45% (22). In Plan1 of our study, V45 and V30 were 44.16% and 62.00%, respectively, to the PGs only, which reduced to 39.18% and 57.41%, respectively, upon involvement of the APG. When the APG was intentionally protected in Plan2, improvements were observed in all dosimetric parameters to the organ, besides V26, which remained higher than the threshold. This may be explained by the large proportion of patients with locally advanced NPC in our study and the relative proximity in location of PG+APG to the target volume.

Dmean, V30, and D50 represent the most critical dosimetric predictors of parotid function impairment in NPC radiotherapy (11). We found that the PG+APG delineation approach resulted in a significant improvement in the aforementioned parameters in both Plan1 and Plan2 ($p < 0.001$). In Plan1, the reductions in the mean value of Dmean and D50 were 1.84 and 3.96 Gy, respectively, while that of V30 was approximately 5%. Among the patients who did not meet the dose constraint, only three patients improved and met the criteria by the addition of APG in Plan1. This may be due to 1) the close location of PGs to the treatment area, resulting in a relatively high volume overlap with PTV54Gy, and 2) a large percentage of level II lymph node involvement. When the APG was outlined and protected in Plan2, the rate that met the dose constraints of the PGs significantly improved from 37.5% to 59.4% ($p < 0.05$), and the mean decreases in Dmean, D50, and V30 were 3.1 Gy, 5 Gy, and approximately 6.5%, respectively, which were greater than those observed in Plan1.

After IMRT, saliva flowrate often significantly decreases in NPC patients (0.10 ml/min vs. 0.57 ml/min at baseline) and only partially recovers a year later (23). Based on the study by Poon et al. (24), approximately 20% of NPC patients developed chronic grade 2–3 grading xerostomia following IMRT, which is consistent with our results (5/30, 16.67%). Grade 3 xerostomia was not observed in our patients. Han et al. demonstrated the difference in the influence of spatial dose patterns on the salivary glands on xerostomia development and recovery, with recovery showing increased importance towards subvolumes that received lower radiation doses (25). Without deliberate protection of the APG, we found that the radiation exposure of the APG ranged between 20 and 30 Gy (Dmean, 24.79 ± 0.85 Gy). By contouring the APG as an OAR, this reduced to 10–

20 Gy (Dmean, 14.22 ± 0.41 Gy). As such, our findings proposed that APG sparing during RT may facilitate better recovery from xerostomia.

In terms of the predictive factors of xerostomia, Gabrys et al. found that Dmean of the PGs failed to recognize patients at risk of grade ≥ 2 xerostomia (26), and no dosimetric parameters (including Dmean, V20, V30, V40, V50, and V60) were reported to significantly associate with xerostomia in the studies by Sommat et al. (27) Our study corroborated with such results and found no significant associations between xerostomia and any of the dose–volume parameters of PG+APG (AUC < 0.700). However, we observed that the AUCs of nearly all dosimetric parameters, especially D50 ($p = 0.050$), of the PG+APG delineation approach tended to improve compared to that of the PG-only delineation approach. Furthermore, a recent study found V25, V30, V35, V45, and Dmean to the PGs as independent predictive factors for xerostomia, although with low assessment ability (AUC < 0.700) (28). Our results may be mainly attributed to the more accurate reflection of the salivary gland volume with the addition of the APG. In Plan2, the dosimetry of seven patients improved to meet the dose restriction standards of the PGs, and five of them exhibited 0–1 grade xerostomia, indicating that inclusion of the APG resulted in increased association between PG+APG dosimetry and xerostomia severity. Given the lack of prospective analyses, the effects of adding APG as an OAR on the prediction of xerostomia require further evaluation. Nonetheless, it is well known that the incidence of xerostomia can be influenced by a multitude of factors, including clinical features and treatment strategies (29). We also found that patients who underwent InC +CRRT were more likely to develop chronic xerostomia. Dosimetric data alone may thus be insufficient for the accurate prediction of late xerostomia. While considerable research effort has been put into this subject (30, 31), further studies involving clinical, molecular, and radiological variables are warranted.

Conclusions

Our study presented a novel approach to PG delineation during RT for NPC by considering the inclusion of the APG. Our results showed that consideration of the APG as a homologous part of the PG resulted in a significant improvement in the dosimetry of the PGs, particularly when the APGs were intentionally protected during RT. None of the dosimetric parameters were predictive for xerostomia; however, the AUCs of the majority of the parameters tended to increase with the PG+APG delineation approach. Our findings thereby suggest the benefits of considering the APG and PGs as a single OAR during RT for NPC and demonstrate its potential to better reflect the long-term outcomes of such patients. Due to the potential biases of a retrospective study, further prospective research is needed to verify our findings.

Data availability statement

The raw data supporting the conclusions of this article will be made available by the authors, without undue reservation.

Ethics statement

The studies involving human participants were reviewed and approved by Sun Yat-sen Memorial Hospital Ethics Committee. The ethics committee waived the requirement of written informed consent for participation.

Author contributions

X-LY and JH: conceptualization and methodology development. X-LC: data analysis and original draft preparation. X-LY, JH, J-TS, and J-SC: data acquisition. X-LY: draft editing. Y-ML and S-MB: methodology supervision and draft revising. All authors contributed to the article and approved the submitted version.

Conflict of interest

The authors declare that the research was conducted in the absence of any commercial or financial relationships that could be construed as a potential conflict of interest.

Publisher's note

References

1. Chen W, Zheng R, Baade PD, Zhang S, Zeng H, Bray F, et al. Cancer statistics in China, 2015. *CA: Cancer J Clin* (2016) 66(2):115–32. doi: 10.3322/caac.21338

2. Siegel RL, Miller KD, Fuchs HE, Jemal A. Cancer statistics, 2021. *CA: Cancer J Clin* (2021) 71(1):7–33. doi: 10.3322/caac.21654

3. Jellema A, Slotman B, Doornaert P, Leemans C, Langendijk J. Impact of radiation-induced xerostomia on quality of life after primary radiotherapy among patients with head and neck cancer. *Int J Radiat Oncol Biol Phys* (2007) 69(3):751–60. doi: 10.1016/j.ijrobp.2007.04.021

4. Liao S, Xie Y, Feng Y, Zhou Y, Pan Y, Fan J, et al. Superiority of intensity-modulated radiation therapy in nasopharyngeal carcinoma with skull-base invasion. *J Cancer Res Clin Oncol* (2020) 146(2):429–39. doi: 10.1007/s00432-019-03067-y

5. Xiao W, Lin Z, Zhang W, Li M, Wu VW. A split-parotid delineation approach for dose optimization in volumetric modulated arc therapy for nasopharyngeal carcinoma patients with parapharyngeal space invasion and level IIa cervical lymph node involvements. *Br J Radiol* (2016) 89(1060):20150635. doi: 10.1259/bjr.20150635

6. Zhang H, Lu X, Huang S, Wang L, Zhao C, Xia W, et al. Superficial parotid lobe-sparing delineation approach: a better method of dose optimization to protect the parotid gland in intensity-modulated radiotherapy for nasopharyngeal carcinoma. *Curr Oncol* (2013) 20(6):e577–584. doi: 10.3747/co.20.1485

7. van Luijk P, Pringle S, Deasy J, Moiseenko V, Faber H, Hovan A, et al. Sparing the region of the salivary gland containing stem cells preserves saliva production after radiotherapy for head and neck cancer. *Sci Transl Med* (2015) 7 (305):305ra147. doi: 10.1126/scitranslmed.aac4441

8. Frommer J. The human accessory parotid gland: its incidence, nature, and significance. *Oral surgery Oral medicine Oral Pathol* (1977) 43(5):671–6. doi: 10.1016/0030-4220(77)90049-4

9. Toh H, Kodama J, Fukuda J, Rittman B, Mackenzie I. Incidence and histology of human accessory parotid glands. *Anat Rec* (1993) 236(3):586–90. doi: 10.1002/ar.1092360319

10. Zhu W, Hu F, Liu X, Guo S, Tao QJ. Role of the accessory parotid gland in the etiology of parotitis: Statistical analysis of sialographic features. *PloS One* (2016) 11(2):e0150212. doi: 10.1371/journal.pone.0150212

11. Lee A, Ng W, Pan J, Poh S, Ahn Y, AlHussain H, et al. International guideline for the delineation of the clinical target volumes (CTV) for nasopharyngeal carcinoma. *Radiotherapy Oncol* (2018) 126(1):25–36. doi: 10.1016/j.radonc.2017.10.032

12. Lee A, Ng W, Pan J, Chiang C, Poh S, Choi H, et al. International guideline on dose prioritization and acceptance criteria in radiation therapy planning for nasopharyngeal carcinoma. *Int J Radiat Oncol Biol Phys* (2019) 105(3):567–80. doi: 10.1016/j.ijrobp.2019.06.2540

13. Bossi P, Chan A, Licitra L, Trama A, Orlandi E, Hui E, et al. Nasopharyngeal carcinoma: ESMO-EURACAN clinical practice guidelines for diagnosis, treatment and follow-up. *Ann Oncol* (2021) 32(4):452–65. doi: 10.1016/j.annonc.2020.12.007

14. Chen A, Lee N, Yang C, Liu T, Narayan S, Vijayakumar S, et al. Comparison of intensity-modulated radiotherapy using helical tomotherapy and segmental multileaf collimator-based techniques for nasopharyngeal carcinoma: dosimetric analysis incorporating quality assurance guidelines from RTOG 0225. *Technol Cancer Res Treat* (2010) 9(3):291–8. doi: 10.1177/153303461000900308

15. Lee NY, Zhang Q, Pfister DG, Kim J, Garden AS, Mechalakos J, et al. Addition of bevacizumab to standard chemoradiation for locoregionally advanced nasopharyngeal carcinoma (RTOG 0615): a phase 2 multi-institutional trial. *Lancet Oncol* (2012) 13(2):172–80. doi: 10.1016/s1470-2045(11)70303-5

16. Cox JD, Stetz J, Pajak TF. Toxicity criteria of the radiation therapy oncology group (RTOG) and the European organization for research and treatment of cancer (EORTC). *Int J Radiat Oncol Biol Phys* (1995) 31(5):1341–6. doi: 10.1016/0360-3016(95)00060-c

17. Eisbruch A, Rhodus N, Rosenthal D, Murphy B, Rasch C, Sonis S, et al. How should we measure and report radiotherapy-induced xerostomia? *Semin Radiat Oncol* (2003) 13(3):226–34. doi: 10.1016/s1053-4296(03)00033-x

18. Rosa M, Łazarz D, Pękala J, Skinningsrud B, Lauritzen S, Solewski B, et al. The accessory parotid gland and its clinical significance. *J Craniofac Surg* (2020) 31 (3):856–60. doi: 10.1097/scs.0000000000006092

19. Ahn D, Yeo CK, Han SY, Kim JK. The accessory parotid gland and facial process of the parotid gland on computed tomography. *PloS One* (2017) 12(9): e0184633. doi: 10.1371/journal.pone.0184633

20. Pujol-Olmo A, Mirapeix RM, Sanudo-Tejero JR, Quer-Agusti M. Description and relationships of the parotid gland levels proposed by the European salivary gland society staging system: an anatomical study. *Surg Radiol Anat* (2020) 42(9):1101–7. doi: 10.1007/s00276-020-02483-x

21. Tower J, Sawan T, Gordon N, BJAsj. P. The aging parotid gland: A longitudinal volumetric study and implications for treatment. *Aesthet Surg J* (2021) 41(4):408–14. doi: 10.1093/asj/sjaa361

22. Eisbruch A, Ten Haken R, Kim H, Marsh L, JJIjoro S. Biology, physics. dose, volume, and function relationships in parotid salivary glands following conformal and intensity-modulated irradiation of head and neck cancer. *Int J Radiat Oncol Biol Phys* (1999) 45(3):577–87. doi: 10.1016/s0360-3016(99)00247-3

23. Lan X, Chan J, Pu J, Qiao W, Pang S, Yang W, et al. Saliva electrolyte analysis and xerostomia-related quality of life in nasopharyngeal carcinoma patients following intensity-modulated radiation therapy. *Radiother Oncol* (2020) 150:97–103. doi: 10.1016/j.radonc.2020.06.016

24. Poon DMC, Kam MKM, Johnson D, Mo F, Tong M, Chan ATC. Durability of the parotid-sparing effect of intensity-modulated radiotherapy (IMRT) in early stage nasopharyngeal carcinoma: A 15-year follow-up of a randomized prospective study of IMRT versus two-dimensional radiotherapy. *Head Neck* (2021) 43 (6):1711–20. doi: 10.1002/hed.26634

25. Han P, Lakshminarayanan P, Jiang W, Shpitser I, Hui X, Lee S, et al. Dose/Volume histogram patterns in salivary gland subvolumes influence xerostomia injury and recovery. *Sci Rep* (2019) 9(1):3616. doi: 10.1038/s41598-019-40228-y

26. Gabryś H, Buettner F, Sterzing F, Hauswald H, Bangert MJ. Parotid gland mean dose as a xerostomia predictor in low-dose domains. *Acta Oncol* (2017) 56 (9):1197–203. doi: 10.1080/0284186x.2017.1324209

27. Sommat K, Hussain A, Ong WS, Yit NLF, Khoo JBK, Soong YL, et al. Clinical and dosimetric predictors of physician and patient reported xerostomia following intensity modulated radiotherapy for nasopharyngeal cancer - a prospective cohort analysis. *Radiother Oncol* (2019) 138:149–57. doi: 10.1016/j.radonc.2019.05.023

28. Xin-Bin P, Yang L, Ling L. Prognostic nomogram of xerostomia for patients with nasopharyngeal carcinoma after intensity-modulated radiotherapy. *Aging (Albany NY)* (2020) 12:1857–66. doi: 10.18632/aging.203308

29. Teguh D, Levendag P, Ghidey W, Van Montfort K, Kwa SJ. Risk model and nomogram for dysphagia and xerostomia prediction in head and neck cancer patients treated by radiotherapy and/or chemotherapy. *Dysphagia* (2013) 28 (3):388–94. doi: 10.1007/s00455-012-9445-6

30. Men K, Geng H, Zhong H, Fan Y, Lin A, YJIjoro X. Biology, physics. a deep learning model for predicting xerostomia due to radiation therapy for head and neck squamous cell carcinoma in the RTOG 0522 clinical trial. *Int J Radiat Oncol Biol Phys* (2019) 105(2):440–7. doi: 10.1016/j.ijrobp.2019.06.009

31. van Dijk L, Brouwer C, van der Laan H, Burgerhof J, Langendijk J, Steenbakkers R, et al. Geometric image biomarker changes of the parotid gland are associated with late xerostomia. *Int J Radiat Oncol Biol Phys* (2017) 99(5):1101–10. doi: 10.1016/j.ijrobp.2017.08.003

frontiers | Frontiers in Oncology

TYPE Original Research
PUBLISHED 01 March 2023
DOI 10.3389/fonc.2023.1147474

OPEN ACCESS

EDITED BY
Giuseppe Carlo Iorio,
University of Turin, Italy

REVIEWED BY
Emma D'Ippolito,
University of Campania Luigi Vanvitelli, Italy
Huan Giap,
Medical University of South Carolina,
United States

*CORRESPONDENCE
Gregory A. Azzam
gxa338@med.miami.edu

SPECIALTY SECTION
This article was submitted to Radiation Oncology, a section of the journal Frontiers in Oncology

RECEIVED 18 January 2023
ACCEPTED 08 February 2023
PUBLISHED 01 March 2023

CITATION
Patel S, Rich BJ, Schumacher L-ED, Sargi ZB, Masforroll M, Washington C, Kwon D, Rueda-Lara MA, Freedman LM, Samuels SE, Abramowitz MC, Samuels MA, Carmona R and Azzam GA (2023) ED visits, hospital admissions and treatment breaks in head/neck cancer patients undergoing radiotherapy.
Front. Oncol. 13:1147474.
doi: 10.3389/fonc.2023.1147474

ED visits, hospital admissions and treatment breaks in head/neck cancer patients undergoing radiotherapy

Shareen Patel[1], Benjamin J. Rich[1], Leif-Erik D. Schumacher[1], Zoukaa B. Sargi[2], Melissa Masforroll[3], Cyrus Washington[1], Deukwoo Kwon[4], Maria A. Rueda-Lara[5], Laura M. Freedman[1], Stuart E. Samuels[1], Matthew C. Abramowitz[1], Michael A. Samuels[1], Ruben Carmona[1] and Gregory A. Azzam[1*]

[1]Department of Radiation Oncology, Sylvester Comprehensive Cancer Center, University of Miami Miller School of Medicine, Miami, FL, United States, [2]Department of Otolaryngology, University of Miami Miller School of Medicine, Miami, FL, United States, [3]Department of Medicine, Florida International University, Miami, FL, United States, [4]Department of Public Health Sciences, Biostatistics and Bioinformatics Shared Resource, Sylvester Comprehensive Cancer Center, University of Miami Miller School of Medicine, Miami, FL, United States, [5]Department of Psychiatry, University of Miami Miller School of Medicine, Miami, FL, United States

Objectives: Radiation therapy (RT) is an integral part of treatment of head/neck cancer (HNC) but is associated with many toxicities. We sought to evaluate sociodemographic, pathologic, and clinical factors associated with emergency department (ED) visits, hospital admissions (HA), and RT breaks in HNC patients undergoing curative-intent RT.

Methods: We completed a Level 3 (Oxford criteria for evidence-based medicine) analysis of a cohort of HNC patients who underwent curative-intent RT at our institution from 2013 to 2017. We collected demographic characteristics and retrospectively assessed for heavy opioid use, ED visits or HA during RT as well as RT breaks. Treatment breaks were defined as total days to RT fractions ratio ≥1.6. Multivariable stepwise logistic regression analyses were done to determine the association of various sociodemographic, pathologic, and clinical characteristics with ED visits, HA and RT treatment breaks.

Results: The cohort included 376 HNC patients (294 male, 82 female, median age 61). On multivariable analysis, significant factors associated with ED visits during RT were heavy opioid use and black race. Receipt of concomitant chemotherapy was the only factor associated with hospital admissions during RT. Advanced age, lower socioeconomic class, glandular site, and receipt of chemotherapy were all independently associated with RT breaks. Lower cancer stage and lack of substance abuse history were independently associated with lack of treatment breaks.

Conclusion: HNC patients with factors such as heavy opioid use, Black race, receipt of concomitant chemotherapy, and lower socioeconomic class may require closer monitoring during RT.

KEYWORDS

head/neck cancer, radiation therapy, hospital admissions, ED visits, treatment breaks, head and neck neoplasms, radiotherapy, hospital admissions

Introduction

Head and neck cancer accounts for approximately 900,000 cases and over 400,000 deaths annually (GLOBOCAN 2020 data) (1). Radiation therapy (RT) is an important part of the multidisciplinary management of head and neck cancer. Unplanned hospitalizations and emergency department (ED) visits during the radiation treatment course can lead to treatment breaks, disproportionately affecting certain vulnerable populations and leading to a financial burden on patients and the healthcare system (2). Overall survival and cancer-specific survival is significantly decreased for head and neck cancer patients hospitalized during radiation therapy, with dehydration and fever the leading causes of admission (3). Moreover, adherence to the radiation treatment timeline is important as unplanned RT breaks and prolongation of the RT period is associated with worse survival and locoregional control of disease, possibly due to rapid repopulation (4–6).

Quality of life scores significantly decrease as patients experience oral complications during or after RT, with pain a major contributor (7). Pain can be prevalent throughout the radiation treatment course and, in some patients, persist 6-12 months post-RT (8). Painful sequelae such as oral mucositis during curative-intent RT for head and neck cancer is a common reason for hospitalizations during treatment (9). In order to optimize pain control amongst head and neck cancer patients, opioids are commonly prescribed (10, 11). Head and neck cancer patients treated with radiotherapy are at risk for long-term opioid use (12, 13), but predicting long-term opioid use is difficult (11).

Although pain and resulting opioid use play a large role in the treatment course of head and neck patients, prior studies evaluating risks for ED visits, unplanned hospitalizations, and treatment breaks in this population have failed to take these important components into account (11). In this study, we sought to analyze the occurrence of ED visits, unplanned hospitalizations, and radiation treatment breaks in head and neck cancer patients undergoing curative-intent radiation therapy in relation to pain and opioid use as well as other clinical, treatment and socioeconomic characteristics.

Materials and methods

This single-institution study was approved by the Institutional Review Board (IRB). We retrospectively identified a group of patients with head and neck cancer at our institution from the Tumor Registry who were treated with curative-intent external beam radiotherapy from 2013 to 2017. Additional inclusion criteria for the cohort included: (a) received RT at our institution, (b) did not have persistent disease or recurrent disease within 18 months, (c) had no history of chronic opioid use for non-cancer pain before cancer presentation or diagnosis, (d) received RT to the primary disease site and (e) had non-metastatic disease. Patients were excluded if they had received prior irradiation or other treatment not part of the current treatment course (indicating recurrent disease).

The electronic medical record (EMR) of eligible patients was reviewed and clinical data was collected in a Research Data Electronic Capture (REDCap) database. Sociodemographic, pathologic, and clinical factors were collected for each patient (Table 1). Additionally, we recorded opioid use, hospitalizations and ED visits within the radiation treatment period and total days to complete radiation therapy from the EMR. Each patient's chart was reviewed for hospitalizations and ED visits in our hospital system as well as documentation of hospitalizations or ED visits outside of our hospital system. Documentation reviewed included weekly on-treatment notes during RT. Planned hospitalizations solely for chemotherapy infusion were excluded unless the hospitalization was extended beyond two days for supportive care related to RT side effects. ED visits leading to a hospital admission were counted as a hospitalization, but not an ED visit. We calculated the ratio of total days from start to completion of RT divided by the fractions completed to assess for a prolonged RT course. Substantial treatment breaks were defined as total days to RT fractions ratio ≥1.6. The ratio cutoff of ≥1.6 days/fraction was chosen based on work by Ho et al. demonstrating a survival significance at this days/fraction ratio (14). In certain cases where an opioid was prescribed, but the patient reported not using opioids, no opioid dose was recorded. Heavy opioid use was defined as >30 morphine milligram equivalents (MME) daily as used elsewhere in the literature (15, 16).

Statistical methods

Continuous variables were summarized with descriptive statistics and categorical variables were summarized using counts and proportions. Univariable and multivariable logistic regression analyses were performed to determine the association of

10.3389/fonc.2023.1147474

socioeconomic class, race, ethnicity, age, marital status, gender, primary language, employment, living situation, chemotherapy, opioid use, non-opioid substance use, history of substance use, chronic pain condition, psychiatric disease, cancer site or cancer stage with ED visits, hospital admissions and RT treatment breaks. Odds ratios (OR) were collected and a p-value <0.05 was considered statistically significant. For the multivariable analysis, we used stepwise variable selection. Statistical analyses were performed with the statistical software package R, version 4.0.5 (R foundation for Statistical Computing).

Results

The institution tumor registry contained a total of 678 patients with head and neck cancer treated with external beam radiation therapy from 2013 to 2017. Our cohort included 376 patients after excluding patients who did not meet our inclusion and exclusion criteria. Table 1 contains patient characteristics of the cohort. The cohort consisted of 78.2% males and 21.8% females with a median age of 61 years. The patients included non-Hispanic white (55.3%), Hispanic white (31.1%), Black (7.2%), Asian (1.3%), Native American (0.5%), and other (4.5%). The majority of patients were married (68.6%), middle class (52.1%), English-speaking (75.5%), living with family members (66%), employed (57.7%), without history of substance abuse (86.2%) or history of psychiatric disorder (91.5%), and with locally advanced disease (71.5% stage III-IV). The most common primary cancer sites were oropharynx (50.5%) and larynx (17.6%). The median radiation therapy dose received was 66 Gy. Of the cohort, 40.4% of patients received chemotherapy during the treatment course and 48.1% of patients received radiation therapy pre- or post-operatively.

In the cohort, 14.9% of the patients had at least one unplanned hospital admission and 5.3% had at least one ED visit not leading to hospitalization. Of the patients who had at least one unplanned hospitalization, 41 (73.2%) patients had one admission, 11 (19.6%) patients had two admissions and 4 (7.1%) patients had three or more admissions. The majority of patients with unplanned hospital admissions had a length of stay greater than 3 days (60.7%). The reasons for unplanned hospital admissions included dehydration (51.8% of admissions), mucositis (17.8%), fever with or without neutropenia (17.8%), intractable nausea or vomiting (3.5%), non-opioid induced constipation (1.8%), diarrhea (1.8%), draining fistula (1.8%), chest pain (1.8%), and urinary tract infection (1.8%). For unplanned hospitalizations, 93% were due to treatment or cancer-related factors and 7% were non-cancer related. The diagnoses for ED visits included dehydration (40%), dysphagia (15%), neutropenic fever (10%), urinary retention (10%), shortness of breath (5%), irritation around PEG tube (5%), depression (5%), constipation (5%), and nephrolithiasis (5%). In total, 80% of ED visits were due to treatment or cancer-related factors and 20% were non-cancer related. The median days to RT fraction ratio was 1.38 days/fraction, with 19 (5.1%) of patients with a ratio ≥ 1.6 days/fraction.

A univariable and multivariable analysis was completed to determine factors associated with ED visits, hospital admissions,

TABLE 1 Patient characteristics.

Characteristic		Patients (N=376)
Age in years – median		61
Sex – n (%)		
	Female	82 (21.8)
	Male	294 (78.2)
Race/Ethnicity – n (%)		
	Non-Hispanic White	208 (55.3)
	Hispanic White	117 (31.1)
	Black	27 (7.2)
	Asian	5 (1.3)
	Native American	2 (0.5)
	Other/Unknown	17 (4.5)
Income class – n (%)		
	Lower	119 (31.6)
	Middle	196 (52.1)
	Upper	51 (13.6)
	Unknown/International Patient	10 (2.7)
Primary Language – n (%)		
	English	284 (75.5)
	Spanish	84 (22.3)
	Other	8 (2.1)
Marital Status – n (%)		
	Married	258 (68.6)
	Not Married	113 (30.1)
	Unknown	5 (1.3)
Living Situation – n (%)		
	Alone	37 (9.8)
	With Family	248 (66.0)
	Unknown	91 (24.2)
Dependent Children – n (%)		
	Yes	116 (30.9)
	No	151 (40.2)
	Unknown	109 (29.0)
Employment – n (%)		
	Employed	217 (57.7)
	Unemployed	107 (28.5)
	Unknown	52 (13.8)
Insurance – n (%)		

(Continued)

10.3389/fonc.2023.1147474

TABLE 1 Continued

Characteristic		Patients (N=376)
	Private	188 (50.0)
	Medicare	157 (41.8
	Medicaid	23 (6.1)
	None Documented	8 (2.1)
Smoking or Tobacco History – n (%)		
	Never	171 (45.5)
	Former	184 (48.9)
	Current	20 (5.3)
Substance Abuse History – n (%)		
	Never	324 (86.2)
	Former	26 (6.9)
	Current	26 (6.9)
History of Psychiatric Disorder – n (%)		
	No	344 (91.5)
	Yes	32 (8.5)
History of chronic pain condition – n (%)		
	No	254 (67.6)
	Yes	122 (32.4)
Cancer Location – n (%)		
	Hypopharynx	7 (1.9)
	Larynx	66 (17.6)
	Nasal Cavity	21 (5.6)
	Nasopharynx	13 (3.5)
	Oral Cavity	43 (11.4)
	Oropharynx	190 (50.5)
	Parotid or Submandibular Gland	26 (6.9)
	Ethmoid or Maxillary Sinus	10 (2.7)
AJCC 7th ed. Cancer Stage – n (%)		
	I	47 (12.5)
	II	46 (12.2)
	III	78 (20.7)
	IV	191 (50.8)
Treatment Modality – n (%)		
	Radiation	376 (100.0)
	Chemotherapy	152 (40.4)
	Surgery	181 (48.1)
Total Radiation Dose – n (%)		
	≤50 Gy	13 (3.5)
	>50 to 60 Gy	95 (25.3)
	>60 to 70 Gy	266 (70.7)
	>70 Gy	2 (0.5)
Gabapentin Use – n (%)		
	No	355 (94.4)
	Yes	21 (5.6)
Mouthwash Use – n (%)		
	No	83 (22.1)
	Yes	293 (77.9)
Patients Admitted to Hospital– n (%)		
	No	320 (85.1)
	Yes	56 (14.9)
Number of Hospital admissions – n (%)		
	0	320 (85.1)
	1	41 (10.9)
	2	11 (2.9)
	3+	4 (1.1)
Total days of hospital admission(s) – n (%)		
	1	4 (1.1)
	2	9 (2.4)
	3	9 (2.4)
	4+	34 (9.0)
Patients with ED visit – n (%)		
	No	356 (94.7)
	Yes	20 (5.3)
Median Days/RT Fractions Ratio		1.38
Days/RT Fractions Ratio		
	<1.6	357 (94.9)
	≥1.6	19 (5.1)

AJCC, American Joint Committee on Cancer; ED, Emergency Department; RT, Radiation Therapy.

and RT treatment breaks. On multivariable analysis, the factors independently associated with ED visits during RT were heavy opioid use (OR 5.39, p<0.01) and black race (OR 6.93, p<0.01) (Table 2). Unplanned hospital admissions during RT were only independently associated with the receipt of concomitant chemotherapy (OR 9.73, p<0.01) (Table 3). Heavy opioid use was associated with hospital admissions on univariable analysis (OR 2.00, p=0.019), but this was not significant on multivariable analysis. On the multivariable analysis, older age (OR 1.08, p<0.01), lower socioeconomic class (OR 4.94, p<0.01), primary salivary tumor site (OR 5.39, p=0.04), and receipt of chemotherapy

(OR 6.86, p=0.01) were all independently associated with RT breaks (Table 4). Lower cancer stage (OR 0.48, p<0.01) and lack of substance abuse history (OR 0.17, p<0.01) were independently associated with lack of treatment breaks. Other socioeconomic, pathologic and clinical treatment variables analyzed in this study did not disclose significant associations.

Discussion

ED visits and unplanned hospitalizations during curative-intent RT for head and neck cancer can lead to significant resource utilization (9, 17)and treatment breaks, which result in worse locoregional disease control and poorer survival (5, 6). Despite the importance of minimizing unplanned hospital encounters and treatment breaks in this patient population, the literature on factors associated with these events is limited and without inclusion of pain or opioid use, both important, quantifiable factors of patient experience during RT. In this large cohort of 376 head and neck cancer patients treated with curative intent RT, heavy opioid use was independently associated with ED visits during RT (OR 5.39, p<0.001), but not unplanned hospitalizations or RT treatment breaks. Pain scores during RT were not independently associated with ED visits, unplanned hospitalizations or RT treatment breaks.

TABLE 2 Factors influencing ED visits.

		Univariable Analysis (UVA)		Multivariable Analysis (MVA)	
Variable	Category	OR (95% CI)	P-value	OR (95% CI)	P-value
Daily Opioid Use	≤ 30 MME	Reference			
	> 30 MME	4.50 (1.79, 12.27)	0.002	5.39 (2.07, 15.53)	<0.001
Age	One year increased	Reference			
		0.98 (0.94, 1.02)	0.352		
Sex	Female	Reference			
	Male	0.83 (0.31, 2.61)	0.723		
Race	White	Reference			
	Black	5.06 (1.54, 14.48)	0.004	6.93 (1.98, 22.30)	0.001
	Native American	NA	0.993		
	More than one race	6.19 (0.30, 51.03)	0.122		
Ethnicity	Hispanic	Reference			
	Non-Hispanic White	1.66 (0.63, 5.21)	0.335		
	Other/Unknown	NA	0.990		
Income class	Upper	Reference			
	Lower	1.47 (0.56, 3.65)	0.412		
Primary language	English	Reference			
	Spanish	0.90 (0.11, 6.63)	0.919		
Marital status	Not Married	Reference			
	Married	0.84 (0.34, 2.29)	0.720		
Employment	Unemployed	Reference			
	Employed	1.38 (0.55, 3.76)	0.499		
Insurance	None	Reference			
	Medicare	1.13 (0.45, 2.81)	0.787		
	Medicaid	0.79 (0.04, 4.11)	0.824		
	Not Documented	NE			
Smoking/tobacco history	Never	Reference			
	Former	0.32 (0.11, 0.87)	0.035		
	Current	0.93 (0.05, 4.89)	0.948		

(Continued)

TABLE 2 Continued

		Univariable Analysis (UVA)		Multivariable Analysis (MVA)	
Substance abuse history	Yes	Reference			
	No	0.90 (0.29, 3.97)	0.876		
Substance abuse at initial visit	Yes	Reference			
	No	1.43 (0.28, 26.31)	0.730		
Site of Disease	Oropharynx	Reference			
	Nasopharynx	3.48 (0.51, 14.28)	0.121		
	Oral Cavity	0.85 (0.13, 3.11)	0.836		
	Sinuses	NE	0.991		
	Larynx and Hypopharynx	NE	0.990		
	Parotid and Submandibular Glands	NE	0.990		
Cancer stage	One stage increased	Reference			
		1.01 (0.94, 1.06)	0.899		
Surgery	No	Reference			
	Yes	0.82 (0.33, 2.08)	0.669		
Chemotherapy	No	Reference			
	Yes	2.50 (0.90, 8.87)	0.107		
Total Radiation Dose	One unit increased	Reference			
		1.05 (0.97, 1.17)	0.294		
Pain scale	One unit increased	Reference			
		1.01 (0.92, 1.10)	0.840		

ED, Emergency Department; MME, morphine milligram equivalent; NE, not evaluatable.

Other socioeconomic and treatment related factors were associated with these events in the cohort. Black race (OR 6.93, p= 0.001) was a significant, independent predictor of ED visits. At least one unexpected hospital admissions occurred in 14.9% of the patients in our cohort (n = 56). Unplanned hospital admissions had a significant association with receipt of concomitant chemotherapy (OR 9.73, p<0.001). 5.1% of patients in the cohort had a significant radiation treatment break. Advanced age, lower socioeconomic status, primary salivary tumor site, lower cancer stage, receipt of chemotherapy, and history of substance abuse were all independently associated with RT breaks (p<0.05).

We found a significant association between ED visits and heavy opioid use, but unplanned hospital admissions and RT breaks did not share this association. Pain was also not an independent risk factor. This may suggest patients requiring heavy opioids require extra counseling or alternative analgesics to prevent unnecessary ED visits. However, patients with heavy opioid use do not appear to be at higher risk of more serious complications leading to hospitalizations or treatment breaks.

The predictors of unplanned hospital encounters found in the present study should be taken into context with existing literature. Like the present study, chemotherapy in the treatment course of head and neck cancer patients has been previously shown to be associated with an increased number of hospital admissions (3, 18, 19). This association is not limited to head and neck patients (20). Our study is the first to report that Black race is associated with ED visits. Other studies have found treatment at a public hospital, comorbidities, radiation dose, smoking status all associated with unplanned hospitalizations (18, 21).

In our cohort, 14.9% of the patients had at least one unplanned hospital admission and 5.3% had at least one ED visit, which is consistent with existing literature showing 20%-36% of patients undergoing curative intent RT for head and neck cancer had at least one hospitalization (3) (18). Unplanned hospital encounters, in addition to treatment breaks and resulting worse cancer outcomes, lead to significant resource utilization (2, 3, 17). In the United States, a 2019 study showed hospitalizations of head and neck cancer patients had an average length of stay of 6.6 days for one admission with an average cost of $18,371 (17).

In the present study, advanced age, lower socioeconomic status, primary salivary tumor site, lower cancer stage, receipt of chemotherapy, and history of substance abuse were all independently associated with RT breaks (p<0.05). The literature reports various patient characteristics associated with treatment

10.3389/fonc.2023.1147474

TABLE 3 Factors Influencing Hospital Admissions.

		Univariable Analysis (UVA)		Multivariable Analysis (MVA)	
Variable	Category	OR (95% CI)	P-value	OR (95% CI)	P-value
Daily Opioid Use	≤ 30 MME	Reference			
	> 30 MME	2.00 (1.11, 3.57)	0.019		
Age	One year increased	Reference			
		1.00 (0.98, 1.03)	0.837		
Sex	Female	Reference			
	Male	0.81 (0.42, 1.61)	0.531		
Race	White	Reference			
	Black	0.69 (0.16, 2.08)	0.569		
	Native American	NE	0.988		
	More than one race	1.92 (0.09, 15.31)	0.575		
Ethnicity	Hispanic	Reference			
	Non-Hispanic White	0.89 (0.49, 1.61)	0.684		
	Other/Unknown	NE	0.989		
Income class	Upper	Reference			
	Lower	1.35 (0.74, 2.44)	0.309		
Primary language	English	Reference			
	Spanish	1.64 (0.86, 3.05)	0.121		
Marital status	Not Married	Reference			
	Married	0.87 (0.48, 1.62)	0.657		
Employment	Unemployed	Reference			
	Employed	1.06 (0.60, 1.91)	0.842		
Insurance	None	Reference			
	Medicare	1.45 (0.82, 2.58)	0.195		
	Medicaid	1.21 (0.34, 3.37)	0.742		
	Not Documented	NE			
Smoking/tobacco history	Never	Reference			
	Former	1.24 (0.70, 2.20)	0.453		
	Current	0.62 (0.10, 2.24)	0.531		
Substance abuse history	Yes	Reference			
	No	0.96 (0.44, 2.30)	0.915		
Substance abuse at initial visit	Yes	Reference			
	No	0.72 (0.28, 2.22)	0.521		
Site of Disease	Oropharynx	Reference			
	Nasopharynx	2.66 (0.70, 8.49)	0.114		
	Oral Cavity	0.73 (0.24, 1.78)	0.524		
	Sinuses	0.63 (0.03, 3.44)	0.662		
	Larynx and Hypopharynx	0.75 (0.32, 1.60)	0.487		
	Parotid and Submandibular Glands	0.46 (0.07, 1.60)	0.297		

(Continued)

TABLE 3 Continued

		Univariable Analysis (UVA)		Multivariable Analysis (MVA)	
Cancer stage	One stage increased	Reference			
		1.01 (0.93, 1.06)	0.720		
Surgery	No	Reference			
	Yes	0.24 (0.13, 0.43)	<0.001		
Chemotherapy	No	Reference			
	Yes	9.73 (3.86, 32.74)	<0.001	9.73 (3.86, 32.74)	<0.001
Total Radiation Dose	One unit increased	Reference			
		1.11 (1.04, 1.20)	0.003		
Pain scale	One unit increased	Reference			
		1.06 (1.00, 1.12)	0.042		

MME, morphine milligram equivalent; NE, not evaluatable.

TABLE 4 Factors influencing radiation treatment breaks.

		Univariable Analysis (UVA)		Multivariable Analysis (MVA)	
Variable	Category	OR (95% CI)	P-value	OR (95% CI)	P-value
Daily Opioid Use	≤ 30 MME	Reference			
	> 30 MME	0.78 (0.25, 2.10)	0.643		
Age	One year increased	Reference			
		1.03 (0.98, 1.08)	0.150	1.08 (1.03, 1.15)	0.006
Sex	Female	Reference			
	Male	0.77 (0.28, 2.44)	0.626		
Race	White	Reference			
	Black	1.56 (0.24, 5.88)	0.565		
	Native American	NE	0.993		
	More than one race	6.56 (0.32, 54.17)	0.111		
Ethnicity	Hispanic	Reference			
	Non-Hispanic White	0.73 (0.29, 1.93)	0.513		
	Other/Unknown	19.78 (0.76, 513.97)	0.038		
Income class	Upper	Reference			
	Lower	3.17 (1.25, 8.40)	0.016	4.94 (1.75, 15.31)	0.003
Primary language	English	Reference			
	Spanish	2.12 (0.77, 5.46)	0.127		
Marital status	Not Married	Reference			
	Married	0.39 (0.15, 0.99)	0.047		
Employment	Unemployed	Reference			
	Employed	0.41 (0.15, 1.04)	0.066		
Insurance	None	Reference			
	Medicare	2.47 (0.97, 6.78)	0.064		

(Continued)

TABLE 4 Continued

		Univariable Analysis (UVA)		Multivariable Analysis (MVA)	
	Medicaid	1.87 (0.28, 7.11)	0.424		
	Not Documented	NE			
Smoking/tobacco history	Never	Reference			
	Former	3.08 (1.15, 9.69)	0.034		
	Current	NE	0.991		
Substance abuse history	Yes	Reference			
	No	0.32 (0.12, 0.95)	0.028	0.17 (0.05, 0.59)	0.004
Substance abuse at initial visit	Yes	Reference			
	No	NE	0.990		
Site of Disease	Oropharynx	Reference			
	Nasopharynx	3.70 (0.55, 15.25)	0.105		
	Oral Cavity	0.91 (0.14, 3.32)	0.898		
	Sinuses	NE	0.991		
	Larynx and Hypopharynx	0.54 (0.08, 1.94)	0.416		
	Parotid and Submandibular Glands	2.72 (0.60, 8.94)	0.132	5.39 (0.94, 27.41)	0.044
Cancer stage	One stage increased	Reference			
		0.78 (0.53, 1.03)	0.235	0.48 (0.27, 0.83)	0.009
Surgery	No	Reference			
	Yes	0.93 (0.37, 2.45)	0.878		
Chemotherapy	No	Reference			
	Yes	1.72 (0.64, 5.43)	0.307	6.86 (1.62, 37.26)	0.015
Total Radiation Dose	One unit increased	Reference			
		1.00 (0.94, 1.08)	0.908		
Pain scale	One unit increased	Reference			
		0.88 (0.78, 0.98)	0.308		

MME, morphine milligram equivalent; NE, not evaluatable.

breaks (22–24). Age is associated with enteral feeding during RT for head and neck cancer and could explain this finding (25). Other studies have found treatment breaks are associated with lower socioeconomic status (23, 24), and this could explain the worse survival seen in head and neck patients with higher baseline financial burden undergoing RT (26). Treatment breaks could also be explained by insurance disparities described elsewhere, although this was not the case for the present study (27).

Nutritional status, hydration status, and feeding tube placement are important factors that can result in unplanned ED visits, hospital admissions and treatment breaks. Among the ED visits in this study, 60% were related to nutritional or hydration status and 52% of unplanned hospital admissions were related to nutritional or hydration status. Early PEG tube placement during head and neck radiotherapy is correlated with a reduction in weight loss and, as a result, hospitalizations for nutritional deficits (28). However, PEG tube placement comes with a variety of complications that could lead to unplanned ED visits or hospitalizations: 12% of all tubes require replacement, with infection rates of approximately 9% and significant pain in 6% of patients (29).

Our study includes several limitations in addition to biases inherent to respective studies. First, the data was collected from the EMR at a single institution. Although all available records were diligently reviewed, outside ED visits or hospitalizations may have been missed if they were not documented in the EMR at out institution. Additionally, the days of treatment to RT fractions ratio may have been affected by holidays, but given the cutoff of ≥1.6 this is unlikely to have much, if any, effect on the categorization of treatment breaks. Lastly, the cohort only included head and neck cancer patients who underwent curative-intent radiation therapy and excluded patients with persistent disease, making the data

collected pertinent only to this subset of patients. This study is strengthened by a relatively large, homogenous number of patients with a robust number of variables collected.

Conclusion

In this analysis of 376 head and neck patients receiving curative-intent RT, we found heavy opioid use to be independently associated with ED visits during RT, but not unplanned hospitalizations or RT treatment breaks. Other factors independently, significantly associated included Black race with ED visits and receipt of chemotherapy with unplanned hospital admissions during RT. RT breaks were associated with advanced age, lower socioeconomic class, primary salivary tumor site, and concomitant chemotherapy. Lower cancer stage and lack of substance abuse history were independently associated with lack of treatment breaks. Head and neck cancer patients with these factors may require extra care during the RT course to prevent ED visits, hospitalizations and treatment breaks.

Data availability statement

The datasets presented in this article are not readily available because not available for public dissemination as per IRB. Requests to access the datasets should be directed to shareen.patel@med.miami.edu.

Author contributions

SP, BR, GA, and MS contributed to conception and design of the study. SP, L-ES, MM organized the database. DK, RC and BR performed the statistical analysis. SP and BR wrote the first draft of the manuscript. MS and GA wrote sections of the manuscript. CW, MR-L, and ZS contributed to investigation. SS, LF, MS and MA contributed to supervision of study. All authors contributed to the article and approved the submitted version.

Conflict of interest

The authors declare that the research was conducted in the absence of any commercial or financial relationships that could be construed as a potential conflict of interest.

Publisher's note

References

1. Sung H, Ferlay J, Siegel RL, Laversanne M, Soerjomataram I, Jemal A, et al. Global cancer statistics 2020 *A Cancer Journal for Clinicians* (2021). (71):3:209-249 doi: 10.3322/caac.21660.

2. Noel CW, Forner D, Wu V, Enepekides D, Irish JC, Husain Z, et al. Predictors of surgical readmission, unplanned hospitalization and emergency department use in head and neck oncology: A systematic review. *Oral Oncol* (2020) 111:105039. doi: 10.1016/J.ORALONCOLOGY.2020.105039

3. Han HR, Hermann GM, Ma SJ, Iovoli AJ, Wooten KE, Arshad H, et al. Matched pair analysis to evaluate the impact of hospitalization during radiation therapy as an early marker of survival in head and neck cancer patients. *Oral Oncol* (2020) 109:104854. doi: 10.1016/J.ORALONCOLOGY.2020.104854

4. Russo G, Haddad R, Posner M, Machtay M. Radiation treatment breaks and ulcerative mucositis in head and neck cancer. *Oncologist* (2008) 13(8):886–98. doi: 10.1634/THEONCOLOGIST.2008-0024

5. McCloskey SA, Jaggernauth W, Rigual NR, Hicks WL, Popat SR, Sullivan M, et al. Radiation treatment interruptions greater than one week and low hemoglobin levels (12 g/dL) are predictors of local regional failure after definitive concurrent chemotherapy and intensity-modulated radiation therapy for squamous cell carcinoma of the head and neck. *Am J Clin Oncol* (2009) 32(6):587–91. doi: 10.1097/COC.0B013E3181967DD0

6. Suntharalingam M, Haas ML, Van Echo DA, Haddad R, Jacobs MC, Levy S, et al. Predictors of response and survival after concurrent chemotherapy and radiation for locally advanced squamous cell carcinomas of the head and neck. *Journal* (2001). doi: 10.1002/1097-0142(20010201)91:3<548::AID-CNCR1033>3.0.CO;2-A

7. Bjordal K, Hammerlid E, Ahlner-Elmqvist M, De Graeff A. Quality of life in head and neck cancer patients: Validation of the European organization for research and treatment of cancer quality of life questionnaire-H&N35 Male cancer view project Utrecht symptom diary view project. *Article J Clin Oncol* (1999). 17:(3):1008–19. doi: 10.1200/JCO.1999.17.3.1008

8. Epstein JB, Stewart KH. Radiation therapy and pain in patients with head and neck cancer. *Eur J Cancer Part B: Oral Oncol* (1993) 29(3):191–9. doi: 10.1016/0964-1955(93)90022-7

9. Murphy BA, Beaumont JL, Isitt J, Garden AS, Gwede CK, Trotti AM, et al. Mucositis-related morbidity and resource utilization in head and neck cancer patients receiving radiation therapy with or without chemotherapy. *J Pain Symptom Manage* (2009) 38(4):522–32. doi: 10.1016/J.JPAINSYMMAN.2008.12.004

10. Sethi RKV, Panth N, Puram SV, Varvares MA. Opioid prescription patterns among patients with head and neck cancer. *JAMA Otolaryngology–Head Neck Surg* (2018) 144(4):382–3. doi: 10.1001/JAMAOTO.2017.3343

11. Rich BJ, Schumacher LED, Sargi ZB, Masforroll M, Kwon D, Zhao W, et al. Opioid use patterns in patients with head and neck cancer receiving radiation therapy: Single-institution retrospective analysis characterizing patients who did not require opioid therapy. *Head Neck* (2021) 43(10):2973–84. doi: 10.1002/HED.26785

12. Bollig CA, Kinealy BP, Gilley DR, Clark AD, Galloway TLI, Zitsch RP, et al. Implications of treatment modality on chronic opioid use following treatment for head and neck cancer. *Otolaryngol - Head Neck Surg (United States)* (2021) 164(4):799–806. doi: 10.1177/0194599820960137

13. Zhao L, Moon DH, Avkshtol V, Siropaides CH, Terauchi S, Day AT, et al. Long-term opioid use in patients treated with head and neck intensity-modulated radiotherapy. *Supportive Care Cancer* (2022) 30(9):7517–25. doi: 10.1007/S00520-022-07155-7

14. Ho AS, Kim S, Tighiouart M, Mita A, Scher KS, Epstein JB, et al. Quantitative survival impact of composite treatment delays in head and neck cancer. *Cancer* (2018) 124(15):3154–62. doi: 10.1002/cncr.31533

15. Denawa Y, Kurtz W, Conermann T. The social and functional implications of high-versus low-dose opioids on chronic non-cancer pain. *Pain Physician* (2019) 22 (4):401–11

16. Fudin J, Raouf M, Wegrzyn EL, Schatman ME. Safety concerns with the centers for disease control opioid calculator. *J Pain Res* (2018) 11:1. doi: 10.2147/JPR.S155444

17. Boakye EA, Johnston KJ, Moulin TA, Buchanan PM, Hinyard L, Tobo BB, et al. Factors associated with head and neck cancer hospitalization cost and length of stay-a national study. *Am J Clin Oncology: Cancer Clin Trials* (2019) 42(2):172–8. doi: 10.1097/COC.0000000000000487

18. Moore ZR, Pham NL, Shah JL, Nedzi L, Sumer BD, Day AT, et al. Risk of unplanned hospital encounters in patients treated with radiotherapy for head and neck squamous cell carcinoma. *J Pain Symptom Manage* (2019) 57(4):738–745.e3. doi: 10.1016/j.jpainsymman.2018.12.337

19. Eskander A, Krzyzanowska MK, Fischer HD, Liu N, Austin PC, Irish JC, et al. Emergency department visits and unplanned hospitalizations in the treatment period for head and neck cancer patients treated with curative intent: A population-based analysis. *Oral Oncol* (2018) 83(January):107–14. doi: 10.1016/j.oraloncology.2018.06.011

20. Waddle MR, Chen RC, Arastu NH, Green RL, Jackson M, Qaqish BF, et al. Unanticipated hospital admissions during or soon after radiation therapy: Incidence and predictive factors. *Pract Radiat Oncol* (2015) 5(3):e245–53. doi: 10.1016/J.PRRO.2014.08.004

21. Ling DC, Kabolizadeh P, Heron DE, Ohr JP, Wang H, Johnson J, et al. Incidence of hospitalization in patients with head and neck cancer treated with intensity-modulated radiation therapy. *Head Neck* (2015) 37(12):1750–5. doi: 10.1002/HED.23821

22. Patel UA, Thakkar KH, Holloway N. Patient compliance to radiation for advanced head and neck cancer at a tertiary care county hospital. *Laryngoscope* (2008) 118(3):428–32. doi: 10.1097/MLG.0B013E31815AE3D2

23. Ohri N, Rapkin BD, Guha D, Haynes-Lewis H, Guha C, Kalnicki S, et al. Predictors of radiation therapy noncompliance in an urban academic cancer center. *Int J Radiat Oncology Biology Phys* (2015) 91(1):232–8. doi: 10.1016/J.IJROBP.2014.09.030

24. Vera-Llonch M, Oster G, Hagiwara M, Sonis S. Oral mucositis in patients undergoing radiation treatment for head and neck carcinoma. *Cancer* (2006) 106 (2):329–36. doi: 10.1002/CNCR.21622

25. Sachdev S, Refaat T, Bacchus ID, Sathiaseelan V, Mittal BB. Age most significant predictor of requiring enteral feeding in head-and-neck cancer patients. *Radiat Oncol (London England)* (2015) 10(1). doi: 10.1186/S13014-015-0408-6

26. Ma SJ, Iovoli AJ, Attwood K, Wooten KE, Arshad H, Gupta V, et al. Association of significant financial burden with survival for head and neck cancer patients treated with radiation therapy. *Oral Oncol* (2021) 115:105196. doi: 10.1016/J.ORALONCOLOGY.2021.105196

27. Thomas K, Martin T, Gao A, Ahn C, Wilhelm H, Schwartz DL. Interruptions of head and neck radiotherapy across insured and indigent patient populations. *J Oncol Pract* (2017) 13(4):e319–28. doi: 10.1200/JOP.2016.017863

28. Rutter CE, Yovino S, Taylor R, Wolf J, Cullen KJ, Ord R, et al. Impact of early percutaneous endoscopic gastrostomy tube placement on nutritional status and hospitalization in patients with head and neck cancer receiving definitive chemoradiation therapy. *Head Neck* (2011) 33(10):1441–7. doi: 10.1002/HED.21624

29. Lawson JD, Gaultney J, Saba N, Grist W, Davis L, Johnstone PAS. Percutaneous feeding tubes in patients with head and neck cancer: Rethinking prophylactic placement for patients undergoing chemoradiation. *Am J Otolaryngol* (2009) 30 (4):244–9. doi: 10.1016/J.AMJOTO.2008.06.010

frontiers | Frontiers in Oncology

TYPE Original Research
PUBLISHED 21 March 2023
DOI 10.3389/fonc.2023.1129918

OPEN ACCESS

EDITED BY
Giuseppe Carlo Iorio,
University of Turin, Italy

REVIEWED BY
Qingtao Qiu,
Shandong Cancer Hospital, China
Chiara Cavallin,
University of Turin, Italy

*CORRESPONDENCE
Yibao Zhang
zhangyibao@pku.edu.cn

†These authors have contributed equally to this work

SPECIALTY SECTION
This article was submitted to Radiation Oncology, a section of the journal Frontiers in Oncology

RECEIVED 22 December 2022
ACCEPTED 13 March 2023
PUBLISHED 21 March 2023

CITATION
Liu H, Zhao D, Huang Y, Li C, Dong Z, Tian H, Sun Y, Lu Y, Chen C, Wu H and Zhang Y (2023) Comprehensive prognostic modeling of locoregional recurrence after radiotherapy for patients with locoregionally advanced hypopharyngeal squamous cell carcinoma. *Front. Oncol.* 13:1129918. doi: 10.3389/fonc.2023.1129918

Comprehensive prognostic modeling of locoregional recurrence after radiotherapy for patients with locoregionally advanced hypopharyngeal squamous cell carcinoma

Hongjia Liu[1,2†], Dan Zhao[2†], Yuliang Huang[2,3†], Chenguang Li[2], Zhengkun Dong[1,2], Hongbo Tian[2], Yijie Sun[4], Yanye Lu[1], Chen Chen[5], Hao Wu[1,2] and Yibao Zhang[1,2*]

[1]Institute of Medical Technology, Peking University Health Science Center, Beijing, China, [2]Key Laboratory of Carcinogenesis and Translational Research (Ministry of Education/Beijing), Department of Radiation Oncology, Peking University Cancer Hospital & Institute, Beijing, China, [3]Centre for Medical Image Computing, Department of Medical Physics and Biomedical Engineering, University College London, London, United Kingdom, [4]School of Basic Medical Sciences, Peking University Health Science Center, Beijing, China, [5]School of Electronics Engineering and Computer Science, Peking University, Beijing, China

Purpose: To propose and evaluate a comprehensive modeling approach combing radiomics, dosiomics and clinical components, for more accurate prediction of locoregional recurrence risk after radiotherapy for patients with locoregionally advanced HPSCC.

Materials and methods: Clinical data of 77 HPSCC patients were retrospectively investigated, whose median follow-up duration was 23.27 (4.83-81.40) months. From the planning CT and dose distribution, 1321 radiomics and dosiomics features were extracted respectively from planning gross tumor volume (PGTV) region each patient. After stability test, feature dimension was further reduced by Principal Component Analysis (PCA), yielding Radiomic and Dosiomic Principal Components (RPCs and DPCs) respectively. Multiple Cox regression models were constructed using various combinations of RPC, DPC and clinical variables as the predictors. Akaike information criterion (AIC) and C-index were used to evaluate the performance of Cox regression models.

Results: PCA was performed on 338 radiomic and 873 dosiomic features that were tested as stable ($ICC_1 > 0.7$ and $ICC_2 > 0.95$), yielding 5 RPCs and DPCs respectively. Three comprehensive features (RPC0, P<0.01, DPC0, P<0.01 and DPC3, P<0.05) were found to be significant in the individual Radiomic or Dosiomic Cox regression models. The model combining the above features and clinical variable (total stage IVB) provided best risk stratification of locoregional recurrence (C-index, 0.815; 95%CI, 0.770-0.859) and prevailing balance between predictive accuracy and complexity (AIC, 143.65) than any other investigated models using either single factors or two combined components.

Conclusion: This study provided quantitative tools and additional evidence for the personalized treatment selection and protocol optimization for HPSCC, a relatively rare cancer. By combining complementary information from radiomics, dosiomics, and clinical variables, the proposed comprehensive model provided more accurate prediction of locoregional recurrence risk after radiotherapy.

KEYWORDS

hypopharyngeal squamous cell carcinoma, radiomics, dosiomics, Cox regression, locoregional recurrence

1 Introduction

Compared with invasive surgery, organ-preserving options such as definitive radiotherapy (RT) are more commonly used for patients with previously untreated, newly diagnosed locoregionally advanced hypopharyngeal squamous carcinoma (HPSCC), achieving comparable if not better long-term survival (1–3). However, due to advanced-stage disease, poor performance status, comorbidities, alcohol abuse, and nutritional problems, the 5-year survival rates of patients with HPSCC were only no greater than 40% as reported in various studies (4, 5). Furthermore, the prognosis was also poor, ascribable to the tumor heterogeneity and large outcome uncertainties after standard treatment (6). To improve the prognosis, personalized risk prediction is clinically desirable to support patient-specific selection and optimization of treatment protocols for better tumor control (7, 8), however, existing clinical experience is very subjective and unstable based on conventional parameters such as smoking, drinking, T stage, and lymph node metastasis etc. (9).

By analyzing high dimensional image features that are invisible to radiologists based on multi-modality images such as MRI (10), PET-CT (11) and CT (12), Radiomics has been demonstrated as a promising approach to stratify patients of various risks due to tumor heterogeneity. Unlike the dominant dependence of chemotherapy outcome on the biological varieties as represented by Radiomics features (12), the radiation dose is another key determinative factor of treatment effectiveness for HPSCC patients receiving radiotherapy. The radiation dose distribution is optimized based on patient-specific characteristics such as the shape, volume and location of the tumor and adjacent organs. However, conventional dose-volume-histograms (DVHs) provided limited dosimetric statistics without spatial information, and the predictive accuracy is unsatisfactory (13). Using similar methods as that of Radiomics, Dosiomics analyzes the spatial features of the 3-dimentional patient-specific dose distribution, hence provides better prediction of radiation-induced results (13, 14).

Considering the therapeutic responses of HPSCC patients treated with radiotherapy depend on both tumor heterogeneity and dosimetric variables, this work hypothesized that combined signatures using both Radiomics and Dosiomics features may have more robust statistical correlation with locoregional recurrence of patients with locoregionally advanced HPSCC treated with radiotherapy, potentially supporting more quantitative and personalized clinical decision making such as strategy selection and protocol optimization, which has not been reported in the literature before and is the purpose of this study.

2 Materials and methods

2.1 Patients

The data of 77 patients pathologically confirmed with HPSCC at our center between October 2011 and July 2020 were retrospectively investigated. The inclusion criteria were (1): lesion located at hypopharynx and pathologically diagnosed squamous cell carcinoma ; (2) administration and completion of laryngeal-preservation treatments: induction chemotherapy (IC)+radical RT or IC+chemoradiation; (3) no postpone, intervention or discontinuation during RT. Data with violation were excluded. All patients underwent disease staging using the American Joint Committee on Cancer Staging System, Eighth Edition (15).

2.2 Image acquisition and target delineation

All patients were immobilized in the supine position using thermoplastic head-neck-shoulder masks. Planning CT with intravenous contrast was acquired for structure delineation on a SIEMENS Sensation Open CT scanner using the following protocols: tube voltage 120kV; tube current 320mAs; reconstruction thickness 3 mm; matrix 512 × 512. Target and organs-at-risk (OARs) delineation was manually performed by experienced radiation oncologists according to NCCN and RTOG guidelines respectively (16, 17). All delineations were double checked and approved by senior radiation oncologists per our clinical protocols.

Intensity-modulated radiation therapy (IMRT) or volumetric modulated arc therapy (VMAT) plans were optimized to deliver a prescription dose of 60 Gy to at least 95% of the planning target volume (PTV) in 33 fractions. The dose limitations to OARs were in accordance with RTOG 0615 protocols (18). Simultaneous-

integrated-boost (SIB) technique was used to deliver 70 Gy to at least 95% of the planning gross tumor volume (PGTV) in the same plan. All patients were treated with one fraction daily, 5 days per week.

2.3 Follow-up protocol and definition of failures

The follow-up was performed at 1 month after the completion of RT, every 3 months during the first 2 years, every 6 months between the third and fifth year, and annually thereafter. At the time of the last follow-up assessment, failure patterns were classified as local, regional, or distant respectively. Local failure was defined as failure of the primary tumor to the treatment. Regional failure was defined as the recurrence in the regional lymph nodes. Distant failure was defined as the appearance of a tumor at any site representing hematogenous dissemination.

2.4 Extraction and selection of radiomic and dosiomic features

The flowchart of building the statistical analysis model is shown in Figure 1 Using PGTV as the volume-of-interest (VOI), radiomic and dosiomic features were extracted from the planning CT images and dose maps respectively using the third-party python library (19) (https://pyradiomics.readthedocs.io). Basic radiomic features included 18 first-order features, 14 shape-and-volume features and 75 texture features. To expand the feature pool, Log of Gaussian filter and wavelet transform were applied on the planning CT images respectively. The aforementioned texture features were then recalculated, generating 1209 more features. In this study, BiorSplines (bior6.8) was used as the main wavelet function (20). Dosiomic features were extracted using the same procedures from the dose maps.

Consistent with other studies (21, 22), this study evaluated the stability of the extracted radiomic features by applying Guassian noise and random ROI boundary perturbance to the original CT images and VOI boundaries respectively. Three levels of standard variations of the Gaussian noise and two levels of the boundary perturbance distances were used, i.e., 10, 50, 100 HU and 0.5, 1 pixel pitch unit respectively. The intraclass correlation coefficient (ICC) (23) was used as an indicator of feature stability between different groups, which was calculated on the original and the counterpart images respectively, using the definitions of ICC (1,1) (ICC_1) and ICC (2,1) (ICC_2) respectively. ICC_1 was used to indicate interrater reliability of the features and ICC_2 was used to indicate non-independence of the features respectively (24). ICC_1 and ICC_2 were calculated as Eq. (1) and Eq. (2):

$$ICC_1 = \frac{MSR - MSW}{MSR + (k+1)*MSW} \quad (1)$$

$$ICC_2 = \frac{MSR - MSW}{MSR} \quad (2)$$

MSR means mean square for rows, MSW means mean square for residual sources of variance and k means the number of raters respectively.

Consistent with the literature, features with $ICC_1 > 0.7$ and $ICC_2 > 0.95$ were considered as reproducible (25) in the existence of image noise and segmentation errors respectively. As the main influential factor of dosiomic feature robustness, only perturbation of ROI boundary was used to assess the stability of dosiomic features in this study, in accordance with Francesco's method (26).

Amongst the screened stable features, the most clinically relevant features were further selected using univariate analysis, according to their capability of stratifying the patients into high and low locoregional recurrence risk rates. Log-rank test (27) was used to examine the statistical significance of the inter-group differences between the survival curves of the two groups. Only significant features with p-values<0.05 (statistically significant) were used for further analysis.

2.5 Modeling and statistical analysis

Dimensionality reduction of the feature space was performed using Principal Component Analysis (PCA). The first five principal components of radiomic and dosiomic features were used as independent variables of two multivariate Cox regression models

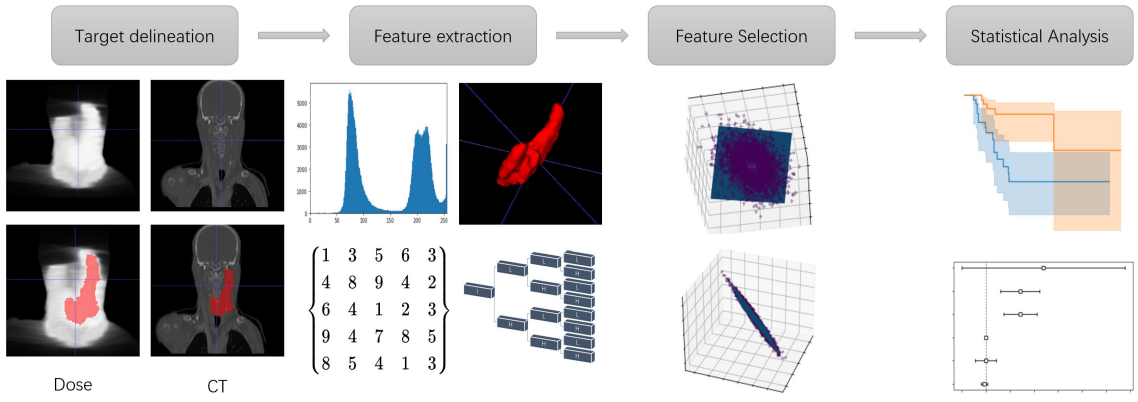

FIGURE 1
The flowchart of building the statistical analysis model.

respectively, noted as the Radiomic Principal Component (RPC) Model and Dosiomic Principal Component (DPC) Model respectively. A multivariate Cox regression model was also constructed on conventional clinical parameters, noted as the Clinical Model. Kaplan-Meier survival analysis and the log-rank test were used to evaluate the predictive capability of each significant Principal Component and clinical variable respectively.

In addition, the principal components with significant hazard ratio ($p< 0.05$) were combined with clinical parameters to construct another three comprehensive multivariate Cox regression models, named as Radiomics+Clinical Model, Dosiomics+Clinical Model, and Radiomics+Dosiomics+Clinical Model respectively. The performance of these comprehensive models were evaluated with the partial Akaike information criterion (AIC) (28) and concordance index (C-index) (29) respectively. Defined as $AIC = 2k - 2ln(\hat{L})$, AIC was proposed to balance the tradeoff between the ability to fit and the simplicity of the model (30), where k means the number of estimated parameters and $\hat{L}$ means the likelihood function which was maximum. Lower AIC values indicate better models with less complexity. The C-index was used to evaluate discriminative performance of each model. Defined as Eq. (3):

$$C - index = \frac{\sum_{i,j} 1_{T_j<T_i} \cdot 1_{\eta_j>\eta_i \cdot \delta_j}}{\sum_{i,j} 1_{T_j<T_i} \cdot \delta_j} \quad (3)$$

C-index (31) presents the proportion of concordant data pairs, where $(i, j)$is a pair of event; $T_n$means event n's observation time; η_n means event n's risk; $1_{Tj<Ti} \cdot 1_{\eta_j>\eta_i}$means when event j's risk is higher than event i, event j's observation time is earlier than event i; $\delta_j$means event j happened in T_j. As a predictive marker and a time-to-event response variable, C-Index values closer to 1 suggest better model performance.

The statistical analysis was conducted using the following packages of R and Python respectively: the survival package (R) and the lifeline package (Python) were used to execute Kaplan–Meier analysis, build the Cox proportional risk models, and calculate the C-index respectively. Local regional recurrence-free survival (LRRFS), metastasis-free survival (MFS), progression-free survival (PFS), and overall survival (OS) rates were estimated using the Kaplan–Meier method and measured from the first day of treatment to the date of the event. All statistical tests were two-sided, and p values< 0.05 were considered as significant.

3 Results

3.1 Patient demography and treatment outcomes

The characteristics of the 77 patients included in this study are presented in Table 1.

The median follow-up duration was 23.27 (range, 4.83–81.40) months. During the study period, 29 patients experienced disease progression, and 30 patients died due to tumor progression (19), local hypopharyngeal haemorrhage (4), infection (5), car accident (1) and secondary primary cancer (1), respectively. The median PFS and OS estimates were 47.07 months and 36.07 months, respectively. Three-year LRRFS, MFS, PFS, and OS rates were 70.6%, 81.7%, 58.3%, and 48.9%, respectively. Of the 29 patients experienced treatment failure at their last follow-up visit, 13, 2, 9, 3, 0, 1 and 1 patients presented with local only, regional only, distant only, local-regional, regional-distant, local-distant, and local-regional-distant failure, respectively.

3.2 Statistical analysis and model evaluation

For each patient, 1321 radiomic features and 1321 dosiomic features were extracted from the planning CT images and dose distributions respectively, from which 338 radiomic features and 873 dosiomic features were identified as stable and reproducible ($ICC_1>0.7$, $ICC_2>0.95$). After PCA, 5 radiomic principal components and 5 dosiomic principal components were obtained respectively. Table 2 shows the hazard ratio (HR) and p-values of each principal component and the AIC of Cox regression, for the Clinical Model, Radiomic Principal Components (RPC) Model and Dosiomic Principal Components (DPC) Model respectively. One clinical variable, one RPC and two DPC had significant hazard ratios in Cox regression (p-value< 0.05) respectively.

For the combined models, the results of Multivariate Cox Regression Analysis are presented in Table 3 for the Radiomic +Clinical Model, Dosiomic+Clinical Model and Radiomic +Dosiomic+Clinical Model respectively.

Figure 2 displays the survival curves of high-risk and low-risk locoregionally advanced patient groups stratified by significant Radiomic and Dosiomic principal components respectively.

TABLE 1 Clinical characteristics of the 77 patients with locoregionally advanced HPSCC involved in this study.

Characteristics	Number of Patients (%)
Gender	
Male	71 (92.2)
Female	6 (7.8)
Age (years old)	
≥58	47 (61.0)
<58	30 (39.0)
Peripheral invasion*	
Yes	55(71.4)
No	22 (28.6)
Total stage (AJCC eighth edition)	
II/III/IVA	55 (71.4)
IVB	22 (28.6)

AJCC, American Joint Committee on Cancer; HPSCC, hypopharyngeal squamous cell carcinoma. *Peripheral invasion: tumor invaded structures surrounding hypopharynx, such as larynx, trachea, oropharynx, and esophagus, et al.

TABLE 2 Multivariate Cox Regression Analysis for the Clinical Model, Radiomic Principal Components (RPC) Model and Dosiomic Principal Components (DPC) Model respectively.

	HR (95% CI)	z	*P* value
Clinical Model (AIC, 158.61; C-index, 0.663; 95% CI, 0.600–0.725)			
Gender	0.68 (0.20-2.35)	-0.61	0.54
Age	0.92 (0.85-1.00)	-1.99	*0.05*
Stage	1.09 (0.38-3.16)	0.16	0.87
Peripheral invasion	1.25 (0.44-3.51)	0.42	0.67
RPC Model (AIC, 150.73; C-index, 0.762; 95% CI, 0.708–0.815)			
RPC0	1.10 (1.04-1.17)	3.26	<0.01
RPC1	1.08 (0.98-1.21)	1.49	0.14
RPC2	0.94 (0.83-1.07)	-0.96	0.34
RPC3	0.94 (0.79-1.12)	-0.68	0.49
RPC4	0.78 (0.60-1.03)	-1.78	0.08
DPC Model (AIC, 146.33; C-index, 0.783; 95% CI, 0.734–0.832)			
DPC0	1.08 (1.03-1.14)	3.33	<0.01
DPC1	1.04 (0.92-1.19)	0.64	0.52
DPC2	0.94 (0.82-1.06)	-1.03	0.30
DPC3	0.76 (0.60-0.97)	-2.16	0.03
DPC4	1.07 (0.90-1.28)	0.80	0.42

HR, hazard ratio; z, Wald statistic value, the ratio of each regression coefficient to its standard error; CI, confidence interval; RPC, Radiomic Principal Component; DPC, Dosiomic Principal Component; RPCn, DPCn, The nth RPC and DPC obtained by principal component analysis and ranked by weight respectively.

TABLE 3 Multivariate Cox Regression Analysis for the Radiomic+Clinical Model, Dosiomic+Clinical Model and Radiomic+Dosiomic+Clinical Model respectively.

	HR (95% CI)	z	*P* value
Radiomic+Clinical Model (AIC, 148.46; C-index, 0.783; 95% CI, 0.734–0.832)			
RPC0	1.11 (1.04-1.19)	3.24	<0.01
gender	0.56 (0.16-2.01)	-0.89	0.37
age	0.92 (0.84-1.01)	-1.83	0.07
total_stage_IVB	0.36 (0.11-1.25)	-1.60	0.11
Peripheral invasion	1.69 (0.55-5.14)	0.92	0.36
Dosiomic+Clinical Model (AIC, 146.63; C-index, 0.782; 95% CI, 0.730–0.833)			
DPC0	1.07 (1.03-1.11)	3.19	<0.01
DPC3	0.7 (0.54-0.91)	-2.64	0.01
gender	0.98 (0.24-4.06)	-0.03	0.98
age	0.94 (0.86-1.03)	-1.32	0.19
total_stage_IVB	0.4 (0.11-1.49)	-1.36	0.17
Peripheral invasion	1.83 (0.58-5.75)	1.04	0.30
Radiomic+Dosiomic+Clinical Model (AIC, 143.65; C-index, 0.815; 95% CI, 0.770-0.859)			
RPC0	1.09 (1.01-1.18)	2.15	0.03

(Continued)

TABLE 3 Continued

	HR (95% CI)	z	*P* value
DPC0	1.04 (0.99-1.08)	1.47	0.14
DPC3	0.7 (0.53-0.93)	-2.47	0.01
gender	0.62 (0.16-2.41)	-0.69	0.49
age	0.91 (0.82-1.01)	-1.76	0.08
total_stage_IVB	0.24 (0.06-0.97)	-2.01	0.04
Peripheral invasion	2.29 (0.73-7.15)	1.43	0.15

HR, hazard ratio; CI, confidence interval; RPC, Radiomic Principal Component; DPC, Dosiomic Principal Component; RPCn, DPCn, The n^{th} RPC and DPC obtained by principal component analysis and ranked by weight respectively.

Figure 3 displays the survival curves stratified by conventional clinical variables such as gender (a), peripheral invasion (b), total stage (c) and age (d) respectively.

4 Discussion

HPSCC is a relatively rare but aggressive malignancy accounting for 5%-10% of head and neck cancer, with high incidence of recurrence and low survival rates (32). There is no sufficient data and evidence to guide precision medicine and prognosis for HPSCC patients. Several clinical prediction models for HPSCC have been published previously (33–35). A reported clinical prediction model for survival in hypopharynx cancer consisted of gender, subsite, TNM classification, Adult Comorbidity Evaluation-27 score (ACE27), body mass index (BMI), hemoglobin, albumin, and leukocyte count. Of these, TNM classification, ACE27, BMI, hemoglobin, and albumin had independent significant associations with survival. But the TNM classification might vary by investigator bias. ACE27 score incorporated 27 ailments which could have mutual effect. Hemoglobin, albumin and leukocyte counts were all baseline data at one time point, and there were 29%, 12% and 2% missing data in the peripheral blood value albumin, leukocyte counts and hemoglobin respectively. All these factors may increase uncertainties of this prediction model (34). The effectiveness and

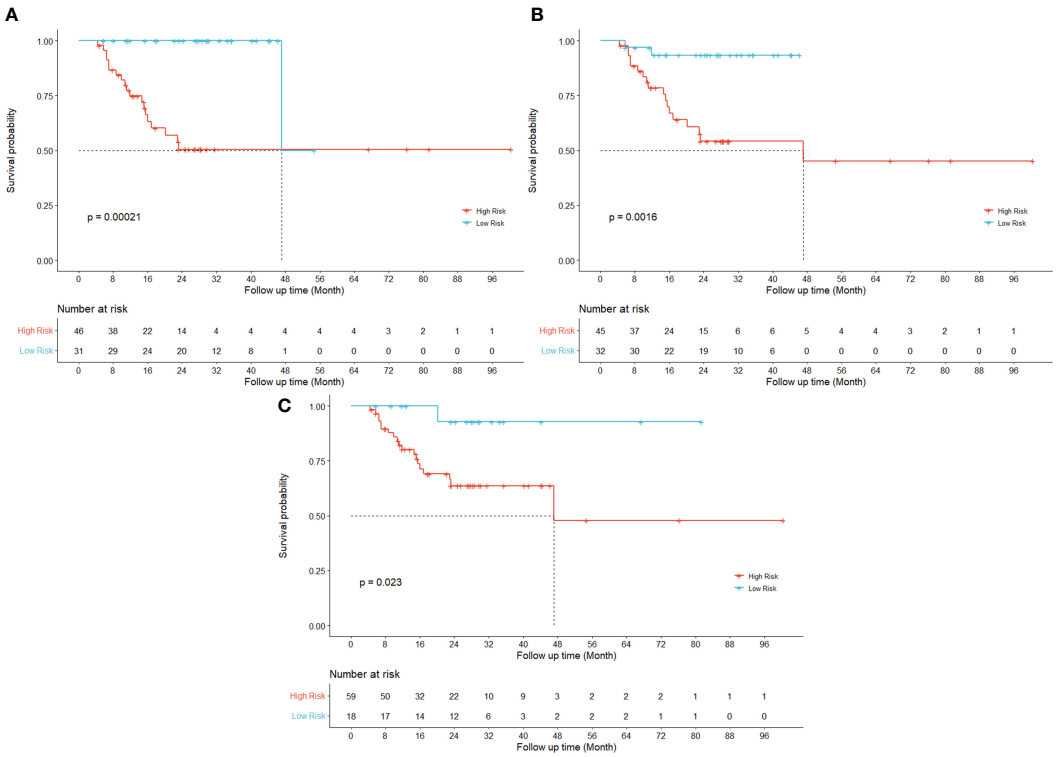

FIGURE 2
Kaplan-Meier curves for LRRFS. Univariate results are shown for three different principal components in radiomic (**(A)** RPC0) and dosiomic (**(B)** DPC0; **(C)** DPC3) features respectively.

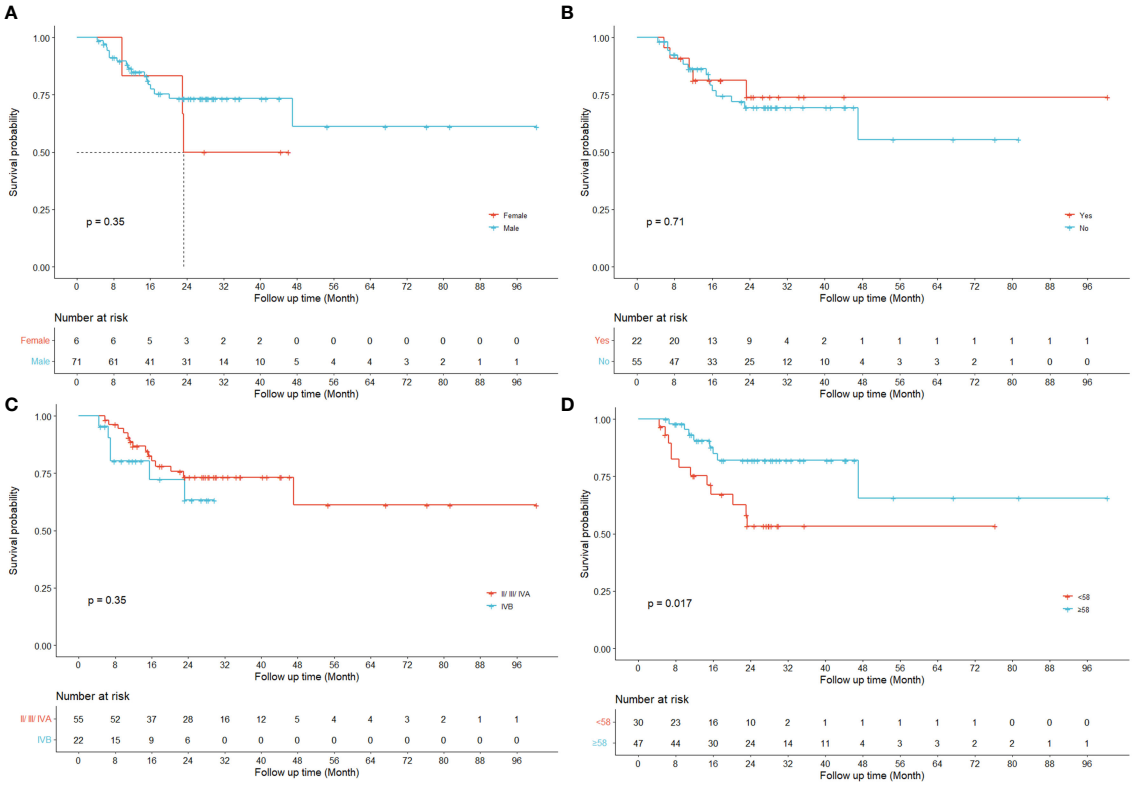

FIGURE 3
Kaplan-Meier curves for LRRFS. Univariate results are shown for four different clinical variables respectively (**(A)** gender; **(B)** peripheral invasion; **(C)** total stage IVB; **(D)** age).

consistency should be further improved in a patient-specific way to assist clinical decision making and treatment protocol optimization.

Previous studies have demonstrated the prognostic values of radiomics features in predicting the risk of HPSCC patients treated with chemoradiation (12, 36) and their key findings were echoed and reconfirmed by our study as shown in the Kaplan-Meier curves for LRRFS (RPC0) in Figure 2A. In addition to radiomics, our work also revealed that the principal components of dosiomic features (DPC0 and DPC3) could also stratify patients with different risk (log-rank P<0.05), as shown in Figures 2B, C. Table 2 suggested that dosiomics principal components (C-index=0.783, 95% CI, 0.734–0.832) achieved better predictive performance than that of radiomics (C-index=0.762, 95% CI, 0.708–0.815), if used alone. In contrast, the prognostic performance of conventional clinical variables was less satisfactory (C-index=0.663, 95% CI, 0.600–0.725), consistent with the Kaplan-Meier curves in Figure 3. The AIC of RPC Model (150.73) and DPC Model (146.33) were also better than that of Clinical Model (158.61), suggesting better balance was achieved between reducing model regression error and complexity by the former two models.

Compared with the aforementioned single models, the predictive performance of the combined models was improved, as suggested by the lower AIC and higher C-index values shown in Tables 2, 3. Consistent with our hypothesis, the comprehensive model combining the radiomics principal components, dosiomics principal components and conventional clinical variables can best stratify the HPSCC patients with different risks of locoregional recurrence after radiotherapy, as suggested by the largest C-index (0.815) than any other models as shown in Tables 2 and 3. This result is also better than that of the previous models using radiomics alone, achieving C-index between 0.690-0.788 (12, 37, 38). Compared with other comprehensive models such as using clinical features + radiomics features by Boot (39) et al (C-index=0.73), and using CT + FDG-PET by Starke (40) et al (C-index=0.80), this work also achieved better reulsts. The comprehensive model also best balanced the ability to fit and the complexity of the model, as suggested by the lowest AIC value (143.65) in Tables 2, 3. We ascribe these improvements to the complementary incorporation of biological heterogeneity as represented by radiomics, personalized treatment intervention as depicted by dosiomics, and empirical evidence as reflected by clinical variables, which were all determinative factors of HPSCC patient outcomes treated with radiotherapy. Firstly, as reported before, the radiomic features are associated with the cancer microenvironment, genetic characteristics, cell growth and histological grading covering the whole tumor area (41–45), providing influential suggestions to the prognosis from the aspects of patient biology. Secondly, as treatment dose distribution was optimized deliberately based on patient-specific anatomies and target prescription, the high-dimensional dosiomic features characterize the personalized specification of treatment intervention. Thirdly, although less robust, clinical variables such as gender, age, stage and peripheral invasion are most familiar to the oncologists, and are broadly used as rule-of-thumb experience to

predict the patient prognosis (46–49). The combined data provide complementary information in the quantitative prediction, which is more accurate than that of single factors.

Regarding accessibility, all the required data for the comprehensive modelling, including the planning CT images, dose distribution of treatment plans and conventional clinical variables are readily available for every patient before the start of radiotherapy, potentially facilitating the clinical application of this approach. It provides prompt suggestions before the start of radiotherapy, enabling possible reconsideration of receiving surgery for patients with high risk of local regional recurrence to achieve longer survival than receiving larynx preservation treatments. For patients that have received larynx preservation treatment but are predicted with high risk of local regional recurrence, our model can support personalized clinical suggestions such as more frequent monitoring and examination after radiotherapy.

Regarding methodologies, this work avoided the interference of collinearity to the radiomic and dosiomic features by using PCA. As reported by Traverso et al. (50), the radiomic features have multicollinearity and are largely dependent on tumor volume. Our approach searched for patterns in the data without assuming any a-priori distribution or condition. This study also avoided the bias from subjective selection of cut-off values, by using Youden index for all continuous variables involved in the Kaplan-Meier analysis, consistent with other researches (51, 52).

Although this work is limited by its retrospective design and the relatively small population due to the low morbidity of HPSCC, it provides additional personalized estimation tools and complementary clinical evidence to stratify patients with various risk of locoregional recurrence after radiotherapy, supporting personalized optimization of precision treatment strategies. For instance, if higher locoregional recurrence risks were predicted for a patient receiving function-preserving radiotherapy, more radical treatment such as total laryngectomy might be considered with multi-disciplinary evaluation.

5 Conclusions

This study demonstrates that comprehensive models combing radiomic, dosiomic and clinical components displayed better predictive values than any single factor for locoregionally advanced HPSCC treated with chemoradiotherapy, potentially supporting more accurate and prompt clinical decision making such as personalized treatment strategy selection and optimization.

Data availability statement

The raw data supporting the conclusions of this article will be made available by the authors, without undue reservation.

Ethics statement

The studies involving human participants were reviewed and approved by Peking University Cancer Hospital (IRB#2019YJZ76). The patients/participants provided their written informed consent to participate in this study.

Author contributions

HL, DZ and YH contributed equally to this work. HL was Responsible for Statistical Analysis (Email: stevendeliu@stu.pku.edu.cn). All authors contributed to the article and approved the submitted version.

Funding

The authors disclosed receipt of the following financial support for the research, authorship, and/or publication of this article: This research was supported by National Natural Science Foundation of China (12275012), Beijing Natural Science Foundation (Z210008); Science Foundation of Peking University Cancer Hospital (2021-1, PY202305, PY202306), Project 2020BD029 supported by PKU-Baidu Fund; Peking University Health Science Center Medical Education Research Funding Project (2020YB34), Peking University Emerging Engineering Interdisciplinary Project/the Fundamental Research Funds for the Central Universities (PKU2022XGK006), National Key R&D Program of China (2019YFF01014405), Open Project funded by Key Laboratory of Carcinogenesis and Translational Research, Ministry of Education/Beijing (2022 Open Project-2) and Inner Mongolia Science & Technology Project Plan (2022YFSH0064).

Acknowledgments

The authors thank Yan Sun, Baomin Zheng, Yichen Pu, Jian Zhang, Zhuolun Liu, Jian Gong, Zhongsu Feng, Fan Jiang, Qiaoqiao Hu, Kaining Yao, Sha Li, Meijiao Wang, Shun Zhou, and Yixiao Du for their assistance.

Conflict of interest

The authors declare that the research was conducted in the absence of any commercial or financial relationships that could be construed as a potential conflict of interest.

Publisher's note

References

1. Bar-Ad V, Palmer J, Yang H, Cognetti D, Curry J, Luginbuhl A, et al. Current management of locally advanced head and neck cancer: The combination of chemotherapy with locoregional treatments. *Semin Oncol* (2014), 41(6):798–806. doi: 10.1053/j.seminoncol.2014.09.018

2. Kuo P, Sosa JA, Burtness BA, Husain ZA, Mehra S, Roman SA, et al. Treatment trends and survival effects of chemotherapy for hypopharyngeal cancer: Analysis of the national cancer data base. *Cancer* (2016) 122:1853–60. doi: 10.1002/cncr.29962

3. Takes RP, Strojan P, Silver CE, Bradley PJ, Haigentz M, Wolf GT, et al. Current trends in initial management of hypopharyngeal cancer: the declining use of open surgery. *Head Neck* (2012) 34:270–81. doi: 10.1002/hed.21613

4. Street W. American Cancer Society. *Cancer facts and figures 2021*. (America: American Cancer Society). (2021).

5. Street W. American Cancer Society. *Cancer facts and figures 2020*. (America: American Cancer Society). (2020).

6. Song L, Zhang S, Yu S, Ma F, Wang B, Zhang C, et al. Cellular heterogeneity landscape in laryngeal squamous cell carcinoma. *Int J Cancer* (2020) 147:2879–90. doi: 10.1002/ijc.33192

7. Department of Veterans Affairs Laryngeal Cancer Study Group. Induction chemotherapy plus radiation compared with surgery plus radiation in patients with advanced laryngeal cancer. *N Engl J Med* (1991) 324:1685–90. doi: 10.1056/NEJM199106133242402

8. Beitler JJ, Zhang Q, Fu KK, Trotti A, Spencer SA, Jones CU, et al. Final results of local-regional control and late toxicity of RTOG 9003: A randomized trial of altered fractionation radiation for locally advanced head and neck cancer. *Int J Radiat Oncol Biol Phys* (2014) 89:13–20. doi: 10.1016/j.ijrobp.2013.12.027

9. Eskander A, Mifsud M, Irish J, Gullane P, Gilbert R, Brown D, et al. Overview of surgery for laryngeal and hypopharyngeal cancer in Ontario, 2003-2010. *Head Neck* (2017) 39:1559–67. doi: 10.1002/hed.24787

10. Yan BC, Li Y, Ma FH, Zhang GF, Feng F, Sun MH, et al. Radiologists with MRI-based radiomics aids to predict the pelvic lymph node metastasis in endometrial cancer: a multicenter study. *Eur Radiol* (2021) 31:411–22. doi: 10.1007/s00330-020-07099-8

11. Oikonomou A, Khalvati F, Tyrrell PN, Haider MA, Tarique U, Jimenez-Juan L, et al. Radiomics analysis at PET/CT contributes to prognosis of recurrence and survival in lung cancer treated with stereotactic body radiotherapy. *Sci Rep* (2018) 8:1–11. doi: 10.1038/s41598-018-22357-y

12. Mo X, Wu X, Dong D, Guo B, Liang C, Luo X, et al. Prognostic value of the radiomics-based model in progression-free survival of hypopharyngeal cancer treated with chemoradiation. *Eur Radiol* (2020) 30:833–43. doi: 10.1007/s00330-019-06452-w

13. Liang B, Yan H, Tian Y, Chen X, Yan L, Zhang T, et al. Dosiomics: Extracting 3D spatial features from dose distribution to predict incidence of radiation pneumonitis. *Front Oncol* (2019) 9:269. doi: 10.3389/fonc.2019.00269

14. Wu A, Li Y, Qi M, Lu X, Jia Q, Guo F, et al. Dosiomics improves prediction of locoregional recurrence for intensity modulated radiotherapy treated head and neck cancer cases. *Oral Oncol* (2020) 104:104625. doi: 10.1016/j.oraloncology.2020.104625

15. Amin MB, Greene FL, Edge SB, Compton CC, Gershenwald JE, Brookland RK, et al. The eighth edition AJCC cancer staging manual: Continuing to build a bridge from a population-based to a more "personalized" approach to cancer staging. *CA: Cancer J Clin* (2017) 67:93–9. doi: 10.3322/caac.21388

16. Grégoire V, Ang K, Budach W, Grau C, Hamoir M, Langendijk JA, et al. Delineation of the neck node levels for head and neck tumors: A 2013 update. DAHANCA, EORTC, HKNPCSG, NCIC CTG, NCRI, RTOG, TROG consensus guidelines. *Radiother Oncol* (2014) 110:172–81. doi: 10.1016/j.radonc.2013.10.010

17. Network NCC. *Nccn clinical practice guidelines in oncology (Nccn guidelines) head and neck cancers version 2.2020*. (America: Journal of the National Comprehensive Cancer Network) (2021).

18. Lee NY, Zhang Q, Pfister DG, Kim J, Garden AS, Mechalakos J, et al. Addition of bevacizumab to standard chemoradiation for locoregionally advanced nasopharyngeal carcinoma (RTOG 0615): A phase 2 multi-institutional trial. *Lancet Oncol* (2012) 13:172–80. doi: 10.1016/S1470-2045(11)70303-5

19. van Griethuysen JJM, Fedorov A, Parmar C, Hosny A, Aucoin N, Narayan V, et al. Computational radiomics system to decode the radiographic phenotype. *Cancer Res* (2017) 77:e104–7. doi: 10.1158/0008-5472.CAN-17-0339

20. Soufi M, Arimura H, Nagami N. Identification of optimal mother wavelets in survival prediction of lung cancer patients using wavelet decomposition-based radiomic features. *Med Phys* (2018) 45:5116–28. doi: 10.1002/mp.13202

21. Traverso A, Kazmierski M, Shi Z, Kalendralis P, Welch M, Nissen HD, et al. Stability of radiomic features of apparent diffusion coefficient (ADC) maps for locally advanced rectal cancer in response to image pre-processing. *Physica Med* (2019) 61:44–51. doi: 10.1016/j.ejmp.2019.04.009

22. Yaşar H, Ceylan M. A new radiomic study on lung CT images of patients with covid-19 using LBP and deep learning (Convolutional neural networks (CNN)). (2020). doi: 10.21203/rs.3.rs-30427/v1

23. Shrout PE, Fleiss JL. Intraclass correlations: Uses in assessing rater reliability. *[J]. Psychological bulletin* (1979), 86(2):420. doi: 10.1037/0033-2909.86.2.420

24. Panth KM, Leijenaar RTH, Carvalho S, Lieuwes NG, Yaromina A, Dubois L, et al. Is there a causal relationship between genetic changes and radiomics-based image features? an *in vivo* preclinical experiment with doxycycline inducible GADD34 tumor cells. *Radiother Oncol* (2015) 116:462–6. doi: 10.1016/j.radonc.2015.06.013

25. LeBreton JM, Senter JL. Answers to 20 questions about interrater reliability and interrater agreement. *Organizat Res Methods* (2008) 11:815–52. doi: 10.1177/1094428106296642

26. Rizzetto F, Calderoni F, De Mattia C, Defeudis A, Giannini V, Mazzetti S, et al. Impact of inter-reader contouring variability on textural radiomics of colorectal liver metastases. *Eur Radiol Exp* (2020) 4:62. doi: 10.1186/s41747-020-00189-8

27. Kleinbaum DG, Klein M. Kaplan-Meier Survival curves and the log-rank test. In: *Survival analysis*. (America: Springer) (2012). p. 55–96.

28. Sakamoto Y, Ishiguro M, Kitagawa G. Akaike information criterion statistics. *Dordrecht Netherlands: D Reidel* (1986) 81:26853. doi: 10.1080/01621459.1988.10478680

29. Harrell FEJr, Lee KL, Califf RM, Pryor DB, Rosati RA. Regression modelling strategies for improved prognostic prediction. *Stat Med* (1984) 3:143–52. doi: 10.1002/sim.4780030207

30. Kuha J. AIC and BIC: Comparisons of assumptions and performance. *Sociological Methods Res* (2004) 33:188–229. doi: 10.1177/0049124103262065

31. Xiang A, Lapuerta P, Ryutov A, Buckley J, Azen S. Comparison of the performance of neural network methods and cox regression for censored survival data. *Comput Stat Data Anal* (2000) 34:243–57. doi: 10.1016/S0167-9473(99)00098-5

32. Bradley PJ. Epidemiology of hypopharyngeal cancer. *Hypopharyngeal Cancer* (2019) 83:1–14. doi: 10.1159/000492299

33. Visini M, Giger R, Shelan M, Elicin O, Anschuetz L. Predicting factors for oncological and functional outcome in hypopharyngeal cancer. *Laryngoscope* (2021) 131:E1543–9. doi: 10.1002/lary.29186

34. Arends CR, Petersen JF, van der Noort V, Timmermans AJ, Leemans CR, de Bree R, et al. Optimizing survival predictions of hypopharynx cancer: development of a clinical prediction model. *Laryngoscope* (2020) 130:2166–72. doi: 10.1002/lary.28345

35. Lin Z, Lin H, Lin C. Dynamic prediction of cancer-specific survival for primary hypopharyngeal squamous cell carcinoma. *Int J Clin Oncol* (2020) 25:1260–9. doi: 10.1007/s10147-020-01671-4

36. Coroller TP, Grossmann P, Hou Y, Rios Velazquez E, Leijenaar RTH, Hermann G, et al. CT-based radiomic signature predicts distant metastasis in lung adenocarcinoma. *Radiother Oncol* (2015) 114:345–50. doi: 10.1016/j.radonc.2015.02.015

37. Aerts HJWL, Velazquez ER, Leijenaar RTH, Parmar C, Grossmann P, Carvalho S, et al. Decoding tumour phenotype by noninvasive imaging using a quantitative radiomics approach. *Nat Commun* (2014) 5:4006. doi: 10.1038/ncomms5006

38. Leger S, Zwanenburg A, Pilz K, Zschaeck S, Zöphel K, Kotzerke J, et al. CT imaging during treatment improves radiomic models for patients with locally advanced head and neck cancer. *Radiother Oncol* (2019) 130:10–7. doi: 10.1016/j.radonc.2018.07.020

39. Boot PA, Mes SW, de Bloeme CM, Martens RM, Leemans CR, Boellaard R, et al. Magnetic resonance imaging based radiomics prediction of human papillomavirus infection status and overall survival in oropharyngeal squamous cell carcinoma. *Oral Oncol* (2023) 137:106307. doi: 10.1016/j.oraloncology.2023.106307

40. Starke S, Zwanenburg A, Leger K, Zöphel K, Kotzerke J, Krause M, et al. Longitudinal and multimodal radiomics models for head and neck cancer outcome prediction. *Cancers (Basel)* (2023) 15:673. doi: 10.3390/cancers15030673

41. Lambin P, Rios-Velazquez E, Leijenaar R, Carvalho S, van Stiphout RGPM, Granton P, et al. Radiomics: Extracting more information from medical images using advanced feature analysis. *Eur J Cancer* (2012) 48:441–6. doi: 10.1016/j.ejca.2011.11.036

42. Chen S-W, Shen W-C, Lin Y-C, Chen R-Y, Hsieh T-C, Yen K-Y, et al. Correlation of pretreatment 18 f-FDG PET tumor textural features with gene expression in pharyngeal cancer and implications for radiotherapy-based treatment outcomes. *Eur J Nucl Med Mol Imaging* (2017) 44:567–80. doi: 10.1007/s00259-016-3580-5

43. Leijenaar RT, Carvalho S, Hoebers FJ, Aerts HJ, Van Elmpt WJ, Huang SH, et al. External validation of a prognostic CT-based radiomic signature in oropharyngeal squamous cell carcinoma. *Acta Oncol* (2015) 54:1423–9. doi: 10.3109/0284186X.2015.1061214

44. Song J, Shi J, Dong D, Fang M, Zhong W, Wang K, et al. A new approach to predict progression-free survival in stage IV EGFR-mutant NSCLC patients with EGFR-TKI therapy. *Clin Cancer Res* (2018) 24:3583–92. doi: 10.1158/1078-0432.CCR-17-2507

45. Gillies RJ, Kinahan PE, Hricak H. Radiomics: Images are more than pictures, they are data. *Radiology* (2016) 278:563–77. doi: 10.1148/radiol.2015151169

46. Kim S-Y, Rho Y-S, Choi E-C, Kim M-S, Woo J-H, Lee DH, et al. Clinicopathological factors influencing the outcomes of surgical treatment in patients with T4a hypopharyngeal cancer. *BMC Cancer* (2017) 17:1–7. doi: 10.1186/s12885-017-3880-6

47. Scherl C, Mantsopoulos K, Semrau S, Fietkau R, Kapsreiter M, Koch M, et al. Management of advanced hypopharyngeal and laryngeal cancer with and without cartilage invasion. *Auris Nasus Larynx* (2017) 44:333–9. doi: 10.1016/j.anl.2016.08.002

48. Gong EJ, Kim DH, Ahn JY, Choi K-S, Jung KW, Lee JH, et al. Routine endoscopic screening for synchronous esophageal neoplasm in patients with head and neck squamous cell carcinoma: A prospective study. *Dis Esophagus* (2016) 29:752–9. doi: 10.1111/dote.12404

49. Patel UA, Howell LK. Local response to chemoradiation in T4 larynx cancer with cartilage invasion. *Laryngoscope* (2011) 121:106–10. doi: 10.1002/lary.21181

50. Traverso A, Kazmierski M, Zhovannik I, Welch M, Wee L, Jaffray D, et al. Machine learning helps identifying volume-confounding effects in radiomics. *Physica Med* (2020) 71:24–30. doi: 10.1016/j.ejmp.2020.02.010

51. Kremer A, Kremer T, Kristiansen G, Tolkach Y. Where is the limit of prostate cancer biomarker research? systematic investigation of potential prognostic and diagnostic biomarkers. *BMC Urol* (2019) 19:1–10. doi: 10.1186/s12894-019-0479-z

52. Chang C, Hsieh M-K, Chang W-Y, Chiang AJ, Chen J. Determining the optimal number and location of cutoff points with application to data of cervical cancer. *PloS One* (2017) 12:e0176231. doi: 10.1371/journal.pone.0176231

frontiers | Frontiers in Oncology

TYPE Original Research
PUBLISHED 06 April 2023
DOI 10.3389/fonc.2023.1137803

OPEN ACCESS

EDITED BY
Giuseppe Carlo Iorio,
University of Turin, Italy

REVIEWED BY
Roberta Grassi,
University of Campania Luigi Vanvitelli, Italy
Donatella Caivano,
Sant'Andrea University Hospital, Sapienza University of Rome, Italy
Matthew Field,
University of New South Wales, Australia

*CORRESPONDENCE
J. John Lucido
lucido.joseph@mayo.edu

SPECIALTY SECTION
This article was submitted to Radiation Oncology, a section of the journal Frontiers in Oncology

RECEIVED 04 January 2023
ACCEPTED 24 March 2023
PUBLISHED 06 April 2023

CITATION
Lucido JJ, DeWees TA, Leavitt TR, Anand A, Beltran CJ, Brooke MD, Buroker JR, Foote RL, Foss OR, Gleason AM, Hodge TL, Hughes CO, Hunzeker AE, Laack NN, Lenz TK, Livne M, Morigami M, Moseley DJ, Undahl LM, Patel Y, Tryggestad EJ, Walker MZ, Zverovitch A and Patel SH (2023) Validation of clinical acceptability of deep-learning-based automated segmentation of organs-at-risk for head-and-neck radiotherapy treatment planning. *Front. Oncol.* 13:1137803. doi: 10.3389/fonc.2023.1137803

Validation of clinical acceptability of deep-learning-based automated segmentation of organs-at-risk for head-and-neck radiotherapy treatment planning

J. John Lucido[1]*, Todd A. DeWees[2], Todd R. Leavitt[2], Aman Anand[3], Chris J. Beltran[4], Mark D. Brooke[5], Justine R. Buroker[6], Robert L. Foote[1], Olivia R. Foss[7], Angela M. Gleason[7], Teresa L. Hodge[1], Cían O. Hughes[5], Ashley E. Hunzeker[1], Nadia N. Laack[1], Tamra K. Lenz[1], Michelle Livne[5], Megumi Morigami[5], Douglas J. Moseley[1], Lisa M. Undahl[1], Yojan Patel[5], Erik J. Tryggestad[1], Megan Z. Walker[5], Alexei Zverovitch[5] and Samir H. Patel[3]

[1]Department of Radiation Oncology, Mayo Clinic, Rochester, MN, United States, [2]Department of Health Sciences Research, Mayo Clinic, Phoenix, AZ, United States, [3]Department of Radiation Oncology, Mayo Clinic, Phoenix, AZ, United States, [4]Department of Radiation Oncology, Mayo Clinic, Jacksonville, FL, United States, [5]Google Health, Mountain View, CA, United States, [6]Research Services, Comprehensive Cancer Center, Mayo Clinic, Rochester, MN, United States, [7]Robert D. and Patricia E. Kern Center for the Science of Health Care Delivery, Mayo Clinic, Rochester, MN, United States

Introduction: Organ-at-risk segmentation for head and neck cancer radiation therapy is a complex and time-consuming process (requiring up to 42 individual structure, and may delay start of treatment or even limit access to function-preserving care. Feasibility of using a deep learning (DL) based autosegmentation model to reduce contouring time without compromising contour accuracy is assessed through a blinded randomized trial of radiation oncologists (ROs) using retrospective, de-identified patient data.

Methods: Two head and neck expert ROs used dedicated time to create gold standard (GS) contours on computed tomography (CT) images. 445 CTs were used to train a custom 3D U-Net DL model covering 42 organs-at-risk, with an additional 20 CTs were held out for the randomized trial. For each held-out patient dataset, one of the eight participant ROs was randomly allocated to review and revise the contours produced by the DL model, while another reviewed contours produced by a medical dosimetry assistant (MDA), both blinded to their origin. Time required for MDAs and ROs to contour was recorded, and the unrevised DL contours, as well as the RO-revised contours by the MDAs and DL model were compared to the GS for that patient.

Results: Mean time for initial MDA contouring was 2.3 hours (range 1.6-3.8 hours) and RO-revision took 1.1 hours (range, 0.4-4.4 hours), compared to 0.7

hours (range 0.1-2.0 hours) for the RO-revisions to DL contours. Total time reduced by 76% (95%-Confidence Interval: 65%-88%) and RO-revision time reduced by 35% (95%-CI,-39%-91%). All geometric and dosimetric metrics computed, agreement with GS was equivalent or significantly greater ($p<0.05$) for RO-revised DL contours compared to the RO-revised MDA contours, including volumetric Dice similarity coefficient (VDSC), surface DSC, added path length, and the 95%-Hausdorff distance. 32 OARs (76%) had mean VDSC greater than 0.8 for the RO-revised DL contours, compared to 20 (48%) for RO-revised MDA contours, and 34 (81%) for the unrevised DL OARs.

Conclusion: DL autosegmentation demonstrated significant time-savings for organ-at-risk contouring while improving agreement with the institutional GS, indicating comparable accuracy of DL model. Integration into the clinical practice with a prospective evaluation is currently underway.

KEYWORDS

deep learning, autosegmentation, head and neck cancer, radiation therapy, clinical validation, comprehensive, organs-at-risk

1 Introduction

Head and Neck (HN) cancer is a significant burden on global health, accounting for an estimated5% of world-wide cancer-related mortality in 2020 (1) – similar in magnitude to breast and pancreas cancers – and it is expected that over 700,000 people will die from HN cancer in 2030 (an increase of 38% from 2016) (2). Unfortunately, this burden is shouldered primarily by low and middle income countries lacking adequate capacity and access to radiation therapy (RT), chemotherapy, and surgery (2). RT plays a critical role in the management of HN cancer: it is indicated in an estimated 74% of HN cancer patients per published guidelines and evidence (3).

Delivering function-preserving, curative HN-RT is challenging due to the complex anatomy and the need to balance the competing objectives of delivering adequate radiation dose to the tumor while sparing adjacent organs-at-risk (OARs). A custom RT treatment plan needs to be designed that finds the optimal balance for an individual patient, and the quality of the treatment plan plays an important role in improving clinical outcomes (4). Furthermore, improved survival has been associated with RT provided by high-volume radiation oncologists (ROs) (5). Integral to this process is the accurate segmentation of the OARs, as radiation injury to OARs can lead to a significant detriment in function and quality of life (6), as seen by the high incidence of suicide in patients with HNC (7, 8). This segmentation must also be comprehensive to mitigate the wide range of potential severe adverse effects, ranging from dysphagia and xerostomia to neuropathy and necrosis. Managing these risks requires segmentation not only of the swallowing structures, mandible, mastoid, and salivary glands, but also neurological organs (brachial plexus, brainstem, cord, optic nerves, optic chiasm, and brain), auditory structures (external auditory canal, and cochlea), and optical structures (eye, lens, lacrimal gland, and retina). It has also been demonstrated that risk of stroke (9) and general cerebrovascular events (10, 11) is associated with RT for HN cancer patients, motivating the need for delineation of carotid arteries (CAs).

High-quality RT for HN cancer patients requires accurate and comprehensive OAR segmentation. Our institutional guidelines define 42 OAR structures that may be contoured for HN cancer patients (see Table S1 in the Supplemental materials). While the specific OAR structures required for treatment planning for each patient varies depending on the site, extent, and staging of the disease, each of these structures has situations in which it is necessary to include it. In addition, having a comprehensive set of contours included in the patient's data set simplifies the collection of dose-volume histogram (DVH) data for outcomes analysis. HN anatomy is complex, and manual segmentation of them is particularly time-consuming and requires significant investment in personnel resources (12). Furthermore, heterogeneity in the quality of manually segmented structures has been widely reported (13–15). Ultimately, the requirements for manual contouring of OARs can be a barrier to patient access for intensity-modulated RT for HN cancer, particularly in low and medium resource environments.

There is great interest in expanding indirect access to high-quality RT *via* autosegmentation tools using deep learning (DL) models informed by expert-level contouring experience (16). These autosegmentation tools have the potential to produce efficiency gains and standardization in the treatment planning process (16). Consequently, there has been much interest in pursuing these models (17–19), but to date there has not been widespread clinical adoption. One limitation is that none of the reported models provides a comprehensive set of all recommended OARs for HN cancer (20). For instance, the brachial plexus (BP) is often not included in the model, despite having both an important role in

treatment planning and generally requiring substantial time to contour (21). In addition, the segmentations produced by these models generally require substantial manual edits of multiple OARs in order to be accurate enough for treatment planning.

One common challenge for deep learning (DL) tools in autosegmentation for RT is the absence of training and validation datasets of sufficient size, consistency, and quality (16). At our institution, all OAR segmentation is governed by a detailed set of institutional standards, primarily based on international consensus guidelines (20). Using these standards, two of the authors (both HN-expert ROs) were given protected time away from clinical responsibilities to contour on retrospectively-collected patient datasets, and without the time constraints experienced during daily clinical practice, spending an average of more than 11 hours per patient dataset (21) (exceeding the typical amount of time available for a clinical case). This effort resulted in a consistent "gold standard" (GS) dataset that best reflects the international consensus and institutional standards for 490 retrospectively-identified patients (21). Using this foundation, a 3D U-Net convolutional neural network (19) was trained using the planning computed tomography (CT) images and curated set of 42 OARs from 445 of these patients.

The standard contouring workflow using humans only is time intensive. We hypothesize that a DL-assisted workflow could significantly reduce contouring time compared to a fully manual workflow. Here, we report the results of a randomized, single-blind observational study comparing the OAR contouring workflow with and without the use of our DL autosegmentation for a hold out (HO) cohort of 20 patients' data available from the GS that had not been previously used for model training, testing, or validation. The study assessed the feasibility of integrating the model into clinical practice and readiness for external validation by measuring the potential time-savings, geometric agreement with the institutional gold standard contours for each patient, and dosimetric impact.

2 Materials and methods

2.1 OAR contouring workflow

Our department has developed a comprehensive set of OAR contouring guidelines that is used for all campuses. The HN OAR guidelines were primarily developed by three of the authors of this study, two HN-expert ROs (SHP and RLF) and a senior certified medical dosimetrist (AEH). It was based on international consensus guidelines (20) and standardized nomenclature (22). Training was provided to all staff involved in contouring after the adoption of the guidelines, and a detailed electronic document was distributed as a reference.

The contouring workflow at our institution starts with initial contouring performed on a patient's planning CT (pCT) by a member of the dosimetry staff: either a CMD or medical dosimetry assistant (MDA). The MDA's role is data preparation for treatment planning, with a large focus on OAR contouring (for which they receive extensive training). The RO reviews and revises the OAR contours and adds the target volumes. These final contours are then used for treatment plan design.

2.2 Selection of patient data sets

This study was conducted at two campuses of Mayo Clinic, a National Cancer Institute-designated comprehensive cancer center within an academic medical center in the United States, with data collected under approval by the Mayo Clinic institutional review board. Retrospective chart data including CTs for adult patients (age > 18 years) receiving HN-RT between January 1, 2016 and October 1, 2020 were collected. Patients were included if they had a pCT for external beam RT (either with x-rays or protons) that was acquired according to the departmental standard protocol with 2 mm slice thickness. Patient data was excluded if the patient was not in a thermoplastic mask, if the pCT contained a proton-specific range-shifting device, or if a small field-of-view reconstruction of the planning CT was not available. Patient data were not automatically excluded on the basis of previous surgery and/or RT; however, each of those cases was reviewed by an author who was a HN-expert RO (RLF or SHP) prior to inclusion to ensure that the anatomical changes associated with the previous treatment still allowed for identification of the majority of OARs of interest. Typical voxel size was 1.27 x 1.27 x 2 mm^3. A total of 490 patient data sets were collected and anonymized for model development and evaluation.

2.3 Curation of gold standard data sets

The same two HN-expert RO-authors (referred to as the RO-As below) who developed the institutional contouring guidelines were given time away from clinical duties to create a set of OAR contours for each of the 490 collected patient data sets, assisted by members of the dosimetry team. The dosimetry team was composed of certified medical dosimetrists and MDAs. The contouring staff had access to the pCT, a small field-of-view reconstruction, and – if available – a contrast-enhanced CT, but not the contours used for the patient's treatment. Due to the protected time, and retrospective nature of the curation, the contouring team was able to spend a mean of 11.6 hours per case during curation. The data curation process and infrastructure is discussed elsewhere (21). The 3D representation and select CT slices with contours for the GS are shown in Figures 1 for a sample patient, with additional representative slices is given in Figure S1 of the Supplemental material (Figure S1).

2.4 Model architecture and training

The deep learning model was based on a single, custom 3D U-Net architecture (Figure 2). This architecture has been shown to be well-adapted to the complexity of medical image segmentation and has been shown to perform very well compared to other architectures and approaches (19, 23, 24). The model was adapted from the model used by Nikolov, et al. (19) and is fully 3D: it operates on 32x512x512 voxel sub-volumes of a CT. This is the largest sub-volumes used by any previously reported 3D autosegmentation model (19, 25–62). The model consists of 6

10.3389/fonc.2023.1137803

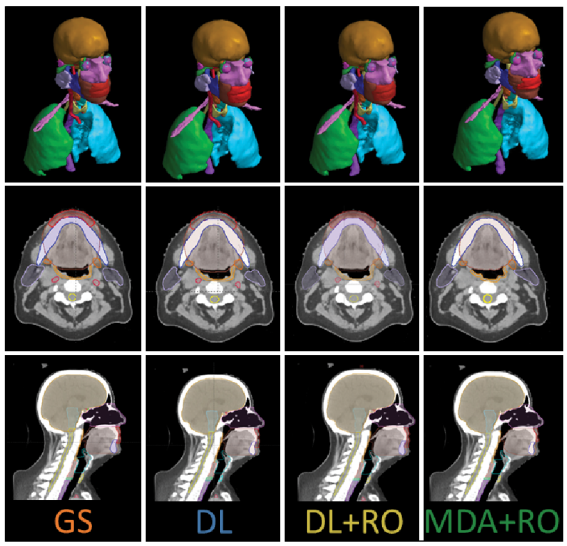

FIGURE 1
3D visualization, and an axial and sagittal slice of the CT with the contours from the gold standard (GS) dataset, as well as the DL, DL+RO, and MDA +RO contours for a representative patient.

convolution blocks each for the encoding and decoding directions, and outputs 42 binary OAR labels for each input voxel (discussed in details in section 2 of the Supplemental material). The number of slices used in each subvolume and the number of convolution blocks was chosen because the authors felt it would achieve a satisfactory balance between providing the model with enough depth to appropriately handle the complexity of the contouring task while also being computationally tractable for model training and inference.

The model was trained on TPUv3 with spatial partitioning using a hybrid loss function consisting of a region-based Dice loss and a voxel-wise focal loss to account for the large variability in OAR sizes. This model was initially re-trained using 544 retrospectively identified patient datasets that were not included in the GS. Training and inference were done using only the GS contours and the planning CT, without access to any additional image series or reconstructions. Some patients were missing structures due to previous surgical excision. In such cases, the DL model was simply presented with an empty contour for the corresponding structure and not given any additional guidance or patient metadata. The empty contours served as negative examples during model training. The model's ability to omit the missing structures was then assessed by computing a contingency table for the presence of the contour compared to the presence in the GS structure set. 312 CTs were used for training, 51 for validation, and 82 for testing (the remaining data sets were held out for the clinical feasibility study reported here). After inference, the binary masks were post-processed to produced vectorized contours that were stored as DICOM-RT Structure Set representations. Further details are provided in the section 2 of the Supplemental material.

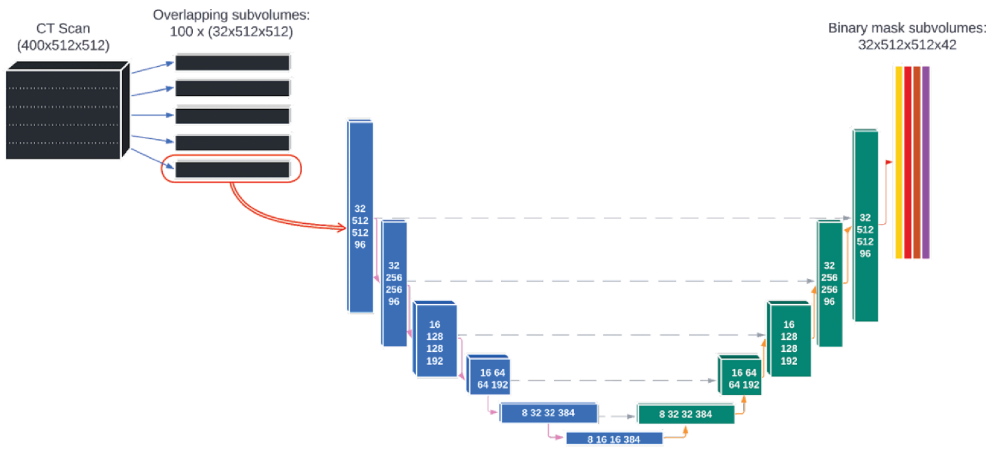

FIGURE 2
The architecture of the deep learning model used for autosegmentation of organ-at-risk for head and neck cancer radiation therapy.

2.5 Study design

Under the approval of the institutional review board, we recruited as participants ROs and MDAs who were staff members with HN contouring expertise at our institution for the observational study. Participants were consented by the departmental clinical trials team. Prior to the recruitment period (11/3-11/10/2021), the model was finalized (AI-HN-v3b) and a study protocol pre-specification was publicly released (63). The staff members were eligible to participate if OAR contouring for HN patients was a part of their regular practice and were excluded if they had been involved in the data curation, model training or validation for this project.

The HO datasets, withheld from model training, testing, and validation, were prospectively selected from a pool of retrospective candidate datasets with an emphasis on diversity in terms of anatomic subsites of disease, surgical status (including both definitive and adjuvant RT), and traditional patient demographical information (race, sex, and ethnicity). 20 patient datasets were selected with patient characteristics given in Table S2 of the Supplemental materials. For each patient data set, one set of OAR contours was created by an MDA participant and a second set was generated by the DL model. Using block randomization without replacement (Figure 1), a RO participant was allocated to review and revise each set of initial contours (blinded to their origin) to make them acceptable for clinical treatment planning. In this way, the initial MDA contours with RO-revisions is the standard arm of the study, representing the fully manual contouring workflow, and the RO-revisions of the DL contours represents the experimental arm. These arms will be referred to as MDA+RO and DL+RO, respectively. To achieve balance between the arms, each participating RO was assigned an equal number of cases for each arm, and the ROs were not assigned to both arms for the same patient to avoid the effects of recall. Randomization was completed by the statistical team and entered in the REDCap database to ensure blinding for the rest of the study team using a REDCap database (REDCap Cloud, Encintas, CA). A CONSORT-AI reporting checklist is provided in the Supplemental materials (section 7).

2.6 Study endpoints

2.6.1 Time savings

The primary endpoint was reduction in the total time to complete OAR contouring for participants. Timing was calculated from manual review of the contouring session recorded using screen-capture software (Capture, Kaltura, New York, NY), excluding any significant period of time without activity (greater than 5 minutes). For the MDA+RO arm, the time required for the MDA to perform initial contours and the RO to revise them was collected, and the total time for both participants was computed.

2.6.2 Evaluation of missing structures

The model's ability to identify and omit missing structures was assessed by computing a contingency table for the presence of the contour compared to the presence in the GS structure set.

2.6.3 Comparison of geometric agreement with gold standard

For each patient, the geometric agreement with the GS contours was assessed with multiple measures for the MDA+RO, and DL+RO contours, as well as the unrevised contours from the autosegmentation model (which will be referred to as the DL arm) with multiple measures: volumetric Dice similarity coefficient (64) (VDSC), surface Dice similarity coefficient (SDCS, with τ=1, 1.5, 2, and 3mm) (19), 95-percentile Hausdorff distance (64) (HD95%), added path length (APL, computed with tolerances of 1, 2, 3, and 5 mm) (65), precision (64), sensitivity (64), contour Dice coefficient (CDC) (66), and the change in volume and centroid of structure.

2.6.4 Comparison of impact on treatment plan dosimetry

To facilitate a comparison of the dosimetric impact of the autosegmentation, a new reference treatment plan was generated for each patient using the OAR structures generated by the DL model before RO revisions. The choice to use the DL contours (without RO revision) for the OARs for the reference plan was made to allow a comparison of the quality of the plan designed using the DL model being evaluated against the GS contours, and to assess the feasibility of running a prospective trial using the unrevised DL contours for treatment planning. The clinical target volumes (CTVs) were taken from the patient's previously delivered treatment plan, and planning target volumes were generated from them by performing a uniform 3mm expansion (cropped to the patient's body surface). Each patient had between one and three prescription dose levels. These OARs were briefly reviewed to detect major defects by MDAs (who were not study participants), and minor post-processing was performed consistent with routine clinical practice. The review and post-processing process was not allowed to take more than 15 minutes, no major defects were noted, and the VDSC was compared before and after the post-processing to ensure that no significant changes were made to the contours. The prescription dose levels for each plan were determined by the RO-As based on the department's guidelines for conventionally fractionated x-ray treatments based on the patient's disease site and treatment intent, ranging from 54 Gy to 72 Gy total dose in fractions of 1.8 to 2.12 Gy. CMDs with significant HN planning experience worked with the RO-As to create a 6 MV volumetric modulated arc therapy treatment plan, with treatment objectives adapted by the RO-As to the specific patient based on institutional guidelines.

Ultimately, HN RT treatment planning is challenging because it involves balancing a complex set of trade-offs to achieve the optimal plan for a given patient. That means assessing the clinical impact of contour accuracy on treatment planning requires looking not just at the impact on one DVH statistic, but also on how it impacts the overall trade-offs that inform plan quality. To quantify this impact, we adapted the concept of the plan quality metric from Nelms, et al. (67). A plan quality metric scoring template was built from DVH statistics for both target volumes and OARs derived from the institutional planning guidelines for HN cancer (see Table S2 in

the Supplemental material). To account for the variation in the number of target levels and OARs between patients within the HO cohort, the plan quality metric score for a given set of contours was reported as the percentage of the maximum possible value of the plan quality metric given the structures present, which we refer to as the normalized plan quality metric (NPQM).

The focus of this study was the agreement of the DVH statistics and NPQM with the GS for the contours on each arm (rather than a plan quality study), so all dosimetric statistics were reported as the absolute value of the difference between the experimental arm and the GS. Using the reference dose distribution for each patient, the mean dose (Dmean) and D0.03cc were computed for the region of the OAR contours that was not overlapping with the PTVs. If the volume of the contour that was non-overlapping with the targets was less than 0.1cc, that contour was excluded from dosimetric analysis. All dose-volume statistics were extracted using a commercial treatment plan quality software (ProKnow Systems, Sanford, FL, USA). The mean value of the absolute difference in the OAR's mean dose (|ΔDmean|) and D0.03cc (|ΔD0.03cc|) between the arms were computed for all structures, and for each individual OAR. In addition, the percent difference in NPQM relative to the GS (|ΔNPQM|) is reported.

2.6.5 Participant survey

Surveys were administered to understand the RO's experience reviewing and revising the contours and their perceived quality. After each case was completed, a survey was administered to the ROs who were still blinded to the origin of the contours. The survey included questions on subjective quality, clinical impact, and task load (68, 69) for that case. After all allocated cases were completed, an exit survey was administered to the RO in which cases were unblinded, allowing ROs to comment on the use of the DL model for autosegmentation.

2.7 Statistical methods

Data analysis was performed using SAS v9.04 and R v3.6.2. Categorical values are reported in terms of absolute and relative frequencies, while continuous variables are described in terms of mean and 95% confidence intervals (95%-CI). Prior to the study, we hypothesized that a 30% time-savings with the deep learning model would be clinically significant. Based on previous internally collected data on timing results showing a reduction in contouring time of approximately 65% (standard deviation 20%), we conservatively estimated that the time-savings in this study would be 50%. From these estimates, we would have 92.4% power to demonstrate that the time-savings was significantly more than 30% (with a one-sided significance level of 0.025) using a sample size of 20 patient datasets. All other group comparisons were performed using independent two-sided paired *t*-tests with significance level of 0.05.

3 Results

3.1 Recruitment and study completion

The study recruited 8 ROs and 8 MDAs to participate. The study was run from 12/6/2021 through 1/31/2022, and two sets of RO-revised contours were obtained for each of the 20 patient data sets. However, one CT dataset had to be excluded from comparison due to unintentional data cross-over during the blinding process. Analyses were performed only on the remaining 19 datasets. Figures 1B shows the contours for a representative patient from both arms, as well as the un-revised contours from the DL and GS contour sets.

3.2 Time savings

The mean contouring times are presented in Table 1. The total contouring time for the MDA+RO contouring time was 3.4 hours, compared to 0.7 hours for the revisions to the DL contours, a time savings of 76% (95% CI: 65% - 88%). In addition, the RO revisions to the DL contours showed a non-significant reduction compared to the revisions of the MDA contours of 35% (95% CI, -39%-91%, p=0.09). For all cases, the DL revision time was less than the combined MDA+RO time.

3.3 Missing structures

The DL model correctly identified the presence of 818 OAR structures and omitted no structures that were present (100% sensitivity). The DL model correctly identified that 15 structures were not present, and incorrectly identified the presence of 7 that were not present (68% specificity).

For clinical cases at our institution, the ROs are responsible for contouring the BPs or CAs. As part of the blinding process, no empty (placeholder) structures for the BP or CA structures in the structure set were added for the MDA-derived contours. The unanticipated result was that for the MDA+RO arm, the ROs did not add the CAs in any cases and only added 13 pairs of BP

TABLE 1 Mean time (95%-CI) for MDA initial contouring, and physician revisions of the MDA and DL contouring for all patients (N=19).

Arm	MDA Contouring (hour)	RO Revision (hour)	Total (hour)
MDA+RO	0.7 (0.6 – 1.6)	1.1 (0.4-4.4)	3.4 (2.9-3.9)
DL+RO	n/a	0.7 (0.6 – 1.6)	0.7 (0.6 – 1.6)
Time Savings	n/a	35% (65% - 88%)	76% (-39% - 91%)*

*Indicates a statistically significant (p<0.05) difference.

contours, although these structures were present in all 19 cases (and were correctly identified by the DL model). As such, the CAs and missing BPs were excluded from all aggregate statistics and comparisons. However, while no comparisons are performed, the geometric similarity of the CAs with the GS is shown for the DL and DL+RO arm for reference.

3.4 Geometric agreement with gold standard

All geometric and dosimetric comparisons and analysis were performed only for structures that were present in all 4 arms for a given patient. With this criteria, there were 777 structures (3108 total contours) that were eligible for analysis from the 19 patients, representing 40 OARs.

3.4.1 DL+RO arm *vs* MDA+RO arm

Comparing the agreement between the final, RO-revised contours from the DL model (DL+RO) to the final contours from the MDA+RO allows us to assess the impact of the DL model on the current workflow. The mean value of the geometric agreement metrics for all experimental contours compared to the GS are given in Table 2 (additional metrics are in section 4 of the Supplemental material). The agreement with the GS of the DL+RO contours was significantly better than for the MDA+RO contours for all geometric metrics except for sensitivity and specificity (for which there was no significant difference). The mean VDSC for the DL +RO contours was 0.86 ± 0.01 compared to 0.78 ± 0.01 for the MDA+RO.

Categorizing the contours by OAR, the mean VDSC, HD95%, APL-1mm, and SDCS-1mm are shown in Figures 3–6 and Table S5 of the Supplemental material l. 32 of the OARs had a mean VDSC greater than 0.8 for DL+RO arm, compared to 20 for the MDA+RO arm. In addition, all OARs showed either a significantly better agreement for the DL+RO contours or no difference, compared to the MDA+RO by all 4 metrics (summarized in Table 3 from the full data provided in Table S5 of the Supplemental material), with one exception (while the pharyngeal constrictor muscles showed better agreement with VDSC and SDCS-1mm for the DL+RO arm and no significant difference as measured by HD95%, there was a better agreement for the MDA+RO as measured by APL-1mm). Better agreement was demonstrated for most OARs for the DL+RO arm using VDSC and APL, while most showed no difference according to HD95%.and SDCS-1mm.

3.4.2 DL+RO arm *vs* DL arm

The comparison of the unrevised (DL) and revised (DL+RO) contours enables an assessment of the quality and consistency of the DL model. The mean agreement with the GS for all contours was significantly better for the unrevised contours compared to the revised ones (Table 2) except for volume and centroid (no statistical differences). Overall, there was very strong agreement with the GS both before and after the revisions: mean VDSC was 0.87 ± 0.01 and 0.86 ± 0.01 for the DL and DL+RO contours, respectively. In addition, before Dean RO-revisions, only 4 of the 777 (<1%) individual contours from the DL model had a VDSC < 0.5 compared to GS, and none of the RO-revisions improved agreement to be greater than 0.5. In addition, there were 3 contours that showed VDSC > 0.5 before RO revisions to the DL model contours, but the revisions reduced agreement below 0.5.

Figures 3–6 also show the agreement with the GS broken down by OAR for both the DL and DL+RO contours (as well as in Table S5 of the Supplemental material). For each of the metrics, none of the OARs showed significantly better agreement with GS after RO revisions compared to before (Table 3): in fact, most showed no differences. However, 2 more OARs had a mean VDSC greater than 0.8 for the DL arm, bringing the total to 34 compared to 32 for the DL+RO arm. The explicit change in geometric agreement with the GS of the RO's revisions is summarized in Figure 7. The mean change in the VDSC compared to GS was not significantly different from zero (p=0.8). There were no individual cases in which the RO-revisions resulted in an improvement of larger than 0.05, and 22 (3%) revisions decreased the agreement by more than 0.1.

TABLE 2 Mean value (95%-CI) of select metrics of geometric agreement between each experimental arm and the GS for all contours for comparison (N=777).

Metric	DL (95%-CI)	DL+RO (95%-CI)	MDA+RO (95%-CI)
VDSC	0.87 (0.01)*	0.86 (0.01)	0.78 (0.01)*
HD95% (mm)	2.2 (0.1)*	2.8 (0.2)	5.3 (1.2)*
APL-1mm (mm)	19.1 (1.9)*	21.6 (2.2)	25.5 (2.5)*
SDCS-1mm	0.81 (0.01)*	0.78 (0.01)	0.70 (0.01)*
ΔVolume (cc)	0.9 (0.6)	1.3 (0.8)	-3.0 (1.2)*
ΔCentroid (mm)	0.8 (0.1)	0.9 (0.1)	1.8 (0.3)*
Precision	0.87 (0.01)*	0.86 (0.01)	0.77 (0.01)*
Sensitivity	0.89 (0.01)*	0.87 (0.01)	0.88 (0.01)
Specificity	1.0 (0.0)*	1.0 (0.0)	1.0 (0.0)
CDC-1mm	0.77 (0.01)*	0.73 (0.01)	0.64 (0.02)*

*Indicates a statistically significant (p<0.05) difference with the DL+RO arm.

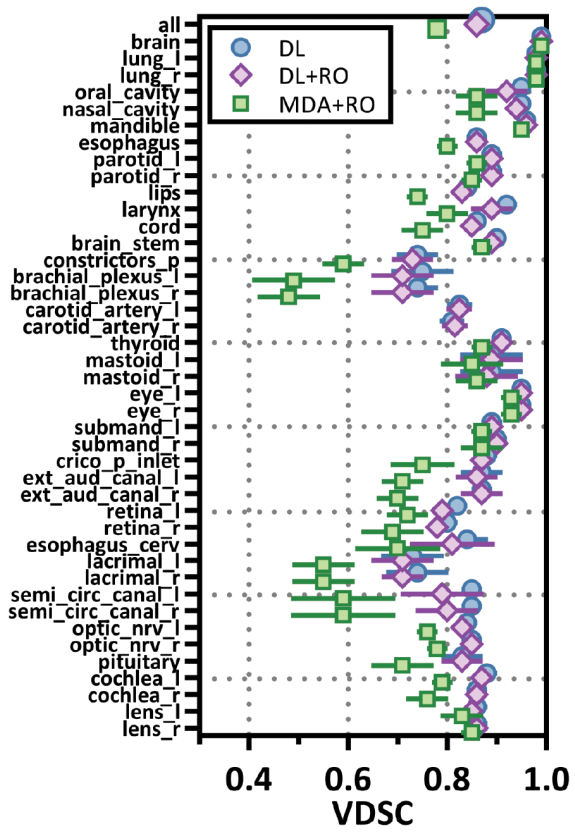

FIGURE 3
Mean volumetric Dice similarity coefficient (VDSC) and 95% confidence intervals for the unrevised deep learning (DL), radiation oncologist (RO) revised deep learning (DL+RO), and RO-revisions to the initial MDA contours (MDA+RO), categorized by organ-at-risk type and for all OARs. OARs listed in order of decreasing volume.

3.5 Dosimetric impact

The average magnitude of the difference of the D0.03cc, mean dose, and NPQM relative to the GS for the DL, DL+RO, MDA+RO contours for all OARs are shown in Table 4. There is no significant difference in the agreement of the NPQM with the GS between the DL+RO contours and either the DL or the MDA+RO contours. In terms of D0.03cc and Dmean, the agreement with the GS was significantly better for the DL+RO contours compared to the MDA +RO contours, (DL contours showed significantly better agreement than DL+RO). The dosimetric data for each OAR are shown in Table S11 of the Supplemental material. The DL+RO contours had significantly better agreement than the MDA+RO contours with the GS in terms of D0.03cc and the mean dose for 5 and 9 of the OARs, respectively, while there was no significant difference in agreement between the DL and DL+RO contours for any OAR.

3.6 Participant survey

While still blinded to the origin of the contours, ROs reported they did not need to make any edits of major clinical significance to the DL contours and reported fewer edits of any significance compared to the MDA contours (Figure 8). ROs rated their subjective impression of the quality of all DL contours from "somewhat satisfied" to "completely satisfied" and all indicated that they were "very interested" in using the DL contours for clinical cases. Complete survey results are available in section 6 of the Supplemental materials.

4 Discussion

The potential of this DL autosegmentation model to be integrated in the clinic and undergo external validation was investigated using a multi-observer randomized trial. Eight ROs with significant experience in HN cancer participated in the study, reviewing and revising two sets of contours (one manually delineated by MDAs, the other from the DL model) for 19 patient datasets. The scale of this study, in terms of both number of participants and patient data sets, is meant to represent the clinical practice at our large institution (and applicability at other institutions). The use of comparisons to an independent GS dataset is a key novelty of this study: created without the demands on the

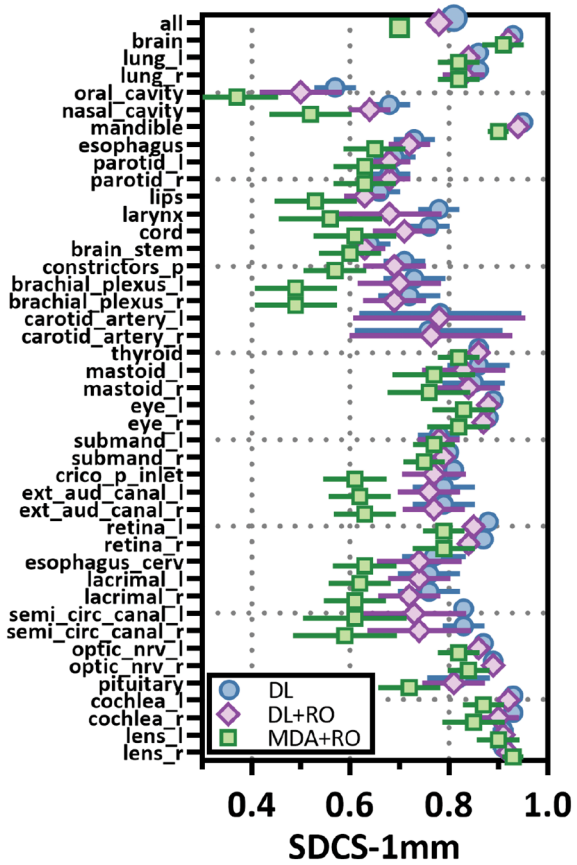

FIGURE 4
Mean surface Dice similarity coefficient (SDSC) with a 1mm tolerance, and 95% confidence intervals for the unrevised deep learning (DL), radiation oncologist (RO) revised deep learning (DL +RO), and RO-revisions to the initial MDA contours (MDA+RO), categorized by organ-at-risk type and for all OARs. OARs listed in order of decreasing volume.

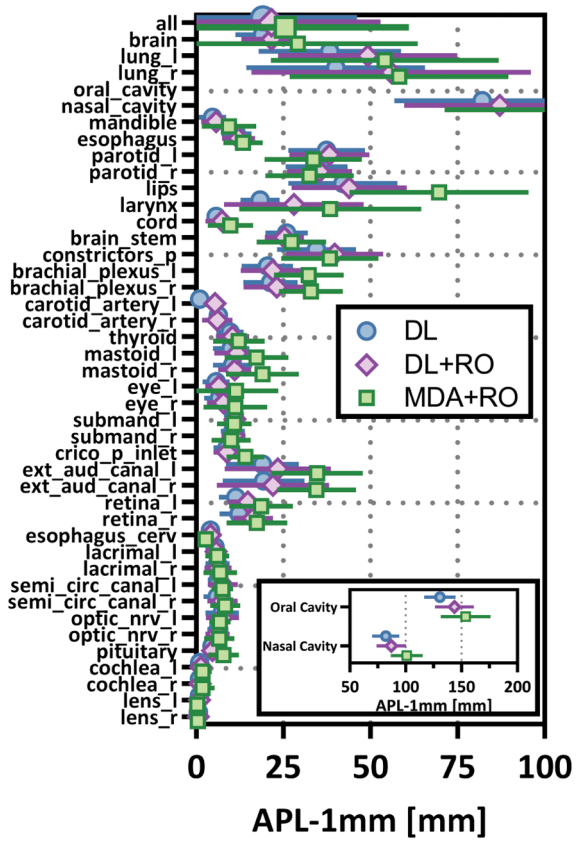

FIGURE 5
Mean added path length (APL) with a 1mm tolerance, and 95% confidence intervals for the unrevised deep learning (DL), radiation oncologist (RO) revised deep learning (DL+RO), and RO-revisions to the initial MDA contours (MDA+RO), categorized by organ-at-risk type and for all OARs. OARs listed in order of decreasing volume.

time that routine clinical practice imposes, the GS in this study represents the realization of the institutional contouring standards derived from international consensus guidelines. The independence of the GS enables us to assess the effect of the DL model in terms of agreement with the institutional standards, in addition to finding differences between the standard and DL-assisted workflows.

The DL-assisted workflow demonstrated significant time savings compared to the standard workflow of 76% reduction (2.7 hours). Furthermore, this reduction in time may underestimate the true time savings, as the CAs and many of the BPs were not contoured in the MDA+RO arm but were reviewed and revised by the ROs on the DL +RO arm. These are complex and often time-consuming OARs to contour: during the GS curation process, it took an average of 33 minutes to manually contour the CAs and 56 minutes for the BPs (21). While all of the OARs may not be required for treatment planning for an individual patient, in our existing workflow the MDAs are expected to contour all of them (except the BP and CA), so this increased efficiency translates to the clinical practice. Crucially, these efficiency gains did not result in lower quality contours. On the contrary, whether for the aggregate statistics for all 777 analyzed structures or categorized by OAR, the geometric and dosimetric agreement with the GS either showed no statistical difference or favored the DL+RO arm relative to the MDA+RO (except for the pharyngeal constrictors, which showed improved agreement for the MDA+RO using APL-1mm but not any other metrics). Ultimately, the DL model has potential to reduce contouring time while improving standardization across the clinic.

The RO's revisions to the DL contours tended to be very minimal, indicating excellent performance by the model. The mean change in VDSC before and after the revisions was not significantly different from zero and there were no revisions resulting in an increase of VDSC greater than 0.06. This finding holds with SDCS-1mm and APL-1mm, which have been shown to have a strong correlation with time-savings (19, 32, 65), and HD95% which is often used to assess treatment planning impact. Importantly, the quality of the DL contours was evident by the fact that the ROs required less time to revise them compared to the MDA contours (an average reduction of 0.4 hours per patient, or 35%). This was also evident in the RO's subjective assessment of contour quality. While still blinded to the origin of the contours, the physicians indicated higher satisfaction with the DL contours and reported that none of the revisions were of major clinical significance. After unblinding, the ROs all expressed interest in using this tool clinically. The contours produced by the DL model have potential to be used for clinical treatment planning with at most minor revisions.

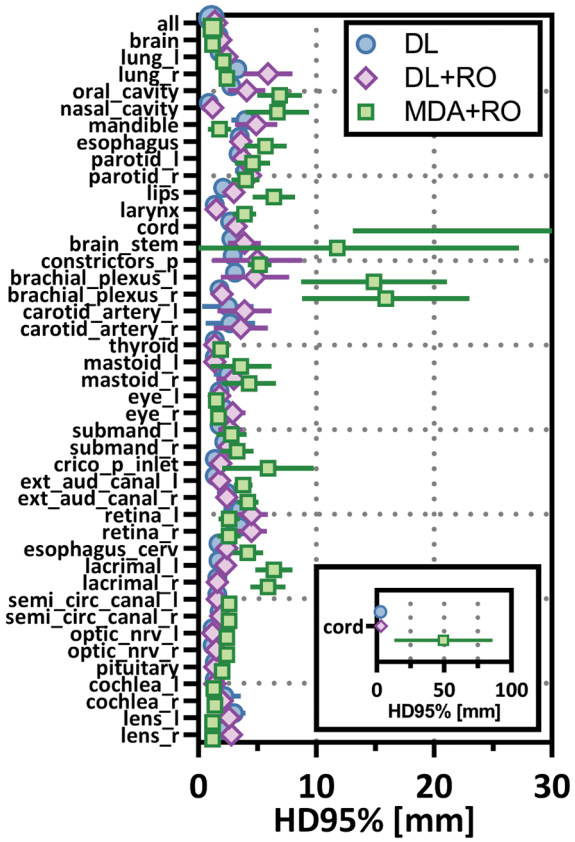

FIGURE 6
Mean 95%-percentile Hausdorff distance (HD95%) with a 1mm tolerance, and 95% confidence intervals for the unrevised deep learning (DL), radiation oncologist (RO) revised deep learning (DL+RO), and RO-revisions to the initial MDA contours (MDA+RO), categorized by organ-at-risk type and for all OARs. OARs listed in order of decreasing volume.

While there have been many published reports of DL-based autosegmentation using 3D U-net architectures, as well as other approaches, the performance of this model is noteworthy (19, 25–62). Model performance was most frequently reported in terms of VDSC, and often a threshold of 0.8 was used for clinical acceptability. In this study, for the 777 analyzed structures, the mean VDSC for the unrevised DL contours was 0.87 ± 0.01, and that 34 of the included OARs showed a mean VDSC of greater than 0.8 (with none less than 0.73). In comparison, none of the other studies report more than 16 OARs which showed a VDSC greater than 0.8 with their reference structures (Figure 9, please see section 5 of the Supplemental materials for further discussion). In addition, this model contains 10 OARs that are not reported elsewhere in the literature. This is the first demonstration of a DL-model that produces the comprehensive set of HN OAR contours needed for treatment planning at our institution: the model demonstrated excellent performance for 42 OARs.

The accuracy, reliability, consistency of this of model for all 42 OARs against the institutional GS reflects well on both the quality and quantity of the curated data as well as the appropriateness of the model architecture and training process. Providing adequate resources to produce a large, standardized, and high-quality dataset provided a strong foundation for both model training and validation. In addition, deep learning in general (and 3D U-Nets

TABLE 3 Number of OARs demonstrating statistically significant differences ($p<0.05$) in agreement with gold standard between arms for select measures of geometric similarity between the DL and DL+RO contours, and MDA+RO and DL+RO contours, and if the difference is significant, which arm showed better agreement with gold standard.

Metric	DL v DL+RO			MDA+RO v DL+RO		
	No Difference	Favor DL	Favor DL+RO	No Difference	Favor DL+RO	Favor MDA+ RO
VDSC	38	2	0	8	32	0
HD95% (mm)	35	5	0	32	8	0
APL-1mm (mm)	29	11	0	32	7	1
SDCS-1mm	30	10	0	27	13	0

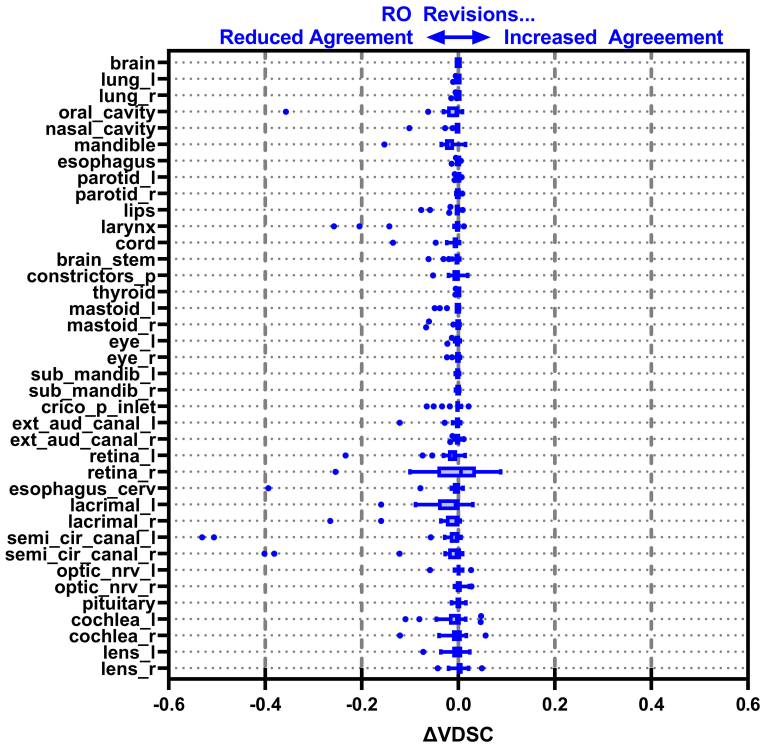

FIGURE 7
Box-and-whisker plot showing the change in agreement with the gold standard (GS) before (DL) and after (DL+RO) the radiation oncologist's (RO's) revisions to the deep learning (DL) contours measured by volumetric Dice similarity coefficient (VDSC). A positive value indicates that the revisions improved agreement with the GS, and a negative value indicates reduced agreement. OARs listed in order of decreasing volume.

TABLE 4 Mean agreement with gold standard using dosimetric comparisons.

Metric	DL (95%-CI)	DL+RO (95%-CI)	MDA+RO (95%-CI)
|ΔD0.03cc| (Gy)	0.6 (0.1)*	0.8 (0.2)	1.2 (0.2)*
|ΔDmean| (Gy)	0.4 (0.1)	0.4 (0.1)	0.8 (0.1)*
|ΔNPQM| (%)	1.3 (0.8)	1.7 (1.2)	3.0 (1.4)

*Indicates a statistically significant ($p<0.05$) difference compared to the DL+RO arm.

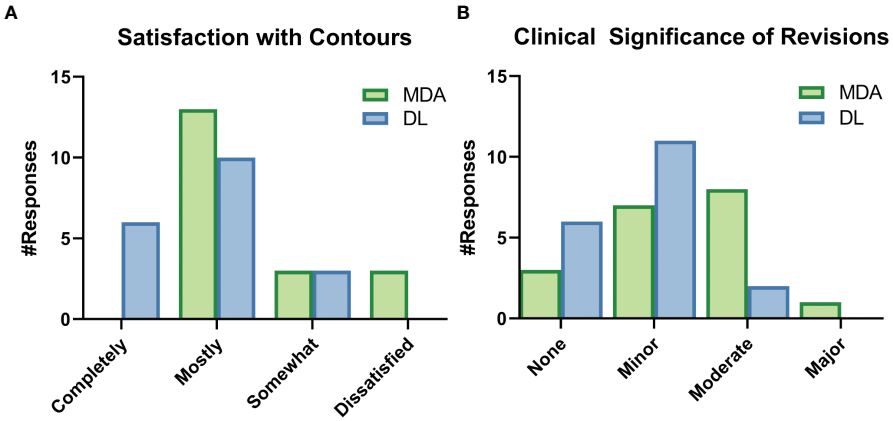

FIGURE 8
Selected results from the survey given to radiation oncologists (ROs) after completion of revision of a particular dataset. These survey questions were asked while the ROs were still blinded to origin of the initial contours, either by a medical dosimetry assistant (MDA) or the deep learning (DL) model. **(A)** The ROs were asked to rate their satisfaction with the initial contours, as well as **(B)** rate the clinical significance of the revisions to the contours.

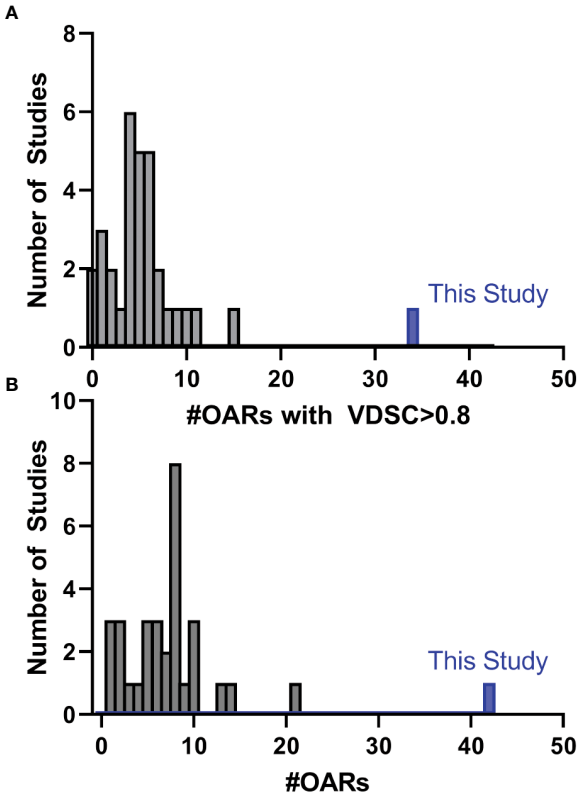

FIGURE 9
Histogram showing the number of studies found during the literature that reported the number of distinct OARs (of those used in this study) that had **(A)** a mean VDSC greater than 0.8 or **(B)** the total number of OARs included in the study that corresponded with those in this study. Detailed discussion is given in section 5 of the Supplemental material.

specifically) have been shown to have advantages over other reported approaches to HN autosegmentation (16, 19, 23, 24, 32, 34). The architecture of this model is unique because of both the size of the 3D sub-volumes it uses and the depth of the network (six layers), which enabled the creation of a model of sufficient complexity to tackle this challenging problem. Ultimately, this process required a very significant investment in terms of curation efforts and model training. In the end, differences in the model architecture, training method, and training data contribute to the differences between this model and previously reported models.

The purpose of this study was to assess whether the current DL model was ready for clinical integration and external validation. As such, although the hold out cohort of 19 patients was selected to be as representative of the US population as possible (and is large compared to other studies), it is still a limited sample size and number of participants (8 ROs). Naturally, this single-institution study on retrospective data is limited in terms of more general applicability: prospective study of the impact on clinical integration in our clinic and an external validation study are in development. Since the institutional standards are based on international consensus guidelines, this model could have applicability for many institutions. The benefits of an accurate and widely available autosegmentation tool would include providing access to comprehensive organ-sparing RT to patients throughout the world, particularly in low-resource environments.

5 Conclusion

A DL model capable of highly accurate autosegmentation of a comprehensive set of 42 HN OARs was demonstrated to provide significant time-savings in a blinded randomized controlled trial involving 19 patient datasets and 8 ROs. The DL contours have the potential to be used for clinical treatment planning with, at most, minor revisions. An interventional clinical trial is being developed to prospectively assess the capability of the model in patient care as well as external validation.

Data availability statement

The raw data supporting the conclusions of this article will be made available by the authors, without undue reservation.

Ethics statement

The studies involving human participants were reviewed and approved by Mayo Clinic Institutional Review Board. The patients/participants provided their written informed consent to participate in this study. Written informed consent was obtained from the individual(s) for the publication of any potentially identifiable images or data included in this article.

Author contributions

All authors were involved in study design, execution of the study, data analysis, writing of the manuscript and final manuscript approval. TD, TL and JL were responsible for statistical analysis. All authors contributed to the article and approved the submitted version.

Acknowledgments

The contributions of project managers LiHong Xi and Arnold Blauert were critical to the timely completion of this enormous study. Prior to the recruitment of study participants, the study design and methods were published as a pre-print on medRxiv (63).

Conflict of interest

The authors declare that the research was conducted in the absence of any commercial or financial relationships that could be construed as a potential conflict of interest.

Publisher's note

Supplementary material

The Supplementary Material for this article can be found online at: https://www.frontiersin.org/articles/10.3389/fonc.2023.1137803/full#supplementary-material

References

1. Sung H, Ferlay J, Siegel RL, Laversanne M, Soerjomataram I, Jemal A, et al. Global cancer statistics 2020: GLOBOCAN estimates of incidence and mortality worldwide for 36 cancers in 185 countries. *CA Cancer J Clin* (2021) 71(3):209–49. doi: 10.3322/caac.21660

2. Patterson RH, Fischman VG, Wasserman I, Siu J, Shrime MG, Fagan JJ, et al. Global burden of head and neck cancer: economic consequences, health, and the role of surgery. *Otolaryngol Head Neck Surg* (2020) 162(3):296–303. doi: 10.1177/0194599819897265

3. Atun R, Jaffray DA, Barton MB, Bray F, Baumann M, Vikram B, et al. Expanding global access to radiotherapy. *Lancet Oncol* (2015) 16(10):1153–86. doi: 10.1016/S1470-2045(15)00222-3

4. Peters LJ, O'Sullivan B, Giralt J, Fitzgerald TJ, Trotti A, Bernier J, et al. Critical impact of radiotherapy protocol compliance and quality in the treatment of advanced head and neck cancer: results from TROG 02.02. *J Clin Oncol* (2010) 28(18):2996–3001. doi: 10.1200/JCO.2009.27.4498

5. Boero IJ, Paravati AJ, Xu B, Cohen EE, Mell LK, Le Q-T, et al. Importance of radiation oncologist experience among patients with head-and-neck cancer treated with intensity-modulated radiation therapy. *J Clin Oncol* (2016) 34(7):684. doi: 10.1200/JCO.2015.63.9898

6. Hawkins PG, Kadam AS, Jackson WC, Eisbruch A. Organ-sparing in radiotherapy for head-and-Neck cancer: Improving quality of life. *Semin Radiat Oncol* (2018) 28(1):46–52. doi: 10.1016/j.semradonc.2017.08.002

7. Kam D, Salib A, Gorgy G, Patel TD, Carniol ET, Eloy JA, et al. Incidence of suicide in patients with head and neck cancer. *JAMA Otolaryngol Head Neck Surg* (2015) 141(12):1075–81. doi: 10.1001/jamaoto.2015.2480

8. Osazuwa-Peters N, Simpson MC, Zhao L, Boakye EA, Olomukoro SI, Deshields T, et al. Suicide risk among cancer survivors: Head and neck versus other cancers. *Cancer* (2018) 124(20):4072–9. doi: 10.1002/cncr.31675

9. Arthurs E, Hanna TP, Zaza K, Peng Y, Hall SF. Stroke after radiation therapy for head and neck cancer: What is the risk? *Int J Radiat Oncol Biol Phys* (2016) 96(3):589–96. doi: 10.1016/j.ijrobp.2016.07.007

10. Smith GL, Smith BD, Buchholz TA, Giordano SH, Garden AS, Woodward WA, et al. Cerebrovascular disease risk in older head and neck cancer patients after radiotherapy. *J Clin Oncol* (2008) 26(31):5119–25. doi: 10.1200/JCO.2008.16.6546

11. Swisher–McClure S, Mitra N, Lin A, Ahn P, Wan F, O'Malley B, et al. Risk of fatal cerebrovascular accidents after external beam radiation therapy for early-stage glottic laryngeal cancer. *Head Neck.* (2014) 36(5):611–6. doi: 10.1002/hed.23342

12. Vorwerk H, Zink K, Schiller R, Budach V, Böhmer D, Kampfer S, et al. Protection of quality and innovation in radiation oncology: the prospective multicenter trial the German society of radiation oncology (DEGRO-QUIRO study). *Strahlenther Onkol.* (2014) 190(5):433–43. doi: 10.1007/s00066-014-0634-0

13. van der Veen J, Gulyban A, Willems S, Maes F, Nuyts S. Interobserver variability in organ at risk delineation in head and neck cancer. *Radiat Oncol* (2021) 16(1):1–11. doi: 10.1186/s13014-020-01677-2

14. Geets X, Daisne J-F, Arcangeli S, Coche E, De Poel M, Duprez T, et al. Inter-observer variability in the delineation of pharyngo-laryngeal tumor, parotid glands and cervical spinal cord: comparison between CT-scan and MRI. *Radiat Oncol* (2005) 77 (1):25–31. doi: 10.1016/j.radonc.2005.04.010

15. Peng Y-l, Chen L, Shen G-z, Li Y-n, Yao J-j, Xiao W-w, et al. Interobserver variations in the delineation of target volumes and organs at risk and their impact on dose distribution in intensity-modulated radiation therapy for nasopharyngeal carcinoma. *Oral Oncol* (2018) 82:1–7. doi: 10.1016/j.oraloncology.2018.04.025

16. Huynh E, Hosny A, Guthier C, Bitterman DS, Petit SF, Haas-Kogan DA, et al. Artificial intelligence in radiation oncology. *Nat Rev Clin Oncol* (2020) 17(12):771–81. doi: 10.1038/s41571-020-0417-8

17. Vrtovec T, Močnik D, Strojan P, Pernuš F, Ibragimov B. Auto-segmentation of organs at risk for head and neck radiotherapy planning: From atlas-based to deep learning methods. *Med Phys* (2020) 47(9):e929–e50. doi: 10.1002/mp.14320

18. Cardenas CE, Yang J, Anderson BM, Court LE, Brock KB. Advances in auto-segmentation. *Semin Radiat Oncol* (2019) 29(3):185–97. doi: 10.1016/j.semradonc.2019.02.001

19. Nikolov S, Blackwell S, Zverovitch A, Mendes R, Livne M, De Fauw J, et al. Clinically applicable segmentation of head and neck anatomy for radiotherapy: deep learning algorithm development and validation study. *J Med Internet Res* (2021) 23(7): e26151. doi: 10.2196/26151

20. Brouwer CL, Steenbakkers RJ, Bourhis J, Budach W, Grau C, Grégoire V, et al. CT-based delineation of organs at risk in the head and neck region: DAHANCA, EORTC, GORTEC, HKNPCSG, NCIC CTG, NCRI, NRG oncology and TROG consensus guidelines. *Radiother Oncol* (2015) 117(1):83–90. doi: 10.1016/j.radonc.2015.07.041

21. Tryggestad E, Anand A, Beltran C, Brooks J, Cimmiyotti J, Grimaldi N, et al. Scalable radiotherapy data curation infrastructure for deep-learning based autosegmentation of organs-at-risk: A case study in head and neck cancer. *Front Oncol* (2022) 12. doi: 10.3389/fonc.2022.936134

22. Mayo CS, Moran JM, Bosch W, Xiao Y, McNutt T, Popple R, et al. American Association of physicists in medicine task group 263: Standardizing nomenclatures in radiation oncology. *Int J Radiat Oncol Biol Phys* (2018) 100(4):1057–66. doi: 10.1016/j.ijrobp.2017.12.013

23. Antonelli M, Reinke A, Bakas S, Farahani K, Kopp-Schneider A, Landman BA, et al. The medical segmentation decathlon. *Nat Commun* (2022) 13(1):4128. doi: 10.1038/s41467-022-30695-9

24. Siddique N, Paheding S, Elkin CP, Devabhaktuni V. U-Net and its variants for medical image segmentation: A review of theory and applications. *IEEE Access*. (2021) 9:82031–57. doi: 10.1109/ACCESS.2021.3086020

25. Zhong Y, Yang Y, Fang Y, Wang J, Hu W. A preliminary experience of implementing deep-learning based auto-segmentation in head and neck cancer: a study on real-world clinical cases. *Front Oncol* (2021) 1572. doi: 10.3389/fonc.2021.638197

26. Van der Veen J, Willems S, Deschuymer S, Robben D, Crijns W, Maes F, et al. Benefits of deep learning for delineation of organs at risk in head and neck cancer. *Radiother Oncol* (2019) 138:68–74. doi: 10.1016/j.radonc.2019.05.010

27. Fang Y, Wang J, Ou X, Ying H, Hu C, Zhang Z, et al. The impact of training sample size on deep learning-based organ auto-segmentation for head-and-neck patients. *Phys Med Biol* (2021) 66(18):185012. doi: 10.1088/1361-6560/ac2206

28. Amjad A, Xu J, Thill D, Lawton C, Hall W, Awan MJ, et al. General and custom deep learning autosegmentation models for organs in head and neck, abdomen, and male pelvis. *Med Phys* (2022) 49(3):1686–700. doi: 10.1002/mp.15507

29. Thor M, Iyer A, Jiang J, Apte A, Veeraraghavan H, Allgood NB, et al. Deep learning auto-segmentation and automated treatment planning for trismus risk reduction in head and neck cancer radiotherapy. *Phys Imaging Radiat Oncol* (2021) 19:96–101. doi: 10.1016/j.phro.2021.07.009

30. Wang W, Wang Q, Jia M, Wang Z, Yang C, Zhang D, et al. Deep learning-augmented head and neck organs at risk segmentation from CT volumes. *Front Phys* (2021) 612. doi: 10.3389/fphy.2021.743190

31. Brunenberg EJ, Steinseifer IK, van den Bosch S, Kaanders JH, Brouwer CL, Gooding MJ, et al. External validation of deep learning-based contouring of head and neck organs at risk. *Phys Imaging Radiat Oncol* (2020) 15:8–15. doi: 10.1016/j.phro.2020.06.006

32. Costea M, Zlate A, Durand M, Baudier T, Grégoire V, Sarrut D, et al. Comparison of atlas-based and deep learning methods for organs at risk delineation on head-and-neck CT images using an automated treatment planning system. *Radiothe Oncol* (2022) 177:61–70. doi: 10.1016/j.radonc.2022.10.029

33. Fritscher K, Raudaschl P, Zaffino P, Spadea MF, Sharp GC, Schubert R. Deep neural networks for fast segmentation of 3D medical images, in: *International Conference on Medical Image Computing and Computer-Assisted Intervention*, (New York, NY, US: Springer Cham) (2016).

34. Ibragimov B, Xing L. Segmentation of organs-at-risks in head and neck CT images using convolutional neural networks. *Med Phys* (2017) 44(2):547–57. doi: 10.1002/mp.12045

35. Močnik D, Ibragimov B, Xing L, Strojan P, Likar B, Pernuš F, et al. Segmentation of parotid glands from registered CT and MR images. *Phys Med* (2018) 52:33–41. doi: 10.1016/j.ejmp.2018.06.012

36. Ren X, Xiang L, Nie D, Shao Y, Zhang H, Shen D, et al. Interleaved 3D-CNNs for joint segmentation of small-volume structures in head and neck CT images. *Med Phys* (2018) 45(5):2063–75. doi: 10.1002/mp.12837

37. Zhong T, Huang X, Tang F, Liang S, Deng X, Zhang Y. Boosting-based cascaded convolutional neural networks for the segmentation of CT organs-at-risk in nasopharyngeal carcinoma. *Med Phys* (2019) 46(12):5602–11. doi: 10.1002/mp.13825

38. Hänsch A, Schwier M, Gass T, Morgas T, Haas B, Klein J, et al. Comparison of different deep learning approaches for parotid gland segmentation from CT images. *Proceeding of SPIE 10575*. Houston, TX, US: SPIE (2018).

39. Zhu W, Huang Y, Tang H, Qian Z, Du N, Fan W, et al. AnatomyNet: Deep 3D squeeze-and-excitation U-nets for fast and fully automated whole-volume anatomical segmentation. *bioRxiv* (2018) 392969:1–14. doi: 10.1101/392969

40. Tong N, Gou S, Yang S, Ruan D, Sheng K. Fully automatic multi-organ segmentation for head and neck cancer radiotherapy using shape representation model constrained fully convolutional neural networks. *Med Phys* (2018) 45 (10):4558–67. doi: 10.1002/mp.13147

41. Liang S, Tang F, Huang X, Yang K, Zhong T, Hu R, et al. Deep-learning-based detection and segmentation of organs at risk in nasopharyngeal carcinoma computed tomographic images for radiotherapy planning. *Eur Radiol* (2019) 29(4):1961–7. doi: 10.1007/s00330-018-5748-9

42. Willems S, Crijns W, Greca Saint-Esteven AL, Veen JVD, Robben D, Depuydt T, et al. Implementation of DeepVoxNet for Auto-Delineation of Organs at Risk in Head and Neck Cancer Patients in Radiotherapy. *In: OR 2.0 Context-aware operating theaters, computer assisted robotic endoscopy, clinical image-based procedures, and skin image analysis*. New York, NY, USA: Springer, Cham (2018) 1104:223–32. doi: 10.1007/978-3-030-01201-4_24

43. Kodym O, Španěl M, Herout A. Segmentation of head and neck organs at risk using cnn with batch dice loss. In: Brox T., Bruhn A., Fritz M. (Eds.) Pattern Recognition. GCPR 2018 - Lecture Notes in Computer Science. Cham: Springer. (2018) 105–114. doi: 10.1007/978-3-030-12939-2_8

44. Wang Y, Zhao L, Wang M, Song Z. Organ at risk segmentation in head and neck CT images using a two-stage segmentation framework based on 3D U-net. *IEEE Access*. (2019) 7:144591–602. doi: 10.1109/ACCESS.2019.2944958

45. Men K, Geng H, Cheng C, Zhong H, Huang M, Fan Y, et al. Technical note: More accurate and efficient segmentation of organs-at-risk in radiotherapy with convolutional neural networks cascades. *Med Phys* (2019) 46(1):286–92. doi: 10.1002/mp.13296

46. Tappeiner E, Pröll S, Hönig M, Raudaschl PF, Zaffino P, Spadea MF, et al. Multi-organ segmentation of the head and neck area: an efficient hierarchical neural networks approach. *Int J Comput Assist Radiol Surg* (2019) 14(5):745–54. doi: 10.1007/s11548-019-01922-4

47. Rhee DJ, Cardenas CE, Elhalawani H, McCarroll R, Zhang L, Yang J, et al. Automatic detection of contouring errors using convolutional neural networks. *Med Phys* (2019) 46(11):5086–97. doi: 10.1002/mp.13814

48. Tang H, Chen X, Liu Y, Lu Z, You J, Yang M, et al. Clinically applicable deep learning framework for organs at risk delineation in CT images. *Nat Mach Intell* (2019) 1(10):480–91. doi: 10.1038/s42256-019-0099-z

49. van Rooij W, Dahele M, Ribeiro Brandao H, Delaney AR, Slotman BJ, Verbakel WF. Deep learning-based delineation of head and neck organs at risk: Geometric and dosimetric evaluation. *Int J Radiat Oncol Biol Phys* (2019) 104(3):677–84. doi: 10.1016/j.ijrobp.2019.02.040

50. Gou S, Tong N, Qi S, Yang S, Chin R, Sheng K. Self-channel-and-spatial-attention neural network for automated multi-organ segmentation on head and neck CT images. *Phys Med Biol* (2020) 65(24):245034. doi: 10.1088/1361-6560/ab79c3

51. Liang S, Thung KH, Nie D, Zhang Y, Shen D. Multi-view spatial aggregation framework for joint localization and segmentation of organs at risk in head and neck CT images. *IEEE Trans Med Imag* (2020) 39(9):2794–805. doi: 10.1109/TMI.2020.2975853

52. Qiu B, Guo J, Kraeima J, Glas HH, Zhang W, Borra RJ, et al. Recurrent convolutional neural networks for 3D mandible segmentation in computed tomography. *J Pers Med* (2021) 11(6):492. doi: 10.3390/jpm11060492

53. Sun S, Liu Y, Bai N, Tang H, Chen X, Huang Q, et al. Attentionanatomy: A unified framework for whole-body organs at risk segmentation using multiple partially annotated datasets, in: *2020 IEEE 17th International Symposium on Biomedical Imaging (ISBI)*, Iowa City, IA, USA: IEEE. (2020) 1-5pp. doi: 10.1109/ISBI45749.2020.9098588.

54. van Dijk LV, Van den Bosch L, Aljabar P, Peressutti D, Both S, J.H.M. Steenbakkers R, et al. Improving automatic delineation for head and neck organs at risk by deep learning contouring. *Radiot Oncol* (2020) 142:115–23. doi: 10.1016/j.radonc.2019.09.022

55. Wong J, Fong A, McVicar N, Smith S, Giambattista J, Wells D, et al. Comparing deep learning-based auto-segmentation of organs at risk and clinical target volumes to expert inter-observer variability in radiotherapy planning. *Radiot Oncol* (2020) 144:152–8. doi: 10.1016/j.radonc.2019.10.019

56. Chan JW, Kearney V, Haaf S, Wu S, Bogdanov M, Reddick M, et al. A convolutional neural network algorithm for automatic segmentation of head and neck organs at risk using deep lifelong learning. *Med Phys* (2019) 46(5):2204–13. doi: 10.1002/mp.13495

57. Gao Y, Huang R, Chen M, Wang Z, Deng J, Chen Y, et al. FocusNet: Imbalanced large and small organ segmentation with an end-to-end deep neural network for head and neck CT images, in: *International Conference on Medical Image Computing and Computer-Assisted Intervention*. New York, NY, USA: Springer. (2019) 829–38pp. doi: 10.1007/978-3-030-32248-9_92

58. Lei W, Wang H, Gu R, Zhang S, Zhang S, Wang G. DeepIGeoS-V2: deep interactive segmentation of multiple organs from head and neck images with lightweight CNNs. In: *Large-Scale annotation of biomedical data and expert label synthesis and hardware aware learning for medical imaging and computer assisted intervention*. New York, NY, USA: Springer (2019). 61–9p.

59. Sun Y, Shi H, Zhang S, Wang P, Zhao W, Zhou X, et al. Accurate and rapid CT image segmentation of the eyes and surrounding organs for precise radiotherapy. *Med Phys* (2019) 46(5):2214–22. doi: 10.1002/mp.13463

60. Tong N, Gou S, Yang S, Cao M, Sheng K. Shape constrained fully convolutional DenseNet with adversarial training for multiorgan segmentation on head and neck CT and low-field MR images. *Med Phys* (2019) 46(6):2669–82. doi: 10.1002/mp.13553

61. Xue Y, Tang H, Qiao Z, Gong G, Yin Y, Qian Z, et al. Shape-aware organ segmentation by predicting signed distance maps, in: *Proceedings of the AAAI Conference on Artificial Intelligence*. (2020) (Washington DC: AAAI). doi: 10.1609/aaai.v34i07.6946

62. Jiang J, Sharif E, Um H, Berry S, Veeraraghavan H. Local block-wise self attention for normal organ segmentation [Internet]. *arXiv [pre-print]* (2019) 1–9. doi: 10.48550/arXiv.1909.05054

63. Anand A, Beltran CJ, Brooke MD, Buroker JR, DeWees TA, Foote RL, et al. Study design: Validation of clinical acceptability of deep-learning-based automated segmentation of organs-at-risk for head-and-neck radiotherapy treatment planning. *medRxiv* (2021) 1–25. doi: 10.1101/2021.12.07.21266421

64. Taha AA, Hanbury A. Metrics for evaluating 3D medical image segmentation: analysis, selection, and tool. *BMC Med Imag* (2015) 15(1):1–28. doi: 10.1186/s12880-015-0068-x

65. Vaassen F, Hazelaar C, Vaniqui A, Gooding M, van der Heyden B, Canters R, et al. Evaluation of measures for assessing time-saving of automatic organ-at-risk segmentation in radiotherapy. *Phys Imaging Radiat Oncol* (2020) 13:1–6. doi: 10.1016/j.phro.2019.12.001

66. Moltz JH, Hänsch A, Lassen-Schmidt B, Haas B, Genghi A, Schreier J, et al. Learning a loss function for segmentation: A feasibility study, in: *2020 IEEE 17th International Symposium on Biomedical Imaging* (New York, NY, USA: IEEE). (2020) 3–7pp.

67. Nelms BE, Robinson G, Markham J, Velasco K, Boyd S, Narayan S, et al. Variation in external beam treatment plan quality: An inter-institutional study of planners and planning systems. *Pract Radiat Oncol* (2012) 2(4):296–305. doi: 10.1016/j.prro.2011.11.012

68. Hart SG, Staveland LE. Development of NASA-TLX (Task load index): Results of empirical and theoretical research. In: Hancock PA, Meshkati N, editors. *Advances in psychology* (Amsterdam, Netherlands: Elsevier Science Publishing) (1988) 58, 139–83.

69. Hart SG. Nasa-task load index (NASA-TLX); 20 years later. *Proc Hum Factors Ergonom Soc Annu Meeting*. (2006) 50(9):904–8. doi: 10.1177/154193120605000909

frontiers | Frontiers in Oncology

TYPE Original Research
PUBLISHED 16 May 2023
DOI 10.3389/fonc.2023.1157584

OPEN ACCESS

EDITED BY
Giuseppe Carlo Iorio,
University of Turin, Italy

REVIEWED BY
Silviu Albu,
University of Medicine and Pharmacy Iuliu Hatieganu, Romania
Valerio Nardone,
University of Campania Luigi Vanvitelli, Italy
Emma D'Ippolito,
University of Campania Luigi Vanvitelli, Italy

*CORRESPONDENCE
Vittorio Rampinelli
vittorio.rampinelli@gmail.com

†These authors have contributed equally to this work and share first authorship

‡These authors have contributed equally to this work and share last authorship

RECEIVED 02 February 2023
ACCEPTED 02 May 2023
PUBLISHED 16 May 2023

CITATION
Rampinelli V, Ferrari M, Mattavelli D, Bonomo P, Lambertoni A, Turri-Zanoni M, D'Angelo E, Alterio D, Cianchetti M, Vischioni B, Rosati R, Tomasoni M, Alparone M, Taboni S, Tomasini D, Maddalo M, Bastia MBdM, Iacovelli NA, Dionisi F, Bignami M, Battaglia P, Bossi P, Deganello A, Piazza C, Schreiber A, Nicolai P, Castelnuovo P and Orlandi E (2023) Treatment of loco-regional recurrence of nasopharyngeal carcinoma in a non-endemic area: oncologic outcomes, morbidity, and proposal of a prognostic nomogram.
Front. Oncol. 13:1157584.
doi: 10.3389/fonc.2023.1157584

Treatment of loco-regional recurrence of nasopharyngeal carcinoma in a non-endemic area: oncologic outcomes, morbidity, and proposal of a prognostic nomogram

Vittorio Rampinelli[1*†], Marco Ferrari[2†], Davide Mattavelli[1], Pierluigi Bonomo[3], Alessia Lambertoni[4], Mario Turri-Zanoni[4], Elisa D'Angelo[5], Daniela Alterio[6], Marco Cianchetti[7], Barbara Vischioni[8], Roberta Rosati[1], Michele Tomasoni[1], Marco Alparone[1], Stefano Taboni[2], Davide Tomasini[9], Marta Maddalo[9], Michela Buglione di Monale Bastia[9], Nicola Alessandro Iacovelli[10], Francesco Dionisi[11], Maurizio Bignami[4], Paolo Battaglia[4], Paolo Bossi[12], Alberto Deganello[13], Cesare Piazza[1], Alberto Schreiber[1‡], Piero Nicolai[2‡], Paolo Castelnuovo[4‡] and Ester Orlandi[8‡]

[1]Unit of Otorhinolaryngology – Head and Neck Surgery, ASST Spedali Civili, Department of Surgical and Medical Specialties, Radiological Sciences, and Public Health, University of Brescia, School of Medicine, Brescia, Italy, [2]Section of Otorhinolaryngology - Head and Neck Surgery, Department of Neurosciences, University of Padova, Padova, Italy, [3]Radiation Oncology, Azienda Ospedaliero-Universitaria Careggi, Florence, Italy, [4]Unit of Otorhinolaryngology and Head & Neck Surgery, Department of Biotechnology and Life Sciences, ASST Sette Laghi, University of Insubria, Varese, Italy, [5]Radiotherapy Unit, Azienda Ospedaliero Universitaria di Modena, Modena, Italy, [6]Division of Radiotherapy, IEO European Institute of Oncology, IRCCS, Milan, Italy, [7]Proton Therapy Unit, Azienda Provinciale Per i Servizi Sanitari, Trento, Italy, [8]Radiation Oncology Clinical Department, National Center for Oncological Hadrontherapy (CNAO), Pavia, Italy, [9]Department of Radiation Oncology, Brescia University, Brescia, Italy, [10]Radiotherapy 2 Unit, Fondazione IRCCS IstitutoTumori, Milan, Italy, [11]Department of Radiation Oncology, IRCCS Regina Elena National Cancer Institute, Rome, Italy, [12]Medical Oncology, Department of Medical and Surgical Specialities, Radiological Sciences, and Public Health, University of Brescia, Brescia, Italy, [13]Otolaryngology Head and Neck Surgery, IRCCS National Cancer Institute (INT), Milan, Italy

Introduction: The study assessed outcomes and toxicities of different treatment modalities for local and/or regional recurrent nasopharyngeal carcinoma (NPC) in a non-endemic area.

Methods: Patients treated with curative intent for recurrent NPC with salvage surgery, photon-based radiotherapy, proton therapy (PT), with or without chemotherapy, at different Italian referral centers between 1998 and 2020 were included. Adverse events and complications were classified according to the Common Terminology Criteria for Adverse Events. Characteristics of the patients, tumors, treatments, and complications are presented along with uni- and multivariate analysis of prognostic factors. A survival predictive nomogram is also provided.

Results: A total of 140 patients treated from 1998 to 2020 were retrospectively assessed. Cases with lower age, comorbidity rate, stage, and shorter disease-free interval (DFI) preferentially underwent endoscopic surgery. More advanced cases underwent re-irradiation, fairly distributed between photon-based radiotherapy and PT. Age and DFI were independent factors influencing overall survival. No independent prognostic effect of treatment modality was observed. No significant difference in the morbidity profile of treatments was observed, with 40% of patients experiencing at least one adverse event classified as G3 or higher.

Conclusion: Recurrent NPC in a non-endemic area has dissimilar aspects compared to its endemic counterpart, suggesting the need for further studies that can guide the choice of the best treatment modality.

KEYWORDS

nasopharyngeal carcinoma, salvage treatment, non-endemic cancer, recurrent tumor, proton therapy, IMRT

Introduction

Despite the intrinsic chemo-radiosensitivity and improvements in radiation techniques and systemic therapies, up to 20% of patients affected by nasopharyngeal carcinoma (NPC) experience persistent or recurrent loco-regional disease after primary radiotherapy (RT) with or without concomitant chemotherapy (1–3).

Unlike for primary treatment, there is no consensus on the therapeutic strategy to be adopted in the recurrent setting, with various options available. These are mainly represented by surgery, highly conformal RT techniques, such as intensity modulated RT (IMRT), stereotactic body RT (SBRT), and proton beam RT (PT), combined or not with concurrent chemotherapy (4, 5).

The recent literature and international recommendations seem to lean in favor of surgical treatment for resectable recurrences (4, 6, 7). Indeed, contemporary case series based on endoscopic surgery have reported similar-to-higher survival outcomes with lower morbidity compared with re-irradiation (re-RT) (8, 9). The only trial offering a head-to-head comparison of surgery vs. re-RT in the management of early-stage local recurrence of NPC demonstrated that endoscopic surgery significantly improved overall survival (OS) compared with IMRT (9). Furthermore, early timing of recurrence and sequelae of the primary treatment may hamper the possibility of curative re-RT.

However, heterogeneity of expertise in endoscopic surgery, variability in radiation oncologist experience and re-RT institutional volume, and lack of extensive knowledge in centers where the disease is not frequent, render the choice of salvage surgery vs. re-RT difficult, as the risk-benefit balance is rarely strongly in favor of one of the two options.

The concept of surgical resectability itself is subjective and frequently relative to the fact that a given procedure may be deemed as too invasive in view of patient's general conditions and prognosis rather than referring to the genuine possibility to completely resect the tumor (10). Liu et al. considered lesions as resectable if limited to the nasopharyngeal cavity, nasal septum, superficial parapharyngeal space, or the base wall of the sphenoid sinus (9). However, these limits can be technically overcome. For instance, endovascular carotid closure or bypass enable the surgeon to extend the resection far laterally and posteriorly (10, 11). Moreover, despite advances in RT techniques, including IMRT, PT, and SRT, the survival benefit of re-RT is still offset by frequent fatal complications, making careful patient selection and re-RT planning and delivery even more mandatory (6). Finally, the availability and integration of other therapeutic options (i.e., neoadjuvant and adjuvant chemotherapy, PT, and immunotherapy) should also be considered in the decision-making process (12).

To further complicate the scenario, there are only few studies focusing on non-endemic NPC recurrence in the literature (13–16), and usually treatment protocols are based on the results of studies performed in endemic areas. Despite the similarities, specific non-endemic traits have been noticed, likely due to distinctive pathogenesis (14). Locoregional and distant recurrences seems to occur more and less frequently compared to endemic cohorts, respectively (13). Moreover, the survival and toxicity predictive models developed for endemic recurrences do not fit with the non-endemic counterpart, as highlighted by Boustani et al. (14). In light of the rarity of the clinical condition in non-typical areas, multicentric efforts should be done to clarify peculiarities and develop valid survival prognostic models.

The present paper analyzes the experience gathered by different referral centers in dealing with locally and/or regionally recurrent/persistent NPC in a non-endemic area, with the aim of analyzing treatment modalities, oncologic and morbidity outcomes, and prognostic factors. Survival predictive nomograms are herein also provided.

Materials and methods

In this multi-institutional, retrospective study, we included locally and/or regionally recurrent/persistent NPC patients, treated with curative intent with salvage surgery or definitive RT at eight Italian referral centers.

The study period was between November 1998 and January 2020. Inclusion criteria were the following: a) having received a curative photon-based treatment for the primary NPC, at a prescribed total dose of at least of 63 Gy with conventional fractionation (corresponding to a biological effective dose (BED) of at least 74.34 Gy (α/β = 10, BED10) and an Equivalent Dose in 2Gy fractions (EQD2) of 61.95 Gy); b) histologically or cytologically-proven local, regional or loco-regional recurrent/persistent NPC confirmed after physical examination and radiological imaging [computed tomography (CT) or magnetic resonance imaging (MRI), and/or positron emission tomography with 2-deoxy-2-[fluorine-18]fluoro-D-glucose/CT (^{18}F-FDG PET/CT)]; c) first and in field recurrences following primary treatment; d) follow-up after salvage therapy of at least 3 months.

Persistent disease was defined as residual disease detected at the first re-staging imaging after completion of (chemo-)RT, within a period of 6 months. Conversely, recurrent disease was defined as relapse beyond 6 months after definitive therapy with radiologic evidence of complete clinical response to primary treatment (3). Recurrent NPCs were classified following the 8th Edition of the TNM staging system (17).

The choice of the treatment between (neo)adjuvant chemotherapy, salvage surgery, and/or re-RT, was based on tumor and patient characteristics as well as expertise of the local multidisciplinary team. Surgery was exclusively performed *via* nasopharyngeal endoscopic resection (NER) and/or neck dissection. Curative re-RT could be delivered in postoperative or definitive setting in the form of IMRT (including volumetric modulated arc therapy, VMAT), PT or SBRT. SBRT included CyberKnife or VMAT with high-precision image-guided system. Brachytherapy (BRT) with High Dose Rate (HDR) or Pulsed Dose Rate (PDR) with ^{192}Ir alone or in combination with photon-based RT was included as treatment strategy. The minimum overall total dose had to be at least 31 Gy and 31 Gy Relative Biological Effectiveness (RBE) EQD2 with photon-based and proton-based approach, using conventional or hypofractionated regimens, respectively.

The following anonymized data were extracted from institutional databases:

- Patient-related variables: age, gender, comorbidities (number, Charlson comorbidity index [CCI]);
- Tumor-related variables (type of relapse, disease-free interval [DFI], histology);
- Treatment-related variables ([neo-]adjuvant treatments, characteristics of surgery and/or re-RT with or without concomitant chemotherapy);
- Adverse events and complications related to salvage treatments were classified according to the Common Terminology Criteria for Adverse Events [CTCAE v5.0] (18).

Statistical analysis

Statistical analysis was performed using RStudio (2022.07.2). Variables assessed in the study were reported with standard descriptive statistics: continuous variables were summarized as median, range, and interquartile range, whereas categorical variables as absolute and percentage distributions. Contingency tables were used to assess the relationship between primary T category and T category at recurrence, and the relationship between clinical and pathological TN categories in patients who underwent salvage surgery. Fisher's exact test, chi-square test or Mann-Whitney test, as appropriate, was used to compare rates of complications relative to the treatment strategy (classified as surgery, re-RT, and combination thereof) and cumulative RT dose.

Survival analysis was conducted considering OS as the primary outcome, and disease-specific (DSS), recurrence-free (RFS), local recurrence-free (LRFS), regional recurrence-free (RRFS), and distant recurrence-free survival (DRFS) as secondary outcomes. Time-to-event observations were determined based on time from diagnosis of recurrence to event occurrence or censor. Events were defined as follows: death of any cause for OS, disease-specific death for DSS, further recurrence for RFS, and further local, regional, or distant recurrence for LRFS, RRFS, and DRFS, respectively. Univariate prognostic analysis was performed with the log-rank test for categorical variables and univariate Cox proportional hazards model for continuous variables. Multivariable analysis was performed with a Cox proportional hazards model. Selection of variables to be included in the model was made *a priori* based on clinical relevance of each factor according to the authors' personal experience. Moreover, variables not selected *a priori* and exhibiting a prognostic effect at univariate analysis were also considered to build the multivariable model. Assumptions of the Cox proportional hazards model were checked as follows: proportional hazards assumption was tested through the global Schoenfeld test, influential observations were checked through deviance residual analysis, and non-linearity was assessed (when needed) by Martingale residual analysis. Multi-collinearity of covariates was assessed with a multi-collinearity test; covariates with a variance inflation factor of 5 or higher were considered as multi-collinear and were excluded from the model. A nomogram predicting OS at 1, 2, 5, and 10 years was created and internally validated at each time point through a 300-repetition bootstrap. Calibration graphs were obtained using the Akaike's Information Criterion as stopping rule. Internal validation was completed by calculating the C-index.

A 4-state multistate model was created, including the following states: alive with neither ≥G3 toxicity nor recurrence, alive with ≥G3 toxicity, alive with recurrence (regardless of the presence of ≥G3 toxicity), dead (absorbing state). A multivariable analysis was performed to identify factors independently favoring transitions from one to another state.

Level of significance was set a 0.05; p values between 0.05 and 0.10 were highlighted with the term "close-to-significant" as not formally significant, but potentially marking clinically relevant associations.

Results

The study included 140 patients. Patients and tumor characteristics are summarized in Table 1. Considering the treatment of the primitive cancer, 99/140 (70.7%) patients underwent concomitant chemo-radiotherapy, the remaining 41/140 (29.3%) only radiotherapy.

EBER (Epstein-Barr virus (EBV)-encoded small RNA) status was not systematically assessed (data available for 65 of 140 patients). When tested, it was found positive at pretreatment biopsy or definitive histological examination in all but one patient (98.5%). A substantial proportion of recurrent tumors (53.7%) showed a different rT category compared with the cT category at presentation. The relationship of T category at primary presentation vs. T category at recurrence is detailed in Table 2. In the subset of patients who underwent surgery as part of their salvage treatment, a considerable match between the clinical and pathological rT category was observed (95.0%). On the contrary, a tendency towards over-diagnosis of nodal involvement was demonstrated (80.5% of tumors classified as rcN+ resulted rpN0). The relationship of rcTN category relative to rpTN category in surgically treated patients is detailed in Table 3.

TABLE 1 Patient and tumor characteristics.

Gender	Male: 102/140 (72.9%) Female: 38/140 (27.1%)
Ethnicity	Caucasian: 134/140 (95.7%) Asian: 3/140 (2.1%) African: 3/140 (2.1%)
Dose of the first RT course (Average; Median; Range)	69.0; 70.0; 63-72 Gy
Age at recurrence date (Average; Median; Range)	52.3; 51.0; 25-81
Comorbidities at time of recurrence	51.5%
Charlson Comorbidity Index (Average; Median; Range)	4.2; 3; 2-16
Type of relapse	Recurrence: 128/140 (91.5%); Persistence: 12/140 (8.5%) Local: 108/140 (77.1%) Regional: 7/140 (5.0%) Locoregional: 24/140 (17.1%) NA: 1/140 (0.1%)
DFI (Average; Median; Range)	45.4; 23; 3-316
rcT (TNM VIII edition)	T0: 7/140 (5.0%) T1: 40/140 (28.6%) T2: 24/140 (17.1%) T3: 31/140 (22.1%) T4: 34/140 (24.3%) NA: 4/140 (2.8%)
rcN (TNM VIII edition)	N0: 108/140 (77.1%) N1: 13/140 (9.3%) N2: 10/140 (7.1%) N3: 3/140 (2.1%) NA: 6/140 (4.3%)
rcStage	I: 38/140 (27.1%) II: 21/140 (15.0%) II: 36/140 (25.7%) IVA: 36/140 (25.7%) IVB: 0/140 (0.0%) NA: 9/140 (6.4%)
Nodal levels involved at recurrence	I: 1/22 (4.5%) II :15/22 (68.2%) III: 5/22 (22.7%) IV: 2/22 (9.0%) V: 1/22 (4.5%) Retropharyngeal: 7/22 (31.8%) NA: 9/31 (29.0%)
Histology of recurrence	Keratinizing NPC: 14/123 (11.4%) Non-keratinizing differentiated NPC: 2/123 (1.6%) Non-keratinizing undifferentiated NPC: 106/123 (86.2%) Basaloid NPC: 1/123 (0.8%) NA: 17/140 (12.1%)

DFI, Disease free interval; NA, Data not available; NPC, Nasopharyngeal carcinoma.

TABLE 2 Contingency table showing the relationship of T category at primary presentation versus T category at recurrence.

Data available for 123 patients		rcT classification				
		T0	T1	T2	T3	T4
cT classification	**T1**	2	22	7	6	7
	T2	2	6	9	3	5
	T3	0	3	3	11	5
	T4	1	6	3	7	15

Treatment

Sixty-five (46.4%) patients received surgery as part of their salvage treatment, whereas the remaining 75 (53.6%) underwent a non-surgical treatment. Neoadjuvant chemotherapy was included in the treatment in 27 (19.3%) patients, whereas adjuvant chemotherapy in 9 (6.4%). Figure 1 and Tables 4, 5 summarize the scheme of treatment and details of each treatment approach. Median prescription RT dose of the first RT course was 70 Gy (84 Gy BED10 and 70 GyEQD2) both for recurrent patients subsequently treated with postoperative re-irradiation and definitive re-irradiation. Adjuvant re-RT was mainly given in case of close or positive margins after surgery (8/10 patients, 80%), with median prescribed radiation dose of 54 Gy (64.8Gy BED10 and 54 GyEQD2) and 58 GyRBE (69.6 GyRBE BED10 and 58 GyRBE EQD2) delivered through IMRT/VMAT and PT, respectively. No patients received re-irradiation after neck dissection. Definitive re-RT was mostly delivered on primary tumor site, less commonly on unresectable retropharyngeal nodes, with median prescribed radiation dose of 56 Gy (67.2 Gy BED10 and 56 GyEQD2) and 54 GyRBE (64.8GyRBE BED10 and 54 GyRBE EQD2) with IMRT/VMAT and PT, respectively. In this setting, 7/77 patients (9.1%) received SBRT with a median prescribed radiation dose of 25 Gy (37.5 Gy BED10 and 31.25 GyEQD2). Only 1 of these 7 patients received a lower SBRT dose (20 Gy, 30 Gy BED10, 25 GyEQD2). Two of 77 (2.6%) patients received PDR-BRT as a boost after a first phase of IMRT. Data about SBRT doses were not available.

Taking into account both the first RT course and photon- and proton-based re-irradiation (excluding BRT), median cumulative prescribed total dose was 126 GyRBE (151.2GyRBE BED10, 126 GyRBE EQD2) and 115 GyRBE (140GyRBE BED10, 115 GyRBE EQD2) in postoperative and definitive settings, respectively.

Survival outcomes

Median duration of follow-up was 29 months [range, 3-160; interquartile range (IQR), 17-63]. At last examination, patients' status was as follows: 67 (47.8%) were alive with no evidence of disease, 22 (15.7%) alive with disease, 46 (32.8%) dead of disease, and 5 (3.6%) dead of other cause. Further recurrences following the first salvage treatment occurred preferentially at the local site. Of a total of 59 further relapses, 38 recurred again at the local sites, 16 on regional lymph nodes, and 5 on both.

Five-year OS, DSS, RFS, LRFS, RRFS, and DRFS were 55.9, 62.1, 41.3, 53.5, 75.9, and 85.9%, respectively. Ten-year OS, DSS, RFS, LRFS, RRFS, and DRFS were 44.2, 49.1, 23.3, 33.3, 69.0, and 82.5%, respectively (Figure 2).

TABLE 3 Contingency table showing the relationship of rcTN category relative to rpTN category in surgically treated patients.

Data available for 60 patients		rpT classification				
		T0	T1	T2	T3	T4
rcT classification	**T0**	3	0	0	0	0
	T1	0	23	2	1	0
	T2	0	0	8	0	0
	T3	0	0	0	20	0
	T4	0	0	0	0	3
Data available for 71 patients		**rpN classification**				
		N0	**N1**	**N2**	**N3**	
rcN classification	**N0**	28	1	1	0	
	N1	18	1	0	0	
	N2	13	5	1	0	
	N3	2	1	0	0	

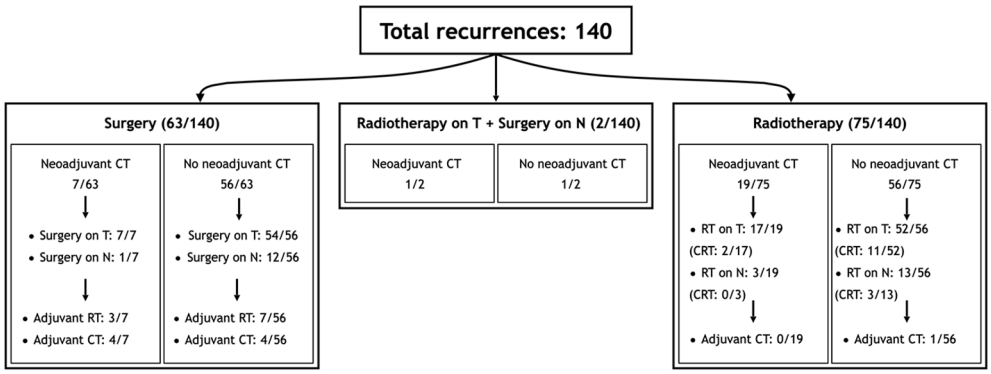

FIGURE 1
Scheme of patient distribution in treatment subgroups. CT, Chemotherapy; CRT, Radiotherapy with concomitant chemotherapy; RT, Radiotherapy.

Univariable survival analysis

At univariable analysis, cT, rcT, and stage at recurrence were factors influencing OS and DSS. Histology, cT, cN, rcT, stage at recurrence, and type of salvage treatment were factors influencing RFS. Margin status influenced both DSS and RFS (Table 6).

Multivariable and multistate survival analysis

At multivariable analysis, age and DFI were independent factors negatively influencing OS and DSS (i.e., higher age/DFI were associated with worse prognosis), in contrast to stage and treatment modality. Primary regional disease, regional recurrence, and induction/adjuvant chemotherapy were independent factors influencing RFS (Table 7). In patients who received local surgery, margin status was not an independent factor affecting RFS.

Figure 3 reports the variables with a statistically significant or close-to-significant impact on status transition at multistate multivariable analysis. In particular, the reconstruction with a vascularized flap displayed a protective effect on the development of ≥G3 toxicity (transition 1 in Figure 3). N category at presentation and rT category significantly affected the risk of developing a recurrence from a toxicity- and disease-free state (transition 2 in Figure 3). On the contrary, use of neoadjuvant and/or adjuvant chemotherapy in the salvage treatment was associated with a protective role towards transition 2. Age, DFI, and TN categories at primary presentation affected the transition between a ≥G3 toxicity state to recurrence (transition 3 in Figure 3). Age, DFI, primary treatment including concomitant chemotherapy, and TN categories of the primary lesion were associated with increased risk of death from a ≥G3 toxicity state (transition 4 in Figure 3). Primary treatment including concomitant chemotherapy was a protective factor with regards to transition from recurrence to death (transition 5 in Figure 3). The cumulative incidence standard and stacked plot (Figure 4) suggest that cancer-specific mortality increased constantly in the first 5 years after salvage treatment, while non-cancer related deaths are concentrated in the first 2 years. Treatment-related adverse events (status alive with ≥G3 toxicity) occurred mainly in the first year.

Figure 5 shows the OS nomogram, which allows estimation of the probability of survival at 1, 2, 5, and 10 years after retreatment. Internal validation of the model showed satisfactory performance of the nomogram (C-index: 0.732) (Figure 6).

Treatment toxicity

Fifty-six (40%) patients experienced at least one adverse event classified as ≥G3; the rate of ≥G3 toxicity was 40.7, 54.5, and 37.3% in the cohorts treated with surgery, surgery + re-RT, and re-RT,

TABLE 4 Details of patient distribution in treatment subgroups.

Patients treated with salvage surgery ± RT (63/140)*	Patients treated with definitive RT (75/140)
Neoadjuvant CT: 7/63 Surgery on T: 61/63 Surgery on N: 13/63 Adjuvant CT: 8/63 Adjuvant RT: 10/63	Neoadjuvant CT: 19/75 Concomitant CT: 16/75 RT on T: 69/75 RT on N: 16/75 Adjuvant CT: 1/75
DFI (median): 18 months Age (median): 51 years Charlson Comorbidity Index (median): 1 rcT distribution: 44.1% T1, 15.5% T2, 35.6% T3, and 5.0% T4	DFI (median): 23 months Age (median): 54 years Charlson Comorbidity Index (median): 2 rcT distribution: 20.6% T1, 22.1% T2, 14.7% T3, and 42.6% T4.

*2/140 Patients underwent RT on T and surgery on N, with neoadjuvant CT in 1 case.
DFI, Disease free interval; CT, Chemotherapy; RT, Radiotherapy.

TABLE 5 Treatment details.

Surgery	**Type of surgery on T**	NER type 1: 6/61 (9.8%) NER type 2: 14/61 (22.9%) NER type 3: 41/61 (67.2%)
	Reconstruction	None: 36/61 (59.0%) TPFF: 6/61 (9.8%) NSF: 19/61 (31.1%)
	Margin status	R0: 52/61 (85.2%) R1: 8/61 (13.1%) R2: 1/61 (1.6%)
Surgery + re-irradiation	**Radiotherapy technique**	IMRT/VMAT: 8/10 (80.0%) PT: 2/10 (20.0%)
	Prescribed radiation doses (Median; Range)	IMRT/VMAT: 54; 54-56 Gy PT: 58; 46-66 GyRBE
	Radiation fractionation (Median; Range)	IMRT/VMAT: 2; 2-2 Gy PT: 2; 1.8-2 GyRBE
Definitive re-irradiation	**Radiotherapy technique**	IMRT/VMAT: 35/77(45.5%) SBRT: 7/77 (9.1%) PT: 33/77 (42.8%) Brachytherapy: 2/77 (2.6%)
	Prescribed radiation doses (Median; Range)	IMRT/VMAT: 56:54-72 SBRT: 25; 20-35 Gy PT: 54; 45-70 GyRBE Brachytherapy (as boost): NA
	Radiation fractionation (Median; Range)	IMRT/VMAT: 2; 1.2-2 Gy SBRT: 5; 3-5 Gy PT: 2; 1.8-3 GyRBE
Neoadjuvant chemotherapy	**Response to neoadjuvant chemotherapy**	CR: 1/27 (5.0%) PR: 7/27 (35.0%) SD: 8/27 (40.0%) PD: 4/27 (20.0%) NA: 7/27 (31.3%)

CR, Complete response; IMRT, Intensity modulated radiotherapy; NA, Data not available; NER, Nasopharyngeal endoscopic resection; NSP, Nasoseptal flap; PD, Progression of disease; PR, Partial response; PT, Proton therapy; RT, Radiotherapy; SBRT, Stereotactic body radiotherapy; SD, Stable disease; TPFF, Temporoparietal fascial flap; VMAT, Volumetric modulated arc therapy.

respectively (p=0.520). Table 8 shows the spectrum of complications classified as ≥G3 observed in the series. The rate of ≥G3 toxicity events was equally frequent in patients who received neoadjuvant chemotherapy (28.6%) and those who did not (29.8%, p=1.000). The total cumulative dose was not statistically different in patients who developed a ≥G3 toxicity event (median: 117 GyRBE) compared with those who did not (median: 110 GyRBE, p=0.662).

Discussion

The present paper collects the experience of different referral centers in dealing with local and/or regional persistence or recurrence of NPC in a non-endemic area, with the aim of analyzing treatment modalities, prognostic factors, and morbidity outcomes. Almost all large NPC series, in fact, are from endemic areas in Asia, with the literature from non-endemic populations being based on heterogeneous and small cohorts (13). Furthermore, these frequently present a share of immigrants from endemic areas that inflates the results of the analysis (13). In our cohort, more than 95% of patients belonged to Caucasian ethnicity, which makes it, to the best of our knowledge, the most homogeneous clinical series of non-endemic recurrent NPC in the current literature.

We observed an average age at recurrence of 52.3 years and a median DFI of 23 months, widely ranging between 3 and 316 months. This observation is in line with the literature coming from endemic areas (3, 14, 19). Of note, more than half of the recurrences in the present study (i.e., candidate to salvage treatment) occurred in the first 2 years after primary (chemo-)RT, which suggests that follow-up strategies should be particularly focused during that time span. On the other hand, the remaining half of recurrences were observed over a wide time frame after 2 years, with the latest representing most likely secondary cancers. This highlights the need for lifetime follow-up in patients treated for NPC.

Our clinical series is focused on relapsed NPCs treated with curative intent in a non-endemic area. As in the curative setting (20, 21), we observed a clear dominance of the non-keratinizing undifferentiated carcinoma (86.2%). Given the more favorable biological profile, non-keratinizing tumors are probably more prone to give treatable relapses, unlike the keratinizing subtypes which behave more aggressively (20).

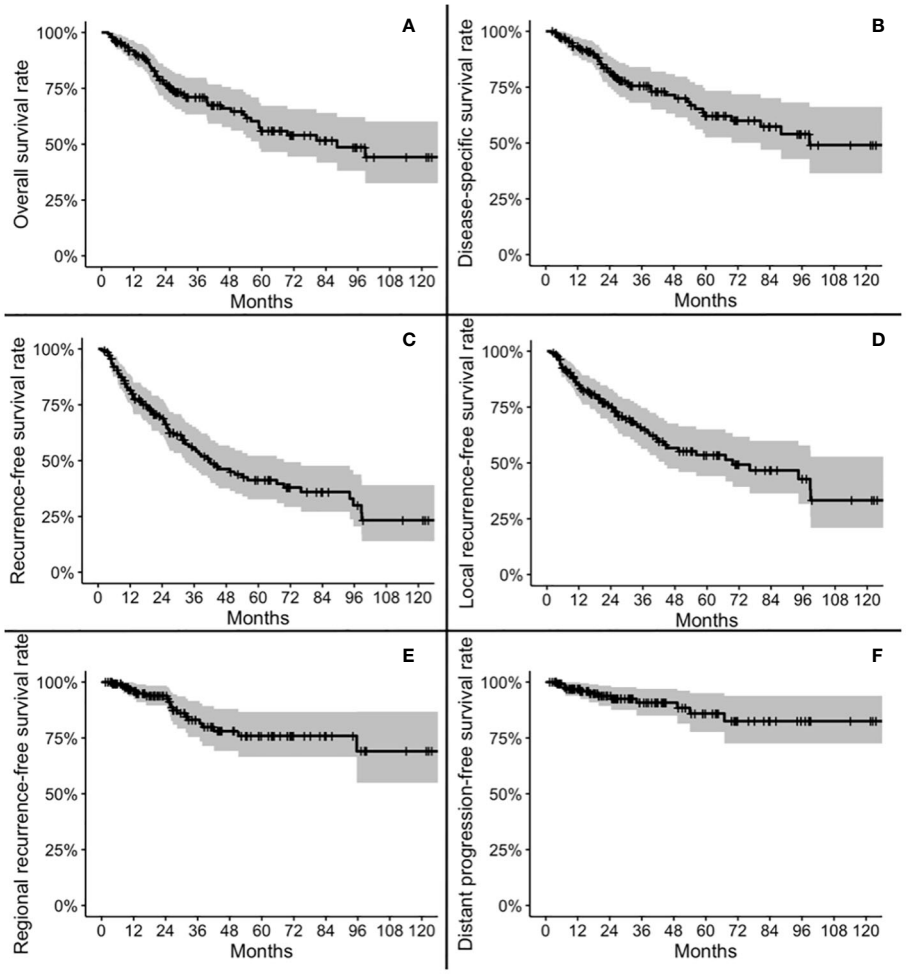

FIGURE 2
Kaplan-Meier plots for overall survival **(A)**, disease-specific survival **(B)**, recurrence-free survival **(C)**, local recurrence-free survival **(D)**, regional recurrence-free survival **(E)**, and distant progression-free survival **(F)**.

T categories at recurrence were distributed homogeneously, with similar rates of rcT from 1 to 4. Furthermore, Table 2 shows that a substantial proportion of recurrent cases (53 of 123, or 46.3%) maintained the T category displayed at presentation. However, several cases were classified with a rT category different to that at presentation. Of note, 22.1% of patients had a nodal recurrence, with only 7 (5%) patients showing isolated nodal recurrence.

The choice of the therapeutic strategy for each patient was based on multiple factors, including the interval after previous RT, morbidity of primary treatment, staging, burden of disease, and experience of the multidisciplinary team, along with general conditions and motivation of the patient.

In the present cohort, all the contemporary curative therapeutic options are represented. The documents guiding the clinical practice, that were cited in the present paper, were mostly focused on endemic populations, since specific prospective trials and guidelines on non-endemic cohorts are lacking. However, when we compare our curative patterns of care with those from endemic regions, we did not find relevant differences. Indeed, in a work by Ng et al. (19) including 272 locally recurrent NPC patients treated in six Hong Kong public hospitals, radical surgery with or without adjuvant RT or chemotherapy (classified as the surgery group) and re-RT with or without induction or concurrent chemotherapy (classified as the re-RT group) were administered with a similar percentage.

Of 140 patients, about 20% underwent neoadjuvant chemotherapy, with a clinical benefit rate (i.e., at least a stable disease) of 80%. The role of induction chemotherapy for recurrent NPC is still debated (22), with the literature lacking in strong evidence. Even in the absence of clear guidelines, the multidisciplinary team may propose selected patients for neoadjuvant chemotherapy in light of the beneficial effects on progression-free survival, OS, loco-regional and distant control observed in patients with primary NPC (23). Furthermore, in cases that are not suitable for re-RT or surgery, it may shrink the tumor and regain the potential for further surgical or radiation treatments, with better outcomes than those observed after chemotherapy (24).

About half of patients underwent surgery on T and/or N. In line with the literature from endemic areas (19), the most common

TABLE 6 Univariate prognostic analysis of patient-, cancer-, and treatment-related variables on overall survival (OS), disease-specific survival (DSS), and recurrence-free survival (RFS).

Variable	5-year OS	P-value	5-year DSS	P-value	5-year RFS	P-value
Gender	Male: 50.7% Female: 58.7%	0.10	Male: 57.7% Female: 62.6%	0.21	Male: 36.3% Female: 58.8%	0.21
Histology	Keratinizing: 53.2% Non–keratinizing differentiated: 60.0%* Non–keratinizing undifferentiated: 55.7%	0.39	Keratinizing: 65.1% Non–keratinizing differentiated: 60.0%* Non–keratinizing undifferentiated: 61.7%	0.57	Keratinizing: 34.0% Non–keratinizing differentiated: 22.9%* Non–keratinizing undifferentiated: 44.9%	**0.014**
cT of primary tumor	T1: 63.1% T2: 84.4% T3: 35.8% T4: 48.3%	**0.047**	T1: 72.2% T2: 87.9% T3: 41.1% T4: 52.0%	**0.043**	T1: 49.0% T2: 59.2% T3: 26.4% T4: 28.6%	**0.038**
cN of primary tumor	N0: 67.9% N1: 16.5% N2: 52.5% N3: 50.0%*	0.49	N0: 79.1% N1: 20.7% N2: 60.5% N3: 50.0%*	0.29	N0: 62.2% N1: 41.3%* N2: 30.8% N3: 33.3%*	**0.0031**
Stage of primary tumor	I: 66.7% II: 79.3% III: 47.5% IV: 33.2%	0.06	I: 100% II: 79.3% III: 53.3% IV: 37.3%	0.066	I: 76.2% II: 50.0% III: 31.4% IV: 19.2%	0.051
rcT	T0: 64.3% T1: 87.6% T2: 61.0% T3: 39.3% T4: 39.4%	**0.0021**	T0: 85.7% T1: 93.1% T2: 64.2% T3: 46.7% T4: 41.1%	**0.00053**	T0: 28.6% T1: 72.0% T2: 31.7% T3: 35.2% T4: 26.6%	**0.00013**
rcN	N0: 57.7% N1: 49.1% N2: 50.0%* N3: 66.7%	0.68	N0: 63.8% N1: 61.4% N2: 50.0%* N3: 66.7%	0.35	N0: 46.4% N1: 23.9%* N2: 25.0%* N3: 33.3%	0.5
rStage	I: 81.7% II: 53.6% III: 37.6% IV: 45.3%	**0.0048**	I: 92.9% II: 59.6% III: 44.3% IV: 47.2%	**0.00079**	I: 71.3% II: 35.6%* III: 30.5% IV: 31.7%	**<0.0001**
Primary tumor treatment	RT: 57.0% CRT: 55.9%	0.47	RT: 68.0% CRT: 60.7%	0.56	RT: 44.7% CRT: 30.1%	0.23
Recurrent tumor treatment	Surgery: 65.6% (C)RT: 48.7% Surgery + (C)RT: 51.1%	0.22	Surgery: 72.5% (C)RT: 55.5% Surgery + (C)RT: 51.1%	0.13	Surgery: 59.1% (C)RT: 28.9% Surgery + (C)RT: 40.9%	**0.0037**
Chemotherapy for recurrent tumor (induction and/or adjuvant)	Yes: 56.7% No: 55.4%	0.73	Yes: 60.2% No: 63.1%	0.94	Yes: 39.8% No: 45.5%	0.82
Margin status	R0: 64.5% R1: 46.7%	0.16	R0: 71.3% R1: 46.7%	**0.048**	R0: 60.4% R1: 40.0%	**0.0035**

*3-year estimate; RT, Radiotherapy; CRT, Radiotherapy with concomitant chemotherapy; CRT - Radiotherapy with or without concomitant chemotherapy.
Words in bolds are statistically significant.

treatment modality for low-stage tumors was surgery, while T4 lesions represented 42.6% of all the lesions treated with re-RT (vs. 5% of the surgical group). Age and CCI were lower in the surgical group, suggesting that selection of patients with favorable conditions did occur. Furthermore, patients with short DFI preferentially underwent surgical resection (Table 4). This is consistent with the evidence that short DFI is associated with lower control rate and higher morbidity if re-RT is indicated (6, 25).

NER represented the surgical approach of choice in all locally recurrent NPC, achieving free resection margins in 85.2% of patients. The preference towards endoscopic approaches was influenced by the many experiences from the literature reporting that survival and morbidity outcomes with a transnasal route are significantly superior to those of open surgery (26). Of note, surgeons operating in non-endemic areas have contributed significantly in the developement and refinement of endoscopic approaches, showing good results on this population (16).

The remaining half of the patients were treated with re-RT, distributed between photon-based RT, with either IMRT or SRT, and PT (54.4% vs. 42.8%, respectively).

All patients in our re-RT series received at least 45Gy/GyRBE, which is historically considered a total dose that is able to control

TABLE 7 Multivariable prognostic analysis of patient-, cancer-, and treatment-related variables on overall survival (OS), disease-specific survival (DSS), and recurrence-free survival (RFS).

Variable	OS		DSS		RFS	
	HR (95% CI)	p	HR (95% CI)	p	HR (95% CI)	p
Age	1.06 (1.02, 1.09)	**<0.001**	1.04 (1.00, 1.08)	**0.03**	/	/
DFI	1.01 (1.00, 1.01)	**0.02**	1.01 (1.00, 1.02)	**0.04**	1.00 (0.99, 1.00)	0.35
cT8						
cT1 or cT2	Reference		Reference		Reference	
cT3 or cT4	1.76 (0.88, 3.53)	0.11	2.04 (0.93, 4.47)	0.08	2.04 (1.12, 3.69)	**0.019**
cN8						
cN0	Reference		Reference		Reference	
cN+	1.56 (0.81, 3.00)	0.18	1.92 (0.91, 4.03)	0.09	2.43 (1.36, 4.34)	**0.003**
rcT8						
rcT0	Reference		Reference		Reference	
rcT1	0.65 (0.10, 4.30)	0.66	0.52 (0.05, 5.36)	0.58	0.22 (0.04, 1.08)	0.06
rcT2	2.29 (0.46, 11.49)	0.31	2.92 (0.44, 19.49)	0.27	0.79 (0.21, 2.98)	0.72
rcT3	2.42 (0.48, 12.20)	0.28	2.73 (0.42, 17.55)	0.29	0.81 (0.20, 3.20)	0.76
rcT4	3.71 (0.80, 17.22)	0.09	5.82 (1.00, 33.90)	**0.05**	0.78 (0.22, 2.78)	0.70
rcN8						
rcN0	Reference		Reference		Reference	
rcN+	1.47 (0.65, 3.33)	0.36	1.74 (0.74, 4.07)	0.20	2.08 (1.00, 4.34)	**0.05**
TREATMENT OF RECURRENCE						
Endoscopic surgery*	Reference		Reference		Reference	
Re–irradiation	0.94 (0.38, 2.34)	0.89	1.02 (0.35, 3.00)	0.97	1.89 (0.79, 4.53)	0.15
Endoscopic surgery + re–irradiation*	1.01 (0.33, 3.10)	0.99	1.71 (0.51, 5.81)	0.39	1.10 (0.37, 3.26)	0.85
CHEMOTHERAPY						
Neither nCT nor aCT	Reference		Reference		Reference	
nCT and/or aCT	0.70 (0.36, 1.38)	0.30	0.66 (0.32, 1.38)	0.27	0.52 (0.29, 0.94)	**0.031**

aCT, adjuvant chemotherapy; DFI, Disease free interval; nCT, neo-adjuvant chemotherapy. *In the multivariable model, no significant difference of the outcomes was observed according to margin status in patients receiving surgery.
Words in bolds are statistically significant.

recurrent disease, although recently international recommendations suggest giving at least 60 Gy (6). So far, although patients with small and potentially resectable recurrences could be efficiently treated with SRT, there is general consensus in using photon-based IMRT or PT, in particular for larger recurrent diseases (6). Due to the paucity of PT facilities worldwide, the choice between IMRT and PT should be ideally based on dosimetric comparison, so that resources are rationally utilized. As in treatment-naive patients, recent publications demonstrated that PT has some dosimetric advantages over IMRT in treating recurrent NPC (27, 28).

In the literature, a wide range of different survival rates is reported for recurrent NPC (9, 19, 29), reflecting the heterogenous stage distribution and treatment modalities. With 29 months median duration of follow-up, we observed a 5-year OS, DSS, and RFS estimates of 55.9, 62.1, and 41.3%, respectively. Our results set at an intermediate level in the wide range of outcomes, with surgical clinical series focusing on low-stage tumors reporting better results [73.8% 5-year OS in Liu et al. (9)] and studies on high-stage recurrent NPC treated with re-RT showing fewer encouraging results [37.0% 5-year OS in Boustani et al. (14)]. This owes to the fact that the full spectrum of stages was included in the present series.

Older patients experienced worse OS and DSS, in line with the literature (1). A shorter DFI influenced positively OS and DSS. Conversely, Tian et al. reported a negative effect on survival in patients whose disease recurred within 24 months from primary treatment (30). In the meta-analysis by Yue et al., however, no significant association was observed between recurrence time interval and OS (31). Our results could be justified by the non-negligible proportion of patients treated with surgery. A short DFI

10.3389/fonc.2023.1157584

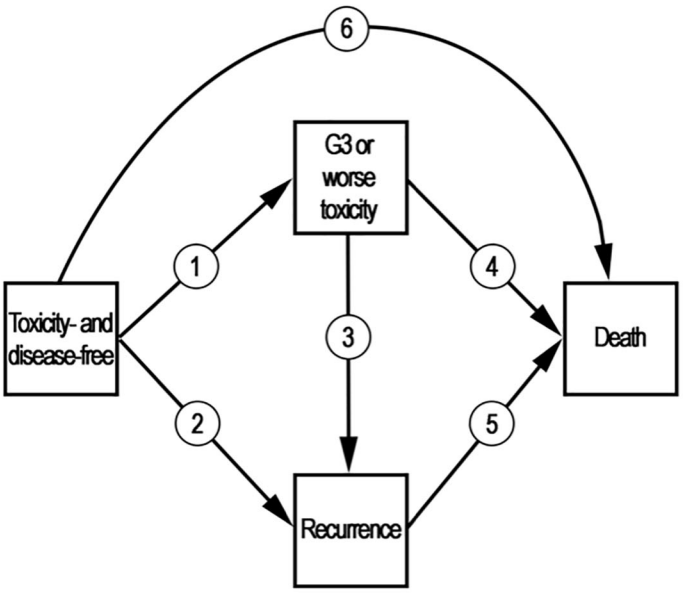

Transition	Variable	Hazard ratio (95%-CI)	p
1	Reconstruction with vascularized flap	0.47 (0.19, 1.16)	0.100
2	cN+ (primary tumor)	2.08 (0.97, 4.48)	0.061
	rT1 (recurrent tumor)	3.64 (1.11, 11.94)	0.033
	rT2 (recurrent tumor)	2.82 (0.93, 8.59)	0.068
	rT3 (recurrent tumor)	4.69 (1.39, 15.80)	0.013
	rT4 (recurrent tumor)	7.99 (0.93, 68.60)	0.058
	Neoadjuvant and/or adjuvant CT	0.33 (0.14, 0.74)	0.007
3	Age at recurrence	1.06 (0.99, 1.13)	0.083
	Disease-free interval	1.01 (1.00, 1.02)	0.084
	cT3 or cT4 (primary tumor)	4.29 (1.57, 11.66)	0.004
	cN+ (primary tumor)	3.45 (1.04, 11.40)	0.042
4	Age at recurrence	1.43 (1.11, 1.85)	0.005
	Disease-free interval	1.03 (1.00, 1.06)	0.046
	Concomitant CRT (primary treatment)	1066.66 (6.66, 170784.56)	0.007
	cT3 or cT4 (primary tumor)	4.53 (1.79, 11.50)	0.001
	cN+ (primary tumor)	2.49 (0.93, 6.69)	0.071
5	Concomitant CRT (primary treatment)	0.04 (0.00, 1.40)	0.076

FIGURE 3
Multistate multivariable analysis. The upper part of the figure represents graphically the 4-state, 6-transition model adopted to analyze the post-treatment course of patients included in the study. Each box represents a state, whereas arrows represent the potential transitions conceived in the model. The lower part of the figure displays a table reporting variables with a statistically significant or close-to-significant impact on state transition. For instance, disease- and toxicity-free patients who underwent a reconstruction based on vascularized tissue as part of their re-treatment had a close-to-significantly lower chance of developing ≥G3 toxicity (transition 1, p=0.100). patients with a nasopharyngeal carcinoma classified as cT3/4 at primary presentation who had a ≥G3 toxicity were more likely to either develop a recurrence (transition 3, p=0.004) or die being disease-free (transition 5, p=0.001) when compared to subjects with cT1/2 primary nasopharyngeal cancer. Transition 6 was not associated with any factor included in the analysis. CI, Confidence interval; CRT, Radiotherapy with concomitant chemotherapy; CT, Chemotherapy.

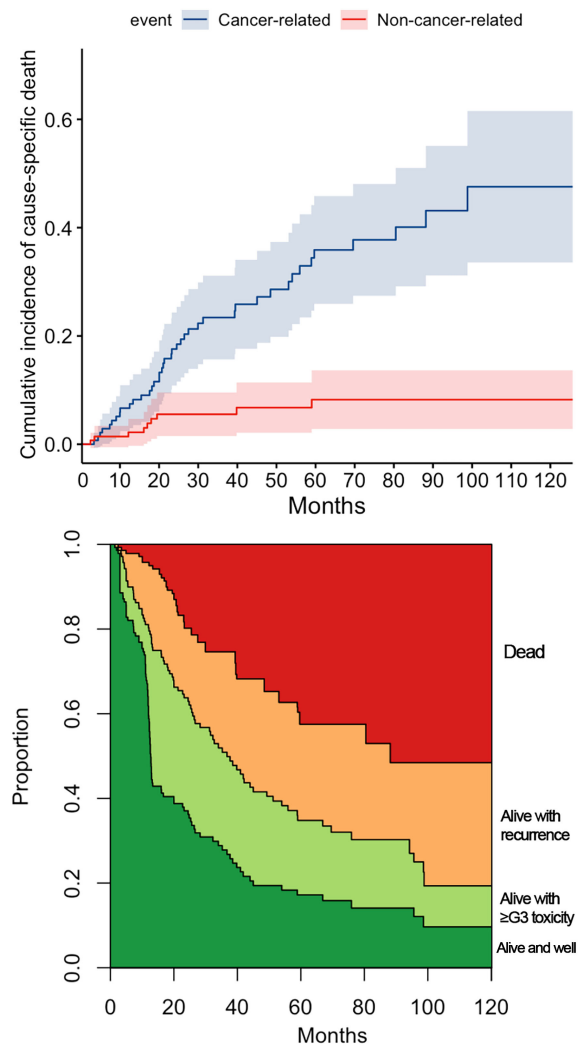

FIGURE 4
The cumulative incidence plot for cancer and non-cancer-related death. The stacked plot depicts the proportion of state (dead, alive with recurrence, alive with ≥G3 toxicity, or alive and well) distribution in the timepoint.

can be considered as an indirect sign of radio-resistance, thus directing the choice of treatment towards surgery. In case of persistence or short-DFI recurrence, an R0 nasopharyngectomy is held to eliminate radioresistant clones, improving survival. On the other hand, re-RT of an early recurring, radiosensitive NPC may correct an inadequate RT dose and/or dose distribution during primary treatment. In both scenarios, early salvage treatment can be considered as completion to primary treatment. Conversely, late relapsing NPCs have several potentially adverse features, including development of secondary cancer, asymptomatic growth to advanced stage, and reduction of patient's global reservoir to receive aggressive treatment.

Many research groups have confirmed the impact of rT classification on survival outcomes, both in surgical and re-RT series (1, 29). Accordingly, at our univariable analysis, primary and recurrent T category significantly influenced OS, DSS, and RFS. However, despite the increasing HR from rcT1 to rcT4, this association was not confirmed at multivariable analysis. RFS after recurrent tumor treatment was worse in cases with nodal involvement. Interestingly, these patients showed further recurrences more frequently on the primary sites instead of neck lymph nodes. This could imply rcT0N+ NPCs are associated with a considerable probability of occult local recurrence that becomes clinically appreciable after a certain time.

Although the RT group was predominantly represented by patients with rT3-4 cancers, no independent prognostic effect of loco-regional treatment modality (definitive re-RT vs. surgery w/o adjuvant therapy) on OS, DSS, or RFS was observed at multivariable analysis. This is partially inconsistent with the literature (9, 19). In our real-world series, the selection of the treatment modality was affected by technological availability together with specific experience of local radiation oncologists. Furthermore, the non-endemic nature of NPCs included in this study might have influenced the biological behavior and response to therapies.

Surgical margin status did not affect OS at univariable analysis. Furthermore, at multivariable analysis, no difference was highlighted between R0 and R1 resections in terms of OS, DSS, and RFS. Being prone to many biases, margin assessment in NER is probably a not reliable estimate of microscopic residual disease. The use of electrocautery or laser leads to shrinkage of the surgical specimen and hampers final pathological analysis. Moreover, the cancer advancement front may be non-homogenous: the effects of primary RT and neoadjuvant chemotherapy are different on cancer cell populations, resulting in potential satellite clones far from the main tumor advancement front (10). Recent consensus guidelines and literature data have reported that opinions vary widely from liberal use of postoperative re-RT to PT in case of involved surgical margins (6, 26). In the present series, according to local multidisciplinary team discussion, re-RT was indicated in case of margin involvement or advanced stage, but the main constraining factor was represented by cumulative dose distribution and estimated risk of toxicity. Thus, positive margins were not always associated with the chance of re-RT, nor did negative margins imply adjuvant re-RT to be automatically excluded from salvage treatment.

Neoadjuvant and/or adjuvant chemotherapy showed a protective effect on RFS, though not determining an impact on OS and DSS. The decreased probability of recurrence is probably counterbalanced by the chemoselection of aggressive clones, so that further recurrences, even if rarer than in patients not receiving chemotherapy in the salvage treatment, might display a more aggressive behavior. On the other hand, one cannot rule out selection bias of treating patients with a higher burden of disease by chemotherapy, and the possibility that in patients who did not receive chemotherapy, its subsequent administration at further relapse may have counterbalanced the positive effect on OS. However, the multistate analysis revealed that chemotherapy had no impact on transitions to death. Overall, chemotherapy showed a positive effect in terms of disease control, but its role in recurrent NPC still needs to be fully elucidated.

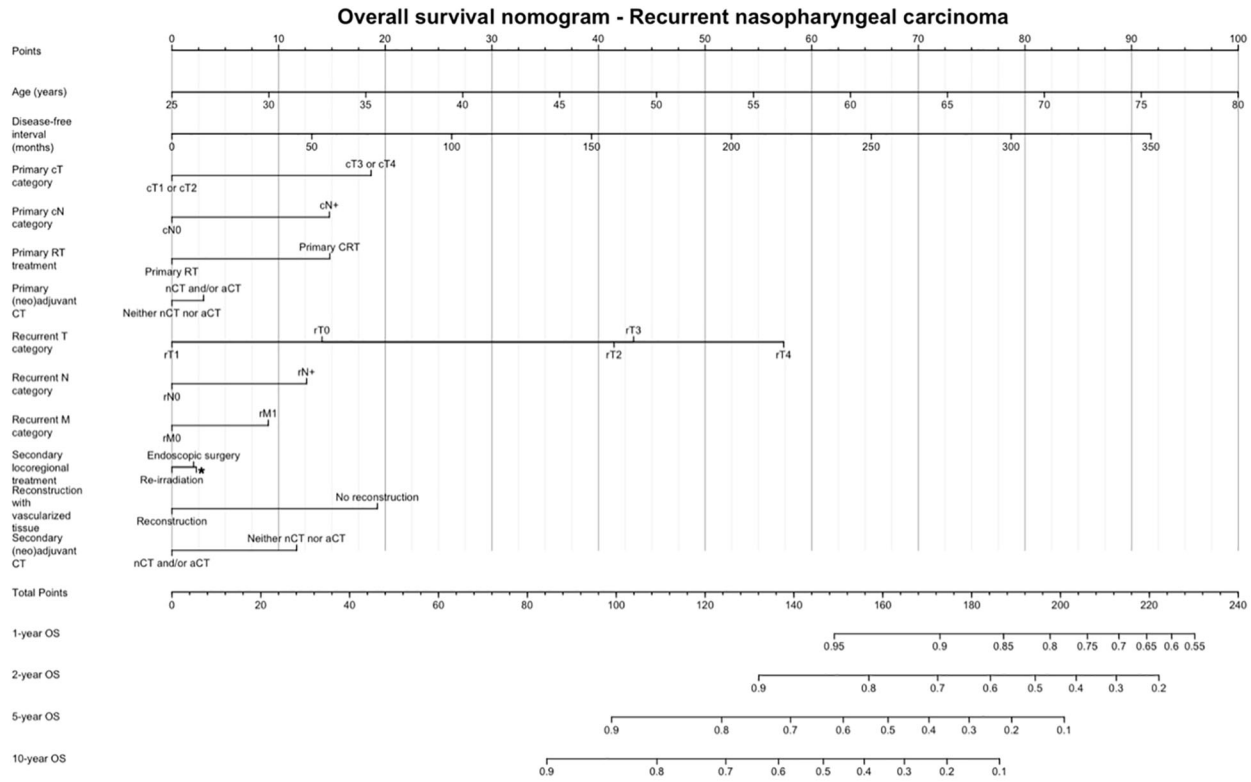

FIGURE 5
Overall survival nomogram, estimating the probability of survival at 1, 2, 5, and 10 years after retreatment. CT, Chemotherapy; RT, Radiotherapy.

We did not find a difference in terms of survival in patients treated with different techniques of re-RT (IMRT/VMAT, SRT, and PT). This might be partly due to the limited cohort size.

In our series, 40% of patients experienced at least one adverse event classified as G3 or higher. As seen at multivariable analysis, age and DFI were independent factors influencing OS. It is likely that toxicity of treatment heavily contributed to this observation. Indeed, multivariable multistate analysis showed that the same covariates were associated with an increased risk of transitioning from a state of ≥G3 toxicity to recurrence-free death. Of note, ≥G3 toxicity occurred constantly over the post-retreatment period, thus underlying the need for close surveillance of these possible adverse effects (Figure 4).

The most frequent late complication in both the surgical and re-RT groups was skull base osteomyelitis. Schreiber et al. demonstrated the correlation between the location and entity of the osteomyelitis with the field and dose of RT (32). This justifies the finding that its frequency is remarkably higher in the re-RT group compared to the surgical group (10 vs. 6 cases, respectively) (22). However, this observation might be related to the fact that the re-RT group included a higher proportion of high-stage diseases. Patients with most advanced recurrences are hardly ever candidates for surgery and usually undergo re-RT, with higher risk of morbidity. Moreover, since high-stage primary lesions are prone to have high-stage recurrence (Table 2), re-irradiated patients had likely already undergone a primary irradiation with a non-negligible toxicity profile.

Of note, all 3 cases of internal carotid artery blowout observed in the re-RT group were treated with PT. In comparison to conformal RT techniques at the same prescription dose, PT planning can result in very high dose hot spots in the target volume, with a potentially high rate of vascular and mucosal complications (27). Moreover, although re-RT planning criteria to ensure both tumor coverage and organs at risk preservation have been proposed with the goal of decreasing radiation-induced life-threatening injuries (thus increasing cure rates) (6, 33), a comprehensive dosimetric analysis of normal tissue complications with more advanced RT techniques, including PT, is lacking. In selected cases, the stenting or occlusion of the carotid artery before starting salvage treatment should be considered to avoid fatal blowouts, although the chance of cerebrovascular and non-cerebrovascular complications should be discussed within the multidisciplinary team (11).

No significant difference in the morbidity profile of treatments was observed. In fact, not only was the rate of ≥G3 adverse events not significantly different among treatment strategies, but multistate multivariable analysis also showed that there was no impact of treatment modality on the transition from the disease- and toxicity-free state to recurrence-free ≥G3 toxicity state. This discrepancy

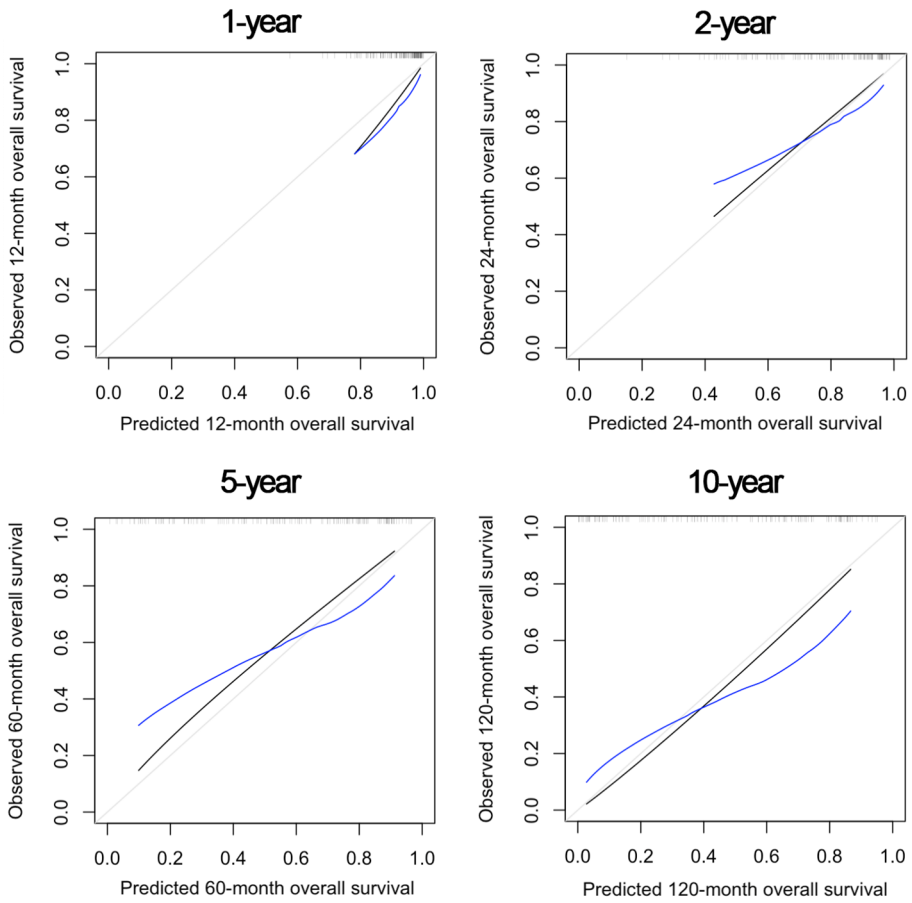

FIGURE 6
Internal validation of the nomogram model at 1, 2, 5, and 10 years after re-treatment timepoints, showing satisfactory predictive performance.

with the literature, where surgery is associated with lower complication rates (9), can be partially explained by the adverse events classification system used in this study. Even if designed to study the adverse effects of RT, the CTCAE system allows for homogeneous and fair assessment of complications and unveiled a more balanced situation between the treatment arms as would have been expected. Of note, in the surgical group, reconstruction with a vascularized flap showed a protective effect on the development of ≥G3 toxicity, thus highlighting the importance of using vascularized tissue to ensure adequate blood supply to previously irradiated tissues, which by definition have impaired microcirculation.

Finally, we provided a prognostic nomogram for non-endemic recurrent NPC, which had adequate accuracy at internal validation. Sun et al. (34) developed a nomogram for patients with endemic local recurrent NPC based on pre-treatment data, thus allowing prediction of OS and guide individualized treatment. We chose to include data in the pre- and post-treatment phases, so that the nomogram can be used: 1) to have a quantitative estimate of chances of survival in a given patient and 2) to appreciate the putative effect of controllable variables (e.g., treatment strategy, use of vascularized reconstruction) on the overall outcome estimate.

The main limits of this study are represented by its retrospective nature and the collection of multiple experience of different referral centers, sharing the same philosophy but not following a common treatment protocol. The precise collection of other recognized prognostic factors, such as performance status, quality of life, and circulating Epstein-Barr virus DNA, was not possible in this retrospective series. Furthermore, the analyses included local, regional, and locoregional recurrences. This makes the results of the present study more complex to be interpreted but brings them closer to a real-world scenario. Overall, taking into consideration the heterogeneity and the rarity of the pathology, this study can be considered as the basis for future prospective trials.

Conclusion

To date, clear evidence guiding the choice of treatment for non-endemic recurrent NPC are lacking. In our series, favorable cases with lower age, comorbidity rate, and stage underwent preferentially endoscopic surgery, as well as patients with shorter DFI from primary treatment. More complex cases underwent re-RT, distributed between photon-based RT and PT.

Age and DFI were independent factors influencing OS. No independent prognostic effect of treatment modality was observed, suggesting that the non-endemic nature of NPCs might have influenced the biological behavior and response to therapies. No statistical difference in the morbidity profile of treatments was

TABLE 8 Spectrum of complications classified as ≥G3 observed in the series.

	Surgery	Surgery + postoperative Re-irradiation	Definitive Re-irradiation
Intraoperative			
Internal carotid artery injury	1	0	0
Early post-treatment (≤30 days)			
Osteomyelitis	0	0	1
Pain	3	1	1
Mucositis	0	0	6
XII nerve palsy	1	0	1
Extraocular muscle paresis	1	1	0
Dysphagia	0	0	1
Neutropenia	0	0	1
Late post-treatment (>30 days)			
Osteomyelitis/osteoradionecrosis	6	2	10
Nasal congestion	3	1	0
Pain	5	3	0
Mucositis	0	2	2
Internal carotid artery blowout	0	0	3
Brain edema	0	1	2
Brain necrosis	1	0	2
Trismus	3	0	1
Hearing loss	1	0	5
Dyspnea	3	0	0

observed, with 40% of patients experiencing at least one adverse event classified as G3 or higher.

The recurrent non-endemic NPC has dissimilar aspects compared to the endemic counterpart, suggesting the need for further survival studies that can guide the choice of the best treatment modality for each patient.

Data availability statement

The raw data supporting the conclusions of this article will be made available by the authors, without undue reservation.

Ethics statement

The studies involving human participants were reviewed and approved by Comitato etico di Brescia, Brescia, Italy. The patients/participants provided their written informed consent to participate in this study.

Author contributions

VR and MF substantially contributed to the conception and design of the work, interpretation of data, and drafting the work. DM, PiB, AL, MT-Z, ED'A, DA, MC, BV, MT, RR, MA, ST, DT, MM, MB, NI, FD, MaBi, AD, PaBa, PaB, and CP substantially contributed to acquisition and interpretation of data. AS, PN, PC, and EO substantially contributed to conception and design of the work, and interpretation of data. All Authors provide approval for publication of the content and agree to be accountable for all aspects of the work in ensuring that questions related to the accuracy or integrity of any part of the work are appropriately investigated and resolved.

Conflict of interest

The authors declare that the research was conducted in the absence of any commercial or financial relationships that could be construed as a potential conflict of interest.

Publisher's note

References

1. Li YQ, Tian YM, Tan SH, Liu MZ, Kusumawidjaja G, Ong EHW, et al. Prognostic model for stratification of radioresistant nasopharynx carcinoma to curative salvage radiotherapy. *J Clin Oncol* (2018) 36(9):891–9. doi: 10.1200/JCO.2017.75.5165

2. Lee AWM, Ng WT, Chan JYW, Corry J, Mäkitie A, Mendenhall WM, et al. Management of locally recurrent nasopharyngeal carcinoma. *Cancer Treat Rev* (2019) 79:101890. doi: 10.1016/j.ctrv.2019.101890

3. Chee J, Ting Y, Ong YK, Chao SS, Loh KS, Lim CM. Relapse status as a prognostic factor in patients receiving salvage surgery for recurrent or residual nasopharyngeal cancer after definitive treatment. *Head Neck* (2016) 38(9):1393–400. doi: 10.1002/hed.24451

4. NCCN. *Guidelines for head and neck cancers V.1*. (2022). Retrieved from: https://www.nccn.org/guidelines

5. Bossi P, Chan AT, Licitra L, Trama A, Orlandi E, Hui EP, et al. ESMO guidelines committee. EURACAN. nasopharyngeal carcinoma: ESMO-EURACAN clinical practice guidelines for diagnosis, treatment and follow-up. *Ann Oncol* (2021) 32(4):452–65. doi: 10.1016/j.annonc.2020.12.007

6. Ng WT, Soong YL, Ahn YC, AlHussain H, Choi HCW, Corry J, et al. International recommendations on reirradiation by intensity modulated radiation therapy for locally recurrent nasopharyngeal carcinoma. *Int J Radiat Oncol Biol Phys* (2021) 110(3):682–95. doi: 10.1016/j.ijrobp.2021.01.041

7. Wang D, Liao M, Wu J, Luo W, Qi S, Liu B, et al. Salvage treatments for locally recurrent nasopharyngeal cancer: a systematic review and meta-analysis. *Head Neck* (2023) 45(2):503–20. doi: 10.1002/hed.27253

8. Hao CY, Hao SP. The management of rNPC: salvage surgery vs. re-irradiation. *Curr Oncol Rep* (2020) 22(9):86. doi: 10.1007/s11912-020-00949-0

9. Liu YP, Wen YH, Tang J, Wei Y, You R, Zhu XL, et al. Endoscopic surgery compared with intensity-modulated radiotherapy in resectable locally recurrent nasopharyngeal carcinoma: a multicentre, open-label, randomised, controlled, phase 3 trial. *Lancet Oncol* (2021) 22(3):381–90. doi: 10.1016/S1470-2045(20)30673-2

10. Ferrari M, Zanoletti E, Taboni S, Cazzador D, Tealdo G, Schreiber A, et al. Resection of the internal carotid artery in selected patients affected by cancer of the skull base. *Head Neck* (2022) 44(4):1030–42. doi: 10.1002/hed.26967

11. Orlandi E, Ferrari M, Lafe E, Preda L, Benazzo M, Vischioni B, et al. When everything revolves around internal carotid artery: analysis of different management strategies in patients with very advanced cancer involving the skull base. *Front Oncol* (2021) 11:781205. doi: 10.3389/fonc.2021.781205

12. Zhu Y, Liu K, Ding D, Wang K, Liu X, Tan X. Chemo-immunotherapy regimes for recurrent or metastatic nasopharyngeal carcinoma: a network meta-analysis and cost-effectiveness analysis. *Front Pharmacol* (2022) 13:858207. doi: 10.3389/fphar.2022.858207

13. Howlett J, Hamilton S, Ye A, Jewett D, Riou-Green B, Prisman E, et al. Treatment and outcomes of nasopharyngeal carcinoma in a unique non-endemic population. *Oral Oncol* (2021) 114:105182. doi: 10.1016/j.oraloncology.2021.105182

14. Boustani J, Ruffier A, Moya-Plana A, Tao Y, Nguyen F, Even C, et al. Long-term outcomes and safety after reirradiation in locally recurrent nasopharyngeal carcinoma in a non-endemic area. *Strahlenther Onkol* (2021) 197(3):188–97. doi: 10.1007/s00066-020-01647-3

15. Karam I, Huang SH, McNiven A, Su J, Xu W, Waldron J, et al. Outcomes after reirradiation for recurrent nasopharyngeal carcinoma: north American experience. *Head Neck* (2016) 38 Suppl 1:E1102–9. doi: 10.1002/hed.24166

16. Castelnuovo P, Nicolai P, Turri-Zanoni M, Battaglia P, Bolzoni Villaret A, Gallo S, et al. Endoscopic endonasal nasopharyngectomy in selected cancers. *Otolaryngol Head Neck Surg* (2013) 149(3):424–30. doi: 10.1177/0194599813493073

17. Amin MB ed. *AJCC cancer staging manual. 8th Edition*. Switzerland: Springer (2017) p. 431–55.

18. US Department of Health and Human Services. *Common terminology criteria for adverse events. version 5.0. Published November 27, 2017*. (2020). Retrieved from: https://ctep.cancer.gov/protocoldevelopment/electronic_applications/docs/ctcae_v5_quick_reference_5x7.pdf

19. Ng WT, Wong ECY, Cheung AKW, Chow JCH, Poon DMC, Lai JWY, et al. Patterns of care and treatment outcomes for local recurrence of NPC after definite IMRT-a study by the HKNPCSG. *Head Neck* (2019) 41(10):3661–9. doi: 10.1002/hed.25892

20. Economopoulou P, Pantazopoulos A, Spathis A, Kotsantis I, Kyriazoglou A, Kavourakis G, et al. Immunotherapy in nonendemic nasopharyngeal carcinoma: real-world data from two nonendemic regions. *Cells* (2021) 11(1):32. doi: 10.3390/cells11010032

21. Bossi P, Trama A, Bernasconi A, Grisanti S, Mohamad I, Galiana IL, et al. Nasopharyngeal cancer portal group of investigators. nasopharyngeal cancer in non-endemic areas: impact of treatment intensity within a large retrospective multicentre cohort. *Eur J Cancer* (2021) 159:194–204. doi: 10.1016/j.ejca.2021.09.005

22. Peng Z, Wang Y, Fan R, Gao K, Xie S, Wang F, et al. Treatment of recurrent nasopharyngeal carcinoma: a sequential challenge. *Cancers (Basel)* (2022) 14(17):4111. doi: 10.3390/cancers14174111

23. Yang SS, Guo JG, Liu JN, Liu ZQ, Chen EN, Chen CY, et al. Effect of induction chemotherapy in nasopharyngeal carcinoma: an updated meta-analysis. *Front Oncol* (2021) 10:591205. doi: 10.3389/fonc.2020.591205

24. Wang Y, Wang ZQ, Jiang YX, Wang FH, Luo HY, Liang Y, et al. A triplet chemotherapy regimen of cisplatin, fluorouracil and paclitaxel for locoregionally recurrent nasopharyngeal carcinoma cases contraindicated for re-irradiation/surgery. *Expert Opin Pharmacother* (2016) 17(12):1585–90. doi: 10.1080/14656566.2016.1204293

25. Leong YH, Soon YY, Lee KM, Wong LC, Tham IWK, Ho FCH. Long-term outcomes after reirradiation in nasopharyngeal carcinoma with intensity-modulated radiotherapy: a meta-analysis. *Head Neck* (2018) 40(3):622–31. doi: 10.1002/hed.24993

26. Na'ara S, Amit M, Billan S, Cohen JT, Gil Z. Outcome of patients undergoing salvage surgery for recurrent nasopharyngeal carcinoma: a meta-analysis. *Ann Surg Oncol* (2014) 21(9):3056–62. doi: 10.1245/s10434-014-3683-9

27. Hung HM, Chan OCM, Mak CH, Hung WM, Ng WT, Lee MCH. Dosimetric comparison of intensity modulated radiotherapy and intensity modulated proton therapy in the treatment of recurrent nasopharyngeal carcinoma. *Med Dosim* (2022) 47(1):14–9. doi: 10.1016/j.meddos.2021.07.002

28. Vai A, Molinelli S, Rossi E, Iacovelli NA, Magro G, Cavallo A, et al. Proton radiation therapy for nasopharyngeal cancer patients: dosimetric and NTCP evaluation supporting clinical decision. *Cancers (Basel)* (2022) 14(5):1109. doi: 10.3390/cancers14051109

29. Yang J, Song X, Sun X, Liu Q, Hu L, Yu H, et al. Outcomes of recurrent nasopharyngeal carcinoma patients treated with endoscopic nasopharyngectomy: a meta-analysis. *Int Forum Allergy Rhinol* (2020) 10(8):1001–11. doi: 10.1002/alr.22552

30. Tian YM, Tian YH, Zeng L, Liu S, Guan Y, Lu TX, et al. Prognostic model for survival of local recurrent nasopharyngeal carcinoma with intensity-modulated radiotherapy. *Br J Cancer* (2014) 110(2):297–303. doi: 10.1038/bjc.2013.715

31. Yue Q, Zhang M, Chen Y, Zheng D, Chen Y, Feng M. Establishment of prognostic factors in recurrent nasopharyngeal carcinoma patients who received salvage intensity-modulated radiotherapy: a meta-analysis. *Oral Oncol* (2018) 81:81–8. doi: 10.1016/j.oraloncology.2018.04.017

32. Schreiber A, Ravanelli M, Rampinelli V, Ferrari M, Vural A, Mattavelli D, et al. Skull base osteomyelitis: clinical and radiologic analysis of a rare and multifaceted pathological entity. *Neurosurg Rev* (2021) 44(1):555–69. doi: 10.1007/s10143-020-01254-x

33. Dionisi F, Fiorica F, D'Angelo E, Maddalo M, Giacomelli I, Tornari E, et al. Organs at risk's tolerance and dose limits for head and neck cancer re-irradiation: a literature review. *Oral Oncol* (2019) 98:35–47. doi: 10.1016/j.oraloncology.2019.08.017

34. Sun XS, Liang YJ, Jia GD, Liu SL, Liu LT, Guo SS, et al. Establishment of a prognostic nomogram to identify optimal candidates for local treatment among patients with local recurrent nasopharyngeal carcinoma. *Oral Oncol* (2020) 106:104711. doi: 10.1016/j.oraloncology.2020.104711

frontiers | Frontiers in Oncology

TYPE Original Research
PUBLISHED 07 June 2023
DOI 10.3389/fonc.2023.1143401

OPEN ACCESS

EDITED BY
Giuseppe Carlo Iorio,
University of Turin,
Italy

REVIEWED BY
Wang-Zhong Li,
First Affiliated Hospital of Guangzhou Medical University, China
Isacco Desideri,
University of Florence, Italy
Ilaria Morelli,
University of Florence, Italy

*CORRESPONDENCE
Feng Liu
liufeng820111@163.com

†These authors have contributed equally to this work and share first authorship

RECEIVED 12 January 2023
ACCEPTED 15 May 2023
PUBLISHED 07 June 2023

CITATION
He L-l, Xiao S, Jiang C-h, Wu X-w, Liu W, Fan C-g, Ye X, Zhao Q, Wu W-q, Li Y-x, Wang H and Liu F (2023) A randomized, controlled trial to investigate cognitive behavioral therapy in prevention and treatment of acute oral mucositis in patients with locoregional advanced nasopharyngeal carcinoma undergoing chemoradiotherapy.
Front. Oncol. 13:1143401.
doi: 10.3389/fonc.2023.1143401

A randomized, controlled trial to investigate cognitive behavioral therapy in prevention and treatment of acute oral mucositis in patients with locoregional advanced nasopharyngeal carcinoma undergoing chemoradiotherapy

Li-li He[1†], Shuai Xiao[1†], Cui-hong Jiang[1], Xiang-wei Wu[1], Wen Liu[1], Chang-gen Fan[1], Xu Ye[1], Qi Zhao[1], Wen-qiong Wu[1], Yan-xian Li[1], Hui Wang[1,2] and Feng Liu[1*]

[1]Department of Radiation Oncology, Hunan Cancer Hospital and The Affiliated Cancer Hospital of Xiangya School of Medicine, Central South University, Changsha, Hunan, China, [2]Hunan Key Laboratory of Translational Radiation Oncology, Hunan Cancer Hospital and The Affiliated Cancer Hospital of Xiangya School of Medicine, Central South University, Changsha, Hunan, China

Purpose: Oral mucositis is a common side effect of concurrent chemoradiotherapy (CCRT). This study aimed to determine whether cognitive behavioral therapy (CBT) could help prevent oral mucositis during chemoradiation therapy for locoregional advanced nasopharyngeal carcinoma (LA-NPC).

Methods and materials: Between July 15, 2020, and January 31, 2022, a randomized controlled phase II trial was conducted. Eligible patients (N=282, 18-70 years old) with pathologically diagnosed LA-NPC were randomly assigned to receive CBT or treatment as usual (TAU) during CCRT (computer-block randomization, 1:1). The primary endpoints were the incidence and latency of oral mucositis.

Results: The incidence of oral mucositis was significantly lower in the CBT group (84.8%; 95% confidence interval [CI], 78.7%-90.9%) than in the TAU group (98.6%; 95% CI, 96.6%-100%; P<0.001). The median latency period was 26 days and 15 days in the CBT and TAU groups, respectively (hazard ratio, 0.16; 95% CI, 0.12-0.22; P<0.001). CBT significantly reduced ≥ grade 3 oral mucositis (71.9% vs. 22.5%, P<0.001), dry mouth (10.8% vs. 3.7%, P=0.021), dysphagia (18% vs. 5.1%, P=0.001), and oral pain (10% vs. 3.6%, P=0.034) compared with TAU. Patients receiving CBT and TAU during CCRT had similar short-term response rates.

Conclusions: CBT reduced the occurrence, latency, and severity of oral mucositis in patients with LA-NPC during CCRT.

KEYWORDS

cognitive behavioral therapy (CBT), chemoradiotherapy, nasopharyngeal carcinoma, acute oral mucositis, toxicities

1 Introduction

Nasopharyngeal carcinoma (NPC) is a malignant tumor with the highest incidence in southern China (1, 2). Concurrent chemoradiotherapy (CCRT) is a major component of curative therapy for locoregional advanced nasopharyngeal carcinoma (LA-NPC) (3, 4); however, it can lead to toxic side effects. The most common complication of NPC related to chemoradiotherapy (CRT) is oral mucositis (OM) (5), and its incidence in patients with NPC ranges from 85% to 100% (6–8). OM commonly reduces the nutritional status and quality of life of patients owing to pain and dysphagia in the mouth (9). Patients with severe oral mucositis (SOM; classified into 3-4 grades according to World Health Organization [WHO]) frequently experience an interruption of treatment and prolonged treatment, both of which negatively affect treatment outcomes (10–13).

Basic oral care is a good clinical practice for oncology patients with mucositis (14). Unfortunately, there is no standard treatment for the prevention of OM. Topical agents (15), oral drugs (16–19), and intravenous drugs (20) have all been studied for the prevention and treatment of OM caused by chemotherapy/radiotherapy; however, none of them can be used as a standard treatment. Photobiomodulation is effective in preventing OM caused by CCRT; however, it can cause cancer in the long run (21, 22).

Consequently, there is an urgent need to develop a feasible and effective management method to take precautions against OM in LA-NPC patients undergoing CCRT. Cognitive behavioral therapy (CBT) has already been confirmed to be an effective psychological treatment to avoid or decrease the occurrence of adverse effects in patients with proven malignancies (23–26). In our previous study, we found that the combination of CBT and CRT significantly reduced acute OM in patients with LA-NPC (27).

To the best of our knowledge, no randomized clinical trials have investigated CBT to prevent and relieve acute chemoradiotherapy-induced OM and improve the survival quality of LA-NPC. Therefore, we performed a randomized controlled trial to assess the preventive and therapeutic effects of CBT on OM in patients with LA-NPC treated with chemoradiotherapy.

2 Methods and materials

2.1 Clinical trial design

This study was a phase II, prospective, randomized, single-center clinical trial. The assay was registered on the chictr.org.cn website (ChiCTR2000034701). This prospective study was approved by the institutional ethics committee and conducted in accordance with the ethical standards formulated in the Declaration of Helsinki. Patients with advanced cancer diagnosed by pathology were selected according to the principles of phase II clinical trial and signed informed consent forms. After checking the eligibility criteria, a computer-generated code was used for randomization. Patients were randomized in a 1:1 ratio to receive either CBT (group A) or treatment as usual (TAU) (group B).

2.2 Eligibility criteria

All the cases were diagnosed as NPC by pathology. Patients with the following baseline characteristics were eligible for the study: WHO pathological types II-III, clinical stage III-IVa (8_{th} American Joint Committee on Cancer); 18-70 years old; Karnofsky physical status ≥ 70; absence of significant oral disease; undergoing 1 to 3 cycles of induction chemotherapy (IC); and normal routine blood cell tests (the total number of leukocytes $\geq 4.0 \times 10^9$/L, absolute neutrophil count $\geq 1.5 \times 10^9$/L, hemoglobin ≥90 g/L, and platelets $\geq 100 \times 10^9$/L), hepatic, and renal function tests. Patients were excluded if they had a history of prior radiation therapy (RT), secondary primary malignant tumor, evidence of distant metastasis, OM or recurrent OM prior to CRT, gingivitis or stomatitis, severe life-threatening illness, psychological or mental health conditions (such as suicidal tendency), and pregnancy or lactating.

2.3 Baseline assessment

Detailed case history of patients with NPC was recorded prior to their treatment. Routine physical examination, hematology and biochemical indices, Epstein-Barr virus (EBV) DNA copies, electro-nasopharyngoscope, nasopharynx and neck enhanced magnetic resonance imaging (MRI), chest enhanced computed tomography (CT), abdominal ultrasound, whole body bone SPECT imaging, and dental and nutritional status were also assessed in our study before IC.

2.4 Radiotherapy

Mask immobilization was performed in all patients using CT simulations and CT-based planning. The CT simulation was

conducted one week after the IC cycle. All patients underwent enhanced MRI before and after IC.

All patients were treated with intensity-modulated radiation therapy (IMRT) at a dose of 70.4 Gy/32 fx and 72.6 Gy/33 fx to the gross tumor volume of the nasopharynx (GTVnx) in stage T1-2 and T3-4 disease, respectively. A total dose of 69.96 to 72.6 Gy was administered to the gross tumor volume of the lymph nodes (GTVnd). Doses prescribed for high-risk subclinical lesions (planning target volume 1, PTV1) and lower-risk subclinical disease (planning target volume 2, PTV2) were 60.06 to 64 Gy/32 to 33 fx and 50.96 to 56.0 Gy/26 to 28 fx, respectively. RT was administered daily from Monday through Friday for 32–33 days. It is important to note that the normal tissue doses were designed according to Radiation Therapy Oncology Group (RTOG) 0615 (28) and RTOG 0225 protocols (29). In our study, onboard image guidance was performed prior to the first five treatments and then weekly thereafter.

2.5 Chemotherapy

The IC regimen consisted of TPF (docetaxel at 60 mg/m^2, d1, intravenous infusion, plus cisplatin at 60 mg/m^2, d1, intravenous infusion, and 5-fluorouracil at 600 mg/m^2, d1-d5, intravenous 120-hour infusion) or TP (docetaxel at 75 mg/m^2, d1, intravenous infusion, plus cisplatin at 75 mg/m^2, d1, intravenous infusion) administered every 3 weeks. Patients were prescribed CCRT with cisplatin alone (80–100 mg/m^2, d1, intravenous infusion) every 3 weeks. All patients planned to receive CCRT, except those who declined treatment or experienced severe adverse events. According to previous studies (30, 31), the cut-off value of cumulated concurrent cisplatin dose was 200 mg/m^2.

2.6 Cognitive behavioral therapy

The large body of empirical data from the work of Ellis (1962) and Beck (1976) (32) and the manual written by Beck et al. (33) supports the efficacy of CBT in treating psychological conditions and associated adverse events. A special treatment plan was designed based on previous studies (24, 34, 35) and the psychological characteristics of patients with NPC. Behavioral, cognitive, and educational strategies were combined into the intervention. The participants in the CBT group received six sessions along with concurrent chemoradiotherapy. The CBT method used in this study is the same as that used in our previous study (27).

The intervention was led by an oncologist doctor, and a multidisciplinary team including a psychotherapist, two oncologists, and two nurses had a 3-day training course. In a group of six participants, CBT was administered once a week in 45 minutes sessions for 6 weeks during concurrent chemoradiotherapy. Prior to the study, all evaluators and therapists received rigorous and uniform training, following Standard Operating Procedures (SOPs) to ensure the quality of this study. To ensure protocol adherence, sessions and scripts were recorded. We randomly selected and assessed the fidelity of the recordings and provided feedback to the psychotherapist. Weekly themes and the main content of the CBT sessions in the present study were the same as those in our previous article (27).

2.7 Treatment as usual

All patients were treated with TAU according to the standards of the oncology radiotherapy department. TAU consists of irregular intervals of educational sessions that include information on health, nutrition, and psychology and provides explanations tailored to the patient or family's problems.

2.8 Concomitant medication

All patients were given conventional oral health guidance and education. All patients underwent oral cleaning immediately after eating. From the first day of chemoradiotherapy, oral cleaning immediately after eating was administered until the entire radiotherapy course was completed. Other medicines for oral mucositis including hormones and antibiotics were not prescribed for patients with grade 1-2 oral mucositis. Sodas and antifungal agents were used in patients with oral cavity fungal infections. Patients could withdraw from the trial if they had grade 3 or higher oral mucositis or if they did not wish to continue the study.

2.9 Evaluation

According to the National Cancer Institute (NCI) Common Terminology Criteria for Adverse Events (CTCAE) version 5.0, oral mucositis is defined as a disorder characterized by ulceration or inflammation of the oral mucosa. The grading criteria of oral mucositis as per CTCAE5.0 were as follows: 1 = Asymptomatic or mild symptoms, intervention not indicated; 2 = Moderate pain or ulcer that does not interfere with oral intake, modified diet indicated; 3 = Severe pain interfering with oral intake; 4 = Life-threatening consequences, urgent intervention indicated; 5 = Death. Oral pain is defined as a sensation of marked discomfort in the mouth, tongue, or lips. The grading criteria of oral pain as per CTCAE5.0 were as follows: 1 = mild pain; 2 = moderate pain, limiting instrumental activities of daily living (ADL); and 3 = severe pain, limiting self-care ADL. Acute oral mucosal toxicity and pain during treatment were carefully observed and assessed daily. The time to the development of grade 3 mucositis was recorded on day 1 of radiotherapy.

Both groups were evaluated for anxiety and depression by a trained psychotherapist using the Hospital Anxiety and Depression Scale (HADS) at baseline (T1) and the end of CCRT (T2). The HADS is a 14-item self-administered questionnaire that measures the symptoms of anxiety (HADS-A) and depression (HADS-D) in patients with somatic illness. The possible scores ranged from 0 to 21 for anxiety and 0 to 21 for depression. This scale has been widely used in cancer research (27, 36). A higher score indicates a more severe level of anxiety and/or depression.

Three months after the completion of chemoradiotherapy, the patients underwent physical examination, nasopharyngoscopy, and MRI to assess tumor response, which was classified according to the Response Evaluation Criteria in Solid Tumors (version 1.1) (37).

2.10 Outcomes

The incidence of oral mucositis and latency to oral mucositis during this study were used as the primary efficacy endpoints. The severity of oral mucositis and accompanying symptoms (e.g., dry mouth, dysphagia, and oral pain) were used as secondary efficacy endpoints.

2.11 Sample size

PASS v11 software was used to calculate the sample size. Two-sided alpha was used in this study. Based on previous randomized studies assessing oral mucositis during chemoradiotherapy for locally advanced NPC, the incidence of ≥ grade 3 oral mucositis ranged from 61.6% to 74.0% (17, 38). The study was designed to detect a 25% difference in the incidence of grade 3 mucositis, assuming an incidence of 70% in the control group. A minimum sample size of 224 (112 in each group) was required for a power of 80% and a significance level (alpha) of 0.05. To allow for a 10% loss rate, the total sample size required in each group was at least 246. One-way ANOVA and chi-square tests were used to compare measurement data and count data between the two groups, respectively.

2.12 Statistical analysis

Fisher's exact test was used to compare the incidence of different degrees of oral mucositis, and 95% confidence intervals (CIs) were calculated. The median time of occurrence of oral mucositis (latency) and 95% confidence interval (CI) was estimated using the Kaplan-Meier method. To compare latencies, the Cox proportional hazards model was used to calculate the hazard ratio and 95% CI values. Secondary efficacy endpoints and toxicities were compared using a 1-way analysis of variance and Fisher's exact test. For HADS scores, the total and subscale scores of each measure at the two time points (T1 and T2) were analyzed using an independent samples t-test. All statistical tests were two-sided, and statistical significance was set at $P < 0.05$. All statistical analyses were performed using the commercial software package SPSS version 25.0 (IBM Corporation, Armonk, NY, USA).

3 Results

From July 15, 2020, to January 31, 2022, 282 patients with LA-NPC were randomly assigned to one of the two study groups (Figure 1). A total of 138 patients in the CBT group received cognitive behavioral therapy, and 139 patients in the TAU group received treatment as usual. The clinical characteristics of the two groups were relatively balanced. Table 1 provides additional information.

*Three patients with distant metastasis, two patients without adequate hematological function, one without adequate renal function, two with hepatotoxicity, and one patient with heart disease. Abbreviations: FAS = full-analysis set; PPS = per-protocol set

3.1 Treatment compliance

One hundred and thirty-seven patients (99.3%) in the CBT group and 137 patients (98.6%) in the TAU group completed at least two cycles of CCRT (Table 2). CCRT was suspended owing to severe hematological toxicity, severe vomiting, and patient refusal. One patient in the CBT group withdrew from the trial in the seventh week of CCRT because of severe leukopenia and fatigue. Two patients in the TAU group who could not tolerate the symptoms of severe OM ended the trial early in the sixth week of CCRT. For patients who withdrew from the trial owing to grade 3 or higher oral mucositis, the standard treatment for severe oral mucositis was applied. All patients in the CBT group completed the planned six sessions of CBT. All but one of the participants received the full planned dose of radiotherapy without any treatment delays > 5 days. The patient in the TAU group received 70.4 Gy (97.0%) of the prescribed RT dose (72.6 Gy planned) and

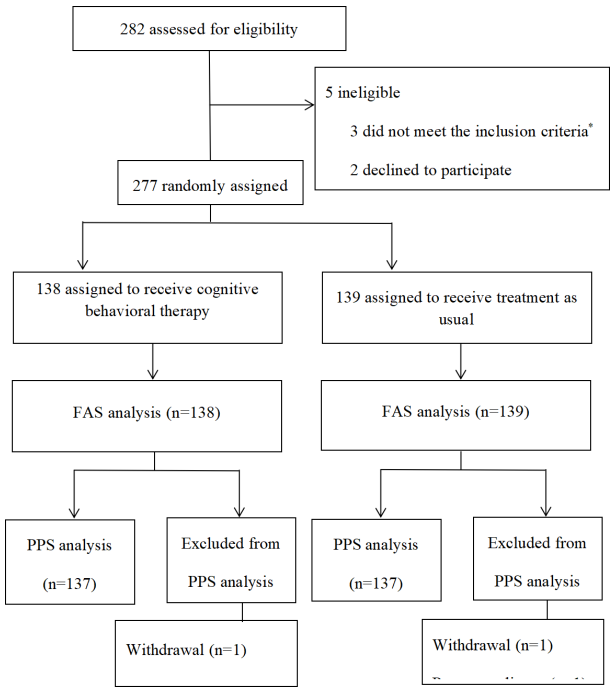

FIGURE 1
Patients included in the study. *Three patients with distant metastasis, two patients without adequate hematological function, one without adequate renal function, two with hepatotoxicity, and one patient with heart disease. FAS = full-analysis set; PPS = per-protocol set.

10.3389/fonc.2023.1143401

TABLE 1 Baseline characteristics.

Characteristics	CBT group	TAU group	
	No. of patients (%)	No. of patients (%)	P value
Total	138	139	
Age, y			
Median	51	52	
Range	18-70	23-70	
Sex			0.358
Male	105 (76.1)	99 (71.2)	
Female	33 (23.9)	40 (28.8)	
Karnofsky scale			0.414
90-100	122 (88.4)	127 (91.4)	
70-80	16 (11.6)	12 (8.6)	
Smoking status			0.572
Never-smoker	40 (29.0)	38 (27.3)	
Cigarette smoker, pack-years			
< 10	22 (15.9)	29 (20.9)	
≥ 10	76 (55.1)	72 (51.8)	
EBV DNA			0.966
≥400 copies/mL	91 (65.9)	93 (66.9)	
<400 copies/mL	47 (34.1)	46 (33.1)	
Pathology			0.644
WHO type II	33 (23.9)	30 (21.6)	
WHO type III	105 (76.1)	109 (78.4)	
T category			0.207
T1	5 (3.6)	6 (4.3)	
T2	43 (31.2)	56 (40.3)	
T3	68 (49.3)	51 (36.7)	
T4	22 (15.9)	26 (18.7)	
N category			0.149
N0	6 (4.3)	5 (3.6)	
N1	12 (8.7)	21 (15.1)	
N2	93 (67.4)	77 (55.4)	
N3	27 (19.6)	36 (25.9)	
Disease stage			0.190
III	90 (65.2)	80 (57.6)	
IVA	48 (34.8)	59 (42.4)	
IC regimen			0.654
TPF	129 (93.5)	128(92.1)	
TP	9 (6.5)	11 (7.9)	
Number of cycles of IC			0.690

(Continued)

TABLE 1 Continued

Characteristics	CBT group	TAU group	
	No. of patients (%)	No. of patients (%)	P value
1 cycle	19 (13.8)	15 (10.8)	
2 cycles	65 (47.1)	71 (51.1)	
3 cycles	54 (41.1)	53 (38.1)	

treatment was suspended due to severe hematological toxicity. No significant differences were observed in cycles of concurrent cisplatin, cumulative concurrent cisplatin dose, radiation treatment delay, and RT dose completion between the two groups (P=0.525, P=0.403, P=0.684, and P=1.000, respectively).

3.2 Incidence and severity of mucositis

The incidence of oral mucositis during the study period was 84.8% (95% CI, 78.7-90.9%) and 98.6% (95% CI, 96.6-100%) in the CBT and TAU groups, respectively. CBT significantly reduced the incidence of oral mucositis (P<0.001). The CBT group also had a lower incidence of grade ≥ 3 mucositis than the TAU group (22.5% vs. 71.9%, P<0.001).

According to the protocol, patients could withdraw from the trial if grade 3 or higher oral mucositis developed and if they are unwilling to continue taking the study drug. The most severe grade of oral mucositis involved in this study was Grade 3. Comparing the TAU group with the CBT group, the incidence of grade 1, 2, and 3 oral mucositis was 98.6% versus 84.8% (P<0.0001), 87.1% versus 58% (P<0.0001), and 71.9% versus 22.5% (P<0.0001), respectively (Table 3).

3.3 Onset time of mucositis

The median latency to onset of oral mucositis was 14.7 days (interquartile range, 12.5-17 days) in the TAU group and 22.6 days (interquartile range, 20-30 days) in the CBT group. Such results showed that CBT significantly delayed the occurrence of oral mucositis (P<.0001, Figure 2). The mean time to onset of grade 2 mucositis was 25± 5.5 days (range, 15–40 days) and 15.5 ± 4 days (range, 7–22 days) in the CBT and TAU groups, respectively (P = 0.001). The onset time of grade 3 mucositis was also significantly longer in the CBT group than in the TAU group (24.5 ± 6 days (10-36 days) vs. 15 ± 4 days (4-30 days), P = 0.001).

3.4 The severity of oral pain

Patients in both groups experienced varying degrees of OM during the treatment (Table 3). The CBT group had a lower incidence of grade 3 pain than the TAU group (3.6% vs. 10%, P = 0.034). Thirty-three patients (14 and 19 in the CBT and TAU groups, respectively) were administered topical anesthesia for grade 2 or 3 oral pain.

TABLE 2 Treatment compliance.

Treatment	No.(%)		
	CBT group (n=138)	TAU group (n=139)	All Patients (N=277)
CCRT			
1 cycle of cisplatin	1 (0.7)	2 (1.4)	3 (1.1)
2 cycles of cisplatin	19 (13.8)	25 (18.0)	15 (15.9)
3 cycles of cisplatin	118 (85.5)	112 (80.6)	230 (83.1)
Cumulated concurrent cisplatin dose			
≥ 200 mg/m^2	128 (92.8)	125 (90)	253(91.3)
< 200 mg/m^2	10 (7.2)	14 (10)	24 (8.7)
Radiotherapy			
Treatment delay, days			
No	136 (98.6)	135 (97.1)	271 (97.8)
≤ 5	2 (1.5)	4 (2.9)	6 (2.2)
> 5	0 (0)	0 (0)	0 (0)
RT dose completed	138 (100)	138 (99.3)	276 (99.6)

TABLE 3 Incidence of different degrees of oral mucositis during the study .

	CBT group		TAU group		
	N	95%CI	N	95%CI	P value
All patients	n=138		n=139		
Grade 1	117 (84.8%)	78.7-90.9	137 (98.6)	96.6-100	<0.0001
Grade 2	80 (58%)	49.6-66.3	121 (87.1)	81.4-92.7	<0.0001
Grade 3	31 (22.5)	15.4-29.5	100 (71.9)	64.4-79.5	<0.0001

CI, confidence interval.

The incidence of ≥ grade 3 symptoms (dry mouth, dysphagia, and mouth pain) of oral mucositis was recorded in both groups. Comparisons of ≥ grade 3 dry mouth (10.8% vs. 3.7%, P=0.021), dysphagia (18% vs. 5.1%, P=0.001), and oral pain (10% vs. 3.6%, P=0.034) showed that the incidence of OM was more likely to be reduced in the CBT group than in the TAU group. The response rates for the TAU and CBT groups were 98.6% (136/138) and 98.6% (137/139, P=1.000), respectively, and the disease control rates of the TAU and CBT groups were 99.0% (137/138) and 99% (138/139), respectively (P=1.000). These results showed that CBT had no effect on the short-term response rate to chemoradiotherapy, and the effect on long-term efficacy is currently being followed up.

3.5 Adverse events

Adverse events were recorded in 136 of the 138 patients (98.6%) in the TAU group and 137 of the 139 patients (98.6%) in the CBT group. Except for oral mucositis, the most common adverse events (≥8%) were leukopenia (8% vs. 8.7%, P=0.814) and neutropenia (8% vs. 6.5%, P=0.654). The incidence of insomnia, fatigue, weight loss, anemia, dry mouth, and serum albumin was significantly lower in the CBT group than in the TAU group. The incidence of other side effects, which were mainly caused by the cytotoxic effects of chemotherapy or radiation therapy, was not different between the two groups (Table 4).

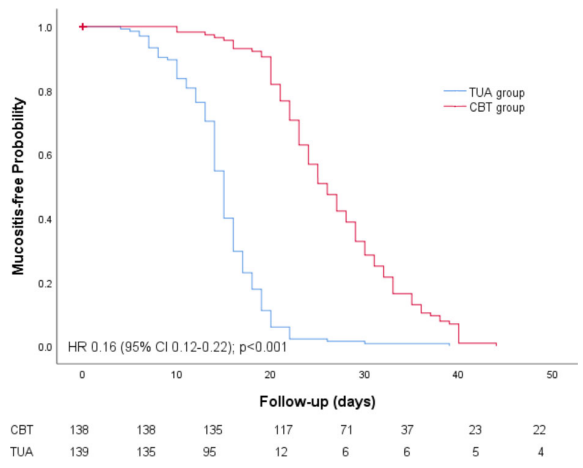

FIGURE 2
Mucositis-free probability CI, confidence interval; HR, hazard ratio.

3.6 Anxiety and depression

As shown in Table 5, there were no significant differences in the mean HADS scores between the CBT and TAU groups at baseline. The HADS scores decreased in both groups at the end of CCRT. Patients in the CBT group showed significantly lower mean total HADS scores and mean HADS scores for depression and anxiety than those in the TAU group at the end of CCRT (P<0.001, P<0.001, and P<0.001, respectively).

4 Discussion

Acute OM, characterized by oral pain, ulceration, necrosis, and pseudomembrane formation, is a common adverse event associated with radiotherapy. It can also be caused by chemotherapy, and usually occurs 7-14 days after the initiation of drug therapy. The severity of oral mucositis is significantly aggravated when radiotherapy and chemotherapy are concomitantly combined (39–43). Recently, induction chemotherapy followed by concurrent chemoradiotherapy has been widely used to treat LA-NPC (44). Since severe mucositis affects treatment compliance and quality of life, management of oral mucositis induced by chemoradiotherapy is important.

Previous studies have shown the efficacy of CBT in reducing treatment-related adverse events (sleep disorders, fatigue, anemia, weight loss, anxiety, depressive symptoms, etc) in survivors of various cancers, including breast, head and neck, and colorectal cancers (26, 45, 46). Garland et al. showed that CBT significantly improved sleep continuity in patients with cancer (47). In a study by Gielissen et al., fatigue in cancer patients was significantly reduced by CBT, and a positive effect was still observed 2 years after the completion of CBT (48). Treatment outcomes for NPC were influenced by pretreatment and mid-treatment hemoglobin (Hb) levels (49). In the present study, the CBT group showed a lower incidence of anemia than the TAU group, which might have had a positive effect on treatment outcomes.

CCRT following IC improved the prognosis of LA-NPC; however, the incidence of OM remained high in patients with NPC undergoing CCRT. Lv et al. (7) found that the incidence of

10.3389/fonc.2023.1143401

TABLE 4 Grade 3–4 acute adverse events.

Grade 3–4 Acute adverse events	CBT group (N=138)	TAU group (N=139)	P-value
Anemia	0 (0%)	6 (4.3%)	0.040
Leukopenia	12 (8.7%)	11 (8.0%)	0.814
Neutropenia	9 (6.5)	11 (8.0%)	0.654
Thrombocytopenia	0 (0%)	4 (2.8%)	0.133
Liver dysfunction	0 (0%)	0 (0%)	–
Nephrotoxicity	0 (0%)	0 (0%)	–
Nausea	0 (0%)	1 (0.7%)	1.000
Vomiting	0 (0%)	2 (1.4%)	0.481
Fatigue	7 (5.1%)	19 (13.7%)	0.014
Dry mouth	5 (3.7%)	15 (10.8%)	0.021
Mucositis	31 (22.5%)	100 (71.9%)	0.001
Dermatitis	0 (0%)	1 (0.7%)	1.000
Dysphagia or odynophagia	7 (5.1%)	25 (18%)	0.001
Oral pain	5 (3.6%)	14 (10%)	0.034
Ototoxicity	0 (0%)	0 (0%)	–
Insomnia	5 (3.6%)	18 (13%)	0.006
Weight loss	5 (3.6%)	16 (11.5%)	0.012
Serum albumin	0 (0%)	6 (4.3%)	0.040

OM in LA-NPC patients treated with CCRT was 97–98%. Another multicenter randomized trial found that the incidence of OM in patients with NPC undergoing CCRT was 97.1% and the incidence of grade 3-4 OM was 32.1% (50). In our present study, patients in the CBT group had lower incidences of OM (84.8%) and SOM (22.5%), compared to that in the TAU group (98.6% and 71.9%, respectively). These results indicate that CBT can reduce the incidence and severity of OM. The median latency period of OM in the CBT group (22.6 days) was significantly longer than that in the TAU group (14.7 days), suggesting that the onset of OM was significantly delayed by CBT.

CBT can improve malnutrition and consequently reduce the incidence of oral mucositis. ROM had strong association with nutritional status which was strongly related to body weight, serum albumin and hemoglobin levels (51–54). Li et al. (51) reported that body weight loss (BWL) was associated with severe acute oral mucositis in LA-NPC patients treated with CCRT. For patients with BWL ≥ 5%, the risk of ≥ grade 3 OM increased by approximately 4 times. Su et al.'s study showed that (52) severe nutritional impairment was an independent risk factor for grade ≥2 oral mucositis of patients with NPC. A prospective study by Shu et al. (54) demonstrated that malnutrition occurred early and

TABLE 5 HADS scores among the two groups.

Time	CBT group	TAU group	
	Mean (SD)	Mean (SD)	P value
Baseline (T1)			
Total	18.03 (3.528)	17.53 (3.397)	0.229
Anxiety	9.16 (1.866)	8.96 (2.028)	0.382
Depression	8.85 (1.843)	8.57 (1.622)	0.178
End of CCRT (T2)			
Total	11.19 (1.971)	13.15 (2.680)	<0.001
Anxiety	4.00 (1.120)	5.76 (1.315)	<0.001
Depression	4.09 (1.162)	5.79 (1.443)	<0.001

worsened continuously during radiotherapy in patients with NPC. Radiation-induced oral mucositis (ROM) was strongly associated with nutritional status, body weight, and serum albumin levels. Huang et al. (51) reported that systematic nutrition management could significantly reduce grade 3-4 oral mucositis during radiotherapy in patients with LA-NPC. Liang et al. (16) reported that thalidomide (THD) treatment reduced the incidence of OM and degree of weight loss and significantly decreased the incidence of vomiting, nausea, and insomnia. Our retrospective previous study (27) showed that CBT significantly reduced the incidences of grade 3 to 4 acute oral mucositis, as well as anemia and weight loss for patients with LA-NPC underwent CRT. In the present study, the CBT group had a lower incidence of BWL, which may be related to its lower incidence of oral mucositis.

The results of the present study also show that the incidence of ≥ grade 3 insomnia and fatigue in NPC patients was significantly reduced by CBT, which is consistent with the findings of Kangas et al. (24) and Gielissen et al. (48). CBT is effective in reducing anxiety and depression in cancer patients (23, 25, 27). Our results also showed that the addition of CBT to chemoradiotherapy significantly reduced depressive and anxiety symptoms.

To the best of our knowledge, no prospective trial has evaluated the effect of CBT plus chemoradiotherapy on response rates in patients with NPC. The CR rate after chemoradiotherapy for LA-NPC is between 82.8% and 98% (55–57). Our previous retrospective study showed that the CBT group had a significantly higher CR rate than the TAU group. The present study showed that CBT tended to increase the CR rate; however, no statistical difference was observed. Liang et al. indicated that THD resulted in a reduction of the incidence of OM, and had no effect on the short-term efficacy of CCRT in NPC patients (16). Weng et al. reported that antibiotics were effective for treating grade 3/4 radiation-induced mucositis but may have potential adverse effects on the prognosis of NPC patients. Compared with antibiotics, CBT can prevent oral mucositis without reducing the treatment response. Further clinical trials are needed to assess the effects of CBT on the treatment response in patients with SOM.

In the present study, patient compliance with CBT was good. None of the patients withdrew from the trial because they were unable or unwilling to undergo CBT. CBT may improve compliance with physicians' instructions (including rinsing the mouth, usage of related medication, and nutritional instruction). We did not assess the effect of CBT on compliance with physicians' instructions in the present study; however, this should be evaluated in future prospective clinical trials. An advantage of CBT is that, as psychotherapy, it does not require oral or intravenous medications. In the present study, no CBT-related adverse events were observed in the CBT group. Other oral drugs (16–19) and intravenous drugs (20) used for prevention and treatment of OM could caused severe adverse events. In a randomized controlled trial by Zheng et al. (17), Shuanghua Baihe tablets (a traditional Chinese medicine) were orally administered to patients with LA-NPC for up to seven weeks during chemoradiotherapy. Shuanghua Baihe tablets significantly reduced the occurrence, severity, and latency of oral mucositis in patients with NPC during chemoradiotherapy. The overall incidence of gastric reactions associated with Shuanghua Baihe tablets was 3.33%. A randomized multicenter trial demonstrated that intravenous actovegin had positive effects on the treatment and prevention of chemoradiotherapy-induced oral mucositis in patients with NPC. Actovegin reduced the incidence of severe OM and decreased the occurrence of severe pain. Actovegin was injected intravenously five times per week during radiotherapy. Two patients withdrew from the study because of vomiting and fever. A multicenter, randomized controlled trial by Liang et al. (16) demonstrated that thalidomide (THD) reduced the incidence of OM but significantly increased the occurrence of constipation and dizziness, and intolerable dizziness caused 2.5% (2/80) of patients in the THD group to drop out of the study. A randomized controlled trial by Yang et al. (58) demonstrated that maxillofacial and oral massage (MOM) significantly attenuated the occurrence of severe radiotherapy-induced oral mucositis (SRTOM), and reduced oral pain, xerostomia, and dysphagia in patients with NPC; however, ≥ grade 3 adverse events were observed in 1.3% of patients during MOM. Weng et al.'s retrospective study (59) analyzed data for 463 patients with NPC with mucositis and found that antibiotics may be effective for the treatment of SRTOM during CRT, but may potentially adversely affect the prognosis (OS and DFS).

The severity of OM is generally associated with the grading score for oral pain. A prospective study by Hua et al. demonstrated that oxycodone (60) effectively reduced moderate-to-severe pain caused by oral mucositis in patients with NPC treated with CCRT. Grade 3 constipation (6.5% and 9.1%) and grade 3-4 vomiting (6.4% and 9.1%) were observed in both the moderate pain and severe pain groups. A prospective study by Guo et al. (61) showed that transdermal fentanyl (TDF) is effective in treating moderate-to-severe pain caused by oral mucositis in NPC patients undergoing chemoradiotherapy, with a 10.26% incidence of nausea and vomiting. Other studies have shown that some drugs, including THD (16), Shuanghua Baihe tablets (17), Actovegin (20), and maxillofacial and oral massage (58), could both prevent oral mucositis and reduce oral pain. In the present study, the most serious oral pain occurred during the severe mucositis phase, and the incidence of serious oral pain was decreased due to the reduced severity of oral mucositis by CBT, which was consistent with the results reported by Liang et al., Zheng et al., Wu et al., and Yang et al. (16, 17, 20, 58). The potential mechanism of CBT in reducing oral pain is that CBT reduces insomnia severity. Yang et al. (62) prospectively evaluated the effect of CBT on pain severity among cancer survivors (including head and neck cancer [HNC] patients) with comorbid pain and insomnia. The result showed that CBT led to pain reductions, possibly achieved by insomnia improvement. In a prospective trial conducted by Garland et al. (63), CBT produced clinically meaningful reductions in pain and insomnia severity in cancer survivors (including HNC patients). Our present study showed that CBT reduced insomnia and oral pain,which was consistent with Yang et al.'s and Garland et al.'s studies (58, 63).

4.1 Limitations

Our study had some limitations. First, it was conducted at a single center rather than at multiple centers, which may limit the generalizability of the findings. Second, due to the limited follow-up duration, late toxicities were not included in the analysis, which

may have important implications for the sustained effectiveness of the intervention. Subsequent investigations incorporating extended follow-up periods and involving multiple medical centers are imperative to comprehensively assess the enduring effects of CBT as well as the potential occurrence of delayed adverse events.

5 Conclusions

Cognitive behavioral therapy reduced the incidence, latency, and severity of oral mucositis in patients with locoregional advanced nasopharyngeal carcinoma during concurrent chemoradiotherapy. Further follow-up and multicenter trials are needed to assess the long-term effects of CBT and late adverse events in NPC patients.

Data availability statement

The original contributions presented in the study are included in the article/supplementary material. Further inquiries can be directed to the corresponding author.

Ethics statement

The studies involving human participants were reviewed and approved by Ethics Committee of Hunan Cancer Hospital. The patients/participants provided their written informed consent to participate in this study. Informed consent was obtained from all participants included in the study during follow-up.

Author contributions

FL designed the study, edited, and submitted the manuscript (FL is the corresponding author). FL, L-LH, SX, C-HJ, X-wW, WL, C-GF, XY, QZ, W-QW, Y-XL, and HW participated in chemotherapy, radiotherapy, treatment as usual, and cognitive behavioral therapy. LH and SX were involved in the design of the study, collection and analysis of the data, and drafting of the manuscript. All authors contributed to the article and approved the submitted version.

Funding

This study was supported by grants from the Science and Technology Department of Hunan Province (No. S2021JJ30426), the Science and Technology Innovation Program of Hunan Province (No. 2021SK51114), the Health Commission of Hunan Province (No. C202309037955), National Natural Science Foundation of China (No. 82272758) and Supported By Hunan Cancer Hospital Climb Plan (No. ZX2020001). The funders had no role in the study design, data collection and analysis, decision to publish, or manuscript preparation.

Conflict of interest

The authors declare that the research was conducted in the absence of any commercial or financial relationships that could be construed as a potential conflict of interest.

Publisher's note

References

1. Chen YP, Chan ATC, Le QT, Blanchard P, Sun Y, Ma J. Nasopharyngeal carcinoma. *Lancet* (2019) 394:64–80. doi: 10.1016/S0140-6736(19)30956-0

2. Wei KR, Zheng RS, Zhang SW, Liang ZH, Li ZM, Chen WQ. Nasopharyngeal carcinoma incidence and mortality in China, 2013. *Chin J Cancer* (2017). doi: 10.1186/S40880-017-0257-9

3. Al- Sarraf M, LeBlanc M, Giri PG, Fu KK, Cooper J, Vuong T, et al. Chemoradiotherapy versus radiotherapy in patients with advanced nasopharyngeal cancer: phase III randomized intergroup study 0099. *J Clin Oncol* (1998) 16:1310–7. doi: 10.1200/JCO.1998.16.4.1310

4. Lee AWM, Lau WH, Tung SY, Chua DTT, Chappell R, Xu L, et al. Preliminary results of a randomized study on therapeutic gain by concurrent chemotherapy for regionally-advanced nasopharyngeal carcinoma: NPC-9901 trial by the Hong Kong nasopharyngeal cancer study group. *J Clin Oncol* (2005) 23::6966–6975. doi: 10.1200/JCO.2004.00.7542

5. Santos RC, Dias RS, Giordani AJ, Segreto RA, Segreto HR. Mucositis in head and neck cancer patients undergoing radiochemotherapy. *Rev Esc Enferm USP* (2011) 45 (6):1338–44. doi: 10.1590/s0080-62342011000600009

6. Xia WX, Lv X, Liang H, Liu GY, Sun R, Zeng Q, et al. A randomized controlled trial comparing two different schedules for cisplatin treatment in patients with locoregionally advanced nasopharyngeal cancer. *Clin Cancer Res* (2021) 27 (15):4186–94. doi: 10.1158/1078-0432.CCR-20-4532

7. Lv X, Cao X, Xia WX, Liu KY, Qiang MY, Guo L, et al. Induction chemotherapy with lobaplatin and fluorouracil versus cisplatin and fluorouracil followed by chemoradiotherapy in patients with stage III-IVB nasopharyngeal carcinoma: an open-label, non-inferiority, randomised, controlled, phase 3 trial. *Lancet Oncol* (2021) 22(5):716–26. doi: 10.1016/S1470-2045(21)00075-9

8. Li WZ, Lv X, Hu D, Lv SH, Liu GY, Liang H, et al. Effect of induction chemotherapy with paclitaxel, cisplatin, and capecitabine vs cisplatin and fluorouracil on failure-free survival for patients with stage IVA to IVB nasopharyngeal carcinoma: a multicenter phase 3 randomized clinical trial. *JAMA Oncol* (2022) 8(5):706–14. doi: 10.1001/jamaoncol.2022.0122

9. McGuire DB, Altomonte V, Peterson DE, Wingard R, Jones RJ, Grochow LB, et al. Patterns of mucositis and pain in patients receiving preparative chemotherapy and bone marrow transplantation. *Oncol Nurs Forum* (1993) 20:1493–502.

10. Li PJ, Li KX, Jin T, Lin HM, Fang JB, Yang SY, et al. Predictive model and precaution for oral mucositis during chemo-radiotherapy in nasopharyngeal carcinoma patients. *Front Oncol* (2020) 10:596822. doi: 10.3389/fonc.2020.596822

11. Trotti A. Toxicity in head and neck cancer: a review of trends and issues. *Int J Radiat Oncol Biol Phys* (2000) 47:1–12. doi: 10.1016/s0360-3016(99)00558-1

12. List MA, Siston A, Haraf D, Schumm P, Kies M, Stenson K, et al. Quality of life and performance in advanced head and neck cancer patients on concomitant

chemoradiotherapy: a pprospective examination. *J Clin Oncol* (1999) 17::1020–8. doi: 10.1200/JCO.1999.17.3.1020

13. Terrell JE, Ronis DL, Fowler KE, Bradford CR, Chepeha DB, Prince ME, et al. Clinical predictors of quality of life in patients with head and neck cancer. *Arch Otolaryngol Head Neck Surg* (2004) 130:401–8. doi: 10.1001/archotol.130.4.401

14. Rajesh VL, Fredrick DA. The MASCC/ISOO mucositis guidelines: dissemination and clinical impact. *Support Care Cancer* (2013) 21:3161–3. doi: 10.1007/s00520-013-1924-2

15. Plevová P. Prevention and treatment of chemotherapy and radiotherapy induced oral mucositis:a review. *Oral Oncol* (1999) 35:453–70. doi: 10.1016/s1368-8375(99)00033-0

16. Liang LF, Liu ZB, Zhu HS, Wang HQ, Wei Y, Ning XY, et al. Efficacy and safety of thalidomide in preventing oral mucositis in patients with nasopharyngeal carcinoma undergoing concurrent chemoradiotherapy: a multicenter, open-label, randomized controlled trial. *Cancer* (2022) 128:1467–1474. doi: 10.1002/cncr.34074

17. Zheng BM, Zhu XD, Liu MZ, Yang ZZ, Yang L, Lang JY, et al. Randomized, double-blind, placebo-controlled trial of shuanghua baihe tablets to prevent oral mucositis in patients with nasopharyngeal cancer undergoing chemoradiation therapy. *Int J Radiat Oncol Biol Phys* (2018) 100(2):418–26. doi: 10.1016/j.ijrobp.2017.10.013

18. Luo Y, Feng M, Fan Z, Zhu X, Jin F, Li R, et al. Effect of kangfuxin solution on Chemo/Radiotherapy-induced mucositis in nasopharyngeal carcinoma patients: a multicenter, prospective randomized phase III clinical study. *Evid Based Complement Alternat Med* (2016), 8692343. doi: 10.1155/2016/8692343

19. Jiang C, Wang H, Xia C, Dong Q, Chen E, Qiu Y, et al. A randomized, double-blind, placebo-controlled trial of probiotics to reduce the severity of oral mucositis induced by chemoradiotherapy for patients with nasopharyngeal carcinoma. *Cancer* (2019) 125(7)::1081–1090. doi: 10.1002/cncr.31907

20. Wu SX, Cui TT, Zhao C, Pan JJ, Xu BY, Tian Y, et al. A prospective, randomized, multi-center trial to investigate actovegin in prevention and treatment of acute oral mucositis caused by chemoradiotherapy for nasopharyngeal carcinoma. *Radiother Oncol* (2010) 97(1):113–8. doi: 10.1016/j.radonc.2010.08.003

21. Sonis ST, Hashemi S, Epstein JB, Nair RG, Raber-Durlacher JE. Could the biological robustness of low level laser therapy (Photobiomodulation) impact its use in the management of mucositis in head and neck cancer patients. *Oral Oncol* (2016) 54::7–14. doi: 10.1016/j.oraloncology.2016.01.005

22. Zadik Y, Arany PR, Fregnani ER, Bossi P, Antunes HS, Bensadoun RJ, et al. Systematic review of photobio-modulation for the management of oral mucositis in cancer patients and clinical practice guidelines. *Support Care Cancer* (2019) 27::3969–3983. doi: 10.1007/s00520-019-04890-2

23. Brothers BM, Yang HC, Strunk DR, Andersen BL. Cancer patients with major depressive disorder: testing a biobehav Ioral/Cognitive behavior intervention. *J Consult Clin Psychol* (2011) 79:253–60. doi: 10.1037/a0022566

24. Kangas M, Milross C, Taylor A, Bryant RA. A pilot randomized controlled trial of a brief early intervention for reducing posttraumatic stress disorder, anxiety and depressive symptoms in newly diagnosed head and neck cancer patients. *Psychooncology* (2013) 22:1665–73. doi: 10.1002/pon.3208

25. Ng TK, Wong DFK. The efficacy of cognitive behavioral therapy for Chinese people: a meta-analysis. *Aust N Z J Psychiatry* (2018) 52:620–37. doi: 10.1177/0004867417741555

26. Ye M, Du K, Zhou J, Zhou Q, Shou M, Hu B, et al. A meta-analysis of the efficacy of cognitive behavior therapy on quality of life and psychological health of breast cancer survivors and patients. *Psychooncology* (2018) 27:1695–703. doi: 10.1002/pon.4687

27. Liu F, Fu SN, Chen YZ, Yan OY, Tong F, Peng WL, et al. Effects of cognitive behavioral therapy for depression and anxiety, response rates and adverse events in patients with locoregional advanced nasopharyngeal carcinoma. *Integr Cancer Ther* (2021) 20:15347354211006179. doi: 10.1177/15347354211006179

28. Lee NY, Zhang Q, Pfister DG, Kim J, Garden AS, Mechalakos J, et al. Addition of bevacizumab to standard chemoradiation for locoregionally advanced nasopharyngeal carcinoma (RTOG 0615): a phase 2 multi-institutional trial. *Lancet Oncol* (2012) 13 (2):172–80. doi: 10.1016/S1470-2045(11)70303-5

29. Lee N, Harris J, Garden AS, Straube W, Glisson B, Xia P, et al. Intensity-modulated radiation therapy with or without chemotherapy for nasopharyngeal carcinoma: radiation therapy oncology group phase II trial 0225. *J Clin Oncol* (2009) 27(22)::3684–90. doi: 10.1200/JCO.2008.19.9109

30. Wen DW, Li ZX, Chen FP, Lin L, Peng BY, Kou J, et al. Individualized cumulative cisplatin dose for locoregionally-advanced nasopharyngeal carcinoma patients receiving induction chemotherapy and concurrent chemoradiotherapy. *Oral Oncol* (2020) 107:104675. doi: 10.1016/j.oraloncology.2020.104675

31. Peng H, Chen L, Zhang Y, Li WF, Mao YP, Zhang F, et al. Prognostic value of the cumulative cisplatin dose during concurrent chemoradiotherapy in locoregionally advanced nasopharyngeal carcinoma: a secondary analysis of a prospective phase III clinical trial. *Oncologist* (2016) 21(11):1369–76. doi: 10.1634/theoncologist.2016-0105

32. Edelman S, Kidman AD. Description of a group cognitive behaviour therapy programme with cancer patients. *Psychooncology* (1999) 8::306–314. doi: 10.1002/(SICI)1099-1611(199907/08)8:4<306::AID-PON387>3.0.CO;2-Y

33. Beck AT, Rush AJ, Shaw BF, Emery G. Cognitive therapy of depression. *Guildford Press* (1979). doi: 10.2147/NDT.S171297

34. Qiu H, Ren W, Yang Y, Zhu X, Mao G, Mao S, et al. Effects of cognitive behavioral therapy for depression on improving insomnia and quality of life in Chinese women with breast cancer: results of a randomized, controlled, multicenter trial. *Neuropsychiatr Dis Treat* (2018) 14::2665–2673. doi: 10.2147/NDT.S171297

35. Ren W, Qiu H, Yang Y, Zhu X, Zhu C, Mao G, et al. Randomized controlled trial of cognitive behavioural therapy for depressive and anxiety symptoms in Chinese women with breast cancer. *Psychiatry Res* (2019) 271:52–9. doi: 10.1016/j.psychres.2018.11.026

36. Wakefield CE, Butow PN, Aaronson NA, Hack TF, HulbertWilliams NJ, Jacobsen PB. Patient-reported depression measures in cancer: a meta-review. *Lancet Psychiatry* (2015) 2:635–47. doi: 10.1016/S2215-0366(15)00168-6

37. Eisenhauer EA, Therasse P, Bogaerts J, Schwartz LH, Sargent D, Ford R, et al. New response evaluation criteria in solid tumours: revised RECIST guideline (version 1.1). *Eur J Cancer* (2009) 45(2)::228–47. doi: 10.1016/j.ejca.2008.10.026

38. Fu S, Li Y, Han Y, Wang H, Chen Y, Yan O, et al. Diffusion-weighted magnetic resonance imaging-guided dose painting in patients with locoregionally advanced nasopharyngeal carcinoma treated with induction chemotherapy plus concurrent chemoradiotherapy: a randomized, controlled clinical trial. *Int J Radiat Oncol Biol Phys* (2022) 113(1)::101–113. doi: 10.1016/j.ijrobp.2021.12.175

39. Merlano M, Corvo R, Margarino G, Benasso M, Rosso R, Sertoli MR, et al. Combined chemotherapy and radiation therapy in advanced inoperable squamous cell carcinoma of the head and neck. *Final Rep A Randomized Trial. Cancer* (1991) 67 (4):915–21. doi: 10.1002/1097-0142(19910215)67:4<915::aid-cncr2820670410>3.0.co;2-8

40. Browman GP, Cripps C, Hodson DI, Eapen L, Sathya J, Levine MN. Placebo-controlled randomized trial of infusional fluorouracil during standard radiotherapy in locally advanced head and neck cancer. *J Clin Oncol* (1994) 12(12)::2648–53. doi: 10.1200/JCO.1994.12.12.2648

41. Bachaud JM, David JM, Boussin G, Daly N. Combined postoperative radiotherapy and weekly cisplatin infusion for locally advanced squamous cell carcinoma of the head and neck: preliminary report of a randomized trial. *Int J Radiat Oncol Biol Phys* (1991) 20(2)::243–6. doi: 10.1016/0360-3016(91)90098-o

42. Taylor SG4, AK M, JM V, Colin P, Dray M, DD C, et al. Randomized comparison of neoadjuvant cisplatin and fluorouracil infusion followed by radiation versus concomitant treatment in advanced head and neck cancer. *J Clin Oncol* (1994) 12(2)::385–95. doi: 10.1200/JCO.1994.12.2.385

43. Trotti A, Bellm LA, Epstein JB, Frame D, Fuchs HJ, Gwede CK, et al. Mucositis incidence, severity and associated outcomes in patients with head and neck cancer receiving radiotherapy with or without chemotherapy: a systematic literature review. *Radiother Oncol* (2003) 66(3):253–62. doi: 10.1016/s0167-8140(02)00404-8

44. Baujat B, Audry H, Bourhis J, Chan AT, Onat H, Chua DT, et al. Chemotherapy in locally advanced nasopharyngeal carcinoma: an individual patient data meta-analysis of eight randomized trials and 1753 patients. *Int J Radiat Oncol Biol* (2003) 66(3):253–62. doi: 10.1016/j.ijrobp.2005.06.037

45. Serfaty M, Wilkinson S, Freeman C, Mannix K, King M. The ToT study: helping with touch or talk (ToT): a pilot randomised controlled trial to examine the clinical effectiveness of aromatherapy massage versus cognitive behaviour therapy for emotional distress in patients in Cancer/Palliative care. *Psychooncology* (2012) 21:563–9. doi: 10.1002/pon.1921

46. Murphy MJ, Newby JM, Butow P, Loughnan SA, Joubert AE, Kirsten L, et al. Randomised controlled trial of Internet-delivered cognitive behaviour therapy for clinical depression and/or anxiety in cancer survivors (iCanADAPT early). *Psychooncology* (2020) 29(1):76–85. doi: 10.1002/pon.5267

47. Garland SN, Roscoe JA, Heckler CE, Barilla H, Gehrman P, Findley JC, et al. Effects of armodafinil and cognitive behavior therapy for insomnia on sleep continuity and daytime sleepiness in cancer survivors. *Sleep Med* (2016) 20:18–24. doi: 10.1016/j.sleep.2015.12.010

48. Gielissen MF, Verhagen CA, Bleijenberg G. Cognitive behaviour therapy for fatigued cancer survivors: long-term follow-up. *Br J Cancer* (2007) 97:612–8. doi: 10.1038/sj.bjc.6603899

49. Guo SS, Tang LQ, Chen QY, Zhang L, Liu LT, Huang PY, et al. Is hemoglobin level in patients with nasopharyngeal carcinoma still a significant prognostic factor in the era of intensity-modulated radiotherapy technology? *PloS One* (2015) 10(8): e0136033. doi: 10.1371/journal.pone.0136033

50. Zhang Y, Chen L, Hu GQ, Zhang N, Zhu XD, Yang KY, et al. Gemcitabine and cisplatin induction chemotherapy in nasopharyngeal carcinoma. *N Engl J Med* (2019) 381(12):1124–35. doi: 10.1056/NEJMoa1905287

51. Li K, Yang L, Xin P, Chen Y, Hu QY, Chen XZ, et al. Impact of dose volume parameters and clinical factors on acute radiation oral mucositis for locally advanced nasopharyngeal carcinoma patients treated with concurrent intensity-modulated radiation therapy and chemoradiotherapy. *Oral Oncol* (2017) 72:32–7. doi: 10.1016/j.oraloncology.2017.06.026

52. Su L, Lin Q, Li R, Hua Y, Zhang H, Song X, et al. Prognostic value of nutritional impairment on treatment-related toxicity and survival in patients with nasopharyngeal carcinoma taking normal nutrition before radiotherapy. *Head Neck.* (2020) 42 (12):3580–9. doi: 10.1002/hed.26426

53. Huang J-F, Sun R-J, Jiang W-J, Wu P, Zhang L, Xu M-Q, et al. Systematic nutrition management for locally advanced nasopharyngeal carcinoma patients undergoing radiotherapy. *Onco Targets Ther* (2019) 12:8379–86. doi: 10.2147/OTT.S213789

54. Shu Z, Zeng Z, Yu B, Huang S, Hua Y, Jin T, et al. Nutritional status and its association with radiation-induced oral mucositis in patients with nasopharyngeal carcinoma during radiotherapy: a prospective study. *Front Oncol* (2020) 10:594687. doi: 10.3389/fonc.2020.594687

55. Hong J, Yao Y, Zhang Y, Tang T, Zhang H, Bao D, et al. Value of magnetic resonance diffusion-weighted imaging for the prediction of radiosensitivity in nasopharyngeal carcinoma. *Otolaryngol Head Neck Surg* (2013) 149(5):707–13. doi: 10.1177/0194599813496537

56. Sun Y, Li WF, Chen NY, Zhang N, Hu GQ, Xie FY, et al. Induction chemotherapy plus concurrent chemoradiotherapy versus concurrent chemoradiotherapy alone in locoregionally advanced nasopharyngeal carcinoma: a phase 3, multicentre, randomised controlled trial. *Lancet Oncol* (2016) 17(11):1509–20. doi: 10.1016/S1470-2045(16)30410-7

57. Zhang Y, Sun Y, Ma J. Induction gemcitabine and cisplatin in locoregionally advanced nasopharyngeal carcinoma. *Cancer Commun (Lond)* (2019) 39(1)::39. doi: 10.1186/s40880-019-0385-5

58. Yang G, Feng D, Li F, Luo B, Zhu J, Yang Q, et al. A rrandomized, controlled phase II trial of maxillofacial and oral massage in attenuating severe radiotherapy-induced oral mucositis and lipid metabolite changes in nasopharyngeal carcinoma. *Radiother Oncol* (2021) 163:76–82. doi: 10.1016/j.radonc.2021.07.024

59. Weng J, Wei J, Li M, Lu J, Qin Y, Liu F, et al. Clinical outcomes of patients with nasopharyngeal carcinoma treated with antibiotics for radiation-induced mucositis: a retrospective study. *J Int Med Res* (2020) 48(3):300060519874899. doi: 10.1177/0300060519874899

60. Hua X, Chen LM, Zhu Q, Hu W, Lin C, Long ZQ, et al. Efficacy of controlled-release oxycodone for reducing pain due to oral mucositis in nasopharyngeal carcinoma patients treated with concurrent chemoradiotherapy: a prospective clinical trial. *Support Care Cancer* (2019) 27(10):3759–67. doi: 10.1007/s00520-019-4643-5

61. Guo SP, Wu SG, Zhou J, Feng HX, Li FY, Wu YJ, et al. Transdermal fentanyl for pain due to chemoradiotherapy induced oral mucositis in nasopharyngeal cancer patients: evaluating efficacy, safety, and improvement in quality of life. *Drug Des Devel Ther* (2014) 8:497–503. doi: 10.2147/DDDT.S60187

62. Yang M, Liou KT, Garland SN, Bao T, Hung TKW, Li SQ, et al. Acupuncture versus cognitive behavioral therapy for pain among cancer survivors with insomnia: an exploratory analysis of a randomized clinical trial. *NPJ Breast Cancer* (2021) 307 (1):148. doi: 10.1038/s41523-021-00355-0

63. Garland SN, Xie SX, DuHamel K, Bao T, Li Q, Barg FK, et al. Acupuncture versus cognitive behavioral therapy for insomnia in cancer survivors: a randomized clinical trial. *JNCI J Natl Cancer Inst* (2019) 111(12):djz050. doi: 10.1093/jnci/djz050

frontiers | Frontiers in Oncology

TYPE Review
PUBLISHED 27 July 2023
DOI 10.3389/fonc.2023.1175578

OPEN ACCESS

EDITED BY
Giuseppe Carlo Iorio,
University of Turin, Italy

REVIEWED BY
Esmeralda Scipilliti,
G. Pascale National Cancer Institute Foundation (IRCCS), Italy
Thorsten Rieckmann,
University Medical Center Hamburg-Eppendorf, Germany

*CORRESPONDENCE
Allen M. Chen
allenmc2@uci.edu

RECEIVED 27 February 2023
ACCEPTED 25 May 2023
PUBLISHED 27 July 2023

CITATION
Chen AM (2023) De-escalated radiation for human papillomavirus virus-related oropharyngeal cancer: evolving paradigms and future strategies.
Front. Oncol. 13:1175578.
doi: 10.3389/fonc.2023.1175578

De-escalated radiation for human papillomavirus virus-related oropharyngeal cancer: evolving paradigms and future strategies

Allen M. Chen*

Department of Radiation Oncology, Chao Family Comprehensive Cancer Center, School of Medicine, University of California- Irvine, Irvine, CA, United States

The incidence of human papillomavirus (HPV)-associated oropharyngeal squamous cell carcinoma has increased dramatically in recent years reaching epidemic-like proportions. Data has emerged not only showing that these cancers are a unique entity with distinct molecular characteristics but that they also have a significantly improved prognosis as a result of their exquisite radiosensitivity compared to their HPV-negative counterparts. This, it has been increasingly suggested that these tumors can be targeted with de-escalated approaches using reduced doses of radiation. The overriding goal of de-escalation is to maintain the high cure and survival rates associated with traditional approaches while reducing the incidence of both short- and long-term toxicity. Although the exact reason for the improved radiosensitivity of HPV-positive oropharyngeal carcinoma is unclear, prospective studies have now been published demonstrating that de-escalated radiation can successfully maintain the high rates of cure and preserve quality of life for appropriately selected patients with this disease. However, these studies have been complicated by such factors as the relatively limited sample sizes, as well as the variability in treatment, inclusion criteria, and follow-up. As the data continues to mature on de-escalation, it is unquestionable that treatment paradigms for this disease will evolve. The ongoing quest to define a standard regimen comprises the subject of this review.

KEYWORDS

HPV, head and neck, cancer, radiation, squamous cell

Introduction

The incidence of human papillomavirus (HPV)-associated oropharyngeal squamous cell carcinoma has risen steadily in recent years reaching epidemic-like proportions. For many patients, radiation therapy is recommended as initial treatment given its longstanding track record and the excellent cure rates generally observed (1).

Historically, this regimen, when used as primary treatment, has consisted of 7 weeks of daily radiation to relatively high doses, often combined with cisplatin chemotherapy. However, due to the anatomical volume of tissue requiring treatment, this regimen can be rigorous and difficult to tolerate with a significant proportion of patients developing long-term toxicity including dysphagia, xerostomia, neuropathy, and/or neck fibrosis (2). Unfortunately, these side effects can be severe, life-altering, and permanent. Indeed, the detrimental effect of treatment on quality of life, psychosocial health, and overall functional capacity has been well-established (3).

A plethora of clinical evidence has accumulated demonstrating that patients with HPV-positive oropharyngeal squamous cell carcinomas have an improved prognosis compared to their counterparts with HPV-negative disease (4–6). Furthermore, the recognition that HPV-positive oropharyngeal cancer responds exquisitely favorably to radiation, both in the pre-clinical and clinical settings, has prompted investigators to suggest that patients with these tumors are possibly over-treated and unnecessarily subjected to the toxicity of intensive chemoradiation with excessively high radiation doses. As a result, prospective trials have been conducted investigating the role of treatment de-escalation with the aim of reducing side effects, particularly those related to swallowing and salivary function, while maintaining the high rates of cure historically observed (7–12). Since patients with HPV-positive oropharyngeal cancer are often healthy, without medical comorbidities, and can potentially survive for decades after treatment, the focus on decreasing long-term complications and optimizing quality of life is particularly germane. For patients who are newly diagnosed with this disease, the focus on preserving function and maximizing well-being has taken on renewed importance. Indeed, the impetus for de-escalation for HPV-positive oropharyngeal carcinoma lies in discovering a new standard that preserves the precious balance between cure and quality of life to the fullest.

Clinical data

Clinico-pathologic biomarker investigations from clinical trials and retrospective studies have so convincingly confirmed HPV status as the single most important predictor of radiation response among oropharyngeal cancer patients that HPV staining (typically through the use of its surrogate, p16) is now standardly performed both in the community and in academic settings. Although HPV testing was initially conducted strictly for purposes of prognostication, its utility to assist with treatment decision-making has become increasingly apparent. Historic data initially published from the Radiation Therapy Oncology Group (RTOG) robustly demonstrated the prognostic importance of HPV. In this analysis, a wide difference was observed in the 3-year rates of local-regional control (86% vs. 65%) and overall survival (82% vs. 57%) between 433 patients with HPV-positive and HPV-negative phenotypes treated prospectively by cisplatin-based chemoradiation (5). Similarly, a subset analysis of 96 patients treated with an induction-concurrent chemoradiation regimen using a taxane-based regimen by the ECOG group showed that patients with HPV-positive tumors had significantly higher response rates (84% vs. 57%), overall survival (95% vs. 62%), and progression-free survival (86% vs. 53%) at 2-years (6). Given the strong link between HPV and radiation response, the American Joint Committee on Cancer (AJCC) created a new (Eighth) staging system in 2016 (Figure 1) specifically for patients diagnosed with HPV-positive oropharyngeal cancer to reflect its favorable prognosis compared to those with HPV-negative disease (13). Interestingly, many tumors that had been previously categorized as stage IV were significantly "down-staged" to stage II or even stage I cancers. This staging system has now been independently validated by numerous studies— overwhelmingly confirming the prognostic significance of HPV (14, 15). It is however important to recognize that the AJCC staging system, similar to most clinical trials, have considered p16-positivity to be equivalent to HPV-positivity. However, it is now established that patients with p16-positive/HPV-negative squamous cell oropharyngeal carcinomas do not have the same favorable prognosis as those with p16-positive/HPV-positive tumors—but rather one that is intermediate those of p16-positive/HPV-positive and p16-negative/HPV-negative cancer (16). As HPV-driven carcinomas are dependent on the permanent over-expression of the HPV E6 and E7 viral oncogene mRNAs, the presence of E6/E7 mRNA is considered to be the gold standard for identifying HPV-positive head and neck cancers (17). From a practical standpoint, mRNA testing is not done in practice because the results from p16 immunohistochemistry and *in situ* hybridization for HPV are generally considered reliable enough for clinical decision-making. It must be recognized, however, that concordance rates between tests can still be variable (17–21).

Furthermore, published data have also suggested that the favorable impact of HPV on prognosis is particularly strong for those patients deemed "never smokers" with several groups showing that the conferred benefit associated with HPV is attenuated for those with an increased smoking history (22). While controversy exists regarding how smoking and its intensity (as well as the impact of quitting) affects prognosis, it is generally accepted that an increased pack-year history and current smoking status are associated with worse outcome (22–25). Table 1 illustrates the improved outcomes for HPV-positive oropharyngeal cancer from the radiation literature. Although the role of HPV in determining prognosis has been unequivocally established, questions persist on how to use this information in the setting of therapeutic decision-making. Indeed, the potential to integrate this biomarker data into treatment paradigms, while promising, is just starting to become explored.

Mechanisms of radio response

How HPV mediates radioresponse in the setting of squamous cell carcinoma of the head and neck is under active investigation and is likely related to a multitude of factors. The most direct explanation is that HPV infection and the subsequent molecular sequestration of the p53 and pRb proteins by the viral products E6 and E7 leads to a cascade of events including the interruption of cell

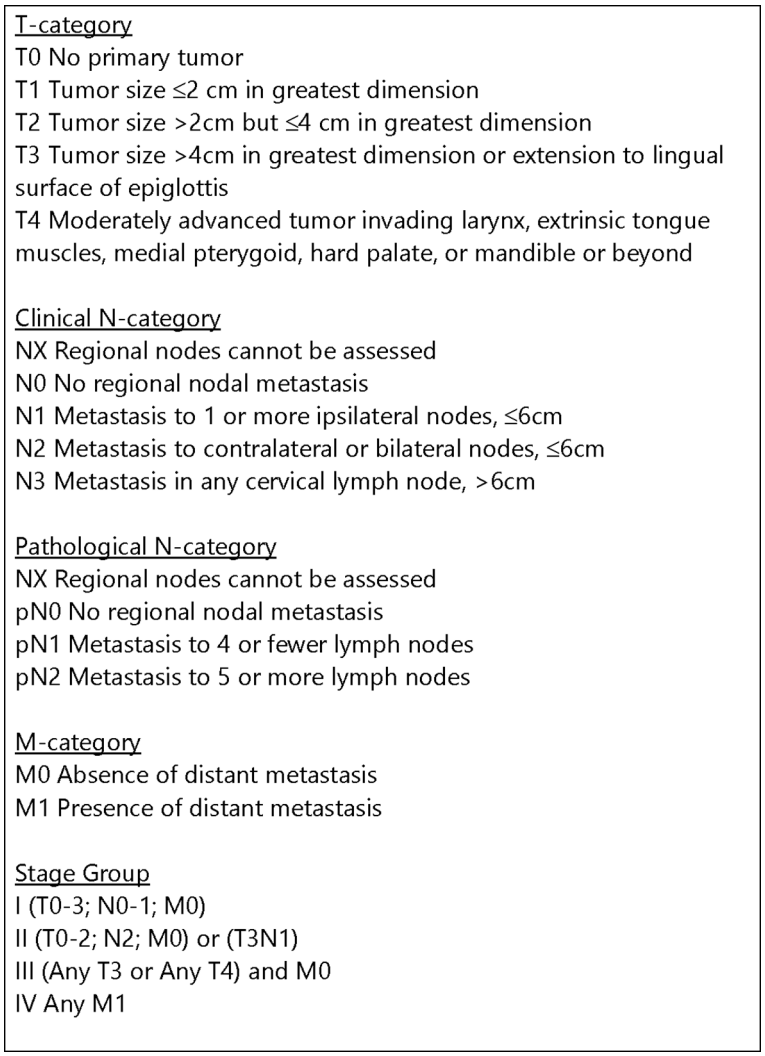

FIGURE 1
AJCC Staging System (Eighth Edition) for HPV-positive (p16-positive) squamous cell carcinoma of the oropharynx (13).

TABLE 1 Subset analysis of prospective trials demonstrating improved prognosis with hpv-related oropharyngeal carcinoma.

Author	N	Dose	Induction	Concurrent	Outcomes
Fakhry (3)	96	70 Gy	Carbo/paclitaxel x2	Paclitaxel	86% vs 53%, 2yr PFS, p=0.02
Rischin (26)	172	70 Gy	None	CDDP +/- Tirapazamine	87% vs 72%, 2yr PFS, p=0.01 93% vs 86%, 2yr LRC, p=0.09
Ang (2)	323	70-72 Gy	None	Cisplatin	74% vs 43%, 3yr PFS, p<0.001 86% vs 65%, 3yr LRC, p<0.001
Lassen (4)	331	66-68 Gy	None	+/- Nimorazole	61% vs 35%, 5yr LRC, p<0.001
Lassen (4)	794	66-68 Gy	None	None	78% vs 64%, 5yr PFS, p=0.001 69% vs 57%, 5yr LRC, p=0.004
Worden (27)	66	70 Gy	Carbo/CDDP+5FU x1	Carbo/CDDP	85% vs 37%, 3yr PFS, p=0.001
Seiwert (28)	110	72 Gy	Carbo/paclitaxel/Cetux x2	Cetux/5-FU/hydroxyurea or Cetuximab/CDDP	84% vs 66%, 5yr PFS, p<0.01

Carbo, Carboplatin; CDDP, Cisplatin; 5FU, 5-fluorouracil; Cetux, Cetuximab; PFS, Progression-free survival; LRC, Local-regional control.

cycle checkpoints and downregulation of cell cycle regulatory proteins culminating in increased genomic instability. As a result, the host tumor cell is left more susceptible to radiation-induced apoptosis. Both *in vitro* and *in vivo* studies, however, have demonstrated, that direct transfer of the E6/E7 genes or gene products into cells did not alter radiation resistance as would be expected (29). Pang et al, however, showed that transfection of the E6 transcript in HPV-negative squamous cell carcinoma cell lines resulted in sensitization to radiation-induced cell death (30).

The data on the interaction between HPV and DNA repair in mediating radiation sensitivity continues to prove provocative. Several studies have shown that the capacity of DNA repair might be hindered by HPV as measured by the persistence of double-strand breaks (31–33). Multiple mechanisms have been proposed as to how HPV might alter DNA repair capacities through homologous recombination and nonhomologous end-joining (34, 35). The role of altered DNA damage response is further supported by the observation that SMG-1, a key protein involved in DNA repair, was negatively correlated with HPV-positive oropharyngeal tumors (36). *In vitro*, decreased SMG-1 expression was seen in cell lines transfected with E6/E7 and such cells had enhanced radiosensitivity.

Other researchers have suggested that radiation has immunogenic properties itself and heightens the host immune response to viral antigens which are expressed on the cancer (37–39). How HPV recruits' immune cells that potentiate the effects of radiation is under active investigation. Numerous studies have confirmed an immunologic mechanism to HPV-mediated radioresponse by demonstrating that the extent of tumor-infiltrating lymphocytes is associated with clinical outcome among patients treated for HPV-positive oropharynx cancer (39, 40). Indeed, the density and pattern of immune infiltrates in the tumor microenvironment is thought to be a byproduct of the HPV activation process in oncogenesis. Relatedly, the presence of regulatory T cells and PD-1(+) T cells and the levels of PD-1(+) cells were positively correlated with a favorable clinical outcome in HPV-positive compared to HPV-negative head and neck cancers (41). While speculative, this may reflect prior immune response in HPV-positive tumors, and radiation may possess a role in helping to re-activate this immune response. Indeed, the presence of tumor-infiltrating lymphocytes may itself be a prognostic marker of improved outcome, regardless of HPV-status (42, 43). The potential role of tumor-associated macrophages and regulatory T cells in mediating HPV-related radioresponse is also increasingly being investigated (38, 44, 45). These studies have demonstrated the importance of the microenvironment and its interaction with tumor cells in mediating radiation response in the setting of HPV-positive oropharyngeal carcinoma.

Regardless of the underlying mechanisms responsible for HPV-mediated radioresponse, laboratory work has confirmed the exquisite radiosensitivity of HPV-positive head and neck squamous cell carcinoma. Gupta et al. conducted a series of experiments using clonogenic survival assays of HPV-positive and HPV-negative cell-lines after exposure to various doses of radiation and showed that the former are characterized by markedly enhanced radiosensitivity (46). Similarly, Kimple et al. demonstrated that HPV-positive cell lines derived from squamous cell head and neck cancer exhibited greater intrinsic radiosensitivity characterized by prolonged G2-M cell-cycle arrest and increased apoptosis compared to HPV-negative cell lines (47). These findings were consistent with those of others showing that cell lines derived from HPV-positive oropharyngeal squamous cell were more frequently in G2 than those from HPV-negative tumors (48). In a series of experiments, Vlashi et al. showed that that the improved radiosensitivity of HPV-positive head and neck cancer might be due to the lower frequency of cancer stem cells and a decreased capacity to engage in radiation-induced dedifferentiation compared to HPV-negative head and neck cancer (49). While none of these studies have directly unraveled the secret of how HPV mediates an enhanced response to radiation, they have confirmed the observations from the clinic and have provided insights into how molecular biology can potentially be exploited to further treatment.

Current treatment

Historically, the current standard for locally advanced HPV-positive and HPV-negative oropharyngeal cancer was identical–regardless of whether primary surgery or radiation therapy was the treatment upfront. As previously described, the HPV biomarker (via its surrogate p16) was not integrated into the staging system until 2016. Although this new system has been useful to categorize patients into varying prognosis based on standard treatment, how to utilize this information for clinical decision-making in the context of de-escalation is largely unknown. While it makes sense that patients with stage I and II (and even stage III) p16-positive oropharyngeal cancer might be the optimal candidates for de-escalation, this notion is speculative at present. Indeed, attempts to identify how treatment recommendations might differ from stage to stage have been hampered by the fact that many of the published studies on de-escalation have used the older staging system, which understandably makes extrapolations challenging (50). As a result, defining new standards of care by stage have remained elusive.

For patients opting for a non-surgical approach, the standard of 70 Gy with high-dose cisplatin chemotherapy has largely remained the same for decades. Alternative chemoradiation regimens which have been studied in the concurrent setting include weekly cisplatin or carboplatin, given alone or in combination with paclitaxel or 5-fluorouracil (51, 52). Concurrent weekly cetuximab with radiation and induction chemotherapy with multi-agent regimens such as taxotere, platinum and 5-fluorouracil followed by concurrent chemoradiation are additional treatment options that have been proposed (53–55). It is important to recognize that prospective trials designed to replace cisplatin with the targeted systemic agent, cetuximab, have shown that this approach may lead to inferior outcomes (56–58). The explanation for the lack of benefit associated with cetuximab might be because HPV-related tumors are less driven by underlying alterations in cell signaling pathways due to the oncogenic properties of HPV-oncoproteins E6 and E7. In other words, compared to HPV-negative carcinoma, HPV-positive oropharyngeal squamous cell carcinoma harbor mutational landscapes that are more devoid of driver mutations or

alterations such as EGFR-overexpression (59). While the eligibility criteria varied between studies, they nonetheless have suggested that cisplatin should continue to be the standard when chemotherapy is utilized with radiation in the definitive treatment of HPV-positive oropharyngeal cancer. Although they do not truly address the question of which patients require chemotherapy for this disease, they nonetheless demonstrate the need for caution with ongoing attempts to pursue de-escalation. It must also be recognized that HPV confirmation was not standardly performed which raises the possibility that some patients with p16-positive disease actually did not have HPV-related disease. Additional studies analyzing whether immunotherapy can be utilized as an alternative are also ongoing (60–62). Although the side effect profiles of these various chemoradiotherapy regimens broadly differ, they generally are considered to be fairly intensive, particularly when combined with 70 Gy of radiation.

Given the provocative evidence attesting to the radiosensitivity of HPV-positive oropharyngeal cancer, an increased amount of attention has focused on ascertaining whether patients with locally advanced HPV-positive oropharyngeal cancer should be treated differently than those with HPV-negative tumors. Investigators from the University of California, Davis (Figure 2) using serial axial imaging to quantify tumor volume obtained longitudinally during the course of radiation to observe *in vivo* patterns of tumor response according to HPV status. This research showed that HPV-positive head and neck cancer tends to regress early during treatment, reaching a plateau by week 5-6, thus providing illustrative evidence that radiation doses can possible be reduced (63). In contrast, HPV-negative tumors were shown to respond relatively later during the course of radiation and more incompletely with respect to volume loss. The robust pattern of tumor reduction described for HPV-positive tumors was noted to be consistent with what was observed in the clinical setting.

The concept of de-escalation encompasses a variety of different strategies intended to make treatment gentler through a reduction in radiation, alteration in chemotherapy regimens, and/or elimination of either modality altogether. The overriding rationale for the interest in de-escalation stemmed from the ability to lessen the intensity of treatment while maintaining survival. However, how to best offer this approach to patients is uncertain, as various methods have been described; and the question of whether de-escalation is even ready for use outside of a clinical trial is hotly debated.

Rationale for de-escalation

The historically observed rates of toxicity from head and neck irradiation are high. Given the understanding that the dose-limiting toxicity from chemoradiation has been related to effects on the mucosal and esophageal surfaces, reducing the radiation dose in selected patients with more favorable biology (e.g. HPV-positive tumors) has been proposed as an attractive option. Indeed, it has been well established that by effectively reducing radiation to the normal structures of the head and neck, there will be a consequent reduction in acute and late side effects—particularly related to swallowing—resulting in improved quality of life. Numerous prospective and retrospective data utilizing sophisticated probability models have demonstrated consistent dose-response relationships predicting toxicity for organs involved in salivary production, swallowing, and mucosal integrity (26–28, 64–67). For xerostomia, it has been long established that the ability to keep mean parotid dose below 26 Gy will significantly reduce the incidence of salivary dryness and preserve quality of life (66). Normal tissue complication probability models have observed that for every 1 Gy in mean dose, the likelihood of xerostomia increases by approximately 5% at 1 year after radiation therapy (67). An abundance of data has similarly shown that dose to anatomical structures thought to be responsible for swallowing is of critical importance in predicting acute and late toxicity from treatment. For instance, multiple studies have demonstrated that minimizing dose to the swallowing apparatus—the pharyngeal constrictor muscles,

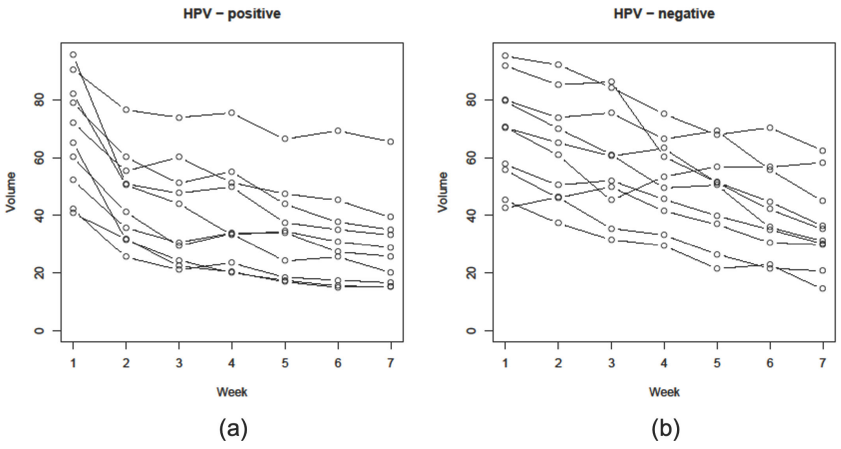

FIGURE 2
Graphical reduction in gross tumor volume (GTV) during a course of definitive radiation therapy for head and neck cancer among 10 patients each with **(A)** HPV-positive and **(B)** HPV-negative oropharyngeal squamous cell carcinomas whom were matched based on clinical and disease characteristics (38).

cervical esophagus, and cricopharyngeal inlet– may decrease the incidence of such side effect as dysphagia, esophageal stricture, trismus, and gastrostomy-tube dependence (26, 27, 64, 65). Between 55 Gy and 70 Gy, a strong linear relationship has been established linking dose to the inferior pharyngeal constrictor muscles and cricopharyngeal inlet with the late grade 3+ dysphagia as defined as gastrostomy-tube dependence (65). These data are consistent with published literature demonstrating that the threshold for radiation-induced long-term dysphagia likely exists at approximately 55 to 60 Gy, and dependent on dose-volume effects (26, 27). These same dosimetric variables have also been linked to complications such as aspiration pneumonia, severe dehydration, unintended weight loss, and malnutrition, as well as to psychosocial distress such as depression and anxiety (68–70). Even for peripheral neuropathy and osteoradionecrosis, presumably due to the development of fibrosis in the neck and/or as a direct effect of radiation-induced vasculitis, probability models have shown an increased likelihood of symptoms with doses exceeding 60 Gy (71, 72).

Given that the probability of developing most radiation-induced complications can be decreased by reducing the intensity and volume of radiation exposure, the potential of de-escalation to improve quality of life for patients undergoing treatment for head and neck cancer is profound. While the use of intensity-modulated and image-guided techniques to deliver radiation in a more customized fashion has become standard and has undoubtedly contributed to improvements in the therapeutic ratio, incidental exposure of radiation to anatomical structures that should be spared still inevitably occurs. This is because the location of many oropharyngeal tumors lie in such close proximity to these organs responsible for swallowing, speaking, and salivating, that it is nearly impossible to avoid subjecting them to radiation. By potentially decreasing toxicity without lowering cure rates, de-escalation of radiation dose for HPV positive tumors has the potential to improve therapeutic ratio by decreasing toxicity while maintaining high rates of disease control.

Quality of life implications

It is increasingly recognized the limiting radiation dose to tissues such as the parotid gland, swallowing structures, larynx, and oral cavity, among others, has the potential to improve quality of life (73). As such, the goal of de-intensification is to improve quality of life while maintaining the excellent rates of cure observed in patients with HPV-positive oropharyngeal cancer. This effort is particularly relevant because traditional treatment using high-dose radiation frequently necessitates unintended breaks, hospitalization, and/or the use of intravenous hydration and enteral feeding. Indeed, it is well-established that concurrent chemoradiation for head and neck cancer has eclipsed the limits of acceptable long-term toxicity. In a combined analysis of late toxicity among patients treated on 3 chemoradiation prospective trials using cisplatin for head and neck cancer, Machtay et al. reported that nearly half of all patients experienced grade 3+ late toxicity related to laryngeal and/or esophageal dysfunction (74). Langendijk et al. similarly showed that the cumulative toxicity of radiation therapy has been shown to contribute to significant quality of life burden with respect to physical and psychosocial functioning (75). A longitudinal analysis by Chen et al. showed that although long-term function has seemingly improved among head and neck cancer patients treated over time due to advances in technology, a significant proportion of patients still rate their quality of life as poor at various points after radiation therapy (76). Consistent with the experiences of others, the less-than-optimal quality of life is related to toxicity largely with respect to swallowing and salivation. It is thus not surprising that the incidence of psychosocial distress has been shown to be high for patients after treatment, despite having long been cured of their disease. These studies, in aggregate, strongly suggest that traditional treatment using high-dose radiation (with or without chemotherapy) is associated with significant quality of life detriments which can unfortunately last a lifetime for patients.

De-escalated radiation

Over the last decade, several prominent prospective trials have been published which have demonstrated promising outcomes with de-escalated radiation regimens using lower than conventionally accepted doses (Table 2). These have consistently shown that de-escalated radiation for HPV-positive oropharyngeal carcinoma can significantly decrease toxicity while maintaining the historically high rates of cure, thus largely validating the premise for which de-escalation was proposed (7–12). The popularity of this approach has been driven by the increasing recognition that HPV-related oropharyngeal cancer is exquisitely sensitive to radiation, as well as the increased desire of patients to avoid side effects.

The evidence in favor of radiation alone for appropriately selected patients with HPV-positive oropharyngeal carcinoma is emerging. Based on historic data from the University of California, Davis and the Princess Margaret Hospital showing that radiation alone (to 70 Gy) is curative for patients with HPV-positive oropharyngeal carcinoma, investigators from Japan recently published a phase 2 trial showing 2-year progression-free survival (PFS) and overall survival (OS) of 94% and 100%, respectively (77–79). In a phase II study, investigators from the University of North Carolina reported on 114 patients who were treated with de-escalated radiation to 60 Gy (8). Notably, patients with higher tumor volume also received low-dose weekly cisplatin. With a median follow-up of 32 months, the 2-year PFS and OS was 86% and 95%, respectively. As importantly, the incidence of grade 3 or higher late toxicity was zero. Results from NRG HN-002, a phase II study of 306 patients randomized to de-escalated chemoradiation versus de-escalated radiation are particularly instructive. The investigators showed that de-escalated radiation alone to 60 Gy, as definitive upfront treatment, for locally advanced HPV-positive oropharyngeal squamous cell carcinoma, delivered using a 6 fraction per week regimen, achieved 2-year PFS and OS of 88% and 97%, respectively (12). Although the heterogenous nature of the subject populations precluded the drawing of definitive conclusions, these studies suggest that some patients with HPV-positive oropharyngeal squamous cell carcinoma can be treated with de-

TABLE 2 Prospective clinical trials on de-escalated radiation as initial treatment for hpv-positive oropharyngeal carcinoma.

First Author (Year)	N	Dose	Chemotherapy	PFS	OS	Time
Chen (2017) (7)	45	54-60 Gy	Induction Carboplatin/Paclitaxel Concurrent Paclitaxel	95%	98%	2-year
Chera (2019) (8)	114	60 Gy	Concurrent Cisplatin or None	86%	95%	2-year
Marur (2017) (10)	51	54 Gy	Induction Cisplatin/Paclitaxel/Cetuximab Concurrent Cisplatin	80%	94%	2-year
Misiukiewicz (2019) (11)	12	56 Gy	Induction Docetaxel/Cisplatin/5-FU Concurrent Carboplatin	83%	83%	3-year
Seiwert (2019) (9)	62	45-75 Gy	Induction Carboplatin/Paclitaxel	95%	98%	2-year
Yom (2021) (12)	150	60 Gy	None	88%	97%	2-year
Yom (2021) (12)	158	60 Gy	Concurrent Cisplatin	91%	97%	2-year

escalation and achieve excellent outcomes. Given the historically high rates of toxicity associated with chemotherapy, the use of radiation alone can be considered an attractive option for appropriate patients.

Indeed, the rationale for the elimination of chemotherapy is driven by the drive to decrease side effects and improve quality of life. The use of concurrent chemotherapy is well-known to dramatically decrease the tolerability of treatment compared to radiation alone (80, 81). In addition to its association with stand-alone side effects such as bone marrow suppression, renal failure, ototoxicity, and neuropathy, among others, the use of chemotherapy combined with radiation has been shown to exacerbate the effects of the latter (82). Studies have shown that the rates of hospitalization, treatment interruptions, and mortality are significantly higher among patients receiving concurrent chemoradiation compared to radiation alone (83, 84).

However, as previously discussed, findings from prospective studies showing that cetuximab is an inadequate substitute for cisplatin for HPV-positive oropharyngeal patients treated by chemoradiation must also be acknowledged. The results of RTOG 1016 conducted in North America randomized 849 patients with locally advanced p16-positive oropharyngeal cancer to radiation with high-dose cisplatin or weekly cetuximab showed inferior OS and PFS for the latter compared with the former (56). Eligibility included patients with T3-T4 tumors or N2a-N3 disease, as defined by the older 7th edition staging system. The estimated 5-year OS was 78% in the cetuximab group versus 85% in the cisplatin group. Investigators from Europe published the "De-ESCALaTE" trial which randomized 334 patients with locally advanced p16-positive oropharyngeal cancer to radiation with high-dose cisplatin or weekly cetuximab (57). Notably, eligibility was defined using the older (7th edition) staging system and included patients with T3-T4 or node-positive disease and minimal smoking history. While OS was not the primary outcome, the study showed a significant difference between cisplatin and cetuximab in 2-year OS (98% versus 89%) and 2-year recurrence (6% versus 16%) favoring cisplatin. The Trans-Tasman Radiation Oncology Group (TROG) randomized 189 patients from Australia and New Zealand to radiation with weekly cisplatin or weekly cetuximab (58). While there was no observed difference in the primary endpoint of symptom severity, the 3-year failure-free survival rates were 93% and 80%, respectively, among patients treated by cisplatin and cetuximab. Eligibility criteria included: AJCC 7th edition stage III (excluding T1-2N1) or stage IV (excluding T4 and/or N3 and/or N2b-c if smoking history >10 pack years and/or distant metastases) p16-positive. While these studies included a generally heterogenous group of patients, notably with respect to tumor volume, clinical stage, and smoking history, they suggest that not all patients might be appropriate for approaches de-intensifying treatment based on the alteration or elimination of radio-sensitizing chemotherapy. If anything, these studies point to a need for caution when designing de-escalation efforts moving forward.

The addition of chemotherapy (administered either before or with) de-escalated radiation is well-studied. Investigators from the University of California performed a multi-center, phase 2 trial, treating 45 patients with locally advanced HPV-positive oropharyngeal squamous cell carcinoma with 2 cycles of induction chemotherapy given 21 days apart, followed by de-escalated radiation to 54 Gy and 60 Gy to complete and partial responders (7). The PFS at 2 years was found to be 92%, and a significantly improved toxicity profile compared with historical regimens using standard radiation doses was observed. The gastrostomy-tube dependence rate at 6-months post-radiation and late dysphagia was zero. As importantly, prospective analysis of quality of life endpoints and pre- and post-therapy swallow studies showed that de-escalation dramatically improved function (85–87). For instance, patients treated by de-escalated radiation had decreased weight loss, depression, and opioid usage compared to contemporary control subjects who opted not to be treated with de-escalation.

The Optima trial was another phase 2 de-escalation study in which 62 patients with HPV-positive oropharyngeal squamous cell carcinoma were treated by induction chemotherapy with 3 cycles of carboplatin and nab-paclitaxel followed by de-escalated radiation (9). The 2-yr PFS was 94% for high-risk patients. The Quarterback trial was a randomized phase 3 study that directly compared reduced dose radiation to standard dose radiation after induction chemotherapy for locally advanced HPV-positive oropharyngeal cancer patients (11). After 3 cycles of docetaxel, cisplatin and 5-fluorouracil induction chemotherapy, patients with a clinical or

radiographic complete/partial response were randomized to receive reduced (56 Gy) or standard (70 Gy) dose radiation with weekly carboplatin. Among the 20 patients randomized, the 3-year PFS rates were not significantly different at 88% and 83% for those receiving standard and reduced dose radiation, respectively. Lastly, NRG HN02 showed excellent rates of survival with concurrent chemoradiation to 60 Gy (12). Notably, in this trial the addition of concurrent cisplatin to de-escalated radiation reduced the 2-year local failure rate from 9% to 3% although it was unclear which subset of patients benefited the most. When the 2-year PFS and OS rates were analyzed, no differences were observed between patients treated by de-escalated radiation with or without chemotherapy.

Lastly, minimally-invasive operative techniques using transoral robotic surgery (TORS) has also been proposed as a means of de-escalating treatment for HPV-positive oropharyngeal cancer (88–90). As an initial treatment, TORS has been shown to be effective in resecting the primary cancer with minimal morbidity. Additional data from the University of Pennsylvania group has further suggested that eliminating postoperative radiotherapy to the primary site for selected patients with oropharyngeal cancer treated by TORS results in high local control and optimal function (91, 92). Another published study from Washington University has suggested that adjuvant chemotherapy may not be necessary for any patients with HPV-related oropharynx cancer, even in the setting of risk factors typically prompting its use such as extracapsular disease spread (93). Enthusiasm for the use of TORS, however, may have been dampened by the results of the ORATOR trial which randomized patients with newly diagnosed HPV-positive oropharyngeal cancer to either initial TORS or to primary radiation (94). While OS and PFS were the same between the 2 arms, patients randomized to TORS had decreased swallowing function at 1-year, which translated into inferior quality of life. Notably, a subsequent randomized trial comparing initial TORS to primary radiation using de-escalated doses was conducted by the same investigators and was halted prematurely due to excessively high grade 5 toxicity in the TORS arm (95). Nonetheless, prospective studies published by the Eastern Cooperative Oncology Group (ECOG) and the Mayo Clinic have shown that reduced doses of radiation (to 30 to 50 Gy) in the post-operative setting may be reasonably delivered after TORS (96, 97).

These prospective trials, in aggregate, have established de-escalated radiation as a feasible treatment option for patients with HPV-positive oropharyngeal cancer. Not only do they demonstrate that de-escalated radiation achieves exceptionally encouraging rates of PFS and OS, but they strongly suggest that de-escalation was associated with meaningful improvements in quality of life and functional outcomes. While preliminary, these data effectively validate the premise underlying de-escalation and provide encouraging evidence that this strategy will be adopted in a more widespread fashion in the future. Notably, a post-hoc analysis of perspectives and attitudes of subjects treated on the University of California de-escalation trial showed that nearly all patients were satisfied with their decision and any regret was nearly non-existent (87). Further evidence supporting de-escalation was provided by Gabani et al. who analyzed data from the National Cancer Database to identify 759 patients with HPV-positive oropharyngeal cancer who were treated with definitive radiation with or without chemotherapy (98). Using a propensity score model to minimize imbalances between arms, the investigators showed no differences in outcome between patients treated to 66 Gy or higher and those treated to lower doses. Furthermore, no benefit to concurrent chemotherapy was observed. Yang et al. similarly conducted a meta-analysis of 13 studies for patients with HPV-positive oropharyngeal cancer and concluded that the 2- and 3-year OS rates in the de-escalated radiation group (96% and 92%, respectively) were superior to those in the standard-dose group (88% and 87%, respectively) leading them to conclude that alleviates the treatment toxicities without compromising survival in this population (99).

De-escalation: next steps

Continued progress to better refine selection criteria as well as to dynamically monitor treatment response will define the evolution of de-escalation for HPV-positive oropharyngeal cancer. At present, the only clinical–pathologic factor (other than AJCC cancer stage) that is used for risk stratification is smoking history. Future advances in de-escalation will need to incorporate a combination of clinical, radiological, and biological data—helping to apply principles of precision medicine to this approach.

The use of cell-free DNA to quantify disease burden and to longitudinally monitor response has been proposed to further individualize care as numerous studies have prospectively demonstrated its utility for prognostication and surveillance purposes for patients treated by radiation for HPV-related oropharyngeal cancer (100–102). The incorporation of other immunologic biomarkers such as PD-1/PDL-1 in conjunction with HPV has also been studied as a more powerful means to refine risk stratification (103, 104). Corredor et al. recently employed image processing and machine learning to develop an imaging biomarker that quantitatively characterized the spatial patterns of tumor-infiltrating lymphocytes and surrounding nucleated cells in digitized hematoxylin and eosin slides of HPV-positive oropharyngeal cancer patients (105). The investigators then showed how this model could be implemented in current staging systems to refine prognostication and to aid in the selection of patients potentially for de-escalation. The utility of pre-treatment circulating leukocytes as a predictive measure of radiation response has also been proposed (106, 107). Unraveling the mechanisms of radiosensitivity may further lead to the development of therapeutic cancer vaccines, which are now being studied (108, 109). The potential of high-yield, next generation sequencing panels to cluster tumors into even more distinct subtypes based on immunogenomics has also been described (110, 111). Others have suggested that expression of cancer stem cell markers in HPV-positive oropharyngeal squamous may help further characterize biological behavior and identify patients who derive the most

benefit from de-escalation (112). Indeed, attempts to discern gene profile signatures that might be useful for risk stratification continue to be explored (113).

The explosion of radiomic information also has the potential to identify who may or may not be eligible for de-escalation, both at diagnosis and midway through radiation. For instance, investigators from China used a radiomics signature of intra-tumoral and peri-tumoral regions to predict which patients might benefit from the addition of chemotherapy to radiation for HPV-related oropharyngeal cancer (114). Another study showed that radiomics can outperform traditionally used clinical factors to characterize HPV-related oropharyngeal squamous cell carcinoma (115). The potential of multi-parametric magnetic resonance imaging (MRI) including diffusion-weighted sequences is also starting to become recognized and may be incorporated into risk stratification schemes in the future (116, 117). Other investigators have suggested that hypoxia monitoring using novel radiotracers can be useful for discerning the most optimal patients for de-escalation (118). In a prospective study utilizing fluoromisonidazole-positron emission tomography (F-MISO-PET) to image hypoxia during radiation, they showed that radical reduction in radiation dose to 30 Gy for those with no pretreatment hypoxia or in whom hypoxia had resolved within the first 2 weeks of initiating radiation might be feasible (119). All in all, tremendous resources are being invested in the identification and development of phenotypic signatures which might predict treatment success for patients opting for de-escalation. The use of machine learning and artificial intelligence is now being investigated as a means to make this process more efficient and clinically practical (120–122).

Conclusion

Given its demonstrated ability to dramatically preserve quality of life and functioning while maintaining high rates of cure, de-escalated radiation has emerged as an attractive option in the management of HPV-positive oropharyngeal cancer. This strategy is seemingly well-supported by the depth and breadth of data that has been published reporting on outcomes of de-escalated radiation for HPV-positive oropharyngeal cancer. Indeed, the reality of clinical decision-making for HPV-positive oropharyngeal cancer has evolved to the point where patients are now routinely demanding de-escalated radiation. Findings from a recent patterns of care analysis demonstrated that de-escalated radiation has become increasingly offered to patients with HPV-positive oropharyngeal cancer as standard treatment (123). Given the preliminary nature of the data to date and the failures of prospective trials attempting to de-escalate treatment with cetuximab, caution must be exercised. However, the fact that patients are demanding and being offered de-escalation outside of clinical trials naturally raises the question of whether a prospective clinical study randomizing subjects to de-escalation versus standard high-dose radiation could ever successfully be performed given that patients, many of whom are educated, are increasingly preferring the former (124).

While is now obvious that HPV-positive and HPV-negative oropharyngeal cancer represent distinct entitle with differing prognosis, the therapeutic implications remain unclear (125–127). While data has steadily emerged, that treatment should be individualized for the subgroup of patients with HPV-related oropharyngeal cancer, exactly how to do so remains uncertain (128). While patients with low-risk disease (low volume and minimal smoking history) can likely be effectively treated with de-escalated radiation alone, those with higher-risk disease (bulky, high-volume disease and/or patients with significant smoking histories), appear to benefit from the addition of chemotherapy to de-escalated radiation. However, these paradigms continue to evolve as studies contribute to an improved understanding of HPV-related oropharyngeal cancer leading to refinement in risk stratification schemes. While enthusiasts argue that the data robustly supports the integration of de-escalation into contemporary practice; skeptics point out that the published data is still relatively preliminary and makes it difficult to make definitive recommendations. Based on the emerging evidence, as well as on the explosion in interest from patients and physicians alike, well-designed clinical trials are urgently needed to better refine selection criteria for de-escalation and to stratify patients with newly diagnosed oropharyngeal cancer into the appropriate means of treatment.

Author contributions

The author confirms being the sole contributor of this work and has approved it for publication.

Conflict of interest

The author declares that the research was conducted in the absence of any commercial or financial relationships that could be construed as a potential conflict of interest.

Publisher's note

References

1. Lassen P, Huang SH, Su J, et al. Treatment outcomes and survival following definitive (chemo)radiotherapy in HPV-positive oropharynx cancer: Large-scale comparison of DAHANCA vs PMH cohorts. *Int J Cancer* (2022) 150:1329–40. doi: 10.1002/ijc.33876

2. Wilkie JR, Mierzwa ML, Yao J, et al. Big data analysis of associations between patient reported outcomes, observer reported toxicities, and overall quality of life in head and neck cancer patients treated with radiation therapy. *Radiother Oncol* (2019) 137:167–74. doi: 10.1016/j.radonc.2019.04.030

3. Van der Laan HP, Van den Bosch L, Schuit E, et al. Impact of radiation-induced toxicities on quality of life of patients treated for head and neck cancer. *Radiother Oncol* (2021) 160:47–53. doi: 10.1016/j.radonc.2021.04.011

4. Lindel K, Beer KT, Laisse J, et al. Human papillomavirus positive squamous cell carcinoma of the oropharynx: a radiosensitive subgroup of head and neck carcinoma. *Cancer* (2001) 92:805–13. doi: 10.1002/1097-0142(20010815)92:4<805::AID-CNCR1386>3.0.CO;2-9

5. Ang KK, Harris J, Wheeler R, et al. Human papillomavirus and survival of patients with oropharyngeal cancer. *N Engl J Med* (2010) 363:24–35. doi: 10.1056/NEJMoa0912217

6. Fakhry C, Westra WH, Li S, et al. Improved survival of patients with human papillomavirus-positive head and neck squamous cell carcinoma in a prospective clinical trial. *J Natl Cancer Inst* (2008) 100:261–9.

7. Chen AM, Felix C, Wang PC, et al. Reduced-dose radiotherapy for human papillomavirus-associated squamous cell carcinoma of the oropharynx: a single-arm, phase 2 study. *Lancet Oncol* (2017) 18:803–11.

8. Chera BS, Amdur RJ, Tepper J, et al. Phase 2 trial of de-intensified chemoradiation therapy for human papillomavirus-associated oropharyngeal squamous cell carcinoma. *J Clin Oncol* (2019) 37:2661–9.

9. Seiwert TY, Foster CC, Blair EA, et al. OPTIMA: a phase II dose and volume de-escalation trial for human papillomavirus-positive oropharyngeal cancer. *Ann Oncol* (2019) 30:297–302.

10. Marur S, Li S, Cmelak AJ, et al. E1308: phase II trial of induction chemotherapy followed by reduced-dose chemotherapy followed by reduced-dose radiation and weekly cetuximab in patients with HPV-associated resectable squamous cell carcinoma of the oropharynx- ECOG-ACRIN cancer research group. *J Clin Oncol* (2017) 35:490–7.

11. Misiukiewicz K, Gupta V, Miles BA, et al. Standard of care versus reduced dose chemoradiation after induction chemotherapy in HPV-positive oropharyngeal carcinoma patients: the quarterback trial. *Oral Oncol* (2019) 95:170–7.

12. Yom SS, Torres-Saavedra P, Caudell JJ, et al. Reduced dose radiation therapy for HPV-associated oropharyngeal carcinoma (NRG 002). *J Clin Oncol* (2021) 39:956–65.

13. Amin MB, Edge SB, Greene FL, et al eds. *American Joint committee on cancer staging manual. 8th ed*. New York: Springer (2017).

14. Cramer JD, Hicks KE, Rademaker AW, et al. Validation of the eighth edition American joint committee on cancer staging system for human papillomavirus-associated oropharyngeal cancer. *Head Neck* (2018) 40:457–66.

15. Zhan KY, Eskander A, Kang SY, et al. Appraisal of the AJCC 8th edition pathologic staging modifications for HPV-positive oropharyngeal cancer, a study of the national cancer data base. *Oral Oncol* (2017) 73:152–9.

16. Mehanna H, Taberna M, Von Buchwald C, et al. Prognostic implications of p16 and HPV discordance in oropharyngeal cancer (HNCIG-EPIC-OPC): a multicentre, multinational, individual patient data analysis. *Lancet Oncol* (2023) 24:239–51.

17. Shi W, Kato H, et al. Comparative prognostic value of HPV16 E6 mRNA compared with *in situ* hybridization for human oropharyngeal squamous carcinoma. *J Clin Oncol* (2009) 27:6213–21.

18. Huanhuan W, Yuyu Z, Wei B, et al. Feasibility of immunohistochemical p16 staining in the diagnosis of human papillomavirus infection in patients with squamous cell carcinoma of the head and neck: a systematic review and meta-analysis. *Front Oncol* (2020) 10:524928.

19. Yang X, Hu C, Zhao H, et al. Aptima HR-HPV testing of cytology specimens is an effective supplement for p16 staining to improve diagnostic accuracy of HPV-related oropharyngeal squamous cell carcinoma. *Acta Cytol* (2022) 13:1–11.

20. Ukpo OC, Flanagan JJ, Ma XJ, et al. High-risk human papillomavirus E6/E7 mRNA detection by a novel *in situ* hybridization assay strongly correlates with p16 expression and patient outcomes in oropharyngeal squamous cell carcinoma. *Am J Surg Pathol* (2011) 35:1343–50.

21. Jordan RC, Lingen MW, Perez-Ordonez B, et al. Validation of methods for oropharyngeal cancer HPV status determination in US cooperative group trials. *Am J Surg Pathol* (2012) 36:945–54.

22. Bouland C, Dequanter D, Lechien J, et al. Prognostic significance of a scoring system combining p16, smoking, and drinking status in a series of 131 patients with oropharyngeal cancers. *Int J Otolaryngol* (2021) 8020826.

23. Beitler JJ, Switchenko JM, Dignam JJ, et al. Smoking, age, nodal disease, T stage, p16 status, and risk of distant metastases in patients with squamous cell cancer of the oropharynx. *Cancer* (2018) 125:704–11.

24. Granata R, Miceli R, Orlandi E, et al. Tumor stage, human papillomavirus and smoking status affect the survival of patients with oropharyngeal cancer: an Italian validation study. *Ann Oncol* (2012) 23:1832–7.

25. Schostag K, Lynch PT, Leavitt T, et al. Smoking and other patient factors in HPV-mediated oropharynx cancer: a retrospective cohort study. *Am J Otolaryngol* (2022) 43:103555.

26. Xu B, Boero IJ, Hwang L, et al. Aspiration pneumonia after concurrent chemoradiotherapy for head-and-neck cancer. *Cancer* (2015) 121:1303–11.

27. Chen AM, Li BQ, Jennelle RL, et al. Late esophageal toxicity after radiation therapy for head and neck cancer. *Head Neck* (2010) 32:178–83.

28. Kamal M, Rock C, Grant S, et al. Dose-volume correlates of the prevalence of patient-reported trismus in long-term survivorship after oropharyngeal IMRT: a cross-sectional dosimetric analysis. *Radiother Oncol* (2020) 149:142–9.

29. DeWeese TL, Walsh JC, Dillehay LE, et al. Human papillomavirus E6 and E7 oncoproteins alter cell cycle progression but not radiosensitivity of carcinoma cells treated with low-dose-rate radiation. *Int J Radiat Oncol Biol Phys* (1997) 37:145–54.

30. Pang E, Delic NC, Hong A, et al. Radiosensitization of oropharyngeal squamous cell carcinoma cells by human papillomavirus 16 oncoprotein E6*I. *Int J Radiat Oncol Biol Phys* (2011) 79:860–5.

31. Zhang M, Hong AM. The human papillomavirus confers radiosensitivity in oropharyngeal cancer cells by enhancing DNA double strand break. *Oncotarget* (2020) 11:1417–26.

32. Kono T, Hoover P, Poropatich K, et al. Activation of DNA damage repair factors in HPV positive oropharyngeal cancers. *Virology* (2020) 547:27–34.

33. Bamps M, Dok R, Nuyts S. The DNA damage response is differentially involved in HPV-positive and HPV-negative radioresistant head and neck squamous cell carcinoma. *Cancers* (2021) 13:3717.

34. Dok R, Kalev P, Limergen EJ, et al. p16INK4a impairs homologous recombination-mediated DNA repair in human papillomavirus-positive head and neck tumors. *Cancer Res* (2014) 74:1739–51.

35. Albert E, Laimins L. Regulation of the human papillomavirus life cycle by DNA damage repair pathways and epigenetic factors. *Viruses* (2020) 12:744.

36. Gubanova E, Brown B, Ivanov SV, et al. Downregulation of SMG-1 in HPV-positive head and neck squamous cell carcinoma due to promoter hypermethylation correlates with improved survival. *Clin Cancer Res* (2012) 18:1257–67.

37. Spanos WC, Nowicki P, Lee DW, et al. Immune response during therapy with cisplatin or radiation for human papillomavirus-related head and neck cancer. *Arch Otolaryngol Head Neck Surg* (2009) 135:1137–46.

38. Chen X, Fu E, Lou H, et al. IL-6 induced M1 type macrophage polarization increases radiosensitivity in HPV positive head and neck cancer. *Cancer Lett* (2019) 456:69–79.

39. Ward MJ, Thirdborough SM, Mellows T, et al. Tumour-infiltrating lymphocytes predict for outcome in HPV-positive oropharyngeal cancer. *Br J Cancer* (2013) 110:489–500.

40. Almangush A, Jouhi L, Atula T, et al. Tumour-infiltrating lymphocytes in oropharyngeal cancer: a validation study according to the criteria of the international immuno-oncology biomarker working group. *Br J Cancer* (2022) 126:1589–94.

41. Lyu X, Zhang M, Li G, et al. PD-1 and PDL-1 expression predicts radiosensitivity and clinical outcomes in head and neck cancer and is associated with HPV infection. *J Cancer* (2019) 10:937–48.

42. Patel JJ, Levy D, Nguyen SA, et al. Impact of PD-L1 expression and human papillomavirus status in anti-PD1/PDL1 immunotherapy for head and neck squamous cell carcinoma–systematic review and meta-analysis. *Head Neck* (2020) 42:774–86.

43. Badoual C, Hans S, Merillon N, et al. PD-1-expressing tumor-infiltrating T cells are a favorable prognostic biomarker in HPV-associated head and neck cancer. *Cancer Res* (2013) 73:128–38.

44. Lee YS, Park JY, Cho KJ, et al. Composition of inflammatory cells regulating the response to concurrent chemoradiation therapy for HPV (+) tonsil cancer. *Oral Oncol* (2015) 51:1113–9.

45. Haave H, Ljokjel B, Lybak H, et al. Tumor HPV status, level of regulatory T cells and macrophage infiltration predict up to 20-year non-disease-specific survival in oropharynx squamous cell carcinoma patients. *Biomedicines* (2022) 10:2484.

46. Gupta AK, Lee JH, Wilke WW, et al. Radiation response in two HPV-infected head and neck cancer cell lines in comparison to non-HPV-infected cell line and relationship to signaling through AKT. *Int J Radiat Oncol Biol Phys* (2009) 74:928–33.

47. Kimple RJ, Smith MA, Blitzer GC, et al. Enhanced radiation sensitivity in HPV-positive head and neck cancer. *Cancer Res* (2013) 73:4791–800. doi: 10.1158/0008-5472.CAN-13-0587

48. Holzhauser S, Pirotte E, Jones J, et al. Sensitivity of human papillomavirus-positive and -negative oropharyngeal cancer cell lines to ionizing irradiation. *Oncol Rep* (2020) 44:1717–26. doi: 10.3892/or.2020.7709

49. Vlashi E, Chen AM, Boyrie S, et al. Radiation-induced dedifferentiation of head and neck cancer cells into cancer stem cells depends on human papillomavirus status. *Int J Radiat Oncol Biol Phys* (2016) 94:1198–206. doi: 10.1016/j.ijrobp.2016.01.005

50. Vijayvargiya P, Trivedi S, Rupji M, et al. Comparison of the seventh and eighth edition of American joint committee on cancer (AJCC) staging for selected and nonselected oropharyngeal squamous cell carcinomas. *Oncologist* (2022) 27:48–56. doi: 10.1093/oncolo/oyab001

51. Perez CA, Wu X, Amsbaugh MJ, et al. High-dose versus weekly cisplatin definitive chemoradiotherapy for HPV-related oropharyngeal squamous cell carcinoma of the head and neck. *Oral Oncol* (2017) 67:24–8. doi: 10.1016/j.oraloncology.2017.01.010

52. Sun L, Candelieri-Surette D, Anglin-Foote T, et al. Cetuximab-based vs carboplatin-based chemoradiotherapy for patients with head and neck cancer. *JAMA Otolaryngol Head Neck Surg* (2022) 148:1022–8. doi: 10.1001/jamaoto.2022.2791

53. Strojan P, Kuhar G, Zumer B, et al. TPF induction chemotherapy and concomitant irradiation with cisplatin and cetuximab in unresectable squamous cell carcinoma of the head and neck. *Head Neck* (2014) 36:1555–61. doi: 10.1002/hed.23506

54. Psyrri A, Fortpied C, Koutsodontis G, et al. Evaluation of the impact of tumor HPV status on outcome in patients with locally advanced unresectable head and neck squamous cell carcinoma (HNSCC) receiving cisplatin, 5-fluorouracil with or without docetaxel: a subset analysis of EORTC 24971 study. *Ann Oncol* (2017) 28:2213–8. doi: 10.1093/annonc/mdx320

55. Swiecicki PL, Li P, Belile E, et al. Paired phase II trials evaluating cetuximab and radiotherapy for low risk HPV associated oropharyngeal cancer and locoregionally advanced squamous cell carcinoma of the head and neck in patients not eligible for cisplatin. *Head Neck* (2020) 42:1728–37. doi: 10.1002/hed.26085

56. Gillison ML, Trotti AM, Harris J, et al. Radiotherapy plus cetuximab or cisplatin in human papillomavirus-positive oropharyngeal cancer (NRG oncology RTOG 1016): a randomised, multicentre, non-inferiority trial. *Lancet* (2019) 393:40–50. doi: 10.1016/S0140-6736(18)32779-X

57. Mehanna H, Robinson M, Hartley A, et al. Radiotherapy plus cisplatin or cetuximab in low-risk human papillomavirus-positive oropharyngeal cancer (De-ESCALaTE HPV): an open-label randomised controlled phase 3 trial. *Lancet* (2019) 393:51–60. doi: 10.1016/S0140-6736(18)32752-1

58. Rischin D, King M, Kenny L, et al. Randomized trial of radiation therapy with weekly cisplatin or cetuximab in low-risk HPV-associated oropharyngeal cancer (TROG 12.01) - a trans-Tasman radiation oncology group study. *Int J Radiat Oncol Biol Phys* (2021) 111:876–86. doi: 10.1016/j.ijrobp.2021.04.015

59. Cancer Genome Atlas Network. Comprehensive genomic characterization of head and neck squamous cell carcinomas. *Nature* (2015) 517:576–82. doi: 10.1038/nature14129

60. Lee NY, Ferris RL, Psyyri A, et al. Avelumab plus standard-of-care chemoradiotherapy versus chemoradiotherapy alone in patients with locally advanced squamous cell carcinoma of the head and neck: a randomised, double-blind, placebo-controlled, multicentre, phase 3 trial. *Lancet Oncol* (2021) 22:450–62. doi: 10.1016/S1470-2045(20)30737-3

61. Aggarwal C, Cohen RB, Morrow MP, et al. Immunotherapy targeting HPV16/18 generates potent immune responses in HPV-associated head and ceck cancer. *Clin Cancer Res* (2019) 25:110–24. doi: 10.1158/1078-0432.CCR-18-1763

62. Leidner R, Crittenden M, Young K, et al. Neoadjuvant immunoradiotherapy results in high rate of complete pathological response and clinical to pathological downstaging in locally advanced head and neck squamous cell carcinoma. *J Immunother Cancer* (2021) 9:e002485. doi: 10.1136/jitc-2021-002485

63. Chen AM, Li J, Beckett LA, et al. Differential response rates to irradiation among patients with human papillomavirus positive and negative oropharyngeal cancer. *Laryngoscope* (2013) 123:152–7. doi: 10.1002/lary.23570

64. Dirix P, Abbeel S, Vanstraelen B, et al. Dysphagia after chemoradiotherapy for head-and-neck squamous cell carcinoma: dose-effect relationships for the swallowing structures. *Int J Radiat Oncol Biol Phys* (2009) 75:385–92. doi: 10.1016/j.ijrobp.2008.11.041

65. Li B, Li D, Lau DH, et al. Clinical-dosimetric analysis of measures of dysphagia including gastrostomy-tube dependence among head and neck cancer patients treated definitively by intensity-modulated radiotherapy with concurrent chemotherapy. *Radiat Oncol* (2009) 4:52–9. doi: 10.1186/1748-717X-4-52

66. Eisbruch A, Ten Haken RK, Kim HM, et al. Dose, volume, and function relationships in parotid salivary glands following conformal and intensity-modulated irradiation of head and neck cancer. *Int J Radiat Oncol Biol Phys* (1999) 45:577–87. doi: 10.1016/S0360-3016(99)00247-3

67. Deasy JO, Moiseenko V, Marks L, et al. Radiotherapy dose-volume effects on salivary gland function. *Int J Radiat Oncol Biol Phys* (2010) 76(S):58–63. doi: 10.1016/j.ijrobp.2009.06.090

68. Cartmill B, Cornwell P, Hons P, et al. Emerging understanding of dosimetric factors impacting on dysphagia and nutrition following radiotherapy for oropharyngeal cancer. *Head Neck* (2013) 35:1211–9. doi: 10.1002/hed.23040

69. Charters EK, Bogaardt H, Freeman-Sanderson AL, et al. Systematic review and meta-analysis of the impact of dosimetry to dysphagia and aspiration related structures. *Head Neck* (2019) 41:1984–98. doi: 10.1002/hed.25631

70. Azzam G, Perlow H, Cerbon D, et al. Quality of life impact and dosimetric predictors of radiation-induced fibrosis of the neck in patients treated for head and neck cancer. *Int J Radiat Oncol Biol Phys* (2020) 106:P1202. doi: 10.1016/j.ijrobp.2019.11.055

71. Chen AM, Hall WH, Li J, et al. Brachial plexus-associated neuropathy after high-dose radiation therapy for head-and-neck cancer. *Int J Radiat Oncol Biol Phys* (2012) 84:165–9. doi: 10.1016/j.ijrobp.2011.11.019

72. Ma C, Gao W, Liu Z, et al. Radiation-induced soft tissue injuries in patients with advanced mandibular osteoradionecrosis: a preliminary evaluation and management of various soft tissue problems around radiation-induced osteonecrosis lesions. *Front Oncol* (2021) 11:641061. doi: 10.3389/fonc.2021.641061

73. Hayakawa T, Kawakami S, Soda I, et al. Dosimetric factors associated with long-term patient-reported outcomes after definitive radiotherapy of patients with head and neck cancer. *Radiat Oncol* (2019) 14:22. doi: 10.1186/s13014-019-1429-3

74. Machtay M, Moughan J, Trotti A, et al. Factors associated with severe late toxicity after concurrent chemoradiation for locally advanced head and neck cancer: an RTOG analysis. *J Clin Oncol* (2008) 26:3582–9. doi: 10.1200/JCO.2007.14.8841

75. Langendijk JA, Doornaert P, Verdonck-de Leeuw IM, et al. Impact of late treatment-related toxicity on quality of life among patients with head and neck cancer treated with radiotherapy. *J Clin Oncol* (2008) 26:3770–6. doi: 10.1200/JCO.2007.14.6647

76. Chen AM, Farwell DG, Luu Q, et al. Intensity-modulated radiotherapy is associated with improved global quality of life among long-term survivors of head-and-neck cancer. *Int J Radiat Oncol Biol Phys* (2012) 84:170–5. doi: 10.1016/j.ijrobp.2011.11.026

77. O'Sullivan B, Huang SH, Perez-Ordonez B, et al. Outcomes of HPV-related oropharyngeal cancer patients treated by radiotherapy alone using altered fractionation. *Radiother Oncol* (2012) 103:49–56. doi: 10.1016/j.radonc.2012.02.009

78. Chen AM, Zahra T, Daly ME, et al. Definitive radiation therapy without chemotherapy for human papillomavirus-positive head and neck cancer. *Head Neck* (2013) 35:1652–6. doi: 10.1002/hed.23209

79. Takemoto N, Seo Y, Nakahara S, et al. Radiation therapy alone for human papillomavirus-related squamous cell carcinoma of the oropharynx: a single-arm, phase 2 study. *Int J Radiat Oncol Biol Phys* (2021) 110:403–11. doi: 10.1016/j.ijrobp.2020.12.025

80. McCusker MG, Mehra R, Amr S, et al. Comparison of efficacy and toxicity of chemoradiation regimens for head and neck squamous cell carcinoma primary treatment. *Head Neck* (2022) 44:749–59. doi: 10.1002/hed.26965

81. Van den Bosch L, van der Laan H, van der Schaaf A, et al. Patient-reported toxicity and quality of life profiles in patients with head and neck cancer treated with definitive radiation therapy or chemoradiation. *Int J Radiat Oncol Biol Phys* (2021) 111:456–67. doi: 10.1016/j.ijrobp.2021.05.114

82. Fahry E, Brooker RC, Fleming JC, et al. A review of unplanned admissions in head and neck cancer patients undergoing oncological treatment. *Support Care Cancer* (2023) 31:328.

83. Patel S, Rich BJ, Schumacher LD, et al. ED visits, hospital admissions and treatment breaks in head/neck cancer patients undergoing radiotherapy. *Front Oncol* (2023) 13:1147474.

84. Eskander A, Krzyanowska MK, Fischer HD, et al. Emergency department visits and unplanned hospitalizations in the treatment period for head and neck cancer patients treated by curative intent: a population-based analysis. *Oral Oncol* (2018) 83:107–14.

85. Hegde JV, Shaverdian N, Daly ME, et al. Patient-reported quality-of-life outcomes after de-escalated chemoradiation for human papillomavirus-positive oropharyngeal carcinoma: findings from a phase 2 trial. *Cancer* (2018) 124:521–9.

86. Hegde JV, Shaverdian N, Felix C, et al. Functional outcomes after de-escalated chemoradiation therapy for human papillomavirus-positive oropharyngeal cancer: secondary analysis of a phase 2 trial. *Int J Radiat Oncol Biol Phys* (2018) 100:647–51.

87. Shaverdian N, Hegde JV, Felix C, et al. Patient perspectives and treatment regret after de-escalated chemoradiation for human papillomavirus-positive oropharyngeal cancer: findings from a phase II trial. *Head Neck* (2019) 10:1012–20. doi: 10.1002/hed.25760

88. Leonhardt FD, Quon H, Abrahao M, et al. Transoral robotic surgery for oropharyngeal carcinoma and its implication on patient-reported quality of life and function. *Head Neck* (2012), 146–54. doi: 10.1002/hed.21688

89. Nichols AC, Lang P, Prisman E, et al. Treatment de-escalation for HPV-associated oropharyngeal squamous cell carcinoma with radiotherapy vs. trans-oral surgery (ORATOR2): study protocol for a randomized phase II trial. *BMC Cancer* (2020) 20:125. doi: 10.1186/s12885-020-6607-z

90. Hilal L, Moukarbel R, Youssef B. Patient selection for surgery versus radiotherapy for early stage oropharyngeal cancer. *Cancer Control* (2021) 28:10732748211050770. doi: 10.1177/10732748211050770

91. Swisher-McClure S, Lukens JN, Aggarwal C, et al. A phase 2 trial of alternative volumes of oropharyngeal irradiation for de-intensification (AVOID): omission of the resected primary tumor bed after transoral robotic surgery for human papilloma virus-related squamous cell carcinoma of the oropharynx. *Int J Radiat Oncol Biol Phys* (2020) 106:725–32. doi: 10.1016/j.ijrobp.2019.11.021

92. Yver CM, Shimunov D, Weinstein GS, et al. Oncologic and survival outcomes for resectable locally-advanced HPV-related oropharyngeal cancer treated with transoral robotic surgery. *Oral Oncol* (2021) 118:105307. doi: 10.1016/j.oraloncology.2021.105307

93. Sinha P, Piccirillo JF, Kallogjeri D, et al. The role of postoperative chemoradiation for oropharynx carcinoma: a critical appraisal of the published literature and national comprehensive cancer network guidelines. *Cancer* (2015) 121:1747–54. doi: 10.1002/cncr.29242

94. Nichols AC, Theurer J, Prisman E, et al. Radiotherapy versus transoral robotic surgery and neck dissection for oropharyngeal squamous cell carcinoma (ORATOR): an open-label, phase 2, randomised trial. *Lancet Oncol* (2019) 20:1349–59. doi: 10.1016/S1470-2045(19)30410-3

95. Palma DA, Prisman E, Berthelet E, et al. Treatement deescalation with radiotherapy vs transoral surgery for HPV-associated oropharyngeal squamous cell carcinoma: the ORATOR2 phase 2 randomized clinical trial. *JAMA Oncol* (2022) 8:1–7. doi: 10.1001/jamaoncol.2022.0615

96. Ma DJ, Price KA, Moore EJ, et al. Phase II evaluation of aggressive dose de-escalation for adjuvant chemoradiotherapy in human papillomavirus-associated oropharynx squamous cell carcinoma. *J Clin Oncol* (2019) 37:1909–18. doi: 10.1200/JCO.19.00463

97. Ferris RL, Flamand Y, Weinstein GS, et al. Phase II randomized trial of transoral surgery and low-dose intensity modulated radiation therapy in resectable p16+ locally advanced oropharynx cancer: an ECOG-ACRIN cancer research group trial (E3311). *J Clin Oncol* (2022) 40:138–49. doi: 10.1200/JCO.21.01752

98. Gabani P, Lin AJ, Barnes J, et al. Radiation therapy dose de-escalation compared to standard dose radiation therapy in definitive treatment of HPV-positive oropharyngeal squamous cell carcinoma. *Radiother Oncol* (2019) 134:81–8. doi: 10.1016/j.radonc.2019.01.016

99. Yang MQ, Liu YC, Sui JD, et al. Reduced-dose radiation in human papillomavirus-associated oropharyngeal carcinoma can improve outcome: a systematic review and meta-analysis. *Ann Transl Med* (2022) 10:1391. doi: 10.21037/atm-22-5935

100. Cao Y, Haring CT, Brummel C, et al. Early HPV ctDNA kinetics and imaging biomarkers predict therapeutic response in p16+ oropharyngeal squamous cell carcinoma. *Clin Cancer Res* (2022) 28:350–9. doi: 10.1158/1078-0432.CCR-21-2338

101. Chera BS, Kumar S, Beaty BT, et al. Rapid clearance profile of plasma circulating tumor HPV type 16 DNA during chemoradiotherapy correlates with disease control in HPV-associated opharyngeal cancer. *Clin Cancer Res* (2019) 25:4682–90. doi: 10.1158/1078-0432.CCR-19-0211

102. Zarrabi KK, Galloway TJ, Flieder DB, et al. Assessing plasma circulating tumor human papillomavirus (HPV) DNA in determining treatment response in HPV-associated oropharyngeal cancer. *Head Neck* (2022) 44:E25–30.

103. Wang J, Sun H, Zeng Q, et al. HPV-positive status associated with inflamed immune microenvironment and improved response to anti-PD-1 therapy in head and neck squamous cell carcinoma. *Sci Rep* (2019) 9:13404.

104. Young RJ, Bressel M, Porceddu S, et al. Validation and characterization of prognostically significant PDL-1+ immune cells in HPV+ oropharyngeal squamous cell carcinoma. *Oral Oncol* (2020) 101:104516.

105. Corredor G, Toro P, Koyuncu C, et al. An imaging biomarker of tumor-infiltrating lymphocytes to risk stratify patients with HPV-associated oropharyngeal cancer. *J Natl Cancer Inst* (2022) 114:609–17.

106. Huang SH, Waldron JN, Milsevic M, et al. Prognostic value of pretreatment circulating neutrophils, monocytes, and lymphocytes in oropharyngeal cancer stratified by human papillomavirus status. *Cancer* (2015) 121:545–55.

107. Meshman J, Velez MA, Wang PC, et al. Immunologic mediators of outcome for irradiated oropharyngeal carcinoma based on human papillomavirus status. *Oral Oncol* (2019) 89:121–6. doi: 10.1016/j.oraloncology.2018.11.030

108. Boilsesn DR, Neckermann P, Muller WT, et al. Efficacy and synergy with cisplatin of an adenovirus vectored therapeutic E12E6E7 vaccine against HPV genome-positive C3 cancers in mice. *Cancer Immunol Res* (2023) 11:261–75. doi: 10.1158/2326-6066.CIR-22-0174

109. Massarelli E, Johnson WW, Kies M, et al. Combining immune checkpoint blockade and tumor-specific vaccine for patients with incurable human papillomavirus 16-related cancer: a phase 2 clinical trial. *JAMA Oncol* (2019) 5:67–73. doi: 10.1001/jamaoncol.2018.4051

110. Mattox AK, D'Souza GD, Khan Z, et al. Comparison of next generation sequencing, droplet digital PCR, and quantitative real-time PCR for the earlier detection and quantification of HPV in HPV-positive oropharyngeal cancer. *Oral Oncol* (2022) 128:105805. doi: 10.1016/j.oraloncology.2022.105805

111. Gao G, Wang J, Kasperbauer JL, et al. Whole genome sequencing reveals complexity in both HPV sequences present and HPV integrations in HPV-positive oropharyngeal squamous cell carcinomas. *BMC Cancer* (2019) 19:352. doi: 10.1186/s12885-019-5536-1

112. Kim SI, Woo SR, Noh JK, et al. Association between cancer stem cell gene expression signatures and prognosis in head and neck squamous cell carcinoma. *BMC Cancer* (2022) 22:1077. doi: 10.1186/s12885-022-10184-4

113. Stepp WH, Farquhar D, Sheth S, et al. RNA Oncoimmune phenotyping of HPV-positive, p16-positive oropharyngeal squamous cell carcinomas by nodal status. *JAMA Otolaryngol Head Neck Surg* (2018) 144:967–75. doi: 10.1001/jamaoto.2018.0602

114. Wang P, Wang X, Zhang M, et al. Combining the radiomics signature and HPV status for the risk strateification of patients with OPC. *Oral Dis* (2022) 00:1–9.

115. Bagher-Ebadian H, Siddiqui F, Ghanem AI, et al. Radiomics outperforms clinical factors in characterizing human papilloma virus (HPV) for patients with oropharyngeal squamous cell carcinomas. *BioMed Phys Eng Express* (2022) 8:045010. doi: 10.1088/2057-1976/ac39ab

116. Suh CH, Lee KH, Choi YJ, et al. Oropharyngeal squamous cell carcinoma: radiomic machine-learning classifiers from multiparametric MR images for determination of HPV infection status. *Sci Rep* (2020) 10:17525. doi: 10.1038/s41598-020-74479-x

117. Ravanelli M, Grammatica A, Maddalo M, et al. Pretreatment DWI with histogram analysis of the ADC in predicting the outcome of advanced oropharyngeal cancer with known human papillomavirus status treated with chemoradiation. *AJNR Am J Neuroradiol* (2020) 41:1473–9. doi: 10.3174/ajnr.A6695

118. Lee N, Schoder H, Beattie B, et al. Strategy of using intratreatment hypoxia imaging to selectively and safely guide radiation dose de-escalation concurrent with chemotherapy for locoregionally advanced human papillomarivus-related oropharyngeal carcinoma. *Int J Radiat Oncol Biol Phys* (2016) 96:9–17. doi: 10.1016/j.ijrobp.2016.04.027

119. Riaz N, Sherman E, Pei X, et al. Precision radiotherapy: reduction in radiation for oropharyngeal cancer in the 30 ROC trial. *J Natl Cancer Inst* (2021) 113:742–51. doi: 10.1093/jnci/djaa184

120. Sohn B, Choi YS, Ahn SS, et al. Machine learning based radiomic HPV phenotyping of oropharyngeal SCC: a feasibility study using MRI. *Laryngoscope* (2021) 131:851–6. doi: 10.1002/lary.28889

121. Alabi RO, Almangush A, Elmusrati M, et al. An interpretable machine learning prognostic system for risk stratification in oropharyngeal cancer. (2022) 168:104896. doi: 10.1016/j.ijmedinf.2022.104896

122. Kim SI, Kang JW, Eun YG, et al. Prediction of survival in oropharyngeal squamous cell carcinoma using machine learning algorithms: a study based on the surveillance, epidemiology, and end results database. *Front Oncol* (2022) 12:974678.

123. Choi KH, Song JH, Kim YS, et al. Survey of radiation field and dose in human papillomavirus-positive oropharyngeal cancer: is de-escalation actually applied in clinical practice? *Radiat Oncol J* (2021) 39:174–83.

124. Nguyen TK, Nguyen EK, Warner A. Failed randomized clinical trials in radiation oncology: what can we learn? *Int J Radiat Oncol Biol Phys* (2018) 101:1018–24.

125. Rischin D, Young RJ, Fisher R, et al. Prognostic significance of p16INK4A and human papillomavirus in patients with oropharyngeal cancer treated on TROG 02.02 phase III trial. *J Clin Oncol* (2010) 28:4142–8.

126. Worden FP, Kumar B, Lee JS, et al. Chemoselection as a strategy for organ preservation in advanced oropharynx cancer: response and survival positively associated with HPV16 copy number. *J Clin Oncol* (2008) 26:3138–46.

127. Seiwert TY, Melotek JM, Blair EA, et al. Final results of a randomized phase 2 trial investigating the addition of cetuximab to induction chemotherapy and accelerated or hyperfractionated chemoradiation for locoregionally advanced head and neck cancer. *Int J Radiat Oncol Biol Phys* (2016) 96:21–9.

128. Cmelak AJ, Ferris RL, Chen AM, et al. Treatment de-intensification for HPV-positive oropharynx cancer: what is currently acceptable? *J Clin Oncol* (2021) 39:2732–3.

frontiers | Frontiers in Oncology

TYPE Original Research
PUBLISHED 05 September 2023
DOI 10.3389/fonc.2023.1228994

OPEN ACCESS

EDITED BY
Giuseppe Carlo Iorio,
University of Turin, Italy

REVIEWED BY
Feng Liu,
Central South University, China
Giuseppe Danilo Di Stasio,
Independent Researcher, Caserta, Italy

*CORRESPONDENCE
Zhen-zhang Chen
czz1976@aliyun.com
Sheng-fu Huang
hsf200902@163.com

RECEIVED 25 May 2023
ACCEPTED 11 August 2023
PUBLISHED 05 September 2023

CITATION
Zong D, Jiang N, Kong C, Wen J, Wang L-j, Guo Y-s, Zhang L-f, He X, Chen Z-z and Huang S-f (2023) Distribution pattern of medial group retropharyngeal lymph nodes and its implication in optimizing clinical target volume in nasopharyngeal carcinoma.
Front. Oncol. 13:1228994.
doi: 10.3389/fonc.2023.1228994

Distribution pattern of medial group retropharyngeal lymph nodes and its implication in optimizing clinical target volume in nasopharyngeal carcinoma

Dan Zong[1], Ning Jiang[1], Cheng Kong[1], Jing Wen[1], Li-jun Wang[1], Ye-song Guo[1], Lan-fang Zhang[2], Xia He[1], Zhen-zhang Chen[1*] and Sheng-fu Huang[1*]

[1]Department of Radiation Oncology, Jiangsu Cancer Hospital, Jiangsu Institute of Cancer Research, Nanjing Medical University Affiliated Cancer Hospital, Nanjing, Jiangsu, China, [2]Department of Medical Imaging, Jiangsu Cancer Hospital, Jiangsu Institute of Cancer Research, Nanjing Medical University Affiliated Cancer Hospital, Nanjing, Jiangsu, China

Purpose: This study aimed to determine the diagnostic value of diffusion-weighted imaging (DWI) and to elucidate the clinical characteristics of medial group retropharyngeal lymph nodes (RLNs) based on multi-modal imaging. Also, we intended to explore the feasibility of optimizing the CTV60 boundary based on the characteristics of medial group RLNs.

Methods: A total of 549 patients with nasopharyngeal carcinoma received magnetic resonance imaging (MRI), DWI, and contrast-enhanced computed tomography (CT) to detect and evaluate clinical characteristics of medial group RLNs. $^{[18F]}$Fluorodeoxyglucose positron emission tomography/computed tomography was utilized to identify fluorodeoxyglucose uptaking and contrast-enhanced CT to ensure the reliability of CTV optimization during radiotherapy. The DESdC (Drinking, Eating, Swallowing Difficulties, and Coughing while Eating or Drinking) score was utilized to evaluate swallowing disability.

Results: Fourteen of 549 patients had medial group RLNs with a transverse diameter of 2.0–19.0 mm, which distributed between the upper margin of 1st cervical vertebra (C1) and the upper one-third of C3. Lasso regression and Pearson chi-square test suggested that its occurrence was associated with stage N, bilateral cervical lymph node metastases, especially when the transverse diameter of cervical lymph nodes was > 3 cm. The sensitivity of DWI, T2 STIR, and contrast-enhanced CT was 100%, 57.1%, and 21.4%, respectively. We optimized CTV60 of medial group RLNs from the base of skull to the upper edge of C2 excluding specific cases. For patients with CTV60 optimization, radiation dose and volume of swallowing structures decreased obviously. Based on our radiotherapy strategy on CTV60, acute toxicities of enrolled patients were well tolerated. Ninety-six of 549 patients had scores with DESdC score. Eighty-three patients scored 1, seven patients scored 2, one patient scored 3, and three patients scored 4. The median interval from the onset of symptoms was 72 (4–114) months. The 5-year overall survival,

progression-free survival, local recurrence-free survival, and distant metastasis-free survival were 87%, 80%, 93%, and 85%, respectively. None of the patients with regional recurrence happened in the optimized region.

Conclusion: DWI possesses superiorities in displaying lymph nodes. Based on the low incidence of the medial RLNs, CTV60 of medial group RLNs from the base of skull to the upper edge of C2 is feasible and has dosimetric advantages for protecting swallowing structures.

KEYWORDS

nasopharyngeal carcinoma, the medial group of retropharyngeal lymph nodes, diffusion-weighed imaging, Lasso regression analysis, swallowing structures

Introduction

The prevalence of nasopharyngeal carcinoma (NPC) varies significantly by area and is particularly high in southern China (1). Intensity-modulated radiotherapy (IMRT) is widely used as the mainstay therapeutic modality due to its biological behavior and radiosensitivity (2). IMRT offered better target conformity and lower doses to surrounding critical organs compared with two- or three-dimensional radiotherapy. With applications of improved radiotherapy techniques and administration of chemotherapy, treatment outcomes and quality of life have been greatly improved in NPC patients (3, 4). However, the high radiotherapy dose and extensive volume coverage determined by particular anatomical position and locoregionally advanced disease result in high incidences of acute mucosal reaction and long-term dysphagia, xerostomia, and cervical fibrosis (5).

As patients survive longer, long-term adverse effects caused by radiotherapy become apparent and a significant factor affecting patients' quality of life. We have initiated a series of studies to explore injuries of essential organs such as the brainstem and temporal lobe after standard treatments according to the protocol of The Radiation Therapy Oncology Group (RTOG) 0225 or 0615. Radiotherapy-induced brain necrosis is one of the severe complications that can lead to cognitive dysfunction, seizure, headache, limb paralysis, and hematencephalon. Our study showed that besides lesion location, brainstem dose per unit volume, D0.1cc, and D1cc should also be considered. Moreover, for patients with microcirculation disturbance, such as diabetes, high blood pressure, and immune disorders, radiotherapy dose-volume parameters should be strictly limited (6, 7).

Dysphagia was identified as a major concern in NPC patients after a long-term follow-up. The incidence of dysphagia after radiotherapy for NPC has been reported to be 54%–95%, and dysphagia will continue to worsen with time (8, 9). Aspiration pneumonia due to dysphagia has become one of the leading causes of death after radiotherapy in patients with NPC (10, 11). The main factor of affecting swallowing function after radiotherapy was impaired swallowing structures (12), including the pharyngeal constrictors, vocal cords, upper larynx of the glottis, and upper esophagus (13). It has been demonstrated that radiotherapy can lead to anatomical changes and dysfunction of swallowing structures (14). In recent years, many studies have been conducted to explore treatment strategies to reduce swallowing dysfunction (15, 16). Researchers advocated reducing the target area V (50) of swallowing structures, but the maximal dose remained high due to surrounding dose coverage (17).

Factors influencing damage to swallowing structures include primary gross tumor and the lateral and medial group retropharyngeal lymph nodes. To date, the understanding of the primary lesions and the lateral group RLNs are relatively mature. The medial group RLNs are the blind spot due to its low incidence and the limitation of imaging technique. The medial group RLNs are close to the center line, located between the pharyngeal constrictor and vertebral front fascia (18). Sun Ying et al. proposed VIIc as the medial group RLNs (19). Since the medial group RLNs are currently recognized as high-risk areas for metastasis, researchers pointed out that no matter how big they were, they should be considered as malignant lesions (20). Because of its low incidence and limited imaging features, clinical characteristics of medial group RLNs are rarely reported.

So far, RTOG 0225/0615 protocols recommend the CTV60 delineation of VIIc, which cover the skull base to the superior border of hyoid bone. Nevertheless, there are controversies regarding the CTV60 boundaries of VIIc in clinical practices. Several cancer institutes have developed feasible guidelines to optimize the target volume of VIIc in China. For example, Sun Ying et al. pointed out that VIIc boundaries extended from skull base to the caudal edge of C2 (19). To date, no consensus guidelines or relevant clinical studies provide strong evidence for the delineation of VIIc boundaries in CTV60. VIIc has the pharyngeal constrictor muscle anteriorly and the long cephalic muscle posteriorly, with the medial border of the VIIa layer laterally and the midline medially (21). The main anatomical structures of VIIc are closely related to swallowing function. We conducted this pilot study to explore the clinical features of medial group RLNs and examine the feasibility of optimizing CTV60 of medial group RLNs from the skull base to the upper margin of C2 to reduce radiotherapy dose of swallowing structures.

Materials and methods

Study subjects

Patients received IMRT from June 2011 to February 2018 in Jiangsu Cancer Hospital. A total of 549 patients were included, and inclusion criteria were as follows: (1) with histologically proven NPC, pathologically diagnosed with non-keratinized undifferentiated carcinoma; (2) patients had not received antitumor treatment before biopsy sampling; (3) clinical stage I-IVa; (4) aged between 18 and 70 years; (5) with complete medical records and regular follow-up, without a history of cancer, and complete treatment. Exclusion criteria were as follows: (1) patients died of other diseases; (2) Other pathological types, such as adenocarcinoma and lymphoepithelial carcinoma; and (3) patients with second primary cancer. They underwent a comprehensive pretreatment evaluation. $^{[18F]}$Positron emission tomography and computed tomography ($^{[18F]}$PET/CT) was performed when necessary. All patients were restaged according to the 8th edition of the American Joint Committee on Cancer (AJCC) staging system based on imaging materials and medical records. The institutional review board approved this study. The Clinical Research Ethics Committee of Jiangsu Cancer Hospital approved the protocol. This study was conducted in accordance with the Declaration of Helsinki. Informed consent was obtained from each participant.

MRI examination

MRI examination was performed using Philips achieva1.5t superconducting MR scanner. Scanning sequences: (1) axial/coronal images: T1WI and STIR; (2) sagittal position: T1WI, T2WI. T1WI, and fat suppression were observed on axial, coronal, and sagittal T1WI after intravenous injection of Magnevist. DWI was performed before the injection of Magnevist, using single-excited spinal-plane echo and STIR sequences. Scanning parameters: The diffusion-sensitive factor b value was 1000s/mm^2, and sensitive gradient pulses were applied to *x*, *y*, and *z* axes to obtain DWI in the 3D workstation. The apparent diffusion coefficient (ADC) images were generated using the software.

Enhanced localization CT and frequent CT examination

A Philips Mx8000 multi-slice spiral CT was used. After intravenous injection of iohexol, patients underwent direct enhanced CT scanning. Frequent CT was defined as enhanced CT scans performed in fractions of 0, 5, 10, 15, and 25 during IMRT.

Image analysis and diagnostic criteria

The images were analyzed independently by two head and neck image diagnostic specialists. The first step was to determine the presence of the medial group RLNs by two physicians on conventional T2 STIR scanning, DWI, and enhanced CT, respectively. The second step was to analyze the sensitivity among T2 STIR, DWI, and enhanced CT.

Treatment

Prior to treatment, patients were immobilized with thermoplastic head and shoulder masks and underwent CT simulation according to standard procedures. MRI and fusion with simulation CT images were performed to assist target delineation. IMRT with 7–9 field fixed angle was adopted. Gross tumor volumes were defined based on MRI, CT, and PET/CT imaging before induction chemotherapy. The specific prescription doses were as follows: planned target area (PTVnx) of the primary tumor (GTVnx), 66–75 Gy for 32–34 times. PTVnd of metastatic cervical lymph node (GTVnd), 66–70 Gy, 32–34 times. PTV1 of CTV1 (high-risk area) and CTV2 (low-risk area) were 60.0 and 50.4 Gy, respectively. Dose limitations for organs at risk were described in detail previously (22). Institutional guidelines recommended only IMRT for stage I NPC and IMRT combined with concurrent chemoradiotherapy ± neoadjuvant/adjuvant chemotherapy for stages II–IVa NPC. Neoadjuvant/adjuvant chemotherapy regimens included TP (docetaxel 80 mg/m^2 and cisplatin 80 mg/m^2, day 1) and TPF (docetaxel 60 mg/m^2 and cisplatin 60 mg/m^2, day 1; fluorouracil 600 mg/m^2/d, days 1–5) every 3 weeks for two to four cycles. Concurrent chemotherapy was weekly cisplatin (40 mg/m^2) during IMRT. When possible, salvage treatments (surgery or chemotherapy) were provided for patients with documented relapse or persistent disease (23).

Principles of optimizing the CTV60 of VIIc regional lymph nodes

The principle of optimizing the CTV60 delineation of the VIIc regional lymph nodes was from the base of the skull to the upper edge of C2 to protect the swallowing structures. The excluded cases were as follows: (1) When the nasopharyngeal lesion involved the oropharynx, the low-separation margin of CTV60 was set at 9–15 mm below the lesion; (2) when the VII regional lymph node was at or below the C1 level, the low separation margin of CTV60 was set at 3–6 mm below the lesion.

$^{[18F]}$Fluorodeoxyglucose positron emission tomography/computed tomography

The 710 DiscoveryTM PET/CT scanner was obtained from GE Healthcare, and 18F-FDG reagent was provided by Nanjing JYAMS, Ltd. Before the examination, patients were asked to empty their stomachs for at least 6h prior to the blood sugar test. After the blood sugar level was confirmed, $^{[18F]}$FDG was injected intravenously at the standard dose. Images were reconstructed after

attenuation correction to obtain 3D CT, PET images, and PET/CT-blending images.

Definition of positive medial RLNs

In the present study, we adopted the professor King AD's definition for positive medial RLNs (20). The criteria for diagnosing positive medial group RLNs were the lymph nodes between the pharyngeal constrictor and the anterior vertebral fascia, regardless of their size.

Dysphagia assessment and end points

This information was collected through telephone interviews. All patients were asked the following four questions about their swallowing disability. Do you have difficulties in (1) drinking; (2) eating; or (3) swallowing; (4) Do you cough when eating or drinking? The answers were recorded as "Yes" or "No". Based on the answers to these questions, we constructed a study-specific categorical symptom score, DESdC (an acronym for difficulty drinking, eating, swallowing, and coughing while eating/drinking), to describe the presence of these symptoms. We also define five categories of DESdC scores ranging from 0 to 4. 0 = *no to all questions*; 1 = *yes to one question*; 2 = *yes to two questions*; 3 = *yes to any three questions*; and 4 = *yes to all four questions* (24).

Follow-up visits

The follow-up period is from the first day of treatment to the last examination or the day of death. Patients were followed up every 3 months for the first 3 years after radiation therapy, every 6 months for the fourth to fifth years, and annually thereafter until death. Follow-up visits included physical examination, hematological and biochemical profiles, EBV-DNA, MRI, CT scan of the chest and abdomen, and whole-body bone scan. $^{[18F]}$ PET/CT was performed when necessary. Local recurrence-free survival (LRFS) was defined as the time from the start of treatment to the first local failure. Progression-free survival (PFS) was defined as the time from initiation of treatment to failure or death from any cause, whichever occurred first. Distant metastasis-free survival (DMFS) was defined as the time from initiation of therapy to first distant failure. Overall survival (OS) was defined as the time from the initiation of therapy to death from any cause.

Statistical methods

SPSS 24.0 software was used for statistical analyses and figures generation. Survival curves were depicted using the Kaplan–Meier method and compared by the log-rank test. The least absolute shrinkage and selection operator (Lasso) is a regression analysis method that performs both variable selection and regularization to improve predictive accuracy and statistical model interpretability. Lasso regression analysis was used to select highly correlated variables that were strongly associated with the occurrence of intermediate RLNs and survival indicators. Two-tailed $P < 0.05$ was considered statistically significant.

Results

A total of 549 NPC patients with clinical stages I–IVa were included in the current study. Deaths caused by other diseases, such as secondary malignancies, cerebral hemorrhage, and liver injury after the use of herbal medicines, were excluded. Specific pathological patterns, such as sarcoma, myoepithelial carcinoma, adenocarcinoma, and mixed pathological patterns, were excluded.

The medium follow-up months were 72 (5–129) months. Of the 549 patients, 14 (2.55%) had medial group RLNs with a transverse diameter of 2.0–19.0 mm. The percentages of those with transverse diameters of 2.0–5.0 mm and > 5 mm were 57.1% (8 of 14) and 42.9% (6 of 14), respectively. Eleven medial group RLNs were distributed between the upper edge of C1 and the upper 1 of 3 of C3. The sensitivities of DWI, T2 STIR and enhanced CT were 100%, 57.1%, and 21.4%, respectively (Table 1). DWI presented an absolute advantage in identifying small lymph nodes and the representative images are shown in Figures 1A–C.

The incidence of medial group RLNs was not associated with age, gender, total clinical stage, T stage, anterior vertebral muscle invasion, or oropharyngeal invasion. The medial group RLNs were also unrelated to the lateral group RLN metastasis, lymph node necrosis, and extracapsular spread, local regional recurrence, or death in the lateral group ($P > 0.05$). However, their incidence were significantly associated with N stage ($P = 0.021$) and bilateral cervical lymph node metastasis ($P = 0.015$). In particular, the incidence of medial group RLNs was significantly higher when the transverse diameter of the patient's cervical lymph nodes > 3 cm ($P = 0.004$), which deserved further clinical attention. In addition, the occurrence of medial group RLNs might also be significantly related to distant metastases ($P = 0.003$) (Table 2).

The lateral RLNs have been explored comprehensively and reached consensus guidelines. In this study, nine serial MRI scans were performed before and after radiotherapy to observe the medial group RLNs and evaluate the treatment responses of the medial RLNs. Thirteen of 14 (92.8%) cases showed completely regression after radiotherapy with or without concurrent chemotherapy; representative case was presented in Figure 1 (before treatment: A–C; After treatment: D–F). Interestingly, one case slightly retreated after treatment, as shown in Figure 2 (before treatment: A–E; after treatment: F–J). It was still identifiable, but the DWI

TABLE 1 Comparison of DWI, T2 STIR and enhanced CT in the display of the medial group of retropharyngeal lymph nodes (n=14).

	Positive	Negative	Sensitivity (%)
DWI	14	0	100
T2 STIR	8	6	57.1
Enhanced CT	3	11	21.4

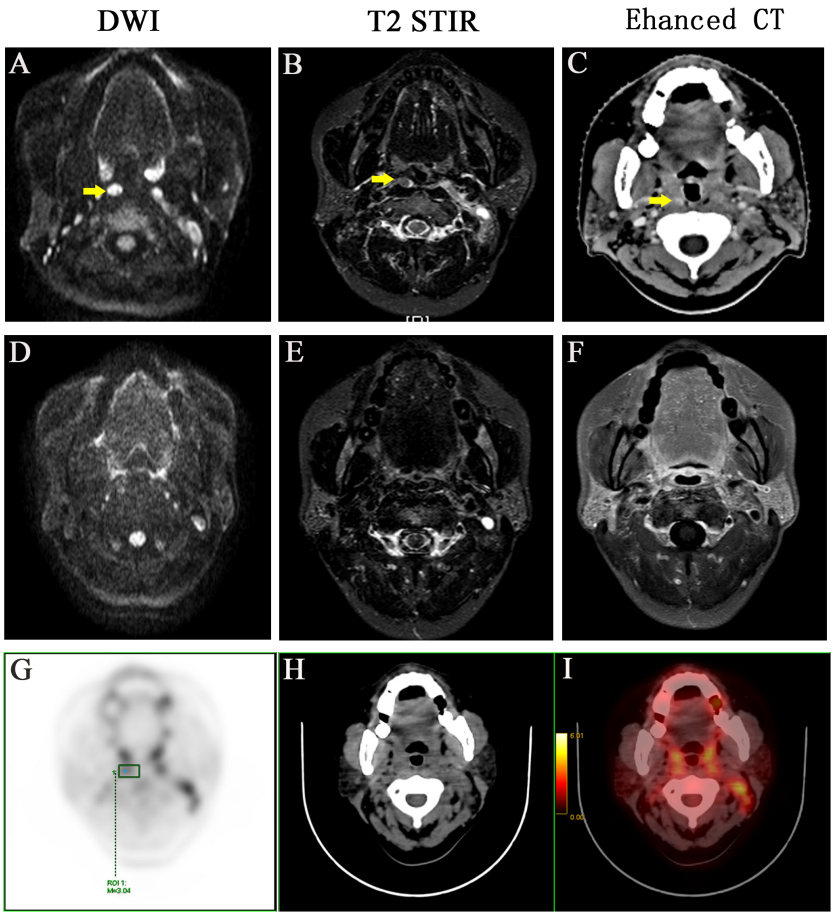

FIGURE 1
A representative case with positive medial group of retropharyngeal lymph node before and after treatment. Before treatment: **(A)** DWI imaging **(B)** T2 STIR **(C)** Enhanced CT. After treatment: **(D)** DWI imaging **(E)** T2 STIR **(F)** Enhanced CT. **(G-I)** PET-CT image before treatment, PET image, CT image, PET/CT blending image, respectively.

TABLE 2 The relationship between clinical characteristics and the medial group of retropharyngeal lymph node.

Clinical Characteristics	The medial group of retropharyngeal lymph nodes		P Value
	Negative,n=535 (%)	Positive, n=14 (%)	
Age			0.722
<50	280 (52.3)	8 (57.1)	
≥50	255 (47.7)	6 (42.9)	
Gender			0.751
Male	402 (75.1)	10 (71.4)	
Female	133 (24.9)	4 (28.6)	
Clinical Stage			0.538
I-II	155 (29.0)	3 (21.4)	
III- IV	380 (71.0)	11 (78.6)	
T Stage			0.837
T1- T2	177 (33.1)	5 (35.7)	
T3- T4	358 (66.9)	9 (64.3)	

(Continued)

TABLE 2 Continued

Clinical Characteristics	The medial group of retropharyngeal lymph nodes		P Value
	Negative,n=535 (%)	Positive, n=14 (%)	
N Stage			**0.021***
N0- N1	317 (59.3)	4 (28.6)	
N2- N3	218 (40.7)	10 (71.4)	
Anterior vertebral muscle invasion			0.766
Yes	246 (46.0)	7 (50.0)	
No	289 (54.0)	7 (50.0)	
Oropharyngeal invasion			
Yes	30 (5.6)	1 (7.1)	
No	505 (94.4)	13 (92.9)	
Bilateral retropharyngeal lymph nodes			0.806
Yes	167 (31.2)	6 (42.9)	
No	368 (68.8)	8 (57.1)	
-Diameter>2cm			0.311
Yes	66 (12.3)	3 (21.4)	
No	469 (87.7)	11 (78.6)	
-Diameter>3cm			0.745
Yes	4 (0.7)	0 (0.0)	
No	531 (99.3)	14 (100)	
Bilateral cervical lymph nodes			**0.015***
Yes	209 (39.1)	10 (71.4)	
No	326 (60.9)	4 (28.6)	
-Diameter>2cm			0.058
Yes	245 (45.8)	10 (71.4)	
No	290 (54.2)	4 (28.6)	
-Diameter>3cm			**0.004***
Yes	100 (18.7)	7 (50.0)	
No	435 (81.3)	7 (50.0)	
Lymph node necrosis			0.239
Yes	152 (28.4)	6 (42.9)	
No	383 (71.6)	8 (57.1)	
Lymph node fusion			0.175
Yes	175 (32.7)	7 (50.0)	
No	360 (67.3)	7 (50.0)	
Local regional recurrence			0.725
Yes	27 (5.0)	1 (7.1)	
No	508 (95.0)	13 (92.9)	
Distant metastasis			**0.003***
Yes	38 (7.1)	4 (28.6)	

(Continued)

TABLE 2 Continued

Clinical Characteristics	The medial group of retropharyngeal lymph nodes		P Value
	Negative,n=535 (%)	Positive, n=14 (%)	
No	497 (92.9)	10 (71.4)	
Death			0.717
Yes	54 (10.1)	1 (7.1)	
No	481 (89.9)	13 (92.9)	

*P-values were calculated using an unadjusted chi-square test.
Bold values means P<0.05.

signal was much weaker than before treatment (Figures 2H, I). $^{[18F]}$ PET/CT was performed to detect FDG accumulation in tumor lesions. As shown in Figures 1G–I, lymph node with standardized uptake value (SUV) 3.04 was completely withdrawn, whereas the lymph node with SUV 3.05 was only reduced in size and DWI signal (Figures 2K–N).

Because of low incidence of the medial group RLNs, to avoid statistical discrepancy, we used Lasso regression analysis to select variables that related to the incidence of medial group RLNs. In addition to the clinical characteristics listed in Table 2, parotid lymph nodes and GTV dose were included in this analysis. The results showed that N stage, bilateral cervical lymph node metastasis, and the diameter of cervical lymph nodes > 3 cm were significantly associated with the incidence of medial group RLNs, which was consistent with the data from Pearson chi-square test (Figure 3A column). Meanwhile, we performed Lasso regression analysis to select factors for predicting prognosis. For OS, clinical stage, T stage, N stage, lymph node necrosis, and extracapsular spread, gender were crucial indicators (Figure 3B column). For LRFS, T stage, oropharyngeal invasion, the diameter of cervical lymph nodes > 2cm and lymph node necrosis were critical predicting markers (Figure 3C column). For DMFS, clinical stage, T stage, N stage, lymph node necrosis and extracapsular spread, oropharyngeal invasion, bilateral retropharyngeal lymph nodes, parotid lymph nodes, and radiation dose were relevant clinical features (Figure 3D column). For PFS, clinical stage, N stage, anterior vertebral muscle invasion, oropharyngeal invasion, lymph node necrosis and extracapsular spread, and parotid lymph nodes were identified as critical indicators (Figure 3E column).

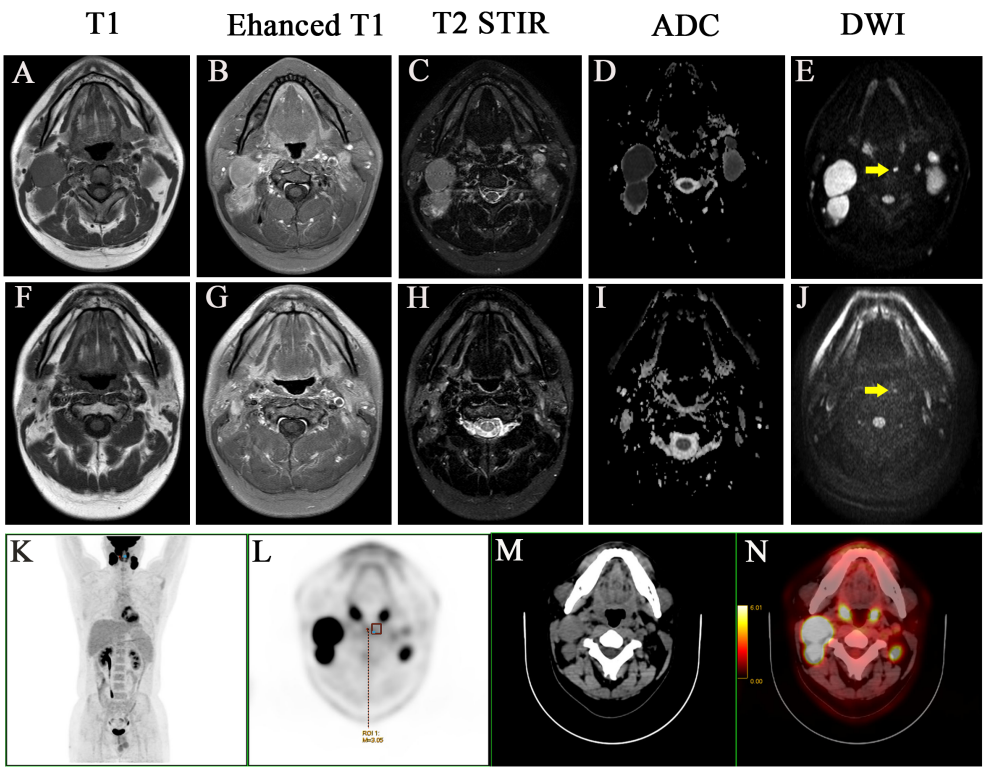

FIGURE 2
A case with the medial group of retropharyngeal lymph node did not retreat completely after treatment and two years follow-up. Before treatment: **(A)** T1 **(B)** Enhanced T1 **(C)** T2 STIR **(D)** ADC **(E)** DWI. After treatment: **(F)** T1 **(G)** Enhanced T1 **(H)** T2 STIR **(I)** ADC **(J)** DWI. **(K-N)** PET-CT image before treatment, MIP image, PET image, CT image, PET/CT blending image, respectively.

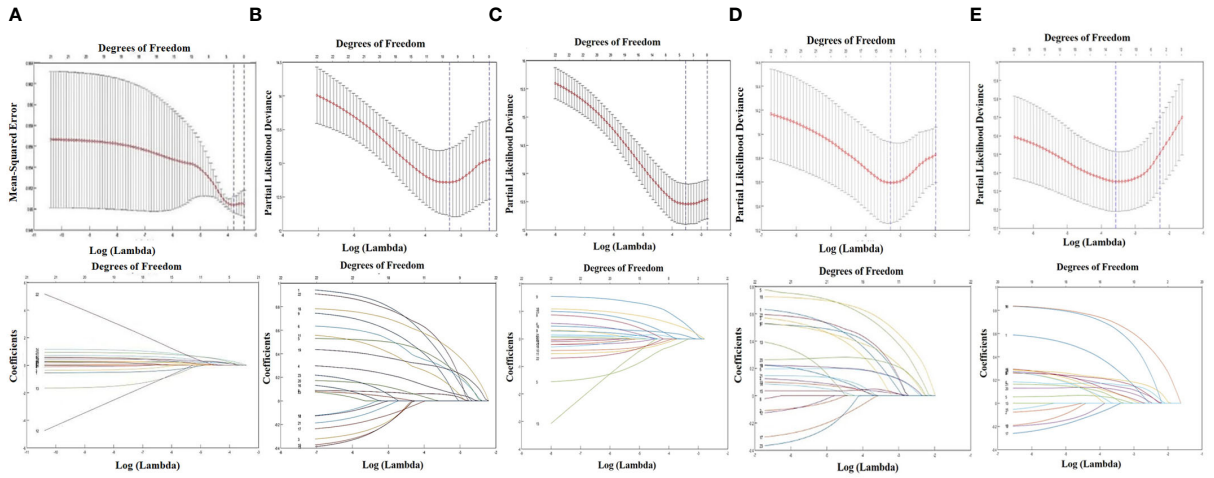

FIGURE 3
LASSO regression analysis about the medial group of retropharyngeal lymph node and survival indicators. **(A)** The relationship between the incidence of retropharyngeal lymph node and the clinical characteristics. **(B)** The relationship between OS and the clinical characteristics. **(C)** The relationship between LRFS and the clinical characteristics. **(D)** The relationship between DMFS and the clinical characteristics. **(E)** The relationship between PFS and the clinical characteristics.

The clinical characteristics of medial group RLNs are crucial for CTV60 delineation. In this study, although a higher incidence of medial group RLNs (2.56%) was found than that in other studies, it was still rare, less than 5% in incidence. Our principles for optimizing CTV60 were discussed and got consistent agreements. The principle of CTV60 delineation for optimizing VIIc was from the skull base to the superior edge of C2 to protect swallowing structures. Our data show that the volume of high-dose radiotherapy (Figure 4B①), the dose and volume of the pharyngeal constrictor muscle (Figure 4B②), vocal cords (Figure 4B③), and supraglottic larynx (Figure 4B④) were significantly reduced compared with the protocol of RTOG 0615 (Figures 4A①–④,C①–④). We delineated one representative patient with RTOG 0615 and our optimized protocol (Supplementary Figure S1). The volume of CTV60 with optimized protocol was reduced significantly compared with RTOG0615 (230.2 cm^3 vs 430.2 cm^3) (Supplementary Figure S1). In addition, we measured the central dose at different typical transverse sections in terms of the upper margin of C2, epiglottis, superior, and inferior margin of hyoid in 50 NPC patients. The mean dose of the upper margin of C2, epiglottis, superior, and inferior margin of hyoid was 36.135, 30.881, 31.135, and 29.451 Gy, respectively (Supplementary Figure S2). For patients with oropharynx invasion and VII regional lymph nodes at or below the C1 level, we suggested a moderately extended boundary of CTV60 as follows. First, when the nasopharyngeal lesion involved oropharynx, the low separation margin of CTV60 was set at 9–15 mm below the lesion. Second, when the lymph nodes of VII region were at or below the C1 level, the low separation margin of CTV60 was set at 3–6 mm below the lesion.

For treatment-related toxicities, acute and late toxicities were assessed during treatment and long-term follow-up. Acute toxicities of radiotherapy and/or chemotherapy were well tolerated. Grades 1 and 2 acute mucositis, dermatitis, and xerostomia were most common. None of the patients discontinued the treatment course due to severe acute toxicity. During long-term follow-up, late toxicities were assessed by telephone interview. We asked patients if they had difficulties in drinking, eating, swallowing, or coughing while eating/drinking. We also scored the combined symptoms ranging from 0 to 4. Ninety-six of 549 patients had difficulties in drinking, eating, swallowing, or coughing when eating/drinking. Of the 96 patients, three patients had difficulty in drinking; 53 patients had difficulties when eating dry food, which can be released by drinking water; 10 patients had difficulties in swallowing; three patients had cough when eating or drinking; and three patients developed serious dysphagia because of its large tumor (Table 3). All of the 96 patients had difficulty in eating and 43 reported difficulty immediately after radiotherapy, which might be due to the damage of salivary glands. Eighty-three patients scored 1, seven patients scored 2, one patient scored 3, and three patients scored 4 (Table 3). The median time from onset of symptoms was 72 (4–114) months. Importantly, there was no regional recurrence in optimized area.

The 5-year OS rates in medial and non-medial groups were 78.6% and 87.3%, respectively (P = 0.12). (Figure 4D). The 5-year PFS rates in medial and non-medial groups were 64.3% and 80.5%, respectively (P = 0.26) (Figure 4E). The 5-year LRFS rates in medial and non-medial groups were 84.4% and 93.0%, respectively (P = 0.15) (Figure 4F). The 5-year DMFS rates in medial and non-medial groups were 71.4% and 85.3%, respectively (P = 0.13) (Figure 4G). The 5-year OS, PFS, LRFS, and DMFS for all enrolled patients were 87%, 80%, 93%, and 85%, respectively.

Discussion

Commonly, nasopharyngeal cancer (NPC) is treated with high-dose radiotherapy in the clinic. Researchers have emerged to standardize tumor target delineation variations and guide dose

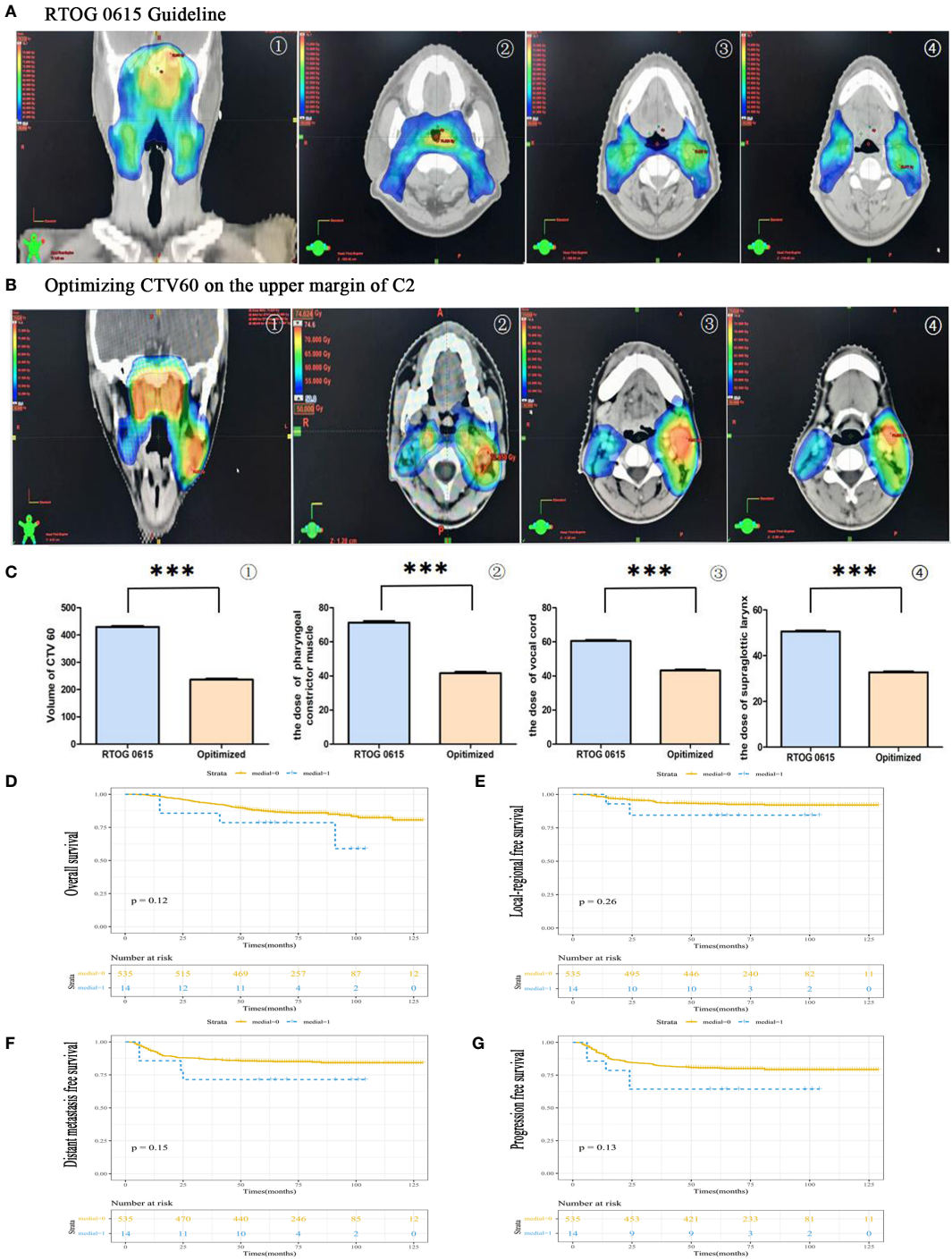

FIGURE 4
The feasibility of CTV60 optimization for VIIc regional lymph node from skull base to the upper margin of C2 to protect swallowing structures. **(A)** The group was delineated according to the protocol of RTOG 0615. The presented images were coronary side of the target volume ①, the layer of pharyngeal constrictor muscle ②, the layer of vocal cords ③ and the layer of supraglottic larynx ④, respectively. **(B)** The group was delineated according to our optimized strategy. The presented images were the coronary side of the target volume ①, the layer of pharyngeal constrictor muscle ②, the layer of vocal cords ③ and the layer of supraglottic larynx, respectively. **(C)** The statistical data of the volume of CTV60 ①, the dose of pharyngeal constrictor muscle ②, the dose of vocal cords ③ and the dose of supraglottic larynx ④. **(D)** Overall survival rate (OS). **(E)** Locoregional recurrence-free survival rate (LRFS). **(F)** Distant-metastasis-free survival rate (DMFS). **(G)** Progression-free survival rate (PFS). ***P<0.0005.

prioritization for NPC radiotherapy. Special efforts are required in the proactive sparing of normal structures to minimize the incidence and severity of radiation-associated complications, many of which may pose lifelong detriments to the life quality in NPC patients. Severe swallowing structures dysfunction might lead to dysphagia (25). Previous study proposed that V60 greater than 12% of the inferior pharyngeal constrictor was significantly associated with increased rate of dysphagia which demanded

TABLE 3 Swallowing dysfunction evaluated with DESdC.

Category	Incidence (%)
DESdC symptoms	
Drinking Difficulties	3/549 (0.5)
Eating Difficulties	96 */549 (17.4)
Swallowing Difficulties	10/549 (1.8)
Coughing while Eating or Drinking	3/549 (0.5)
DESdC Score	
0	453/549 (82.5)
1	83/549 (15.1)
2	7/549 (1.3)
3	1/549 (0.2)
4	3/549 (0.5)

*43 of the 96 patients had difficulty immediately after radiotherapy, which might be due to the damage of salivary glands.

enteral nutritional supporting treatment (26). Dysphagia after radiotherapy has been reported in NPC cohorts (27). Emerging studies showed that dysphagia had a significantly detrimental effect on health-related quality of life. Although the exact incidence of dysphagia is uncertain, some investigators have suggested that up to 50% of patients undergoing chemoradiotherapy for head and neck cancer may experience long-term dysphagia. It not only significantly diminished patients' quality of life but it might also result in severe pulmonary complications, which might be a major cause of death (28, 29). In this study, we illustrated the clinical characteristics of medial group RLNs. Meanwhile, based on the primary tumor and VII regional lymph node, we proposed the optimization of CTV60 delineation to protect swallowing structures.

This study revealed that the medial group RLNs were generally small, and 57.1% of them were with a transverse diameter of < 5 mm, which distributed between the upper edge of C1 and upper third of C3. Some scholars suggested that the incidence of medial group RLNs was 0.3% (19), whereas others suggested that the incidence was 0.2% (30). The conclusions were all based on conventional MRI imaging. Of note, even conventional MRI imaging is capable of discriminating soft tissue, but detecting small lymph nodes remains a challenge (18). We made use of multi-modal imaging approaches including contrast-enhanced CT, MRI, and $^{[18F]}$PET-CT, which offered the most comprehensive anatomic depiction of tumor extent. These diagnostic images can be imported into radiation treatment planning systems and registered with simulation scans to facilitate contouring target volumes. DWI is a technology of MRI functional imaging systems. The basis of DWI is the diffusion motion of water molecules. At a certain value of b, the diffusion motion of water molecules is measured to predict changes of internal microstructure state. At a low b value, DWI is not sensitive enough to the diffusion of water molecules, and is easily affected by T2 penetration effect. With the increase of b value, the diffusion weight and contrast of DWI increase, and the sensitivity of small lymph nodes is improved. Based on the imaging of DWI, our results showed that the incidence of medial group RLNs was nearly 3%, which was much higher than previous studies (31). Among DWI, T2 STIR and enhanced CT, the sensitivity of DWI is least affected by the size of lymph nodes, rendering DWI an advantage in detecting small lymph nodes. We also performed $^{[18F]}$PET-CT to identify and ascertain the SUV of medial group RLNs. However, it did not show obvious advantage in presenting the small lymph nodes with diameter < 5 mm. PET-CT has its limitations, which can recognize lesions larger than 4 mm. When lesions are less than 4 mm, its diagnostic accuracy decrease obviously. In addition, the size limitation, researchers demonstrated that PET-CT imaging might also show false-positive lymph node due to concurrent infection (32). Based on the sensitivity and location of DWI, it showed high FDG uptake in medial group RLNs, which could help to distinguish the essence of the lesion.

According to the results of the Pearson chi-square test and Lasso regression analysis, the incidence of medial group RLNs was associated with N stage and bilateral cervical lymph node metastasis, especially when the transverse diameter of cervical lymph nodes was > 3 cm. We also performed Lasso regression analysis to select factors for predicting prognosis. For OS, clinical stage, T stage, N stage, lymph node necrosis, and extracapsular spread, gender were crucial indicators. For LRFS, T stage, oropharyngeal invasion, diameter of cervical lymph nodes > 2 cm and lymph node necrosis were important predicting markers. For DMFS, clinical stage, T stage, N stage, lymph node necrosis and extracapsular spread, oropharyngeal invasion, bilateral RLNs, parotid lymph nodes, and radiation dose were involved. For PFS, clinical stage, N stage, anterior vertebral muscle invasion, oropharyngeal invasion, lymph node necrosis, and extracapsular spread and parotid lymph nodes were critical indicators. Based on results from Lasso regression analysis, the medial group RLNs did not act as an independent prognostic indicator. All the above indicators may help us to construct predictive models that can be used to classify patients into different risk for individual treatment.

Lam and King suggested that the medial group RLNs should be considered as malignant lesions (18, 20). In this study, we found that 92.86% (13 of 14) of the cases showed complete regression following treatment while the remaining one only showed partial regression. The lymph node was present continuously during 3 years follow-up, which might suggest that the medial group RLNs might not be indicator of malignant lesions.

RTOG 0225/0615 are main guidelines for the delineation of NPC. Compared with RTOG 0225, RTOG 0615 mainly reduced the target volume of CTV anterior boundary and posterior boundary. Moreover, considering the low incidence of Ib region lymph nodes (about 3%), the revised guideline proposed that only positive lymph node should be irradiated (33). However, there were no changes about CTV60 of medial group RLNs, which was from the skull base to the superior margin of hyoid. Optimizing CTV60 of medial group RLNs in NPC patients are favorable in reducing swallowing dysfunction. In this study, we optimized CTV60 of medial group RLNs from skull base to the upper margin of C2 to protect swallowing structures, except two special lesions as described previously. Using this strategy, the dose and volume of pharyngeal constrictor muscle, vocal cords, and the glottis,

especially the volume of high dose radiotherapy, were significantly reduced compared with the protocol of RTOG 0615. The 5-year OS, LRFS, DMFS, and PFS rates in medial group and no medial group showed no significant differences. The 5-year OS, LRFS, DMFS, and PFS survival probabilities of enrolled patients were 87%, 80%, 93%, and 85%, respectively, which was consistent with previous survival rates (1, 23, 34–36). None of regional recurrence occurred within optimized target region. Excellent outcomes supported the feasibility of individualized CTV60 delineation. Our result reached the consistent conclusion compared with a multicenter randomized phase 3 trial initiated by Jun Ma, in which all patients was 1:1 assigned to sparing group and standard group (37). Their conclusion included the following: (1) There were no significant difference in terms of 3-year OS, DMFS, and LRFS; (2) the acute and long-term side effect in sparing group were better than standard group, and patients could have a much better quality life. However, they did not clarify which patients could benefit from the sparing radiotherapy and which patients could undergo this kind of target optimization. Also, they randomised the patients 1:1 to two groups, which might ignore the individual clinical features as the NPC was of high heterogeneity. To some extent, our results provide supplementary clinical data to this clinical research. We not only clarified the characteristics of the medial group RLNs but also proposed individualized CTV60 delineation approach in different subtypes.

Compared with standardized treatments, all enrolled patients had a considerably improved quality of life both during and after therapy. Acute toxicities during radiotherapy were well tolerated. Ninety-six of 549 (17.5%) patients had symptoms in terms of difficulties in drinking, eating, swallowing, or coughing when eating/drinking. Eighty-three patients scored 1, seven patients scored 2, one patient scored 3, and three patients scored 4. Related symptoms occurred in 43 patients immediately after radiotherapy, which might due to the damage of salivary glands. The median interval from onset of symptoms in the rest 53 patients was 72 (4–114) months. To visualize dosimetric changes in target volumes and OARs, we performed CT scans on fractions of 0, 5, 15, and 25 throughout radiotherapy. We were able to not only replan the target volume according to the altered body contour and shifting tumor position but also monitor the optimization's correctness and safety.

In summary, our result showed much higher incidence of medial group RLNs based on multi-model imaging. We should combine clinical features and multi-imaging records to comprehensively identify the essence of medial group RLNs. Considering the low incidence of medial group RLNs, optimizing CTV60 for VIIc from skull base to the upper edge of C2 is safe and feasible. This study had longer follow-up time and much more concrete optimized strategy of medial group RLNs, which might supplement the findings of the prospective clinical trial NCT03346109 (37). Moreover, this study clarified the advantage of DWI in presenting small lymph nodes. This study have several limitations, such as deficient number of cases, single-center retrospective study, and unvalidated questionnaires. As a single-center retrospective study, the results of this study need relevant prospective studies to verify. With increased awareness of long-term radiation complications and the advances in chemoradiotherapy, researchers will strive to reduce radiation dose and volume to improve the quality of life in NPC.

Data availability statement

The raw data supporting the conclusions of this article will be made available by the authors, without undue reservation.

Ethics statement

The studies involving humans were approved by the Clinical Research Ethics Committee of Jiangsu Cancer Hospital. The studies were conducted in accordance with the local legislation and institutional requirements. The participants provided their written informed consent to participate in this study.

Author contributions

DZ and NJ collected the clinical data and wrote the manuscript. CK guided the statistical analysis. JW, L-JW, and Y-SG read images and delineated the CTV 60. L-FZ read images and helped finish data acquisition. XH read images and revised the manuscript. Z-ZC and S-FH designed and defined the intellectual content. All authors contributed to the article and approved the submitted version.

Funding

National Natural Science Foundation of China (82172804), China Postdoctoral Science Foundation (NO. 2017M621679), The Young Talents Program of Jiangsu Cancer Hospital (QL201802), The Talents Program of Jiangsu Cancer Hospital (NO.LGY2018070). Science and Technology Development Fund of Jiangsu Cancer Hospital (ZL202105) and Nasopharyngeal Carcinoma Cohort Program of Nanjing Medical University [No.NMUC2021011A].

Conflict of interest

The authors declare that the research was conducted in the absence of any commercial or financial relationships that could be construed as a potential conflict of interest.

Publisher's note

All claims expressed in this article are solely those of the authors and do not necessarily represent those of their affiliated

organizations, or those of the publisher, the editors and the reviewers. Any product that may be evaluated in this article, or claim that may be made by its manufacturer, is not guaranteed or endorsed by the publisher.

Supplementary material

The Supplementary Material for this article can be found online at: https://www.frontiersin.org/articles/10.3389/fonc.2023.1228994/full#supplementary-material

References

1. Zhou GQ, Wu CF, Deng B, Gao TS, Lv JW, Lin L, et al. An optimal posttreatment surveillance strategy for cancer survivors based on an individualized risk-based approach. *Nat Commun* (2020) 11(1):3872. doi: 10.1038/s41467-020-17672-w

2. Co J, Mejia MB, Dizon JM. Evidence on effectiveness of intensity-modulated radiotherapy versus 2-dimensional radiotherapy in the treatment of nasopharyngeal carcinoma: Meta-analysis and a systematic review of the literature. *Head Neck* (2016) 38 Suppl 1:E2130–2142. doi: 10.1002/hed.23977

3. Li WF, Sun Y, Chen M, Tang LL, Liu LZ, Mao YP, et al. Locoregional extension patterns of nasopharyngeal carcinoma and suggestions for clinical target volume delineation. *Chin J Cancer* (2012) 31(12):579–87. doi: 10.5732/cjc.012.10095

4. Chow JCH, Cheung KM, Au KH, Zee BCY, Lee J, Ngan RKC, et al. Radiation-induced hypoglossal nerve palsy after definitive radiotherapy for nasopharyngeal carcinoma: Clinical predictors and dose-toxicity relationship. *Radiother Oncol* (2019) 138:93–8. doi: 10.1016/j.radonc.2019.06.011

5. Jin X, Han C, Zhou Y, Yi J, Yan H, Xie C, et al. A modified VMAT adaptive radiotherapy for nasopharyngeal cancer patients based on CT-CT image fusion. *Radiat Oncol* (2013) 8:277. doi: 10.1186/1748-717X-8-277

6. Yao CY, Zhou GR, Wang LJ, Xu JH, Ye JJ, Zhang LF, et al. A retrospective dosimetry study of intensity-modulated radiotherapy for nasopharyngeal carcinoma: radiation-induced brainstem injury and dose-volume analysis. *Radiat Oncol* (2018) 13 (1):194. doi: 10.1186/s13014-018-1105-z

7. Kong C, Zhu XZ, Lee TF, Feng PB, Xu JH, Qian PD, et al. LASSO-based NTCP model for radiation-induced temporal lobe injury developing after intensity-modulated radiotherapy of nasopharyngeal carcinoma. *Sci Rep* (2016) 6:26378. doi: 10.1038/srep26378

8. Nguyen NP, Moltz CC, Frank C, Vos P, Smith HJ, Karlsson U, et al. Dysphagia following chemoradiation for locally advanced head and neck cancer. *Ann Oncol* (2004) 15 (3):383–8. doi: 10.1093/annonc/mdh101

9. Karsten RT, van der Molen L, Hamming-Vrieze O, van Son R, Hilgers FJM, van den Brekel MWM, et al. Long-term swallowing, trismus, and speech outcomes after combined chemoradiotherapy and preventive rehabilitation for head and neck cancer; 10-year plus update. *Head Neck* (2020) 42(8):1907–18. doi: 10.1002/hed.26120

10. Krisciunas GP, Sokoloff W, Stepas K, Langmore SE. Survey of usual practice: dysphagia therapy in head and neck cancer patients. *Dysphagia* (2012) 27(4):538–49. doi: 10.1007/s00455-012-9404-2

11. Wang JJ, Jiang RS, Yen TT, Liang KL. Risk factors for recurrent pneumonia in post-irradiated patients with nasopharyngeal carcinoma. *J Chin Med Assoc* (2017) 80 (9):558–62. doi: 10.1016/j.jcma.2017.01.006

12. Chiu YH, Tseng WH, Ko JY, Wang TG. Radiation-induced swallowing dysfunction in patients with head and neck cancer: A literature review. *J Formosan Med Assoc = Taiwan yi zhi* (2022) 121(1 Pt 1):3–13. doi: 10.1016/j.jfma.2021.06.020

13. Hutchison AR, Cartmill B, Wall LR, Ward EC, Hargrave C, Brown E, et al. Practices, knowledge and inter-professional relationships between speech pathologists and radiation therapists managing patients with head and neck cancer. *J Med Radiat Sci* (2019) 66(2):103–111. doi: 10.1002/jmrs.332

14. Gensheimer MF, Nyflot M, Laramore GE, Liao JJ, Parvathaneni U. Contribution of submandibular gland and swallowing structure sparing to post-radiation therapy PEG dependence in oropharynx cancer patients treated with split-neck IMRT technique. *Radiat Oncol* (2016) 11(1):151. doi: 10.1186/s13014-016-0726-3

15. Carnaby-Mann G, Crary MA, Schmalfuss I, Amdur R. "Pharyngocise": randomized controlled trial of preventative exercises to maintain muscle structure and swallowing function during head-and-neck chemoradiotherapy. *Int J Radiat Oncol Biol Phys* (2012) 83(1):210–9. doi: 10.1016/j.ijrobp.2011.06.1954

16. Barnhart MK, Cartmill B, Ward EC, Brown E, Sim J, Saade G, et al. Optimising Radiation Therapy Dose to the Swallowing Organs at Risk: An In Silico Study of feasibility for Patients with Oropharyngeal Tumours. *Dysphagia* (2019) 34(6):869–878. doi: 10.1007/s00455-019-09983-y

17. Petkar I, Rooney K, Roe JW, Patterson JM, Bernstein D, Tyler JM, et al. DARS: a phase III randomised multicentre study of dysphagia- optimised intensity- modulated radiotherapy (Do-IMRT) versus standard intensity- modulated radiotherapy (S-IMRT) in head and neck cancer. *BMC Cancer* (2016) 16(1):770. doi: 10.1186/s12885-016-2813-0

18. Lam WW, Chan YL, Leung SF, Metreweli C. Retropharyngeal lymphadenopathy in nasopharyngeal carcinoma. *Head Neck* (1997) 19(3):176–81. doi: 10.1002/(sici)1097-0347(199705)19:3<176::aid-hed2>3.0.co;2-#.

19. Lin L, Lu Y, Wang XJ, Chen H, Yu S, Tian J, et al. Delineation of neck clinical target volume specific to nasopharyngeal carcinoma based on lymph node distribution and the international consensus guidelines. *Int J Radiat Oncol Biol Phys* (2018) 100 (4):891–902. doi: 10.1016/j.ijrobp.2017.11.004

20. King AD, Ahuja AT, Leung SF, Lam WW, Teo P, Chan YL, et al. Neck node metastases from nasopharyngeal carcinoma: MR imaging of patterns of disease. *Head Neck* (2000) 22 (3):275–81. doi: 10.1002/(sici)1097-0347(200005)22:3<275::aid-hed10>3.0.co;2-n

21. Tang LL, Chen YP, Chen CB, Chen MY, Chen NY, Chen XZ, et al. The Chinese Society of Clinical Oncology (CSCO) clinical guidelines for the diagnosis and treatment of nasopharyngeal carcinoma. *Cancer Commun (Lond)* (2021) 41(11):1195–227. doi: 10.1002/cac2.12218

22. Zong D, Jiang N, Xu JH, Wang DJ, Zhu HF, Wu LR, et al. ZNF488 is an independent prognostic indicator in nasopharyngeal carcinoma and promotes cell adhesion and proliferation *via* collagen IV/FAK/AKT/Cyclin D1 pathway. *Cancer Manag Res* (2019) 11:5871–82. doi: 10.2147/CMAR.S200001

23. Tang SQ, Xu C, Wang XS, Tang LL, Li WF, Chen L, et al. Induction versus adjuvant chemotherapy combined with concurrent chemoradiotherapy in locoregionally advanced nasopharyngeal carcinoma: A propensity score-matched analysis. *Oral Oncol* (2020) 105:104686. doi: 10.1016/j.oraloncology.2020.104686

24. Hedstrom J, Tuomi L, Finizia C, Olsson C. Correlations between patient-reported dysphagia screening and penetration-aspiration scores in head and neck cancer patients post-oncological treatment. *Dysphagia* (2018) 33(2):206–15. doi: 10.1007/s00455-017-9847-6

25. Liu WS, Chien JC, Huang YH, Chen PC, Huang WL, Chiang SW, et al. High superior-middle pharyngeal constrictor muscle mean dose correlates with severe late lung infection and survival in nasopharyngeal cancer patients. *Cancer Manag Res* (2022) 14:1063–73. doi: 10.2147/CMAR.S350714

26. Caudell JJ, Schaner PE, Desmond RA, Meredith RF, Spencer SA, Bonner JA, et al. Dosimetric factors associated with long-term dysphagia after definitive radiotherapy for squamous cell carcinoma of the head and neck. *Int J Radiat Oncol Biol Phys* (2010) 76(2):403–9. doi: 10.1016/j.ijrobp.2009.02.017

27. Zhao Y, Liang J, Ou H, Zhang J, Huang H, Feng H, et al. Effects of swallowing rehabilitation training with a balloon dilation therapy on the deglutition function and quality of life of patients with dysphagia after radiotherapy for nasopharyngeal carcinoma. *Evid Based Complement Alternat Med* (2022) 2022:7496753. doi: 10.1155/2022/7496753

28. Xiong J, Krishnaswamy G, Raynor S, Loh KS, Kwa AL, Lim CM, et al. Risk of swallowing-related chest infections in patients with nasopharyngeal carcinoma treated with definitive intensity-modulated radiotherapy. *Head Neck* (2016) 38 Suppl 1:E1660–1665. doi: 10.1002/hed.24296

29. Xu B, Boero IJ, Hwang L, Le QT, Moiseenko V, Sanghvi PR, et al. Aspiration pneumonia after concurrent chemoradiotherapy for head and neck cancer. *Cancer* (2015) 121(8):1303–11. doi: 10.1002/cncr.29207

30. Wang X, Hu C, Ying H, He X, Zhu G, et al. Patterns of lymph node metastasis from nasopharyngeal carcinoma based on the 2013 updated consensus guidelines for neck node levels. *Radiother Oncol* (2015) 115(1):41–5. doi: 10.1016/j.radonc.2015.02.017

31. Li L, Li Y, Zhang J, Wu Q, Yu H, Li Z, et al. Optimization of cervical lymph node clinical target volume delineation in nasopharyngeal carcinoma: a single center experience and recommendation. *Oncotarget* (2018) 9(43):26980–9. doi: 10.18632/oncotarget.23723

32. Vaarwerk B, Breunis WB, Haveman LM, de Keizer B, Jehanno N, Borgwardt L, et al. Fluorine-18-fluorodeoxyglucose (FDG) positron emission tomography (PET) computed tomography (CT) for the detection of bone, lung, and lymph node metastases in rhabdomyosarcoma. *Cochrane Database systematic Rev* (2021) 11(11): Cd012325. doi: 10.1002/14651858.CD012325.pub2

33. Lee AW, Ng WT, Pan JJ, Poh SS, Ahn YC, AlHussain H, et al. International guideline for the delineation of the clinical target volumes (CTV) for nasopharyngeal carcinoma. *Radiother Oncol* (2018) 126(1):25–36. doi: 10.1016/j.radonc.2017.10.032

34. Wu S, Quan R, Han L, Zhang H, Zhang B, Xu G, et al. Analysis of intensity-modulated radiotherapy for patients with nasopharyngeal carcinoma. *Med (Baltimore)* (2020) 99(30):e21325. doi: 10.1097/MD.0000000000021325

35. Bongiovanni A, Vagheggini A, Fausti V, Mercatali L, Calpona S, Di Menna G, et al. Induction chemotherapy plus concomitant chemoradiotherapy in nasopharyngeal carcinoma: An updated network meta-analysis. *Crit Rev Oncol Hematol* (2021) 160:103244. doi: 10.1016/j.critrevonc.2021.103244

36. Tang LL, Guo R, Zhang N, Deng B, Chen L, Cheng ZB, et al. Effect of radiotherapy alone vs radiotherapy with concurrent chemoradiotherapy on survival without disease relapse in patients with low-risk nasopharyngeal carcinoma: A randomized clinical trial. *JAMA* (2022) 328(8):728–36. doi: 10.1001/jama.2022.13997

37. Mao YP, Wang SX, Gao TS, Zhang N, Liang XY, Xie FY, et al. Medial retropharyngeal nodal region sparing radiotherapy versus standard radiotherapy in patients with nasopharyngeal carcinoma: open label, non-inferiority, multicentre, randomised, phase 3 trial. *BMJ* (2023) 380:e072133. doi: 10.1136/bmj-2022-072133

frontiers | Frontiers in Oncology

TYPE Original Research
PUBLISHED 26 September 2023
DOI 10.3389/fonc.2023.1251132

OPEN ACCESS

EDITED BY
Giuseppe Carlo Iorio,
University of Turin, Italy

REVIEWED BY
Giuseppe Danilo Di Stasio,
Independent researcher, Torino, Italy
Ciprian Camil Mirestean,
University of Medicine and Pharmacy of Craiova, Romania

*CORRESPONDENCE
Xiaojin Gu
x.gu@amsterdamumc.nl

†These authors have contributed equally to this work and share first authorship

RECEIVED 30 June 2023
ACCEPTED 25 August 2023
PUBLISHED 26 September 2023

CITATION
Gu X, Strijbis VIJ, Slotman BJ, Dahele MR and Verbakel WFAR (2023) Dose distribution prediction for head-and-neck cancer radiotherapy using a generative adversarial network: influence of input data.
Front. Oncol. 13:1251132.
doi: 10.3389/fonc.2023.1251132

Dose distribution prediction for head-and-neck cancer radiotherapy using a generative adversarial network: influence of input data

Xiaojin Gu[1,2*†], Victor I. J. Strijbis[1,2†], Ben J. Slotman[1,2], Max R. Dahele[1,2] and Wilko F. A. R. Verbakel[1,2]

[1]Department of Radiation Oncology, Amsterdam UMC Location Vrije Universiteit Amsterdam, Amsterdam, Netherlands, [2]Cancer Center Amsterdam, Cancer Treatment and Quality of Life, Amsterdam, Netherlands

Purpose: A three-dimensional deep generative adversarial network (GAN) was used to predict dose distributions for locally advanced head and neck cancer radiotherapy. Given the labor- and time-intensive nature of manual planning target volume (PTV) and organ-at-risk (OAR) segmentation, we investigated whether dose distributions could be predicted without the need for fully segmented datasets.

Materials and methods: GANs were trained/validated/tested using 320/30/35 previously segmented CT datasets and treatment plans. The following input combinations were used to train and test the models: CT-scan only (C); CT +PTVboost/elective (CP); CT+PTVs+OARs+body structure (CPOB); PTVs+OARs +body structure (POB); PTVs+body structure (PB). Mean absolute errors (MAEs) for the predicted dose distribution and mean doses to individual OARs (individual salivary glands, individual swallowing structures) were analyzed.

Results: For the five models listed, MAEs were 7.3 Gy, 3.5 Gy, 3.4 Gy, 3.4 Gy, and 3.5 Gy, respectively, without significant differences among CP-CPOB, CP-POB, CP-PB, among CPOB-POB. Dose volume histograms showed that all four models that included PTV contours predicted dose distributions that had a high level of agreement with clinical treatment plans. The best model CPOB and the worst model PB (except model C) predicted mean dose to within $\pm$3 Gy of the clinical dose, for 82.6%/88.6%/82.9% and 71.4%/67.1%/72.2% of all OARs, parotid glands (PG), and submandibular glands (SMG), respectively. The R^2 values (0.17/0.96/0.97/0.95/0.95) of OAR mean doses for each model also indicated that except for model C, the predictions correlated highly with the clinical dose distributions. Interestingly model C could reasonably predict the dose in eight patients, but on average, it performed inadequately.

Conclusion: We demonstrated the influence of the CT scan, and PTV and OAR contours on dose prediction. Model CP was not statistically different from model

CPOB and represents the minimum data statistically required to adequately predict the clinical dose distribution in a group of patients.

KEYWORDS

artificial intelligence, machine learning, deep learning, generative adversarial network (GAN), dose prediction, OAR sparing, radiotherapy

Introduction

Head and neck cancer (HNC) radiotherapy treatment planning is complex, due to large and irregular planning target volumes (PTV), multiple prescription/PTV dose levels (e.g., primary tumor and nodal areas), and a large range of organs at risk (OARs) in close proximity to the PTVs. It requires extensive contouring of all relevant target and OAR structures on a planning computed tomography (CT) scan, which is a labor- and time-intensive process subject to inter- and intra-observer variation. The treatment planning process can take several hours to complete (1), and the dose distribution is dependent on the skills and experience of the planner and the institution (2, 3). In order to increase efficiency and reduce variation in quality, automated treatment planning technologies have been introduced in recent years (4–6).

Traditionally, automated approaches relied on modeling spatial relationships between target volumes and OARs (e.g., overlap volume histograms (7, 8), distance-to-target histograms) in combination with machine learning algorithms to identify correlations between predictive volumetric or spatial features and dosimetry. Important limitations of such knowledge-based planning approaches are the limited predictability in cases where the clinical situation is not adequately represented by the library of patient plans.

More recently, deep learning (DL) has been investigated for automated treatment planning by using convolutional neural networks (CNNs) that incorporate contextual information with precise localization to solve a wide variety of imaging-related problems (e.g., U-Net (9), ResNet (10)). Given the non-linearity of source inputs (e.g., CT, PTV, and OAR contours) and the target output (dose distribution), dose prediction may be regarded as an image synthesis task (11). While U-Net and its derivatives have been widely used for dose distribution prediction (12–17), generative adversarial networks (GANs) are a method to implicitly learn density functions that estimate the probability distribution from training data through adversarial learning. A GAN uses two concurrent generative and discriminative neural networks to generate realistic predictions (18, 19). The objective of the generative network is to increase the error rate of the discriminative network, whereas the discriminator tries to classify realism. As a result, the GAN learns features of a realistic dose distribution for given anatomical characteristics and may be more capable than CNN-based neural networks of predicting dose distributions (20–22). Therefore, for this piece of work, we have selected a GAN-based approach.

In most previous works (11, 20, 21, 23, 24), dose prediction was based on an input of CT, PTV contours, and OAR contours. In contrast, we investigated if clinically acceptable, realistic HNC dose distributions could be predicted from the patient CT and primary tumor and lymph node PTVs, without explicit prior knowledge of the relevant OARs, in comparison with CT scan with OAR contours. This could circumvent the laborious and error-prone process of OAR contouring and be of relevance to routine clinical care, and in other scenarios like the rapid selection of patients most suitable for proton therapy (25). In addition, we investigated the added value of the CT itself, and if the neural network (NN) could recognize the tumor and OARs in the CT without providing any contours. In total, five different models trained with different combinations of input data were evaluated.

Materials and methods

Data acquisition

The dataset consisted of 350 patients who had previously been treated for locally advanced HNC between 2013 and 2018, and 35 patients treated in 2019 that were used as an independent test set. Each patient had a treatment plan consisting of two full volumetric modulated arc therapy (VMAT) arcs, delivering 35 fractions of 2 Gy to PTV-boost (PTV-B) and 1.55 Gy to PTV-elective (PTV-E). All tumor sites were included. During the selected time period, plans were made with different versions of the Eclipse treatment planning system; however, they all consistently aimed to achieve a low mean dose to the individual salivary glands and swallowing structures. The volume receiving 95% of the prescribed dose (V95) was ≥99% for PTV-B and ≥98% for PTV-E. From 2013 to 2014, plans were made by manually interactively adapting OAR optimization objectives during optimization. From 2014 to 2017, plans were made using in-house-developed automated interactive optimization (AIO) software, which automatically performed what planners previously had to do manually (6, 26). From 2017, plans were made using RapidPlan (Varian, a Siemens Healthineers Company, Palo Alto, CA, USA), which used a model based on previous AIO-generated plans. It was previously shown that treatment plans improved over time (27). Oral cavity mean dose reduction was introduced around 2016 and intensified in 2019.

10.3389/fonc.2023.1251132

Each patient in the dataset contains a three-dimensional (3D) planning CT scan, structure set, and dose distribution. Patients had to have at least one OAR structure available out of all the individual salivary glands and swallowing structures (Table 1). CT acquisition resolutions were [0.80,1.27] mm in-plane and 2.5 mm longitudinal, and acquisition dimensions were 512 × 512 × [97,228] voxels. The dose distribution resolutions were 2.5 mm isotropic. OAR contours of salivary glands and swallowing structures were grouped and unified into composite salivary glands (CSG) and composite swallowing structures (CSS), respectively (Table 1). In total, six structures were used for model training, validation, and testing: CSG, CSS, spinal canal (SC), PTV-E, PTV-B, and body contour.

Preprocessing

CT Hounsfield units were window-leveled from −200 to +300, similar to what would be used for head and neck automated segmentation tasks (28). Dose was capped at a maximum of 79 Gy. CTs and doses were normalized to [0,1], and structures were binarized as masks. To accommodate hardware limitations, the dataset was cropped from the original images. Based on the smallest number of slices for all patients, the most central 96 slices from each CT scan were selected and the data was cropped in left–right to retain the middle 256 out of 512 voxels (entire head and neck remained included, shoulders were removed). Then, in the vertical direction, 256 voxels starting from the tip of the nose were retained. Finally, this volume was resized to a 128 × 128 × 64 grid using trilinear and nearest-neighbor interpolation for the real-valued volumes (CT and dose) and binary valued structure masks, respectively, where the final voxel size was [1.60, 2.55] × [1.60, 2.55] × 3.75 mm. Cropping occasionally resulted in the loss of some caudal PTV and OAR containing slices resulting in the loss of 5% of OAR voxels, on average.

TABLE 1 Overview of the relevant structures and their percentage prevalence in the RT data set.

Structure	Occurrence
Composite salivary glands*	
Parotid gland (L/R)	99%
Submandibular gland (L/R)	83%
Composite swallowing structures*	
Lower larynx	76%
Upper larynx	68%
Cricopharynx	70%
Esophagus	61%
Trachea	60%
Thyroid	62%
Upper esophageal sphincter	73%
Inferior pharyngeal constrictor muscle	76%
Medial pharyngeal constrictor muscle	69%
Superior pharyngeal constrictor muscle	73%
Nervous structures	
Spinal canal*	98%
Brain stem	44%
Planning target volumes	
PTV-E*	100%
PTV-B*	100%
Individual structures	
Oral cavity	90%
Body*	100%

* used as single-channel 3D images for model training, validation, and testing. Composite salivary glands (CSG) and composite swallowing structures (CSS) were unified structures of the respective subsequent individual structures.

Model architecture

Figure 1 shows the architectures of the GAN. The generator is an adapted deep 3D U-Net. It can take any combinations of CT, PTVs (PTV-B and PTV-E), OAR structures, and the body contour as input and outputs a predicted dose distribution. The discriminator takes the same input channels as the generator together with the clinical dose distribution as training target and outputs the probability that the predicted dose cannot be distinguished from a clinical dose distribution. The discriminator is discarded after training; only the generator is used for dose prediction.

Model training

The 350 patients in the dataset were randomly split into sets of 320 and 30 for training and validation, respectively. Model training was done on four NVIDIA GeForce GTX 2080 Ti graphics processor units (GPUs), each having 11 GB of GPU RAM, using PyTorch 1.11 and Python 3.9.16. The generator was trained using the ADAM optimizer (29) with $\beta_1 = 0.5$ and $\beta_2 = 0.999$, and the discriminator was trained with stochastic gradient descent (SGD). The initial learning rates were 0.001 for both networks, and a learning rate scheduler to decay by 10% every 20 epochs was applied to the generator. Batch size = 4 was the maximum number that could fit in the combined GPU memory. The conditional GAN's objective is given by a weighted combination of the adversarial and reconstruction losses:

$$L_{cGAN}(G, D) = L_{adv}(G, D) + \lambda \; L_{rec}(G),$$

where the adversarial loss L_{adv} is given by the binary cross-entropy loss (19) and the reconstruction loss L_{rec} is a weighted combination of the 1 × L1 loss (mean absolute error) and 0.5 × L2 loss (mean squared error) functions, which we named elastic loss, motivated by the elastic net regularization. The weighting hyperparameter λ was chosen as 10, which gave the best empirical results among the values of 1, 10, and 100 we experimented with. For data augmentation, we used random horizontal flipping to increase the number of training samples.

After model development and hyperparameter tuning based on the evaluation of the validation set, five experiments were conducted. All experiments used the same NN architecture with the same hyperparameters, trained and tested on the same patients; the only difference was the patient information data used as input. The experiments were as follows: 1. Model C used only CT as input data, 2. Model CP used CT and PTVs. 3. Model CPOB used CT, PTVs, OARs, and body contour. 4. Model POB used PTVs, OARS, and body contour (but no CT). 5. Model PB used PTVs and body contour as input data (and no CT). All models were trained for 400 epochs with the same random seed. The composite OAR contours were used for model training to provide extra geometric information and were not used in the loss function.

Models were designed to answer the following questions: (C) How much can an NN learn when only the CT scan is provided as input? (CP-CPOB) Does the presence of the OAR contours in the training result in a statistically significant influence on dose prediction? (CPOB-POB) Does CT data offer significant improvements for the models? (PB) In case CT data makes a better model, does it learn from CT pixels where the OARs are, or does it estimate an approximate position of OARs based on all the average position of all training data?

Evaluation

Predicted dose distributions for the 35 test patients by the five models trained with different input data were compared with doses from the clinical plans. The mean OAR dose and the mean absolute dose difference (MAE) in a volume of interest (VOI) were compared, 2D dose distributions were selected, and dose volume histograms (DVH) are presented. The VOI consisted of the part of the body for slices containing PTV-E, and where the PTV-E did not reach the cranial or caudal ends of the crop, two additional slices were added (7.5 mm). The VOI did not contain any background air and is the volume, which contains most of the dose. We also performed a significance test of the MAE in the VOI, to evaluate the statistical influence of the different types of input data. Wilcoxon significance test was used for each model tested against the other four models, $\alpha = 0.05$, with a Bonferroni correction per set of tests to adjust the p-values.

Figure 2 shows the flowchart of the experiment setup. The different combinations of the input data were used to train different models. The five models were then tested on the same test set to make dose predictions. Finally, the five sets of prediction were evaluated based on the metrics.

Results

Dose volume histograms

Figure 3 shows the dose volume histograms (DVH) for all five models for four patients, selected from the following: the best case, q1 (lower quartile), q2 (median), and q3 (upper quartile) of the average MAE for CPOB in the VOI.

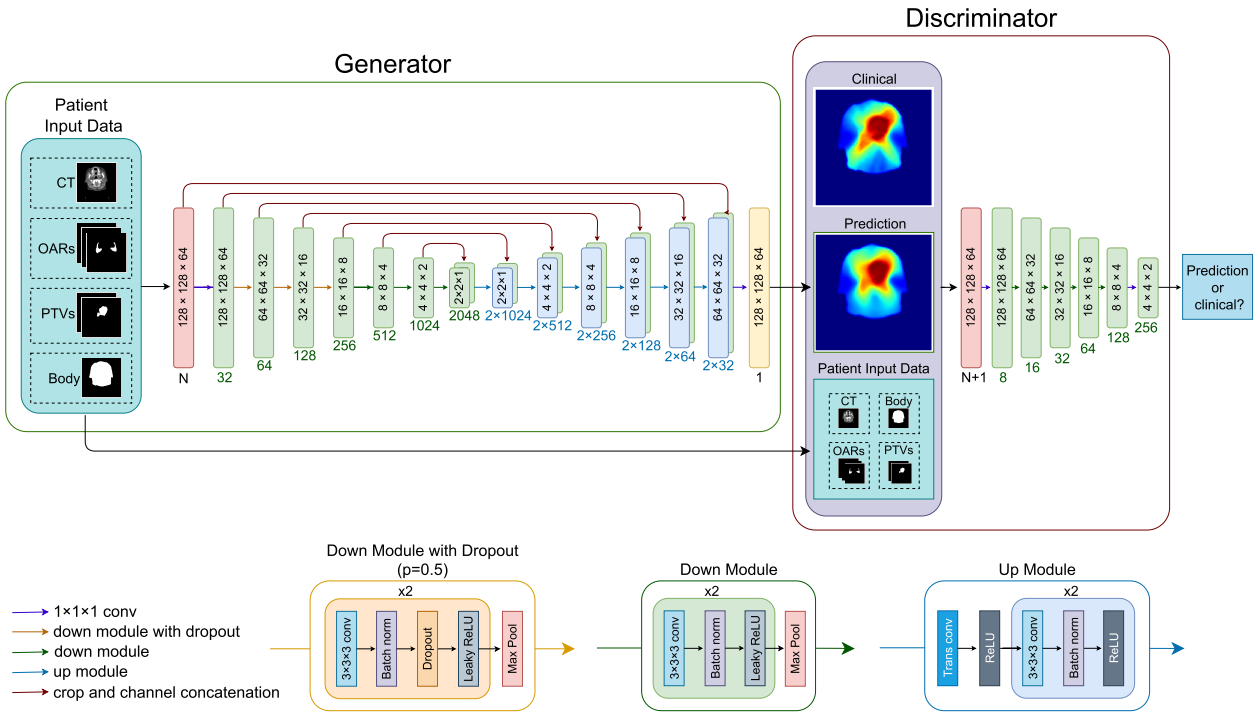

FIGURE 1
Overview of the neural network architecture for a forward pass. Blocks inside the generator and discriminator indicate the image dimensions (block sizes not in scale), numbers below the blocks indicate channel numbers. The neural network can take any combination of the patient input data, CT (one channel), OARs (three channels), PTV-E and PTV-B (two channels), and body contour (one channel), where N is the number of channels of the combined input data. LeakyReLU negative slope = 0.2, dropout rate = 0.5. CT, computed tomography; OAR, organ at risk; PTV, planning target volume; conv, convolutional layer; trans conv, transposed convolution; batch norm, batch normalization; ReLU, rectified linear activation unit.

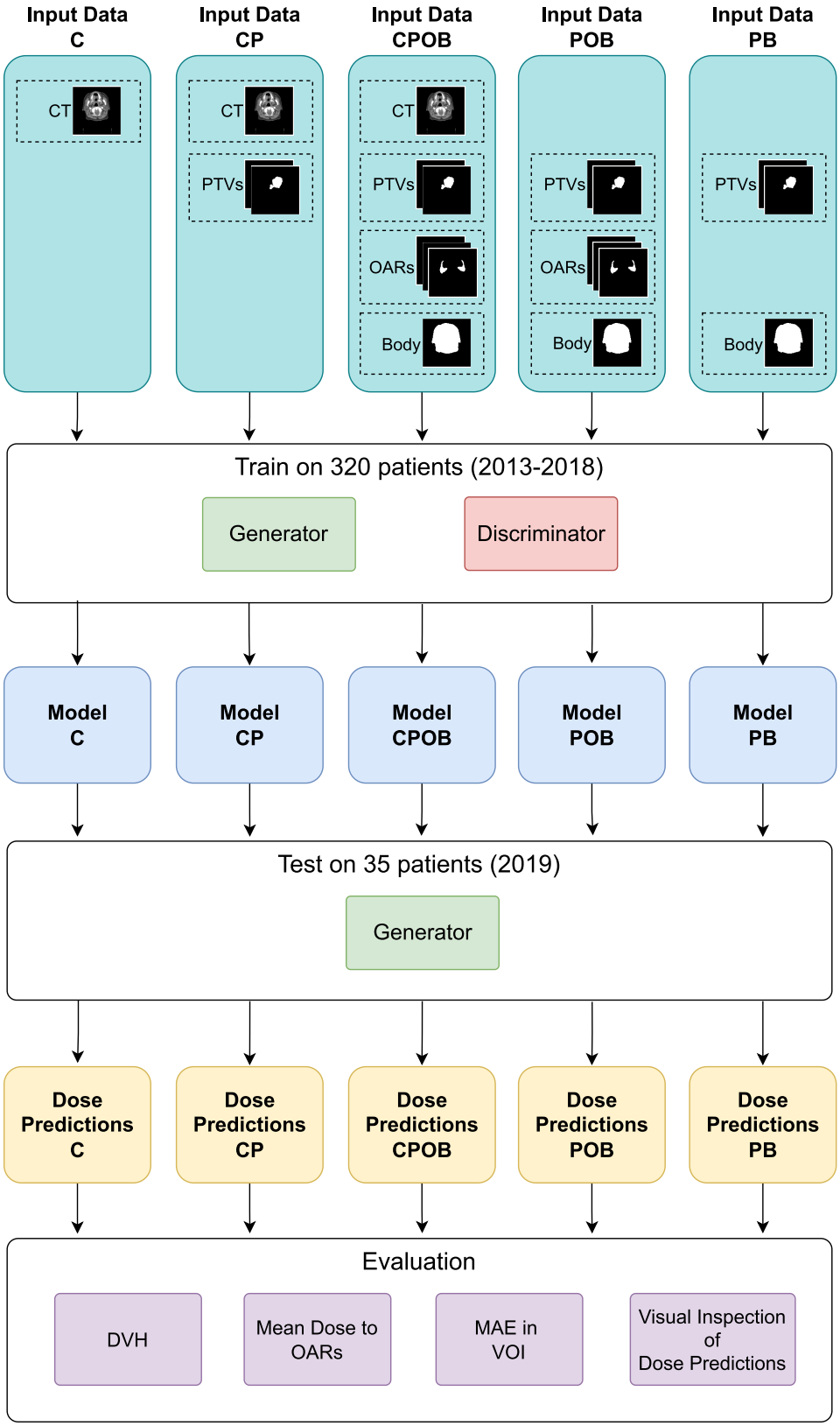

FIGURE 2
The flowchart of the experiments. The five combinations of the input data of CT, PTVs, OARs, and body contour were used to train the five models. Thereafter, the models were tested on the same test set to make the dose predictions. Finally, the predicted doses were evaluated by the metrics of dose volume histogram (DVH), mean dose to OARs, mean absolute error (MAE) in the volume of interest (VOI), and qualitative visual inspection on the predicted doses.

Mean dose to OARs

Figure 4 shows the mean dose per structure compared with the clinical mean doses, where none of the OARs above were trained and tested individually. The R^2 scores indicate that the predictions were highly correlated with the clinical dose distributions; the mean squared errors illustrate the spread of the predictions. Models CPOB and POB had the highest correlation and the lowest spread for all OARs. CPOB achieved for most patients a predicted mean dose within ±3 Gy from the clinical dose, 82.6%, 88.6%, and 82.9% for all OARs, PG, and SMG, respectively, whereas POB had for most patients a deviation within ±6 Gy: 95.1%, 95.7%, and 94.3% for all OARs, PG, and SMG, respectively.

Mean dose error

Figure 5A shows the mean dose difference between the clinical and predicted doses for different structures. The greatest differences were produced by model C where it was clear that if the model could not predict the correct tumor extent, it was impossible to predict the correct dose distribution resulting in PTV mean doses that were too low and incorrect OAR mean doses. The other four models showed a mean dose difference close to 0 and less spread. Models CP and PB, the models without OARs, led to doses in the OARs higher than in clinical plans, whereas models CPOB and POB, the models with OARs, more accurately predicted OAR doses. Figure 5B shows the MAE of the dose in all the voxels in the VOI, which excludes voxels outside the body and voxels in slices away from PTV-E, whereas the mean absolute dose errors over the entire dose distribution volume, i.e., 128 × 128 × 64 voxels, of the five models were 2.45, 1.35, 1.32, 1.31, and 1.35 Gy, respectively. Excluding model C, the remaining four models had comparable results. Model CPOB trained with the most comprehensive input data had both the lowest mean and median and performed significantly better than model PB (p = 0.007, Supplementary Material Table 2). Although model C has in general a very high MAE, there are a few patients with much lower MAE where this model manages to predict reasonable dose

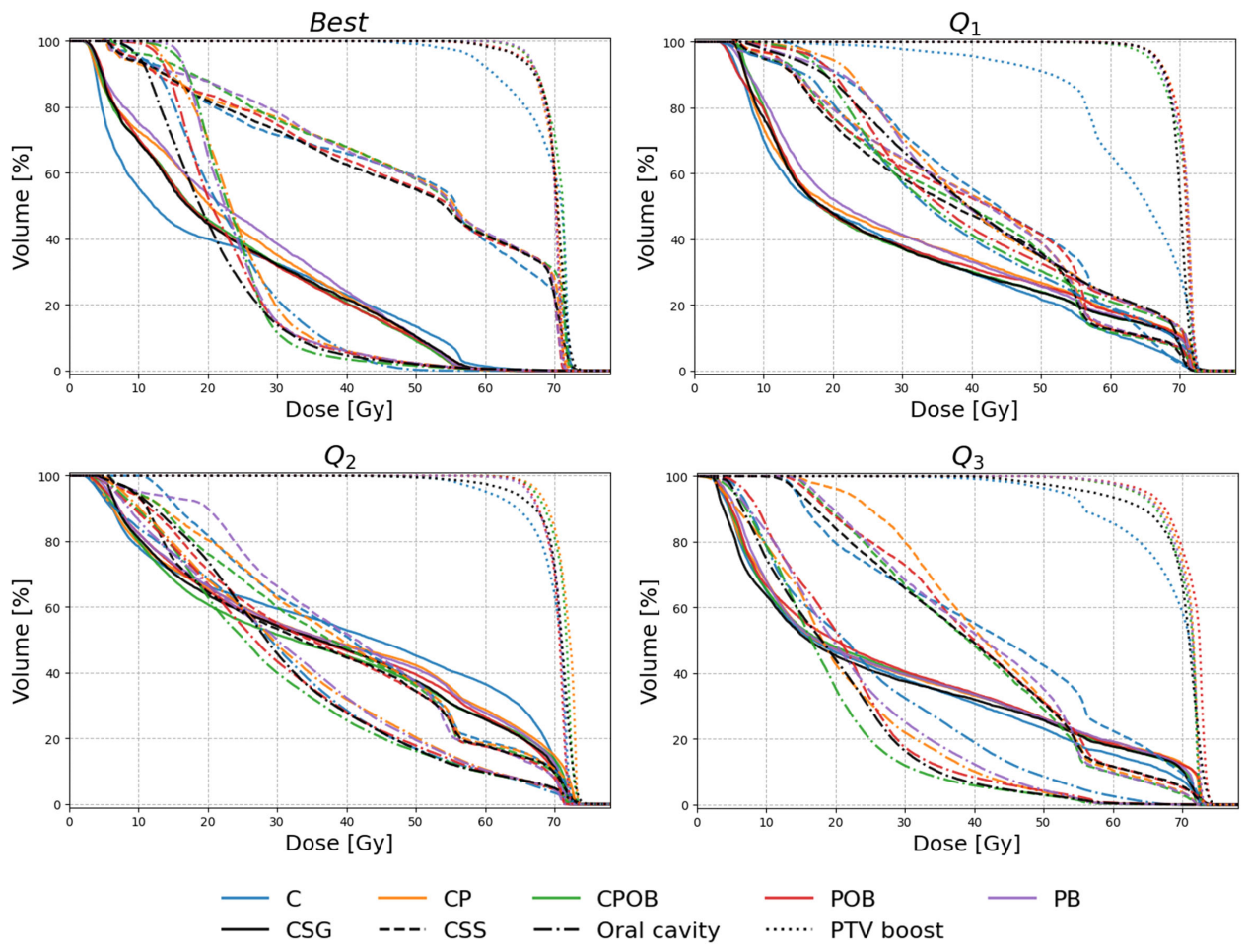

FIGURE 3
Dose volume histogram (DVH) of four selected patients for the models C, CP, CPOB, POB, and PB. The patients were selected to show a range of performances of the CPOB mean absolute error (best/Q_1/Q_2/Q_3) in the volume of interest (VOI: slices containing PTV-E with a 7.5-mm margin in the body contour). The clinical DVHs are in black color, and the predicted DVHs of the five models are in blue, orange, green, red, and purple, respectively, for composite salivary glands (CSG, solid), composite swallowing structures (CSS, dashed), oral cavity (dash-dotted), and PTV-B (dotted). DVHs for individual OARs and PTV-E for Q_1 and Q_2 can be found in Figures 2 and 3, Supplementary Material.

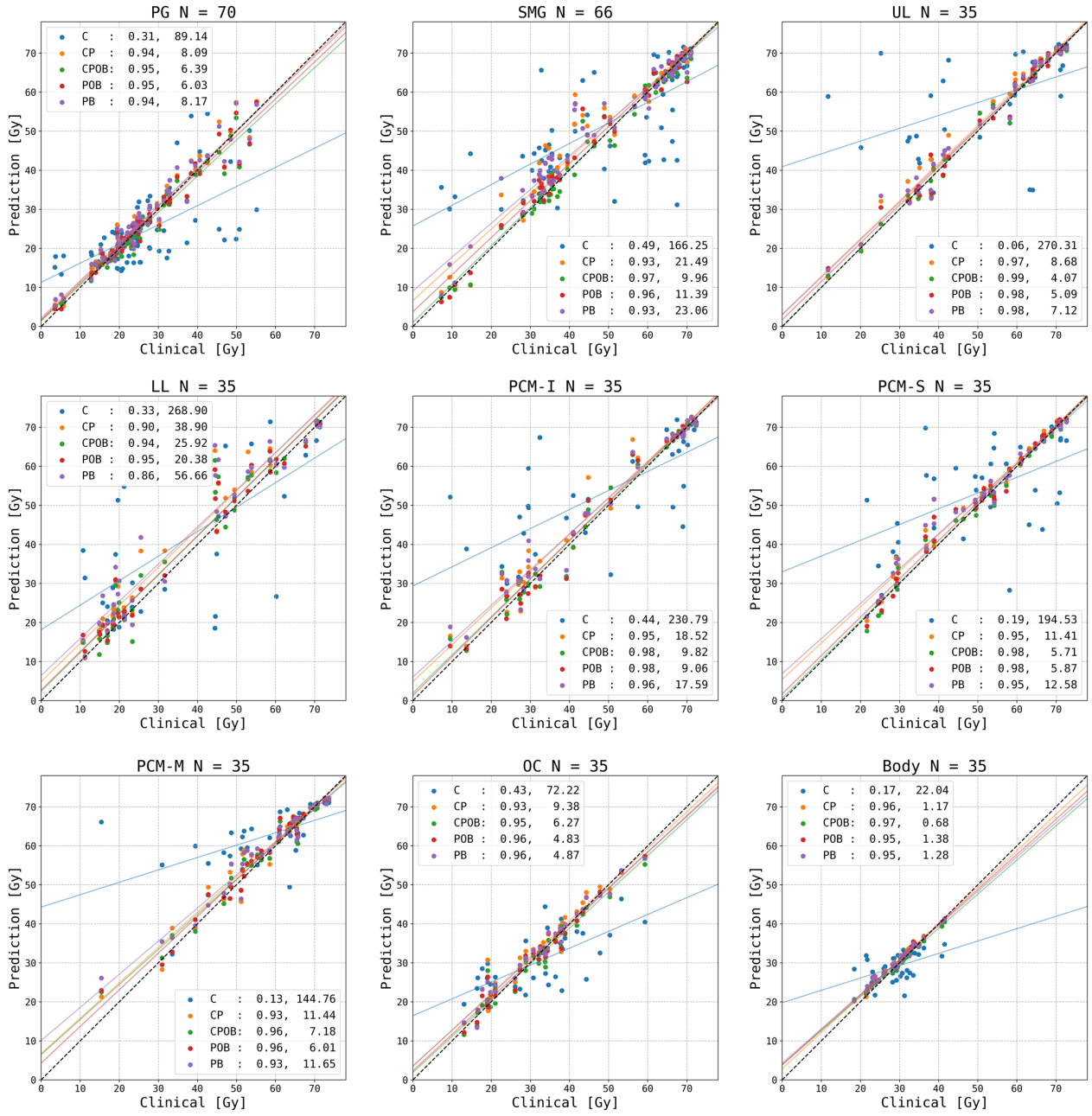

FIGURE 4
Predicted versus clinical mean dose to organs at risk (OARs). From left upper to right lower: parotid gland (PG) left and right combined, submandibular gland (SMG) left and right combined, upper larynx (UL), lower larynx (LL), oral cavity (OC), inferior pharyngeal constrictor muscle (PCM-I), medial pharyngeal constrictor muscle (PCM-M), superior pharyngeal constrictor muscle (PCM-S), and the entire body contour. Each data point represents the dose for one OAR for each of the 35 patients in the test set. N indicates the number of clinical contoured OARs. The vertical distance to the diagonal line shows the error between the predicted and clinical mean doses. For each model, an R^2 correlation (left) and a residual measured in mean squared error (right) are in the legend. The colored lines are the regression lines for mean dose of each model.

distributions. For the models trained with PTVs, the predicted PTV-E and PTV-B had minimal mean dose differences and the coverage was comparable with the clinical plans (Figure 3).

Figure 6A shows examples of the predicted in comparison with the clinical dose distributions for three patients. There are notable differences between CT only and other results, whereas the differences among the other four models are small. For most patients, model C (CT only) was able to find the location of the tumor but was often inaccurate in predicting the extension of the PTVs. Figures 6B, C demonstrate examples of predicted dose distributions by model C with low and high MAEs in the VOI, respectively.

10.3389/fonc.2023.1251132

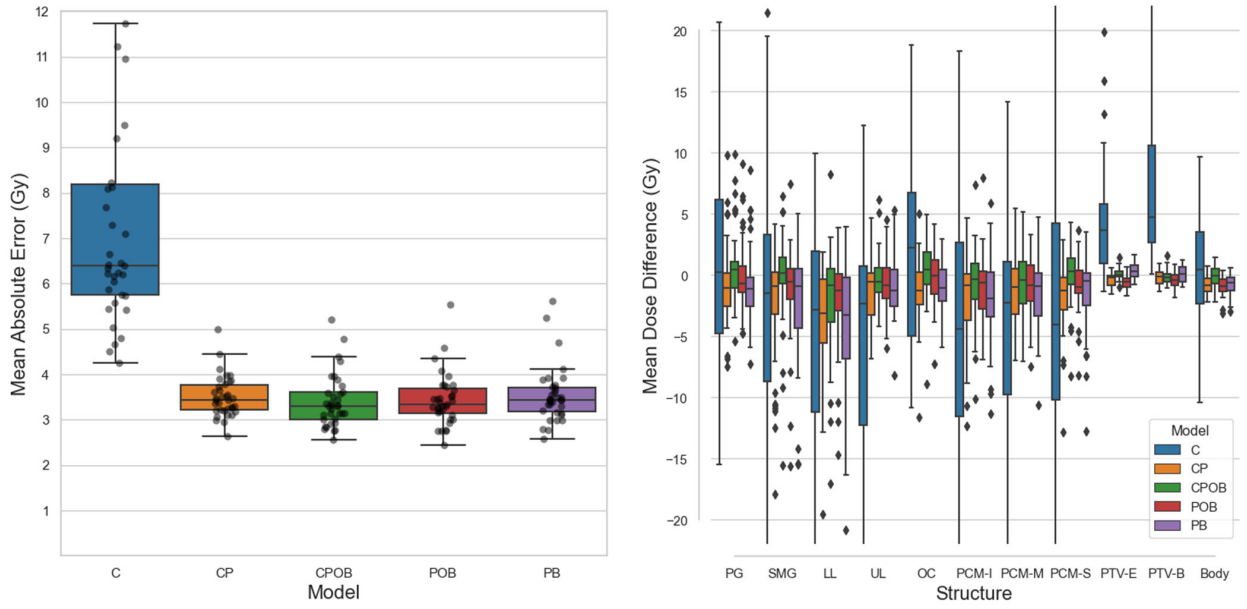

FIGURE 5
(A) (Left): Mean absolute dose error (MAE) over all voxels in the volume of interest for all five models on the test set. Mean values of each boxplot were 7.3, 3.5, 3.4, 3.4, and 3.5 Gy. Each dot represents a patient in the test set. The vertical axis shows the voxel-wise MAE between the clinical and predicted doses. In the boxplots, the lower and upper whiskers indicate the 1.5× the interquartile range<Q1 and >Q3, respectively, the data points outside the whiskers are considered outliers. **(B)** (Right): Mean dose differences (clinical – predicted) of individual structures. CPOB had the lowest mean dose differences for the OARs: 2.8, 2.8, 4.6, 2.7, 4.1, 3.1, 3.1, and 2.7 Gy. G, parotid gland (left and right combined); SMG, submandibular gland (left and right combined); LL, lower larynx; UL, upper larynx; OC, oral cavity: PCM-I, inferior pharyngeal constrictor muscle; medial pharyngeal constrictor muscle; PCM-S, superior pharyngeal constrictor muscle.

Discussion

Deep learning for radiotherapy dose prediction has been reported for different tumor sites, but to the best of our knowledge, the influence of multiple different levels of input information on the ability to predict dose has not been (adequately) investigated. We demonstrated that all four models that included PTV contours predicted dose distributions that had a high level of agreement with clinical treatment plans. Although model CPOB, trained with the most comprehensive input data, produced the best dose predictions, even model CP, trained with patient CTs and primary tumor and lymph node PTVs and without explicit prior knowledge of the relevant OARs, achieved results that were not significantly different than those from the best model. The results and significance tests showed that for head and neck cancer, use of CT scans in training and testing adds little to dose prediction when OARs or PTVs are also used in model training. Somewhat surprisingly, using only the PTVs and the body contour (model PB) provided sufficient information for dose prediction, and presumably the shapes of the dose distributions were learnt and CT scans had limited added value for model training.

The mean dose to OARs and the shape of the DVHs demonstrated that the majority of predictions of all models except model C were consistently in line with the clinical doses and the PTVs. From the composite OAR structures, the models CPOB and POB had explicitly learned the OAR locations and sizes and more accurately predicted doses both in the individual OARs and in the VOI than the other three models. Although on average the predicted OAR doses were comparable with the clinical doses, there were individual patients with up to 17 Gy higher predicted dose than clinical, e.g., for the SMG that clinically received 41.4 Gy (Figure 4). All models predicted too high doses. This SMG was partly inside the PTV-B; the dose gradient was not steep enough, unlike the patients in Figure 6A. The overprediction could be caused by the downsampling resulting in larger voxel sizes, or by the fact that training samples from 2013 to 2015 had a less aggressive SMG sparing than in later years. Model POB and PB predicted comparable results as other models trained with the CT. As expected, the OARs provided significant information for OAR sparing (p = .015, Supplementary Material Table 2); however, for the model PB, with no knowledge of CT nor OARs, it had comparable results for both the DVH and mean dose to OARs.

While most other research using deep learning for dose prediction has used CT scans together with PTVs and OARs (14, 20), similar to our model CPOB, we observed from models CP and CPOB that when the CT was present in training and testing, the OAR contours did not result a statistically significant influence (p = .175, Supplementary Material Table 2) in the VOI. However, when the CT was absent, OAR structures made a statistically significant difference (p = .015, Supplementary Material Table 2) of the dose prediction for model POB over PB. There are limited published data demonstrating that NNs are capable of dose prediction without the need of the CT scans (17, 30). The results suggest that sufficient information had already been distilled from the CT in the OAR contours to predict dose distributions close to the clinically accepted ones. When CT scans are excluded from the training, the data

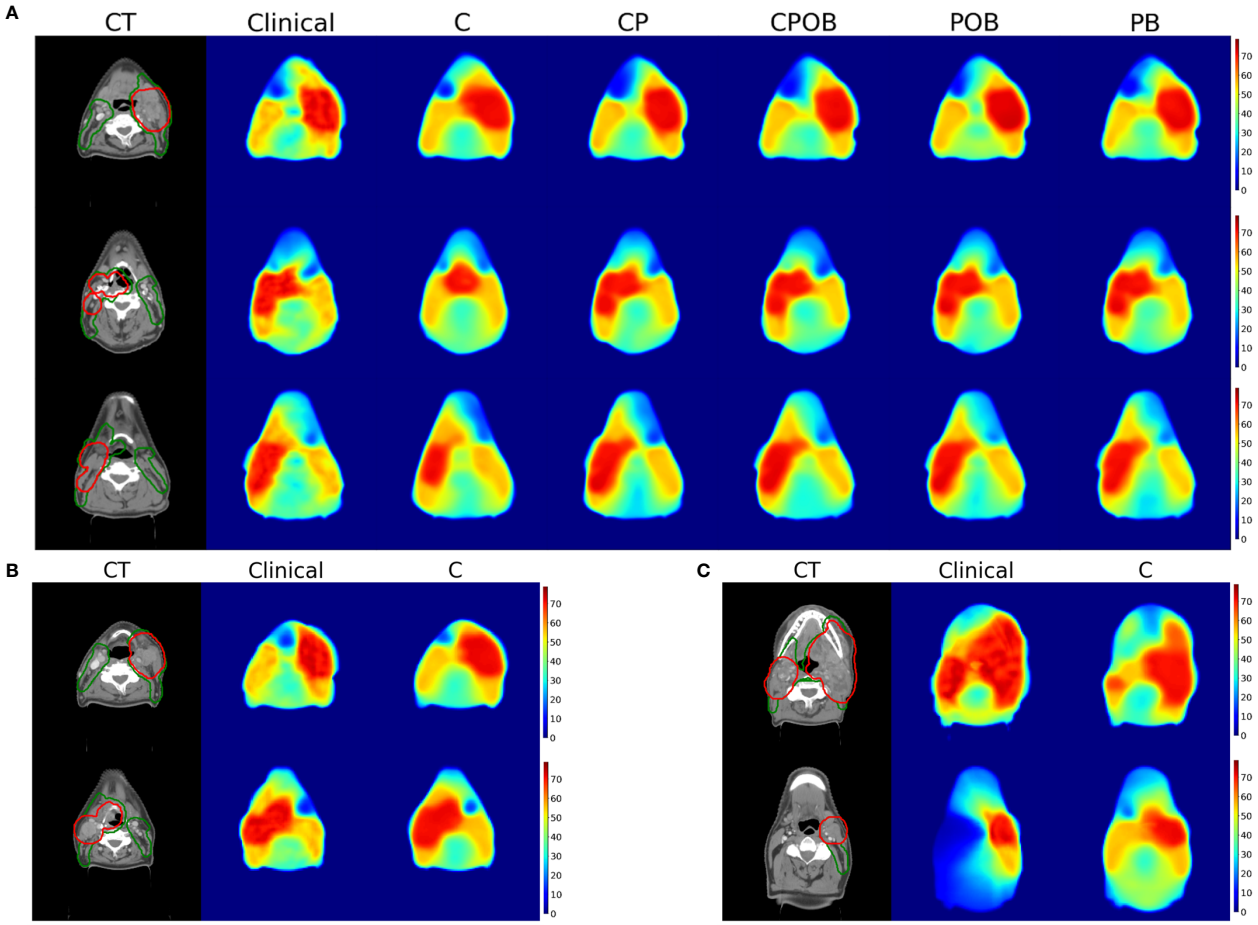

FIGURE 6
(A) (Up): Dose prediction comparison for a single slice for 3 patients with mean absolute dose errors in the volume of interest for model CPOB around the mean (3.62, 3.32, and 3.29 Gy). From left to right, CT with PTV-elective (green) and PTV-boost (red) contours, dose distributions of clinical, models C, CP, CPOB, POB, and PB. The CT scans above are displayed in the original resolution, which is better than the input to the models. **(B)** (Down-Left): Dose distributions predicted by model C of two patients with a small MAE in VOI (4.7 and 4.8 Gy). **(C)** (Down-right): Dose distributions predicted by model C of two patients with a large MAE in VOI (11.2 and 12.4 Gy). CT, computed tomography; OAR, organ at risk; PTV, planning target volume; MAE, mean absolute error; VOI, volume of interest.

distribution of PTV and OAR contours becomes binary resulting in a lower complexity and stronger gradients to update the parameters in the NNs. When the OARs are not part of the input, the model can learn their location and size from the CT scan and the PTV but seems to do this only to a limited extent (CP results were worse than CPOB). The results of the PB model indicated that the model has implicitly learned the typical location of OAR and the locations where the dose needs a steeper gradient, only from the PTV and body contours. The reason that this model performed slightly worse than model POB is probably that the exact location and size of the OAR cannot be estimated for individual patients.

When CT was the only input for our architecture, the majority of the dose predictions were not adequate. Large deviations in PTV-B were observed in the DVH, and predicted dose distributions of all 35 test patients assumed a bilateral PTV-E, which resulted in a high mean dose error when the PTV-E was unilateral, probably because most training cases had a bilateral PTV-E. Although the model seemed to recognize the location of the primary tumor for 25 out of 35 test patients based on visual inspection, it had difficulties in detecting from only the CT scan the extent of the tumor and which lymph node levels needed to be included for elective irradiation. In a minority of cases (8 out of 35 test patients, with lowest MAEs, Figure 5A), the model was able to better locate the tumor position and extent and the predicted-clinical DVH were in closer agreement. While others have investigated dose prediction using CT scans only and achieved good results (21, 24), this was for rectum and prostate cancer. Both have rather less complex PTVs than HNC and fewer OARs. For HNC, the extent of lymph node irradiation depends on the size and location of primary tumor and the presence of positive lymph nodes are more difficult to determine from only a CT scan. The performance of a model without any contours could possibly be improved with the addition of magnetic resonance imaging (MRI) data, which in general better shows the extent of the tumor. The enhanced tissue-tumor contrast of MRI could also provide extra information, and different types of MRI scans can highlight different types of tissues that could help the models to detect gross tumor volume (GTV). Including other modalities such as positron emission tomography (PET) can

further improve GTV segmentation (31). In practice, incorporating MRI may pose challenges, including that (1) MRIs may not be available for all patients; (2) many centers do not acquire MRIs in the same position as the planning CTs, which makes registration more difficult; (3) clinical MRIs may not image the same volume as the CTs and may not image the entire PTV; and (4) there are many possible MRI sequences, delivering all differences in images, and different sequences may have been used for different patients.

We used composite OAR structures to better generalize the DVH analysis for individual patients. Plans often need to make a trade-off between OARs to spare, e.g., parotid or submandibular glands, sparing at the cost of the oral cavity and pharyngeal constructor muscles. Without this knowledge for individual patients, the use of composite structures may represent the overall quality of the dose prediction better than if individual OARs had been used, and it requires fewer input channels for training. Over time, OAR sparing has evolved in complexity and now includes many more OARs as the focus changes from sparing only the parotid glands to also minimizing the risk of damage to the submandibular glands, to reduce xerostomia and minimize the dose to the swallowing apparatus in order to reduce dysphagia. Even without using individual OARs for training and testing, the predicted mean doses evaluated on individual OARs were close to those of the clinical plans (Figure 5). For the best model, only 17.4% of all OARs deviated by more than 3 Gy from the clinical plans. This is better than the dose prediction using RapidPlan, a knowledge-based planning system, where 22.5% of head and neck OAR deviated by more than 3 Gy (27). The variations in our deep learning dose prediction were also substantially lower than the variation in planning between radiation therapy centers (3).

Models C, CP, and PB had to learn the position of OARs implicitly from the clinical dose distributions. Using two individual NNs for OAR segmentation and dose prediction could achieve better performance, because the weights of the NNs can be independent for the corresponding tasks. Since our study is meant to investigate the influence of input data for dose prediction, we have not yet experimented if our methods would benefit segmentation tasks. The models were trained with elastic loss function, a combination of the L1 and the L2 loss, which penalizes highly predicted doses on OARs in L2 loss's quadratic term to encourage OAR sparing (for details, see Supplementary Material).

This study has its limitations. First, dose distribution has been predicted, but we have not shown how to convert this to a deliverable treatment plan. Second, the dataset was cropped and had larger voxel sizes than the original. This could be particularly a limitation for smaller OARs. However, we have not tested the influence of voxel size. Third, we used the central 96 slices in this study, with the length of 24 cm, such that on average 5% of OARs were excluded from the dataset, although the greatest dose differences were not observed at the caudal end. Furthermore, the clinical plans in the training and validation sets were drawn from a time span of 7 years, and the ability of OAR sparing may have changed overtime (32). As it was not known how many cases were needed for training, we opted for a sufficiently large training set, which necessitated the long period. Finally, none of the clinical plans used for training and testing were curated to ensure an optimal OAR sparing. Having a curated, consistent training and test set could possibly improve the models (and facilitate a smaller dataset). However, we have assumed that by having a sufficiently large training set, we could mitigate this.

Our model CP, trained only with CT scans and PTVs, was not statistically different from model CPOB, which was trained with OAR contours. This represents the minimum data statistically required to adequately predict the clinical dose distribution. This paper takes one step forward in (1) understanding how AI dose prediction works (i.e., what input data is important) and (2) achieving fully autonomous AI generated head and neck treatment plans, which could help to overcome limitations in time, manpower, experience, and financing. All the clinician need to do is to generate GTV/CTV boost (33), and CTV elective and OARs can be automatically generated (34, 35).

Conclusions

In this study, we used deep generative adversarial networks to predict dose distributions for head and neck radiotherapy treatment planning and achieved results that were highly similar to the clinical plans. We demonstrated the influence of the CT scan and PTV and OAR contours and showed that CT scans give limited additional benefit when OARs were used; PTVs provide sufficient information for OAR sparing; and models trained together with OARs have the lowest mean absolute dose differences. Our model CP, trained only with CT scans and PTVs, was not statistically different from model CPOB, which was trained with OAR contours.

Data availability statement

The original contributions presented in the study are included in the article/Supplementary Material, further inquiries can be directed to the corresponding author.

Ethics statement

This study was reviewed by the Medical Ethics Review Committee of VU University Medical Center. Due to the retrospective nature of this study which does not include tests or different treatments on human individuals, and the use of anonymized data, it was concluded by the Medical Ethics Review Committee that the Medical Research involving Human Subjects Act (WMO) does not apply to this study and that official approval of this study by the committee is not required. The study was conducted in accordance with the local legislation and institutional requirements.

Author contributions

XG and VS contributed equally to this work and share first authorship. All authors contributed to the article and approved the submitted version.

Conflict of interest

MD declares honoraria and research funding from Varian, a Siemens Healthineers Company Palo Alto, CA, USA, WV declares honoraria and travel expenses with Varian, XG and VS's are funded by a research grant from Varian. Since 1 May 2023, WV is employed by Varian.

The remaining author declares that the research was conducted in the absence of any commercial or financial relationships that could be construed as a potential conflict of interest.

Publisher's note

Supplementary material

The Supplementary Material for this article can be found online at: https://www.frontiersin.org/articles/10.3389/fonc.2023.1251132/full#supplementary-material

References

1. Craft DL, Hong TS, Shih HA, Bortfeld TR. Improved planning time and plan quality through multicriteria optimization for intensity-modulated radiotherapy. *Int J Radiat Oncol Biol Phys* (2012) 82(1):e83–90. doi: 10.1016/j.ijrobp.2010.12.007

2. Nelms BE, Robinson G, Markham J, Velasco K, Boyd S, Narayan S, et al. Variation in external beam treatment plan quality: An inter-institutional study of planners and planning systems. *Pract Radiat Oncol* (2012) 2(4):296–305. doi: 10.1016/j.prro.2011.11.012

3. Verbakel WFAR, Doornaert PAH, Raaijmakers CPJ, Bos LJ, Essers M, van de Kamer JB, et al. Targeted intervention to improve the quality of head and neck radiation therapy treatment planning in the Netherlands: Short and long-term impact. *Int J Radiat OncologyBiologyPhysics* (2019) 105(3):514–24. doi: 10.1016/j.ijrobp.2019.07.005

4. Delaney AR, Dahele M, Tol JP, Kuijper IT, Slotman BJ, Verbakel W. Using a knowledge-based planning solution to select patients for proton therapy. *Radiother Oncol* (2017) 124(2):263–70. doi: 10.1016/j.radonc.2017.03.020

5. Krayenbuehl J, Zamburlini M, Ghandour S, Pachoud M, Tanadini-Lang S, Tol J, et al. Planning comparison of five automated treatment planning solutions for locally advanced head and neck cancer. *Radiat Oncol* (2018) 13(1):170. doi: 10.1186/s13014-018-1113-z

6. Tol JP, Delaney AR, Dahele M, Slotman BJ, Verbakel WFAR. Evaluation of a knowledge-based planning solution for head and neck cancer. *Int J Radiat OncologyBiologyPhysics* (2015) 91(3):612–20. doi: 10.1016/j.ijrobp.2014.11.014

7. Wu B, Ricchetti F, Sanguineti G, Kazhdan M, Simari P, Jacques R, et al. Data-driven approach to generating achievable dose–volume histogram objectives in intensity-modulated radiotherapy planning. *Int J Radiat OncologyBiologyPhysics* (2011) 79(4):1241–7. doi: 10.1016/j.ijrobp.2010.05.026

8. Kaderka R, Hild SJ, Bry VN, Cornell M, Ray XJ, Murphy JD, et al. Wide-scale clinical implementation of knowledge-based planning: An investigation of workforce efficiency, need for post-automation refinement, and data-driven model maintenance. *Int J Radiat Oncol Biol Phys* (2021) 111(3):705–15. doi: 10.1016/j.ijrobp.2021.06.028

9. Ronneberger O, Fischer P, Brox T. *U-net: Convolutional networks for biomedical image segmentation. Lecture Notes in Computer Science (including subseries Lecture Notes in Artificial Intelligence and Lecture*. Springer Verlag (2015) 9341. doi: 10.1007/978-3-319-24574-4_28

10. He K, Zhang X, Ren S, Sun J. Deep residual learning for image recognition. (2015) 770-8. doi: 10.1109/CVPR.2016.90

11. Zhan B, Xiao J, Cao C, Peng X, Zu C, Zhou J, et al. Multi-constraint generative adversarial network for dose prediction in radiotherapy. *Med Image Analysis* (2022) 77:102339–. doi: 10.1016/j.media.2021.102339

12. Liu Y, Chen Z, Wang J, Wang X, Qu B, Ma L, et al. Dose prediction using a three-dimensional convolutional neural network for nasopharyngeal carcinoma with tomotherapy. *Front Oncol* (2021) 11. doi: 10.3389/fonc.2021.752007

13. Kearney V, Chan JW, Haaf S, Descovich M, Solberg TD. DoseNet: a volumetric dose prediction algorithm using 3D fully-convolutional neural networks. *Phys Med Biol* (2018) 63(23):235022–. doi: 10.1088/1361-6560/aaef74

14. Nguyen D, Long T, Jia X, Lu W, Gu X, Iqbal Z, et al. A feasibility study for predicting optimal radiation therapy dose distributions of prostate cancer patients from patient anatomy using deep learning. *Sci Rep* (2019) 9(1):1076–. doi: 10.1038/s41598-018-37741-x

15. Gronberg MP, Gay SS, Netherton TJ, Rhee DJ, Court LE, Cardenas CE. Technical Note: Dose prediction for head and neck radiotherapy using a three-dimensional dense dilated U-net architecture. *Med Physics* (2021) 48(9):5567–73. doi: 10.1002/mp.14827

16. Yan H, Liu S, Zhang J, Liu J, Li T. Utilizing pre-determined beam orientation information in dose prediction by 3D fully-connected network for intensity modulated radiotherapy. *Quantitative Imaging Med Surgery* (2021) 11(12):4742–52. doi: 10.21037/qims-20-1076

17. Nguyen D, Jia X, Sher D, Lin M-H, Iqbal Z, Liu H, et al. Three-dimensional radiotherapy dose prediction on head and neck cancer patients with a hierarchically densely connected U-net deep learning architecture. *Phys Med Biol* 64(6):065020. doi: 10.1088/1361-6560/ab039b

18. Goodfellow IJ, Pouget-Abadie J, Mirza M, Xu B, Warde-Farley D, Ozair S, et al. Generative adversarial networks. In Advances in neural information processing systems. (2014) 2672–80. doi: 10.48550/arXiv.1406.2661

19. Isola P, Zhu J-Y, Zhou T, Efros AA. Image-to-image translation with conditional adversarial networks. (2016) 5967–76. doi: 10.1109/CVPR.2017.632

20. Babier A, Mahmood R, McNiven AL, Diamant A, Chan TCY. Knowledge-based automated planning with three-dimensional generative adversarial networks. *Med Physics* (2020) 47(2):297–306. doi: 10.1002/mp.13896

21. Cui J, Jiao Z, Wei Z, Hu X, Wang Y, Xiao J, et al. CT-only radiotherapy: An exploratory study for automatic dose prediction on rectal cancer patients *via* deep adversarial network. *Front Oncol* (2022) 12:875661. doi: 10.3389/fonc.2022.875661

22. Kalantar R, Messiou C, Winfield JM, Renn A, Latifoltojar A, Downey K, et al. CT-based pelvic T(1)-weighted MR image synthesis using UNet, UNet++ and cycle-consistent generative adversarial network (Cycle-GAN). *Front Oncol* (2021) 11:665807. doi: 10.3389/fonc.2021.665807

23. Kearney V, Chan JW, Wang T, Perry A, Descovich M, Morin O, et al. DoseGAN: a generative adversarial network for synthetic dose prediction using attention-gated discrimination and generation. *Sci Rep* (2020) 10(1):11073–. doi: 10.1038/s41598-020-68062-7

24. Murakami Y, Magome T, Matsumoto K, Sato T, Yoshioka Y, Oguchi M. Fully automated dose prediction using generative adversarial networks in prostate cancer patients. *PloS One* (2020) 15(5):e0232697–e. doi: 10.1371/journal.pone.0232697

25. Hytonen R, Vergeer MR, Vanderstraeten R, Koponen TK, Smith C, Verbakel W. Fast, automated, knowledge-based treatment planning for selecting patients for proton therapy based on normal tissue complication probabilities. *Adv Radiat Oncol* (2022) 7(4):100903. doi: 10.1016/j.adro.2022.100903

26. Tol JP, Dahele M, Doornaert P, Slotman BJ, Verbakel WFAR. Toward optimal organ at risk sparing in complex volumetric modulated arc therapy: An exponential trade-off with target volume dose homogeneity. *Med Physics* (2014) 41(2):021722–. doi: 10.1118/1.4862521

27. Tol JP, Dahele M, Gregoire V, Overgaard J, Slotman BJ, Verbakel WFAR. Analysis of EORTC-1219-DAHANCA-29 trial plans demonstrates the potential of knowledge-based planning to provide patient-specific treatment plan quality assurance. *Radiotherapy Oncol* (2019) 130:75–81. doi: 10.1016/j.radonc.2018.10.005

28. van Rooij W, Verbakel WF, Slotman BJ, Dahele M. Using spatial probability maps to highlight potential inaccuracies in deep learning-based contours: Facilitating online adaptive radiation therapy. *Adv Radiat Oncol* (2021) 6(2):100658–. doi: 10.1016/j.adro.2021.100658

29. Kingma DP, Ba J. *Adam: A Method for Stochastic Optimization.* CoRR, abs/1412.6980. doi: 10.48550/arXiv.1412.6980 (2014).

30. Mashayekhi M, Tapia IR, Balagopal A, Zhong X, Barkousaraie AS, McBeth R, et al. Site-agnostic 3D dose distribution prediction with deep learning neural networks. *Med Physics* (2022) 49(3):1391–406. doi: 10.1002/mp.15461

31. Ren J, Eriksen JG, Nijkamp J, Korreman SS. PET and MRI multi-modality image combinations for deep learning-based head and neck tumor segmentation. *Acta Oncol* (2021) 60(11):1399–406. doi: 10.1080/0284186X.2021.1949034

32. Tol JP, Doornaert P, Witte BI, Dahele M, Slotman BJ, Verbakel WF. A longitudinal evaluation of improvements in radiotherapy treatment plan quality for head and neck cancer patients. *Radiother Oncol* (2016) 119(2):337–43. doi: 10.1016/j.radonc.2016.04.011

33. De Biase A, Sijtsema NM, van Dijk LV, Langendijk JA, van Ooijen PMA. Deep learning aided oropharyngeal cancer segmentation with adaptive thresholding for predicted tumor probability in FDG PET and CT images. *Phys Med Biol* (2023) 68(5). doi: 10.1088/1361-6560/acb9cf

34. Strijbis VIJ, Dahele M, Gurney-Champion OJ, Blom GJ, Vergeer MR, Slotman BJ, et al. Deep learning for automated elective lymph node level segmentation for head and neck cancer radiotherapy. *Cancers (Basel)* (2022) 14(22). doi: 10.3390/cancers14225501

35. van Rooij W, Dahele M, Ribeiro Brandao H, Delaney AR, Slotman BJ, Verbakel WF. Deep learning-based delineation of head and neck organs at risk: geometric and dosimetric evaluation. *Int J Radiat Oncol Biol Phys* (2019) 104(3):677–84. doi: 10.1016/j.ijrobp.2019.02.040

frontiers | Frontiers in Oncology

TYPE Original Research
PUBLISHED 20 October 2023
DOI 10.3389/fonc.2023.1177788

OPEN ACCESS

EDITED BY
Giuseppe Carlo Iorio,
University of Turin, Italy

REVIEWED BY
Kuo Men,
Chinese Academy of Medical Sciences and Peking Union Medical College, China
Guangjun Li,
Sichuan University, China

*CORRESPONDENCE
Benpeng Zhu
benpengzhu@hust.edu.cn
Yi Ding
dingyi_hbch@163.com
Xudong Xue
xuexudong511@163.com
Wei Wei
weiwei_hbch@163.com

RECEIVED 08 March 2023
ACCEPTED 03 October 2023
PUBLISHED 20 October 2023

CITATION
Luan S, Wei C, Ding Y, Xue X, Wei W, Yu X, Wang X, Ma C and Zhu B (2023) PCG-net: feature adaptive deep learning for automated head and neck organs-at-risk segmentation.
Front. Oncol. 13:1177788.
doi: 10.3389/fonc.2023.1177788

PCG-net: feature adaptive deep learning for automated head and neck organs-at-risk segmentation

Shunyao Luan[1], Changchao Wei[2], Yi Ding[3]*, Xudong Xue[3]*, Wei Wei[3]*, Xiao Yu[4], Xiao Wang[5], Chi Ma[5] and Benpeng Zhu[1]*

[1]School of Integrated Circuit, Wuhan National Laboratory for Optoelectronics, Huazhong University of Science and Technology, Wuhan, China, [2]Key Laboratory of Artificial Micro and Nano-structures of Ministry of Education, Center for Theoretical Physics, School of Physics and Technology, Wuhan University, Wuhan, China, [3]Department of Radiation Oncology, Hubei Cancer Hospital, TongJi Medical College, Huazhong University of Science and Technology, Wuhan, Hubei, China, [4]Department of Radiation Oncology, The First Affiliated Hospital of University of Science and Technology of China, Division of Life Sciences and Medicine, University of Science and Technology of China, Hefei, Anhui, China, [5]Department of Radiation Oncology, Rutgers-Cancer Institute of New Jersey, Rutgers-Robert Wood Johnson Medical School, New Brunswick, NJ, United States

Introduction: Radiation therapy is a common treatment option for Head and Neck Cancer (HNC), where the accurate segmentation of Head and Neck (HN) Organs-AtRisks (OARs) is critical for effective treatment planning. Manual labeling of HN OARs is time-consuming and subjective. Therefore, deep learning segmentation methods have been widely used. However, it is still a challenging task for HN OARs segmentation due to some small-sized OARs such as optic chiasm and optic nerve.

Methods: To address this challenge, we propose a parallel network architecture called PCG-Net, which incorporates both convolutional neural networks (CNN) and a Gate-Axial-Transformer (GAT) to effectively capture local information and global context. Additionally, we employ a cascade graph module (CGM) to enhance feature fusion through message-passing functions and information aggregation strategies. We conducted extensive experiments to evaluate the effectiveness of PCG-Net and its robustness in three different downstream tasks.

Results: The results show that PCG-Net outperforms other methods, improves the accuracy of HN OARs segmentation, which can potentially improve treatment planning for HNC patients.

Discussion: In summary, the PCG-Net model effectively establishes the dependency between local information and global context and employs CGM to enhance feature fusion for accurate segment HN OARs. The results demonstrate the superiority of PCGNet over other methods, making it a promising approach for HNC treatment planning.

KEYWORDS

head and neck cancer, radiation therapy, medical image, deep learning, automated segmentation

1 Introduction

Head and neck cancer (HNC) is the seventh most common cancer worldwide, resulting in an estimated 50,000 deaths in 2018 (1). Radiotherapy is the most commonly prescribed curative treatment option. Evidence showed that it took about 2.7 to 3 hours to delineate a full set of necessary structures in one HNC patient (2), including 0.5 to 1 hour's organs-at-risk (OARs) delineation. Nowadays, the delineation process is usually performed manually on treatment planning system (TPS). Manual delineation exists inter-variability, which is highly related to knowledge, experience, and preference of the radiation oncologists (3). The OARs auto-segmentation system can save the contouring time from at least half hour to only several minutes. However, the accuracy of commercial auto-segmentation system still needs to be evaluated and improved (4).

Traditional techniques including atlas-based methods (5, 6) and hybrid model-based methods (7, 8) have been used in clinical practice to improve the efficacy and accuracy. The atlas-based process implements segmentation by aligning a fixed set of manually labeled examples with the new images. Hybrid model-based approaches were done by statistical analysis of ground truth contours and imposed prior shape constraints in the segmentation process. These methods may be limited due to large anatomical variations of human organs or local uncertainty of deformable registration (9, 10).

Currently, deep learning represented by deep convolutional neural networks (CNNs) has shown great success in computer science and medical image analysis. There have been many studies which applied CNNs to segment various organs and substructures in radiotherapy for various disease sites and various types of image data (11–16). Given the varying sizes of the OARs) within the head and neck region, we opted to use this particular set of OARs for evaluating the segmentation performance of our deep neural network model. This choice enables a comprehensive assessment of the model's segmentation abilities across a range of anatomical structures, contributing to a more robust and clinically relevant evaluation. Ibragimov first performed the convolutional neural networks to segment the OARs in head and neck (HN) CT images, and the DSC varied from 37.4% for optic chiasm to 89.5% for mandible (17). Sun et al. developed a first locating then segmentation approach for accurate CT image segmentation of eyes and surrounding organs, which is accurate, efficient, and suitable for clinical use (18). Zhu et al. proposed an end-to-end atlas-free and fully automated deep learning model for anatomy segmentation from HN CT images, which introduced a new encoding scheme, 3D squeeze-and-excitation residual blocks, and combined loss. The experiments showed that compared to the prior state-of-the-art results achieved during the MICCAI 2015 competition, their model exhibited an average increase of 3.3% in the Dice similarity coefficient (19).

However, firstly, traditional deep learning segmentation requires large amounts of annotated datasets, while obtaining the annotated datasets in medical image analysis requires manual layer-by-layer annotation by experienced clinicians (20). Moreover, different institutions have different imaging modalities/protocols and different annotation approaches. Therefore, it is extremely hard to achieve cross-institution tasks by only using supervised training strategies. Secondly, OARs contain regions of variable sizes, including some OARs with very small sizes, such as optic chiasm and optic nerves. Accurately segmenting these small OARs structures is always a challenge.

To address above challenge, we attempted to utilize contrastive pre-learning strategies to alleviate medical image tasks with small annotated datasets and serious deviations in the distribution of cross-institutional data, to strengthen model feature extraction capability. Then we propose a parallel multiscale progressive refinement graph neural network (PCG-Net) for segment HN OARs, which contains A parallel encoder (PE), a cascade graph module (CGM), and a progressive refinement module (PRM). In addition, we proposed a new loss function based on the combination of dice scores and focal losses, for better segmenting small OARs structures.

To evaluate the performance of PCG-Net, we conducted experiments using two publicly available datasets and two local datasets for HN OARs segmentation. We performed a systematic analysis of various components of PCG-Net and compared them with other segmentation methods to demonstrate the effectiveness of PCG-Net's components. Furthermore, we utilized three distinct downstream tasks to evaluate the robustness of PCG-Net. The evaluation of PCG-Net indicating its potential for HNC treatment and various clinical applications.

2 Related works

2.1 Siamese-contrastive learning

The overall architecture of Siamese contrastive learning is shown in Figure 1. Two randomly augmented feature maps x_1 and x_2 from the input image x are fed to the encoder f, which includes a backbone network (CNN or Transformer) and a multi-layer perceptron *MLP* for performing prediction functions. The two output vectors are denoted as $z_i \triangleq P_r(f(x_i))$ and $p_i \triangleq f(x_i)$, where i represents the input number and P_r represents *MLP* for performing prediction. The difference between p_i and z_i is minimized with negative cosine similarity as in equation (1), with optimizing encoder f by Siamese-loss function as in equation (2), where $||\cdot||_2$ is ℓ_2-norm, $\mathcal{S}$ is the stop-gradient operation. $\mathcal{S}$ specifically presents as $\mathcal{S}(p_1, \ stopgrad(z_2))$, and $\mathcal{S}(p_2, stopgrad(z_1))$, which means the gradient of z_i is replaced by constant. Therefore, equation (2) can be updated to equation (3), expressed as the encoded network on x_1 receiving the back-propagation gradient from p_1 in the first term, while receiving no back-propagation gradient from z_1 in the second term (and vice versa for x_2).

$$S(p_1, z_2) = -\frac{p_1}{\| p_1 \|_2} \cdot \frac{z_2}{\| z_2 \|_2}$$
$$S(p_2, z_1) = -\frac{p_2}{\| p_2 \|_2} \cdot \frac{z_1}{\| z_1 \|_2} \quad (1)$$

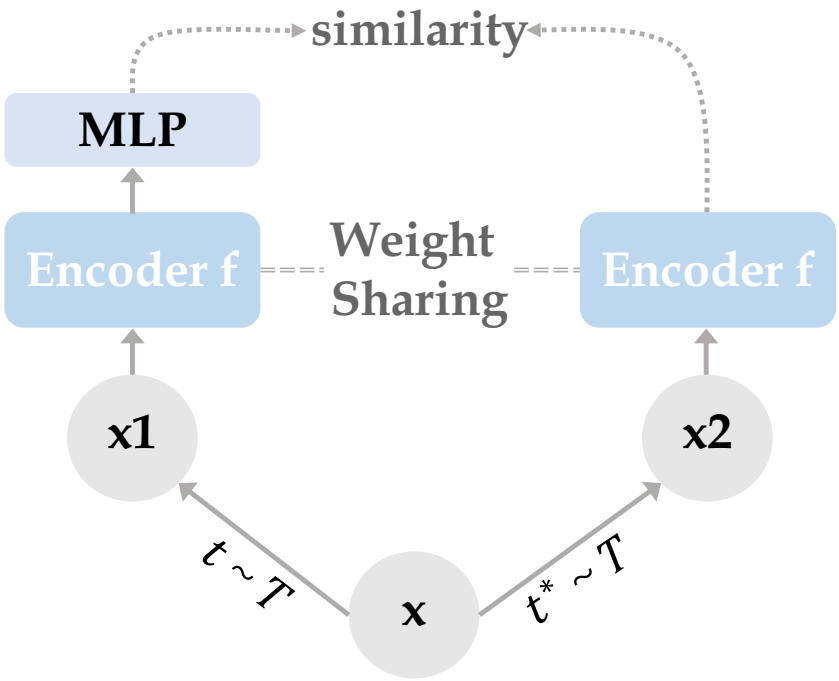

FIGURE 1
Two mutually independent augmentation operators *t*, *t** are randomly sampled from the data augmentations cluster *T*, and applied to the input x to obtain two correlated views x1, x2. Two identical encoder f (CNN/Transformer + MLP) are trained using x1 and x2, then the predicted MLP is applied on one side while the other side stops the gradient update, using the negative cosine similarity to minimize the feature difference of the two output results. After completing the training, we remove all MLP layers and use CNN or Transformer encoder for downstream tasks.

$$\mathcal{L} = \frac{1}{2}\mathcal{S}(p_1, z_2) + \frac{1}{2}\mathcal{S}(p_2, z_1) \tag{2}$$

$$\mathcal{L} = \frac{1}{2}\mathcal{S}(p_1, \text{stopgrad}\,(z_2)) + \frac{1}{2}\mathcal{S}(p_2, \text{stopgrad}\,(z_1)) \tag{3}$$

3 Method

The parallel multiscale progressive refinement graph neural network PCG-Net based on Siamese-contrastive learning is shown in Figure 2. PCG-Net uses parallel encoder (PE) and cascade graph module (CGM) to extract and fusion local features and global contextual information, respectively (Further details are available in the Supplementary Materials). In addition, the prediction results are progressively refined from lower resolution to higher resolution by the progressive refinement module (PRM) to optimize segmentation details.

3.1 Parallel encoder

3.1.1 Gated-axial transformer encoder

In this work, the traditional self-attention layers were replaced by two axial modules, which performed self-attention operations on the height-axis and width-axis, respectively, as shown in Figure 3. Specifically, the 2D spatial operation of the traditional self-attention layer was transformed into a 1D axial operation, and self-attention encoding was performed for the height and width axes sequentially. A multiple-headed attention mechanism was employed for both axis modules to optimize encoding performance. In addition, we define three positional bias matrices r_{ij}^{q}, r_{ij}^{k}, $r_{ij}^{v} \in R^{W\times W}$ to encode positional parameters q_{ij}, k_{ij}, v_{ij} to accurately capture more accurate positional information, respectively, where q_{ij}, k_{ij}, v_{ij}, represent the query, key and value, respectively. These bias matrices can participate in the gradient descent of neural networks to update the weights parameters. Finally, we introduced the gate mechanism to adaptively control the effect of the position bias on the output y_{ij} during the self-attention encoding process, the width-axis self-attention operations is shown in equation (4), where $G_Q, G_K, G_{V1}, G_{V2} \in R$ are learnable parameters which forms the gate bias.

$$y_{ij}(x_{ij}) = \sum_{w=1}^{W} \text{softmax}\left(q_{iw}^{T}k_{iw} + G_Q q_{iw}^{T} r_{iw}^{q} + G_K k_{iw}^{T} r_{iw}^{k}\right)\left(G_{V1} v_{iw} + G_{V2} r_{iw}^{v}\right) \tag{4}$$

3.1.2 CNN encoder

Although the transformer architecture enables sufficient extraction of global information, due to the self-attention mechanism, the transformer is prone to ignore local details. Without excellent feature extraction capability from the local to global, the organ contours cannot be accurately segmented. To

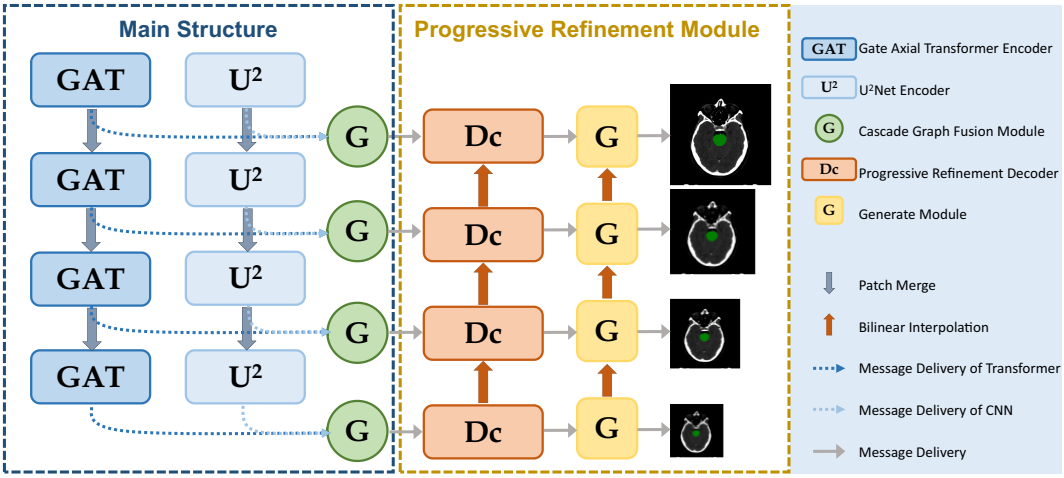

FIGURE 2
PCG-Net extracts local features and global contextual information through a parallel encoder, progressive refinement architecture for resolution-by-resolution spatial information recovery to achieve efficient feature decoding, cascade graph modules embedded in skip-connections adaptively refine high-level representations between different semantic information to achieve feature fusion and transfer. (The meanings of different modules represented in the figure are given in the legend).

extract both local features and global context information, the CNN encoder was utilized to compensate for the deficiencies of the transformer encoder. The U-shaped architecture has already been widely used in medical artificial intelligence, which usually builds U-shaped cascades based on sequential stacking of VGG architectures. But it has been demonstrated that single-level U-shaped architectures are susceptible to losing semantic details in deeper networks (21). Therefore, an $U^n Net$ encoder was introduced to alleviate the gradient loss problem, where n could be set as any positive integer to achieve multi-level or single-level nesting. Here, we set n as 2 to build the $U^2 Net$ encoder. Its exterior is semi-U-shaped with top-down compression of spatial information into channel information. Each module internally is independently U-shaped nested, which can effectively extract intra-stage multi-scale features and aggregate inter-stage multi-level features.

3.2 Cascade graph module

We use CGM for fusing high-level semantic information extracted based on the transformer encoder and CNN encoder, as shown in Figure 4. We first define two types of nodes: global feature nodes $V_1 = \{t_1, t_2, \ldots, t_n\}$ and local feature nodes $V_2 = \{c_1, c_2, \ldots, c_n\}$, where n represents the nodes number, t_i and c_i represents feature node. their initial feature scales are both $t_i^{(0)}, c_i^{(0)} \in R^{c \times h \times w}$, where c, h, w are the number of node channels, height, and width, respectively. For capturing feature information at different receptive fields, 2n nodes are obtained by using n different dilated convolutions with different dilated rates applied to two different types of feature maps. The integral node encoding can be represented as equation (5). where δ^m denotes the dilated convolution, m denotes the dilated rate, and $\chi_{h \times w}$ ensures the spatial dimension of the feature map after interpolation is $h \times w$.

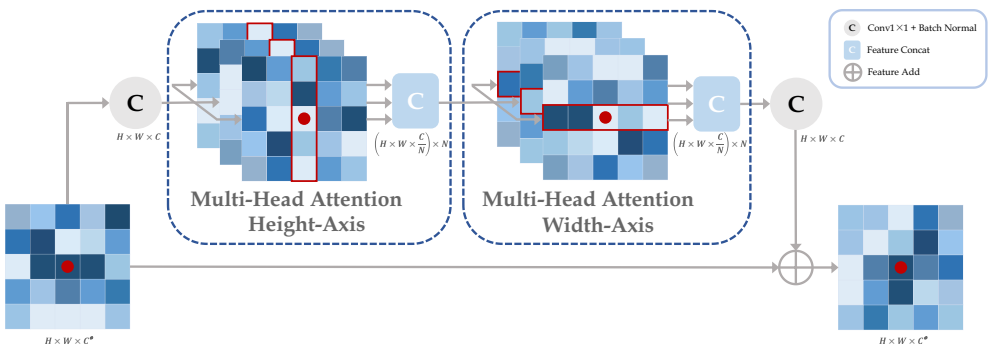

FIGURE 3
The axial attention module is composed by cascading the attention layers in height and width axis. Taking the red point as an example, it performs a multi-headed self-attention calculation with other points along specific columns and specific rows in sequence. Ultimately, the red point features contain all the information about the row and column in which it is located. where H, W, C, and N represent the height, width, channel, and attention head of the feature map, respectively, and C^* represents the original input channel.

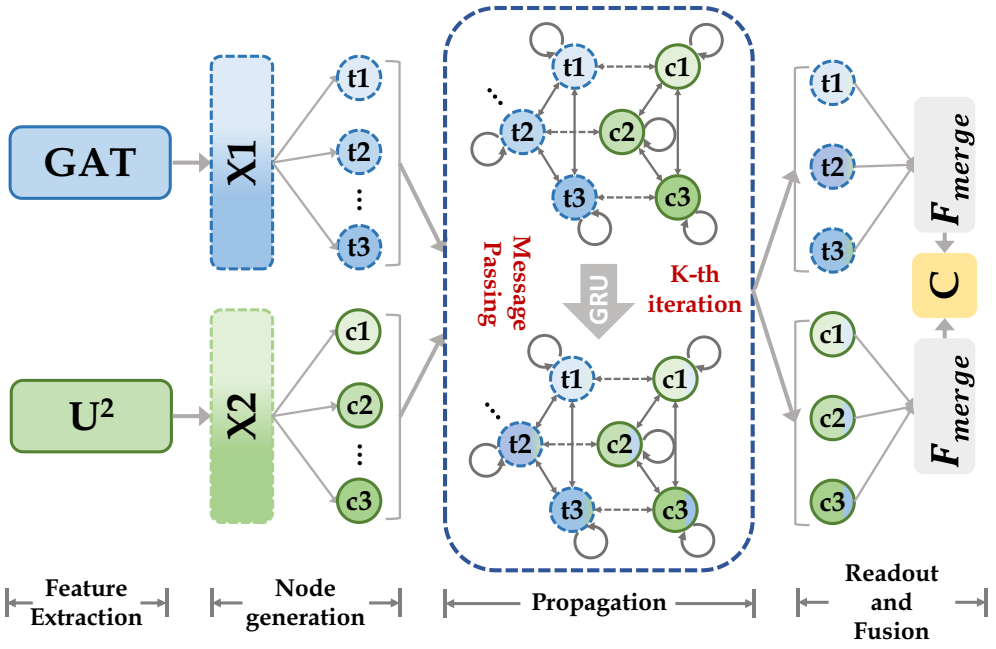

FIGURE 4
Our cascade graph module is built on two different categories of feature extractors (CNN and Transformer). Node features are updated by message-passing functions and gated recurrent neural networks, they enable inference of high-level relationships between different semantic space nodes and construct more powerful feature representations.

$$t_i^{(0)} = \chi_{h\times w}(Conv_\delta^m(X_1;\delta^m))$$
$$c_i^{(0)} = \chi_{h\times w}(Conv_\delta^m(X_2;\delta^m)) \quad (5)$$

Then we defined two types of edge e_1 and e_2 to update node state. For e_1, the relationship function is represented as equation (6), where ϑ is defined as the aggregation function between the same type of nodes, which can be represented by $\vartheta(t_i, t_j) = \alpha t_i + \beta t_j$, where i and j denote the node numbers. The connection relation $t_i \leftrightarrow c_i$ was defined as e_2, which can be expressed by the function f_ξ, with the overall process shown in equation (7), where $\alpha, \beta \in R$ is the learnable gating unit.

$$e_1 = Conv\{\sum_{i=1}^{n}\sum_{j=1}^{n}\vartheta[(t_i, t_j)or(c_i, c_j)]\} \in R^{c\times h\times w} \quad (6)$$

$$e_2 = f_\xi(V_1, V_2) = Conv[\sum_{i=1}^{n}\sum_{j=1}^{n}(\alpha t_i + \beta c_j)] \in R^{c\times h\times w} \quad (7)$$

Finally, we defined two types message passing function M (same feature node aggregation M_1 and different feature node aggregation M_2) for aggregating information from neighboring nodes to update the central node, as shown in equation (8), where δ is the *sigmoid* function. Gated Recurrent Unit (GRU) was used to update the node state as shown in equation (9). After the t message passing steps, every node in nodes set contains the feature information from neighboring nodes to achieve the effect of feature fusion. Finally, all the updated nodes were merged to generate dense mapping of the feature map, as shown in equation (10), where F_{merge} is the 3 × 3 convolutional layer and X^Θ is the output after GNN feature fusion.

$$M_1^{(t-1)} = \sum_{i=1}^{2} V_i[\delta(e_1^{(t-1)})]$$
$$M_2^{(t-1)} = V[\delta(e_2^{(t-1)})] \quad (8)$$

$$V^{(t)} = F_{GRU}(V^{(t-1)}, M^{(t-1)}) \quad (9)$$

$$X^\Theta = Conv_{C^\kappa}(F_{merge}(V_1, V_2)) \in R^{C^\kappa\times h\times w} \quad (10)$$

3.3 Progressive refinement module

The decoder contains a series of up-sampling modules to gradually recover spatial information. For each decoding block, the feature map scale resolution increases by a factor of 2 and skip-connects with the output of CGM, which not only introduces multi-dimensional spatial information but also alleviates the common gradient problem in deep learning. Usually, low resolution compared to high resolution makes reconstruction easier and focuses more on global features (22). Therefore, PRM was introduced to gradually add detailed information during decoding to generate more accurate predictions. Specifically, each prediction branch of the decoding module contains a generator G to generate target region contours φ_i^G of scale $n_i \times n_i$. Each generator consists of two successive series γ_i (convolution, batch normalization, ReLu activation function) and a feature dimension-adjusted convolution σ_i. The successive series γ_i at low resolution, after bilinear interpolation up-sampling with the scale factor of 2,

are fed to the higher scale prediction branch to perform elementwise addition with the output of successive series γ_{i+1} at higher resolution, and the targets' contours φ_{i+1}^{G} at the current scale resolution are obtained by dimension-adjusted convolution σ_{i+1}. The overall progressive refinement branch is shown in equation (11), where $\oplus$ is the elementwise addition and U is the up-sampling operation.

$$\varphi_i^G = \begin{cases} \sigma_i(\gamma)_i, & i = 1 \\ \sigma_{i+1}(\gamma_{i+1} \oplus U(\gamma_i)), & i = 2,3,4 \end{cases} \tag{11}$$

3.4 Loss function

The number of voxels within the small target volume is considerably fewer than the number of voxels outside, which means the data distribution is unbalanced and could lead to difficulty in training. Therefore, small target segmentation has always been a challenge in semantic segmentation. To address the above issues, the loss function fusion algorithm was employed to make the model fit target volume contours more accurately. The dice loss (23) enables converting the voxels-by-voxels labeling problem into minimizing the class-level distribution distance, which can alleviate the shortcoming in small target volume contributing slightly to the loss function. The focal loss (24) is the extension based on the cross-entropy loss function, which can adaptively apply different weights to distinct voxels to further alleviate the problems of difficulty imbalance in segmentation. In PCG-Net, the dice loss l_{DSC} was used to reduce the imbalance voxel problem, focal loss l_{Focal} was used to strengthen the model to focus on misclassified voxels, in order to design and build the focal-dice loss function l_{DF}, as shown in equation (12), where $FP_p(m)$, $FN_p(m)$ and $TP_p(m)$ are the false positives, false negatives and true positives of class m based on the predicted probabilities, respectively. $p_n(m)$ is the predicted probability that voxel n belongs to class m, and $g_n(m)$ is the ground truth that voxel n belongs to class m, where m is the total number of OARs structures plus one (background), and n is the total number of voxels in the CT image. $\alpha = 2$ is a weight parameter to balance between l_{DSC} and l_{Focal}. $\beta = 1$ and $\eta = 1$ are the trade-offs of penalties for false negatives and false positives.

$$\begin{aligned} TP_p(m) &= \sum_{n=1}^{N} p_n(m) g_n(m) \\ FN_p(m) &= \sum_{n=1}^{N} g_n(m)(1 - p_n(m)) \\ FP_p(m) &= \sum_{n=1}^{N} (1 - g_n(m)) p_n(m) \\ l_{DF} &= l_{DSC} + \alpha l_{Focal} \\ &= M - \sum_{m=0}^{m-1} \frac{TP_p(m)}{TP_p(m) + \beta FN_p(m) + \eta FP_p(m)} \\ &\quad - \alpha \frac{1}{N} \sum_{m=0}^{m-1} \sum_{n=1}^{N} g_n(m)(1 - p_n(m))^2 \log(p_n(m)) \end{aligned} \tag{12}$$

4 Experiment

4.1 Dataset

In the HN OARs segmentation task, our data include two publicly available datasets: DATASET 1 (177 samples) consisting of CT images from four different institutions in Quebec, Canada, and DATASET 2 (46 samples) consisting of CT images from the Head-Neck Cetuximab collection, as well as two local datasets: DATASET 3 (60 samples) provided by the Department of Radiology, Hubei Cancer Hospital, and DATASET 4 (100 samples) provided by the Radiotherapy Center of Anhui Provincial Hospital. Each dataset contains five organs: brain stem, mandible, parotid, optic chiasm, and optic nerve. Please note that for detailed information on publicly available datasets (DATASET 1 and DATASET 2), please refer to reference (25). The explanations about the acquisition of local CT datasets (DATASET 3 and DATASET 4) are as follows: During CT simulation, patients were immobilized in supine position with a thermoplastic mask and underwent contrast-enhanced CT scan on the CT scanning system (Philips Brilliance Big Bore, GE LightSpeed 16, and GE Discovery CT590 RT). The resolution, and thickness of CT images were 512 × 512× (0.9766-1.1719mm), and 2.5mm-3 mm, respectively.

The two publicly available datasets contain CT images from five different institutions, which have significant data complexity. Therefore, during the contrastive experiments shown in Section 5.3, contrastive learning was performed based on the public dataset (223 samples) to pre-train the encoder for improving the robustness and feature extraction capability of the encoder. DATASET 4 was used as the training dataset for supervised learning to fine-tune the weight distribution of the neural network. DATASET 3 was used to validate and test the effectiveness of the algorithm. In particular, the pre-training process requires only CT images without corresponding manually delineation, whereas the training and validation processes both require HN CT images and corresponding manually delineated OARs. It was ensured that the above four datasets are not overlapping with each other to avoid any potential overfitting.

To demonstrate the heterogeneity between the public dataset and the local dataset, the following features were extracted from each image using the gray-level co-occurrence matrix: sum entropy, difference entropy, sum average, correlation, contrast, homogeneity, sum variance, and variance, then the statistical differences were analyzed between the datasets. The p-value of each statistic was then obtained using the Mann-Whitney U test. The results in Table 1

TABLE 1 Analysis of the statistical differences.

Textural Features	p-value	Textural Features	p-value
Sum entropy	< 0.001	Difference entropy	< 0.001
Sum average	< 0.001	Correlation	< 0.001
Contrast	< 0.001	Homogeneity	< 0.001
Sum variance	< 0.001	Variance	< 0.001

show that eight statistics have p-values less than 0.001, hence there are serious adaptation issues between the two types of datasets which require more powerful pre-training methods with segmentation algorithms to adapt to both datasets.

To further test our algorithm's efficacy in different downstream tasks, more datasets were collected, including 1) Liver Tumor Segmentation Challenge (LITS) liver cancer public dataset, with 131 patient samples, 2) Lung Nodule Analysis 16 (LUNA16) lung cancer public dataset, with 888 patient samples, and 3) (Blood Cell Classification Datasets) BCCD blood cell classification public dataset, containing 12,500 blood cell enhanced images (JPEG format).

4.2 Evaluation metrics

The segmentation performance was evaluated by calculating the Dice Similarity coefficient (DSC), which is defined as $DSC(p,z) = \frac{2\times|p\cap z|}{|p|+|z|} \times 100\,\%$, where p is the voxel mask predicted by the network and z is the ground truth. The DSC values are between 0 and 1, where the closer DSC is to 1, the better the segmentation performance. In addition, to evaluate the segmentation results from multiple perspectives, the Hausdorff Distance (HD), the Average Symmetric Surface Distance (ASSD), and the Jaccard Coefficient (Jaccard) were further utilized as supplementary metrics. Generally, the DSC and Jaccard are considered more sensitive to the voxel details inside the contour which reflects the segmentation integrity, while the HD and ASSD are more sensitive to the contour surface which can characterize the segmentation surface contour accuracy. The four-evaluation metrics complement each other and enable a comprehensive assessment of segmentation results. Please note that the p-value of each statistic in our work was derived by other methods with PCG-Net based on the T-test: Two-tailed critical value for paired sample mean analysis.

4.3 Experimental details

The neural network using PyTorch was implemented and experiments were performed on a small NVIDIA RTX3090Ti workstation equipped with 24GB of RAM. To enhance data consistency and improve model training efficiency, all CT images and mask labels were preprocessed in the same way. Using the linear interpolation method to adjust the pixel spacing of different institutions' images, each slice pixel spacing was adjusted to 1mm, and the original CT images and the masked images were padded to 512×512 uniformly. Image morphing is to rotate, translate, mirror, and affine transform each CT image with its corresponding label to enhance the complexity of the data. The grayscale float uses the current voxel grayscale value superimposed with random initialization numbers, which in turn generates CT images with noise, thus effectively improving the model's anti-interference capability. Please refer to the Supplementary Material for more details on about image preprocessing and grayscale float.

For the contrastive learning pre-trained encoder, the SGD optimizer was used for pre-training. Linear scaling learning rate (26) was used with a base $l_r = 0.05$, and the learning rate has a cosine decay schedule (27). The weight decay was 0.0001 and the SGD momentum was 0.9. Considering the computational complexity, the batch size was set to 32 and the epoch size was set to 50. For training PCG-NET, Adam with a weight decay of 0.0001 was utilized to optimize network parameters, with the initial learning rate set to 0.0001, and the "ploy" strategy with 0.9 power as adjustment. The batch size was set to 32 and the epoch size was set to 150 due to hardware limitations.

5 Results

To demonstrate the benefits brought by each module and the superiority of PCG-Net, the following experiments were performed: the benefits of gated-axial transformer encoder, cascade graph feature fusion architecture, and progressive refinement decoder on PCG-Net through ablation study was demonstrated in Section 5.1; the superiority of PCG-Net's was verified by comparing it with three advanced segmentation algorithms, U^2Net, CPFNet, and MedT in Section 5.2; the effectiveness of Siamese contrastive learning pre-trained encoder was demonstrated in Section 5.3; the universality and generalization ability of PCG-Net by other medical tasks was demonstrated in Section 5.4.

It's worth noting that in Sections 5.1 and Sections 5.2, the contrastive learning strategy was not utilized to pre-train the PCG-Net's encoder, while the overall training method was the supervised task, with DATASET 4 as the training dataset, and DATASET 3 as the validation and test dataset. In Section 5.3, in order to discuss the importance of contrastive learning, the encoder was first pre-trained by DATASET 1 and DATASET 2, which was an unsupervised task. Secondly, the pre-trained encoder weights were transferred to PCG-Net, during which the MLP layer necessary for the contrastive learning task was removed, and end-to-end training of the PCG-Net by DATASET 4 was performed based on a supervised strategy, with DATASET 3 as the validation and testing dataset. Please note that all the results are the mean values on the test datasets after ten-fold cross-validation. In addition, the detailed processing times for all deep learning models handling the same image can be found in the Supplementary Materials.

5.1 Ablation study

To demonstrate the effectiveness of different modules, ablation experiments were performed to compare the gains from each module. Using the U^2*Net* (28) as a baseline, unlike traditional U^2*Net* which contains 6 encoder/decoder blocks, a 4 encoder/decoder blocks structure was employed to reduce the computational complexity. For better performance, the pooling layer was replaced by the patch merging layer (29) for minimizing the semantic information loss caused by the traditional pooling layer. During the ablation study, all competitors were conducted in the same computing environment and under the same data enhancement to ensure a fair comparison.

By replacing the corresponding components in the baseline network with the gated-axial transformer, the cascaded graph

module, and the progressive refinement decoder, respectively, it was possible to obtain: level1 (progressive refinement decoder replacing the baseline decoder), level2 (gated-axial transformer encoder replacing the baseline encoder), and level3 (parallel encoder replacing the baseline encoder). Further, the following was obtained by simultaneous replacement for two or three components in the baseline network: level4 (parallel encoder replacing the baseline encoder, cascade graph module replacing the baseline skip connection), level5 (parallel encoder replacing the baseline encoder, progressive refinement decoder replacing the baseline decoder, cascade graph module replacing the baseline skip connection). Five methods equipped with different modules were evaluated on the HN dataset, with the segmentation results shown in Figure 5. Compared with the baseline method, the level1, level2, and level3 methods have improvements in processing segmentation tasks. Compared to adding only a single module to the baseline, the combination based on two or more modules can obtain more accurate segmentation results, especially for small volume OARs. The statistical results are shown in Table 2.

Compared with the baseline network, the mean DSC of the level1 and level2 methods improved by approximately 0.7% (from 73.2% to 73.9%) and 0.02% (from 73.2% to 73.22%), respectively, which proved contribution of the progressive refinement module and the gated-axial transformer module in feature decoding and feature encoding. Compared with the baseline model and level2, the mean DSC and mean Jaccard of the level3 method improved by 4.32% (from 73.2% to 77.52%), 4.26% (from 66.0% to 70.26%) and 4.3% (from 73.22% to 77.52%), 4.74% (from 65.52% to 70.26%), respectively, while the mean DSC and mean Jaccard of the small volume OARs (optic chiasm and optic nerve) improved by 4.1% (from 58.85% to 62.95%), 5.3% (from 57.65% to 62.95%) and 2.95% (from 51.15% to 54.1%), 6.3% (from 47.8% to 54.1%), respectively, demonstrating that the parallel encoder is superior to the single-branch encoder in segmentation accuracy, which enables adequate

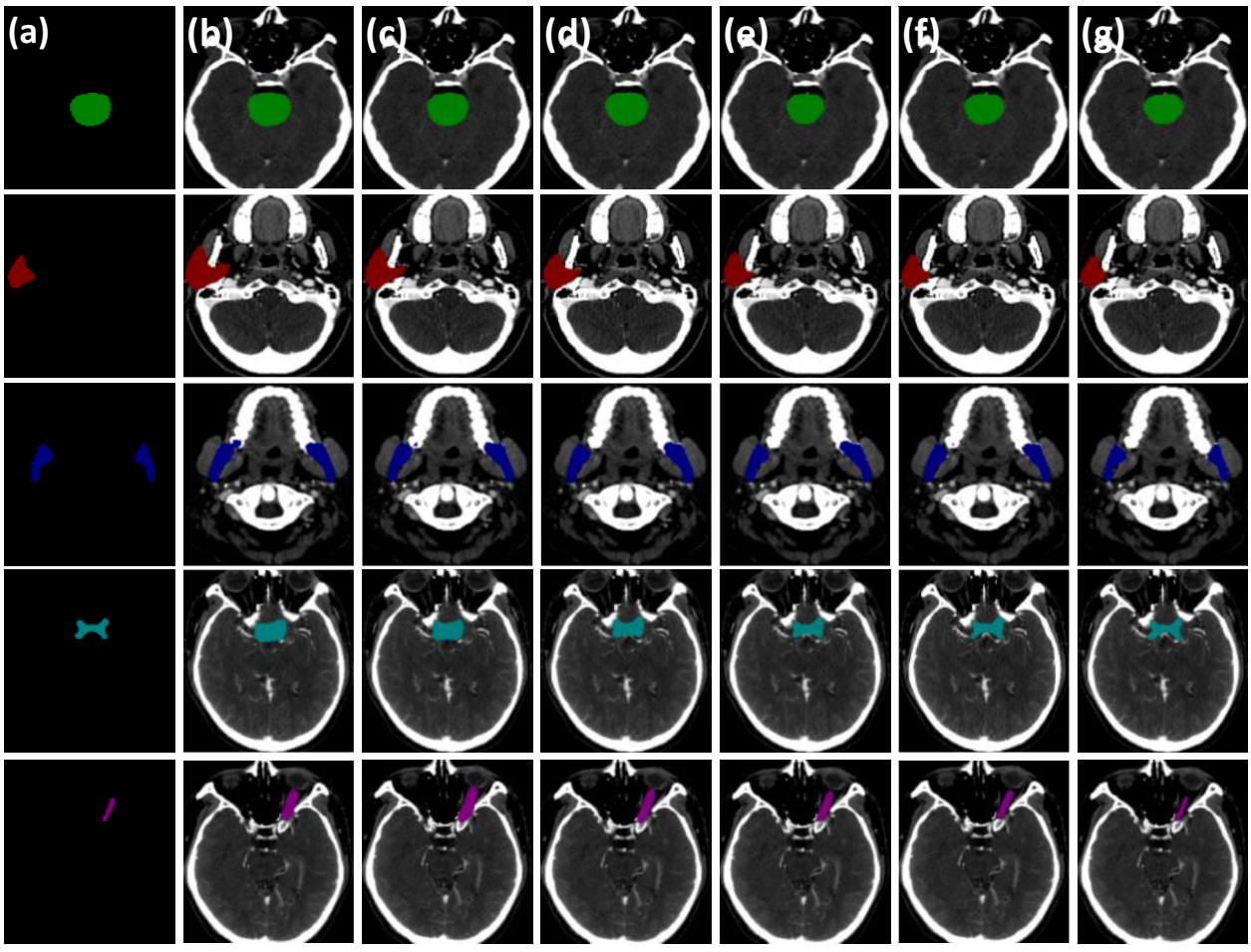

FIGURE 5
Visual comparison of three critical modules of the PCG-Net ablation study. **(A)** Ground truth. **(B)** Baseline model. **(C)** The progressive refinement decoder replaces the baseline decoder. **(D)** Gated-axial transformer encoder replaces the baseline encoder. **(E)** The parallel encoder replaces the baseline encoder. **(F)** The parallel encoder replaces the baseline encoder and cascade graph module replaces the baseline skip connection. **(G)** The parallel encoder replaces the baseline encoder, the progressive refinement decoder replaces the baseline decoder, and the cascade graph module replaces the baseline skip connection. To facilitate visual representation, we used different color masks to represent different organ-at-risks, where green mask is the brainstem, red mask is the parotid, blue mask is the mandible, cyan mask is the optic chiasm, and purple mask is the optic nerve.

TABLE 2 Statistical comparisons of ablation studies for the three main modules in PCG-Net.

	Brain Stem	Mandible	Parotid	Optic Nerve	Optic Chiasm	Mean	Mean (small volume OARs)
Baseline	84.3% ± 2.6%	85.2% ± 3.1%	78.8% ± 3.7%	65.5% ± 7.8%	52.2% ± 14.3%	73.2% ± 6.3%	58.85% ± 11.05%
	77.2% ± 2.1%	76.3% ± 2.7%	74.4% ± 3.1%	58.2% ± 6.9%	44.1% ± 10.2%	66.0% ± 5%	51.15% ± 8.55%
	3.123 ± 1.1	3.211 ± 0.9	4.212 ± 1.7	2.979 ± 0.6	4.811 ± 1.2	3.67 ± 1.1	3.895 ± 0.9
	1.217 ± 0.4	1.334 ± 0.5	1.899 ± 0.7	0.886 ± 0.3	1.577 ± 0.6	1.38 ± 0.5	1.2315 ± 0.45
Level 1	85.1% ± 2.1%	85.9% ± 2.2%	79.3% ± 3.1%	66.1% ± 7.3%	53.1% ± 12.9%	73.90% ± 5.5%	59.6% ± 10.1%
	77.9% ± 1.8%	78.1% ± 2.3%	74.7% ± 3.3%	58.8% ± 7.1%	45.7% ± 11.4%	67.04% ± 5.2%	52.25% ± 9.25%
	3.013 ± 1.3	3.313 ± 1.2	3.991 ± 1.9	2.876 ± 0.9	4.792 ± 1.3	3.60 ± 1.3	3.834 ± 1.1
	1.155 ± 0.4	1.270 ± 0.4	1.792 ± 0.8	0.878 ± 0.3	1.565 ± 0.6	1.33 ± 0.5	1.221 ± 0.45
Level 2	84.9% ± 2.3%	85.8% ± 2.4%	80.1% ± 3.2%	65.9% ± 7.1%	49.4% ± 16.3%	73.22% ± 6.3%	57.65% ± 11.7%
	78.2% ± 2.0%	78.7% ± 2.5%	75.1% ± 2.9%	54.3% ± 9.2%	41.3% ± 14.2%	65.52% ± 6.2%	47.8% ± 11.7%
	2.992 ± 0.9	3.172 ± 0.9	3.876 ± 1.5	2.878 ± 0.9	5.137 ± 1.9	3.61 ± 1.22	4.008 ± 1.4
	1.143 ± 0.3	1.233 ± 0.5	1.786 ± 0.7	0.924 ± 0.4	1.669 ± 0.9	1.35 ± 0.56	1.296 ± 0.65
Level 3	87.1% ± 2.6%	88.7% ± 1.9%	85.9% ± 2.7%	68.8% ± 6.7%	57.1% ± 9.2%	77.52% ± 4.6%	62.95% ± 7.95%
	81.8% ± 2.3%	82.5% ± 1.9%	78.8% ± 3.0%	60.2% ± 5.5%	48.0% ± 8.3%	70.26% ± 4.2%	54.1% ± 6.9%
	2.633 ± 1.2	3.017 ± 1.3	3.663 ± 1.6	2.531 ± 0.5	4.331 ± 1.1	3.24 ± 1.1	3.431 ± 0.8
	0.983 ± 0.3	1.005 ± 0.5	1.594 ± 0.5	0.775 ± 0.2	1.347 ± 0.4	1.14 ± 0.4	1.061 ± 0.3
Level 4	88.9% ± 1.9%	90.7% ± 2.1%	87.9% ± 2.9%	70.2% ± 6.5%	57.7% ± 10.7%	79.08% ± 4.8%	63.95% ± 8.6%
	82.2% ± 2.2%	83.3% ± 2.3%	79.2% ± 2.7%	61.9% ± 6.1%	48.8% ± 9.1%	71.08% ± 4.5%	55.35% ± 7.6%
	2.455 ± 0.8	2.967 ± 0.9	3.532 ± 1.3	2.411 ± 0.6	4.299 ± 1.3	3.13 ± 1.0	3.355 ± 0.95
	0.916 ± 0.4	1.005 ± 0.4	1.511 ± 0.6	0.701 ± 0.2	1.210 ± 0.5	1.07 ± 0.4	0.955 ± 0.35
Level 5	89.2% ± 1.9%	91.8% ± 2.1%	89.1% ± 2.6%	71.7% ± 6.9%	58.1% ± 12.1%	79.98% ± 5.1%	64.9% ± 9.5%
	82.9% ± 1.9%	84.1% ± 2.0%	79.7% ± 2.5%	63.1% ± 5.7%	49.1% ± 7.9%	71.78% ± 4.0%	56.1% ± 6.8%
	2.406 ± 0.9	2.655 ± 1.1	3.317 ± 1.4	2.389 ± 0.5	4.221 ± 1.1	3.00 ± 1	3.305 ± 0.8
	0.881 ± 0.3	0.993 ± 0.3	1.470 ± 0.6	0.677 ± 0.2	1.112 ± 0.4	1.03 ± 0.4	0.894 ± 0.3

In each ablation experiment, the first and second rows represent the DSC values (mean ± variance) and Jaccard values (mean ± variance) in the test datasets, respectively; the third and fourth rows represent the $HD_{(mm)}$ values (mean ± variance) and $ASSD_{(mm)}$ values (mean ± variance) in the test datasets, respectively. The results in the table are the mean values on the test datasets after ten-fold cross-validation.

extraction of the local information while fitting the global information. Compared with the level3 method, the segmentation accuracy for the level4 method further improved, with the mean DSC and mean Jaccard improving by 1.56% (from 77.52% to 79.08%) and 0.82% (from 70.26% to 71.08%), respectively. For the small volume OARs (optic chiasm and optic nerve), the mean DSC and mean Jaccard improved by 1.00% (from 62.95% to 63.95%) and 1.25% (from 54.1% to 55.35%), respectively, revealing the excellent feature fusion and relationship modeling capabilities of the cascade graph module. The level5 method, simultaneously integrating three modules, achieved the best global prediction results, with the mean DSC and mean Jaccard improving by 6.78% (from 73.2% to 79.98%) and 5.78% (from 66.0% to 71.78%) compared to the baseline model. In the small volume OARs segmentation (optic chiasm and optic nerve), the improvement was particularly significant compared with the baseline model, with the mean DSC and mean Jaccard for optic chiasm improving by 6.05% (from 58.85% to 64.9%) and 4.95% (from 51.15% to 56.1%).

5.2 Model horizontal comparison

PCG-Net was horizontally compared with three other advanced segmentation approaches, including U^2Net (28), CPFNet (30), and MedT (31). In the comparison experiments, all competitors were performing under the same computational environment and the same data enhancement to ensure a fair comparison. Table 3 depicts the segmentation results by different methods on the HN OARs. Our model achieved the most excellent results on most metrics, with mean DSC, mean Jaccard, mean HD, and mean ASSD of 79.98%, 71.78%, 3.00, and 1.03, respectively. On small volume OARs segmentation, compared to the MedT, the mean DSC,

TABLE 3 Statistical comparison with different state-of-the-art methods.

	Brain Stem	Mandible	Parotid	Optic Nerve	Optic Chiasm	Mean
U²Net(×)	84.3% ± 2.6%*	85.2% ± 3.1%*	78.8% ± 3.7%**	65.5% ± 7.8%*	52.2% ± 14.3%*	73.20% ± 6.30%*
	77.2% ± 2.1%**	76.3% ± 2.7%*	74.4% ± 3.1%*	58.2% ± 6.9%#	44.1% ± 10.2%***	66.04% ± 5.00%#
	3.123 ± 1.1*	3.211 ± 0.9*	4.212 ± 1.7**	2.979 ± 0.6*	4.811 ± 1.2*	3.67 ± 1.10*
	1.217 ± 0.4*	1.334 ± 0.5**	1.899 ± 0.7***	0.886 ± 0.3*	1.577 ± 0.6*	1.38 ± 0.50#
CPFNet(×)	88.1% ± 2.4%**	88.7% ± 2.7%#	85.1% ± 2.9%**	70.3% ± 7.1%*	56.2% ± 13.3%*	77.68% ± 5.68%**
	80.5% ± 2.1%*	83.1% ± 2.3%*	77.2% ± 3.7%*	61.1% ± 6.2%*	47.8% ± 8.0%***	69.94% ± 4.46%*
	2.662 ± 0.8*	2.932 ± 0.9**	3.636 ± 1.5*	**2.377 ± 0.6****	4.667 ± 1.1*	3.25 ± 0.98**
	1.003 ± 0.3*	1.113 ± 0.3*	1.517 ± 0.6**	0.689 ± 0.2**	1.225 ± 0.4*	1.11 ± 0.36#
MedT(×)	**89.5% ± 1.7%***	90.6% ± 1.9%***	88.6% ± 3.1%*	68.1% ± 8.8%*	57.7% ± 12.9%*	78.90% ± 5.68%***
	82.2% ± 2.1%*	83.7% ± 2.2%*	78.3% ± 2.9%*	59.2% ± 6.7%*	48.0% ± 7.5%*	70.28% ± 4.28%*
	2.513 ± 0.9*	2.717 ± 1.1#	3.379 ± 1.4*	2.511 ± 0.5*	4.375 ± 1.2**	3.10 ± 1.02**
	0.879 ± 0.2*	1.059 ± 0.4*	**1.447 ± 0.5***	0.703 ± 0.4*	1.169 ± 0.3*	1.05 ± 0.36*
PCG-Net (×)	89.2% ± 1.9%	**91.8% ± 2.1%**	**89.1% ± 2.6%**	**71.7% ± 6.9%**	**58.1% ± 12.1%**	79.98% ± 5.12%
	82.9% ± 1.9%	**84.1% ± 2.0%**	**79.7% ± 2.5%**	**63.1% ± 5.7%**	**49.1% ± 7.9%**	71.78% ± 4.00%
	2.406 ± 0.9	**2.655 ± 1.1**	**3.317 ± 1.4**	2.389 ± 0.5	**4.221 ± 1.1**	3.00 ± 1.00
	0.881 ± 0.3	**0.993 ± 0.3**	1.470 ± 0.6	**0.677 ± 0.2**	**1.112 ± 0.4**	1.03 ± 0.36
U²Net(√)	84.7% ± 2.3%* 77.9% ± 1.6%*	85.6% ± 3.0%*	79.3% ± 3.5%*	66.7% ± 6.8%*	53.7% ± 11.9%*	74.00% ± 5.50%*
		76.9% ± 2.5%*	74.9% ± 3.2%*	59.5% ± 5.4%***	45.3% ± 8.8%*	66.90% ± 4.30%***
	3.112 ± 1.2*	3.157 ± 0.7*	4.106 ± 1.5**	2.858 ± 0.5*	4.551 ± 1.1*	3.56 ± 1.00**
	1.179 ± 0.3*	1.298 ± 0.4*	1.847 ± 0.7*	0.831 ± 0.2**	1.436 ± 0.3*	1.32 ± 0.38*
CPFNet(√)	88.3% ± 2.2%*	89.1% ± 2.7%**	85.8% ± 2.3%*	71.2% ± 6.7%*	58.3% ± 10.7%#	78.54% ± 4.92%*
	81.2% ± 2.0%*	83.6% ± 2.3%#	77.9% ± 3.5%*	63.3% ± 6.1%*	48.2% ± 8.2%#	70.84% ± 4.42%*
	2.636 ± 0.8*	2.919 ± 0.7*	3.596 ± 1.2*	2.290 ± 0.5**	4.544 ± 0.9*	3.20 ± 0.82**
	0.997 ± 0.2**	1.107 ± 0.3*	1.403 ± 0.5*	0.676 ± 0.2*	1.193 ± 0.3*	1.08 ± 0.30#
MedT(√)	89.9% ± 1.6%*	91.2% ± 1.8%*	89.1% ± 2.7%**	69.4% ± 7.9%*	58.6% ± 10.9%*	79.64% ± 4.98%**
	82.7% ± 2.0%*	84.2% ± 1.9%*	78.9% ± 2.6%*	60.1% ± 6.8%*	49.3% ± 8.1%**	71.04% ± 4.28%*
	2.479 ± 0.8#	2.699 ± 1.0*	3.293 ± 1.5*	2.410 ± 0.7#	4.132 ± 1.5*	3.00 ± 1.10**
	0.873 ± 0.3*	1.016 ± 0.3*	1.431 ± 0.4***	0.688 ± 0.3*	1.027 ± 0.4*	1.01 ± 0.34*
PCG-Net (√)	***90.1% ± 2.2%***	***92.3% ± 1.9%***	***89.9% ± 2.4%***	***73.2% ± 7.3%***	***59.9% ± 11.3%***	81.08% ± 5.02%
	83.3% ± 1.7%	***84.7% ± 1.8%***	***80.2% ± 2.1%***	***64.6% ± 6.1%***	***50.7% ± 7.2%***	72.70% ± 3.78%
	2.377 ± 0.8	***2.613 ± 1.0***	***3.288 ± 1.1***	***2.157 ± 0.4***	***4.023 ± 1.3***	2.89 ± 0.92
	0.868 ± 0.3	***0.986 ± 0.3***	***1.436 ± 0.5***	***0.619 ± 0.3***	***1.013 ± 0.3***	0.98 ± 0.34

In each comparison experiment, the first and second rows represent the DSC values (mean ± variance) and Jaccard values (mean ± variance) in the test datasets, respectively; the third and fourth rows represent the HD $_{(mm)}$ values (mean ± variance) and ASSD $_{(mm)}$ values (mean ± variance) in the test datasets, respectively. The symbols at the bottom of the models in the first column represent with/without contrastive pre-training strategy, where (×) indicates without contrastive learning pre-training strategy and (√) indicates with contrastive learning pre-training strategy. The black bold font indicates the optimal value among the four models without the contrastive learning pre-training strategy. The black bold italic font indicates the optimal value among the four models with the contrastive learning pretraining strategy. Please note that "***" to indicate p< 0.05, "**" for p< 0.01, "*" for p< 0.001, and "#" for p > 0.05.

mean Recall, mean HD, and mean ASD of our model improved by 1.08%, 1.5%, 3.23%, and 1.90%, respectively.

For visual comparison, the results of different segmentation algorithms are shown in Figure 6. Significant superiority can be observed for our algorithm compared to other competitors, especially for the more accurate identification of the small volume OARs. Combining Figure 6 with Table 3, PCG-Net effectively extracted local features and global context information by parallel encoder, fused features by cascaded module, and used progressive refinement decoder gradually refines the spatial dimension.

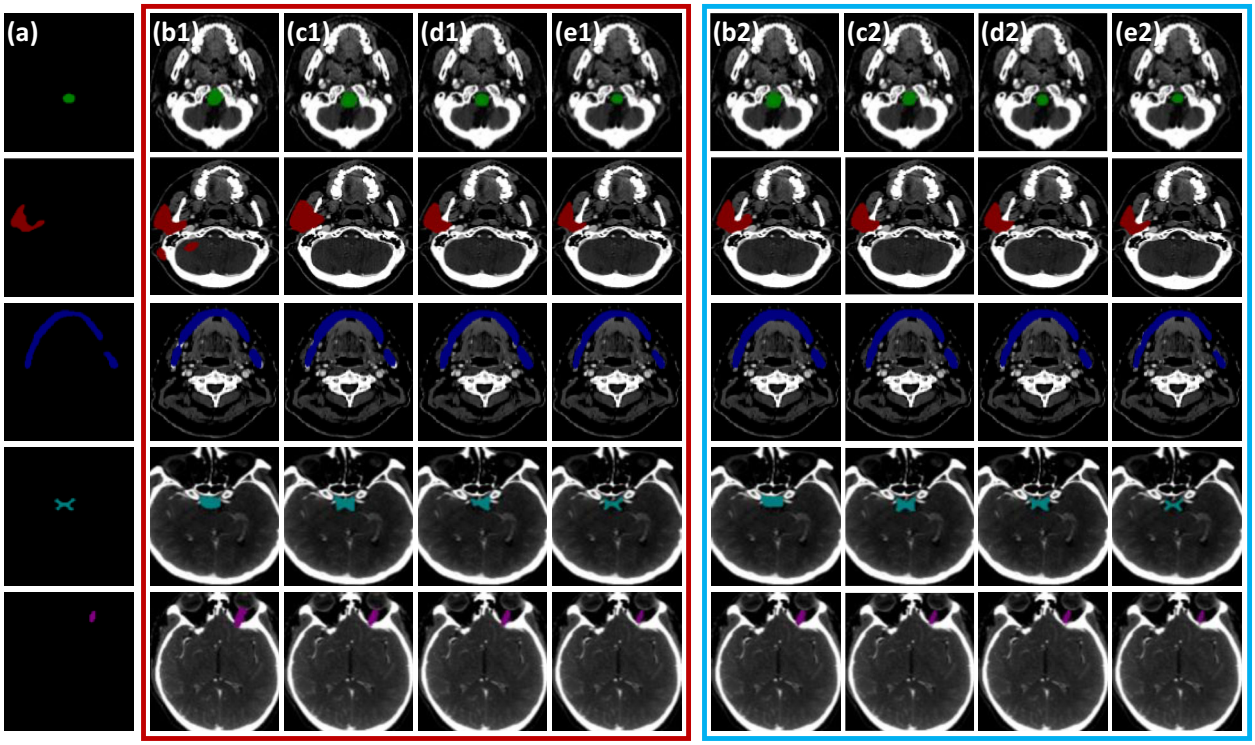

FIGURE 6
Horizontal visual comparison of PCG-Net with different state-of-the-art algorithms. Where the red box represents the segmentation result without a contrastive learning pre-training strategy, and the blue box represents the segmentation result with a contrastive learning pre-training strategy. **(A)** Ground truth. **(B)** U^{2}Net. **(C)** CPFNet. **(D)** MedT. **(E)** PCG-Net. To facilitate visual representation, we used different color masks to represent different organ-at-risks, where green mask is the brainstem, red mask is the parotid, blue mask is the mandible, cyan mask is the optic chiasm, and purple mask is the optic nerve.

Therefore, our segmentation accuracy was superior compared with other competitors, especially in the case of small volume OARs and blurred foreground and background boundaries.

5.3 Contrastive learning evaluation

The unsupervised strategy of contrastive learning was applied to the current main segmentation algorithms, including U^{2}Net (28), CPFNet (30), and MedT (31). All competitors were performing under the same computing environment and the same data enhancement throughout the experiment to ensure fair comparisons. The experimental algorithms were classified into two categories: one using contrastive learning pre-training strategy and the other without contrastive learning pre-training strategy. The overall results of the comparison of the gain of the four different main segmentation algorithms with difference in whether contrastive learning was imposed are shown in Table 3. After applying the contrastive learning strategy, the models showed slightly improved segmentation accuracy for large volume OARs. For example, for the brainstem and mandible, the mean DSC of the four models improved by 0.45% and 0.475%, respectively. The segmentation accuracy significantly improved for small volume OARs. For example, for optic nerve and optic chiasm, the mean DSC of the four models improved by 1.225% and 1.575% after using contrastive learning, respectively. This may be because the unsupervised paradigm of contrastive learning enables effective extraction of the similar features from large amounts of data to improve the neural network's weight distribution. The mean DSC values versus epoch for different OARs based on contrastive learning strategies using supervised tasks to fine-tune the four neural network weights is plotted in Figure 7. The accuracy of each algorithm reached the optimal value of the contrastive-free learning strategy after about 40 epochs. This fully demonstrated the feasibility of using contrastive learning to perform unsupervised training on large medical unlabeled samples and transferring the pre-trained model to supervised tasks for weight fine-tuning. This strategy greatly solved the problem of medical tasks with few annotated data. The experiment results further verified that contrastive learning has a strong generalization ability, which can find common-solution in distinct datasets with statistically significant differences to optimize feature extraction module weights. With the epoch gradually increasing, the accuracy of MedT and U^{2}Net gradually stabilizes, while the accuracy of CPFNet slightly decreases, which is probably caused by model overfitting. Compared with the competitors, the accuracy of PCG-Net has been steadily improving, and its mean DSC always remains at the highest level, which fully verifies the advanced performance of PCG-Net.

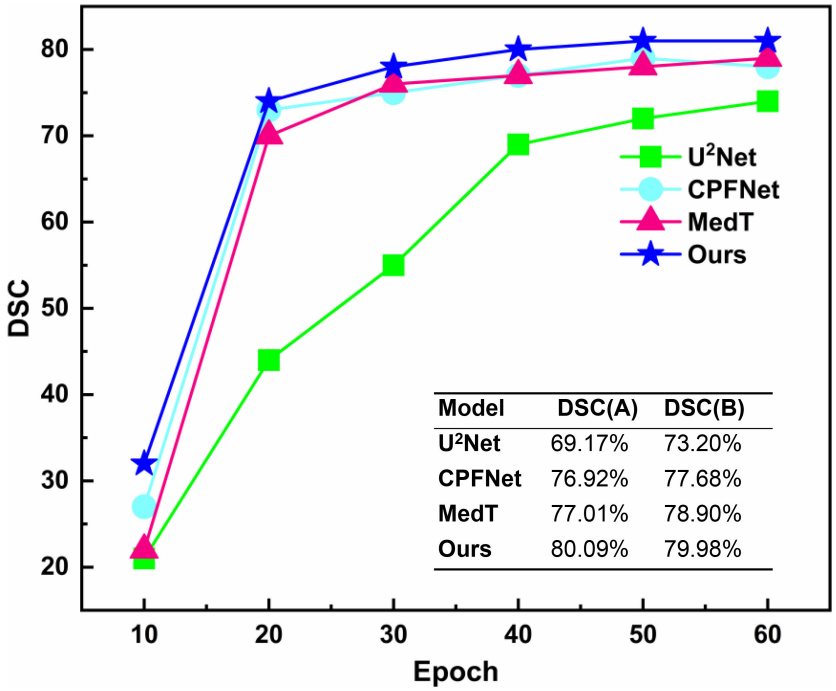

FIGURE 7
Mean DSC versus epoch for automatic head and neck organ-at-risks segmentation of the test datasets by different neural network models based on contrastive learning strategy. DSC(A) represents the mean DSC value of the head and neck organs-at-risks in the test datasets when different models were trained to the 40_th epoch under the contrastive pre-training strategy. DSC(B) represents the mean DSC values of the head and neck organ-at-risks in the test datasets when different models were trained to the end (150_th epochs) without the contrastive pre-training strategy.

5.4 Other medical assignments

The contrastive-learning-based PCG-Net achieved excellent results on the HN segmentation task, which can not only accurately delineate large volume OARs such as parotid gland and brainstem, but also accurately identify small volume samples such as optic chiasm and optic nerve. However, the HN segmentation tasks alone cannot fully demonstrate the superiority of PCG-Net. Therefore, three different medical image challenge tasks were chosen, including segmentation, classification, and object detection, to further validate the generalization ability of PCG-Net. For different downstream tasks, different decoders were used while ensuring the feature extraction module remaining constant. For example, in classification tasks, the progressive refinement decoder was replaced by the fully connected layer, and the final output was the mapping of category numbers. To perform the object detection task, the progressive refinement decoder was replaced by the YOLOV3 decoder, and output was in three different scales of detection windows to achieve object detection for different sizes. All experiments were performed in the same computing environment and data enhancement to ensure fairness.

5.4.1 Liver tumor segmentation

A horizontal comparison experiment for liver tumor segmentation was performed on the LiTS dataset, where the training, validation, and testing sets were divided with the ratio of 7:2:1, using SGD optimizer with momentum of 0.9 and linear scaling learning rate with weight decay of 0.0001, with focal-dice loss as loss function, batch size set to 32, epoch set to 150, using DSC, VOE, and ASSD as evaluation metrics. The LiTS dataset includes primary and secondary liver tumors with strong heterogeneity and diffuseness. Therefore, it can be fully verified whether the algorithm can effectively extract features from the region of interest to achieve end-to-end mapping under the circumstances of blurred boundaries, complex structure, diverse distribution, and grayscale diversity.

PCG-Net was compared with four currently popular segmentation methods, including SFF-Net (32), H-Dense UNet (33), and FAT-Net (34). The segmentation results of applying different algorithms on the LiTS dataset are shown in Table 4,

TABLE 4 Horizontal comparison experiment of liver tumor segmentation based on Lits dataset, where ↑ indicates the larger value the better, and ↓ indicates the smaller value the better.

	DSC (%)↑	VOE (%)↓	ASSD (mm) ↓
SFF-Net	61.3% ± 11.8%*	39.8% ± 14.3%**	1.885 ± 0.5*
H-Dense UNet	71.3% ± 10.9%**	25.7% ± 13.6%#	1.331 ± 0.3*
FAT-Net	72.3% ± 15.2%**	24.26% ± 14.1%***	1.371 ± 0.2*
PCG-Net	**73.6% ± 7.8%**	**21.19% ± 9.7%**	**1.118 ± 0.2**

Please note that "***" to indicate p< 0.05, "**" for p< 0.01, "*" for p< 0.001, and "#" for p > 0.05. The bold values denote the optimal result.

including accuracy and computational complexity evaluation metrics. The SFF-Net based on a multi-scale feature pyramid and feature fusion module obtained relatively accurate results for the large tumor (diameter larger than 10 mm) segmentation problem. However, the performance was unsatisfactory for the segmentation of small tumors (diameter less than 5 mm) and multiple tumors. The H-Dense UNet, which relies on the fusion of 2D features with 3D features to increase the spatial region of interest, achieved comparable performance to the FAT-Net method. However, both methods underperformed in edge-complex multi-tumor semantic segmentation problems. On the contrary, PCG-Net based on a parallel encoder, cascade graph module, and progressive refinement decoder can effectively reconstruct the dependencies between different features and achieve end-to-end mapping by layer-by-layer refinement. PCG-Net performed better than other competitors in general, with the highest mean DSC of 73.6%, and mean VOE and mean ASSD metrics of 21.19% and 1.118, respectively. Meanwhile, the parametric number of PCG-Net was lower than average, indicating PCG-Net reduced the computational complexity without losing segmentation accuracy. In addition, the visualization of comparison of segmentation results between different algorithms is demonstrated in Figure 8. For most samples with extremely complex blurred boundaries and diverse grayscales, PCG-Net still obtained the best segmentation results.

5.4.2 Lung nodule object detection

A horizontal comparison experiment for lung nodule object detection was performed on the LUNA16 dataset, where the training, validation, and testing sets were divided in 7:2:1, using an SGD optimizer with a momentum of 0.9 and linear scaling learning rate with weight decay of 0.0001, using EIoU as the loss function (35), with batch size set to 32 and epoch size set to 150. The model performance was evaluated by CPM competitive performance metrics. The LUNA16 lung nodule dataset is challenging for object detection because of the extremely complex brightness distribution and blurred boundaries. The YOLOV3 encoder was replaced with the PCG-Net encoder, Att-UNet encoder (36), U2Net encoder (28), ViT encoder (37), and Swin (29) encoder, respectively, to demonstrate the feature extraction capability of the PCG-Net encoder. The results of object detection

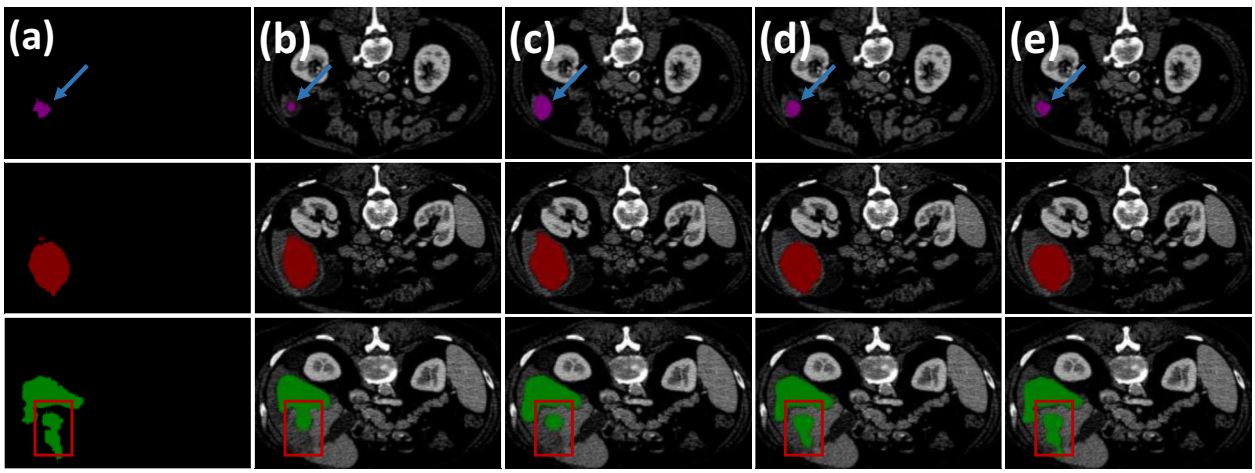

FIGURE 8
Visual comparison of PCG-Net on the LiTS dataset with different state-of-the-art methods. **(A)** Ground truth. **(B)** U^{2}Net. **(C)** SFF-Net. **(D)** H-Dense UNet. **(E)** PCG-Net. Three different types of tumors were selected to fully demonstrate PCG-Net's effectiveness: small tumors (purple mask), large tumors (red mask), and multiple tumors (green mask). The blue arrow highlights PCG-Net's ability to accurately identify the irregular boundary contours of small tumors compared to other algorithms, and the red box highlights PCG-Net's ability to correctly capture multiple tumors.

TABLE 5 Horizontal comparison experiment for lung nodule object detection based on the LUNA16 dataset.

Model	Number of FPs/scan (%)							CPM(%)↑
	A (%)	B (%)	C (%)	D (%)	E (%)	F (%)	G (%)	
Att-UNet Encoder	71.2%	81.1%	85.7%	88.6%	91.2%	93.3%	94.1%	86.5%
U^{2}Net Encoder	68.8%	72.6%	81.3%	86.5%	89.9%	93.0%	94.7%	83.8%
ViT Encoder	78.8%	87.3%	91.7%	92.2%	92.9%	93.6%	94.5%	90.1%
Swin Encoder	79.5%	87.8%	92.1%	92.6%	93.1%	93.7%	94.6%	90.4%
PCG-Net Encoder	**80.3%**	**87.9%**	**90.2%**	**93.2%**	**96.2%**	**97.7%**	**98.5%**	**92.0%**

In the table, A, B, C, D, E, F, and G represent the sensitivity of detection at an average number of false positives of 0.125, 0.25, 0.5, 1, 2, 4, and 8 in each group of CT images, respectively. For a fair comparison, we deploy the opponent's model locally, and train them employing the same preprocessing, optimizer, loss function, and training epochs, where ↑ indicates that the larger value the better. The bold values denote the optimal result.

applying different encoders on the LUNA16 dataset, including the sensitivity to the seven average number of false positives per scan and the corresponding computational complexity evaluation metrics, are shown in Table 5. The U2Net, which introduced U-shaped nested architecture with multi-level and multi-scale feature extraction modules, achieved more accurate object recognition results than AttU-Net. The ViT based on long-distance feature modeling had significantly higher computational complexity and slightly lower detection accuracy compared to the traditional feature extraction modules AttU-Net and U2Net. Swin alleviated the high computational complexity of ViT through the shift-window mechanism, hierarchical structure, and window self-attention. However, the results in Table 5 demonstrate that Swin still performed poorly on few-sample medical object detection tasks. PCG-Net can effectively solve the latter three problems by trainable positional bias and gated-axial transformer encoder, and alleviate the first problems by the parallel encoder. Therefore, through the parallel encoder and cascaded graph neural networks, it is capable to accurately capture and model local features and global context information, meanwhile reducing overfitting risks. It is observed from Table 5 that our algorithm performed better than other competitors, with the highest mean CPM at 92.0%.

5.4.3 Classification of blood cells

A horizontal comparison experiment for blood cell classification was performed on the BCCD dataset. The BCCD dataset includes four different types of cells: neutrophils, monocytes, lymphocytes, and eosinophils. Blood disease diagnosis usually involves classifying blood cell subtypes, having very important clinical significance. A four-classified fully connected layer was used as decoder, using ResNet50 (38), RepLKNet (39), ViT (36), and ConvNeXt (40) as encoder to verify the feature extraction capability of PCG-Net. Because of the few samples of the BCCD dataset, it is prone to overfitting when the BCCD dataset was directly used for training. Therefore, contrastive learning was employed to pre-train the encoder of five different models on the LIDC-IDRI dataset, then the BCCD dataset was used to fine-tune encoder weights. The training, validation, and testing sets were divided in the ratio of 7:2:1, using an SGD optimizer with a momentum of 0.9 and linear scaling learning rate with a weight decay of 0.0001, using cross entropy as the loss function, with batch size set to 32 and epoch size set to 150. The results of the blood cell classification task applying different encoders on the BCCD dataset are shown in Table 6, including accuracy and computational complexity evaluation metrics. Using large convolutional kernels enabled RepLKNet and ConvNeXt to increase the receptive field more efficiently than ResNet50, while avoiding optimization difficulties caused by the increase of model depth, therefore, the classification accuracy was significantly improved. However, large convolution kernels increased the computational complexity, which cannot balance accuracy and speed. The ViT, which is the classical classification architecture of the transformer, had mediocre performance, with no improvement in classification accuracy despite the increase in computational complexity. Our structure utilized small convolutional kernels of CNN to efficiently extract local semantic information, gated axial self-attention architecture to reduce computational complexity without losing receptive fields, and cascaded graph module as feature fusion architecture to achieve efficient information aggregation. It can be observed in Table 6 that PCG-Net achieved the highest scores under most evaluation metrics, especially the two major metrics, Accuracy and Spec, which reached 98.6% and 99.0%, respectively.

TABLE 6 Horizontal comparison experiment of blood cell classification based on BCCD dataset.

	ACC(%)↑	Spec(%)↑	Sens(%)↑
ResNet50	93.6% ± 1.9%*	79.3% ± 6.3%*	98.8% ± 1.3%**
RepLKNet	98.0% ± 0.8%***	97.1% ± 2.3%**	**98.4% ± 1.3%***
ViT	94.3% ± 1.7%*	96.6% ± 5.5%*	92.1% ± 1.1%**
ConvNext	98.3% ± 0.7%#	98.3% ± 0.9%*	98.2% ± 1.2%*
PCG-Net	**98.6% ± 0.3%**	**99.0% ± 1.0%**	98.3% ± 0.7%

For a fair comparison, we deploy the opponent's model locally, and train them employing the same preprocessing, optimizer, loss function, and training epochs, where ↑ indicates that the larger value the better. Please note that "**" to indicate $p< 0.05$, "**" for $p< 0.01$, "*" for $p< 0.001$, and "#" for $p > 0.05$. The bold values denote the optimal result.

6 Discussion

In this study, a Siamese-contrastive learning strategy was used to pre-train encoder weights on public datasets and transfer them to local tasks for fine-tuning. It can be seen from the results that this pre-training strategy can be used to fit local tasks by using prior knowledge of public datasets, which can be crucial in the case of sparse annotation samples. The essence of deep learning is extraction and generalization for large amounts of features. Annotated samples enable the model to extract more reliable information from datasets, however medical data require manual annotation by numerous professional physicians, which is extremely costly. Therefore, learning efficient visual representation without annotated samples is the focus of the medical task. Currently, the unsupervised tasks were mainly based on generative or contrastive learning. Generative learning, represented by self-encoders (41), generates or models pixels in the input space (42), yet the pixel-level generation consumes considerable computational resources. The contrastive learning method (43) uses the loss function similar to supervised tasks to optimize the weight distribution, which can autonomously learn the mapping relationships among large amounts of data and ignore the complex details of instances, therefore the optimization of model becomes simpler (44).

Encoder-decoder architectures have been widely used in medical artificial intelligence tasks, but most algorithms used a single type codec to extract features, such as UNet (45) for pure CNN architectures and MedT (31) for pure transformer architectures, thereby not being able to simultaneously capture local features and global contextual information. Fused CNN and transformer architectures such as Confomer (46) and CoTNet (47) are difficult to be applied directly in local datasets, although they have achieved state-of-the-art results in their fields, both requiring

pre-training with large amounts of data to fit the neural network. Other parallel encoding algorithms such as FAT-Net (34) have achieved state-of-the-art results in dermatological segmentation. However, FAT-Net does not employ an effective feature fusion method, only stacking the CNN's and transformer's high-dimensional semantic features at the bottom of the encoder, which ignores the importance of features under parallel encoders of different scales. In summary, those methods still failed to effectively fuse local features and global long-term dependencies. Furthermore, traditional transformer algorithms require enormous data, making it difficult for direct application to medical few-sample tasks. Therefore, most available methods still failed to accurately infer the small volume OARs of the lesion areas with blurred boundaries. To obtain better feature extraction capability, balance local information with global context information, and applicability to few-sample datasets, we integrated CNN and axial transformer branches for a parallel encoder, making local and global information supplement each other to achieve accurate feature extraction, where the transformer branch adopts cascaded axial architecture, which can alleviate the computational complexity (48) without losing spatially distant features, and effectively solve the problems of heavy expenses and resource consumption of traditional self-attention mechanism. The advantages were clearly demonstrated by the ablation studies and comparison experiments conducted in Section 5.1.

Although abundant local features and global contextual information were extracted by a parallel encoder, accurate target segmentation is impossible if they cannot be aggregated by an effective message-passing method. Therefore, a cascaded graph neural network model was used to refine the high-level relationship between two different feature spaces to improve the model representation. Extensive work have been done to improve segmentation performance by fusing semantic information under different feature spaces. For instance, DCA (49) directly stacked and spliced two features to improve the semantic representation, and FSSD (50) extracted various scale features from a different layer of the model for contact. However, these methods only focused on information transfer and ignored modeling and reasoning between different features, which makes them difficult to fully utilize features of different spatial resolutions or different semantic categories to overcome complex medical tasks. Numerous experiments have demonstrated GNNs to be sensitive to relational modeling and feature inference (51–53), so the cascaded graph neural network model used in this study enabled aggregating different feature information by learning powerful and dense feature embeddings. It is proved that this cascade graph model can capture detailed regions and overcome ambiguities by employing the complementary information of multi-level features.

Finally, a novel parallel multiscale progressive refinement graph neural network PCG-Net was proposed to achieve accurate OARs segmentation in the presence of unbalanced data and few annotated samples to assist physicians clinically. To evaluate the contribution of each module to the PCG-Net, ablation studies were performed for each module to demonstrate their effectiveness. Comparing with the advanced segmentation algorithms U^2Net (28), SFF-Net (32), H-Dense UNet (33), and FAT-Net (34), PCG-Net showed stronger feature extraction capability and robustness. To verify PCG-Net's fitting ability for different tasks, the encoder of PCG-Net was applied to the three main vision downstream tasks respectively. In the context of head and neck segmentation tasks, when compared to the commonly used medical image segmentation algorithm, MedT, PCG-Net demonstrates notable improvements in the segmentation of small organs, specifically the optic nerve and optic chiasm. PCG-Net achieves a 1.08% increase in DSC, a 1.5% improvement in Recall, a 1.5% reduction in HD, and a 1.9% decrease in ASD. Furthermore, in various downstream medical image tasks, PCG-Net consistently delivers outstanding results. For instance, in the context of liver cancer segmentation, PCG-Net outperforms all listed models, achieving a DSC, VOE, and ASSD of 73.6%, 21.19%, and 1.118, respectively. In comparison to SSF-Net, PCG-Net exhibits substantial improvements of 16%, 46.7%, and 40.6%, significantly enhancing liver cancer recognition capabilities. The results proved that PCG-Net had strong generalization ability for different tasks. Note that the encoder of PCG-Net can be used as a backbone feature extraction module for different medical tasks in different datasets. Meanwhile, the pre-training approach based on contrastive learning can effectively overcome the weakness of insufficient annotated data in medical tasks, and this may be the priority method for processing medical tasks in the future.

The PCG-Net proposed in this study still has limitations. Similar to most existing neural network models, PCG-Net can only be trained for specific tasks due to local computing power and algorithmic constraints. In practical applications, it requires pre-trained models with different data to handle different downstream tasks, which greatly increases resource consumption and workload. In addition, contrastive learning can significantly reduce the amount of annotated data required by neural networks, however, during the model training process, it still requires fine-tuning model weights with annotated samples to fit the ground truth, which cannot completely achieve unsupervised training. In the future work, we will focus on the study of model generalization and unsupervised tasks.

7 Conclusion

A PCG-Net was proposed to solve the problems of few clinical medical images, lack of annotated data, and difficulty in segmenting small volume OARs. Using the contrastive learning pre-training strategy, the local task was fitted by prior knowledge from large unannotated datasets, which greatly alleviates the model robustness problem caused by sample scarcity. Unlike traditional single-branch encoders, our parallel encoder can infer semantic features from two different dimensions, effectively extracting global contextual information while preserving local receptive fields. In addition, the cascade graph architecture could allow better utilization of abundant complementary information in multi-level features compared to traditional fusion methods. Extensive experiments were conducted to evaluate PCG-Net on different medical tasks and compare it horizontally with the current main approaches in

different downstream tasks, further demonstrating the excellent inference performance and generalization capability of PCG-Net. It is believed that the novel design in this paper could be effectively used for clinical applications and treatment.

Data availability statement

The raw data supporting the conclusions of this article will be made available by the authors, without undue reservation.

Ethics statement

Written informed consent was obtained from the individual(s) for the publication of any potentially identifiable images or data included in this article.

Author contributions

SL: Conceptualization, Methodology, Writing – original draft, Writing –review and editing. CW: Conceptualization, Methodology, Writing – original draft, Writing –review and editing. YD: Conceptualization, Methodology, Writing – original draft, Writing –review and editing. XX: Conceptualization, Methodology, Funding acquisition, Writing –review and editing. WW: Conceptualization, Funding acquisition, Project administration, Methodology, Writing – original draft, Writing – review and editing. XY: Methodology. XW: Methodology, Writing – review and editing. CM: Methodology, Writing –review and editing. BZ: Conceptualization, Methodology, Writing – original draft, Writing –review and editing, Project administration.

Funding

This study was supported by the National Natural Science Foundation of China (No.12075095), the Natural Science Foundation of China (No.U22A20259), the Health Commission of Hubei Province scientific research project (No.WJ2021M192), the Natural Science Foundation of Hubei Province (No.2022CFB938), and the Shenzhen Basic Science Research (No.JCYJ20200109110006136).

Conflict of interest

The authors declare that the research was conducted in the absence of any commercial or financial relationships that could be construed as a potential conflict of interest.

Publisher's note

Supplementary material

The Supplementary Material for this article can be found online at: https://www.frontiersin.org/articles/10.3389/fonc.2023.1177788/full#supplementary-material

References

1. Chow LQM. Head and neck cancer. *N Engl J Med* (2020) 382(1):60–72. doi: 10.1056/NEJMra1715715

2. Kosmin M, Ledsam J, Romera-Paredes B, Mendes R, Moinuddin S, de Souza D, et al. Rapid advances in auto-segmentation of organs at risk and target volumes in head and neck cancer. *Radiother Oncol* (2019) 135:130–40. doi: 10.1016/j.radonc.2019.03.004

3. Voet PW, Dirkx ML, Teguh DN, Hoogeman MS, Levendag PC, Heijmen BJ. Does atlas-based autosegmentation of neck levels require subsequent manual contour editing to avoid risk of severe target underdosage? A dosimetric analysis. *Radiother Oncol* (2011) 98(3):373–7. doi: 10.1016/j.radonc.2010.11.017

4. Chen X, Sun S, Bai N, Han K, Liu Q, Yao S, et al. A deep learning-based auto-segmentation system for organs-at-risk on whole-body computed tomography images for radiation therapy. *Radiother Oncol* (2021) 160:175–84. doi: 10.1016/j.radonc.2021.04.019

5. Cabezas M, Oliver A, Lladoí X, Freixenet J, Cuadra MB. A review of atlas-based segmentation for magnetic resonance brain images. *Comput Methods Programs BioMed* (2011) 104(3):e158–77. doi: 10.1016/j.cmpb.2011.07.015

6. Cuadra MB, Duay V, Iran JP. *Atlas-Based Segmentation. Handbook of Biomedical Imaging*. USA: Springer (2015) p. 221–44.

7. Hoogeman MS, Han X, Teguh DN, Voet P, Nowak P, Wolf T, et al. Atlas-based auto-segmentation of CT images in head and neck cancer: what is the best approach? *Int J Radiat Oncol Biol Phys* (2008) 72:S591. doi: 10.1016/j.ijrobp.2008.06.196

8. Tsuji SY, Hwang A, Weinberg V, Yom SS, Quivey JM, Xia P. Dosimetric evaluation of automatic segmentation for adaptive IMRT for head-and-neck cancer. *Int J Radiat Oncol Biol Phys* (2010) 77(3):707–14. doi: 10.1016/j.ijrobp.2009.06.012

9. Chen X, Sun S, Bai N, Han K, Liu Q, Yao S, et al. A deep learning-based auto-segmentation system for organs-at-risk on whole-body computed tomography images for radiation therapy. *Radiother Oncol* (2021) 160:175–84. doi: 10.1016/j.radonc.2021.04.019

10. Vrtovec T, Močnik D, Strojan P, Pernuš F, Ibragimov B. Auto-segmentation of organs at risk for head and neck radiotherapy planning: from atlas-based to deep learning methods. *Med Phys* (2020) 47(9):e929–50. doi: 10.1002/mp.14320

11. Wang J, Lu J, Qin G, Shen L, Sun Y, Ying H, et al. A deep learning-based autosegmentation of rectal tumors in MR images. *Med Phys* (2018) 45(6):2560–4. doi: 10.1002/mp.12918

12. Cha KH, Hadjiiski LM, Samala RK, Chan HP, Cohan RH, Caoili EM, et al. Bladder cancer segmentation in CT for treatment response assessment: application of deep-learning convolution neural network—a pilot study. *Tomography* (2016) 2 (4):421–9. doi: 10.18383/j.tom.2016.00184

13. Wang B, Lei Y, Tian S, Wang T, Liu Y, Patel P, et al. Deeply supervised 3D fully convolutional networks with group dilated convolution for automatic MRI prostate segmentation. *Med Phys* (2019) 46(4):1707–18. doi: 10.1002/mp.13416

14. Men K, Chen X, Zhang Y, Zhang T, Dai J, Yi J, et al. Deep deconvolutional neural network for target segmentation of nasopharyngeal cancer in planning computed tomography images. *Front Oncol* (2017) 7:315. doi: 10.3389/fonc.2017.00315

15. Lin L, Dou Q, Jin YM, Zhou GQ, Tang YQ, Chen WL, et al. Deep learning for automated contouring of primary tumor volumes by MRI for nasopharyngeal carcinoma. *Radiology* (2019) 291(3):677–86. doi: 10.1148/radiol.2019182012

16. Han S, Kang HK, Jeong JY, Park MH, Kim W, Bang WC, et al. A deep learning framework for supporting the classification of breast lesions in ultrasound images. *Phys Med Biol* (2017) 62(19):77. doi: 10.1088/1361-6560/aa82ec

17. Ibragimov B, Xing L. Segmentation of organs-at-risks in head and neck CT images using convolutional neural networks. *Med Phys* (2017) 44(2):547–57. doi: 10.1002/mp.12045

18. Sun Y, Shi H, Zhang S, Wang P, Zhao W, Zhou X, et al. Accurate and rapid CT image segmentation of the eyes and surrounding organs for precise radiotherapy. *Med Phys* (2019) 46(5):2214–22. doi: 10.1002/mp.13463

19. Zhu W, Huang Y, Zeng L, Chen X, Liu Y, Qian Z, et al. AnatomyNet: Deep learning for fast and fully automated whole-volume segmentation of head and neck anatomy. *Med Phys* (2019) 46(2):576–89. doi: 10.1002/mp.13300

20. Razzak MI, Naz S, Zaib A. Deep learning for medical image processing: Overview, challenges and the future. *Classification BioApps* (2018), 323–50. doi: 10.1007/978-3-319-65981-7_12

21. Huang H, Lin L, Tong R, Hu H, Zhang Q, Iwamoto Y, et al. Unet 3+: A full-scale connected unet for medical image segmentation, in: *ICASSP 2020-2020 IEEE International Conference on Acoustics, Speech and Signal Processing (ICASSP)*. (2020) IEEE, 1055–9.

22. Wang J, Hu J, Song Y, Wang Q, Zhang X, Bai S, et al. VMAT dose prediction in radiotherapy by using progressive refinement UNet. *Neurocomputing* (2022) 488:528–39. doi: 10.1016/j.neucom.2021.11.061

23. Sudre CH, Li W, Vercauteren T, Ourselin S, Jorge Cardoso M. Generalised dice overlap as a deep learning loss function for highly unbalanced segmentations. In: *Deep learning in medical image analysis and multimodal learning for clinical decision support*. Cham: Springer International Publishing (2017). p. 240–8.

24. Lin T-Y, Goyal P, Girshick R, He K, Dollár P. (2017). Focal loss for dense object detection. In: *Proceedings of the IEEE international conference on computer vision*, 2980–8.

25. Clark K, Vendt B, Smith K, Freymann J, Kirby J, Koppel P, et al. The Cancer Imaging Archive (TCIA): maintaining and operating a public information repository. *J Digital Imaging* (2013) 26:1045–57. doi: 10.1007/s10278-013-9622-7

26. Priya G, Piotr D, Ross G, Pieter N, Lukasz W, Aapo K, et al. Accurate, large minibatch SGD: Training ImageNet in 1 hour. *arXiv preprint arXiv:1706.02677* (2017).

27. Loshchilov I, Frank H. Sgdr: Stochastic gradient descent with warm restarts. *Proceedings of the 5th Int. Conf. Learning Representations* (2016).

28. Qin X, Zhang Z, Huang C, Dehghan M, Zaiane OR, Jagersand M. U2-Net: Going deeper with nested U-structure for salient object detection. *Pattern Recognit* (2020) 106:107404. doi: 10.1016/j.patcog.2020.107404

29. Liu Z, Lin Y, Cao Y, Hu H, Wei Y, Zhang Z, et al. Swin transformer: Hierarchical vision transformer using shifted windows. In: *Proceedings of the IEEE/CVF International Conference on Computer Vision*. (2021) 10012–22.

30. Feng S, Zhao H, Shi F, Cheng X, Wang M, Ma Y, et al. CPFNet: Context pyramid fusion network for medical image segmentation, in: *IEEE transactions on medical imaging*. (2020) 39 (10), 3008–18.

31. Valanarasu JMJ, Oza P, Hacihaliloglu I, Patel VM. Medical transformer: Gated axial-attention for medical image segmentation. In: *International Conference on Medical Image Computing and Computer-Assisted Intervention*. Cham: Springer International Publishing (2021).

32. Liu T, Liu J, Ma Y, He J, Han J, Ding X, et al. Spatial feature fusion convolutional network for liver and liver tumor segmentation from CT images. *Med Phys* (2021) 48 (1):264–72. doi: 10.1002/mp.14585

33. Li X, Chen H, Qi X, Dou Q, Fu CW, Heng PA. H-DenseUNet: hybrid densely connected UNet for liver and tumor segmentation from CT volumes. *IEEE Trans Med Imaging* (2018) 37(12):2663–74. doi: 10.1109/TMI.2018.2845918

34. Wu H, Chen S, Chen G, Wang W, Lei B, Wen Z. FAT-Net: Feature adaptive transformers for automated skin lesion segmentation. *Med Image Anal* (2022) 76:102327. doi: 10.1016/j.media.2021.102327

35. Wang Z, **n J, Sun P, Lin Z, Yao Y, Gao X. Improved lung nodule diagnosis accuracy using lung CT images with uncertain class. *Comput Methods Programs Biomed* (2018) 162:197–209. doi: 10.1016/j.cmpb.2018.05.028

36. Schlemper J, Oktay O, Schaap M, Heinrich M, Kainz B, Glocker B, et al. Attention gated networks: Learning to leverage salient regions in medical images. *Med Image Anal* (2019) 53:197–207. doi: 10.1016/j.media.2019.01.012

37. Dosovitskiy A, Beyer L, Kolesnikov A, Weissenborn D, Zhai X, Unterthiner T, et al. An image is worth 16x16 words: Transformers for image recognition at scale. *arXiv preprint arXiv:2010.11929* (2020).

38. He K, Zhang X, Ren S, Sun J. Deep residual learning for image recognition, in: *Proceedings of the IEEE conference on computer vision and pattern recognition*. (2016) 770–8.

39. Ding X, Zhang X, Han J, Ding G. Scaling up your kernels to 31x31: Revisiting large kernel design in cnns. In: *Proceedings of the IEEE/CVF Conference on Computer Vision and Pattern Recognition* (2022) 11963–75.

40. Liu Z, Mao H, Wu CY, Feichtenhofer C, Darrell T, **e S. A convnet for the 2020s. In: *Proceedings of the IEEE/CVF Conference on Computer Vision and Pattern Recognition*. (2022) 11976–86.

41. Lyu Z, Ali S, Breazeal C. Introducing Variational Autoencoders to High School Students. In *Proceedings of the AAAI Conference on Artificial Intelligence*. (2022) 36 (11), 12801–9. doi: 10.4324/9780429470790-1

42. Sewak M, Sanjay K, Hemant R. An overview of deep learning architecture of deep neural networks and autoencoders. *J Comput Theor Nanosci* (2020) 17:182–8. doi: 10.1166/jctn.2020.8648

43. Caron M, Misra I, Mairal J, Goyal P, Bojanowski P, Joulin A. Unsupervised learning of visual features by contrasting cluster assignments. *Adv Neural Inf Process Syst* (2020) 33:9912–24.

44. Chen X, Kaiming H. Exploring simple siamese representation learning. In: *Proceedings of the IEEE/CVF Conference on Computer Vision and Pattern Recognition*. (2021) 15750–8.

45. Ronneberger O, Philipp F, Thomas B. U-net: Convolutional networks for biomedical image segmentation. In: *International Conference on Medical image computing and computer-assisted intervention*. Cham: Springer (2015).

46. Peng Z, Huang W, Gu S, **e L, Wang Y, Jiao J, et al. Conformer: Local features coupling global representations for visual recognition, in: *Proceedings of the IEEE/CVF International Conference on Computer Vision*. (2021) 367–76.

47. Li Y, Yao T, Pan Y, Mei T. Contextual transformer networks for visual recognition. *IEEE Trans Pattern Anal Mach Intell* (Cham: Springer International Publishing) (2022) 45 (2), 1489–500. doi: 10.1109/TPAMI.2022.3164083

48. Wang H, Zhu Y, Green B, Adam H, Yuille A, Chen LC. Axial-deeplab: Stand-alone axial-attention for panoptic segmentation. In: *European conference on computer vision*. Cham: Springer International Publishing (2020) 108–26.

49. Chaib S, Liu H, Gu Y, Yao H. Deep feature fusion for VHR remote sensing scene classification. *IEEE Trans Geosci Remote Sens* (2017) 55(8):4775–84. doi: 10.1109/TGRS.2017.2700322

50. Li Z, Fuqiang Z. FSSD: feature fusion single shot multibox detector. *arXiv preprint arXiv* (2017) 1712:00960.

51. Xu K, Hu W, Leskovec J, Jegelka S. How powerful are graph neural networks? *arXiv preprint arXiv:1810.00826* (2018).

52. Zhao L, Peng X, Tian Y, Kapadia M, Metaxas DN. (2019). Semantic graph convolutional networks for 3d human pose regression. In: *Proceedings of the IEEE/CVF conference on computer vision and pattern recognition*, 3425–35.

53. Chen Y, Rohrbach M, Yan Z, Shuicheng Y, Feng J, Kalantidis Y. (2019). Graph-based global reasoning networks, in: *Proceedings of the IEEE/CVF Conference on Computer Vision and Pattern Recognition*, 433–42.

frontiers | Frontiers in Oncology

TYPE Original Research
PUBLISHED 25 October 2023
DOI 10.3389/fonc.2023.1168995

OPEN ACCESS

EDITED BY
Giuseppe Carlo Iorio,
University of Turin, Italy

REVIEWED BY
Giuseppe Danilo Di Stasio,
Independent Researcher, Caserta, Italy
Wei Huang,
Shandong University, China

*CORRESPONDENCE
Xiaoxue Xie
xiexiaoxue@hnca.org.cn
Zijian Zhang
wanzzj@csu.edu.cn

†These authors share first authorship

RECEIVED 18 February 2023
ACCEPTED 12 September 2023
PUBLISHED 25 October 2023

CITATION
Huang Q, Yang C, Pang J, Zeng B, Yang P, Zhou R, Wu H, Shen L, Zhang R, Lou F, Jin Y, Abdilim A, Jin H, Zhang Z and Xie X (2023) CT-based dosiomics and radiomics model predicts radiation-induced lymphopenia in nasopharyngeal carcinoma patients.
Front. Oncol. 13:1168995.
doi: 10.3389/fonc.2023.1168995

CT-based dosiomics and radiomics model predicts radiation-induced lymphopenia in nasopharyngeal carcinoma patients

Qingfang Huang[1,2†], Chao Yang[3,4†], Jinmeng Pang[1,2], Biao Zeng[1,2], Pei Yang[1,2], Rongrong Zhou[3,5], Haijun Wu[3,5], Liangfang Shen[3,5], Rong Zhang[1,2], Fan Lou[1,2], Yi Jin[1,2], Albert Abdilim[1,2], Hekun Jin[1,2], Zijian Zhang[3,5*] and Xiaoxue Xie[1,2*]

[1]Department of Radiation Oncology Hunan Cancer Hospital/The Affiliated Hospital of Xiangya School of Medicine, Central South University Changsha, Hunan, China, [2]Key Laboratory of Translational Radiation Oncology, Department of Radiation Oncology, Hunan Cancer Hospital, Changsha, Hunan, China, [3]Department of Radiation Oncology, Xiangya Hospital, Central South University, Changsha, Hunan, China, [4]College of Physics and Electronic Science, Shandong Normal University, Jinan, China, [5]National Clinical Research Center for Geriatric Disorders, Xiangya Hospital, Central South University, Changsha, China

Purpose: This study aims to develop and validate a model predictive for the incidence of grade 4 radiation-induced lymphopenia (G4RIL), based on dosiomics features and radiomics features from the planning CT of nasopharyngeal carcinoma (NPC) treated by radiation therapy.

Methods: The dataset of 125 NPC patients treated with radiotherapy from August 2018 to March 2019 was randomly divided into two sets—an 85-sample training set and a 40-sample test set. Dosiomics features and radiomics features of the CT image within the skull bone and cervical vertebrae were extracted. A feature selection process of multiple steps was employed to identify the features that most accurately forecast the data and eliminate superfluous or insignificant ones. A support vector machine learning classifier with correction for imbalanced data was trained on the patient dataset for prediction of RIL (positive classifier for G4RIL, negative otherwise). The model's predictive capability was gauged by gauging its sensitivity (the likelihood of a positive test being administered to patients with G4RIL) and specificity in the test set. The area beneath the ROC curve (AUC) was utilized to explore the association of characteristics with the occurrence of G4RIL.

Results: Three clinical features, three dosiomics features, and three radiomics features exhibited significant correlations with G4RIL. Those features were then used for model construction. The combination model, based on nine robust features, yielded the most impressive results with an ACC value of 0.88 in the test set, while the dosiomics model, with three dosiomics features, had an ACC value

of 0.82, the radiomics model, with three radiomics features, had an ACC value of 0.82, and the clinical model, with its initial features, had an ACC value of 0.6 for prediction performance.

Conclusion: The findings show that radiomics and dosiomics features are correlated with the G4RIL of NPC patients. The model incorporating radiomics features and dosiomics features from planning CT can predict the incidence of G4RIL in NPC patients.

KEYWORDS

radiation-induced lymphopenia, nasopharyngeal carcinoma, radiomics, dosiomics, machine learning

Introduction

RT, the primary treatment for nasopharyngeal carcinoma, has been found to provide a satisfactory 5-year overall survival rate (OS) (1). Although RT is locally targeted at the tumor and damages DNA in the cells to suppress tumor growth, it unavoidably exposes normal tissues to some radiation and causes complications (2). One of the common side effects induced by RT is lymphopenia. The toxicity of radiotherapy, as evidenced by increasing evidence, has been identified as radiation-induced lymphopenia (RIL) (3) and has been reported to be a detrimental prognostic factor in those receiving radiotherapy for various solid tumors, including NPC (4–6).

The treatment strategy for cancer patients undergoing radiation therapy must take into account the issue of minimizing the occurrence of RIL. Current studies have made some efforts to explore possible factors related to RIL, including the dose–volume histogram (DVH) of lymphocyte-related organs at risk (LOARs) (7). Adults' primary hematopoiesis site is the bone marrow, with the pelvis, cervical vertebrae, thoracic vertebrae, lumbar vertebrae, sacrum, skull, sternum, and ribs/clavicle contributing around 25%, 4%, 20%, 17%, 9%, 3%, 3%, and 9%, respectively (8). The elimination of resident lymphocytes and progenitor cells in bone marrow is likely a factor in lymphopenia. It was found that the relative volume of sternum bone marrow irradiated by more than 20 Gy could obviously affect the peripheral blood lymphocytes in patients with ESCC (9). WU et al. (10) found that there was a significant association between lymphopenia of grade 3 or higher and the radiation doses received by the thoracic vertebrae and ribs in patients with esophageal cancer who underwent neoadjuvant chemoradiotherapy. Specifically, they observed a correlation between lymphopenia and the average dose and V5-30 of the thoracic vertebrae, as well as the average dose and V5-20 of the ribs. Sini et al. (11) found a correlation between elevated BM V40 and an increased risk of acute grade 3 or late grade 2 lymphopenia in prostate cancer patients treated with whole-pelvis RT. However, no study has been conducted to identify dosimetry factors for RIL in NPC patients to date.

It has been realized that the dose–volume factors are only discrete points on the DVH curve and cannot take full advantage of the information deeply concealed in dose distributions. The 3D dose distribution's dosiomics (dose shape) features, extracted with great optimism, surpass the restrictions of the DVH curve and uncover many of the hidden spatial features of the dose distribution (12). Dosiomics is born directly as an extension of radiomics, which refers to the automatic extraction of quantitative imaging features to develop predictive models (13). The usability of the dosiomics features' granularity and quantity of data, in comparison to standard parameters such as DVH, DVH metrics, and visual assessment of the 3D dose distribution, could potentially be more advantageous in supporting clinical decisions. Dosiomics has been shown to be useful in predicting radiation therapy response in several studies (14, 15). However, neither radiomics nor dosiomics biomarkers for RIL prediction in NPC patients have ever been developed to date.

In this study, we first used radiomics and dosiomics analysis to predict RIL incidence in NPC patients. In the dataset of 125 NPC patients who had undergone radiotherapy, the performance of prediction models, based on dosiomics, radiomatics, clinical factors, and all other factors was assessed and compared.

Materials and methods

The workflow diagram for this study is shown in Figure 1. We extracted data from records of patients who received definitive

Abbreviations: RT, radiotherapy; NPC, nasopharyngeal carcinoma; OS, overall survival; DVH, dose–volume histogram; LOARs, lymphocyte-related organs at risk; HIS, hospital information system; VMAT, volumetric-modulated arc therapy; IMRT, intensity-modulated radiation therapy; TPS, treatment planning systems; OARs, organs at risk; G4RIL, grade 4 RT-induced lymphopenia; ROI, region of interest; GLCM, Gray Level Co-occurrence Matrix; GLRLM, Gray Level Run Length Matrix; GLSZM, Gray Level Size Zone Matrix; GLDM, Gray Level Dependence Matrix; LASSO, least absolute shrinkage and selection operator; VIF, variance inflation factor; RFE, recursive feature elimination; SVM, support vector machine; SMOTE, Synthetic Minority Over-Sampling Technique; AUC, the area under the curve; ACC, accuracy; MSE, mean squared error; CI, confidence interval; ROC, the receiver operating characteristic; CV, cross-validation.

10.3389/fonc.2023.1168995

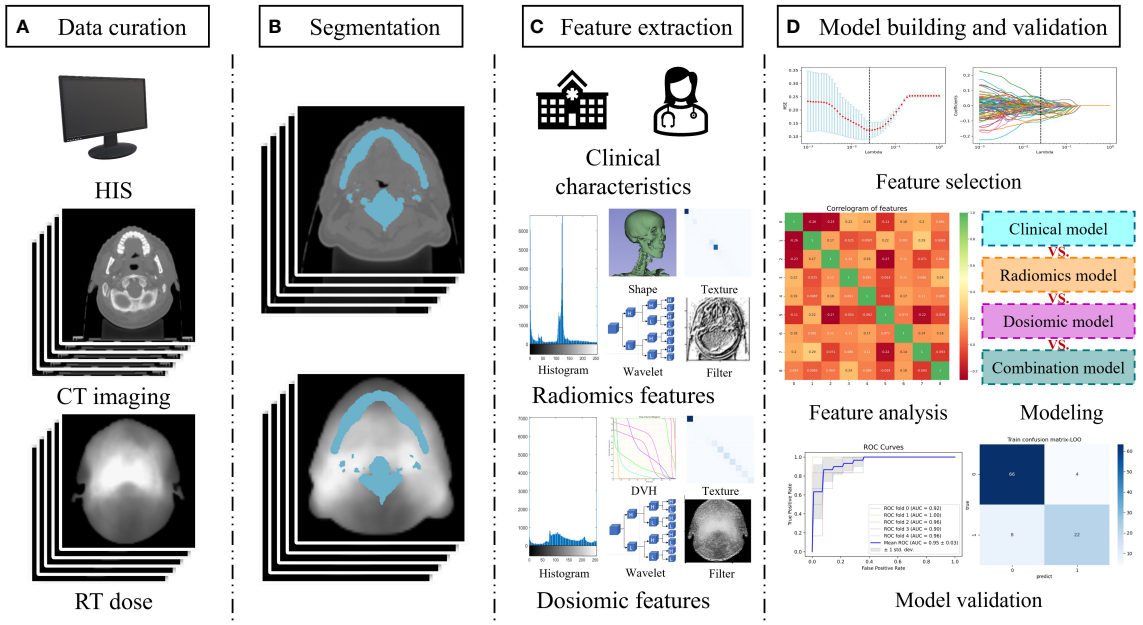

FIGURE 1
Study workflow overview. **(A)** Data acquisition; **(B)** Segmentation of the region of interest by radiologists; **(C)** Feature extraction including clinical characteristics, radiomics feature, and dosiomic feature; **(D)** Model building and validation. Abbreviation: HIS, hospital information system; DVH, dose volume histogram.

radiation therapy (with or without chemotherapy) for biopsy-proven nasopharyngeal cancer between August 2018 and March 2019. Exclusion criteria included planned total radiation doses other than 70–74 Gy, split-course RT, simultaneous irradiation of a second primary tumor, missing records in baseline blood sample data or less than 5-week-documented ALC values during the treatment, and the unavailability of planning CT or planned biological dose maps.

Treatment and endpoint

The Varian-600CD linear accelerator (Varian Medical Systems, Palo Alto, CA, USA) was utilized to administer volumetric-modulated arc therapy (VMAT) or intensity-modulated radiation therapy (IMRT) to all patients, with a dose of 70–74 Gy in 31–33 fractions. The RT plans were designed on Eclipse treatment planning system (TPS) (Varian Medical Systems, Palo Alto, CA). CT datasets with a 3-mm-slice thickness can be employed in either the Madison, WI, USA-based Pinnacle3 (v9.2) or the Philips Fitchburg, WI, USA-based TPS treatment planning systems. The grid size (spatial resolution of the dose distribution) in these two planning systems was 0.3 $cm^3 \times 0.3\ cm^3 \times 0.3\ cm^3$. The beam energy for all plans was 6 MV, and the dose rate in Varian-600CD is 600 MU/min. The ultimate aim of treatment planning was to ensure a consistent and sufficient dose was delivered to the PTV and to minimize the dose to organs at risk. All patients were treated according to the principles of NPC treatment at our institute.

The endpoint of this study is the occurrence of grade 4 RT-induced lymphopenia (G4RIL), which was defined as an ALC of less than 200 cells/μL during and immediately following the course of RT.

Delineation of ROI

This study considers the region of interest (ROI) to be the skull bone and cervical vertebrae, excluding GTV. The ROI was retrospectively delineated on plan CT with the bone windows (W2000Hu, L500Hu) and modified layer by layer with the soft tissue window (W250Hu, L50Hu). After a decade of expertise in radiation oncology, the CT images were manually segmented, and the outcomes were then evaluated by a senior radiologist. The ROIs of the CT images were all manually segmented using ITK-SNAP software (version 3.8.0; www.itksnap.org).

Radiomics feature extraction

The incorporated CT images were normalized before extracting features. We extracted 1,734 radiomics features from ROI using PyRadiomics (Version 3.0.1, https://pyradiomics.readthedocs.io/). The original features, such as shape, first order, texture, Laplacian of Gaussian, wavelet, logarithm, gradient, square root, exponential, and 3D Local Binary Pattern, are all included in the io/matrix. Texture features include the Gray Level Co-occurrence Matrix (GLCM), Gray Level Run Length Matrix (GLRLM), Gray Level

Size Zone Matrix (GLSZM), and Gray Level Dependence Matrix (GLDM).

Dosiomics feature extraction

Normalize before extracting the dosiomics feature. After normalization, we used PyRadiomics (Version 3.0.1, https://pyradiomics.readthedocs.io/). From the dose distribution, the dosiomics features of the ROI can be extracted. A total of 1,476 dosiomics features were extracted from the ROI of the dose distribution, which contained 100 original features and 1,376 filtered features. Shape, first order, texture, Laplacian of Gaussian, wavelet, gradient, square root, logarithm, and exponential features are all extracted from the dosiomics. Texture features include GLDM, GLCM, GLRLM, and GLSZM.

Feature selection

The selection of features was done to prevent overfitting, as the amount of extracted features is far greater than the amount of patients. In this study, we used a multistep-by-step feature selection method for the extracted radiomics features and dosiomics features. Utilizing a *t*-test to detect features with noteworthy distinctions, we initiated the feature selection process. Subsequently, the least absolute shrinkage and selection operator (LASSO) algorithm was applied to eliminate features that had regression coefficients that decreased to nothing as the penalty rose. Lastly, the variance inflation factor (VIF) was employed in the third step of feature selection to eliminate features with multicollinearity. Recursive feature elimination (RFE) based on support vector machines (SVM) is employed in the fourth step of feature selection, allowing for the assessment of feature prediction performance and the selection of features with superior prediction performance for modeling through iterative construction of the model. We used RFE to select clinical features with better predictive performance for modeling analysis in this study.

Model construction and validation

The sample sizes of the two cohorts in this study were unbalanced, with the number of G4 RIL patients being much lower than the other cohort of G2–3 RIL patients. By utilizing the Borderline Synthetic Minority Over-Sampling Technique (SMOTE) algorithm, we augmented the G4 RIL patients, thereby achieving a more balanced sample size (16).

Before building the classification model, each feature extracted is normalized. The study builds predictive models based on SVM. We constructed a multivariate clinical model, a radiomics model, a dosiomics model, and a combination model that incorporated clinical, radiomics, and dosiomics components.

In this study, data enhancement was conducted on the training set in order to enhance the classification performance of the model. To assess the model's performance, we split the test set into five subsets, four of which were used for training and one for testing. To validate the training set, fivefold or 10-fold cross-validation was conducted. After five repetitions of the process, the model's performance was assessed by the mean. The 10-fold cross-validation process was comparable to the fivefold cross-validation process. We assessed the performance of each classification model by means of the receiver operating characteristic (ROC) curve, the area under the curve (AUC), accuracy (ACC), precision, sensitivity, and specificity metrics on both the training and test sets. By employing the DeLong test, we compared the statistical disparities between the various ROC curves.

Statistical analysis

Using IBM SPSS Statistics (version 25; IBM Corporation, Armonk, NY, USA), a statistical analysis was conducted, utilizing Python (version 3.7.3, https://www.python.org) and R (https://cran.r-project.org/). The Spearman rank correlation was used to evaluate the correlation of features. The ROC curves between the different models were tested using the DeLong test, and generally, p-values < 0.05 were considered statistically significant.

Results

Patient characteristics

This study included 125 patients, with 85 in the training set and 40 in the test set. Table 1 displays the characteristics of the patients. The training set was composed of 70 individuals with G2–3 RIL and 15 with G4 RIL, while the test set was composed of 30 individuals with G2–3 RIL and 10 with G4 RIL.

Features selection

We performed data augmentation by using the Borderline SMOTE algorithm on G4 RIL patients in the training set. After the multistep-by-step feature selection process, nine features were finally obtained for model construction. These nine features were identified as robust features, and the correlation heat map is shown in Figure 2, which contained three radiomics features, three dosiomics features, and three clinical features. Figure 3 illustrates the LASSO algorithm's selection process for features that minimize the loss function through parameter alteration.

Development and evaluation of the model

We built a radiomics model based on radiomics features, a dosiomics model based on dosiomics features, and a clinical model based on clinical features for this study. By blending radiomics, dosiomics, and clinical characteristics, a model of amalgamation was created.

10.3389/fonc.2023.1168995

TABLE 1 Patient characteristics.

Characteristic	All-data set (*N* = 125)	Training set (*N* = 85)	Test set (*N* = 40)
	No. (%)	No. (%)	No. (%)
Age (year)			
Median (range)	51 (27–74)	52 (27–74)	51 (28–68)
Gender			
Men	92 (73.6)	63 (74.1)	29 (72.5)
Women	33 (26.4)	22 (25.9)	11 (27.5)
T-stage[a]			
T1	14 (11.2)	8 (9.4)	6 (15.0)
T2	37 (29.6)	26 (30.6)	11 (27.5)
T3	46 (36.8)	31 (36.5)	15 (37.5)
T4	28 (22.4)	20 (23.5)	8 (20)
N-stage[a]			
N0	5 (4.0)	5 (5.9)	0 (0.0)
N1	19 (15.2)	16 (18.8)	3 (7.5)
N2	78 (62.4)	51 (60.0)	27 (67.5)
N3	23 (18.4)	13 (15.3)	10 (25.0)
Clinical staging[a]			
I	1 (0.8)	1 (1.2)	0 (0.0)
II	10 (8)	10 (11.8)	0 (0.0)
III	70 (56)	45 (52.9)	25 (62.5)
IV	44 (35.2)	29 (34.1)	15 (37.5)
EGFR			
Yes	19 (15.2)	13 (15.3)	6 (15.0)
No	106 (84.8)	72 (84.7)	34 (85.0)
RIL grade			
G2	15	12	3
G3	85	58	27
G4	25	15	10

[a]According to the eighth edition of the International Union against Cancer/American Joint Committee on Cancer (UICC/AJCC) staging manual.

Figure 4 displays the ROC curves of the four models for predicting RIL in NPC. Figure 4A demonstrates the fivefold cross-validation in the training set, with the radiomics model having an AUC of 0.82 (95% confidence interval (CI): 0.72–0.92), the dosiomics model having 0.83 (95% CI: 0.74–0.92), the clinical model having 0.66 (95% CI: 0.55–0.77), and the combination model having 0.95 (95% CI: 0.92–0.98). The radiomics model, dosiomics model, clinical model, and combination model all had AUC values significantly higher than the clinical model ($p < 0.05$), as Figure 4B demonstrates. The radiomics model had an AUC of 0.87, the dosiomics model had 0.88, the clinical model had 0.57, and the combination model had 0.93. The difference between the combination model and the radiomics model was significant ($p < 0.05$). No statistically significant difference was found between the combination model and the dosiomics model ($p = 0.09$), yet the combination model still proved to be superior (AUC, 0.93 vs. 0.89; ACC, 0.88 vs. 0.82). The performance of the four prediction models was summarized in detail in Table 2.

The best RIL prediction model was the combination model, which contained three radiomics features, three dosiomics features, and three clinical features (age, baseline_ALC, and volume of GTVnx). A combination model's AUC of 0.95 (95% CI: 0.92–0.98) was revealed by both a fivefold and 10-fold cross-validation of the training set. The AUC of the combination model in the test set was 0.93 (accuracy: 0.88; specificity: 0.9). The combination model's ROC curves for fivefold cross-validation (Figure 4C), 10-fold cross-validation (Figure 4D), and test set (Figure 4E) are depicted in Figure 4, and Table 2 gives the evaluated performance of the model.

Discussion

In the study, three clinical features, three dosiomics features, and three radiomics features were extracted from cervical vertebrae and skull bone to build prediction models for G4RIL in NPC. Using only clinical features, dosiomics features, radiomics features, and a combination of all, four models were constructed. We found that the best performance was achieved when all features were added in, and the combination model provides an expected strategic evaluation method for the radiation plans of NPC. This is the first study that has built an RIL prediction model based on dosiomics analysis.

After examining the study's outcomes, we discovered that relying solely on clinical factors like GTVnx volume, the age of the patients, and the ALC before RT had limited predictive power for G4RIL. The AUC of the clinical model was 0.66 in the training set and 0.57 in the test set. The results suggest that more information about patients' physiopathological characteristic and treatment process should not be omitted. Therefore, the radiomics and dosiomics methods were considered effective tools for quantitative information analysis from images and 3D RT-dose distribution in our study.

The rapid expansion of radiomics research has enabled the extraction of feature data from medical images with high throughput, and it is a noninvasive quantitative technique (17, 18). The general hypothesis of radiomics is that imaging characteristics reflect physiopathological tissue information, which is thus made accessible through quantitative features (19). Radiomics, taking radiomics features from medical images and transforming them into data that can be utilized (17, 20), is a field of study. Several studies on radiomics have shown that texture features can provide more predictive information (21–23), and some transformations may enhance texture features. In the study, three predictive radiomics features for RIL include wavelet-LHL_glcm_Idn, logarithm_glszm_gray level nonuniformity normalized, and wavelet-HHL_glcm_maximum probability. The radiomics model's AUC, as depicted in Figure 4, was 0.82 in the training set and 0.87 in the test set.

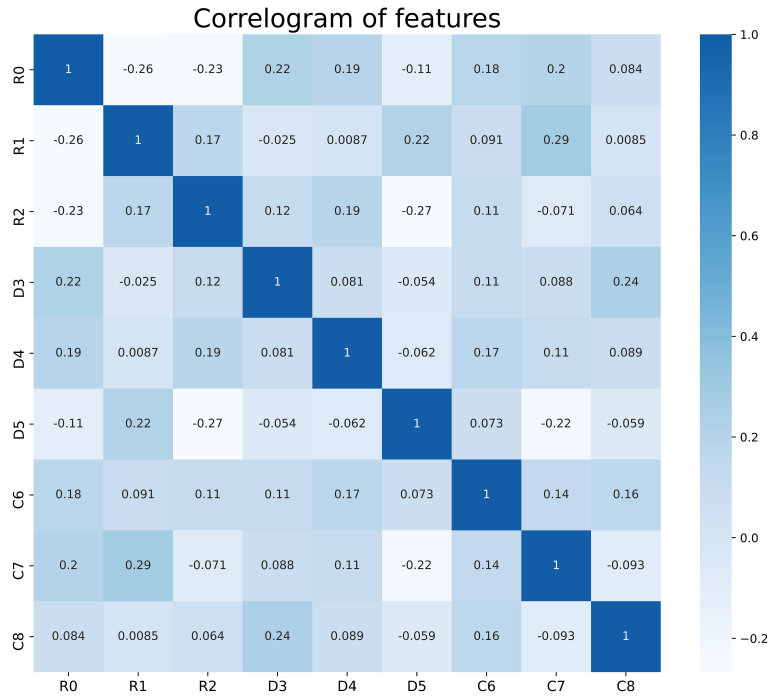

FIGURE 2
Correlation analysis of the features used in the model, there is no correlation between these features. R0- R2 are radiological features; D3- D5 are dosiomic features; C6- C8 are clinical features. R0, wavelet-LHL_glcm_Idn; R1, logarithm_glszm_Gray Level NonUniformity Normalized; R2, wavelet-HHL_glcm_Maximum Probability; D3, original_shape_Major Axis Length; D4, log-sigma-4-0-mm-3D_glszm_Small Area Emphasis; D5, wavelet-LLH_firstorder_Mean; C6, Age; C7, baseline_ALC; C8, Volume of GTVnx.

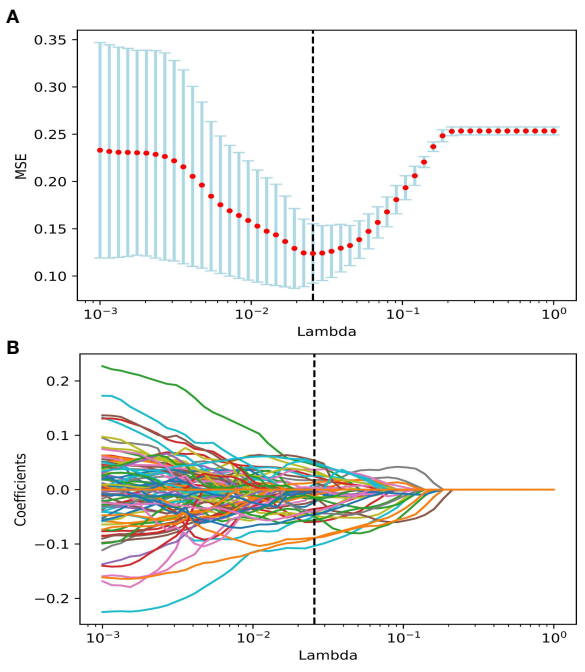

FIGURE 3
The features were selected using the LASSO regression model. **(A)** Selection of the regulation parameter lambda (λ). The vertical black dashed line defines the optimal λ at the minimum MSE. **(B)** LASSO coefficient curves of features. Vertical black dashed lines are drawn at the best lambda in **(A)**, non-zero features under the best λ are selected. Abbreviation: LASSO, the least absolute shrinkage and selection operator; MSE, Mean Squared Error.

Compared to traditional dosimetry analysis, dosimetry analysis demonstrated more promising results, e.g., after IMRT for head and neck cancer, locoregional recurrence has been documented (24), carbon-ion radiotherapy in skull-base chordoma has been linked to local control (25), lung cancer patients treated with radiotherapy have experienced acute-phase weight loss (26), and radiation pneumonitis has been linked to lung stereotactic body radiation therapy (27). In the study, three predictive dosiomics features for RIL include original_shape_major axis length, log-sigma-4-0-mm-3D_glszm_small area emphasis, and wavelet-LLH_firstorder_mean. As shown in Figure 4, the AUC of the dosiomics model was 0.83 in the training set and 0.88 in the test set.

Through the analysis of big data information from images and 3D RT dose, both radiomics and dosiomics models showed stronger predictive power than traditional clinical models. However, the robustness of the models based only on radiomics or dosiomics features in this study needs to be improved, and the error range of cross-validation is relatively large. Without a doubt, the RIL predictive models, which were based solely on radiomics or dosiomics features, were significantly enhanced in both predictive power and robustness when all features were amalgamated. The difference between the combination model and either radiomics or dosiomics models was significant ($p < 0.05$). In the training set, the AUC of the combination model was 0.95, as depicted in Figure 4; however, in the test set, it was 0.93. We successfully established G4RIL predictive models on NPC cancer cases by introducing dosiomics from RT three-dimensional dose distribution to an

10.3389/fonc.2023.1168995

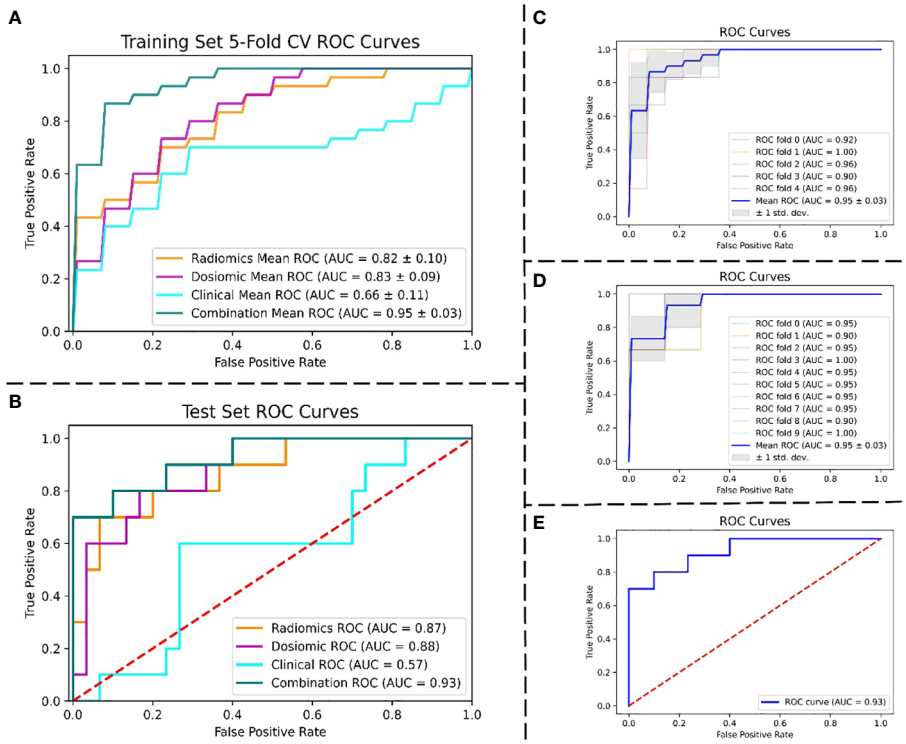

FIGURE 4
Performance of the ROC curves. **(A)** ROC curves of four models were compared using 5-fold CV in the training set. **(B)** ROC curves of four models were compared in the test set. **(C)** 5-fold CV ROC curves for the combined model in the training set. **(D)** 10-fold cross-validation ROC curves for the combined model in the training set. **(E)** ROC curve for the combined model in the test set. Abbreviation: ROC, the receiver operating characteristic; AUC, the area under the curve; CV, cross-validation.

image-based radiomics strategy. This research is the first of its kind to contemplate 3D dose distribution in NPC RIL forecasting, to our knowledge.

The outcome prediction using radiomics and dosiomics analysis based on medical images and spatial dose distribution is helpful in developing clinical decision-making for the personalization of patients' treatment. Accordingly, for NPC patients with a high predicted G4RIL risk, the therapeutic scheme may need to protect cervical vertebrae and skull bone appropriately while focusing on killing cells in the tumor area.

We have to admit that the patient dataset for this study is limited. First and foremost, the dosiomics features demonstrate good prediction ability, while the understanding of these features is still qualitative. The main reason is that the process of transforming dose distribution into GLCM, GLRLM, GLSZM, and GLDM cannot be accurately described with analytic function. Therefore, the features based on GLCM, GLRLM, GLSZM, and GLDM are not as simple and straightforward as dosimetry factors. Therefore, how to utilize the features for treatment plan design is not quite clear. In other words, currently, the dosiomics-based prediction model can only be used to evaluate an RT plan rather than help make an RT plan. It is anticipated that by gaining a more profound comprehension and accurate application of those features, this future predictive model could be used to revolutionize cancer treatment by providing clinicians with valuable tools for treatment planning, dosimetry optimization, and patient stratification. (1) The expected predictive models developed in the study can provide valuable insights into these aspects of cancer

TABLE 2 Performance comparison of four models: radiomics model, dosiomics model, clinical model, and combination model.

Model	Training set	Test set				
	Mean AUC (95% CI)	AUC	ACC	Precision	Sensitivity	Specificity
Radiomics	0.82 (95% CI, 0.72–0.92)	0.87	0.82	**1**	0.3	**1**
Dosiomics	0.83 (95% CI, 0.74–0.92)	0.88	0.82	0.64	0.7	0.87
Clinical	0.66 (95% CI, 0.55–0.77)	0.57	0.6	0.13	0.1	0.77
Combination	0.95 (95% CI, 0.92–0.98)	**0.93**	**0.88**	0.73	**0.8**	0.9

CI, confidence interval; AUC, the area under the receiver operating characteristic curve; ACC, accuracy. The values denoted in bold within the table signifies the best values of performance.

treatment. By utilizing the predictive models, clinicians can gain a better understanding of the potential outcomes of different treatment options. This information can help guide treatment planning decisions by providing insights into the likelihood of treatment success or failure. For example, if the models predict a high probability of treatment failure, clinicians may consider alternative treatment strategies or adjust the treatment plan to improve the chances of success. (2) Dosimetry optimization is another area where the future study's findings can have a significant impact. Optimizing dosimetry involves finding the best balance between delivering an effective dose to the tumor and minimizing radiation exposure to healthy tissues. The predictive models should assist in this process by providing information on the expected response of the tumor to different radiation doses. This can help clinicians optimize the radiation dose distribution to maximize tumor control while minimizing the risk of side effects. (3) Patient stratification based on risk is an essential aspect of personalized medicine. The predictive models developed in future studies should aid in identifying patients who are at higher risk of treatment failure or experiencing severe side effects. By stratifying patients based on their individual risk profiles, clinicians can tailor treatment plans to suit each patient's specific needs.

Another limitation that should never be overlooked is the limited sample size in this study. There are several potential strategies to expand the dataset or conduct external validation through future research to evaluate the generalizability of the predictive model, including multicenter studies, retrospective studies, multimodal datasets, data sharing, and external validation. For the multimodal dataset, other than radiation therapy dose, other parameters related to radiation therapy, such as patient's age, gender, and pathological type, can also be considered. By collecting these multimodal data, a more comprehensive predictive model can be constructed, and the size of the dataset can be increased. By sharing the dataset with other research teams, institutions can expand the dataset through collaboration. This collaboration can be achieved through data-sharing agreements or data-sharing platforms, allowing more researchers to use the data for model validation and evaluation. For external validation, independent datasets should be used to validate the generalizability of the predictive model. These datasets can come from other research teams' studies or publicly available clinical databases. By validating the model on different datasets, its performance and reliability in different samples can be assessed. In our further study, we will employ the above strategies to improve the reliability and generalizability of the predictive model and better evaluate the predictive effect of radiation therapy dose on radiation-related lymphocyte toxicity.

Conclusion

Radiomics and dosiomics analyses predicting the risk of G4RIL in NPC patients were implemented for the first time, integrating CT, dose maps, and clinical features. Demonstrating that radiomics and dosiomics features can be beneficial for risk modeling of G4RIL in NPC patients in a highly conformal regime of modern radiotherapy, we still require thorough validation before they can be put into practice.

Data availability statement

Due to further research needs, the data will not be made public within three years. After three years, the dataset may be made available upon request to the corresponding author.

Ethics statement

The studies involving humans were approved by Ethics Committee of Xiangya Hospital, Central South University/Hunan Cancer Hospital. The studies were conducted in accordance with the local legislation and institutional requirements. Written informed consent for participation was not required from the participants or the participants' legal guardians/next of kin in accordance with the national legislation and institutional requirements.

Author contributions

XX and ZZ wrote the main manuscript text and CY and QH prepared figures and tables. CY did the statistical analysis and QH collected the primary data. All authors reviewed the manuscript. All authors contributed to the article and approved the submitted version.

Funding

The work is supported by the Natural Science Foundation of Hunan Province (2022JJ30363), the National Natural Science Foundation of China (62071176), and the Hunan Cancer Hospital Climb Plan (2020ITTB002).

Acknowledgments

This work was supported in part by the High-Performance Computing Center of Central South University.

Conflict of interest

The authors declare that the research was conducted in the absence of any commercial or financial relationships that could be construed as a potential conflict of interest.

Publisher's note

References

1. Chen YP, Chan ATC, Le QT, Blanchard P, Sun Y, Ma J. Nasopharyngeal carcinoma. *Lancet* (2019) 394(10192):64–80. doi: 10.1016/S0140-6736(19)30956-0

2. Burman C, Kutcher GJ, Emami B and Goitein M. Fitting of normal tissue tolerance data to an analytic function Int. *J Radiat Oncol Biol Phys* (1991) 21:123–35. doi: 10.1016/0360-3016(91)90172-Z

3. Venkatesulu BP, Mallick S, Lin SH, Krishnan S. A systematic review of the influence of radiation-induced lymphopenia on survival outcomes in solid tumors. *Crit Rev Oncol/Hematol* (2018) 123:42–51. doi: 10.1016/j.critrevonc.2018.01.003

4. Xie X, Gong S, Jin H, Yang P, Xu T, Cai Y, et al. Radiation-induced lymphopenia correlates with survival in nasopharyngeal carcinoma: impact of treatment modality and the baseline lymphocyte count. *Radiat Oncol* (2020) 15(1):1–10. doi: 10.1186/s13014-020-01494-7

5. Liu LT, Chen QY, Tang LQ, Guo SS, Guo L, Mo HY, et al. The prognostic value of treatment-related lymphopenia in nasopharyngeal carcinoma patients. *Cancer Res Treat* (2018) 50(1):19–29. doi: 10.4143/crt.2016.595

6. Cho O, Oh Y-T, Chun M, Noh O-K, Hoe J-S, Kim H. Minimum absolute lymphocyte count during radiotherapy as a new prognostic factor for nasopharyngeal cancer. *Head Neck* (2016) 38 Suppl 1:E1061–7. doi: 10.1002/hed.24158

7. Vrisekoop N, den Braber I, de Boer AB, Ruiter AF, Ackermans MT, van der Crabben SN, et al. Sparse production but preferential incorporation of recently produced naive T cells in the human peripheral pool. *Proc Natl Acad Sci USA* (2008) 105(16):6115–20. doi: 10.1073/pnas.0709713105

8. Hayman JA, Callahan JW, Herschtal A, Everitt S, Binns DS, Hicks RJ, et al. Distribution of proliferating bone marrow in adult cancer patients determined using FLT-PET imaging. *Int J Radiat Oncol Biol Phys* (2011) 79(3):847–52. doi: 10.1016/j.ijrobp.2009.11.040

9. Wang Q, Qiu Q, Zhang Z, Zhang J, Yang G, Liu C, et al. Bone marrow dosimetric analysis of lymphopenia in patients with esophageal squamous cell carcinoma treated with chemoradiotherapy. *Cancer Med* (2021) 10(17):5847–58. doi: 10.1002/cam4.4131

10. Lee J, Lin JB, Sun FJ, Lu KW, Lee CH, Chen YJ, et al. Dosimetric predictors of acute haematological toxicity in oesophageal cancer patients treated with neoadjuvant chemoradiotherapy. *Br J Radiol* (2016) 89(1066):20160350. doi: 10.1259/bjr.20160350

11. Sini C, Fiorino C, Perna L, Noris Chiorda B, Deantoni CL, Bianchi M, et al. Dose-volume effects for pelvic bone marrow in predicting hematological toxicity in prostate cancer radiotherapy with pelvic node irradiation. *Radiother Oncol* (2016) 118 (1):79–84. doi: 10.1016/j.radonc.2015.11.020

12. Liang B, Yan H, Tian Y, Chen X, Yan L, Zhang T, et al. Dosiomics: extracting 3D spatial features from dose distribution to predict incidence of radiation pneumonitis. *Front Oncol* (2019) 9:269. doi: 10.3389/fonc.2019.00269

13. Lambin P, Leijenaar RTH, Deist TM, Peerlings J, de Jong EEC, van Timmeren J, et al. Radiomics: the bridge between medical imaging and personalized medicine. *Nat Rev Clin Oncol* (2017) 14:749–62. doi: 10.1038/nrclinonc.2017.141

14. Gabrys HS, Buettner F, Sterzing F, Hauswald H, Bangert M. Design and selection of machine learning methods using radiomics and dosiomics for normal tissue complication probability modeling of xerostomia. *Front Oncol* (2018) 8:35. doi: 10.3389/fonc.2018.00035

15. Zhen X, Chen J, Zhong Z, Hrycushko B, Zhou L, Jiang S, et al. Deep convolutional neural network with transfer learning for rectum toxicity prediction in cervical cancer radiotherapy: a feasibility study. *Phys Med Biol* (2017) 62:8246–63. doi: 10.1088/1361-6560/aa8d09

16. Han H, Wang W-Y, Mao B-H. Borderline-SMOTE: a new over-sampling method in imbalanced data sets learning. In: *International conference on intelligent computing*. (Berlin, Heidelberg: Springer) (2005). p. 878–87.

17. Bibault JE, Xing L, Giraud P, El Ayachy R, Giraud N, Decazes P, et al. Radiomics: A primer for the radiation oncologist. *Cancer Radiother* (2020) 24:403–10. doi: 10.1016/j.canrad.2020.01.011

18. Mayerhoefer ME, Materka A, Langs G, Häggström I, Szczypiński P, Gibbs P, et al. Introduction to radiomics. *J Nucl Med* (2020) 61(4):488. doi: 10.2967/jnumed.118.222893

19. Gillies RJ, Kinahan PE, Hricak H. Radiomics: images are more than pictures, they are data. *Radiology* (2016) 278(2):563–77. doi: 10.1148/radiol.2015151169

20. Aerts HJ, Velazquez ER, Leijenaar RT, Parmar C, Grossmann P, Carvalho S, et al. Decoding tumour phenotype by noninvasive imaging using a quantitative radiomics approach. *Nat Commun* (2014) 5:4006. doi: 10.1038/ncomms5006

21. Zhang X, Xu XP, Tian Q, Li B, Wu Y, Yang Z, et al. Radiomics assessment of bladder cancer grade using texture features from diffusion-weighted imaging. *J Magn Reson Imaging* (2017) 46(5):1281–8. doi: 10.1002/jmri.25669

22. Cunliffe A, Armato SG, Castillo R, Pham N, Guerrero T, Al-Hallaq HA. Lung texture in serial thoracic computed tomography scans: correlation of radiomics-based features with radiation therapy dose and radiation pneumonitis development. *Int J Radiat Oncol* (2015) 91(5):1048–56. doi: 10.1016/j.ijrobp.2014.11.030

23. Tian Q, Yan LF, Zhang X, Zhang X, Hu YC, Han Y, et al. Radiomics strategy for glioma grading using texture features from multiparametric MRI. *J Magn Reson Imaging* (2018) 48(6):1518–28. doi: 10.1002/jmri.26010

24. Wu A, Li Y, Qi M, Lu X, Jia Q, Guo F, et al. Dosiomics improves prediction of locoregional recurrence for intensity modulated radiotherapy treated head and neck cancer cases. *Oral Oncol* (2020) 104:104625. doi: 10.1016/j.oraloncology.2020.104625

25. Buizza G, Paganelli C, D'Ippolito E, Fontana G, Molinelli S, Preda L, et al. Radiomics and dosiomics for predicting local control after carbon-ion radiotherapy in skull-base chordoma. *Cancers* (2021) 13:339. doi: 10.3390/cancers13020339

26. Rossi L, Bijman R, Schillemans W, Aluwini S, Cavedon C, Witte M, et al. Texture analysis of 3D dose distributions for predictive modelling of toxicity rates in radiotherapy. *Radiother Oncol* (2018) 129(3):548–53. doi: 10.1016/j.radonc.2018.07.027

27. Adachi T, Nakamura M, Shintani T, Mitsuyoshi T, Kakino R, Ogata T, et al. Multi-institutional dose-segmented dosiomic analysis for predicting radiation pneumonitis after lung stereotactic body radiation therapy. *Med Phys* (2021) 48 (4):1781–91. doi: 10.1002/mp.14769

frontiers | Frontiers in Oncology

TYPE Opinion
PUBLISHED 09 January 2024
DOI 10.3389/fonc.2023.1240913

OPEN ACCESS

EDITED BY
Dirk Van Gestel,
Universitélibre de Bruxelles,
Belgium

REVIEWED BY
Nerina Denaro,
IRCCS Ca 'Granda Foundation Maggiore Policlinico Hospital, Italy
Cathy Lazarus,
Icahn School of Medicine at Mount Sinai, United States

*CORRESPONDENCE
Niccolò Bertini
niccolo.bertini@unifi.it

RECEIVED 16 June 2023
ACCEPTED 14 December 2023
PUBLISHED 09 January 2024

CITATION
Santo B, Bertini N, Cattaneo CG, De Matteis S, De Franco P, Grassi R, Iorio GC, Longo S, Boldrini L, Piras A, Desideri I, De Felice F and Salvestrini V (2024) Nutritional counselling for head and neck cancer patients treated with (chemo)radiation therapy: why, how, when, and what?
Front. Oncol. 13:1240913.
doi: 10.3389/fonc.2023.1240913

Nutritional counselling for head and neck cancer patients treated with (chemo)radiation therapy: why, how, when, and what?

Bianca Santo[1], Niccolò Bertini[2*], Carlo Guglielmo Cattaneo[3], Sara De Matteis[1], Paola De Franco[1], Roberta Grassi[4], Giuseppe Carlo Iorio[5], Silvia Longo[6], Luca Boldrini[6], Antonio Piras[7,8,9], Isacco Desideri[2], Francesca De Felice[3] and Viola Salvestrini[10]

[1]Radiation Oncology Unit, Dipartimento di Oncoematologia, Ospedale "Vito Fazzi", Lecce, Italy, [2]Radiation Oncology Unit, Azienda Ospedaliero-Universitaria Careggi, Department of Experimental and Clinical Biomedical Sciences, University of Florence, Florence, Italy, [3]Department of Radiotherapy, Policlinico Umberto I, Department of Radiological, Oncological and Pathological Sciences, "Sapienza" University of Rome, Rome, Italy, [4]Department of Precision Medicine, University of Campania "L. Vanvitelli", Naples, Italy, [5]Department of Oncology, Radiation Oncology, University of Turin, Turin, Italy, [6]Unità Operativa Complessa (UOC) Radioterapia Oncologica, Fondazione Policlinico Universitario Istituto di Ricovero e Cura a Carattere Scientifico (IRCCS) "A. Gemelli", Roma, Italy, [7]Unità Operativa (UO) Radioterapia Oncologica, Villa Santa Teresa, Palermo, Italy, [8]Department of Biomedical Image Processing and Analysis, Ri.Med Foundation, Palermo, Italy, [9]Department of Health Promotion, Mother and Child Care, Internal Medicine and Medical Specialties, Molecular and Clinical Medicine, University of Palermo, Palermo, Italy, [10]Radiation Oncology Unit, Centro Cyberknife, Istituto Fiorentino di Cura e Assistenza, Florence, Italy

KEYWORDS

head and neck, nutrition, chemotherapy, radiation therapy, weight

Introduction

Weight loss is a frequent occurrence among patients with head and neck cancer (HNC) and can be observed before, during, and after cancer treatment, especially radiation therapy (RT) with or without concurrent chemotherapy (CRT). Patients with HNC are at a high risk of malnutrition at the time of diagnosis, and nutritional support or intervention is often needed during and after RT or concurrent CRT. Given the severe consequences of malnutrition and cachexia on treatment outcomes, mortality, morbidity, and quality of life, it is essential to identify patients who are at higher risk of developing this condition. The nutritional status of patients is a crucial factor in terms of adherence to treatment and recovery. Malnutrition may have a significant impact on treatment outcomes and, consequently, tumor progression. However, in clinical practice, identifying and standardizing nutritional interventions can be challenging. In this commentary, we aim to identify the components of screening and assessment that are commonly used in both literature and clinical practice and suggest the appropriate timing for nutritional interventions in patients with HNC undergoing RT or CRT.

At the time of diagnosis, 35%–60% of head and neck cancer (HNC) patients are malnourished due to cancer-related impairment such as pain, obstruction, or loss of appetite (1, 2). Compared to patients with other primary neoplasms, HNC patients are at a higher risk of malnutrition due to the location of the tumor and the impact of the treatment-related side effects on quality of life (3, 4). Indeed, malnutrition can cause a range of clinical symptoms, including metabolic and electrolytic imbalances, immune system depression, and increased morbidity and mortality (5). Weight loss can lead to discontinue cancer treatments and to a negative impact on oncological outcomes, with approximately 55% of patients losing an additional 10% or more of their body weight during RT or CRT (5–7). This note aims to provide an overview on the role of nutritional counseling in HNC patients undergoing CRT, either in an exclusive or adjuvant setting.

Screening

Malnutrition screening is an essential component of multimodal care in HNC patients. It involves the systematic identification of patients who are at risk of malnutrition and the provision of appropriate interventions to prevent or treat malnutrition (8). In this regard, the European Society for Clinical Nutrition and Metabolism (ESPEN) guidelines for screening suggests that the purpose of nutritional screening is to predict the outcome and the impact of nutritional intervention (9).There are no standardized guidelines regarding nutritional screening. Screening should occur at the time of diagnosis, before treatment begins, and at regular intervals throughout treatment and follow-up. This allows for early identification of malnutrition and timely intervention to prevent or treat it. Despite its acknowledged role, there are no standardized guidelines regarding nutritional screening.

Nutritional assessment

The risk of malnutrition is frequent in HNC patients, and for this reason, it is mandatory to primarily identify patients at higher risk. Currently, standardized parameters are adopted, and although there is not a single assessment tool, we suggest that the use of a standardized assessment is essential to identify patients at risk at baseline. The commonly used nutrition assessment tools are the following:

1. Mini Nutrition Assessment (MNA) includes anthropometric, general, dietary, and autonomy of food self-assessments (self-perception of health and nutrition) (10–12).
2. Nutritional Risk Screening 2002 (NRS2002) detects the presence or the risk of undernutrition (9, 13).
3. Patient-Generated Subjective Globe Assessment (PG-SGA) is focused on the preeminent interdisciplinary patient assessment and allows for triaging of nutrition interventions (14).
4. Malnutrition Universal Screening Tool (MUST) is a five-step screening tool to identify malnourished adults (15, 16).

The appropriate nutritional assessment should be performed for all patients before CRT. For defining the severity of malnutrition, we recommend the use of the new GLIM (Global Leadership Initiative on Malnutrition) score, already adopted by ESPEN, ASPEN, FELANPE, and PENSA. In particular, the GLIM includes three phenotypical criteria (weight loss, low BMI, and reduced muscle mass) and two etiological criteria (reduced food intake or absorption and increased disease burden or inflammation) (17).

Nutritional intervention

The aim of the nutritional intervention is to improve the subjective quality of life, enhance anti-tumor treatment effects, reduce the adverse effects of oncological care, prevent the interruption of therapy, and treat RT/CRT-related undernutrition. In this regard, Table 1 summarizes the main studies analyzing the impact of nutritional counseling and nutritional intervention strategies in HNC patients (18–32). The onset of oral mucositis in HNC patients during RT or CRT may result in weight loss and intensive dietary counseling, and oral nutrition support is recommended. This is also advised to prevent interruptions to CRT (33). There are different types of nutritional support that can be adopted to reach the needs of the patient. Main options of nutritional support are oral, enteral, and parenteral. Nutritional interventions include relaxation of previous therapeutic diets, to minimize further nutritional compromise and to positively influence quality of life outcomes (34). However, this may not necessarily be appropriate, due to the side effects and intensity of treatment regimens. Patients may require more intensive nutritional support methods from the beginning of treatment over and above traditional food fortification methods with the early use of oral nutrition support. The choice of feeding route in HNC patients will depend upon local arrangements; however, clinical considerations should include site of primary tumor, treatment plan and intent, predicted duration of enteral feeding, and patient choice (35, 36). Tube feeding is recommended if swallowing is impaired or if mucositis is anticipated, which may interfere with oral and/or pharyngeal functionality. If enteral feeding is expected to be required for longer than 4 weeks, then gastrostomy insertion is recommended but not in a prevention way, except for limited cases (37). The optimal method of tube feeding still remains unclear, and any approach should be discussed with the patient in order to ensure an individualized nutritional care. Moreover, the optimal screening and assessment for suitability and method of gastrostomy insertion by endoscopic, radiological, or surgical approach is essential. Assessment of co-morbidities and contraindications should be taken into account to prevent complications prior to oncological treatment (35, 36).

The type and volume of enteral nutrition will depend upon patients' symptoms and current intake and is likely to change throughout and after treatment. There are no data to suggest a

TABLE 1 Nutritional counseling and intervention strategies in HNC patients.

Author/ Year	Study Type	Treatment	Population (Number)	Time to Intervention	Outcomes	Conclusions
Britton et al. (18) 2019	Randomized controlled trial	RT/CRT	307	Oncology dietitians delivered EAT (Eating As Treatment) during their usual consultations with a weekly exposure while the patient was receiving RT, and then fortnightly thereafter.	NS at end of treatment.	NS participants exhibited better nutrition, less weight loss, lower depression scores, fewer RT interruptions, and better QoL scores. The EAT intervention is an effective and achievable intervention.
Orell et al. (19) 2019	Randomized trial	CRT/RT	65	Prophylactic PEG is inserted to almost all HNC patients either prior to surgery or before the start of (C)RT.	NSt (PG-SGA), weight loss, handgrip strength (HGS), body composition, and survival.	Individualized on-demand NC is efficacious as intensive counseling in preventing deterioration of NSt and incidence of malnutrition during (C)RT
Sandmael, J.A. et al. (20) 2017	Randomized controlled pilot trial	RT	41	Exercise and NI during RT or after RT.	Feasibility, efficacy.	Exercise and NI is feasible for patients with HNC during RT, and the intervention is potentially effective in mitigating loss of muscle mass both during and after RT.
Capozzi et al. (21) 2016	Randomized trial	RT/CRT	60	Patients were randomly assigned to either the 12-week immediate lifestyle intervention group or the 12-week delayed lifestyle intervention group.	PO: body composition SO: fitness, quality of life, depression, and NSt.	Common interventions to manage side effects focus on NC, although NC alone does not significantly mitigate muscle and functional loss. Physical activity has been recognized as an important intervention for general cancer populations, helping patients to manage side effects throughout treatment.
Lønbro, S. et al. (22) 2013	Randomized, stratified and parallel-grouped feasibility trial	RT/CRT	30	12-week immediate lifestyle intervention vs. 12-week delayed intervention.	Whole body lean body mass and fat mass.	Progressive resistance training increase body mass, muscle strength, and functional performance in both groups.
Cereda et al. (23) 2018	Randomized, pragmatic, parallel-group controlled trial	RT/CRT	159	NC in combination with ONS or without ONS from the start of RT and continuing for up to 3 months after its end.	PO: change in body weight at the end of RT SO: changes in protein–calorie intake, muscle strength, phase angle, and QoL and anticancer treatment tolerance.	ONS results in better weight maintenance, increased protein–calorie intake, improved QoL, and was associated with better anti-cancer treatment tolerance.
Jiang et al. (24) 2018	Randomized trial	CRT	100	Each measurement were assessed within 1 week before CRT (baseline), within 3 days before the end of CRT and 3 months after the end of CRT. Patients were examined once a week to assess the severity of mucositis.	To determine the effect of ONS on the outcomes of weight, fat-free mass, fat-free mass index, and laboratory parameters, the dependent	ONS had beneficial outcomes in terms of reducing weight loss, minimizing BMI decrease and increasing protein intake in loco-regionally advanced

(Continued)

TABLE 1 Continued

Author/ Year	Study Type	Treatment	Population (Number)	Time to Intervention	Outcomes	Conclusions
					continuous variable, analysis of covariate variance was used to compare the ONS group.with the control group.	nasopharyngeal cancer patients during CRT.
Machon et al. (25) 2012	Prospective non-controlled phase II pilot study	CRT	46	Patients were followed up by a dietician and a radiotherapist once a week during RCT and for the following 2 months post-CRT.	Effects of an NS containing amino acids, ω-3 fatty acids, and ribonucleic acids on inflammatory and oxidative markers status before and during CRT.	NS could improve inflammatory state and could prevent severe acute mucositis in HNC patients.
Sykes et al. (26) 2022	Prospective, randomized controlled trial	Surgery	49	Optimization of NSt was attempted via a multimodal intervention: (1) Preoperative Dietitian Consultation (2) ONS	The scored PG-SGA was validated to triage NI in oncology patients. Participants completed the MD Anderson Dysphagia Inventory to assess swallowing-related factors. Data were collected during the inpatient hospital course and up to 30 days following discharge from the hospital.	Preoperative nutrition optimization shows potential to reduce weight loss normally experienced by patients with HNC prior to surgical extirpation, especially among those with subjective dysphagia.
Blake et al. (27) 2021	Prospective cohort study	RT/CRT	111	All high risk patients were referred to an oncology dietitian for an "early" 1-h pre-treatment counseling session, which was aimed to be delivered at least 2 weeks prior to treatment commencement. Patients who proceeded with prophylactic gastrostomy placement were recommended to commence the proactive EN protocol as soon as safe to do so post gastrostomy insertion, ideally prior to treatment commencement.	PO: percentage weight change. SO: changes in percentage fat mass and percentage fat-free mass and change in SGA category.	A new pre-treatment model of nutrition care that combined early dietary counselling with a proactive EN protocol was effective in generating a clinically important reduction in weight loss and reduced decline in NSt.
Ho et al. (28) 2021	Prospective cohort study	CRT	243	Questionnaire including lifestyle habits (smoking, alcohol drinking, and use of betel quid), comorbidity, and NSt assessment within 7 days of CRT initiation. NC was provided by a registered dietician to each patient using face-to-face interviews at least every 2 weeks during CRT.	OS, Comparison of body weight change during concurrent CRT, treatment completeness and CRT related death according to the different nutritional counseling groups.	HNC patients, regardless of pretreatment NSt, should immediately receive NC prior to CRT.
Jantharapattana and Orapipatpong (29) 2019	Randomized controlled trial	Surgery	62	All patients were scheduled for surgery within 7–14 days after receiving a preoperative evaluation to prevent the treatment delay. During the perioperative period, the patients were assigned to receive their NSu at least 7 days before surgery and then 14 days postoperatively. At 14 days, 2 months, and 4 months postoperatively, the weight, BMI, lean body mass, and body compositions of all participants were measured or	Effect on body weight changes, on lean body mass and body composition, on hematology and biochemistry, and complications related to surgery and hospitalization	Body weight changes in malnourished patients with HNC following surgery were not influenced by Eicosapentaenoic acid additives to perioperative NSu. The NSt and postoperative morbidities of the malnourished patients primarily depended on

(Continued)

TABLE 1 Continued

Author/ Year	Study Type	Treatment	Population (Number)	Time to Intervention	Outcomes	Conclusions
				calculated, and blood tests was analyzed.		the adequacy of caloric intake.
Boisselier et al. (30) 2020	Phase III double-blind multicenter study	CRT	172	ONS of either a formula enriched with l-arginine and omega-3 fatty and ribonucleic acids (experimental arm), or an isocaloric isonitrogenous control (control arm), for 5 days before each of three cycles of cisplatin. Intention-to-treat and per-protocol analyses were undertaken, along with subgroup analyses of ≥75% compliant patients, to compare the incidence of acute mucositis and 36-month survival.	PO: efficacy of the same immunonutrient supplement on severe mucositis. SO: tolerance, compliance to oral supplementation, chemotherapy interruptions and delays, quality of life, and progression-free survival and overall survival at 1, 2, and 3 years	Immunomodulating formula failed to reduce severe mucositis during CRT, but the long-term survival of compliant HNC patients was improved.
Carvalho et al. (31) 2017	Randomized controlled trial	CT	53	The control group received powdered HH supplement during 4 weeks. The experimental group received liquid HH supplement, ready for consumption, enriched with EPA from fish oil (2 g/440 ml) for the same period. The adherence to the supplementation was evaluated weekly through phone calls and in the return visits after 4 weeks of NI.	Inflammatory profile	Effect of NS with HH formula enriched with EPA on the inflammatory profile of patients with oral cavity cancer in antineoplastic pretreatment. However, the supplementation during 4 weeks was not able to promote significant changes in the inflammatory profile of the patients.
Brown et al. (32) 2017	Randomized controlled trial	Surgery/ RT/CRT	131	All patients received education on the care of their feeding tube during their overnight elective admission for gastrostomy placement. In the standard care arm, patients were commenced on EN via their prophylactic gastrostomy by the dietitian when indicated. For patients in the intervention group, this meant initiation of enteral nutrition via their prophylactic gastrostomy immediately following tube placement prior to commencement of treatment, until completion of treatment. Patients were asked to maintain a self-reporting diary of their daily prescribed enteral nutrition intake, and any barriers to this prescription.	PO: percentage weight change with additional nutrition outcomes, including body composition (fat mass and fat-free mass) and nutritional status. SO: quality of life, tertiary endpoints: tolerance to (C)RT, rate of unplanned hospital admissions and gastrostomy complications.	The early NI did not improve outcomes, but poor adherence to nutrition recommendations impacted on potential outcomes.

PO, primary outcome; S, second outcome; OR, oral nutrition; NS, nutritional support; QoL, quality of life; BMI, Body Mass Index; NI, nutrition intervention; NSt, nutritional status; NC, nutrition counseling; ONS, oral nutritional supplements; HH, hypercaloric and hyperproteic; NSu, nutritional supplement; EN, enteral nutrition; EN, enteral nutrition.

role for cancer-specific enteral formulae. Monitoring nutritional intervention is essential, as compliance with recommendations can be a problem and should be organized weekly during CRT. Supplementation with immunonutrient-enriched formulas such as arginine, nucleotides (RNA), and omega-3 fatty acids up to the end of (C)RT or until withdrawal in HNC patients during RT and CRT may improve or maintain nutrition status (37–39). Moreover, it can delay the onset of oral mucositis and reduce the incidence of severe oral mucositis (38–40). Much evidence is showing a possible beneficial effect of immunonutrition on the control of the onset of local recurrences of the disease after esophagectomy, an improvement in immunosurveillance mechanisms, and a reduction in inflammatory status. Finally, by modulating gene expression, the immunonutrition may make it easier for the body to adapt to systemic inflammation and oxidative stress induced by RCTs and may improve 3-year survival (25, 30, 41, 42). However, further studies focusing on the timing, dosage, and duration of immunonutrition in HNC patients are awaited.

Conclusion

In conclusion, HNC patients undergoing cancer treatment are at high risk of malnutrition before, during, and after oncological care. The nutritional screening, assessment, and support play a crucial role on the maintenance of nutritional status providing specific interventions such as oral nutritional supplements increasing dietary intake and preventing therapy-associated weight loss. It is well-reported in the literature that the interruption of CRT may contribute to worse oncological outcomes. In this regard, the present overview highlighted that an adequate nutritional screening, assessment, and interventions might increase the adherence of HNC patients to oncological treatments and encourages radiation oncologists to set up multidisciplinary care paths.

Author contributions

BS: Conceptualization, Methodology, Validation, Formal analysis, Data curation, Writing - original draft, Writing - review and editing, Supervision. NB: Methodology, Data curation, Writing – original draft, Writing – review and editing, Visualization. CC: Methodology, Data curation, Writing – original draft, Writing – review and editing, Visualization. SM: Methodology, Data curation, Writing – original draft, Writing – review and editing, Visualization. PF: Conceptualization, Validation, Formal analysis, Writing – review and editing, Visualization, Supervision. RG: Conceptualization, Validation, Formal analysis, Writing – review and editing, Visualization, Supervision. GCI: Conceptualization, Validation, Formal analysis, Writing – review and editing, Visualization, Supervision. SL: Data curation, Writing – original draft, Writing – review and editing. LB: Conceptualization, Validation, Formal analysis, Writing – review and editing, Visualization, Supervision. AP: Conceptualization, Validation, Formal analysis, Writing – review and editing, Visualization, Supervision. ID: Conceptualization, Validation, Formal analysis, Writing – review and editing, Visualization, Supervision. FF: Conceptualization, Validation, Formal analysis, Writing – review and editing, Visualization, Supervision. VS: Conceptualization, Methodology, Data curation, Writing – original draft, Writing – review and editing. All authors contributed to the article and approved the submitted version.

Conflict of interest

The authors declare that the research was conducted in the absence of any commercial or financial relationships that could be construed as a potential conflict of interest.

The reviewer ND is currently organizing a Research Topic with the authors GCI, ID.

Publisher's note

References

1. Isenring EA, Capra S, Bauer JD. Nutrition intervention is beneficial in oncology outpatients receiving radiotherapy to the gastrointestinal or head and neck area. *Br J Cancer* (2004) 91:447–52. doi: 10.1038/sj.bjc.6601962

2. Beer KT, Krause KB, Zuercher T, Stanga Z. Early percutaneous endoscopic gastrostomy insertion maintains nutritional state in patients with aerodigestive tract cancer. *Nutr Cancer* (2005) 52:29–34. doi: 10.1207/s15327914nc5201_4

3. Kruizenga HM, Wierdsma NJ, Van Bokhorst MAE, De van der Schueren MAE, Hollander HJ, Jonkers-Schuitema CF, et al. Screening of nutritional status in the Netherlands. *Clin Nutr* (2003) 22:147–52. doi: 10.1054/clnu.2002.0611

4. Datema FR, Ferrier MB, Baatenburg De Jong RJ. Impact of severe malnutrition on short-term mortality and overall survival in head and neck cancer. *Oral Oncol* (2011) 47:910–4. doi: 10.1016/j.oraloncology.2011.06.510

5. Ehrsson YT, Hellström PM, Brismar K, Sharp L, Langius-Eklöf A, Laurell G. Explorative study on the predictive value of systematic inflammatory and metabolic markers on weight loss in head and neck cancer patients undergoing radiotherapy. *Support Care Cancer* (2010) 18:1385–91. doi: 10.1007/s00520-009-0758-4

6. Silvestris N, Falzone L, Elasbali AM, Minoia C, Romito F, Dellino M, et al. Article 1270 psychological distress in outpatients with lymphoma during the COVID-19 pandemic. *Front Oncol* (2020) 1:1270. doi: 10.3389/fonc.2020.01270

7. Vera-Llonch M, Oster G, Hagiwara M, Sonis S. Oral mucositis in patients undergoing radiation treatment for head and neck carcinoma: Risk factors and clinical consequences. *Cancer* (2006) 106:329–36. doi: 10.1002/cncr.21622

8. Talwar B, Donnelly R, Skelly R, Donaldson M. Nutritional management in head and neck cancer: United Kingdom National Multidisciplinary Guidelines. *J Laryngol Otol* (2016) 130:S32–40. doi: 10.1017/s0022215116000402

9. Kondrup J, Allison SP, Elia M, Vellas B, Plauth M. ESPEN guidelines for nutrition screening 2002. *Clin Nutr* (2003) 22:415–21. doi: 10.1016/S0261-5614(03)00098-0

10. Vellas B, Guigoz Y, Baumgartner M, Garry PJ, Lauque S, Albarede JL. Relationships between nutritional markets and the mini-nutritional assessment in 155 older persons. *J Am Geriatr Soc* (2000) 48:1300–9. doi: 10.1111/j.1532-5415.2000.tb02605.x

11. Vellas B, Guigoz Y, Garry PJ, Nourhashemi F, Bennahum D, Lauque S, et al. The mini nutritional assessment (mna) and its use in grading the nutritional state of elderly patients. *Nutrition* (1999) 15(2):116-22. doi: 10.1016/s0899-9007(98)00171-3

12. Villars H, Soto M, Morley JE. *Overview of the MNA-Its history and challenges Aging Issues and Culture, Nationality, and Ethnicity View project The SITLESS project: Exercise Referral Schemes enhanced by Self-Management Strategies to battle sedentary behaviour in older adults View project* (2005). Available at: https://www.researchgate.net/publication/6617786.

13. Kondrup J, Ramussen HH, Hamberg O, Stanga Z, Camilo M, Richardson R, et al. Nutritional risk screening (NRS 2002): A new method based on an analysis of controlled clinical trials. *Clin Nutr* (2003) 22:321–36. doi: 10.1016/S0261-5614(02)00214-5

14. Correira Pereira MA, Santos CA, Almeida Brito J, Fonseca J. Evaluación global subjetiva del estado de nutrición generada por el paciente, albúmina y transferrina en pacientes con cáncer de cabeza o cuello alimentados por gastrostomía. *Nutr Hosp* (2014) 29:420–6. doi: 10.3305/nh.2014.29.2.7066

15. Boléo-Tomé C, Monteiro-Grillo I, Camilo M, Ravasco P. Validation of the malnutrition universal screening tool (MUST) in cancer. *Br J Nutr* (2012) 108:343–8. doi: 10.1017/S000711451100571X

16. Amaral TF, Antunes A, Cabral S, Alves P, Kent-Smith L. An evaluation of three nutritional screening tools in a Portuguese oncology centre. *J Hum Nutr Diet* (2008) 21:575–83. doi: 10.1111/j.1365-277X.2008.00917.x

17. Cederholm T, Jensen GL, Correia MITD, Gonzalez MC, Fukushima R, Higashiguchi T, et al. GLIM criteria for the diagnosis of malnutrition – A consensus report from the global clinical nutrition community. *Clin Nutr* (2019) 38:1–9. doi: 10.1016/j.clnu.2018.08.002

18. Britton B, Baker AL, Wolfenden L, Wratten C, Bauer J, Beck AK, et al. Eating as treatment (EAT): A stepped-wedge, randomized controlled trial of a health behavior change intervention provided by dietitians to improve nutrition in patients with head and neck cancer undergoing radiation therapy (TROG 12.03). *Int J Radiat Oncol Biol Phys* (2019) 103:353–62. doi: 10.1016/j.ijrobp.2018.09.027

19. Orell H, Schwab U, Saarilahti K, Österlund P, Ravasco P, Mäkitie A. Nutritional counseling for head and neck cancer patients undergoing (chemo) radiotherapy—a prospective randomized trial. *Front Nutr* (2019) 6:22. doi: 10.3389/fnut.2019.00022

20. Sandmæl JA, Bye A, Solheim TS, Stene GB, Thorsen L, Kaasa S, et al. Feasibility and preliminary effects of resistance training and nutritional supplements during versus after radiotherapy in patients with head and neck cancer: A pilot randomized trial. *Cancer* (2017) 123:4440–8. doi: 10.1002/cncr.30901

21. Capozzi LC, McNeely ML, Lau HY, Reimer RA, Giese-Davis J, Fung TS, et al. Patient-reported outcomes, body composition, and nutrition status in patients with head and neck cancer: Results from an exploratory randomized controlled exercise trial. *Cancer* (2016) 122:1185–200. doi: 10.1002/cncr.29863

22. Lonbro S, Dalgas U, Primdahl H, Overgaard J, Overgaard K. Feasibility and efficacy of progressive resistance training and dietary supplements in radiotherapy treated head and neck cancer patients-the DAHANCA 25A study. *Acta Oncol (Madr)* (2013) 52:310–8. doi: 10.3109/0284186X.2012.741325

23. Cereda E, Cappello S, Colombo S, Klersy C, Imarisio I, Turri A, et al. Nutritional counseling with or without systematic use of oral nutritional supplements in head and neck cancer patients undergoing radiotherapy. *Radiother Oncol* (2018) 126:81–8. doi: 10.1016/j.radonc.2017.10.015

24. Jiang W, Ding H, Li W, Ling Y, Hu C, Shen C. Benefits of oral nutritional supplements in patients with locally advanced nasopharyngeal cancer during concurrent chemoradiotherapy: an exploratory prospective randomized trial. *Nutr Cancer* (2018) 70:1299–307. doi: 10.1080/01635581.2018.1557222

25. MacHon C, Thezenas S, Dupuy AM, Assenat E, Michel F, Mas E, et al. Immunonutrition before and during radiochemotherapy: Improvement of inflammatory parameters in head and neck cancer patients. *Support Care Cancer* (2012) 20:3129–35. doi: 10.1007/s00520-012-1444-5

26. Sykes KJ, Gibbs H, Farrokhian N, Arthur A, Flynn J, Shnayder Y, et al. Pilot randomized, controlled, preoperative intervention for nutrition trial in head and neck cancer. *Head Neck* (2023) 45:156–66. doi: 10.1002/hed.27220

27. Blake C, Edwards A, Treleaven E, Brown T, Hughes B, Lin C, et al. Evaluation of a novel pre-treatment model of nutrition care for patients with head and neck cancer receiving chemoradiotherapy. *Nutr Diet* (2022) 79:206–16. doi: 10.1111/1747-0080.12714

28. Ho YW, Yeh KY, Hsueh SW, Hung CY, Lu CH, Tsang NM, et al. Impact of early nutrition counseling in head and neck cancer patients with normal nutritional status. *Support Care Cancer* (2021) 29:2777–85. doi: 10.1007/s00520-020-05804-3

29. Jantharapattana K, Orapipatpong O. Efficacy of EPA-enriched supplement compared with standard formula on body weight changes in malnourished patients with head and neck cancer undergone surgery: a randomized study. *Head Neck* (2020) 42:188–97. doi: 10.1002/hed.25987

30. Boisselier P, Kaminsky MC, Thézenas S, Gallocher O, Lavau-Denes S, Garcia-Ramirez M, et al. A double-blind phase III trial of immunomodulating nutritional formula during adjuvant chemoradiotherapy in head and neck cancer patients: IMPATOX. *Am J Clin Nutr* (2020) 112:1523–31. doi: 10.1093/ajcn/nqaa227

31. Carvalho TC, Cruz BCS, Viana MS, Martucci RB, Saraiva DCA, Reis PF. Effect of nutritional supplementation enriched with eicosapentaenoic acid on inflammatory profile of patients with oral cavity cancer in antineoplastic pretreatment: A controlled and randomized clinical trial. *Nutr Cancer* (2017) 69:428–35. doi: 10.1080/01635581.2017.1274406

32. Brown TE, Banks MD, Hughes BGM, Lin CY, Kenny LM, Bauer JD. Randomised controlled trial of early prophylactic feeding vs standard care in patients with head and neck cancer. *Br J Cancer* (2017) 117:15–24. doi: 10.1038/bjc.2017.138

33. Giddings A. Treatment interruptions in radiation therapy for head-and-neck cancer: Rates and causes. *J Med Imaging Radiat Sci* (2010) 41:222–9. doi: 10.1016/j.jmir.2010.08.002

34. Ravasco P, Monteiro-Grillo I, Vidal PM, Camilo ME. Impact of nutrition on outcome: A prospective randomized controlled trial in patients with head and neck cancer undergoing radiotherapy. *Head Neck* (2005) 27:659–68. doi: 10.1002/hed.20221

35. Talwar B, Findlay M. When is the optimal time for placing a gastrostomy in patients undergoing treatment for head and neck cancer? *Curr Opin Support Palliat Care* (2012) 6:41–53. doi: 10.1097/SPC.0b013e32834feafd

36. Bradley PT, Brown T, Paleri V. Gastrostomy in head and neck cancer: Current literature, controversies and research. *Curr Opin Otolaryngol Head Neck Surg* (2015) 23:162–70. doi: 10.1097/MOO.0000000000000135

37. NICE group. *Nutrition support for adults: oral nutrition support, enteral tube feeding and parenteral nutrition*. London: National Institute for Health and Care Excellence (NICE); NICE Clinical Guidelines (2022).

38. Reber E, Schönenberger KA, Vasiloglou MF, Stanga Z. Nutritional risk screening in cancer patients: the first step toward better clinical outcome. *Front Nutr* (2021) 8:603936. doi: 10.3389/fnut.2021.603936

39. Caccialanza R, Cereda E, Orlandi E, Filippi AR, Comoli P, Alberti A, et al. Immunonutrition in head and neck cancer patients undergoing chemoradiotherapy: an alternative approach for overcoming potential bias. *Am J Clin* (2021) 113 (4):1053–54.

40. Caccialanza R, Cereda E, Klersy C, Nardi M, Masi S, Crotti S, et al. The efficacy of immunonutrition in improving tolerance to chemoradiotherapy in patients with head and neck cancer, receiving nutritional counseling: study protocol of a randomized, open-label, parallel group, bicentric pilot study. *Ther Adv Med Oncol* (2021) 13. doi: 10.1177/17588359211025872

41. Scarpa M, Kotsafti A, Fassan M, Scarpa M, Cavallin F, Nardi T, et al. Immunonutrition before esophagectomy: Impact on immune surveillance mechanisms. *Tumor Biol* (2017) 39:1–9. doi: 10.1177/1010428317728683

42. Talvas J, Garrait G, Goncalves-Mendes N, Rouanet J, Vergnaud-Gauduchon J, Kwiatkowski F, et al. Immunonutrition stimulates immune functions and antioxidant defense capacities of leukocytes in radiochemotherapy-treated head & neck and esophageal cancer patients: A double-blind randomized clinical trial. *Clin Nutr* (2015) 34:810–7. doi: 10.1016/j.clnu.2014.12.002

Frontiers in Oncology

Advances knowledge of carcinogenesis and tumor progression for better treatment and management

The third most-cited oncology journal, which highlights research in carcinogenesis and tumor progression, bridging the gap between basic research and applications to imrpove diagnosis, therapeutics and management strategies.

Discover the latest Research Topics

See more →

Frontiers

Avenue du Tribunal-Fédéral 34
1005 Lausanne, Switzerland
frontiersin.org

Contact us

+41 (0)21 510 17 00
frontiersin.org/about/contact